frontiers | Research Topics

Bone marrow adiposity: Contributions to bone, aging, and beyond

Edited by
Jason Horton, Andre J. van Wijnen and Sarah Beck-Cormier

Published in
Frontiers in Endocrinology

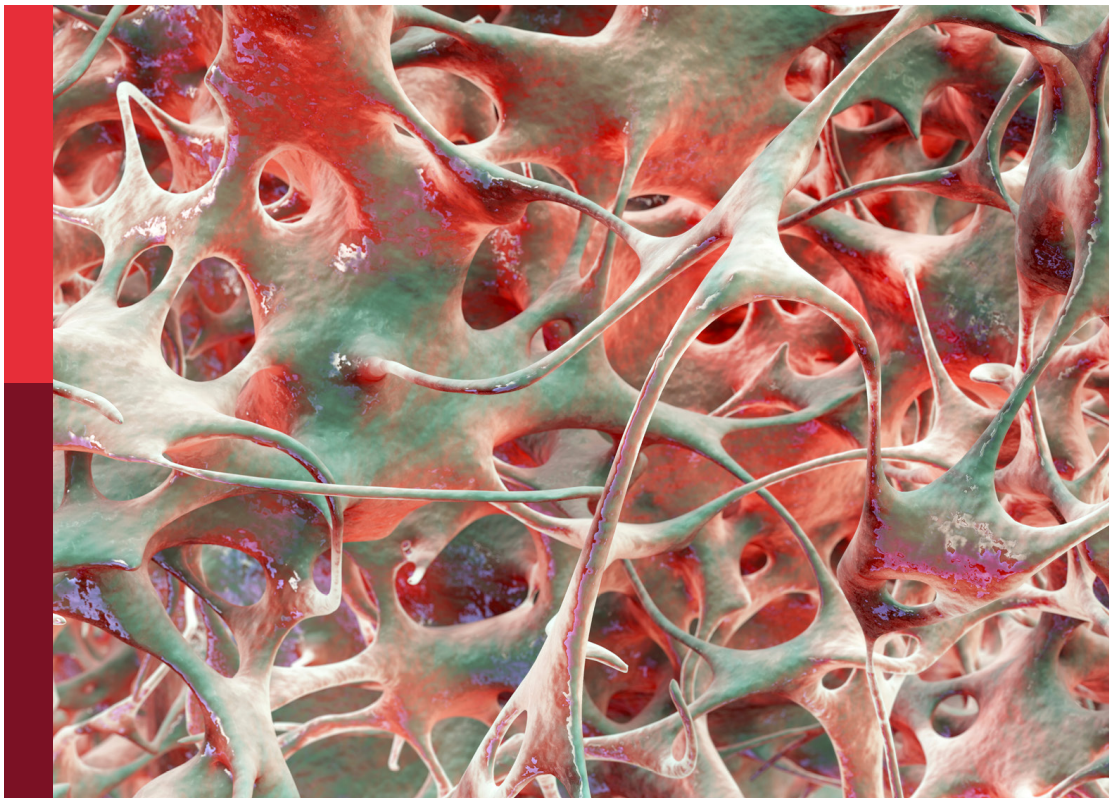

THE INTERNATIONAL BONE MARROW ADIPOSITY SOCIETY
AT THE CROSSROADS OF FAT, BLOOD AND BONE

ISSN 1664-8714
ISBN 978-2-8325-2382-7
DOI 10.3389/978-2-8325-2382-7

About Frontiers

Frontiers is more than just an open access publisher of scholarly articles: it is a pioneering approach to the world of academia, radically improving the way scholarly research is managed. The grand vision of Frontiers is a world where all people have an equal opportunity to seek, share and generate knowledge. Frontiers provides immediate and permanent online open access to all its publications, but this alone is not enough to realize our grand goals.

Frontiers journal series

The Frontiers journal series is a multi-tier and interdisciplinary set of open-access, online journals, promising a paradigm shift from the current review, selection and dissemination processes in academic publishing. All Frontiers journals are driven by researchers for researchers; therefore, they constitute a service to the scholarly community. At the same time, the *Frontiers journal series* operates on a revolutionary invention, the tiered publishing system, initially addressing specific communities of scholars, and gradually climbing up to broader public understanding, thus serving the interests of the lay society, too.

Dedication to quality

Each Frontiers article is a landmark of the highest quality, thanks to genuinely collaborative interactions between authors and review editors, who include some of the world's best academicians. Research must be certified by peers before entering a stream of knowledge that may eventually reach the public - and shape society; therefore, Frontiers only applies the most rigorous and unbiased reviews. Frontiers revolutionizes research publishing by freely delivering the most outstanding research, evaluated with no bias from both the academic and social point of view. By applying the most advanced information technologies, Frontiers is catapulting scholarly publishing into a new generation.

What are Frontiers Research Topics?

Frontiers Research Topics are very popular trademarks of the *Frontiers journals series*: they are collections of at least ten articles, all centered on a particular subject. With their unique mix of varied contributions from Original Research to Review Articles, Frontiers Research Topics unify the most influential researchers, the latest key findings and historical advances in a hot research area.

Find out more on how to host your own Frontiers Research Topic or contribute to one as an author by contacting the Frontiers editorial office: frontiersin.org/about/contact

Bone marrow adiposity: Contributions to bone, aging, and beyond

Topic editors

Jason Horton — Upstate Medical University, United States

Andre J. van Wijnen — University of Vermont, United States

Sarah Beck-Cormier — INSERM U1229 Médecine Régénératrice et Squelette (RMeS), France

Citation

Horton, J., van Wijnen, A. J., Beck-Cormier, S., eds. (2023). *Bone marrow adiposity: Contributions to bone, aging, and beyond*. Lausanne: Frontiers Media SA. doi: 10.3389/978-2-8325-2382-7

This research topic was sponsored by the International Bone Marrow Adiposity Society (BMAS, https://bma-society.org/) and is published in collaboration with Frontiers in Endocrinology. The guest editors and BMAS membership wish to gratefully acknowledge the efforts of the authors and peer-reviewers in making this e-book possible.

Table of contents

frontiers | Frontiers in Endocrinology

TYPE Editorial
PUBLISHED 02 February 2023
DOI 10.3389/fendo.2023.1144163

OPEN ACCESS

EDITED AND REVIEWED BY
Jonathan H. Tobias,
University of Bristol, United Kingdom

*CORRESPONDENCE
Jason A. Horton
hortonj@upstate.edu

SPECIALTY SECTION
This article was submitted to Bone Research, a section of the journal Frontiers in Endocrinology

RECEIVED 13 January 2023
ACCEPTED 25 January 2023
PUBLISHED 02 February 2023

CITATION
Horton JA, Beck-Cormier S and van Wijnen AJ (2023) Editorial: Bone marrow adiposity - contributions to bone, aging and beyond. *Front. Endocrinol.* 14:1144163. doi: 10.3389/fendo.2023.1144163

Editorial: Bone marrow adiposity - contributions to bone, aging and beyond

Jason A. Horton[1]*, Sarah Beck-Cormier[2] and Andre J. van Wijnen[3]

[1]Deparment of Orthopedic Surgery, State University of New York (SUNY) Upstate Medical University, Syracuse, NY, United States, [2]Nantes Université, The National Center for Scientific Research (CNRS), The National Institute of Health and Medical Research (INSERM), l'institut du thorax, Nantes, France, [3]Department of Biochemistry, University of Vermont, Burlington, VT, United States

KEYWORDS

bone marrow adipose tissue (BMAT), osteoporosis, diabetes, adipocyte biology, bone biology and physiology

Editorial on the Research Topic
Bone marrow adiposity - contributions to bone, aging, and beyond

Introduction

Bone marrow adipose tissue (BMAT) plays a complex role in regulating various biological processes, including metabolism, endocrine and immune functions, hematopoeisis and skeletal homeostasis. However, our understanding of the physiological and pathological roles of BMAT remains limited. For this Special Issue on BMAT, we selected 14 articles that provide a comprehensive overview of BMAT, including 4 reviews, 8 original research papers and 2 conference reports. The articles cover a range of topics related to the biology of BMAT in health and disease, and include validated methodologies and overviews of concepts relevant to researchers in the field.

Realizing the vision of the International Bone Marrow Adiposity Society

The International Bone Marrow Adiposity Society (BMAS) has held 7 annual meetings since 2015, with the sixth meeting held virtually in 2020 due to the COVID-19 pandemic (Scheller et al.). The meeting was attended by nearly 200 people from 18 countries and featured presentations, networking opportunities and career development. The BMAS also held its inaugural Summer School in 2021, which was aimed at early-career researchers and featured lectures, workshops and career development sessions (Labella et al.). The Biobanking Working Group of the BMAS has developed best practices for preparing, preserving and distributing biomaterials and related cells and tissues as biospecimens for research, including protocols and guidelines for ethical, legal and social issues (Lucas et al.). These best practices aim to ensure the rigor and collaborations in the field of BMAT research.

Origins and phenotypes of BMAT in development and aging

This Special Issue contains two informative studies that assess lineage commitment of mesenchymal stem cells. Matsushita et al. reviewed data from single-cell RNA sequencing and lineage tracing studies to build a framework for understanding how bipotent bone marrow stromal cell (BMSC) progenitors differentiate along adipocytic or osteogenic trajectories. This study discussed the inverse relationship between marrow adiposity and bone formation rate and the authors propose that these lineages may be plastic and dynamic, rather than mutually exclusive and static. Evidence of this was presented by Lee et al. whom used a lineage tracing approach the relationship bone marrow adipocytes (BMAd) and osteoblasts. The authors examined mice with a fluorescent osteocyte-specific lineage tracer (i.e., tamoxifen-induced DMP1Cre-driven GFP reporter). In these mice, exposure to the thiazolidinedione (TZD) drug rosiglitazone, which activates Peroxisome-Proliferator Activated Receptor Gamma (PPARγ/PPARG), leads to an expansion of BMAT that is positive for perilipin 1 (PLIN1), a definitive adipocyte marker. However, a small fraction (~5%) of these cells also expressed GFP, which was not observed in control mice, suggesting that osteocytes can convert into adipocytes. The osteoanabolic drug Romosozumab slightly reduced BMAT expansion and eliminated the GFP+/PLIN1+ population. These findings may have implications for the management of co-occurring skeletal and metabolic conditions. Future studies will need to refine how control of cell fate determination of mesenchymal stem cells relates to trans-differentiation of phenotypically committed cells.

Tratwal et al. used single-cell raman microspectroscopy to characterize the lipid saturation profile of murine BMSC-like OP9 cells under induced and spontaneous adipogenic differentiation conditions and compared it to human primary samples with predominantly hematopoietic marrow (iliac crest) or fatty marrow (femoral head). They found that the lipid profile of spontaneously differentiated OP9 cells closely resembled that of hematopoiesis-supportive regulated marrow adipocytes (rMAd), while chemically-induced differentiation promoted a constitutive marrow adipocyte (cMAd)-like phenotype that did not effectively support hematopoiesis. These results offer a new way to differentiate rMAd and cMAd that may be useful for further study of their development and functional differences.

Aaron et al. reviewed the effects of BMAT expansion on bone homeostasis, immune and endocrine function, BMSC biology and bone regeneration during aging. They discuss how BMAT can either support or suppress the growth and differentiation of hematopoietic stem cells (HSCs) and can induce pro-inflammatory cytokines and ROS that contribute to senescence in BMSCs and impair their function. The review suggests potential strategies, such as senolytics, miRNAs and antioxidants, to improve the function of BMSCs and reduce the negative effects of aging on the bone marrow microenvironment, paving the way for further research.

Identification of new regulators for bone and adipose tissues is important for the ageing population being more susceptible to bone loss and fat gain. Considering the deleterious effect of the PiT2 sodium-phosphate co-transporter (SLC20A2) deficiency in bone, Frangi et al. addressed whether the BMAT could also be affected in PiT2/Scl20a2 knockout mice. They found that PiT2-deficient young mice have high level of BMAT, but that this volume does not increase into adulthood, leading to lower BMAT volume in older PiT2-deficient mice. However, the absence of PiT2 did not prevent an increase in BMAT volume in a model of bone loss induced by ovariectomy. PiT2-deficient mice did not have differences in serum phosphate levels or key markers of phosphate regulation, suggesting that the observed defects in BMAT were not related to serum phosphate levels. Their findings suggest that PiT2 plays a role in the maintenance of both bone and BMAT, probably independently of systemic phosphate homeostasis although the cellular and molecular mechanisms remain to be identified.

Role and responses of BMAT in pathophysiology

Ali et al. examined how conditions such as hormone deficiency, obesity and type 2 diabetes can contribute to the development of osteoporosis by increasing the negative impact of BMAT on bone health. They discussed several mechanisms involved in these effects, including transcription factors, DNA damage and the production of inflammatory cytokines that alter the fate of BMSCs. The authors also discussed lifestyle modifications, including diet and exercise, as strategies to improve bone parameters and modulate BMAT in patients with metabolic diseases. They noted that antiresorptive drugs may not be effective in all patients with metabolic diseases and discussed research suggesting that Denosumab may improve insulin sensitivity, bone formation and muscle strength in some cases, but emphasized that need for further research is needed to understand how these co-morbid conditions may be best managed.

Sollmann et al. used advanced image analysis techniques to improve the accuracy of fracture risk prediction in patients with osteoporosis. The authors suggest that incorporating texture analysis of CT and MRI T2* data based on Proton Density Fat fraction (PDFF) may be more effective at predicting and differentiating between patients with and without osteoporotic vertebral fractures compared to bone mineral density (BMD) and PDFF alone.

Janus kinase inhibitors such as Tofacitinib are used to control systemic inflammatory disorders such as rheumatoid arthritis (RA), and may have beneficial effects on bone, but their effect on BMAds is unknown. Letarouilly et al. investigated the effects Tofacitinib, on BMAd and osteoblasts derived from human BMSCs and in RA patients treated with Tofacitinib. Tofacitinib increased BMAd differentiation and decreased osteoblast differentiation of primary cells under non-inflammatory conditions. In RA patients, Tofacitinb increased lumbar spine PDFF and had no effect on BMD or body composition over a 6-month period. These results suggest that Tofacitinib has a stimulatory effect on BMAd commitment and differentiation, which may not support its beneficial effects on the bone microenvironment. Further studies are needed to determine whether this is a class effect of Janus kinase inhibitors or specific to Tofacitinib.

Dello Spedale Venti et al. compared the histopathologic characteristics of BMAds in patients with bone metastasis and myeloproliferative neoplasia to age-matched controls. They found that in both neoplastic conditions, there was a significant reduction in the number and size of BMAds, as well as changes in the expression of certain proteins. They also observed an unusual morphology in BMAds from a patient with metastasis of a malignant glioma. These findings suggest that BMAds undergo significant changes in neoplastic conditions, which may have an impact on the microenvironment and could potentially be used as markers for diagnosis and understanding of these diseases. Further research is needed to understand the mechanisms behind these changes and their clinical implications.

Turner et al. studied the relationship between thermoregulation, BMAT and the hormone leptin in mice. They found that higher housing temperatures led to higher levels of BMAT, white adipose tissue mass and serum leptin in mice and that the administration of leptin led to lower BMAT and higher bone formation in the distal femur metaphysis of mice. However, these effects were not observed in pair-fed mice. They also found that increased housing temperature led to an increase in BMAT in both wild type and leptin-deficient mice, but this increase was attenuated in leptin-deficient mice treated with leptin. These results suggest that both increased housing temperature and increased leptin have independent but opposing effects on BMAT in mice.

Avilkina et al. used a mouse model of anorexia to study the effects of different levels of weight loss on bone density and the expression of the NAD-dependent protein deacetylase Sirtuin 1 (Sirt1) in BMSCs. They found that more severe and prolonged weight loss was associated with decreased bone density and decreased Sirt1 expression in the bone marrow. They also found that Sirt1 expression may influence the differentiation of bone marrow cells into either fat or bone cells, which could further affect bone density. This study suggests that the severity and duration of energy deficits related to anorexia can have important effects on bone density and Sirt1 expression in the bone marrow.

Conclusions and perspective

This Research Topic presents the latest research and comprehensive reviews on the origins, pathology and systemic physiology of BMAT. It includes conference reports, best practices and insights from a community of scientists dedicated to advancing research in this field. The peer review process and membership of the Bone Marrow Adiposity Society contribute to the rigor of this research. The Research Topic highlights the growing interest of research in BMAT function and reveals the importance of future studies aimed at understanding the developmental, homeostatic and endocrinological intricacies of BMAT that impact metabolic disorders, bone health and beyond.

Author contributions

JH prepared the first draft and final manuscript; SB-C and AW edited the manuscript. All authors contributed to the article and approved the submitted version.

Conflict of interest

The authors declare that the research was conducted in the absence of any commercial or financial relationships that could be construed as a potential conflict of interest.

Publisher's note

frontiers in Endocrinology

POLICY AND PRACTICE REVIEWS
published: 16 July 2021
doi: 10.3389/fendo.2021.712088

Report From the 6th International Meeting on Bone Marrow Adiposity (BMA2020)

Erica L. Scheller[1], Meghan E. McGee-Lawrence[2]* and Beata Lecka-Czernik[3]**

[1] Division of Bone and Mineral Diseases, Department of Medicine, Washington University, Saint Louis, MO, United States, [2] Department of Cellular Biology and Anatomy, Medical College of Georgia, Augusta University, Augusta, GA, United States, [3] Departments of Orthopaedic Surgery, Physiology and Pharmacology, Center for Diabetes and Endocrine Research, University of Toledo, Toledo, OH, United States

The 6th International Meeting on Bone Marrow Adiposity (BMA) entitled "Marrow Adiposity: Bone, Aging, and Beyond" (BMA2020) was held virtually on September 9th and 10th, 2020. The mission of this meeting was to facilitate communication and collaboration among scientists from around the world who are interested in different aspects of bone marrow adiposity in health and disease. The BMA2020 meeting brought together 198 attendees from diverse research and clinical backgrounds spanning fields including bone biology, endocrinology, stem cell biology, metabolism, oncology, aging, and hematopoiesis. The congress featured an invited keynote address by Ormond MacDougald and ten invited speakers, in addition to 20 short talks, 35 posters, and several training and networking sessions. This report summarizes and highlights the scientific content of the meeting and the progress of the working groups of the BMA society (http://bma-society.org/).

Keywords: bone marrow adiposity, bone marrow adipocyte, marrow fat, yellow marrow, bone metabolism, bone marrow adiposity society (BMAS)

OPEN ACCESS

Edited by:
Jason Horton,
Upstate Medical University,
United States

Reviewed by:
Eleni Douni,
Agricultural University of Athens,
Greece
William Peter Cawthorn,
University of Edinburgh,
United Kingdom

****Correspondence:***
Erica L. Scheller
scheller@wustl.edu
Meghan E. McGee-Lawrence
mmcgeelawrence@augusta.edu
Beata Lecka-Czernik
beata.leckaczernik@utoledo.edu

Specialty section:
This article was submitted to Bone Research, a section of the journal Frontiers in Endocrinology

Received: *19 May 2021*
Accepted: *21 June 2021*
Published: *16 July 2021*

Citation:
Scheller EL, McGee-Lawrence ME and Lecka-Czernik B (2021) Report From the 6th International Meeting on Bone Marrow Adiposity (BMA2020). Front. Endocrinol. 12:712088. doi: 10.3389/fendo.2021.712088

INTRODUCTION

The primary goal of the 6th international meeting on Bone Marrow Adiposity, "Marrow Adiposity: Bone, Aging, and Beyond" (BMA2020), was to provide a forum for basic, translational, and clinical scientists from around the world to discuss different aspects of bone marrow adiposity in health and disease. The Bone Marrow Adiposity Society (BMAS) conferences are greatly enhanced by the broad research and training backgrounds among conference organizers, speakers, and attendees that promote diverse perspectives and opportunities for collaboration. The field of bone marrow adipose tissue (BMAT) research is growing, which was reflected in the BMA2020 program. Besides a specific focus on aging and osteoporosis, the BMA2020 meeting program included sessions related to the role of BMAT in hematopoiesis, regulation of systemic energy metabolism, cancer development and metastasis, and response to environmental cues including nutrition and exercise (See **Figure 1**).

The BMA2020 meeting was hosted in partnership with the American Society for Bone and Mineral Research (ASBMR) and was co-organized by Drs. Erica Scheller (Washington University), Meghan McGee-Lawrence (Augusta University), and Beata Lecka-Czernik (The University of Toledo). BMA2020 was originally scheduled to take place in Seattle, Washington as the first BMA

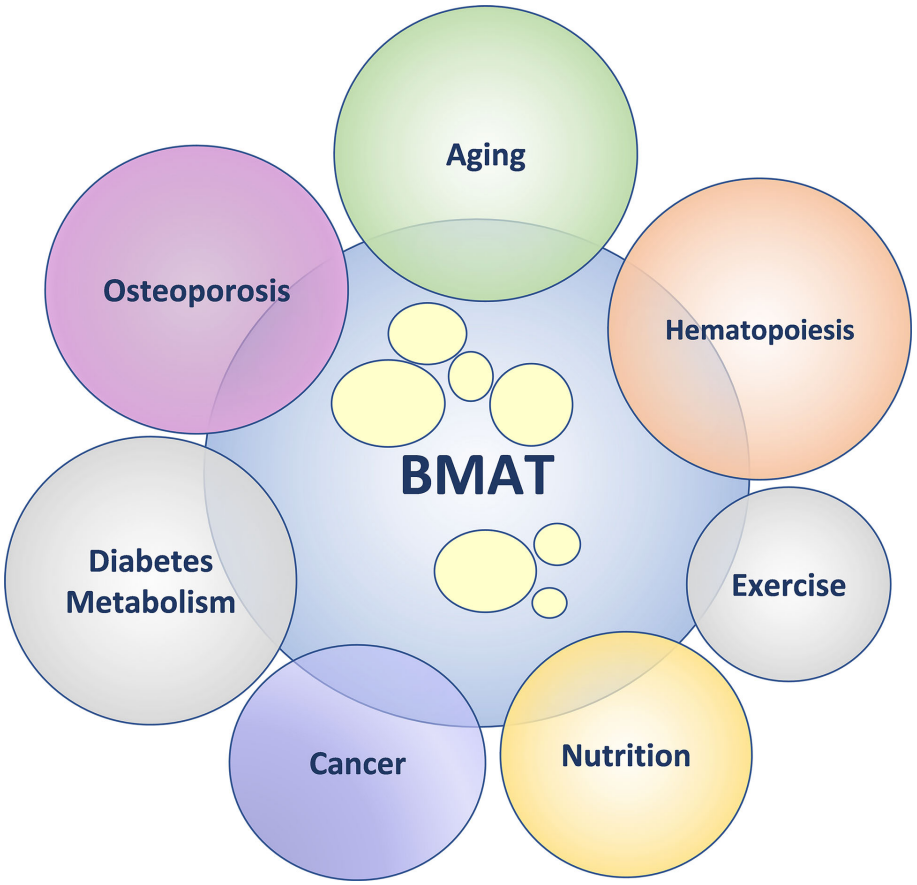

FIGURE 1 | Bone marrow adipose tissue (BMAT) – friend or foe? In health, BMAT supports physiological homeostasis. In pathological states, BMAT augments dysregulation of physiological homeostasis. The diagram depicts the emerging topics within the field of BMAT research.

meeting in the United States. However, due to the global COVID-19 pandemic, the congress was instead hosted entirely online in a mixed live/asynchronous format to promote both networking and accessibility. With great thanks to the dedication of our BMAS members, both established and new, this meeting ended up being our largest event to date with 11 invited speakers, 55 submitted abstracts, and 198 registered attendees from 18 different countries around the world. The congress featured 53 sessions and sub-sessions, 35 posters, and 14 lab highlights that were viewed collectively more than 7,000 times. In direct evidence of the collaborative nature of the meeting, there were also 63 photos shared and 1,391 in-app messages sent between colleagues. In all, despite the change in format, the BMA2020 meeting succeeded in bringing together clinicians and scientists studying all aspects of bone marrow adiposity, contributing to the advancement of the field.

SCIENTIFIC SESSIONS

The scientific sessions at BMA2020 included bone marrow adipocyte (BMAd) dynamics and bone mass in aging, obesity and malnutrition, as well as BMAd progenitors and lineage tracing, metabolism, hematopoiesis, metastasis, leukemia and myeloma, endocrine regulation, exercise, and advanced methods of BMAd imaging and analysis, as discussed below. A full list of talks and speakers is available in **Supplemental Table 1**. Where available, references to recently published related manuscripts are provided below.

Keynote Address

BMA2020 opened with a welcome address from the conference organizers, followed immediately by a keynote presentation by Ormond MacDougald (University of Michigan) entitled "Bone marrow adipose tissue biology, endocrine physiology and metabolism – unique and common traits with peripheral adipose tissue depots". In his talk, Dr. MacDougald highlighted the basis of BMAd cell biology and physiology as grounded in the broader field of adipose tissue biology. He went on to discuss the nature of regulated and constitutive BMAT clusters (rBMAT and cBMAT, respectively), the discovery of which ultimately provided bases for in-depth analysis of the unique metabolic regulation of BMAT relative to other fat depots in the body (1). Thus, rBMAT located in proximal skeletal elements and closer to

body core temperature is interspersed with hematopoietic, stromal and vascular cells and changes its volume in response to hormonal, nutritional and pharmacological challenges. In contrast, cBMAT, which is located distally and relatively further from the body core temperature, shares similar characteristics with white adipose tissue and is largely resistant to environmental stimuli (2). However, cBMAT volume in humans may change after bariatric surgery and in certain hematologic conditions (3). Dr. MacDougald also introduced the first animal model that specifically targets marrow adipocytes by expressing both adipocyte-targeted (adiponectin) and osteoblast-targeted (osterix) markers, a combination that is characteristic for BMAds. This conditional model may ultimately help the field to understand BMAT function in diverse settings of bone loss, as well as its contributions to systemic energy metabolism. In summary, this keynote presentation was a perfect introduction to the entire conference by highlighting the unique position of BMAT among other fat depots, which may explain its divergent functions in health and disease as explored in the subsequent sessions.

Session I: Bone Marrow Adipose Tissue, Aging, and Skeletal Homeostasis

The first session featured an invited talk by Sundeep Khosla (Mayo Clinic) that covered aspects of BMAT, aging, senolytics and skeletal health. A key focus of his presentation was that cellular senescence may play a causal role in reducing osteoblastogenesis and increasing adipogenesis during the process of aging, suggesting that senolytic drugs have potential to target this aspect of skeletal aging biology (4). The invited talk was followed by four short talks from Anuj Sharma (Augusta University), Abhishek Chandra (Mayo Clinic), Thomas Ambrosi (Stanford University), and Vagelis Rinotas (Agricultural University of Athens) that covered topics including sex differences in marrow adiposity induced by glucocorticoid signaling, radiation-associated bone marrow adiposity, skeletal stem cell diversity, and the role of RANKL in development of BMAd expansion and osteoporosis. The session was moderated by Bram van der Eerden (Erasmus University Rotterdam) and Rosella Labella (Columbia University). The presentation content, and subsequent discussion, focused heavily on mechanisms of cross-talk between cells, and the influence of the bone marrow niche environment (particularly with aging) on mechanisms of increasing marrow adiposity. The first short talk highlighted the sexually dimorphic low bone mass and high BMAT phenotype of mice with conditional deletion of the glucocorticoid receptor in osteoprogenitor cells (5). The second talk demonstrated the time course of molecular events leading to enhanced marrow adiposity following irradiation of bone, and highlighted similarities in mechanisms of senescence between aging and irradiated bone that precede fatty infiltration of the bone marrow cavity (6). In the third talk, single cell RNA-sequencing was used to show alterations in the skeletal stem cell populations that promote a pro-inflammatory, pro-resorptive, pro-adipogenic, and anti-osteogenic environment within the bone marrow niche that could be pharmacologically targeted (7). The fourth and final short talk characterized marrow adiposity and BMSC differentiation patterns in two different RANKL transgenic mouse models and explored the molecular mechanisms underlying the observed phenotypes (8).

Session II: Environmental Regulation of Bone and Marrow Adipose Tissue

The second session included two invited talks by Pouneh Fazeli (University of Pittsburgh) and Janet Rubin (University of North Carolina), followed by a short talk from Piotr Czernik (The University of Toledo). It was moderated by Anne Schafer (University of California San Francisco) and Rebecca Schill (University of Michigan). The session was concentrated on regulators of BMAT volume including nutrition, exercise and gut microbiota. Dr. Fazeli reviewed research focused on the paradox of increased BMAT volume in anorexia nervosa, a clinical condition of chronic undernutrition, with a take home message that BMAT serves different functions in states of nutrient sufficiency as compared to nutrient insufficiency (9). In addition, she emphasized the important function of BMAT in regulation of hematopoiesis by demonstrating that BMAT is inversely associated with white and red blood cell counts in premenopausal women, and by showing that in women with anorexia treated with transdermal estrogen, decreases in BMAT were significantly associated with increases in both red blood cells and hematocrit (10). Dr. Rubin focused her presentation on the effect of exercise on adaptive changes in bone, including decreases in BMAT volume and increases in osteogenesis. This presentation added new information to the ongoing discussion on sequestration of β-catenin and Wnt pathway activity in regards to the BMSC lineage commitment and identified EZH2 as key to preservation of BMSC multipotentiality *via* β-catenin (11, 12). To conclude the session, a short talk by Piotr Czernik revealed that reconstitution of the gut microbiome in germ-free rats increased marrow adipocyte number and altered their cell size distribution toward smaller adipocytes. His work suggests that gut microbiota deliver powerful signals to the skeleton to regulate bone marrow adipocyte differentiation and function and that *de novo* expansion of small adipocytes synergizes with new bone formation in conditions of acute nutrient utilization in the gut (13).

Session III: Endocrine Regulation of Bone Marrow Adipose Tissue in Health and Disease

Session III began with an invited talk by Clifford Rosen (Maine Medical Center Research Institute). This presentation focused on the role of hormones, especially parathyroid hormone, in the regulation of BMAT *via* mechanisms such as lineage recruitment and lipolysis (14, 15). The invited talk was followed by three short talks by Nikki Aaron (Columbia University), Sudipta Baroi (The University of Toledo), and Li Chen (Southern Denmark University) that covered topics including novel adipokines, osteocytic control of marrow adiposity *via* sclerostin production, and crosstalk between the immune system and bone. This session was moderated by Laura McCabe (Michigan State University) and Biagio Palmisano (Columbia University). The first short talk reported the role of the novel adipokine adipsin and its ability

to activate the immune complement system in BMAT expansion promoted by caloric restriction or thiazolidinedione treatment (16). The second short talk described the role of PPARγ in osteocytes, showing that the sclerostin gene is regulated by PPARγ and that osteocyte-specific conditional knockout mice have a high bone mass and low BMAT phenotype (17). The third and final short talk in this session examined the regulatory role of the immune system complement factor H in bone and BMAT homeostasis (18).

Session IV: Advanced Methods for Clinical and Pre-Clinical Assessment of Bone Marrow Adiposity and Skeletal Health

This methods-focused session started with two invited speakers, Gustavo Duque (University of Melbourne) and Greet Kerckhofs (Université Catholique de Louvain), followed by two short talks from Kisoo Pahk (Korea University Anam Hospital) and Josefine Tratwal (Ecole Polytechnique Fédérale de Lausanne). Session IV was moderated by Jean-Francois Budzik (Groupement des Hôpitaux de l'Institut Catholique de Lille) and Ahmed Al Saedi (University of Melbourne). Dr. Duque discussed secreted factors that couple bone marrow adipocytes to the surrounding skeletal cells and their implications for the pathophysiology of osteoporosis. In addition, he provided information about key technical approaches that can be used to study aspects of bone marrow adipocyte function and lipotoxicity both *in vitro* and *ex vivo* (19, 20). After this, Dr. Kerckhofs demonstrated how novel contrast agents such as polyoxometalate can be used to visualize and to quantify bone marrow adipocytes in three dimensions, in addition to relating this information to bone and vascular quantifications using high-resolution computed tomography (21). Next, Kisoo Pahk reported the use of 18F-FDG PET/CT for the evaluation of adipose tissue metabolic activity in patients with osteoporosis, demonstrating that metabolic activity of visceral *vs* subcutaneous adipose tissue is predictive of bone mineral density (22). Last, Josefine Tratwal gave an overview of a new injectable, three-dimensional tissue engineered model of bone marrow adipogenesis and hematopoiesis that can be used to accelerate studies on the regeneration of the bone marrow niche for treatment of blood and other marrow-related disorders (23).

Session V: Bone Marrow Adipose Tissue, Cancer, and Hematopoiesis

The invited speakers for Session V were Olaia Naiveras (École Polytechnique Fédérale de Lausanne) and Izabela Podgorski (Wayne State University). Short talks were given by Emma Morris (University of Oxford), Sonia Severin (Inserm U1048 and Paul Sabatier University), and Mariah Farrell (Maine Medical Center Research Institute). The session was moderated by Michaela Reagan (Maine Medical Center Research Institute) and Josefine Tratwal (Ecole Polytechnique Fédérale de Lausanne). Session V focused on mechanisms by which BMAT regulates hematopoiesis and cancer progression. Olaia Naveiras summarized the effects of BMAT on hematopoiesis, including use of MarrowQuant, a new tool for quantification of bone marrow compartments in histologic sections (24). This presentation concluded that marrow adiposity correlates inversely with hematopoiesis in health and pathologic conditions, and that the degree of adipocyte maturation correlates inversely with the proliferation of hematopoietic precursors. In addition, Dr. Naiveras identified loss of SCF upon differentiation of BMAT progenitor cells as responsible for decreased support of hematopoiesis (25). After this, Izabela Podgorski showed that BMAT fuels and supports growth of prostate cancer metastasis to bone by serving as an abundant source of lipids and signaling molecules. She demonstrated that metastatic tumor cells engage in reciprocal interactions with bone marrow adipocytes to evade therapy and provided evidence that targeting IL-1β or lipolysis improves tumor cell response to anti-cancer therapy with docetaxel (26). Dr. Podgorski concluded her talk by stressing an importance of understanding the role of BMAT in tumor adaptation and survival in bone, as a tool to reveal novel, mechanistic targets for therapies for prostate and breast bone-metastatic diseases, which continue to be incurable (27). After this, Emma Morris discussed the effects of PPARγ agonist BAGDE on myeloma cells and bone marrow adipocytes (28), Sonia Severin showed a functional link between marrow adipocytes and the development of megakaryocytes (29), and Mariah Farrell revealed that bone marrow adipocytes support multiple myeloma drug resistance and induce adipocyte mimicry, increasing cell survival (30, 31). Overall, this session stressed an importance of understanding the role of BMAT in hematopoiesis and cancer cell survival in bone, while underscoring a prominent role of adipocytes in the regulation of different components of hematopoietic niche.

Session VI: Bone Marrow Adipose Tissue Origins and Maturation

This session featured an invited talk by Moustapha Kassem (University of Southern Denmark) and three short talks by Russell Turner (Oregon State University), Leilei Zhong (University of Pennsylvania), and Xiao Zhang (Washington University). Session VI was moderated by Michaela Tencerova (University of Southern Denmark) and Sudipta Baroi (The University of Toledo). Dr. Kassem opened the session by reviewing the mechanisms underlying lineage commitment of multipotent bone marrow stromal (skeletal) stem cells to adipocytes with an emphasis on the role of KIAA1199 (32). Next, Dr. Turner presented data showing that c-kit expression in hematopoietic and mesenchymal cells contributes to the maturation of bone marrow adipocytes (33). After this, Leilei Zhong presented new data that defines a stromal/perivascular, adiponectin-expressing bone marrow adipocyte progenitor, termed the marrow adipogenic lineage precursor (MALP) and its role in the maintenance of the bone marrow vasculature (34, 35). Last, Xiao Zhang showed that a unique population of maladapted bone marrow adipocytes was retained in an otherwise 'fat free' lipodystrophic mouse, revealing the existence of a bone-specific, compensatory adipogenesis pathway that is activated in states of metabolic stress (36). Overall, this session contributed to our understanding of the unique cellular origins of

bone marrow adipocytes during development and metabolic disease, in addition to providing new information about the molecular signals regulating the maturation of committed pre-adipocytes within the bone marrow.

Session VII: Bone Marrow Adipocyte Differentiation, Metabolism and the Skeletal Niche

The final session started with an invited talk by Courtney Karner (University of Texas Southwestern Medical Center), followed by four short talks by Ziru Li (University of Michigan), Ayyoub Salmi (MABlab), Amit Chougule (University of Toledo), and Wei Yu (University of Pennsylvania). The session was moderated by Christophe Chauveau (MABLab) and Thomas Ambrosi (Stanford University). Dr. Karner presented on the role of glutamine metabolism in the fate specification of bone marrow adipocytes from mesenchymal precursor cells, providing support for a model by which inhibition of glutamine metabolism or glutathione biosynthesis increases oxidative stress and promotes adipocyte differentiation (37). After this, Dr. Li presented work in a conditional adipose triglyceride lipase knockout mouse demonstrating roles for bone marrow adipocyte lipolysis in states of nutrient deficiency. Next, Ayyoub Salmi presented evidence in support of the capacity for osteoblasts to transdifferentiate to adipocyte-like cells following co-culture with adipocytes, emphasizing the plasticity and intercellular communication of cell populations within bone (38). This was followed by a presentation from Amit Chougule showing that activation of PPARα in the osteocyte lineage suppresses bone marrow adipose tissue expansion in regions of hematopoietic marrow. Last, Wei Yu demonstrated that adiponectin-expressing MALP cells are a critical source of osteoclast-regulatory factor RANKL, contributing directly to osteoclast formation and bone turnover (35). The questions and discussion in this diverse session centered on Cre specificity and the use of Cre-dependent lineage tracing when compared to surface marker strategies for characterization of bone marrow adipocyte progenitors. In addition, the group emphasized the need to continue to work together to unify our models and definitions to promote the advancement of future work in the field.

POSTERS

Posters consisted of a pre-recorded video presentation of up to 5-minutes in length. Virtual posters were highlighted in the exhibitor center and could be viewed asynchronously by congress attendees. A live poster session was also held on the first day of the conference where attendees and presenters could post and respond to questions in real time. The highlighted topics of the posters fell into several main categories including aging, BMAT dynamics and bone mass, endocrine regulation, imaging and advanced methods, metabolism, metastasis, myeloma and hematopoiesis, obesity and malnutrition, and progenitors and lineage tracing. A detailed list of posters and presenters is available in **Supplemental Table 2**.

NETWORKING AND PROFESSIONAL DEVELOPMENT

The Bone Marrow Adiposity Society is committed to fostering collaborations between members and to the development of trainees and fellows to support the growth and advancement of the field. Consistent with this mission, the BMA2020 meeting featured several trainee discussion sessions and networking events. All members were invited to participate in an open discussion with keynote speaker Dr. Ormond MacDougald, a question-and-answer session with leaders from the National Institutes of Health, and a BMA2020 'After Hours Trivia' social event hosted by Don't Tell Comedy. In addition, there were two trainee-specific sessions focused on topics including publishing, preprints, and open access (led by William Cawthorn, The University of Edinburgh) and planning for life and job opportunities after research training (led by Gina Woods, UCSD, Hai-Bin Ruan, University of Minnesota, and Christa Maes, KU Leuven). The meeting organizers would like to provide special thanks to Andrea Lovdel and Biagio Palmisano for their contributions to the development of the trainee-focused content and trivia event of the BMA2020 meeting.

BMAS WORKING GROUPS

In addition to networking and scientific content, the BMA2020 symposium provided a forum for meetings of the six BMAS working groups (WG). Additional information on the activities of the working groups can also be obtained by following BMAS on twitter (@BMA_Society).

WG1 – Nomenclature. The nomenclature working group position paper reporting Standardized Nomenclature, Abbreviations, and Units for the Study of Bone Marrow Adiposity was published in 2020 (39). The current goal of WG1 is to promote the awareness and application of these guidelines among researchers, journal editors and publishers, and to continue monitoring the emergence of new terms and methods to ensure that the guidelines are updated as the field continues to develop.

WG2 – Methodologies. The goal of the methodologies working group is to encourage the use of standardized methodologies for the assessment of bone marrow adipocytes. The methodologies working group recently published a review on standardization in methodology for the study of bone marrow adiposity (40). After welcoming new members, the methodologies working group decided on new projects. In the coming years the group will focus on in-depth review and discussion of *in vivo* imaging methods and *in vitro* systems in the study of bone marrow adiposity, leading to future publications on the topic to promote the standard application of methods in the field.

WG3 – Biobanking. The aim of the biobanking working group is to establish the use of standardized protocols for the collection and storage of materials related to bone marrow adipocytes. WG3 is currently preparing a position paper on biobanking of BMAd-related material. This position paper will cover several aspects of biobanking including introduction to

biobanking with a focus on BMAd-related material, patient information, pseudonymization and ethics, types of tissues/sources from which BMAd-related material can be obtained, and isolation protocols to collect bone marrow adipocytes and bone marrow mesenchymal stromal cells for future applications. With this, WG3 aims to reach clinicians and scientists involved in biobanking of BMAd-related material by providing considerations on the collection, storage and use of BMAd-samples.

WG4 - Public Engagement. The working group on public engagement focuses on ways to educate target groups outside the society, including other societies, patient organizations and the public. Since the start of the working group, fruitful collaborations have been set up with affiliating societies, such as ECTS and ASBMR. Finally, WG4 is involved in managing the social media (Twitter, LinkedIn) of BMAS.

WG5 – Repositories. The working group on repositories aims to identify currently existing repositories that contain expression data related to BMAd. Ultimately, this information can be distributed among BMAS members to gain access to the BMAd-related repositories for their research.

WG6 – Sponsoring. The aim of the sponsoring working group is to find partners in industry and academia to financially liaise with BMAS. This committee is tasked with developing a strategy to ensure stable sponsorships for BMAS.

AWARDS

Awards were presented during the conclusion of the BMA2020 meeting for the highest scoring clinical research and basic/translational research short talks and poster presentations. In addition, to promote scientific discourse and interaction during the virtual meeting, awards were also presented for the "audience choice" best poster presentation, a social media-based photo contest, a community engagement award, and a trivia contest. For the abstract-based scientific awards, all abstract submissions underwent blinded review and scoring by three to five independent reviewers. Abstracts were categorized as "clinical research" or "basic/translational research", and awards were administered proportionally to the volume of abstracts received in each category; seven such awards were presented for basic/translational research, and three for clinical science. For the short talk and poster presentation awards during the meeting, presentations were scored by representatives from the BMAS Scientific Board on the overall presentation quality, the speaker's responses during the question and answer session, the impact of the data, and the overall communication of the message. A full list of scientific awards and recipients is provided in **Supplemental Table 3**.

CONCLUDING REMARKS AND PERSPECTIVES

BMA2020 was the 6th International Meeting of the Bone Marrow Adiposity Society. This was an important forum for discussion within the diverse, growing field of bone marrow adiposity research. The success of the transition to a virtual format has prompted discussions regarding the future integration of both in-person and virtual events to support the attendance of those that are not able to travel to the on-site destination. Moving forward, the BMAS meetings will be held once every 2-years with the next BMA2022 meeting currently scheduled to take place in Greece under the direction of Eleni Douni. In addition to this, several trainees and members within BMAS have come together to organize a virtual training seminar entitled "BMAS Summer School 2021". This training seminar will take place over three half-days in September of 2021 and feature topical lectures from international experts, skill-based workshops, group discussions, and presentations that will promote the career development of trainees in the field. In conclusion, we are thankful for the overall success of the BMA2020 symposia and the connections made between colleagues despite the global COVID-19 pandemic. Though bone marrow adipocytes are gaining increasing attention as an endocrine cell and key component of the skeletal niche, much remains to be discovered to harness their potential in anti-osteoporotic, metabolic, cancer, hematological, or regenerative therapies. The research highlighted at this meeting and the new collaborations formed between colleagues will undoubtedly contribute to these efforts.

AUTHOR CONTRIBUTIONS

ES, MM-L, and BL-C served as co-organizers of the BMA2020 meeting and worked together to develop the conference report herein. All authors contributed to the article and approved the submitted version.

FUNDING

The authors declare that this research conference received funding from Radius Heath Inc., Kubtec, The Jackson Laboratory, Progen, Washington University Musculoskeletal Research Center, and BioQuant. The funders were not involved in the conference design, the writing of this article or the decision to submit it for publication.

ACKNOWLEDGMENTS

Grant support for the BMA2020 meeting was received from the National Institute on Aging (primary) with secondary support from the National Institute of Arthritis and Musculoskeletal and Skin Diseases (R13AG069353-01; Lecka-Czernik, McGee-Lawrence, and Scheller). Additional financial support was provided by the following companies: Radius Heath Inc., Kubtec, The Jackson Laboratory, Progen, Washington University Musculoskeletal Research Center, and BioQuant. The organizers of the BMA2020 meeting would like to thank our partner society, the American Society for Bone and Mineral Research (ASBMR), for meeting promotion. Technical support was provided by Joey Daoud from

NewTerritory Media and the Whova virtual meeting platform. In addition, the organizers would like to thank administrators Linda Mudd and Kena King (Washington University) and Jeff Lewandowski (University of Toledo) for their important contributions to the success of the BMA2020 meeting.

SUPPLEMENTARY MATERIAL

The Supplementary Material for this article can be found online at: https://www.frontiersin.org/articles/10.3389/fendo.2021.712088/full#supplementary-material

REFERENCES

1. Scheller EL, Doucette CR, Learman BS, Cawthorn WP, Khandaker S, Schell B, et al. Region-Specific Variation in the Properties of Skeletal Adipocytes Reveals Regulated and Constitutive Marrow Adipose Tissues. *Nat Commun* (2015) 6:7808. doi: 10.1038/ncomms8808
2. Mori H, Dugan CE, Nishii A, Benchamana A, Li Z, Cadenhead TS, et al. The Molecular and Metabolic Program by Which White Adipocytes Adapt to Cool Physiologic Temperatures. *PLoS Biol* (2021) 19(5):e3000988. doi: 10.1371/journal.pbio.3000988
3. Li Z, Hardij J, Evers SS, Hutch CR, Choi SM, Shao Y, et al. G-CSF Partially Mediates Effects of Sleeve Gastrectomy on the Bone Marrow Niche. *J Clin Invest* (2019) 129(6):2404–16. doi: 10.1172/JCI126173
4. Khosla S, Farr JN, Tchkonia T, Kirkland JL. The Role of Cellular Senescence in Ageing and Endocrine Disease. *Nat Rev Endocrinol* (2020) 16(5):263–75. doi: 10.1038/s41574-020-0335-y
5. Pierce JL, Ding KH, Xu J, Sharma AK, Yu K, Del Mazo Arbona N, et al. The Glucocorticoid Receptor in Osteoprogenitors Regulates Bone Mass and Marrow Fat. *J Endocrinol* (2019) 243(1):27–42. doi: 10.1530/JOE-19-0230
6. Chandra A, Lagnado AB, Farr JN, Monroe DG, Park S, Hachfeld C, et al. Targeted Reduction of Senescent Cell Burden Alleviates Focal Radiotherapy-Related Bone Loss. *J Bone Miner Res* (2020) 35(6):1119–31. doi: 10.1002/jbmr.3978
7. Ambrosi TH, Goodnough LH, Chan CKF. Human Skeletal Stem Cell Aging. *Aging* (2020) 12(17):16669–71. doi: 10.18632/aging.104034
8. Rinotas V, Niti A, Dacquin R, Bonnet N, Stolina M, Han CY, et al. Novel Genetic Models of Osteoporosis by Overexpression of Human RANKL in Transgenic Mice. *J Bone Miner Res* (2014) 29(5):1158–69. doi: 10.1002/jbmr.2112
9. Fazeli PK, Klibanski A. The Paradox of Marrow Adipose Tissue in Anorexia Nervosa. *Bone* (2019) 118:47–52. doi: 10.1016/j.bone.2018.02.013
10. Polineni S, Resulaj M, Faje AT, Meenaghan E, Bredella MA, Bouxsein M, et al. Red and White Blood Cell Counts Are Associated With Bone Marrow Adipose Tissue, Bone Mineral Density, and Bone Microarchitecture in Premenopausal Women. *J Bone Miner Res* (2020) 35(6):1031–9. doi: 10.1002/jbmr.3986
11. Sen B, Paradise CR, Xie Z, Sankaran J, Uzer G, Styner M, et al. β-Catenin Preserves the Stem State of Murine Bone Marrow Stromal Cells Through Activation of EZH2. *J Bone Miner Res* (2020) 35(6):1149–62. doi: 10.1002/jbmr.3975
12. Pagnotti GM, Styner M, Uzer G, Patel VS, Wright LE, Ness KK, et al. Combating Osteoporosis and Obesity With Exercise: Leveraging Cell Mechanosensitivity. *Nat Rev Endocrinol* (2019) 15(6):339–55. doi: 10.1038/s41574-019-0170-1
13. Czernik PJ, Golonka RM, Chakraborty S, Yeoh BS, Abokor A, Saha P, et al. Reconstitution of the Host Holobiont in Germ-Free Rats Acutely Increases Bone Growth and Affects Marrow Cellular Content. *BioRxiv* (2020). doi: 10.1101/2020.07.15.201657
14. Le PT, Liu H, Alabdulaaly L, Vegting Y, Calle IL, Gori F, et al. The Role of Zfp467 in Mediating the Pro-Osteogenic and Anti-Adipogenic Effects on Bone and Bone Marrow Niche. *Bone* (2021) 144:115832. doi: 10.1016/j.bone.2020.115832
15. Maridas DE, Rendina-Ruedy E, Helderman RC, DeMambro VE, Brooks D, Guntur AR, et al. Progenitor Recruitment and Adipogenic Lipolysis Contribute to the Anabolic Actions of Parathyroid Hormone on the Skeleton. *FASEB J* (2019) 33(2):2885–98. doi: 10.1096/fj.201800948RR
16. Aaron N, Kraakman MJ, Zhou Q, Liu Q, Yang J, Liu L, et al. Adipsin Promotes Bone Marrow Adiposity by Priming Mesenchymal Stem Cells. *eLife* (2021) 10:e69209. doi: 10.7554/eLife.69209
17. Baroi S, Czernik PJ, Chougule A, Griffin PR, Lecka-Czernik B. PPARG in Osteocytes Controls Sclerostin Expression, Bone Mass, Marrow Adiposity and Mediates TZD-Induced Bone Loss. *Bone* (2021) 147:115913. doi: 10.1016/j.bone.2021.115913
18. Kristensen LP, Chen L, Nielsen MO, Qanie DW, Kratchmarova I, Kassem M, et al. Temporal Profiling and Pulsed SILAC Labeling Identify Novel Secreted Proteins During *Ex Vivo* Osteoblast Differentiation of Human Stromal Stem Cells. *Mol Cell Proteomics* (2012) 11(10):989–1007. doi: 10.1074/mcp.M111.012138
19. Bani Hassan E, Ghasem-Zadeh A, Imani M, Kutaiba N, Wright DK, Sepehrizadeh T, et al. Bone Marrow Adipose Tissue Quantification by Imaging. *Curr Osteoporos Rep* (2019) 17(6):416–28. doi: 10.1007/s11914-019-00539-5
20. Al Saedi A, Chen L, Phu S, Vogrin S, Miao D, Ferland G, et al. Age-Related Increases in Marrow Fat Volumes Have Regional Impacts on Bone Cell Numbers and Structure. *Calcif Tissue Int* (2020) 107(2):126–34. doi: 10.1007/s00223-020-00700-8
21. De Bournonville S, Vangrunderbeeck S, Ly HGT, Geeroms C, De Borggraeve WM, Parac-Vogt TN, et al. Exploring Polyoxometalates as Non-Destructive Staining Agents for Contrast-Enhanced Microfocus Computed Tomography of Biological Tissues. *Acta Biomater* (2020) 105:253–62. doi: 10.1016/j.actbio.2020.01.038
22. Kim S. Visceral Fat Metabolic Activity Evaluated by 18F-FDG PET. *J Nucl Med* (2020) 61(supplement 1):46–6. doi: 10.1016/j.orcp.2020.05.008
23. Tavakol DN, Tratwal J, Bonini F, Genta M, Campos V, Burch P, et al. Injectable, Scalable 3D Tissue-Engineered Model of Marrow Hematopoiesis. *Biomaterials* (2020) 232:119665. doi: 10.1016/j.biomaterials.2019.119665
24. Tratwal J, Bekri D, Boussema C, Sarkis R, Kunz N, Koliqi T, et al. Marrowquant Across Aging and Aplasia: A Digital Pathology Workflow for Quantification of Bone Marrow Compartments in Histological Sections. *Front Endocrinol (Lausanne)* (2020) 24:11:480. doi: 10.3389/fendo.2020.00480
25. Zhou BO, Yu H, Yue R, Zhao Z, Rios JJ, Naveiras O, et al. Bone Marrow Adipocytes Promote the Regeneration of Stem Cells and Haematopoiesis by Secreting SCF. *Nat Cell Biol* (2017) 19(8):891–903. doi: 10.1038/ncb3570
26. Herroon MK, Diedrich JD, Rajagurubandara E, Martin C, Maddipati KR, Kim S, et al. Prostate Tumor Cell-Derived Il1β Induces an Inflammatory Phenotype in Bone Marrow Adipocytes and Reduces Sensitivity to Docetaxel *via* Lipolysis-Dependent Mechanisms. *Mol Cancer Res* (2019) 17(12):2508–21. doi: 10.1158/1541-7786.MCR-19-0540
27. Diedrich JD, Herroon MK, Rajagurubandara E, Podgorski I. The Lipid Side of Bone Marrow Adipocytes: How Tumor Cells Adapt and Survive in Bone. *Curr Osteoporos Rep* (2018) 16(4):443–57. doi: 10.1007/s11914-018-0453-9
28. Morris EV, Edwards CM. Bone Marrow Adiposity and Multiple Myeloma. *Bone* (2019) 118:42–6. doi: 10.1016/j.bone.2018.03.011
29. Valet C, Batut A, Vauclard A, Dortignac A, Bellio M, Payrastre B, et al. Adipocyte Fatty Acid Transfer Supports Megakaryocyte Maturation. *Cell Rep* (2020) 32(1):107875. doi: 10.1016/j.celrep.2020.107875
30. Fairfield H, Dudakovic A, Khatib CM, Farrell M, Costa S, Falank C, et al. Myeloma-Modified Adipocytes Exhibit Metabolic Dysfunction and a Senescence-Associated Secretory Phenotype. *Cancer Res* (2021) 81(3):634–47. doi: 10.1158/0008-5472.CAN-20-1088
31. Fairfield H, Costa S, Falank C, Farrell M, Murphy CS, D'Amico A, et al. Multiple Myeloma Cells Alter Adipogenesis, Increase Senescence-Related and Inflammatory Gene Transcript Expression, and Alter Metabolism in Preadipocytes. *Front Oncol* (2020) 10:584683. doi: 10.3389/fonc.2020.584683
32. Chen L, Shi K, Andersen TL, Qiu W, Kassem M. KIAA1199 Is a Secreted Molecule That Enhances Osteoblastic Stem Cell Migration and Recruitment. *Cell Death Dis* (2019) 10(2):126. doi: 10.1038/s41419-018-1202-9
33. Turner RT, Wong CP, Iwaniec UT. Effect of Reduced C-Kit Signaling on Bone Marrow Adiposity. *Anat Rec (Hoboken)* (2011) 294(7):1126–34. doi: 10.1002/ar.21409
34. Zhong L, Yao L, Tower RJ, Wei Y, Miao Z, Park J, et al. Single Cell Transcriptomics Identifies a Unique Adipose Lineage Cell Population That Regulates Bone Marrow Environment. *elife* (2020) 9:e54695. doi: 10.7554/eLife.54695

35. Yu W, Zhong L, Yao L, Wei Y, Gui T, Li Z, et al. Bone Marrow Adipogenic Lineage Precursors (MALPs) Promote Osteoclastogenesis in Bone Remodeling and Pathologic Bone Loss. *J Clin Invest* (2020) 131(2):e140214. doi: 10.1101/2020.08.01.231829
36. Robles H, Zhang X, Magee KL, Lorenz MR, Wang Z, Harris CA, et al. A Novel Skeletal-Specific Adipogenesis Pathway Defines Key Origins and Adaptations of Bone Marrow Adipocytes With Age and Disease. *BioRxiv* (2021). doi: 10.1101/2021.01.05.425449
37. Yu Y, Newman H, Shen L, Sharma D, Hu G, Mirando AJ, et al. Glutamine Metabolism Regulates Proliferation and Lineage Allocation in Skeletal Stem Cells. *Cell Metab* (2019) 29(4):966–78.e4. doi: 10.1016/j.cmet.2019.01.016
38. Clabaut A, Grare C, Rolland-Valognes G, Letarouilly JG, Bourrier C, Andersen TL, et al. Adipocyte-Induced Transdifferentiation of Osteoblasts and Its Potential Role in Age-Related Bone Loss. *PLoS One* (2021) 16(1): e0245014. doi: 10.1371/journal.pone.0245014
39. Bravenboer N, Bredella MA, Chauveau C, Corsi A, Douni E, Ferris WF, et al. Standardised Nomenclature, Abbreviations, and Units for the Study of Bone Marrow Adiposity: Report of the Nomenclature Working Group of the International Bone Marrow Adiposity Society. *Front Endocrinol (Lausanne)* (2019) 10:923. doi: 10.3389/fendo.2019.00923
40. Tratwal J, Labella R, Bravenboer N, Kerckhofs G, Douni E, Scheller EL, et al. Reporting Guidelines, Review of Methodological Standards, and Challenges Toward Harmonization in Bone Marrow Adiposity Research. Report of the Methodologies Working Group of the International Bone Marrow Adiposity Society. *Front Endocrinol (Lausanne)* (2020) 11:65. doi: 10.3389/fendo.2020.00065

Conflict of Interest: The authors declare that the research was conducted in the absence of any commercial or financial relationships that could be construed as a potential conflict of interest.

The reviewer WC declared a past collaboration with one of the authors ES to the handling editor.

frontiers in Endocrinology

REVIEW
published: 27 September 2021
doi: 10.3389/fendo.2021.744527

Guidelines for Biobanking of Bone Marrow Adipose Tissue and Related Cell Types: Report of the Biobanking Working Group of the International Bone Marrow Adiposity Society

Stephanie Lucas[1†], Michaela Tencerova[2†], Benoit von der Weid[3,4,5†], Thomas Levin Andersen[6,7,8,9], Camille Attané[10,11], Friederike Behler-Janbeck[12,13], William P. Cawthorn[14], Kaisa K. Ivaska[15], Olaia Naveiras[5,16], Izabela Podgorski[17], Michaela R. Reagan[18,19] and Bram C. J. van der Eerden[20] the Biobanking Working Group for the International Bone Marrow Adiposity Society (BMAS)*

[1] Marrow Adiposity and Bone Lab-MABLab ULR4490, Univ. Littoral Côte d'Opale, Boulogne-sur-Mer, Univ. Lille, CHU Lille, Lille, France, [2] Molecular Physiology of Bone, Institute of Physiology of the Czech Academy of Sciences, Prague, Czechia, [3] School of Life Sciences, École Polytechnique Fédérale de Lausanne, Lausanne, Switzerland, [4] Swiss Institute of Bioinformatics, Lausanne, Switzerland, [5] Department of Biomedical Sciences, Faculty of Biology and Medicine, Université de Lausanne, Lausanne, Switzerland, [6] Clinical Cell Biology, Department of Pathology, Odense University Hospital, Odense, Denmark, [7] Clinical Cell Biology, Pathology Research Unit, Department of Clinical Research, University of Southern Denmark, Odense, Denmark, [8] Department of Molecular Medicine, University of Southern Denmark, Odense, Denmark, [9] Department of Forensic Medicine, Aarhus University, Aarhus, Denmark, [10] Institute of Pharmacology and Structural Biology, Université de Toulouse, CNRS UMR 5089, Toulouse, France, [11] Equipe labellisée Ligue contre le cancer, Toulouse, France, [12] Department of Biochemistry and Molecular Cell Biology, University Medical Center Hamburg-Eppendorf, Hamburg, Germany, [13] Department of Orthopedics, University Medical Center Hamburg-Eppendorf, Hamburg, Germany, [14] British Heart Foundation Centre for Cardiovascular Science, The Queen's Medical Research Institute, University of Edinburgh, Edinburgh, United Kingdom, [15] Institute of Biomedicine, University of Turku, Turku, Finland, [16] Hematology Service, Departments of Oncology and Laboratory Medicine, Lausanne University Hospital (CHUV), Université de Lausanne, Lausanne, Switzerland, [17] Department of Pharmacology, Wayne State University School of Medicine and Karmanos Cancer Institute, Detroit, MI, United States, [18] Center for Molecular Medicine, Maine Medical Center Research Institute, Scarborough, ME, United States, [19] Graduate School for Biomedical Science, Tufts University, Boston, MA, United States, [20] Laboratory for Calcium and Bone Metabolism, Department of Internal Medicine, Erasmus University Medical Center, Rotterdam, Netherlands

OPEN ACCESS

Edited by:
Jason Horton, Upstate Medical University, United States

Reviewed by:
Sang Wan Kim, Seoul National University, South Korea
Yong-Can Huang, Peking University Shenzhen Hospital, China

***Correspondence:**
Bram C. J. van der Eerden
b.vandereerden@erasmusmc.nl

[†]These authors have contributed equally to this work

Specialty section:
This article was submitted to Bone Research, a section of the journal Frontiers in Endocrinology

Received: *20 July 2021*
Accepted: *24 August 2021*
Published: *27 September 2021*

Citation:
Lucas S, Tencerova M, von der Weid B, Andersen TL, Attané C, Behler-Janbeck F, Cawthorn WP, Ivaska KK, Naveiras O, Podgorski I, Reagan MR and van der Eerden BCJ (2021) Guidelines for Biobanking of Bone Marrow Adipose Tissue and Related Cell Types: Report of the Biobanking Working Group of the International Bone Marrow Adiposity Society. Front. Endocrinol. 12:744527. doi: 10.3389/fendo.2021.744527

Over the last two decades, increased interest of scientists to study bone marrow adiposity (BMA) in relation to bone and adipose tissue physiology has expanded the number of publications using different sources of bone marrow adipose tissue (BMAT). However, each source of BMAT has its limitations in the number of downstream analyses for which it can be used. Based on this increased scientific demand, the International Bone Marrow Adiposity Society (BMAS) established a Biobanking Working Group to identify the challenges of biobanking for human BMA-related samples and to develop guidelines to advance establishment of biobanks for BMA research. BMA is a young, growing field with increased interest among many diverse scientific communities. These bring new perspectives and important biological questions on how to improve and build an international community with biobank databases that can be used and shared all over the world. However, to create internationally accessible biobanks, several practical and

legislative issues must be addressed to create a general ethical protocol used in all institutes, to allow for exchange of biological material internationally. In this position paper, the BMAS Biobanking Working Group describes similarities and differences of patient information (PIF) and consent forms from different institutes and addresses a possibility to create uniform documents for BMA biobanking purposes. Further, based on discussion among Working Group members, we report an overview of the current isolation protocols for human bone marrow adipocytes (BMAds) and bone marrow stromal cells (BMSCs, formerly mesenchymal), highlighting the specific points crucial for effective isolation. Although we remain far from a unified BMAd isolation protocol and PIF, we have summarized all of these important aspects, which are needed to build a BMA biobank. In conclusion, we believe that harmonizing isolation protocols and PIF globally will help to build international collaborations and improve the quality and interpretation of BMA research outcomes.

Keywords: bone marrow adiposity, bone marrow adipocytes, bone marrow stromal cells, biobanking, cell isolation protocols, international research networks, patient information, clinical studies

1 INTRODUCTION

Over the last two decades there has been an increased interest by researchers to study bone marrow adipose tissue (BMAT) in relation to bone and adipose tissue physiology, which expanded the number of publications in the literature. Researchers have used different sources of BMAT to address the major questions in the bone marrow adiposity (BMA) field including: 1) What is the role of BMAT and how does its function change in different physiological and pathophysiological conditions compared to white or brown adipose tissues? and 2) How do we employ bone marrow adipocytes (BMAds) and bone marrow stromal cells (BMSCs) to enrich our knowledge about BMA? However, the methods used to isolate BMAT, BMAds and BMSCs, and the anatomical site(s) from which these are obtained, may influence their biological properties and the downstream analyses for which they can be used reliably. BMA is a young field that has recently received increasing attention among numerous scientific communities (1–5). The goal of this BMA biobanking position paper is to make protocols accessible for all interested researchers and to support researchers in designing their biobanks, sharing their samples and expertise to accelerate progress in BMA research. By facilitating the exchange of knowledge and biological samples, we aim to enhance BMA research worldwide. The BMA biobanking initiative was formed based on discussions among scientists involved in the International Bone Marrow Adiposity Society (BMAS), who created a BMAS Working Group (WG) focused on a need to coordinate biobanking activities in the field; develop guidelines and steps to advance establishment of biobanks for BMA research; and to enhance transparency about differences in BMA-related protocols used among the growing BMA research community. Our Biobanking WG identified currently used collection procedures related to BMAT, BMAds and BMSCs isolated from bone marrow (BM) aspirates, BM plasma and bone tissues. Since samples might be shared among international collaborators, it is critical to consider aligning procedures as much as possible for all sites participating in BMA research, and where access to samples and data will be subject to the strictest scientific and ethical scrutiny. The WG realizes that this is currently impossible to achieve, but as first attempts towards harmonization for biobanks have been successfully employed to access cross-institutional data (6), we aim to report here on the uniformities and discrepancies between protocols and storage of materials related to BMA. Our effort is in line with the recently published BMAS guidelines on nomenclature, abbreviations and units (7), as well as data reporting guidelines and methodological standards (8), produced by the BMAS working groups on Nomenclature and Methodologies, respectively.

Ethical, legal and social issues are complex, affect many biobanking aspects, and have not been fully resolved by the scientific community. In this review, we will also address guidelines in regard to BMA-related biobanking issues, such as informed consent, and compare differences in biobanking procedures and institutional patient information forms (PIFs).

The main goal, therefore, of this paper is to describe the current uniformities and discrepancies for the collection, use, storage and monitoring of BMA-related samples. A stepwise approach going from medical ethical approval through collecting and storing samples to the characterization and analysis of BMA-related samples is depicted in **Figure 1**. Although we are still far from a global harmonization of protocols, achieving this

Abbreviations: ADIPOQ, Adiponectin; ADSC, Adipose tissue-Derived Stromal Cell; ALPL, Alkaline Phosphatase; BM, Bone Marrow; BMA, Bone Marrow Adiposity; BMAd, Bone Marrow Adipocyte; BMAS, Bone Marrow Adiposity Society; BMAT, Bone Marrow Adipose Tissue; BMI, Body Mass Index; BMSC, Bone Marrow Stromal Cell; BSA, Bovine Serum Albumin; CFU, Colony Forming Unit; DMEM, Dulbecco's Modified Eagle's Medium; FBS, Fetal Bovine Serum; IF, Immunofluorescence; ITGA5, Integrin alpha 5; KRH, Krebs Ringer HEPES; LEP, Leptin; LPL, Lipoprotein Lipase; MEM, Minimum Essential Medium; PBS, Phosphate Buffered Saline; PIF, Patient Information Form; PLIN1, Perilipin 1; PPARG, Peroxisome Proliferator Activated Receptor Gamma; RUNX2, Runt-related transcription factor 2; scRNA-Seq, Single Cell RNA Sequencing; WAT, White Adipose Tissue; WG, Working Group.

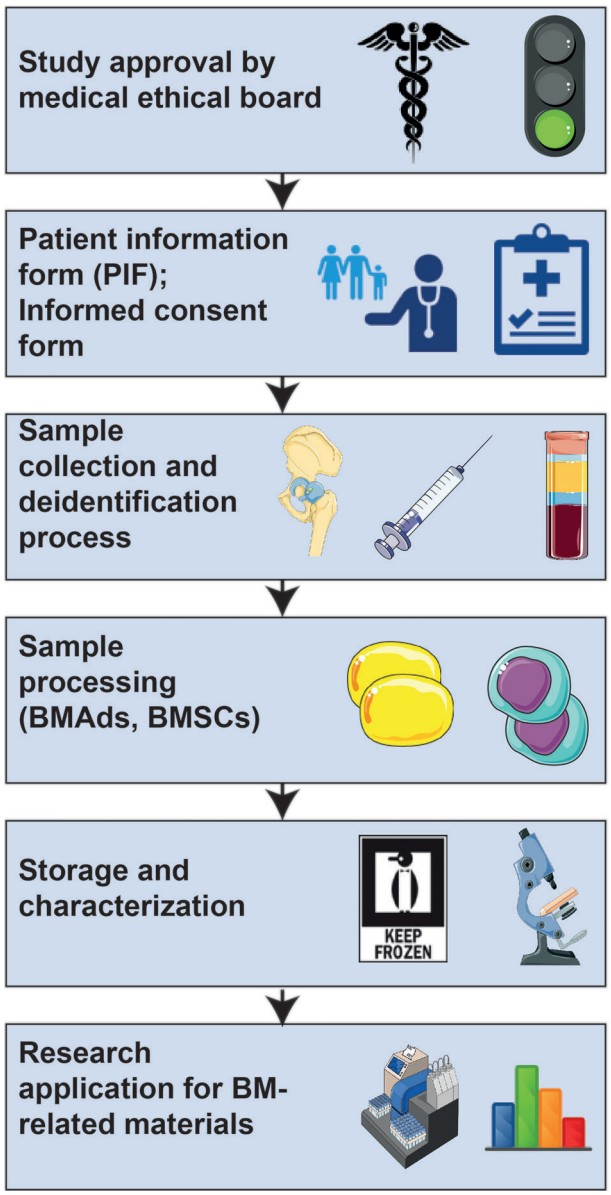

FIGURE 1 | Workflow for BMA-related research.

would greatly enhance the quality and interpretation of BMA-associated outcomes and increase the impact of BMA research. In fact, broad consent for future research may facilitate harmonization as well and, as it is ethically valid, this should be recommended for biobank research (9).

1.1 Introduction to Biobanking

Biological collections and collection-based science was first described by Carl von Linné in the 18th century when he proposed the first system of classification for all biological species on earth (10, 11). The term "biobank" was used for the first time by Loft and Poulsen in 1996 when they suggested the use of human biological material to study a risk factor in cancer (12). Ever since, the field of biobanking has been expanding and it is now a fundamental and indispensable infrastructure for global health research (13–15). However, a BMA biobank has not yet been created. In general, a "biobank" includes large collections of biological samples such as DNA, cells, solid tissues or blood samples (16, 17), which are often stored for a long period of time and used only once a certain number of samples have been collected. They can also be processed, distributed, and used immediately. Samples are used by a variety of research projects and end-users, for example in population-based cohorts for diagnostic or interventional clinical trials, for medical needs/treatments, or for basic researchers validating their findings in human samples. Biobanks can be hospital-, government- or academic-based; networked or more isolated; and for profit or non-profit organizations (16–18). The population-based UK Biobank, between 2006 and 2010 collected biological samples from 500,000 volunteers without specific inclusion/exclusion criteria. Its aim was to investigate the influence of individual genetic susceptibility and exposure to external factors (19). In contrast, disease-oriented biobanks collect disease-specific specimens and non-diseased controls (20). Therefore, the definition of "biobank" varies greatly due to different types and components/purpose of biobanks, and because many biobanks evolved in a local and decentralized manner (13, 17, 21). Different national regulations established by local governance such as ethical guidelines or data protection provoke heterogeneity with regard to biobanking; however, for sharing biological samples with the scientific community, standard procedures for harmonization are required (21). Major advantages of the centralization of processing and standardization are the reduction of costs, increased throughput, and improved accuracy of sample handling and picking (22). The Organization for Economic Cooperation and Development (OECD) recommendations on Human Biobanks and Genetic Research Databases (HBGRD), published in 2009, provide guidelines for the establishment, management, governance, operation, access, use and discontinuation of human biobanks and genetic research databases (23). The structural key elements for sustainable international scientific infrastructure are named Biological Resource Centers (BRCs) as defined by the OECD (24). In addition, the International Organization for Standardization publishes standards for biobanks and bio-resources in ISO 20387 (ISO 20387:2018 "Biobanking – General requirements for biobanking") to harmonize the biobank procedures. It also provides a professional environment for handling not only biological samples but also animal, plant and microorganism resources. Besides quality control of samples, ISO 20387: 2018 also includes validation of methods and competences of personnel (21, 25). In addition to the biobank infrastructure itself, the term "biobank" also covers bioethical and legal issues including ownership, informed consent and privacy – anonymization (17).

2 INFORMED CONSENT FORM FOR BMA-RELATED RESEARCH

2.1 Providing Information Before Donation

Informed consent is a first, critical step in any tissue donation. Informed consent is not merely a disclosure form confirmed by a signature, it must also promote participant's understanding of the research project and emphasize the voluntary nature of participation (26). The informed consent form consists of two parts: the informed consent certificate (containing approval of participant) and the Patient Information Form (PIF). Generally, the patient/donor is presented with the consent form after they have familiarized themselves with the PIF (see below). However, some institutions administer both consent form and the PIF simultaneously. The consent form should state that the patient had time and the opportunity to consider the information contained in the PIF, to ask questions, and obtain satisfactory answers to those questions. The consent form should explicitly state that the risks and benefits of the study have been clearly explained to the participant. The forms can be broad or specific to BMA research; the advantage of a broad consent form is that the collected samples can be used for a number of research projects that do not have to be specified at the time of consent. This breadth may be particularly useful for BMA research, which spans numerous other research fields. On the other hand, formulating the consent form specific for BMA research might make it easier for a donor to agree to participate, as they will know precisely what their samples will be used for. In fact, there is not yet a consensus on the policy regarding consent issues (27). The potential use of biobanked samples for translational work that may involve industrial collaborations and eventual commercial applications should also be discussed, as this may require explicit consent. For this reason, some countries have opted to include on their informed consent template a clause specifying that the patient waives future commercial rights.

Participants should realize that they are signing the consent to allow the storage and use of their specific biospecimens and any data resulting from the research using those specimens. Thus, it should be clear that only approved research studies can gain access to a donor's de-identified data and samples. Studies that utilize the specimens and/or data need to receive prior scientific and ethical approval by the relevant committees, such as the IRB (Institutional Review Board), and they need to fit within the general requirements of the biobank and align with the consent form.

2.2 Deidentification as Prerequisite Before Consenting

Deidentification of data is a critical component of any research study involving human subjects. The procedures that will be used to protect the privacy and confidentiality of the subject's data need to be clear to the potential donor prior to consenting. Unfortunately, biobank participants are not always made aware of the confidentiality risks associated with participation, which is a major ethical concern (28). Therefore, the donor needs to clearly understand how records will be secured, who will have access to the identifiable data, and whether names or ID numbers will be used. The procedure for securing the file linking the codes to individual subjects needs to be explained and participants should be informed about these issues while discussing the informed consent (29). Not all institutions include a Data Privacy Statement as part of their consenting protocol, and it is critical that this procedure is standardized across all institutions participating in BMA biobanking.

2.3 Possibility of Withdrawal From a Clinical Study

The consent form should state that the donor can withdraw from the study at any point and the acceptable ways to withdraw (e.g., email, phone call, letter) should be indicated. It should be clearly explained that upon withdrawal, identifiable samples and the associated data will be destroyed, unless the data have already been used for research. This is in line with the guidelines of the International Bioethics Committee (UNESCO) stating that handling of data and biological samples should follow the wishes of the donor unless they are irretrievably unlinked, making it impossible to do so (30). Accordingly, the consent form should indicate that the code that enables re-linking the samples with personal information will be deleted and only the signed consent form and a copy of the withdrawal letter will be kept as a record. These steps will prevent information about the donor contributing to further research and analyses.

3 PATIENT INFORMATION FORM AS BASIS FOR BMA-RELATED BIOBANKING AND ETHICS DISCUSSION

Many research institutes have templates for patient information and informed consent forms, and The Research Ethics Review Committee of WHO provides general templates and recommendations that can be adapted to specific needs (31). Within a PIF, the participant taking part in the study should be accurately informed about the planned study, what material will be collected and how it will be stored and used for research purposes. Although not every detail of the study has to be provided, the donor should have a rough idea of what will be done with his/her material and know that the collected samples will be handled with the utmost care and adherence to the various regulations, including those according to the General Data Protection Regulation (GDPR). The consent process can be improved by using clear and simple language in the documents (26, 32). Discussions between investigator and patient are encouraged to improve participant comprehension and ensure consent to participate (32). Below is a list of items that the WG believes should be mentioned in the PIF and which will be elaborated upon briefly, point by point (**Table 1**).

3.1 Positive Disadvantages or Risks and Benefits of Donation

With every medical treatment or procedure there is some risk involved. Thus, the sample procurement procedure should be

TABLE 1 | Issues to be considered in patient information and informed consent forms.

Item	Patient information form (PIF) (presented to the participant before donation)	Informed consent form (signed by the participant, after considering the information in PIF)
a. Information about the planned study	*1. What is the purpose of the study?* - Background information and simple description of the study (broad or specific to BMA research) - Clear description of goals and expected results will help to increase the participation rates - Study is approved by Research Ethics Committee/Institutional Review Board *2. What sample material will be collected?* - BM sample (tissues/cells) - Reference samples (eg. subcutaneous fat, blood) *3. How it will be collected?* - Sampling procedure (surgery/biopsy/aspirate) - Risks and disadvantages related to BM sampling *4. What the sample will be used for?* - Broad purpose (unspecified projects) or BMA-specific purpose - General risks related to the sample donation and storage (eg. storage of genetic information)	Donor has had enough time to familiarize him/herself to the information provided in the PIF Donor has had a possibility to ask questions after considering the information in the PIF Donor understands the risks and benefits of participation Risks - General risks of sample donation - BMA-specific risks (e.g. risks related to the BM sampling procedure), blood sampling, or surgery. Benefits - No direct health benefits or financial benefits - Indirect benefits *via* promoting BMA-related research (and e.g. development of novel therapies in the future) Donor provides information about his/her clinical condition - Current diseases and treatments - Past diseases and treatments - Age, metabolic status and lifestyle habits (according to the study)
b. Sample and data storage	*5. Who can access the biological samples and the data obtained?* - Only approved research studies (with ethical approval) may have access to the samples - Tissue/cells that is left over from this study will be stored for future research to learn more about BMA	Donor allows the use of 1) biological samples and 2) the data resulting from the research using these samples. - The permission to store unused samples for possible future research should be separately requested.
c. Anonymization	*6. What procedures will be used to protect the privacy and confidentiality of the data?* - Explain what personal data is collected and how the data is anonymized - Sample material (and the data resulting from these samples) cannot be traced back to any of the person-related data	Donor understands 1) what data is collected and 2) how the data will be secured (Data Privacy Statement). Donor understands he/she will not have later access to his/her own data as all data is deidentified.
d. Withdrawal	*7. How to withdraw from the study?* - Participation is always voluntary - Provide contact information for withdrawal from the study (email, phone number, website) - Explain how the samples and associated data will be destroyed after withdrawal: new data cannot be obtained and that existing data will be maintained in a non-identifiable form	Sample is donated to biobank voluntarily. Donor can withdraw from the study later at any time and without any reason. - Explain how the withdrawal should be signaled to the researchers (eg. email, letter, phone call)

sufficiently risk-assessed and communicated to the donor. Standard donation through tissue biopsies or blood drawing constitutes minimal risk, while BM biopsies or aspirations are more invasive and have an increased risk of various complications that need to be specified. Complications are rare, but as with any procedure involving a tissue biopsy, there is a small risk of bleeding and/or bruising from the sampling site. Moreover, there are descriptions of rare cases of deep tissue infections, severe internal bleeding or bone fracture associated to the BM biopsy/aspiration procedure. In the case of sampling as a byproduct during knee/hip surgery, there are no other risks beyond those usually associated with surgery. In all cases, there should be a lead doctor or research nurse involved to answer questions surrounding the tissue/cell collection. Moreover, donors should be informed about the potential risk of not being able to use the material, for example by unanticipated loss or low quality of the material obtained.

Benefits also have to be addressed towards the donor, with the general message that no direct benefits (e.g. financial or material) can be obtained from participating in a study. Having said that, being a donor contributes to the general understanding of diseases or tissues, such as BMAT, which may lead to future development of new, effective treatments, and thereby may benefit patients. In addition, healthy control donors are often compensated for their involvement in a research study in the form of a small fee for the incremental inconvenience, burden or risk associated to dedicated tissue collection, as opposed to the often-uncompensated donation of residual tissue obtained upon routine medical procedures (33–35). Providing relevant background information about the goals of the study and the expected results is key and will increase participation rates. This will lead to more impactful studies with more reliable conclusions on BMA-related outcomes.

3.2 Constraints and Safeguards of Biobanking

For any clinical study to start, two critical steps are required. Firstly, approval of a medical ethical board is required within the institute where the study is conducted. When a study is multi-centered, there should be an additional approval from the cooperating institutes, but this could be partial or less stringent as long as the coordinating center has a full approval.

Secondly, a valid, written consent is needed before the acquisition or use of the intended BMA-related sample or associated clinical data. By definition, the donor's participation is always voluntary and he/she can always withdraw from the study. The participant will never have access to his/her own data as all data are anonymized. In fact, as soon as a sample is obtained, it should be fully deidentified through encoding in any biobank. None of the users employing the samples or analyzing data belonging to the study can trace back any of the material to any of the person-related data belonging to the donor. This is one of the primary requirements for any medical study involving patient or participant biomaterial and all effort should be taken to prevent any breach of confidentiality.

3.3 Differences Between Institutional PIFs and Biobanking Procedures

In preparation of this position paper, the BMAS Biobanking WG has scrutinized and compared PIFs derived from seven different institutes across Europe and the US. It became evident that there are differences regarding the various aspects described above, especially in the context of the actual content and the level of detail of the proposed research, but also with respect to which measures have to be taken to safeguard the anonymity of the participant in the study and the protection of the acquired data. We thus realized that there are many hurdles to overcome in an attempt to harmonize protocols and procedures across the globe.

4 BIOLOGICAL MATERIALS RELEVANT FOR BMA-RELATED RESEARCH

The types of tissue/cell that will be collected for BMA-related studies are primarily driven by the sample accessibility. Bone and BM samples can often be obtained during invasive procedures, such as surgeries (joint replacement, amputations, open-heart or spinal surgery), autopsies, BM biopsies and BM aspirates (8). The nature of the research depends on the surgery and biopsy type, which determines the anatomical site, patient characteristics (underlying pathology, age, sex, etc., as reviewed below), quantity and quality of sample, and transportation/storage capabilities. Other tissues, such as subcutaneous white adipose tissue (WAT) and venous blood, can also be collected in parallel, but only waste/discarded material, or small samples that cause minimal risk, should be used. Subcutaneous WAT is relatively easily obtained at the site of surgery and can be used as a reference for BMAT analyses, and serum/plasma can be assessed for relevant biomarkers, for example for metabolic function and bone remodeling (biochemical analyses).

The presence of BMAds is variable depending on the surgery site but could be also due to patient heterogeneity (**Figures 2A–I**). For example, as demonstrated from Magnetic Resonance Imaging analyses, the femoral head is expected to be more enriched for BMAds compared to the ilium, while the femoral or tibial diaphysis are expected to have even greater BMA than the femoral head (36). The pathophysiological context can also be a source of heterogeneity in BMAd development and phenotype, and can consequently influence the BMAd isolation, analysis, and study outcomes. Indeed, age, sex, lifestyle habits, metabolic status (e.g. obesity, diabetes, anorexia), medications (e.g. thiazolidinediones, glucocorticoid analogs, hormonal substitutive therapy, radio- or chemo-therapy) and the pathology underlying the orthopedic surgery (osteoporotic fractures, osteoarthritis, osteonecrosis, etc.) are conditions known to modify the BMAd component [as reviewed in (37–41)]. Therefore, it is important to collect donor clinical characteristics, including age, sex, body mass index (BMI), medication history, and incidence of fractures in order to better define the heterogeneity of clinical material (**Table 1**).

In this context, it is very challenging to establish a harmonized "healthy" control set for biobanking as the definition of "healthy control" varies among different studies, depending on the clinical sampling, the aim and biological questions. The "healthy control" samples are ideally obtained by BM biopsies and aspirates from healthy volunteer donors. Yet, as emphasized above, ilium may not represent the most reliable bone site to study BMAds. Orthopedic surgery of healthy patients (not diagnosed with BM diseases or necrosis) following trauma or amputation are an exception, while it is sometimes possible to get "healthy" samples considered as debris during surgery. In fact, this type of surgery currently delivers most of the "healthy" samples. Post-mortem sampling from organ donors can also be considered if the subsequent analyses (such as adipocyte histomorphometry) are compatible with a delayed processing; however, BMAd molecular characteristics are likely to be compromised in such post-mortem samples. It is the responsibility of the research team to clearly establish and describe the inclusion and exclusion criteria, which subsequently allows for categorization of "healthy" or "control" *versus* "study" group(s). Alternatively, a referent cell type (e.g. subcutaneous adipocytes, BMSCs from another bone site) isolated from the same patient can be used for comparisons.

4.1 Choice of BMA Relevant Biological Materials and Their Use

Due to the various types of tissue and cell types relevant to BMA, the unclear definitions of cell populations and the relatively recent emergence of the field, the methodology behind collecting BMAT, BMAds and BMSCs is heterogeneous as recently reviewed (8). It is important, for all samples that have been collected, to specify if screenings have been performed for viral diseases (typically HIV, HBV and HCV), as in some countries a negative test is a prerequisite to allow usage of the samples in research facilities. So, for the future of biobanking it is important to keep track of these variables.

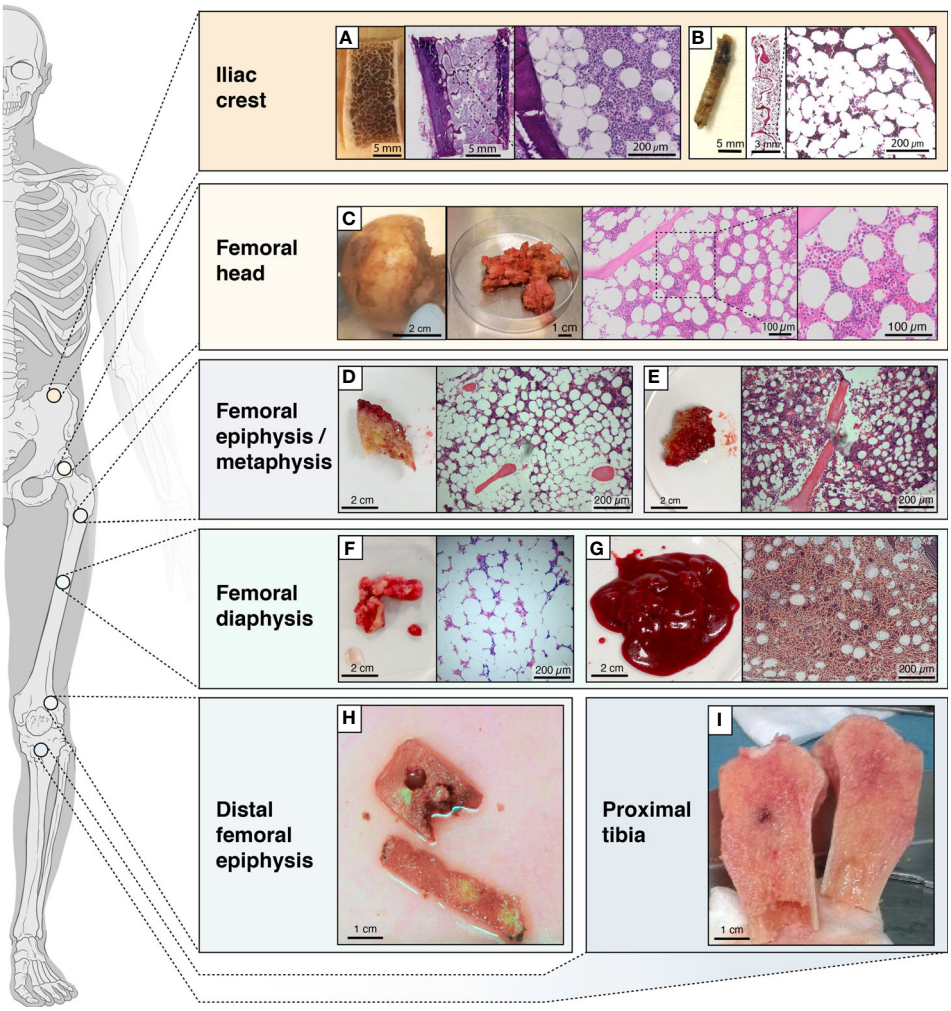

FIGURE 2 | Schematic figure showing the locations from which BMAT is obtained. Locations from which BMAT is obtained, heterogeneity in tissues (e.g. more fatty *vs* less fatty) and collected fractions. **(A)** transiliac bone autopsy obtained with a Bordier trephine and **(B)** iliac bone marrow biopsies obtained with a Jamshidi trephine; **(C)** femoral head autopsy; **(D)** epiphyseal or **(E)** metaphyseal tissue from femur; **(F)** diaphyseal bone or **(G)** bone marrow from femur; **(H)** tissue from the distal femoral epiphysis; **(I)** bone tissue from the proximal tibia.

4.1.1 Operation Specimens and Autopsies

A reliable method to obtain fresh BMA-relevant biological material is during orthopedic surgeries, such as knee and hip replacements, reconstructions, corrections and amputations. During these operations, a key part of the surgical procedure is removal of bone and BM that is often discarded after the surgery. It is possible to recover this biological material for BMA-related research and biobanking. A good example is hip replacement surgery, where the femoral head and part of the trabecular bone cavity are removed and simply discarded, if not transferred to a bone bank as allograft material. With these surgical specimens, it is possible to process samples for downstream detailed histology (see BM biopsies) (**Figures 2A–I**) or to isolate almost all desired adipocytic, stromal and hematopoietic BM cell types; see also section 4.2.

Post-mortem autopsies offer a unique opportunity to obtain BMA-relevant biological materials from several skeletal sites, and not only the classical sites undergoing orthopedic surgery or BM biopsies. As mentioned earlier, these autopsies are useful only for simple adipocyte histology and histomorphometry, and ex vivo imaging by micro-computed tomography (µCT); they are not suitable for molecular analysis and cell isolation (unlike for fresh operation specimens and BM biopsies). Nevertheless, histomorphometry and imaging of autopsy samples are still useful as they allow for analysis of the BM compartment to analyze the BMAd content, morphology and size (**Figure 2A**). High quality tissue may however be banked in the exceptional context of systematic bone tissue collection from post-mortem organ donors.

4.1.2 Bone Marrow Biopsies

Transiliac bone biopsies obtained with a Meunier/Bordier trephine (inner diameter 5-8 mm) have for decades been the

gold standard within bone research and diagnostics. These biopsies are obtained under a quite invasive procedure, usually performed under general anesthesia. For BMA-related research, it is sufficient to obtain iliac BM biopsies with a Jamshidi trephine [inner diameter 3 mm, recommended length 2 cm (42)]; this is a much-less-invasive procedure usually performed under local anesthesia, which also allows for collection of a BM aspirate (**Figure 2B**). These 3-mm bone marrow biopsies are the gold standard in hematology research and diagnostics, and due to their less-invasive nature they are more justifiable from an ethical perspective. The usability of these biopsies is versatile for BMA-related research, as it is for surgery specimens. For BMA-related research by histology there is no need to embed the undecalcified specimens/biopsies in plastic, as done for classical bone histomorphometry. Instead, the specimens/biopsies can be fixed, decalcified and paraffin- or frozen-embedded. *Ex vivo* imaging by μCT or similar method can be performed before the specimens/biopsies are decalcified. The embedded specimens/biopsies are then usable not only for adipose histomorphometry (see autopsies), but also for more advanced molecular histology, like multiplex immunostaining, *in situ* hybridization, laser microdissection and spatial transcriptomics (8). This facilitates detailed analysis of BMAd spatial distribution, gene expression profile, and interaction with other cell types in the BM.

4.1.3 Bone Marrow Aspirates

BM aspirates are primarily taken from the iliac crest or femoral BM biopsy (occasionally from femoral epiphyses) site, usually following the biopsy under local anesthesia. This is a less-invasive procedure and allows for relatively easy collection of BM fluid containing various cell types, including adipocytes (43–45). The BM aspiration procedure is not necessarily familiar to the participant and the PIF should describe what happens during sampling on a step-by-step basis, including injection of the local anaesthetic into the location where the sample is to be taken from. BM aspirates are especially useful for the collection of various cell types, including a BMAd-enriched fraction (see *Section 5*) and BMSCs (8). The cells can be directly cultured following collection, or they can be prepared for storage to be analyzed later. Typically, the different BMSC-related cultures are employed to study cell behavior, differentiation, marker expression and/or their interaction with other cell types (mimicking the situation in BM). BMAd-enriched fractions can be extemporaneously used or stored for further molecular and biochemical analyses. Although no cell type or tissue collection is involved, *in vivo* analyses of BM are increasingly available and provide a good source of information on BMA content, composition, spatial and temporal distribution (etc.), and it would be very helpful to compare these *in vivo* analyses to biobank data (8).

4.1.4 Subcutaneous Fat

Subcutaneous WAT can be collected at the surgery site and provides a rich source of adipocytes and Adipose tissue-Derived Stromal Cells [ADSCs, nomenclature according to (7)], that can be used for reference, for example for comparison with BMAds and BMSCs.

4.1.5 Blood Samples

Venous blood can be collected in different ways depending on the research question but most often is stored in the form of serum (for measurement of biochemical parameters e.g. lipids, growth factors, hormones or plasma collected in the presence of anti-clotting agents (e.g. EDTA or Heparin) (for molecular analyses, chemistry, or cell culture). Quantification of metabolites in blood samples requires standardization of pre-analytical processing and rapid cooling down, as reviewed here (46–48). If blood samples are obtained in the fasted state, it is also possible to investigate the level of bone resorption and formation using markers like P1NP, CTX, NTX and TRAcP, and link this to the bone metabolic state (49).

4.2 Isolated Human Primary BMAds and BMSCs

BMAds are present scattered or more packed within the BM of different bones in humans (**Figures 2A–I**). Accessibility of the BM cavity is obviously required to isolate BMAds, which restricts the bone sites available to obtain samples [i.e., BM biopsy sites, resected bone pieces and BM aspirates of long bones obtained during orthopedic surgery (**Figures 2A–C, 2E** and **2G**)]. So far, BMAds and BMSCs have been obtained from different locations including the femoral head (50, 51), the diaphyseal end of the femur or tibia (52), BM aspirates from the femur (53) and the iliac crest (54, 55) (**Figures 2A–C, F–G, I** and **4**).

Specific procedures for the collection of BMAds are relatively novel (*see below*), and in some cases freshly isolated BMAds may be needed for immediate analysis. However, BM fragments and BMSCs have been successfully collected and biobanked, followed by optimized characterization of the cryopreserved material (56, 57).

The process of sampling is also variable and influences the quality of BMAd isolation. For example, for hip arthroplasty the femoral head is removed using a surgical saw and, prior to insertion of the artificial hip, the medullary canal is cleared using a reaming tool before aspiration of the BM. These steps are often done using electric saws and reamers, but non-electric tools can also be used. Similarly, some electric reamers simultaneously aspirate the BM cavity, but aspiration can also be done manually, post-reaming, using a syringe and soft cannula. These different methods (i.e. electric *vs* non-electric) can affect the quality of BMAds as a result of differences in heat production and/or mechanical stress (51, 53, 58).

Thorough discussions with the surgeons are thus instrumental to determine the optimal processes and to adapt surgical techniques, when possible, for BMAT sampling.

As previously encouraged (8), a detailed description of the source of BMAds is consequently required for biobanking purposes and study comparisons. Firstly, minimal information should state the original skeletal location, i.e. distal/proximal bone site, trabecular bone or BM (**Table 2**). Secondly, patient characteristics should be reported including the distribution by age, sex and BMI as well as the pathophysiological context, i.e. the presence of bone disease, osteo-articular disease, hematological disease, malignancies, and their related treatment.

TABLE 2 | Summary of critical steps for BMAd and BMSC isolation to highlight differences between protocols.

Main steps	EDIN	TOUL	LILL	LAUS	PRAG
Material					
Bone site of sampling	Femoral proximal metaphysis and diaphysis Femoral head	Femoral proximal metaphysis and diaphysis	Trabecular bone from distal femoral epiphysis	Femoral head (epiphysis + variable quantity of metaphysis) Iliac crest	Iliac crest
Sample type	BM aspirates	BM aspirates	Cancellous bone	BM aspirates	BM aspirates
Final material obtained	BMAds	BMAds	BMAds	BMSCs and BMAd-enriched fraction	BMSCs and BMAd-enriched fraction
Digestion					
Buffer	KRH, 5.5 mM glucose 3% BSA	PBS 2% BSA	DMEM, 5.5 mM glucose 3% BSA	DMEM, 10% FBS	-
Collagenase type, manufacturer (reference number)	Type 1, Worthington Biochemicals (LS004196)	from *C. histolyticum*, Sigma Aldrich (C6885)	NB 4 standard grade, SERVA Electrophoresis (17454)	Type I, Gibco (#17100-017)	-
Collagenase concentration		250 UI/mL	0.2 to 0.3 UI/mL	1 UI/ml	-
Digestion time	45min	Max. 20 min	15-30 min	45 min -1h	-
Washing					
Buffer	KRBH 5.5 mM glucose	KRBH 0.5% BSA	DMEM, 5.5 mM glucose/ 3% BSA	PBS/1% BSA	PBS/1% BSA

Different protocols have been set up to isolate BMAds (from 3 institutes: EDIN, TOUL, LILL) or BMSCs (from 2 institutes: LAUS, PRAG). Differences related to biological material, digestion and washing parameters are highlighted.

Abbrevations referring to institute cities of members within BMAS Biobanking WG. EDIN: Edinburgh (WC); TOUL: Toulouse (CA); LILL: Lille (SL), LAUS: Lausanne (ON); PRAG: Prague (MT).

According to the studied questions, other specific parameters (such as BMI, metabolic status when relating to energetic metabolism perturbations for example) are also expected. Thirdly, how the original clinical sample is obtained (i.e., use of electric or non-electric surgical tools, use of digestion or other sample processing and any other relevant details) should also be described.

5 METHODOLOGY OF BMA-RELATED CELL ISOLATION AND ANALYSIS

Various protocols for human BMSC isolation (55–57, 59–61) and, to a lesser extent, for BMAd isolation (50–54, 62–64) have been published. Isolated BMSCs are classically used *in vitro* to analyze their differentiation capacity into different lineages, to study BM cell interactions, to characterize progenitor markers, to analyze BMSC senescence and to compare their molecular and cellular characteristics to different sources of stem cells, including peripheral ADMSCs. Thus far, applications for isolated BMAds are devoted to characterizing their specific phenotype by comparison with extramedullary adipocytes, such as subcutaneous WAT adipocytes, using RNA analyses, proteomics or lipidomics. The downstream analyses, as well as the research context encompassing the biological questions, the clinical sampling and the type of comparative/referent samples, have to be taken into consideration for the choice of the isolation method.

In this review we provide dedicated protocols for isolation of BMAds and/or BMSCs. As discussed within each section, the absence of other contaminant cells, the cell integrity and the cell yield determine the success of the method. Considering the great heterogeneity in patients and samplings, it is advised to file a small piece of the initial tissue for histological analysis (**Figure 2**). Besides, BMSCs can be obtained, though in small amount, during the BMAd isolation procedure. In addition, a floating lipid-loaded cell layer is often observed following the processing of BM aspirates or trabecular bone samples before any collagenase digestion (**Figure 3A**). This cell fraction most likely results from the surgical procedure that allows the release of BMAds that are loosely attached and contains both BMAds and contaminant cells from the hematopoietic and the stromal compartment. We suggest referring to this as a BMAd-enriched fraction (i.e. fraction that is obtained from BM but without collagenase digestion, as illustrated in **Figure 3B**), which could be used for lipid analysis. Yet, this BMAd-enriched fraction should be used only after digestion and washing steps if pure BMAds have to be analyzed. This floating lipid-loaded cell layer is not to be confounded with the free lipid layer that results from spontaneous cell lysis upon excessive mechanical processing, excessive ambient temperature or handling time (**Figure 4**).

5.1 Isolation of BMAds

Various laboratories have already started working on BMAds isolated from BM aspirates, from femoral diaphysis (51–53, 64), from trabecular bone of the proximal femoral metaphysis/epiphysis (51), the femoral head (50, 62, 65), femoral BM fluid (62), the proximal tibia (52) or the iliac crest (54) (**Figures 2A–I**). Within our working group, three protocols were set up and validated to isolate and purify BMAds, and accordingly, the critical steps to obtain pure primary BMAds for different analyses are depicted here. These main steps are based on protocols commonly used for the isolation of adipocytes from peripheral WAT, which have been adapted from the initial work of Rodbell (66). Tissue digestion is commonly performed using collagenase to release BMAds from the extracellular matrix,

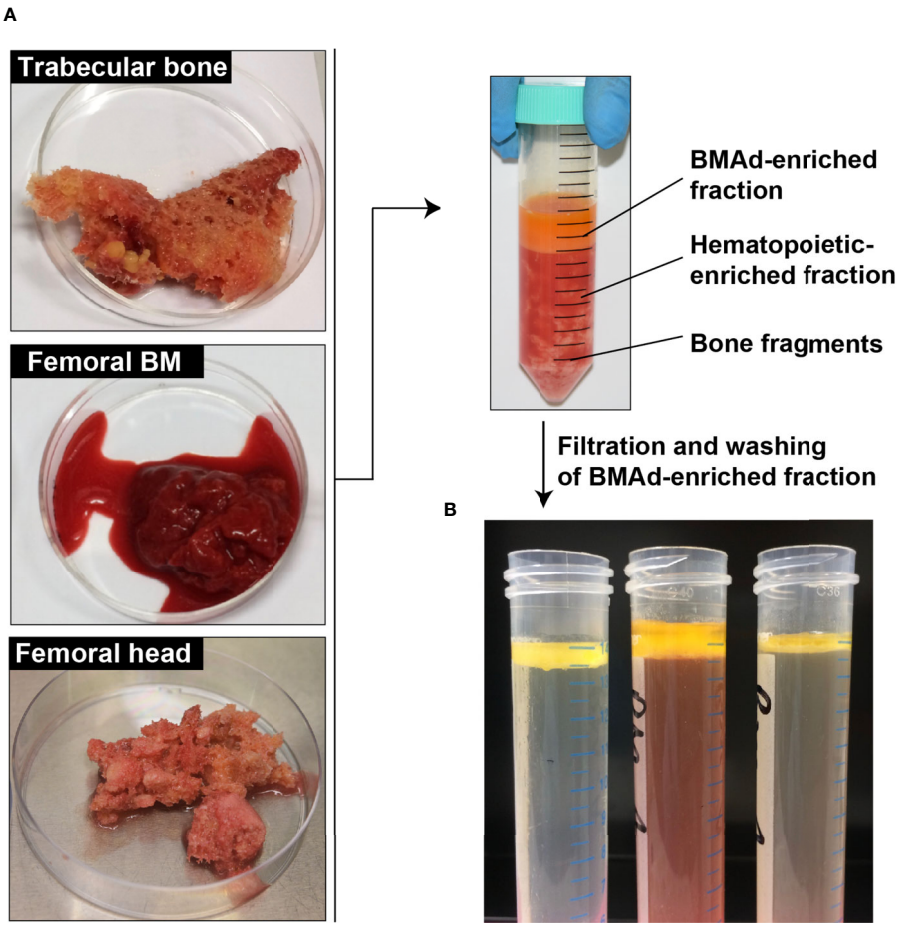

FIGURE 3 | Processing of the BMAd-enriched fraction without digestion step. **(A)** Samples are received from surgeries into their transport buffer. The adipocyte-enriched layer is harvested, filtered and washed. **(B)** Several examples of BMAd-enriched fractions after washing are shown.

which is mainly composed of collagen fibers (67). Indeed, if the study relies on a comparison between isolated BMAds and WAT adipocytes, a similar method based on collagenase digestion should be performed. However, this enzyme-based isolation is not required if the study focuses on characterizing only BMSCs. Within the following sections we describe how the clinical sample is obtained and provide a general protocol to process these samples with joined notes to discuss key aspects. The main differences between our three protocols relate to reagents, as highlighted in **Tables 2**, **3**. It is important to emphasize that each protocol has been tested and established separately. As combining reagents between the protocols has not been validated, it is recommended to strictly use the advised reagents for the selected protocol.

5.1.1 Isolation and Transport of Samples

As mentioned above, BMAds are isolated from femoral head, BM aspirates of femoral proximal metaphysis/diaphysis or trabecular bone from distal femoral epiphysis (**Figure 4**).

The femoral head is removed with an electric bone saw and stored in buffer or processed immediately in the surgical theater and the bone fragments obtained by mechanical processing stored in transport buffer. To obtain BMAds from the femoral head (51, 65), the trabecular core is first exposed by bisecting the femoral head longitudinally using an electric bone saw. A sterile spoon spatula is then used to cut and scoop out ~1 cm^3 portions of the trabecular bone from within the femoral head. The medullary cavity of the proximal femoral metaphysis and diaphysis is then cleared of trabecular bone by using a manual reaming tool, with a bone mallet used to drive the reamer into the medullary canal. To obtain BMAds from it, portions of trabecular bone are then removed from the reaming tool, washed and stored in buffer (51) (**Figures 4A, B**).

To obtain BMAds from the proximal diaphysis, BM from this region is aspirated using a soft cannula attached to a manually operated syringe. The aspirate is then transferred to a sterile petri dish or specimen tube prior to washing and storing in buffer (51, 53, 64) (**Figures 4A, B**).

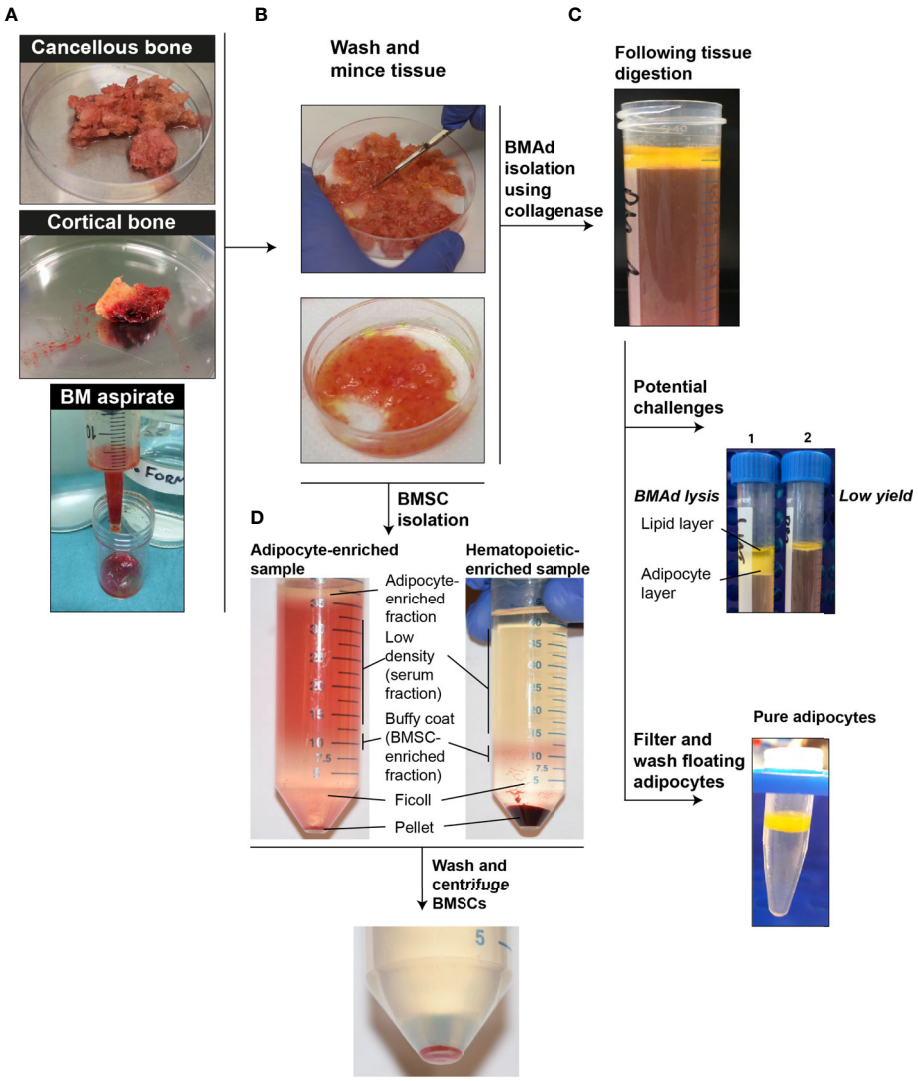

FIGURE 4 | Schematic protocol for isolation of BMAds and BMSCs. **(A)** Strategy to recover BMAds and BMSCs depending of the tissue source. **(B)** Wash and mince the selected tissue. **(C)** Digestion strategy using collagenase digestion to increase the release and the purity of BMAds. Some encountered challenges are shown such as the lysis (1) and low yield (2) of BMAds. At the end of the process pure BMAds are obtained. **(D)** BMSCs isolation with tubes showing the variation observed between samples. BMSCs are obtained after centrifugation of the serum fraction and the BSMC-enriched fraction.

To obtain trabecular bone from distal femoral epiphysis, 1 cm^3 of cancellous bone square is taken in the center of the femoral epiphysis using adapted cold chisels after the first distal femoral cut during knee prosthetic surgery (**Figures 2D–H**).

As soon as the sample is harvested, it must be placed in transportation buffer (**Table 3**) and transferred to the laboratory in the quickest possible manner[1,2,3].

Notes:

1- Different buffers are used in our laboratories and the composition of these buffers is detailed in **Table 3**. *All these media should be at pH 7.4 (buffered with HEPES and/or bicarbonate) and contain inorganic salts and glucose as nutrients are needed to maintain tissue integrity.*

2- It is recommended to transport the sample at room temperature (~20°C) and to minimize strong temperature changes. Yet, for some applications such as molecular analysis (RNA expression, protein or lipid content characterization), keeping samples at 4°C (on ice) can be advised as reported in (51). *For biobanking purposes, the effect of transport/storage conditions on cell properties and on any post-isolation changes still remains to be tested. At the moment, we recommend documenting the transport/storage conditions for every sample.*

3- Ideally the transportation should be achieved within 30-60 minutes since the reduction of oxygenation and nutrient deprivation at the center of the sample may compromise tissue integrity, as already reported for other adipose tissues (53, 64).

TABLE 3 | Composition of buffers used for sample transportation.

Buffer name	EDIN KRH	TOUL KRBH	LILL DMEM	LAUS PBS 1X + EDTA 1 mM	PRAG MEM
$MgCl_2$; 6H2O	N/A	0,5	N/A	N/A	N/A
$MgSO_4$	0,6	N/A	0.8	N/A	0.8
KCl	2	4,6	5.4	2.7	5.3
NaCl	120	120	110	137	117.24
Na_2HPO_4 (anhydrous)	N/A	0,7	N/A	10	N/A
NaH_2PO_4 (anhydrous)	N/A	1,5	1	N/A	1
KH_2PO_4	1	N/A	N/A	1.8	N/A
$CaCl_2$; $2H_2O$	1	N/A	1.8	N/A	1.8
D-Glucose	5,5	10	5.5	N/A	5.5
$NaHCO_3$	N/A	150	44	N/A	26.2
HEPES	81,6	10	N/A	N/A	N/A
Bovine Serum Albumin (BSA)	1%	0.5%	N/A	0	N/A

Five different buffers have been used for sample transportation: Krebs Ringer Bicarbonate HEPES buffer (KRBH), Krebs Ringer HEPES (KRH) and Dulbecco's Modified Eagle's Medium (DMEM, Dutscher, L0064). The concentrations of the different components are indicated in mM, except for BSA.
Abbreviations referring to institute cities of members within BMAS Biobanking WG. EDIN, Edinburgh (WC); TOUL, Toulouse (CA); LILL, Lille (SL); LAUS, Lausanne (ON); PRAG, Prague (MT).

5.1.2 General Protocol for BMAd Isolation

Reagents and Equipment:

- digestion buffer with collagenase (composition in **Table 2**), pre-warmed at 37°C
- washing buffer (composition in **Table 2**), pre-warmed at 37°C
- shaking water bath at 37°C
- Polypropylene tubes[4]
- cell strainer (100 μm) or a Nylon mesh (porosity between 150 to 300 μm)
- classical instruments and lab pipets/tips

Notes:

4- To limit the lysis of BMAds we recommend working only with plastic, because glass tubes cause lysis of adipocytes.

General Protocol (Figures 4B, C)[5]:

Rinse the tissue several times in the transport buffer (**Table 2**) to remove tissue debris and clotted pieces.

Mince the tissue in small pieces to facilitate digestion[6] and add tissue pieces in the digestion buffer[7,8] containing collagenase[9].

Digest the tissue at 37°C in a water bath under gentle shaking (from 120 to 200 rpm) with a careful and continuous monitoring of the incubation time[10].

At the end of digestion[11], filter the cell suspension, either on a cell strainer or a Nylon mesh over a tube. The strainer or mesh should have a pore size of at least 100 μm, given the large size of adipocytes.

Add washing buffer to dilute the collagenase and to rapidly stop the collagenase action.

Allow the adipocytes to then float in the filtered suspension either storing upright the tubes or centrifuging (5min, 300 g).

Aspirate the infranatant and the cell pellet[12].

Wash 3 times the floating adipocytes by adding washing buffer and centrifuging for 5 min at 300 g to pellet contaminant cells[13,14,15].

Collect the BMAds in this floating layer using a micropipette[16] or by removing the remaining washing buffer as much as possible following a short centrifugation step to pack the floating cells[17].

Notes:

5- The isolation protocol is performed at room temperature with the exception of the digestion step. Please be aware that in poorly temperature-controlled environments (for example in the summer months), BMAd viability may be considerably compromised.

6- Unless the tissue is already partly dislocated, such as for the BM aspirates, the other tissue types (e.g. cancellous bones) are then minced in small pieces to facilitate digestion. Cancellous bone from the femoral epiphysis or metaphysis is for example transferred in a small flat plastic dish and kept immersed in digestion buffer to be cut using a scalpel or scissors to get pieces of ~5mm^3. During cutting, the bone can be held in place using cutting clamp or forceps, as needed.

7- The digestion is favored by an appropriate balance between the volume of digestion buffer and the amount of tissue fragments. We recommend the use of two buffer volumes for each sample volume or, if preferred, 2 mL buffer per gram of tissue.

*8- Digestion buffer can vary from PBS, Dulbecco's Modified Eagle's Medium (DMEM) to Krebs Ringer HEPES (KRH), highlighting the importance of a basic ionic strength (**Table 2**). The presence of glucose may not be necessary during a short digestion duration but can be advised to minimize changes following transportation or when metabolic features of BMAds are studied. Importantly, the presence of fatty-acid-free Bovine Serum Albumin (BSA) at classical concentrations of 2 to 3% (w/v) is instrumental: BSA binds the released fatty acids and prevents their detergent action on cell membrane* (68).

*9- Different collagenases can be used with yet a careful choice (**Table 2**). Indeed, collagenase preparations differ between manufacturers and from batch to batch. Thus, our labs first*

check the efficiency of the collagenase batch they use and determine the collagenase amount and the digestion duration to obtain a BMAd suspension. BMAds are more fragile and loosely associated compared to adipocytes from WAT. Thus, digestion time for BM tissue can be reduced; however, it remains unclear how differences in digestion duration affect the final properties of the BMAds and WAT adipocytes.

10- An optimal shaking should provide the appropriate diffusion of the collagenase with the whole tissue fragments while mixing the fatty acids with BSA, and yet should also avoid BMAd lysis. This shaking can modulate the digestion duration and can also be adapted according to the samples. As a general rule, shaking force should be highest at the beginning and reduced with time. Incubation time can vary between 15 and 45 minutes.

11- Digestion occurs when increased turbidity appears. The medium becomes more and more opaque because of BMAds which, once released, float at the surface (especially evident once the tube is no longer being shaken). This step should be continuously monitored and stopped when cell release from bone pieces seems reduced. Besides, the digestion must be stopped when large amounts of lipids are released (i.e., oil appearance in the suspension meaning that adipocytes burst).

12- The cell pellet contains BMSCs, which can be harvested at this step. After removing the adipocytes, the remaining buffer with collagenase is aspirated. In a sterile hood, pellet is resuspended in red blood cell lysis buffer according to the manufacturer's instructions: add 1ml of buffer, vigorously pipette to mix, let sit for 1 min, add 15 ml of KRH buffer (without BSA), pipette to mix. Then, split cell resuspension into two 14 mL falcon tubes and centrifuge at 300 g for 10 minutes prior to remove the supernatant. Then the pellet is resuspended in appropriate culture medium as described in the BMSC section (5.2.3).

13- Even after cell dissociation with collagenase and separation of adipocytes by flotation, some contaminant cells can remain attached to adipocytes. Thus, to purify adipocytes, it is important to wash and centrifuge the adipocyte suspension to pellet contaminant cells.

14- BMAds are fragile and can burst during the washing steps so we recommend doing this step as quickly and gently as possible.

15- For Western blots or proteomic analyses, BSA must be removed to allow a correct protein quantification of the samples. To do so, it is important to wash twice with PBS.

16- If using a pipette, it is recommended to cut the tip using a scalpel to increase the bore size of the pipette tip; this prevents shear stress and lysis of the BMAds.

17- If BMAds are to be used only for downstream molecular analysis, it can be advised to store the tube on ice to facilitate formation of the floating adipocyte layer, to use ice-cold washing buffer to minimize any further molecular changes and to centrifuge at 4 °C. In that case, the use of glass pipettes to homogenize in the RNA extracting reagent is beneficial because this promotes BMAd lysis and prevents adherence of the cells to the pipette, thereby increasing yields.

5.1.3 Freezing and Storage of BMAd Samples

The isolated BMAds can then be frozen according to the future analyses[18] as indicated in the overview in **Table 4**. Special attention should be paid to the cell volume to adapt the volume of RNA extraction reagent (about 1:6 or 1:10 v/v) and to remove lipids. As for adipocytes from WAT, excessive lipid can prevent efficient RNA isolation. Thus, following initial cell lysis, it is helpful to allow the homogenate to settle on ice, resulting in a formation of a floating lipid layer. This lipid layer can then be removed and discarded, to be replaced by a similar volume of RNA extraction reagent.

For untargeted lipidomics, BMAds can be frozen in methanol to allow a better stability of lipids. For targeted lipidomics, the extraction buffer is different depending on lipid classes. Thus, we recommend freezing samples directly in the appropriate extraction buffer. In other cases, BMAds can be frozen without extraction buffer but under nitrogen gas to prevent the oxidation of lipids.

Notes:

18- We recommend freezing a known volume of adipocytes in liquid nitrogen and keeping samples at -80°C until use. When subsequent analyses are already planned, samples can be stored in specific media for better stability.

5.1.4 Approaches to Check Purity and Viability

One issue with BMAd isolation is that non-BMAd populations may contaminate the layer of floating cells. As an example, human BMAds can have direct interactions with osteoclast precursors (62). Considering that macrophages are contaminants of isolated WAT adipocytes, other surrounding cells (e.g. BMSCs, endothelial cells, hematopoietic or immune

TABLE 4 | Recommended storage of isolated BMSC and BMAd samples.

Storage of the samples	BMSCs	BMAds
Cell cryopreservation	One million cells in freezing media (per vial: 80% FBS, 10% DMSO, 10% MEM or 50% MEM, 40% FBS, 10% DMSO) in liquid nitrogen).	Impossible to keep viable frozen BMAds. Frozen isolated BMAds can be snap-frozen in liquid nitrogen and stored at least at-80°C for further analyses.
RNA	In Trizol (or similar) at -80°C	In Trizol (or similar) at -80°C
Protein	In protein lysis buffer at -80°C	In protein lysis buffer at -80°C
Lipids	Flash freezing in liquid nitrogen within 4 hours after surgery. Store at -80°C	Flash freezing in liquid nitrogen within 4 hours after surgery. Store at -80°C

cells) may remain attached to the floating BMAds. In addition, the evaluation of BMAd viability may be beneficial to discard cell alteration from the isolation procedure or for subsequent functional analysis.

Evaluation of Cell Purity

Immunofluorescence (IF) imaging is suitable to check both the morphology preservation following isolation and the size of BMAds, as well as potential contaminants. For good IF imaging it is better to embed BMAds in a matrix of fibrin gel (53). BMAds should contain a large lipid droplet filled with lipids, which can be stained using a fluorescent dye for neutral lipids such as BODIPY or LipidTox (**Figure 5A**), or the lipid-droplet marker Perilipin 1 (PLIN1) (53, 63). Nuclear staining (using DAPI, Topro 3 or Hoechst) can inform on the presence of contaminant cells that could remain attached to BMAds (**Figure 5B**) (53, 64). Though not yet reported for human BMAds, the presence of specific markers such as CD45 for leukocytes and CD11b for myeloid cells has already been performed for mouse isolated BMAds using immunostaining to discard monocyte or macrophage contaminants (69). Alternatively, flow cytometry analysis following immunolabeling for markers of endothelial cells (CD31), stromal cells (CD105, CD90, CD24) has also been reported to validate the purity of human BMAds (63, 70).

BMAd purity is usually assessed by analyzing the expression of typical transcripts. Adiponectin *(ADIPOQ)*, PPARγ (*PPARG*), leptin (*LEP*) (69) and *PLIN1* (63) are used as classical adipocyte markers. Other genes such as integrin alpha-5 (*ITGA5*), *CD11B* (encoded by *ITGAM*) and CD45 (encoded by *PTPRC*) have also been used, respectively, as markers of stromal cells (both for BMSCs and stromal vascular cells within WAT), leukocytes and other hematopoietic cells (51, 65). Based on the specifics of the conducted study, other markers for osteoblasts [e.g. *RUNX2*, Osteocalcin (62)] and for osteoclasts (TRAcP, Cathepsin K) can also be helpful to test cell purity.

Evaluation of Cell Viability

Based on previous studies investigating functional assays on BMAds (e.g. lipolysis) (53), metabolic studies require at least 50 µl suspension (around 50,000 cells) per condition and several experimental conditions (with and without pharmacological agents) are needed. However, the number of BMAds at the end

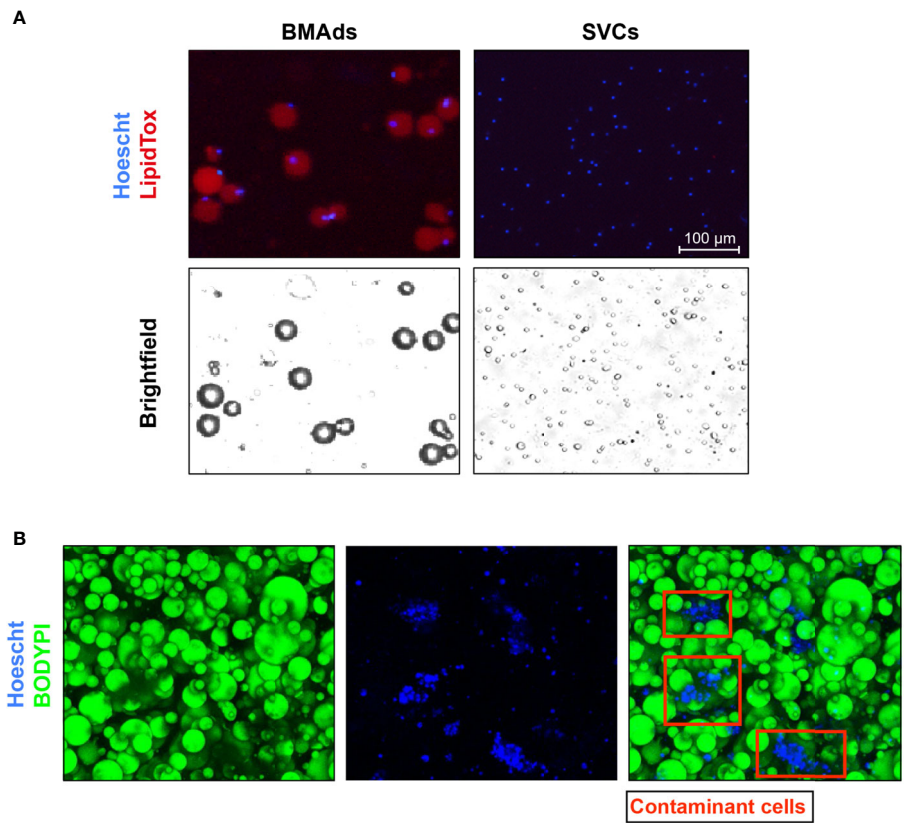

FIGURE 5 | Histological images demonstrating the purity of the BMAds. **(A)** BMAds were stained with Hoechst and LipidTox DeepRed. Stromal-vascular cells (SVCs) were included as a negative control for LipidTox staining. Stained cells were then analysed using a Nexcelom Vision Cellometer. Adipocyte images confirm that all nuclei are associated with unilocular lipid droplets and there are no lipid-free nuclei, suggesting an absence of contaminating non-adipose cell types. Analysis of the SVC fraction confirms that the LipidTox signal is dependent on the presence of lipid droplets. Scale bar represents 100 µm. **(B)** BMAds were stained with BODIPY and Topro 3 to verify by IF the integrity of BMAds (BODIPY staining) and the purity of the adipocyte suspension. Nucleus staining show the presence of contaminant cells attached to adipocytes (red squares).

of the purification process is generally limited and they are very fragile. Of note, other functional tests with isolated BMAds have already been performed following a 24h culture in various media (62, 63) or ceiling culture (54, 65), yet the impact of this subculture has not been clearly assessed. Therefore, it should be emphasized that these functional metabolic assays are difficult to set up and do not seem appropriate to rapidly check the viability of BMAds. Other developments of functional tests are thus to be pursued based on our growing knowledge of BMAd metabolism.

5.2 Isolation and Culture of BMSCs

Within our working group, we reviewed two protocols for the isolation of BMSCs and BMAd-enriched fraction and validation of the purity of BMSCs obtained by BM aspirates from iliac crest or femoral head (55) (**Table 2**). Based on the source of BM aspirate, the yield of isolated BMSCs can differ (BM aspirate under local anesthesia *vs* BM aspirate taken during an orthopedic surgery procedure). In the following paragraphs, we describe a general protocol accompanied with the notes to highlight the critical steps and remarks which need to be considered during isolation.

5.2.1 Isolation and Transports

BMSCs are isolated from BM of "healthy volunteers" (non-relevant diagnosis prior to surgery), from hematological patients at the iliac crest, or from orthopedic patients upon gentle washing of the femoral head (obtained and fragmented into pieces during hip replacement surgery) (**Figures 4B, D**). An aliquot of one ml of BM diluted with heparin can be centrifuged 2,000 g, 10 min at 4°C to preserve BM plasma. After centrifugation, the supernatant (BM plasma) is transferred to a new tube and frozen at -80°C for subsequent analyses.

BM aspirates are obtained by aspiration of 5-10 mL from the iliac crest after infiltration of the area with local anesthetic (lidocaine, 10 mg/mL), in a 20 mL syringe and mixed 1:1 with basal media containing heparin (100 U/mL) or EDTA (1 mM)[1,2].

After the isolation of the BM aspirate, the samples are transferred to a tube prepared with buffer containing anticoagulant and directly processed for isolation of BMSCs and BMAd-enriched fraction. The BM samples should be processed within a couple of hours, otherwise the viability of the cells can be compromised[3].

***Notes*:**

1- We do not observe a huge difference between heparin or EDTA as a source of anticoagulant in the buffer for transport of BM aspirates regarding the yield and viability of isolated BMSCs. Similar results are obtained by collecting BM aspirates into commercial EDTA tubes or by using 1 mM of EDTA (replacing Heparin) into PBS.

2- Before the procedure, Minimum Essential Medium (MEM) is prepared with heparin (100 U/ml) or with 1 mM EDTA and kept at 4°C.

3- The BM samples should be ideally transferred at room temperature and processed within two hours. The transport duration and temperature should be recorded, as described previously.

5.2.2 General Procedure for BMSC and BMAd-Enriched Fraction Isolation

Reagents and Equipment:

- Lymphoprep (StemCell, Scintila) (stored at RT, protected from a light) OR Ficoll (Ficoll-Paque™ PLUS (#17-1440-03, GE Healthcare)
- MEM (Invitrogen cat.no. 04193013M, stored at 4°C)
- MEM + 10% Fetal Bovine Serum (FBS) + 1% Penicilin/ Streptamycin (stored at 4°C)
- Human Fibroblast Growth Factor (FGF)-2 (R&D system, # 233-FB-010) to add directly to the medium at 1 ng/mL (optional)
- Heparin (1,000 U/ml; stored at 4°C)
- Sterile filter (0.2 μM)
- 10 ml syringe
- Basket filter 100 μM
- Kwill or Falcon plastic tubes
- Small disposable needles
- Pasteur pipette
- Centrifuge with cooling and setting for non-break spinning

General Protocol (Figure 4):

- Dilute harvested BM aspirate 1:1 in PBS (with Ca and Mg), mix gently and immediately divide into two 50 ml Falcon tubes[4].
- Add 10 ml Lymphoprep or 15 ml Ficoll by the kwill plastic tubes, which is placed at the bottom of the tube in order to create a gradient for the separation[5].
- To obtain a floating BMAd-enriched fraction centrifuge samples at 1,050 g for 25-30 minutes at **RT without brake**. For BMSCs, centrifuge samples at 300g 30 min at **RT without brake.** After centrifugation, collect the BMAd-enriched fraction on the top by a pipette (**Figures 3B**, **4C**) and follow the steps of washing and harvest in appropriate buffer depending on the subsequent analyses[6,7].
- For the mononuclear cell component containing the BMSC fraction, isolate the buffy coat with a Pasteur pipette and transfer to the prepared 50 ml Falcon tube with preheated MEM medium. The buffy coats from both tubes are combined[8]. Higher BMSC yield can be obtained by also recovering the "serum" fraction above the buffy coat and below the floating BMAd-enriched fraction, which contains less cells but relatively enriched in BMSCs.
- Centrifuge tube at 1,050g for BMAds or at 300g for BMSCs for 10 min. Aspirate supernatant, disperse cell pellet in fresh complete medium (~ 20 ml), count the cells and seed them for *in vitro* cultivation[9].

Notes:

4- Before the gradient separation (by Lymphoprep or Ficoll), the BM sample is filtered with a cell strainer (100 μm) to remove big clumps that can cause disturbances in the gradient. We apply a sterile plunger the filter to break the small aggregates and cell clusters.

5- Lymphoprep or Ficoll are aspirated from the bottle with a small disposable needle, which is changed to the kwill plastic needle appropriate for making the gradient.

6- BMAd-enriched fraction is washed 2-3 times with PBS/1%BSA and then aliquoted for RNA and protein sample by preservation in Trizol or protein lysis buffer, respectively, and stored at -80°C (more details in **Table 4***). Note that this fraction contains a very significant amount of contaminating hematopoietic and immune cells, but it is the only source of enriched BMAd from iliac crest BM aspirates remaining from diagnostic procedures in hematological patients. Results associated to this fraction have to be interpreted within this context.*

7- The BMAd-enriched fraction can also be preserved for lipid storage. For this purpose, the BMAd-enriched fraction is transferred to an Eppendorf tube, centrifuged at maximum speed for 5 minutes followed by collecting the lipid supernatant into a clean Eppendorf tube, flash freezing by submersion in liquid nitrogen and store at -80°C. Lipid extraction is performed at a subsequent step prior to further analysis (HPLC, lipidomics).

8- The serum fraction above the buffy coat can also be collected, as it contains a significant number of BMSCs.

9- To improve cell growth, we add hFGF2 to the medium (at 1 ng/ml).

5.2.3 BMSC Cultivation

BMSCs are cultured at a density $1x10^5$ cells/cm^2 ($1x10^6$ cells per chamber slide)[10] in MEM containing 10% fetal bovine serum (FBS, GIBCO) and antibiotics at 1% (penicillin/streptomycin) incubated at 5% CO_2 and 37°C followed by completely changing the medium once a week[11], while passaging at 70-80% confluence. The cells from passage 0 are cryopreserved in freezing media containing FBS, MEM and DMSO[12] (**Table 4**). For cryopreservation, cells in freezing media are immediately transferred into freezer at -80°C for 24 hours before storing them in liquid nitrogen.

Cultured cells are sub-cultured[13] and further used for quality control tests (CFU-F, purity assessment, as described below (Section 5.2.5) and in previous literature (8) and subsequently studied in differentiation conditions when appropriate to induce adipogenesis, osteogenesis and/or chondrogenesis. Passage number should be recorded for all experiments[13].

Notes:

10- We usually seed 10 million cells per T75 flask.

11- After 4-7 days the stromal cells have attached and started making colonies. Change medium without disturbing or perturbing cells. Media can be switched to Super-MEM (10% FBS/1% pen/strep/glutamax/nonessential amino acids/sodium pyruvate) to enrich the media for essential components needed for BMSC proliferation.

*12- There are several options to prepare freezing media e.g. 80% FBS, 10% MEM and 10% DMSO (***Table 4***) or a variant recipe with 50% MEM, 40% FBS and 10% DMSO.*

13- The cultured cells from passage 0 are usually sub-cultured 1:2 in order to expand for further analyses and functional assays. Primary BMSCs are easily capable of passaging up to passage 6-7 but with each passage their capacity to proliferate and differentiate into different cell types is decreased, which affects their cellular and molecular properties. Also, they become more senescent as noticed when cells do not double within 4-5 days (71, 72).

5.2.4 Sample Storage

Storage of BMSCs and BMAd-enriched samples depends on the purpose of the intended analyses (more details in **Table 4**). The stability of RNA or protein samples is superior when the samples are processed completely, rather than storing them in RNA or protein lysis buffer as specified in **Table 4**. The storage of BMSCs is more stable in liquid nitrogen compared to -80°C.

5.2.5 Quality Controls

There are several methods available to check the quality of isolated BMSC samples [as detailed in (8)]. Representative pictures of validated methods are depicted in **Figures 6**, **7**.

Cell Viability

The cell viability of isolated BMSCs can be verified by Trypan blue staining or by flow cytometry using 7-AAD staining (7- amino-actinomycin D; marker of dead cells) or Live/dead viability assay (73).

Purity (Hematopoietic, Endothelial Cell Contamination)

The purity of BMSCs can be checked by flow cytometry using CD markers for BMSCs (e.g. CD73, CD271, CD146, CD90, CD105), hematopoietic cells (e.g. CD45 neg), erythroid cells (e.g. CD235a neg) and monocytes/macrophages (e.g. CD14 neg, CD16 neg) (**Figure 6** for representative dot plots for BMSC purity) (56, 59–61).

CFU-F Assay

In order to test stem cell potency of isolated BMSCs (**Figure 7A**), we perform a CFU-F assay, i.e. capability of stem/progenitor cells to form colonies. We seed around 1 million isolated BMSC cells in T25 flask and count number of colonies grown after 14 days. CFU-F assays are done through dilution of the test BMSC population and counting at day 14 after fixation and staining with either methylene blue or crystal violet (**Figure 7B**) (56, 59–61).

Bi/Tri-Lineage Differentiation Assay

To test differentiation potential of isolated BMSCs (70, 74), we seed and culture the cells in the conditions to differentiate into osteoblast (bone forming cells), adipocyte (BMAT forming cells), chondrocyte (cartilage forming cells) (**Figures 7C–E**). Each of these differentiation protocols can vary among different laboratories (8). For evaluation of osteoblast differentiation, we perform alkaline phosphatase (ALP) activity assay, Alizarin/ALP staining, gene expression of osteoblast genes (e.g. *RUNX*2, Osteocalcin (*BGLAP*), *ALPL*); for adipocyte differentiation these are Oil Red O or Nile Red staining, gene expression of adipocyte genes (*PPARG, LPL, ADIPOQ, LEP*), and for chondrocyte differentiation these are Alcian Blue staining, gene expression of chondrocyte genes (e.g. *SOX9, COL2A1, ACAN*) are evaluated (56, 59–61, 70, 74).

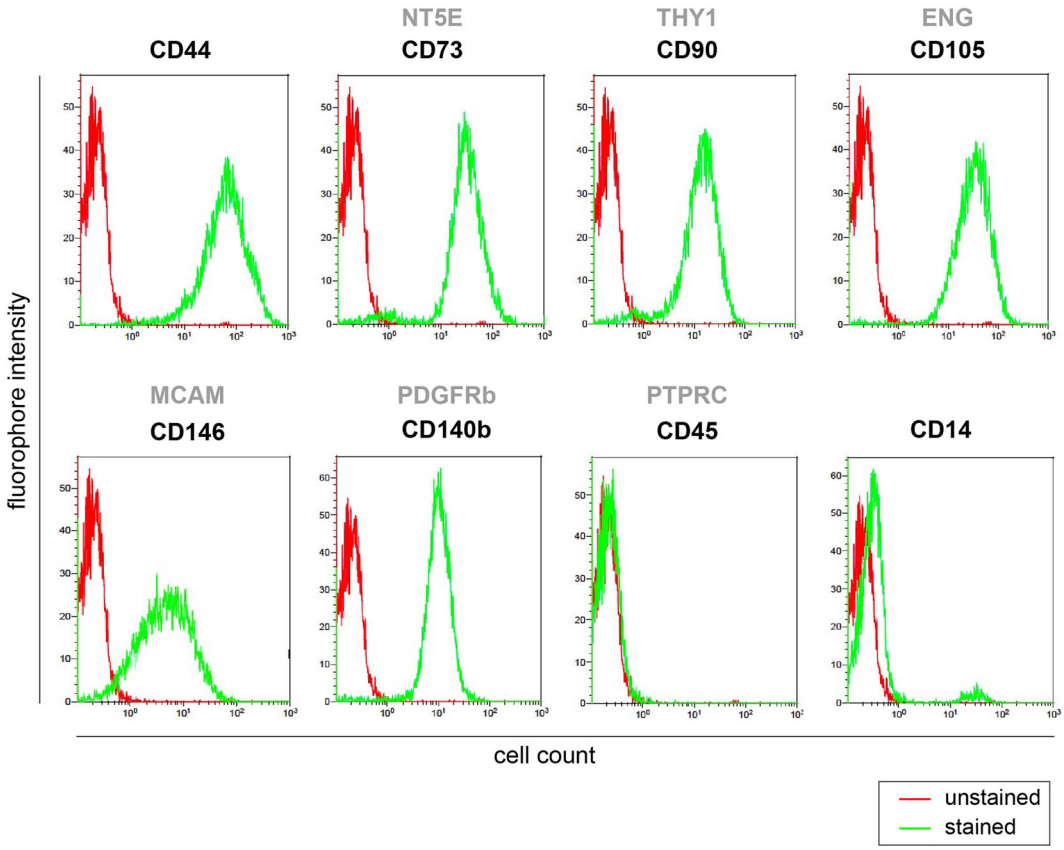

FIGURE 6 | BMSC purity assessment by flow cytometry. Screening of stem cell surface markers expression (positive for CD44, CD73, CD90, CD146, CD140b, CD105, and negative for CD45 and CD14) measured by flow cytometry in primary human BMSCs isolated from iliac crest cultured *in vitro* at passage p0.

For the purpose of biobanking it is important to keep all necessary information related to the quality of BMSC samples. However, additional comparative studies are still needed to define the crucial parameters that influence BMSC quality, and which therefore are needed for interpreting the analyses of biobank samples.

6 BMAS STRATEGY TO HARMONIZE BMA-RELATED BIOBANKING AND FUTURE PERSPECTIVES

Increased numbers of BMA-related publications in recent years using different sources of BMAT raised important questions about how to compare and reproduce the data in such a young and dynamic field. This raises an opportunity to create BMA biobanks that can provide material for other researchers and generate improved harmonization in future studies. Therefore, a standard protocol would be preferred to allow comparison of samples obtained from different institutions with specifications of critical points, which have been raised in this position paper based on the evaluation of the current literature.

While isolation protocols and collections for BMSCs have been proposed from various laboratories and private companies for long standing, those relative to BMAds are more recent and heterogenous. We currently validated three protocols from which we generated a general procedure to isolate BMAds using collagenase. Yet, it can be acknowledged that this digestion step (i.e. type of collagenase, duration of collagenase treatment, etc.) has to be further standardized and its impact on adipocyte selection, viability and functionality further characterized. When pure BMAd suspension is required or if the BMAds are to be compared with WAT adipocytes, the use of collagenase is recommended to prevent contamination from other cell types and to ensure that differences between adipocyte isolation procedures is not a confounding factor (65).

As technical developments in transcriptomics and other -omics approaches performed in various other tissues could be relevant for future BMAd analyses, we provide the following suggestions regarding next generation sequencing approaches based on preliminary and often unpublished results from different laboratories belonging to the consortium. Indeed, several factors have been determined as critical for single cell RNA sequencing (scRNA-seq) and other -omics approaches. We suggest to minimize as much as possible manipulation of the cell prior to any -omics or

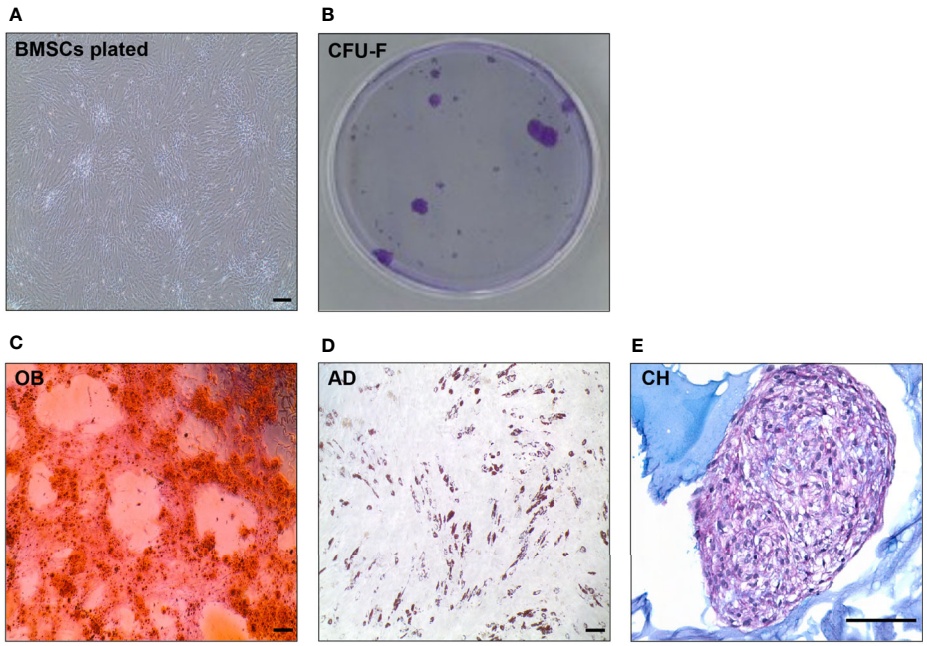

FIGURE 7 | *In vitro* evaluation of BMSC quality (BMSC culture, CFU-C, tri-differentiation). **(A)** Representative picture of spindle-like shape cells in *in vitro* culture of human BMSCs. **(B)** CFU-F of BMSCs after 14 days *in vitro* culture visualized by Violet Blue in a petri dish. **(C)** Alizarin staining of mineralized matrix in 10 days osteoblast (OB) culture differentiated from primary BMSCs. **(D)** Oil Red O staining of neutral lipids in a 10 days adipocyte (AD) culture differentiated from primary BMSCs. **(E)** Alcian Blue staining of a 21 days chondrocyte (CH) culture differentiated from BMSCs. Scale bar represents 200 μm in all the pictures.

transcriptomic approach. A very recent studies suggest that routine steps such as collagenase digestion can have a detrimental effect on the cell's transcriptome for all single cell analyses and other omics approaches. If to be used, the time of collagenase treatment or other digestion enzymes should be as short as possible as it has been shown to drastically affect the transcriptome, resulting in that the most important gene signature is the digestion itself (75).

Furthermore, a recent study determined that flash freezing (cryopreservation) of cells from BM aspirates prior to scRNA-seq does not affect the transcriptome (76). By doing so, multiple BM samples can be analyzed simultaneously, which would drastically reduce the batch effect that is often visible for single cell RNA-sequencing experiments. Since currently available scRNA-seq analyses are thus far challenging (77), the compatibility of cryopreservation with single nuclei RNA-seq could constitute a very interesting approach to determine and better characterize the BMAT transcriptional landscape. Indeed, it is today impossible to process an entire adipocyte by standard scRNA-seq, since current technologies use pure oil to create the encapsulation droplets. Partial adipocyte lysis, which is hard to avoid due to their natural fragility, prevents the formation of the droplet emulsion and ruins the chip for further use. However, nuclei extraction from BMAds is still very challenging and current procedures still need to be improved. Altogether, the WG suggests to limit the use of collagenase digestion as much as possible while collecting BMAT for these specific transcriptomic analyses since an absolute cell purity is not required and such a digestion step could interfere with subsequent analyses.

Finally, critical differences between our protocols should be further discussed and validated (e.g. precise requirements and specifications for clinical sample isolation and transportation) or improved (easier and standardized assays to assess the quality of samples, increased yield of isolated materials) for harmonization purposes. Meanwhile our current work paves the way for BMAT biobanking perspectives and next generation sequencing. We thus strongly encourage future publications to provide a detailed description of patient characteristics, BMA source and sampling, isolation procedures and validity tests to enhance standardization in the field.

Last but not least, we should pay attention to clinical/molecular data and the anonymization of participants` personal information as they are aimed to be shared among different institutes. At all times, the utmost care should be taken to deidentify the samples obtained from study participants (as discussed in *Section 2.2*). The technological advancements to perform genetic analyses have advanced to such an extent that certain approaches, such as RNA sequencing and single cell sequencing can allow for identification of the individual. Therefore, there is a task at hand to create awareness among researchers to minimize risks of deidentification.

Future Perspectives

Although we are still several steps away from achieving this, harmonizing protocols globally would greatly enhance the quality and interpretation of BMA-associated outcomes and yield increased impact in the field. A longer-term goal of this

WG is to establish a common protocol or minimal conditions that everyone could use. In an attempt to achieve this, one action of the WG will be to setup a study in which the same material will be processed in different labs, using an identical protocol followed by careful evaluation of the outcomes.

It is important to emphasize that at the beginning of creating a BMA biobank one needs to think about preparation of broad consent for future research, which may help to facilitate harmonization as well and, as it is ethically valid, this should be recommended for biobank research (9). In addition, harmonizing sample collection and storage will facilitate medical ethical boards of institutes of collaborating universities about the synchronous sample characteristics of incoming or outgoing samples in case of international studies. One of the other things that the BMAS WG on Biobanking has in mind is to develop a Global Material Transfer Agreement (GMTA) that would allow for easier acceptance and transport of BMA-related samples between institutes across the globe.

Altogether, this position paper should create awareness and facilitate scientists involved in BMA that plan to or continue studies in which collection, storage and analysis of BMA-related samples are involved.

AUTHOR CONTRIBUTIONS

SL, MT, BW and BE coordinated the writing and wrote the section on BMAS strategy. FBJ, KI, IP and BE wrote sections on background, informed consent and patient information. TLA with SL and MT wrote the section on biological materials. SL, MT, MR, BW, ON, CA and WC wrote the section on methodology of cell isolation and analysis. FB-J generated the reference library. WC, SL, TA, CA, MT, BW and BE contributed to and composed the figures. All authors contributed to the article and approved the submitted version.

FUNDING

MR was funded by the NIH/NIGMS (P20GM121301 and U54GM115516), NIH/NCI (1R37CA245330-01A1), and the American Cancer Society (#133077-RSG-19-037-01-LIB). MT was funded by the Czech Science Foundation (GACR 20-03586S), EFSD/NovoNordisk foundation Future leaders award (NNF20SA0066174). ON and BW were funded by the Swiss National Science Foundation Sinergia program (CRSII5_186271). SL was funded by MSD Avenir Foundation (ADIMETABONE project) and the University of Littoral-Côte d'Opale (ULCO). WC was funded by the Medical Research Council (MR/M021394/1 and MR/S010505/1). CA was funded by La Ligue contre le cancer (Equipe Labellisée) and INCa PLBIO20-028. IP was funded by NIH/NCI (1R01 CA251394 and 1R01 CA181189). KI was funded by the Academy of Finland (325498). TA was funded by the VELUX foundation (25723) and the Region of Southern Denmark (20/14282).

ACKNOWLEDGMENTS

Acknowledgments to Dr. Li Chen, KMEB, Odense, DK for representative pictures of Alcian Blue stained chondrocytes of human BMSCs and to David Estève, Toulouse, France for the representative picture of BMAd staining with BODIPY and Topro 3 to evaluate cell contamination. The involvements of orthopaedic surgeons – Dr Stéphane Cherix (Department of orthopaedic and traumatology, Lausanne University Hospital, CHUV, Switzerland), Prof Gilles Pasquier (CHU Lille, France), Gavin Macpherson (Department of Orthopaedic Surgery, Royal Infirmary of Edinburgh, UK), Dr Charlotte Ejersted and Dr Bjarke Viberg (Department of Endocrinology and Department of Orthopaedic Surgery, Odense University Hospital, Denmark), Dr Lene W.T. Boel (Department of Forensic Medicine, Aarhus University, Denmark), Prof Moustapha Kassem, Dr Morten Frost and Dr Jens-Jacob Lauterlein (Department of Endocrinology, Odense University Hospital, Denmark), Prof Nicolas Reina (Department of orthopaedic and traumatology, CHU Toulouse, France) and BRC staff – Dr Patrick Gele and Bertrand Accart (Lille, France) and the Lausanne University Hospital, CHUV, Bone Marrow diagnostic lab and Hematology staff (Prof. Olivier Spertini, Dr Sabine Blum, Dr Mariangela Costanza, Valentin Basset, Stéphane Quarroz) are all esteemed and acknowledged. We are extremely grateful to all the patients and families who have generously consented to sample and data collection, making our research possible.

REFERENCES

1. Bani Hassan E, Ghasem-Zadeh A, Imani M, Kutaiba N, Wright DK, Sepehrizadeh T, et al. Bone Marrow Adipose Tissue Quantification by Imaging. *Curr Osteoporos Rep* (2019) 17(6):416–28. doi: 10.1007/s11914-019-00539-5
2. de Paula FJA, Rosen CJ. Marrow Adipocytes: Origin, Structure, and Function. *Annu Rev Physiol* (2020) 82:461–84. doi: 10.1146/annurev-physiol-021119-034513
3. Penel G, Kerckhofs G, Chauveau C. Brief Report From the 4th International Meeting on Bone Marrow Adiposity (Bma2018). *Front Endocrinol (Lausanne)* (2019) 10:691. doi: 10.3389/fendo.2019.00691
4. Sebo ZL, Rendina-Ruedy E, Ables GP, Lindskog DM, Rodeheffer MS, Fazeli PK, et al. Bone Marrow Adiposity: Basic and Clinical Implications. *Endocr Rev* (2019) 40(5):1187–206. doi: 10.1210/er.2018-00138
5. Bartelt A, Koehne T, Todter K, Reimer R, Muller B, Behler-Janbeck F, et al. Quantification of Bone Fatty Acid Metabolism and Its Regulation by Adipocyte Lipoprotein Lipase. *Int J Mol Sci* (2017) 18(6):1264. doi: 10.3390/ijms18061264
6. Mate S, Kampf M, Rodle W, Kraus S, Proynova R, Silander K, et al. Pan-European Data Harmonization for Biobanks in. *Appl Clin Inform* (2019) 10 (4):679–92. doi: 10.1055/s-0039-1695793
7. Bravenboer N, Bredella MA, Chauveau C, Corsi A, Douni E, Ferris WF, et al. Standardised Nomenclature, Abbreviations, and Units for the Study of Bone Marrow Adiposity: Report of the Nomenclature Working Group of the International Bone Marrow Adiposity Society. *Front Endocrinol (Lausanne)* (2019) 10:923. doi: 10.3389/fendo.2019.00923
8. Tratwal J, Labella R, Bravenboer N, Kerckhofs G, Douni E, Scheller EL, et al. Reporting Guidelines, Review of Methodological Standards, and Challenges Toward Harmonization in Bone Marrow Adiposity Research. Report of the

Methodologies Working Group of the International Bone Marrow Adiposity Society. *Front Endocrinol* (2020) 11:65. doi: 10.3389/fendo.2020.00065
9. Hansson MG, Dillner J, Bartram CR, Carlson JA, Helgesson G. Should Donors be Allowed to Give Broad Consent to Future Biobank Research? *Lancet Oncol* (2006) 7(3):266–9. doi: 10.1016/S1470-2045(06)70618-0
10. Charmantier I. Carl Linnaeus and the Visual Representation of Nature. *Hist Stud Nat Sci* (2011) 41(4):365–404. doi: 10.1525/hsns.2011.41.4.365
11. Funk VA. Collections-Based Science in the 21st Century. *J Syst Evol* (2018) 56 (3):175–93. doi: 10.1111/jse.12315
12. Loft S, Poulsen HE. Cancer Risk and Oxidative DNA Damage in Man. *J Mol Med (Berl)* (1996) 74(6):297–312. doi: 10.1007/BF00207507
13. Hewitt R, Watson P. Defining Biobank. *Biopreserv Biobank* (2013) 11(5):309–15. doi: 10.1089/bio.2013.0042
14. Larsson A. The Need for Research Infrastructures: A Narrative Review of Large-Scale Research Infrastructures in Biobanking. *Biopreserv Biobank* (2017) 15(4):375–83. doi: 10.1089/bio.2016.0103
15. Mayrhofer MT, Holub P, Wutte A, Litton JE. BBMRI-ERIC: The Novel Gateway to Biobanks. From Humans to Humans. *Bundesgesundheitsblatt Gesundheitsforschung Gesundheitsschutz* (2016) 59(3):379–84. doi: 10.1007/s00103-015-2301-8
16. Kinkorova J. Biobanks in the Era of Personalized Medicine: Objectives, Challenges, and Innovation: Overview. *EPMA J* (2015) 7:4. doi: 10.1186/s13167-016-0053-7
17. Paskal W, Paskal AM, Debski T, Gryziak M, Jaworowski J. Aspects of Modern Biobank Activity - Comprehensive Review. *Pathol Oncol Res* (2018) 24 (4):771–85. doi: 10.1007/s12253-018-0418-4
18. Fransson MN, Rial-Sebbag E, Brochhausen M, Litton JE. Toward a Common Language for Biobanking. *Eur J Hum Genet* (2015) 23(1):22–8. doi: 10.1038/ejhg.2014.45
19. Sudlow C, Gallacher J, Allen N, Beral V, Burton P, Danesh J, et al. UK Biobank: An Open Access Resource for Identifying the Causes of a Wide Range of Complex Diseases of Middle and Old Age. *PloS Med* (2015) 12(3): e1001779. doi: 10.1371/journal.pmed.1001779
20. Gottweis H, Zatloukal K. Biobank Governance: Trends and Perspectives. *Pathobiology* (2007) 74(4):206–11. doi: 10.1159/000104446
21. Coppola L, Cianflone A, Grimaldi AM, Incoronato M, Bevilacqua P, Messina F, et al. Biobanking in Health Care: Evolution and Future Directions. *J Transl Med* (2019) 17(1):172. doi: 10.1186/s12967-019-1922-3
22. Peakman T, Elliott P. Current Standards for the Storage of Human Samples in Biobanks. *Genome Med* (2010) 2(10):72. doi: 10.1186/gm193
23. OECD. *OECD Guidelines on Human Biobanks and Genetic Research Databases* (2009). Available at: http://www.oecd.org/sti/emerging-tech/44054609.pdf (Accessed 6th of August 2020).
24. OECD. *OECD Best Practice Guidelines for Biological Resource Centres* (2007). Available at: http://www.oecd.org/sti/emerging-tech/38777417.pdf (Accessed 6th of August 2020).
25. Muller H, Dagher G, Loibner M, Stumptner C, Kungl P, Zatloukal K. Biobanks for Life Sciences and Personalized Medicine: Importance of Standardization, Biosafety, Biosecurity, and Data Management. *Curr Opin Biotechnol* (2020) 65:45–51. doi: 10.1016/j.copbio.2019.12.004
26. Jefford M, Moore R. Improvement of Informed Consent and the Quality of Consent Documents. *Lancet Oncol* (2008) 9(5):485–93. doi: 10.1016/S1470-2045(08)70128-1
27. Master Z, Nelson E, Murdoch B, Caulfield T. Biobanks, Consent and Claims of Consensus. *Nat Methods* (2012) 9(9):885–8. doi: 10.1038/nmeth.2142
28. Siminoff LA, Wilson-Genderson M, Mosavel M, Barker L, Trgina J, Traino HM. Confidentiality in Biobanking Research: A Comparison of Donor and Nondonor Families' Understanding of Risks. *Genet Test Mol Biomark* (2017) 21(3):171–7. doi: 10.1089/gtmb.2016.0407
29. Udesky JO, Boronow KE, Brown P, Perovich LJ, Brody JG. Perceived Risks, Benefits, and Interest in Participating in Environmental Health Studies That Share Personal Exposure Data: A U.S. Survey of Prospective Participants. *J Empir Res Hum Res Ethics* (2020) 15(5):425–42. doi: 10.1177/1556264620903595
30. Abbing HD. Unesco. International Declaration on Human Genetic Data. *Eur J Health Law* (2004) 11(1):93–107. doi: 10.1163/157180904323042399
31. WHO. *Templates for Informed Consent Forms* (2020). Available at: https://www.who.int/groups/research-ethics-review-committee/guidelines-on-submitting-research-proposals-for-ethics-review/templates-for-informed-consent-forms (Accessed 30th of November 2020).
32. Bleiberg H, Decoster G, de Gramont A, Rougier P, Sobrero A, Benson A, et al. A Need to Simplify Informed Consent Documents in Cancer Clinical Trials. A Position Paper of the ARCAD Group. *Ann Oncol* (2017) 28(5):922–30. doi: 10.1093/annonc/mdx050
33. Council of Europe. *Guide for the Implementationof the Principle of Prohibition of Financial Gain With Respect to the Human Body and Its Parts From Living or Deceased Donors* (2018). Available at: https://rm.coe.int/guide-financial-gain/16807bfc9a (Accessed 06th of May 2021).
34. Hayflick L. Paying for Tissue: The Case of WI-38. *Science* (2012) 337 (6100):1292. doi: 10.1126/science.337.6100.1292-a
35. Truog RD, Kesselheim AS, Joffe S. Research Ethics. Paying Patients for Their Tissue: The Legacy of Henrietta Lacks. *Science* (2012) 337(6090):37–8. doi: 10.1126/science.1216888
36. Le Ster C, Lasbleiz J, Kannengiesser S, Guillin R, Gambarota G, Saint-Jalmes H. A Fast Method for the Quantification of Fat Fraction and Relaxation Times: Comparison of Five Sites of Bone Marrow. *Magnet Reson Imaging* (2017) 39:157–61. doi: 10.1016/j.mri.2017.03.001
37. Costa S, Reagan MR. Therapeutic Irradiation: Consequences for Bone and Bone Marrow Adipose Tissue. *Front Endocrinol* (2019) 10:587. doi: 10.3389/fendo.2019.00587
38. Rharass T, Lucas S. Mechanisms in Endocrinology: Bone Marrow Adiposity and Bone, a Bad Romance? *Eur J Endocrinol* (2018) 179(4):R165–78. doi: 10.1530/EJE-18-0182
39. Suchacki KJ, Cawthorn WP. Molecular Interaction of Bone Marrow Adipose Tissue With Energy Metabolism. *Curr Mol Biol Rep* (2018) 4(2):41–9. doi: 10.1007/s40610-018-0096-8
40. Vande Berg BC, Gilon R, Malghem J, Lecouvet F, Depresseux G, et al. Correlation Between Baseline Femoral Neck Marrow Status and the Development of Femoral Head Osteonecrosis in Corticosteroid-Treated Patients: A Longitudinal Study by MR Imaging. *Eur J Radiol* (2006) 58 (3):444–9. doi: 10.1016/j.ejrad.2006.01.009
41. Veldhuis-Vlug AG, Rosen CJ. Clinical Implications of Bone Marrow Adiposity. *J Intern Med* (2018) 283(2):121–39. doi: 10.1111/joim.12718
42. Lee SH, Erber WN, Porwit A, Tomonaga M, Peterson LC. ICSH Guidelines for the Standardization of Bone Marrow Specimens and Reports. *Int Jnl Lab Hem* (2008) 30:349–64. doi: 10.1111/j.1751-553X.2008.01100.x
43. Gillet C, Dalla Valle A, Gaspard N, Spruyt D, Vertongen P, Lechanteur J, et al. Osteonecrosis of the Femoral Head: Lipotoxicity Exacerbation in MSC and Modifications of the Bone Marrow Fluid. *Endocrinology* (2017) 158(3):490–502. doi: 10.1210/en.2016-1687
44. Miranda M, Pino AM, Fuenzalida K, Rosen CJ, Seitz G, Rodriguez JP. Characterization of Fatty Acid Composition in Bone Marrow Fluid From Postmenopausal Women: Modification After Hip Fracture. *J Cell Biochem* (2016) 117(10):2370–6. doi: 10.1002/jcb.25534
45. Pino AM, Rios S, Astudillo P, Fernandez M, Figueroa P, Seitz G, et al. Concentration of Adipogenic and Proinflammatory Cytokines in the Bone Marrow Supernatant Fluid of Osteoporotic Women. *J Bone Miner Res* (2010) 25(3):492–8. doi: 10.1359/jbmr.090802
46. Kirwan JA, Brennan L, Broadhurst D, Fiehn O, Cascante M, Dunn WB, et al. Preanalytical Processing and Biobanking Procedures of Biological Samples for Metabolomics Research: A White Paper, Community Perspective (for "Precision Medicine and Pharmacometabolomics Task Group"-The Metabolomics Society Initiative). *Clin Chem* (2018) 64(8):1158–82. doi: 10.1373/clinchem.2018.287045
47. Yin P, Peter A, Franken H, Zhao X, Neukamm SS, Rosenbaum L, et al. Preanalytical Aspects and Sample Quality Assessment in Metabolomics Studies of Human Blood. *Clin Chem* (2013) 59(5):833–45. doi: 10.1373/clinchem.2012.199257
48. Gonzalez-Dominguez R, Gonzalez-Dominguez A, Sayago A, Fernandez-Recamales A. Recommendations and Best Practices for Standardizing the Pre-Analytical Processing of Blood and Urine Samples in Metabolomics. *Metabolites* (2020) 10(6):229. doi: 10.3390/metabo10060229
49. Vasikaran S, Eastell R, Bruyere O, Foldes AJ, Garnero P, Griesmacher A, et al. Markers of Bone Turnover for the Prediction of Fracture Risk and Monitoring of Osteoporosis Treatment: A Need for International Reference Standards. *Osteoporos Int* (2011) 22(2):391–420. doi: 10.1007/s00198-010-1501-1

50. Ferland-McCollough D, Masseli D, Spinetti G, Sambataro M, Sullivan N, Blom A, et al. MCP-1 Feedback Loop Between Adipocytes and Mesenchymal Stromal Cells Causes Fat Accumulation and Contributes to Hematopoietic Stem Cell Rarefaction in the Bone Marrow of Diabetic Patients. *Diabetes* (2018) 67(7):1380–94. doi: 10.2337/db18-0044
51. Suchacki KJ, Tavares AAS, Mattiucci D, Scheller EL, Papanastasiou G, Gray C, et al. Bone Marrow Adipose Tissue Is a Unique Adipose Subtype With Distinct Roles in Glucose Homeostasis. *Nat Commun* (2020) 11(1):3097. doi: 10.1038/s41467-020-16878-2
52. Griffith JF, Yeung DKW, Ahuja AT, Choy CWY, Mei WY, Lam SSL, et al. A Study of Bone Marrow and Subcutaneous Fatty Acid Composition in Subjects of Varying Bone Mineral Density. *Bone* (2009) 44(6):1092–6. doi: 10.1016/j.bone.2009.02.022
53. Attané C, Estève D, Chaoui K, Iacovoni JS, Corre J, Moutahir M, et al. Human Bone Marrow Is Comprised of Adipocytes With Specific Lipid Metabolism. *Cell Rep* (2020) 30(4):949–58.e6. doi: 10.1016/j.celrep.2019.12.089
54. Poloni A, Maurizi G, Serrani F, Mancini S, Zingaretti MC, Frontini A, et al. Molecular and Functional Characterization of Human Bone Marrow Adipocytes. *Exp Hematol* (2013) 41(6):558–66.e2. doi: 10.1016/j.exphem.2013.02.005
55. Tencerova M, Frost M, Figeac F, Nielsen TK, Ali D, Lauterlein JL, et al. Obesity-Associated Hypermetabolism and Accelerated Senescence of Bone Marrow Stromal Stem Cells Suggest a Potential Mechanism for Bone Fragility. *Cell Rep* (2019) 27(7):2050–62.e6. doi: 10.1016/j.celrep.2019.04.066
56. Caplan AI. Mesenchymal Stem Cells. *J Orthop Res* (1991) 9(5):641–50. doi: 10.1002/jor.1100090504
57. Tanavde V, Vaz C, Rao MS, Vemuri MC, Pochampally RR. Research Using Mesenchymal Stem/Stromal Cells: Quality Metric Towards Developing a Reference Material. *Cytotherapy* (2015) 17(9):1169–77. doi: 10.1016/j.jcyt.2015.07.008
58. Pham TT, Ivaska KK, Hannukainen JC, Virtanen KA, Lidell ME, Enerback S, et al. Human Bone Marrow Adipose Tissue Is a Metabolically Active and Insulin-Sensitive Distinct Fat Depot. *J Clin Endocrinol Metab* (2020) 105(7):2300–10. doi: 10.1210/clinem/dgaa216
59. Bianco P, Gehron Robey P. Marrow Stromal Stem Cells. *J Clin Invest* (2000) 105(12):1663–8. doi: 10.1172/JCI10413
60. Bianco P, Riminucci M, Gronthos S, Robey PG. Bone Marrow Stromal Stem Cells: Nature, Biology, and Potential Applications. *Stem Cells (Dayton Ohio)* (2001) 19(3):180–92. doi: 10.1634/stemcells.19-3-180
61. Bianco P, Robey PG, Simmons PJ. Mesenchymal Stem Cells: Revisiting History, Concepts, and Assays. *Cell Stem Cell* (2008) 2(4):313–9. doi: 10.1016/j.stem.2008.03.002
62. Goto H, Hozumi A, Osaki M, Fukushima T, Sakamoto K, Yonekura A, et al. Primary Human Bone Marrow Adipocytes Support TNF-α-Induced Osteoclast Differentiation and Function Through RANKL Expression. *Cytokine* (2011) 56(3):662–8. doi: 10.1016/j.cyto.2011.09.005
63. Miggitsch C, Meryk A, Naismith E, Pangrazzi L, Ejaz A, Jenewein B, et al. Human Bone Marrow Adipocytes Display Distinct Immune Regulatory Properties. *EBioMedicine* (2019) 46:387–98. doi: 10.1016/j.ebiom.2019.07.023
64. Attané C, Estève D, Moutahir M, Reina N, Muller C. A Protocol for Human Bone Marrow Adipocyte Isolation and Purification. *Star Protoc* (2021) 2(3). doi: 10.1016/j.xpro.2021.100629
65. Mattiucci D, Maurizi G, Izzi V, Cenci L, Ciarlantini M, Mancini S, et al. Bone Marrow Adipocytes Support Hematopoietic Stem Cell Survival. *J Cell Physiol* (2018) 233(2):1500–11. doi: 10.1002/jcp.26037
66. Rodbell M. Localization of Lipoprotein Lipase in Fat Cells of Rat Adipose Tissue. *J Biol Chem* (1964) 239:753–5.
67. Craft CS, Scheller EL. Evolution of the Marrow Adipose Tissue Microenvironment. *Calcif Tissue Int* (2016) 100:461–75. doi: 10.1007/s00223-016-0168-9
68. Lafontan M. Historical Perspectives in Fat Cell Biology: The Fat Cell as a Model for the Investigation of Hormonal and Metabolic Pathways. *Am J Physiol Cell Physiol* (2012) 302(2):C327–59. doi: 10.1152/ajpcell.00168.2011
69. Liu L-F, Shen W-J, Ueno M, Patel S, Kraemer FB. Characterization of Age-Related Gene Expression Profiling in Bone Marrow and Epididymal Adipocytes. *BMC Genomics* (2011) 12:212. doi: 10.1186/1471-2164-12-212
70. Dominici M, Le Blanc K, Mueller I, Slaper-Cortenbach I, Marini F, Krause D, et al. Minimal Criteria for Defining Multipotent Mesenchymal Stromal Cells. The International Society for Cellular Therapy Position Statement. *Cytotherapy* (2006) 8(4):315–7. doi: 10.1080/14653240600855905
71. Andrzejewska A, Catar R, Schoon J, Qazi HT, Sass FA, Jacobi D, et al. Multi-Parameter Analysis of Biobanked Human Bone Marrow Stromal Cells Shows Little Influence for Donor Age and Mild Comorbidities on Phenotypic and Functional Properties. *Front Immunol* (2019) 10:2474. doi: 10.3389/fimmu.2019.02474
72. Vidal MA, Walker NJ, Napoli E, Borjesson DL. Evaluation of Senescence in Mesenchymal Stem Cells Isolated From Equine Bone Marrow, Adipose Tissue, and Umbilical Cord Tissue. *Stem Cells Dev* (2012) 21(2):273–83. doi: 10.1089/scd.2010.0589
73. Xiao M, Dooley DC. Assessment of Cell Viability and Apoptosis in Human Umbilical Cord Blood Following Storage. *J Hematother Stem Cell Res* (2003) 12(1):115–22. doi: 10.1089/152581603321210190
74. Viswanathan S, Shi Y, Galipeau J, Krampera M, Leblanc K, Martin I, et al. Mesenchymal Stem *Versus* Stromal Cells: International Society for Cell & Gene Therapy (ISCT®) Mesenchymal Stromal Cell Committee Position Statement on Nomenclature. *Cytotherapy* (2019) 21(10):1019–24. doi: 10.1016/j.jcyt.2019.08.002
75. Machado L, Geara P, Camps J, Dos Santos M, Teixeira-Clerc F, Van Herck J, et al. Tissue Damage Induces a Conserved Stress Response That Initiates Quiescent Muscle Stem Cell Activation. *Cell Stem Cell* (2021) 28(6):1125–35. doi: 10.1016/j.stem.2021.01.017
76. Chen D, Abu Zaid MI, Reiter JL, Czader M, Wang L, McGuire P, et al. Cryopreservation Preserves Cell-Type Composition and Gene Expression Profiles in Bone Marrow Aspirates From Multiple Myeloma Patients. *Front Genet* (2021) 12:663487. doi: 10.3389/fgene.2021.663487
77. Deutsch A, Feng D, Pessin JE, Shinoda K. The Impact of Single-Cell Genomics on Adipose Tissue Research. *Int J Mol Sci* (2020) 21(13):4773. doi: 10.3390/ijms21134773

Conflict of Interest: BE is chair and coordinator of the BMAS Working Group on Biobanking. All authors are members of the BMAS Working Group on Biobanking. BE, WC and ON are members of the BMAS Executive Board. SL, MR and MT are members of the BMAS Scientific Board.

Publisher's Note: All claims expressed in this article are solely those of the authors and do not necessarily represent those of their affiliated organizations, or those of the publisher, the editors and the reviewers. Any product that may be evaluated in this article, or claim that may be made by its manufacturer, is not guaranteed or endorsed by the publisher.

frontiers in Endocrinology

ORIGINAL RESEARCH
published: 03 December 2021
doi: 10.3389/fendo.2021.766254

Bone Lining Cells Could Be Sources of Bone Marrow Adipocytes

Ji Yeon Lee[1,2], *Jae-Yeon Yang*[1,2] *and Sang Wan Kim*[1,3]*

[1] Department of Internal Medicine, Seoul National University College of Medicine, Seoul, South Korea, [2] Department of Research and Experiment, Seoul National University Hospital Biomedical Research Institute, Seoul, South Korea, [3] Division of Endocrinology and Metabolism, Seoul Metropolitan Government Boramae Medical Center, Seoul, South Korea

Background: Recently, lineage-tracing studies demonstrated that parathyroid hormone and anti-sclerostin antibody (Scl-Ab) can convert bone lining cells (BLCs) into active osteoblasts. However, BLCs might also be differentiated into other lineages. Here we investigated whether BLCs could differentiate into bone marrow adipocytes (BMAds) and whether Scl-Ab could suppress this process.

Methods: Dmp1-CreERt2:mTmG mice were injected with 0.5 mg of 4-hydroxytamoxifen once weekly from postnatal week 4 to week 8. The mice were treated with either vehicle or rosiglitazone for 8 weeks (weeks 12–20). Moreover, they were administered either vehicle or Scl-Ab (50 mg/kg) twice weekly for 4 weeks (weeks 16–20, N = 4–6/group). We chased the GFP+ cells from the endosteal surface to the bone marrow (BM) of the femur. Using immunohistochemical staining, the numbers of perilipin+ or GFP+/perilipin double+ cells in the BM were quantified. In addition, serum N-terminal propeptide of type I procollagen (P1NP) levels were measured at each time point, and bone mass was analyzed at 20 weeks using micro-computed tomography.

Results: Scl-Ab administration significantly reversed the decreases in bone parameters induced by rosiglitazone. Plump GFP+ cells, presumably active osteoblasts, and extremely flat GFP+ cells, presumably BLCs, were present on the endosteal surface of the femur at 8 and 12 weeks, respectively, in line with prior findings. When we chased the GFP+ cells, rosiglitazone significantly increased the number of GFP/perilipin double+ BMAds compared to the effects of the vehicle ($P < 0.001$), and overlapping Scl-Ab administration decreased the number of GFP/perilipin double + BMAd compared to rosiglitazone alone ($P < 0.001$). In addition, we found that osteoblast lineage cells such as BLCs might express PPARγ on immunohistochemical staining. When rosiglitazone was administered to Rip-Cre:mTmG mice, GFP+ cells were not present on the endosteal surface or in the BM of the femur; however, they were present in the pancreas.

Conclusion: BLCs could be sources of BMAds, and rosiglitazone could stimulate the differentiation of osteoblast lineage cells into BMAds. Suppression of the differentiation of osteoblast lineage cells into BMAds might contribute to anabolic effects resulting from the pharmacologic inhibition of sclerostin.

Keywords: bone marrow adipocyte, bone lining cell, anti-sclerostin antibody, rosiglitazone, osteoblast

OPEN ACCESS

Edited by:
Sarah Beck-Cormier, INSERM U1229 Médecine Régénératrice et Squelette (INSERM), France

Reviewed by:
Noriaki Ono, University of Texas Health Science Center at Houston, United States
Bram van der Eerden, Erasmus Medical Center, Netherlands
Michelle Mcdonald, Garvan Institute of Medical Research, Australia

***Correspondence:**
Sang Wan Kim
swkimmd@snu.ac.kr

Specialty section:
This article was submitted to Bone Research, a section of the journal Frontiers in Endocrinology

Received: *28 August 2021*
Accepted: *15 November 2021*
Published: *03 December 2021*

Citation:
Lee JY, Yang JY and Kim SW (2021) Bone Lining Cells Could Be Sources of Bone Marrow Adipocytes. Front. Endocrinol. 12:766254. doi: 10.3389/fendo.2021.766254

INTRODUCTION

Bone marrow adiposity (BMA) is a specific fat depot in bone cavities. BMA increases with age, and it is caused by a variety of induction signals including thiazolidinediones, glucocorticoids, high-fat diet feeding, and irradiation exposure (1). Under these conditions, bone marrow adipose tissue (BMAT) could replace hematopoietic/osteogenic marrow in the long bones. A large body of research has revealed an inverse relationship between BMA and bone mineral density (BMD) in young or elderly men and women (2–5). In addition, postmenopausal women can exhibit the most consistent association compared to old men (2, 3). Furthermore, vertebral fractures were associated with a higher BMA volume in women with postmenopausal osteoporosis, and BMA was also associated with measures of decreased bone integrity (6, 7). Interestingly, 1 year of teriparatide treatment resulted in decreased vertebral BMAT with concomitant increases in lumbar spine BMD in postmenopausal women (8).

Bone marrow adipocytes (BMAds) are distinct from white or beige adipocytes in terms of localization, function, and origin (9–11). Previous lineage-tracing studies demonstrated that BMAds do not share the same progenitors as extramedullary adipocytes, and they might be derived from bone marrow (BM) (12, 13). The definite origin of BMAds remains unclear. Recent studies revealed that BMAds are derived from skeletal stem cells (SSCs) in BM, and Osx+, LepR+, and Nes+ SSC populations are capable of generating BMAds (14–16). Thus, the origin of BMAds might be heterogeneous.

Bone lining cells (BLCs) are quiescent osteoblasts covering bone surfaces. BLCs are sources of active osteoblasts and target cells for anabolic agents. Short-term treatment with parathyroid hormone (PTH) or anti-sclerostin antibody (Scl-Ab) can induce the conversion of BLCs into active osteoblasts (17, 18). In addition, BLCs express stem cell-like genetic markers (19). Those studies suggested that BLCs have the potential to differentiate into other lineages (20). Thus, we investigated whether BLCs could represent one source of BMAds. In addition, we examined whether Scl-Ab administration could suppress the possible transdifferentiation of BLCs into BMAds. To better understand the response of BLCs to adipogenic signals and follow their subsequent differentiation, we conducted a lineage-tracing study using inducible transgenic mice.

MATERIALS AND METHODS

Mice

Temporally controlled transgene expression was used to trace cells of the osteoblast lineage using Dmp1-CreERt2 and mTmG mice. We used the mouse 10-kb Dmp1 promoter to drive the expression of the inducible CreERt2 in transgenic mice because it is expressed not only in osteocytes but also in mature osteoblast cell populations. The mutated ERt domain responds only to the synthetic estrogen receptor ligand tamoxifen. Administration of tamoxifen induces transient nuclear translocation and CreERt-mediated gene recombination. Dmp1-CreERt2 mice were crossed with mTmG mice, a double fluorescent reporter mouse strain. A reporter gene, such as the Rosa26R mTmG reporter transgene, can visualize the recombination since the expression of cre-recombinase induces the permanent excision of the upstream cassette encoding the membrane-targeted dTomato (mT) reporter protein to allow expression of a downstream cassette encoding a membrane targeted eGFP (mG) reporter protein (21, 22). In this manner, cells expressing cre-recombinase are indicative of mG expression. Then, mG is expressed continuously in the target cells and all possible progeny. Therefore, in this system, we can chase the fate of GFP-expressing cells such as from osteoblast lineage cells to BMAds (12). The 10-kb Dmp1-CreERt2 mice the Rip-Cre mice were kindly provided by Dr. Henry Kronenberg (Endocrine unit, Massachusetts General Hospital, USA) and Dr. Hye Seung Jung (Seoul National University Hospital). The 10-kb Dmp1-CreERt2 mice were generated by nuclear injections of a transgene encoding CreERt2 under the control of a 10-kb fragment of Dmp1 in B6C3F1 hybrid mice (Taconic, Hudson, NY, USA). Reporter mice (*Gt (ROSA)26Sortm4(ACTB-tdTomato,-EGFP)Luo/J*, stock no. 007576) were purchased from The Jackson Laboratory (Bar Harbor, Maine, USA).

These studies were approved by the Institutional Animal Care and Use Committee of Seoul National University.

Tamoxifen Administration

For experiments with Dmp1-CreERt2:mTmG mice, 4-hydroxytamoxifen (4-OHTam, Takeda, Osaka, Japan) was used. For 4-OHTam injections, 2.5 mg of 4-OHTam were dissolved in 100 mL of dimethylformamide (Thermo Fisher Scientific, Waltham, MA, USA) and then diluted to 2.5 mg/mL in corn oil (Sigma-Aldrich, St. Louis, MO, USA). Dmp1-CreERt2 were injected with 0.5 mg of 4-OHTam once weekly in postnatal weeks 4–8.

Rosiglitazone and Sclerostin Antibody (Scl-Ab) Administration

In postnatal week 12, the mice were fed a 20 mg/kg/day rosiglitazone-supplemented diet (containing 140 mg rosiglitazone/kg diet; R0106, Tokyo Chemical Industry, Japan) or chow diet ad libitum for 8 weeks (randomly assorted into cages and group-housed), weighed, humanely euthanized, and analyzed. In addition, mice were injected subcutaneously with vehicle (phosphate-buffered saline [PBS]) or 50 mg/kg Scl-Ab (ratized antibody; Amgen Inc., Thousand Oaks, CA, USA; UCB, Brussels, Belgium) twice weekly for 4 weeks starting in postnatal week 16 (**Figure 1**). Mice were sacrificed in postnatal weeks 8 (+2 days), 12, 16, and 20.

Serum Biochemistry

Blood was collected *via* orbital sinus puncture before animals were euthanized. The serum levels of N-terminal propeptide of

Abbreviations: BM, Bone marrow; BMA, Bone marrow adiposity; BMAd, Bone marrow adipocyte; BMAT, Bone marrow adipose Tissue; BMD, Bone mineral density; BV/TV, Bone volume/total volume; BS/TV, Bone surface/total volume; Tb. Th, Trabecular thickness; Tb. N, Trabecular number; Tb. Sp, Trabecular separation.

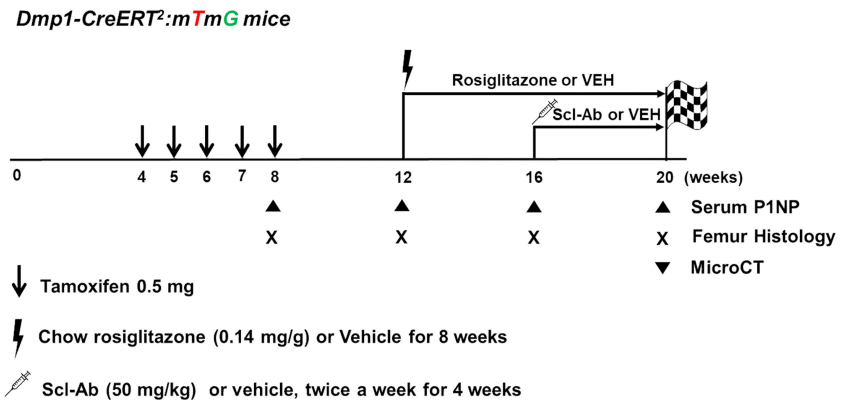

FIGURE 1 | Experimental design. Dmp1-CreERt2:mTmG mice were injected with 0.5 mg 4-OHTam on postnatal weeks 4, 5, 6, 7, and 8. The mice were treated with either vehicle or rosiglitazone for 8 weeks (weeks 12–20). Moreover, they were administered either vehicle or Scl-Ab (50 mg/kg) twice weekly for 4 weeks (weeks 16–20, N = 4–6/group). We chased the GFP+ cells from the endosteal surface to the bone marrow of the femur. Animals were euthanized on postnatal week 8 or 12 (2 days or 4 weeks after the last 4-OHTam treatment), as well as on week 16 and 20 to evaluate the impact of rosiglitazone or Scl-Ab administration.

type I procollagen (P1NP) were measured using an ELISA kit (Immunodiagnostic Systems, Fountain Hills, AZ, USA).

Micro-Computed Tomography (micro-CT)

Whole femurs were harvested from the mice after euthanasia, fixed in formaldehyde solution for 48 h, placed in 70% ethanol, and stored at 4°C until imaging. The distal femur from each mouse was scanned using high-resolution micro-CT (SkyScan 1173, Bruker microCT, Kontich, Belgium) at 90 kV and 88 µA with an isotropic voxel size of 7.1 µm using a 1.0-mm aluminum filter. For the metaphyseal tibia, a 1.5-mm section (starting 500 µm below the growth plate) was analyzed. Scanned images were reconstructed using NRecon v.1.6 software (Bruker microCT) by correcting for beam hardening and ring artifacts. Data were analyzed using CT Analyzer version1.6 (Bruker microCT). For trabecular bone regions, bone volume density (BV/TV), trabecular thickness (Tb.Th), trabecular separation (Tb.Sp), and trabecular number (Tb.N) were assessed.

Histology and Immunohistochemical Staining

Samples were dissected to remove soft tissues, fixed in 4% paraformaldehyde, incubated overnight at 4°C, and then decalcified in 15% EDTA for 7–14 days. Decalcified samples were cryoprotected in 30% sucrose/PBS followed by a 30% sucrose/PBS : OCT (1:1) solution, each performed overnight at 4°C. Samples were then embedded in OCT and cryosectioned at 8 µm (Leica, CM3050S). Images were captured using an epifluorescence microscope (Leica DMI 6000 [Inverted]) with prefigured triple-band filter settings for DAPI/FITC/TRITC and an automated fluorescent microscope with a whole-slide scanning platform. Confocal images were acquired using LEICA TCS SP8 STED CW and LAS X (Leica) software with lasers and corresponding band-pass filters for DAPI (Ex. 405 nm, BP 420–480), GFP (Ex. 488 nm, BP 505–530), and tomato (Ex. 543 nm, BP 565–595). Representative images of at least three independent biological samples are presented in the figures. Routine H&E staining was performed using previously published protocols.

Paraffin sections were postfixed in 4% paraformaldehyde for 10 min, blocked with 2% BSA for 30 min, and incubated with mouse anti-GFP monoclonal antibody (1:250, ab6673, Abcam), and anti-perilipin antibody (1:250, ab3526, Abcam) overnight at 4°C followed by Alexa Fluor 488-conjugated donkey anti-goat IgG (1:250, ab150129, Abcam) and Alexa Fluor 594-conjugated donkey anti-rabbit IgG H&L (1:250, ab150076, Abcam) for 1 h at room temperature. Sections were further incubated with DAPI to stain nuclei and observed under a microscope. Immunohistochemical staining of PPARγ (1:100, MBS8241690, Mybiosource) was performed as previously described (23). Adipocyte sizes were determined using Image J, as described previously (24).

Statistical Analysis

The results were presented as the mean ± standard deviation. Statistical evaluation was performed *via* a nonparametric two-tailed Student's *t*-test using GraphPad Prism version 6 (www.graphpad.com). Bonferroni's correction for multiple testing was used for **Figures 4** and **5**. $P < 0.05$ was considered significant.

RESULTS

A Lineage-Tracing System to Label Endosteal Osteoblasts

Figure 1 outlines the protocol used for this experiment. As found in previous studies, large numbers of GFP+ (direct fluorescence from mG) plump osteoblasts (yellow arrow) were identified on the endosteal surfaces of the femur 2 days after the last 4-OHTam injection in postnatal week 8 (**Figure 2**). Four weeks after the last 4-OHTam injection (12-week-old mice), the GFP+ cells, presumably BLCs (white arrow), became flat and less

numerous on the endosteal surface of the femur. A few GFP+ osteocytes are shown in **Figure 2** (asterisk). The flat GFP+ cells persisted on the endosteal surface in mice at week 16. Therefore, we could label mature osteoblasts and BLCs in the 10-kb Dmp1-CreERt2:mTmG mice. Additionally, to characterize the targeting specificity of 10-kb Dmp1-CreERt2:mTmG, we analyzed GFP expression in sections of the tibia at 2 weeks of age (**Figure 3**). The Dmp1-CreERt2:mTmG mice showed strong GFP signals in the tibia but not in the BM (**Figure 3A**). As expected, the tibia sections from CreERt2(-):mTmG mice did not exhibit any GFP activity (**Figure 3B**). Furthermore, GFP+ cells were not detected on the bone sections of Dmp1-CreERT2:mTmG mice without 4-OHTam(**Figure 3C**). Within the tibia, Dmp1-CreERt2 marked not only endocortical osteoblasts (**Figure 3D**) but also trabecular osteoblasts (**Figure 3E**) and the adjacent skeletal muscle (**Figure 3F**).

Scl-Ab Reverses the Negative Effects of Rosiglitazone on Bone Parameters

We first analyzed the skeletal effects of 8 weeks of exposure to rosiglitazone by measuring microCT parameters of the distal femur. Significant decreases in BV/TV (**Figure 4A**), bone surface density (BS/TV) (**Figure 4B**), and Tb.N (**Figure 4C**), and increases in Tb.Sp (**Figure 4D**) were noted after 8 weeks of rosiglitazone administration compared to the effects of the vehicle ($P < 0.05$). We then examined the effects of Scl-Ab in rosiglitazone-treated and control mice. Scl-Ab administration significantly improved trabecular parameters induced by rosiglitazone (BV/TV and Tb.Th: $P < 0.01$; BS/TV, Tb.N, Tb.Sp, and serum P1NP levels: $P < 0.05$) (**Figure 4**). The combined use of rosiglitazone and Scl-Ab did not lead to significant differences in these parameters compared to the effects of Scl-Ab alone. Serum P1NP levels significantly

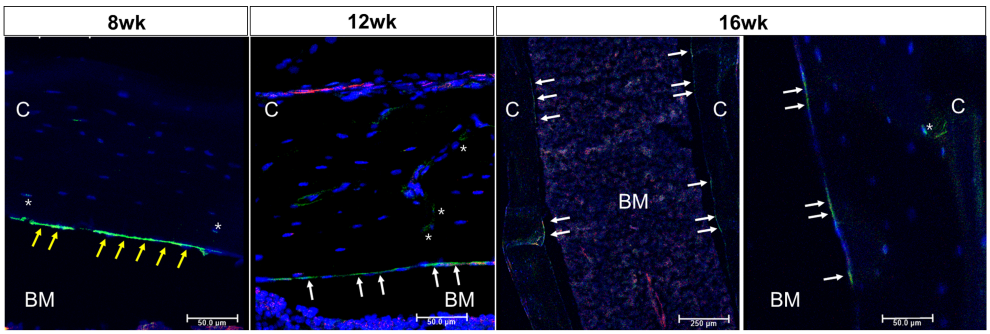

FIGURE 2 | Osteoblast lineage cells are labeled in 10-kb Dmp1- CreERt2:mTmG mice Representative confocal microscopy images of endocortical surface of the femur from Dmp1- CreERt2:mTmG mice at the indicated experimental groups(the left panel at 16 weeks shows low power field). BM, bone marrow; C, cortical bone; white arrow, bone lining cell; yellow arrow, active osteoblast; asterisk, osteocyte; red, mTomato; green, mGFP; blue, DAPI staining of nuclei. Red and green protein fluorescence were captured directly. Scale bar: 50 μm.

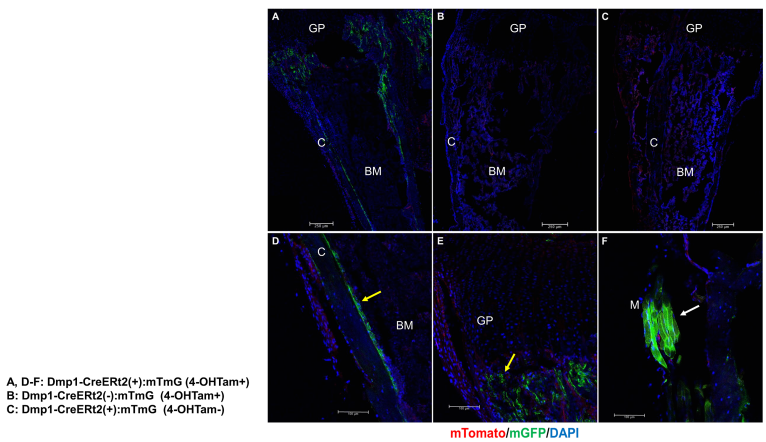

FIGURE 3 | 10-kb Dmp1- CreERt2 targets osteoblast lineage cells and skeletal muscle, but not bone marrow cells in 2-week-old mice. **(A–C)** Confocal microscopy images of direct fluorescence on longitudinal sections of the tibia at the indicated experimental groups. **(D–F)** Images at a higher magnification for different areas of bone as indicated. C, cortical bone; GP, growth plate; M, skeletal muscle; yellow arrow, osteoblast; white arrow, muscle; red, mTomato; green, mGFP; blue, DAPI staining of nuclei. Red and green protein fluorescence were captured directly.

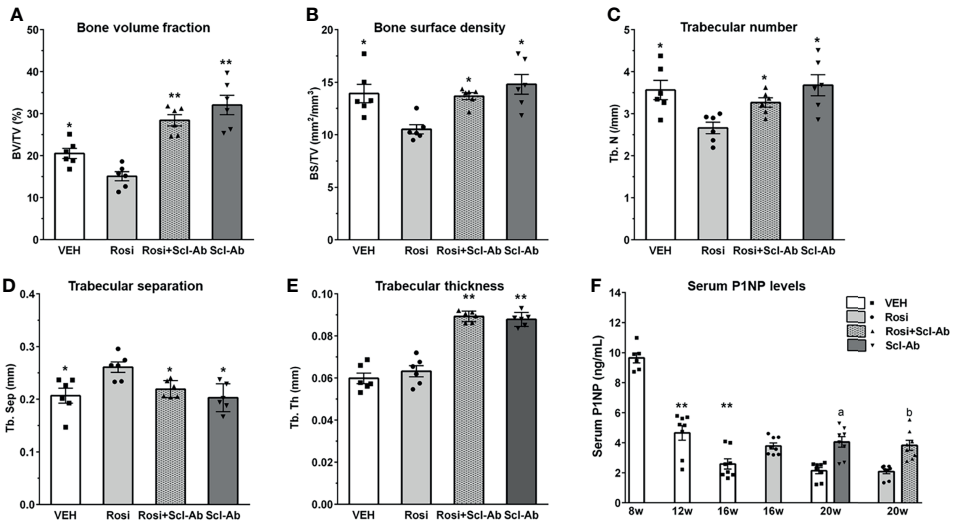

FIGURE 4 | Scl-Ab rescues the negative effects of rosiglitazone on bone parameters. **(A–E)** MicroCT quantification of trabecular bone. Each data represents the mean, and error bars represent the standard error (*, P < 0.05 vs. rosiglitazone; **, P < 0.01 vs. rosiglitazone, N = 6/group). BV, bone volume; TV, total volume; BS, bone surface, Tb.N, trabeculae number; Tb.Sp, trabeculae separation; Tb.Th, trabeculae thickness. **(F)** Serum P1NP measurements from mice in the indicated groups. Each data represents the mean, and error bars represent the standard error (**, P < 0.01 vs. 8 week; a, P < 0.05 vs. vehicle; b, P < 0.05 vs. rosiglitazone, N = 6–8/group). Vehicle, white; rosiglitazone, gray; Scl-Ab, dark gray; Scl-Ab/rosiglitazone, gray pattern.

decreased from 8 to 12 weeks (P < 0.01). Scl-Ab significantly increased serum P1NP levels versus the vehicle (P < 0.05). In addition, 4 weeks of overlapping Scl-Ab treatment significantly increased serum P1NP levels compared to the effects of rosiglitazone alone (P < 0.05, **Figure 4F**).

Rosiglitazone Increases GFP/Perilipin Double+ BMAds, Whereas Scl-Ab Modestly Suppresses This Effect

To determine whether rosiglitazone could stimulate the differentiation of osteoblast lineage cells into BMAds, we chased GFP+ cells on the endosteal surface of the femur after 8 weeks of rosiglitazone administration. To better characterize and quantify the number of BMAds, we performed immunohistochemical staining using anti-perilipin antibody and anti-GFP antibody. Therefore, BMAds were visualized with anti-perilipin antibody, and GFP/perilipin double+ BMAds should be derived from osteoblast lineage cells. Representative histological images of BMAds in the femur in each group are shown in **Figure 5A**. After a 4-week chase period (16 weeks), some perilipin+ BMAds were detected in the BM but no GFP/perilipin double+ BMAds were detected. After an 8-week chase period, GFP/perilipin dual expression was detected from a few BMAds (yellow arrow) in the rosiglitazone group, and very few GFP/perilipin double+ BMAds were detected in the rosiglitazone/Scl-Ab group (N = 4–6/group). As shown in **Figure 5B**, rosiglitazone significantly increased the overall number of adipocytes (perilipin + BMAds) in the femur BM (rosiglitazone 543.5 ± 205.9/mm^2 vs. vehicle 3.1 ± 2.1/mm^2; P < 0.001, **Figure 5A**). Moreover, some GFP/perilipin double+ BMAds were identified near the endosteal surface (rosiglitazone 20.5 ± 11.2/mm^2 vs. vehicle 0/mm^2; P < 0.001, **Figure 5B**). Collectively, these data suggest that a small subpopulation of endosteal osteoblast lineage cells could differentiate into BMAds during rosiglitazone treatment compared to the vehicle findings (rosiglitazone 4.3 ± 2.8% vs. vehicle 0%; P < 0.001, **Figure 5B**).

We then tested whether Scl-Ab could modulate this effect of rosiglitazone on BMAds and thereby alter the total number of BMAds and the number of GFP/perilipin double+ BMAds in rosiglitazone-treated mice. When 8 weeks of rosiglitazone was overlapped by 4 weeks of Scl-Ab treatment, the total number of BMAds was not significantly decreased compared to the effects of 4 weeks of vehicle treatment (rosiglitazone 543.5 ± 205.9/mm^2 vs. Scl-Ab/rosiglitazone 487.3 ± 175.2/mm^2, **Figure 5B**). Additionally, Scl-Ab did not decrease the adipocyte size significantly (rosiglitazone 1612.2 ± 490.1 μm^2 vs. Scl-Ab/rosiglitazone 1498.5 ± 286.6 μm^2, **Figure 5C**). Interestingly, Scl-Ab significantly decreased the number of GFP/perilipin double+ BMAds in the femur BM relative to the vehicle (rosiglitazone 20.5 ± 11.2/mm^2 vs. Scl-Ab/rosiglitazone 2.8 ± 3.7/mm^2; P < 0.001, **Figure 5B**). Collectively, when we quantified the contribution of the differentiation of osteoblast lineage cells into adipocytes to the entire BM adipogenesis process by counting the number of GFP/perilipin double+ BMAds and total perilipin+ BMAds, Scl-Ab preferentially suppressed the differentiation of osteoblast lineage cells into adipocytes (rosiglitazone 4.3 ± 2.8% vs. Scl-Ab/rosiglitazone 0.6 ± 0.9%; P < 0.001, **Figure 5B**). In addition, as found in previous studies, more GFP+ endosteal cells appeared plumper in the Scl-Ab or Rosi+Scl-Ab treatment groups than in the vehicle or Rosi alone groups (**Figure 5D**).

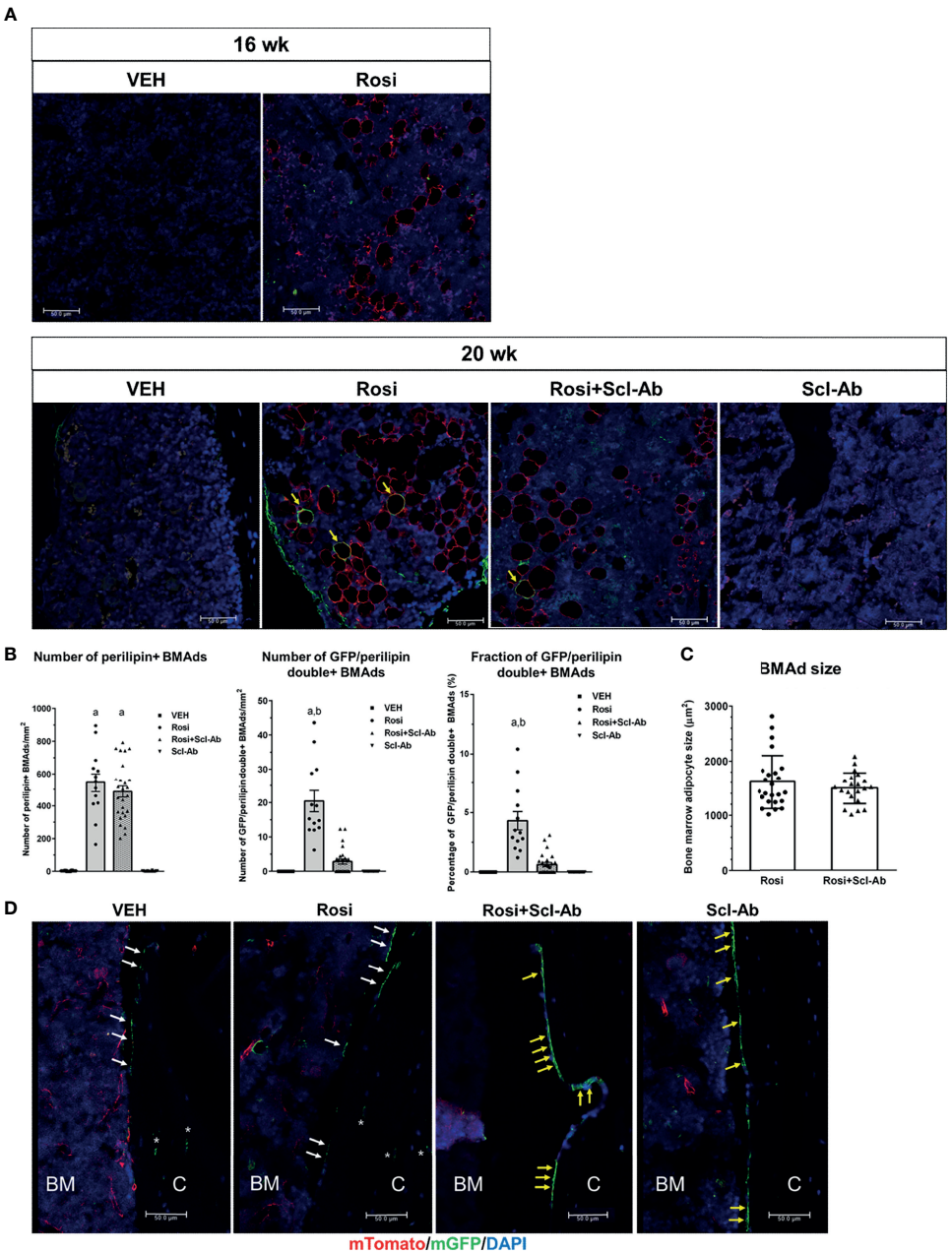

FIGURE 5 | Rosiglitazone increases GFP/perilipin double positive bone marrow adipocytes, whereas Scl-Ab suppresses the effect of rosiglitazone on them. **(A)** Representative immunostaining against GFP and perilipin on sections of femoral bone marrow from Dmp1- CreERt2:mTmG mice in the indicated experimental groups. Scale bar: 50 μm. Red, perilipin+ bone marrow adipocytes (BMAds); yellow arrow, GFP/perilipin double positive BMAds; blue, DAPI staining of nuclei. **(B)** Quantification of total perilipin+ or GFP/perilipin double+ BMAds. a, $P < 0.001$ vs. vehicle or Scl-Ab; b, $P < 0.001$ vs. rosiglitazone + Scl-Ab; N=4–6/group. **(C)** Quantification of perilipin+ BMAd size in the indicated experimental groups (N = 4–6/group). **(D)** Representative confocal images showing direct fluorescence in cells on endocortical surfaces of the femur from the indicated experimental groups. BM, bone marrow; C, cortical bone; white arrow, bone lining cell; yellow arrow, active osteoblast; asterisk, osteocyte; red, mTomato; green, mGFP; blue, DAPI staining of nuclei. Red and green protein fluorescence were captured directly. Scale bar: 50 μm.

To exclude the possibility that rosiglitazone affected endogenous GFP expression, Rip-Cre:mTmG mice were also treated with rosiglitazone. In Rip-Cre transgenic mice, the rat insulin II promoter drives cre expression in both β cells in the pancreas and some neurons in the brain (25). Co-immunostaining experiments showed that rosiglitazone also increased the number of perilipin+BMAds in Rip-Cre:mTmG mice, but GFP/perilipin double+ cells were not detected on the

endosteal surface or in the BM of the femur (**Figure 6A**). As expected, Rip-Cre mice targeted islet cells in the pancreas (**Figure 6B**), and no GFP signals were detected in the pancreas sections obtained from Rip-Cre(-):mTmG mice (**Figure 6C**). Thus, rosiglitazone did not increase endogenous GFP expression.

Osteoblasts and BLCs Express PPARγ

To explore the adipogenic characteristics of osteoblast lineage cells in response to rosiglitazone treatment, we examined PPARγ expression. Immunohistochemical staining revealed numerous PPARγ–expressing cells in the trabecular and cortical bones, which were likely to be osteoblasts and BLCs in the femur at 8 and 12 weeks, respectively (**Figure 7**).

DISCUSSION

In this study, we demonstrated that rosiglitazone could stimulate the transdifferentiation of endosteal osteoblast lineage cells such as BLCs into BMAds, which appeared to contribute to increased BMA. In addition, overlapping Scl-Ab administration could suppress this effect. To the best of our knowledge, this is the first report to reveal that BLCs serve as sources of BMAds using a lineage-tracing study.

In the present study, rosiglitazone increased the number of BMAds and concurrently decreased bone mass. These data further strengthened the association between BMA and bone mass. In humans, pioglitazone, another PPARγ agonist, has also been demonstrated to influence both BMA and bone mass (26). A previous 12-month study recorded a statistically significant correlation between the increase in femoral BMA and decrease in hip BMD (26). Although the association between BMA and BMD appears clear, the mechanism of action has not been clarified. One likely possibility is that intrinsic and extrinsic signals determine mesenchymal stem cell (MSC) lineage differentiation into osteoblasts or adipocytes (27–29). Most rosiglitazone-induced BMAds are proposed to be derived from MSCs. Although the molecular mechanisms by which MSCs differentiate to adipocytes remain unclear, multiple transcription factors have been demonstrated to be critical for the differentiation of MSCs into adipocytes. PPARγ and C/EBPs are involved in the adipogenic differentiation of MSCs (30–33). Alternatively, the dedifferentiation or transdifferentiation of osteoblast lineage cells could be a potential route to BMAds (20). In this study, we observed that a small subpopulation of osteoblast lineage cells has the capacity to differentiate into BMAds. However, this result does not completely exclude the possibility that mature osteoblasts or osteocytes directly differentiate into BMAds. In addition, we could not detect cells that have characteristics of both osteoblasts and adipocytes undergoing the transition from BLCs to BMAds in the BM. Although it remains unclear that BLCs directly transdifferentiate into BMAds, BLCs could be a promising source of BMAds. In previous lineage tracing studies, we demonstrated that Dmp1-CreERt2 or osteocalcin-CreERt2 mature osteoblasts differentiate into BLCs *in vivo* (17, 18). Mature osteoblasts could become inactive in the first step so that they transdifferentiate into BMAds. Additionally, osteocyte dedifferentiation into osteoblasts or BLCs could be possible, but this has not been reported to occur in physiologic *in vivo* settings. Collectively, mature osteoblasts and their progeny could be a source of BMAds.

The mechanism by which osteoblast lineage cells differentiate into BMAds is unclear. In a previous study, we found that PPARγ-overexpressed preosteoblasts can transdifferentiate into adipocyte-like cells *in vitro* (34). Furthermore, we demonstrated that PPARγ activation inhibits osteocalcin expression both by suppressing Runx2 expression and interfering with the transactivation of Runx2 in osteoblast cell lines (35). In this study, we found that even endosteal lining cells can express PPARγ. BLCs could express cell-surface markers characteristic of mesenchymal stem/progenitors (19). Collectively, some subpopulations of osteoblast lineage cells containing MSC-like

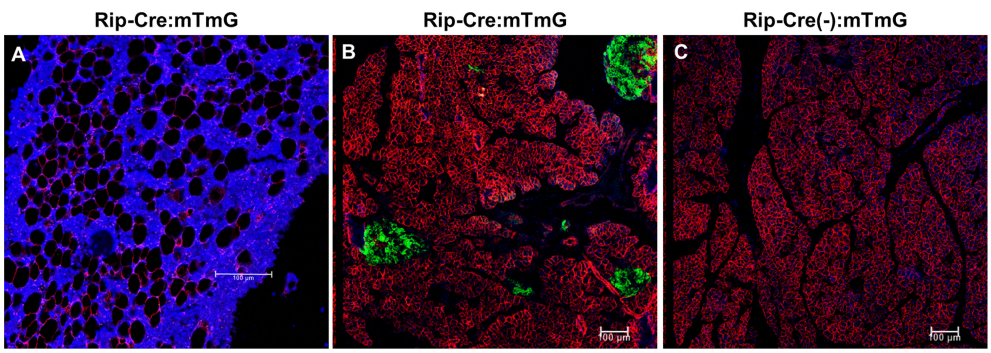

FIGURE 6 | Rosiglitazone does not increase endogenous GFP expression. **(A)** Representative immunostaining against GFP and perilipin on sections of femoral bone marrow from Rip-Cre:mTmG mice that had received rosiglitazone for 8 weeks. Red, perilipin+ bone marrow adipocytes; blue, DAPI staining of nuclei. **(B, C)** Representative confocal images of the pancreas from Rip-Cre:mTmG mice or Rip-Cre(-):mTmG mice that had received rosiglitazone for 8 weeks. Red, mTomato; green, mGFP; blue, DAPI staining of nuclei. Rip-Cre transgene, a 668 bp fragment of the rat insulin II promoter. Red and green protein fluorescence were captured directly. Scale bar: 100 μm.

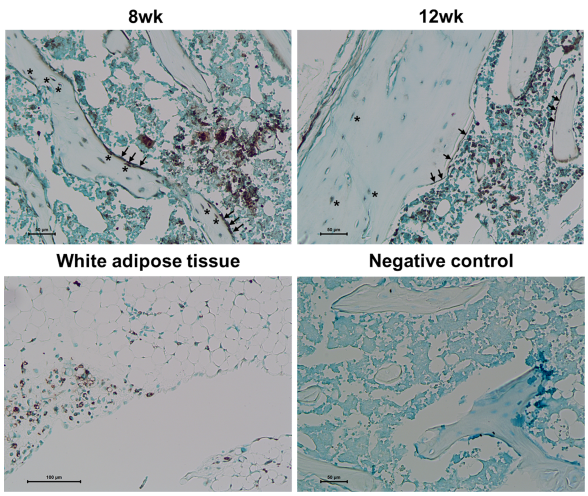

FIGURE 7 | PPARγ expression in osteoblasts and bone lining cells. Representative images for PPARγ immunohistochemical staining of osteoblast lineage cells (arrow) and osteocytes (asterisk) in the femur at 8 and 12 weeks. Immunostaining is shown as a brown color in white adipose tissue. Staining was absent in a negative control section. The primary antibody was replaced with nonimmune serum (1: 100) for negative control slides. Tissues were counterstained with methyl green (N = 3/each group).

characteristics or expressing PPARγ might respond to external signals that stimulate differentiation into adipocytes.

We found that Scl-Ab significantly suppressed the transdifferentiation of osteoblast lineage cells into BMAds. The anabolic action of Scl-Ab is predominantly modeling-based bone formation (36). One primary cellular mechanism of modeling-based bone formation is the reactivation of inactive BLCs into active osteoblasts (17). The mechanism by which this suppressive effect of Scl-Ab on the adipogenic differentiation of osteoblast lineage cells could contribute to anabolic action is unclear. The conditional deletion of Sost in Prx1-expressing cells recapitulated the global high-bone-mass phenotype of Sost KO mice, whereas both Col1- and Dmp1-specific deletions of Sost induced milder increases in bone formation (37). Thus, although cell populations of osteoblasts at various differentiation stages could be targets of Scl-Ab, MSCs or mesenchymal progenitor cells appear to be the main targets.

Few studies have revealed a link between sclerostin and the regulation of BMAT development. Recombinant Sost or Sost in osteocyte-conditioned medium stimulated BM adipogenesis (38). Furthermore, Scl-Ab treatment reversed the increase in marrow adiposity in ovariectomized rabbits (39). A recent lineage tracing study showed that Scl-Ab administration suppresses adipogenesis by suppressing the differentiation of Sox9+ skeletal precursors into BMAds *in vivo* (40).

Several questions remain to be addressed. Overlap of 4 week-Scl-Ab administration failed to inhibit the increase in BMAd counts of the femur induced by 8 weeks of rosiglitazone administration, whereas the negative effect on bone was significantly improved. However, a recent study revealed that Scl-Ab significantly decreased rosiglitazone-induced BMAT in the femur (41). The discrepancy could have resulted from differences of the doses or administration schedules of Scl-Ab. In the current study, we focused on the possibility that BLCs could transdifferentiate into BMAds. Thus, we adopted distinct administration schedules of rosiglitazone and Scl-Ab from other studies. Another possibility of the discrepancy is that osteoblasts lineage cells could have distinct responses to rosiglitazone in the adipogenic differentiation from that of MSCs. In this study, after a 4-week chase period (16 weeks), some perilipin+ BMAds were detected in the BM but there were no GFP/perilipin double+ BMAds. Therefore, osteoblast lineage cell differentiation into BMAds in response to rosiglitazone could require more time compared to MSCs. Furthermore, we did not use osmium tetroxide micro-CT analysis to evaluate adipose tissue volume. Next, in this experiment, we focused on presumably regulated BMAT (rBMAT) in the femur because it might be more dynamic than constitutive BMAT (cBMAT). Previous studies revealed the presence of cBMAT and rBMAT as distinct BMAT subpopulations in different periods of development in rodents (42). rBMAT has been proposed to be preferentially distributed within the mid-to-proximal tibia, femur, and lumbar vertebrae, whereas cBMAT develops in the distal tibia and caudal vertebrae from an early stage (11). However, further studies are required to determine whether cBMAT and rBMAT are differentially regulated by Sost. In addition, there was an issue of targeting of Dmp1-CreERt2. We could not detect GFP+ cells in the BM of Dmp1-CreERt2:mT/mG mice at 8 weeks, 12 weeks, and 16 weeks. Additionally, there were no GFP+ cells in the BM of RIP-Cre:mTmG mouse treated with rosiglitazone for 8 weeks. However, this do not completely exclude ectopic expression of the current 10kb Dmp1-CreERt2 in BM. Previous studies suggested that the 14kb Dmp1-Cre targets not only osteoblasts and osteocytes but also osteoblast precursors at an earlier stage (43). However, the cre activity was not detected in BMAds in that study. Therefore, it is most unlikely that the 10kb Dmp1-CreERt2 exists in BMAd precursors.

Moreover, we could not identify the genetic characteristics of osteoblast lineage cells that could differentiate to BMAds. It would be more valuable to compare the genetic characteristics of osteoblast-derived and MSC-derived adipocytes. Finally, we observed weak immunostaining of PPARγ in osteoblast lineage cells. More sophisticated experiments are necessary to confirm this result.

In conclusion, BLCs could represent sources of BMAds, and the pharmacologic inhibition of sclerostin might suppress the differentiation of osteoblast lineage cells into BMAds in response to BM adipogenic signals.

DATA AVAILABILITY STATEMENT

The original contributions presented in the study are included in the article/supplementary material. Further inquiries can be directed to the corresponding author.

ETHICS STATEMENT

The animal study was reviewed and approved by the Institutional Animal Care and Use Committee of Seoul National University.

AUTHOR CONTRIBUTIONS

All authors designed experiments and interpreted experiments. JL and JY performed experiments. SK wrote the manuscript. All authors contributed to the article and approved the submitted version.

FUNDING

This work was supported by grants from the National Research Foundation of Korea (2017R1A2B2004708).

ACKNOWLEDGMENTS

Dmp1-CreERt2 mice and Rip-Cre mice were kindly provided by Dr. Hank Kronenberg (Massachusetts General Hospital) and Dr. Hye Seung Jung (Seoul National University Hospital), respectively.

REFERENCES

1. Sebo ZL, Rendina-Ruedy E, Ables GP, Lindskog DM, Rodeheffer MS, Fazeli PK, et al. Bone Marrow Adiposity: Basic and Clinical Implications. *Endocr Rev* (2019) 40(5):1187–206. doi: 10.1210/er.2018-00138
2. Li GW, Xu Z, Chen QW, Tian YN, Wang XY, Zhou L, et al. Quantitative Evaluation of Vertebral Marrow Adipose Tissue in Postmenopausal Female Using MRI Chemical Shift-Based Water–Fat Separation. *Clin Radiol* (2014) 69(3):254–62. doi: 10.1016/j.crad.2013.10.005
3. Schwartz AV, Sigurdsson S, Hue TF, Lang TF, Harris TB, Rosen CJ, et al. Vertebral Bone Marrow Fat Associated With Lower Trabecular BMD and Prevalent Vertebral Fracture in Older Adults. *J Clin Endocrinol Metab* (2013) 98(6):2294–300. doi: 10.1210/jc.2012-3949
4. Shen W, Chen J, Gantz M, Punyanitya M, Heymsfield SB, Gallagher D, et al. MRI-Measured Pelvic Bone Marrow Adipose Tissue Is Inversely Related to DXA-Measured Bone Mineral in Younger and Older Adults. *Eur J Clin Nutr* (2012) 66(9):983–8. doi: 10.1038/ejcn.2012.35
5. Shen W, Chen J, Punyanitya M, Shapses S, Heshka S, Heymsfield SB. MRI-Measured Bone Marrow Adipose Tissue Is Inversely Related to DXA-Measured Bone Mineral in Caucasian Women. *Osteoporos Int* (2007) 18 (5):641–7. doi: 10.1007/s00198-006-0285-9
6. Schellinger D, Lin CS, Hatipoglu HG, Fertikh D. Potential Value of Vertebral Proton MR Spectroscopy in Determining Bone Weakness. *AJNR Am J Neuroradiol* (2001) 22(8):1620–7.
7. Beekman KM, Veldhuis-Vlug AG, den Heijer M, Maas M, Oleksik AM, Tanck MW, et al. The Effect of Raloxifene on Bone Marrow Adipose Tissue and Bone Turnover in Postmenopausal Women With Osteoporosis. *Bone* (2019) 118:62–8. doi: 10.1016/j.bone.2017.10.011
8. Yang Y, Luo X, Xie X, Yan F, Chen G, Zhao W, et al. Influences of Teriparatide Administration on Marrow Fat Content in Postmenopausal Osteopenic Women Using MR Spectroscopy. *Climacteric* (2016) 19(3):285–91. doi: 10.3109/13697137.2015.1126576
9. Atit R, Sgaier SK, Mohamed OA, Taketo MM, Dufort D, Joyner AL, et al. Beta-Catenin Activation Is Necessary and Sufficient to Specify the Dorsal Dermal Fate in the Mouse. *Dev Biol* (2006) 296(1):164–76. doi: 10.1016/j.ydbio.2006.04.449
10. Lass A, Zimmermann R, Oberer M, Zechner R. Lipolysis - a Highly Regulated Multi-Enzyme Complex Mediates the Catabolism of Cellular Fat Stores. *Prog Lipid Res* (2011) 50(1):14–27. doi: 10.1016/j.plipres.2010.10.004
11. Scheller EL, Cawthorn WP, Burr AA, Horowitz MC, MacDougald OA. Marrow Adipose Tissue: Trimming the Fat. *Trends Endocrinol Metab* (2016) 27(6):392–403. doi: 10.1016/j.tem.2016.03.016
12. Horowitz MC, Berry R, Holtrup B, Sebo Z, Nelson T, Fretz JA, et al. Bone Marrow Adipocytes. *Adipocyte* (2017) 6(3):193–204. doi: 10.1080/21623945.2017.1367881
13. Li Q, Wu Y, Kang N. Marrow Adipose Tissue: Its Origin, Function, and Regulation in Bone Remodeling and Regeneration. *Stem Cells Int* (2018) 2018:7098456. doi: 10.1155/2018/7098456
14. Mohamed FF, Franceschi RT. Skeletal Stem Cells: Origins, Functions and Uncertainties. *Curr Mol Biol Rep* (2017) 3(4):236–46. doi: 10.1007/s40610-017-0075-5
15. Yue R, Zhou BO, Shimada IS, Zhao Z, Morrison SJ. Leptin Receptor Promotes Adipogenesis and Reduces Osteogenesis by Regulating Mesenchymal Stromal Cells in Adult Bone Marrow. *Cell Stem Cell* (2016) 18(6):782–96. doi: 10.1016/j.stem.2016.02.015
16. Zhou BO, Yue R, Murphy MM, Peyer JG, Morrison SJ. Leptin-Receptor-Expressing Mesenchymal Stromal Cells Represent the Main Source of Bone Formed by Adult Bone Marrow. *Cell Stem Cell* (2014) 15(2):154–68. doi: 10.1016/j.stem.2014.06.008
17. Kim SW, Lu Y, Williams EA, Lai F, Lee JY, Enishi T, et al. Sclerostin Antibody Administration Converts Bone Lining Cells Into Active Osteoblasts. *J Bone Miner Res* (2017) 32(5):892–901. doi: 10.1002/jbmr.3038
18. Kim SW, Pajevic PD, Selig M, Barry KJ, Yang JY, Shin CS, et al. Intermittent Parathyroid Hormone Administration Converts Quiescent Lining Cells to Active Osteoblasts. *J Bone Miner Res* (2012) 27(10):2075–84. doi: 10.1002/jbmr.1665
19. Matic I, Matthews BG, Wang X, Dyment NA, Worthley DL, Rowe DW, et al. Quiescent Bone Lining Cells Are a Major Source of Osteoblasts During Adulthood. *Stem Cells* (2016) 34(12):2930–42. doi: 10.1002/stem.2474
20. Fan Y, Hanai J-i, Le PT, Bi R, Maridas D, DeMambro V, et al. Parathyroid Hormone Directs Bone Marrow Mesenchymal Cell Fate. *Cell Metab* (2017) 25 (3):661–72. doi: 10.1016/j.cmet.2017.01.001
21. Berry R, Rodeheffer MS. Characterization of the Adipocyte Cellular Lineage *In Vivo*. *Nat Cell Biol* (2013) 15(3):302–8. doi: 10.1038/ncb2696
22. Muzumdar MD, Tasic B, Miyamichi K, Li L, Luo L. A Global Double-Fluorescent Cre Reporter Mouse. *Genesis* (2007) 45(9):593–605. doi: 10.1002/dvg.20335
23. Yates T, Davies MJ, Henson J, Edwardson C, Webb D, Bodicoat DH, et al. Effect of the PPARG2 Pro12Ala Polymorphism on Associations of Physical Activity and Sedentary Time With Markers of Insulin Sensitivity in Those With an Elevated Risk of Type 2 Diabetes. *PLoS One* (2015) 10(5):e0124062. doi: 10.1371/journal.pone.0124062
24. Costa S, Fairfield H, Reagan MR. Inverse Correlation Between Trabecular Bone Volume and Bone Marrow Adipose Tissue in Rats Treated With Osteoanabolic Agents. *Bone* (2019) 123:211–23. doi: 10.1016/j.bone.2019.03.038
25. Postic C, Shiota M, Niswender KD, Jetton TL, Chen Y, Moates JM, et al. Dual Roles for Glucokinase in Glucose Homeostasis as Determined by Liver and Pancreatic Beta Cell-Specific Gene Knock-Outs Using Cre Recombinase. *J Biol Chem* (1999) 274(1):305–15. doi: 10.1074/jbc.274.1.305
26. Pop LM, Lingvay I, Yuan Q, Li X, Adams-Huet B, Maalouf NM. Impact of Pioglitazone on Bone Mineral Density and Bone Marrow Fat Content. *Osteoporos Int* (2017) 28(11):3261–9. doi: 10.1007/s00198-017-4164-3
27. Abdallah BM, Haack-Sorensen M, Fink T, Kassem M. Inhibition of Osteoblast Differentiation But Not Adipocyte Differentiation of Mesenchymal Stem Cells by Sera Obtained From Aged Females. *Bone* (2006) 39(1):181–8. doi: 10.1016/j.bone.2005.12.082
28. Moerman EJ, Teng K, Lipschitz DA, Lecka-Czernik B. Aging Activates Adipogenic and Suppresses Osteogenic Programs in Mesenchymal Marrow Stroma/Stem Cells: The Role of PPAR-Gamma2 Transcription Factor and TGF-Beta/BMP Signaling Pathways. *Aging Cell* (2004) 3(6):379–89. doi: 10.1111/j.1474-9728.2004.00127.x

29. Stenderup K, Justesen J, Clausen C, Kassem M. Aging Is Associated With Decreased Maximal Life Span and Accelerated Senescence of Bone Marrow Stromal Cells. *Bone* (2003) 33(6):919–26. doi: 10.1016/j.bone.2003.07.005
30. Kushwaha P, Khedgikar V, Gautam J, Dixit P, Chillara R, Verma A, et al. A Novel Therapeutic Approach With Caviunin-Based Isoflavonoid That En Routes Bone Marrow Cells to Bone Formation *via* BMP2/Wnt-Beta-Catenin Signaling. *Cell Death Dis* (2014) 5:e1422. doi: 10.1038/cddis.2014.350
31. Kim J, Ko J. A Novel PPARgamma2 Modulator sLZIP Controls the Balance Between Adipogenesis and Osteogenesis During Mesenchymal Stem Cell Differentiation. *Cell Death Differ* (2014) 21(10):1642–55. doi: 10.1038/cdd.2014.80
32. Lefterova MI, Zhang Y, Steger DJ, Schupp M, Schug J, Cristancho A, et al. PPARgamma and C/EBP Factors Orchestrate Adipocyte Biology *via* Adjacent Binding on a Genome-Wide Scale. *Genes Dev* (2008) 22(21):2941–52. doi: 10.1101/gad.1709008
33. Cao Z, Umek RM, McKnight SL. Regulated Expression of Three C/EBP Isoforms During Adipose Conversion of 3T3-L1 Cells. *Genes Dev* (1991) 5 (9):1538–52. doi: 10.1101/gad.5.9.1538
34. Kim SW, Her SJ, Kim SY, Shin CS. Ectopic Overexpression of Adipogenic Transcription Factors Induces Transdifferentiation of MC3T3-E1 Osteoblasts. *Biochem Biophys Res Commun* (2005) 327(3):811–9. doi: 10.1016/j.bbrc.2004.12.076
35. Jeon MJ, Kim JA, Kwon SH, Kim SW, Park KS, Park SW, et al. Activation of Peroxisome Proliferator-Activated Receptor-Gamma Inhibits the Runx2-Mediated Transcription of Osteocalcin in Osteoblasts. *J Biol Chem* (2003) 278(26):23270–7. doi: 10.1074/jbc.M211610200
36. Ominsky MS, Niu QT, Li C, Li X, Ke HZ. Tissue-Level Mechanisms Responsible for the Increase in Bone Formation and Bone Volume by Sclerostin Antibody. *J Bone Miner Res* (2014) 29(6):1424–30. doi: 10.1002/jbmr.2152
37. Yee CS, Manilay JO, Chang JC, Hum NR, Murugesh DK, Bajwa J, et al. Conditional Deletion of Sost in MSC-Derived Lineages Identifies Specific Cell-Type Contributions to Bone Mass and B-Cell Development. *J Bone Miner Res* (2018) 33(10):1748–59. doi: 10.1002/jbmr.3467
38. Fairfield H, Falank C, Harris E, Demambro V, McDonald M, Pettitt JA, et al. The Skeletal Cell-Derived Molecule Sclerostin Drives Bone Marrow Adipogenesis. *J Cell Physiol* (2018) 233(2):1156–67. doi: 10.1002/jcp.25976
39. Li S, Huang B, Jiang B, Gu M, Yang X, Yin Y. Sclerostin Antibody Mitigates Estrogen Deficiency-Inducted Marrow Lipid Accumulation Assessed by Proton MR Spectroscopy. *Front Endocrinol (Lausanne)* (2019) 10:159. doi: 10.3389/fendo.2019.00159
40. Balani DH, Trinh S, Xu M, Kronenberg HM. Sclerostin Antibody Administration Increases the Numbers of Sox9creER+ Skeletal Precursors and Their Progeny. *J Bone Miner Res* (2021) 36(4):757–67. doi: 10.1002/jbmr.4238
41. Farrell M, Fairfield H, Costa S, D'Amico A, Falank C, Brooks DJ, et al. Sclerostin-Neutralizing Antibody Treatment Rescues Negative Effects of Rosiglitazone on Mouse Bone Parameters. *J Bone Miner Res* (2021) 36 (1):158–69. doi: 10.1002/jbmr.4170
42. Rharass T, Lucas S. MECHANISMS IN ENDOCRINOLOGY: Bone Marrow Adiposity and Bone, a Bad Romance? *Eur J Endocrinol* (2018) 179(4):R165. doi: 10.1530/eje-18-0182
43. Lim J, Burclaff J, He G, Mills JC, Long F. Unintended Targeting of Dmp1-Cre Reveals a Critical Role for Bmpr1a Signaling in the Gastrointestinal Mesenchyme of Adult Mice. *Bone Res* (2017) 5:16049. doi: 10.1038/boneres.2016.49

Conflict of Interest: The authors declare that the research was conducted in the absence of any commercial or financial relationships that could be construed as a potential conflict of interest.

Publisher's Note: All claims expressed in this article are solely those of the authors and do not necessarily represent those of their affiliated organizations, or those of the publisher, the editors and the reviewers. Any product that may be evaluated in this article, or claim that may be made by its manufacturer, is not guaranteed or endorsed by the publisher.

frontiers in Endocrinology

ORIGINAL RESEARCH
published: 04 January 2022
doi: 10.3389/fendo.2021.778537

Texture Analysis Using CT and Chemical Shift Encoding-Based Water-Fat MRI Can Improve Differentiation Between Patients With and Without Osteoporotic Vertebral Fractures

Nico Sollmann[1,2,3,4†], Edoardo A. Becherucci[3†], Christof Boehm[5], Malek El Husseini[3], Stefan Ruschke[5], Egon Burian[3], Jan S. Kirschke[3,4], Thomas M. Link[2], Karupppasamy Subburaj[6,7], Dimitrios C. Karampinos[5], Roland Krug[2], Thomas Baum[3] and Michael Dieckmeyer[3]*

[1] Department of Diagnostic and Interventional Radiology, University Hospital Ulm, Ulm, Germany, [2] Department of Radiology and Biomedical Imaging, University of California San Francisco, San Francisco, CA, United States, [3] Department of Diagnostic and Interventional Neuroradiology, School of Medicine, Klinikum rechts der Isar, Technical University of Munich, Munich, Germany, [4] TUM-Neuroimaging Center, Klinikum rechts der Isar, Technical University of Munich, Munich, Germany, [5] Department of Diagnostic and Interventional Radiology, School of Medicine, Klinikum rechts der Isar, Technical University of Munich, Munich, Germany, [6] Engineering Product Development (EPD) Pillar, Singapore University of Technology and Design (SUTD), Singapore, Singapore, [7] Changi General Hospital, Singapore, Singapore

Purpose: Osteoporosis is a highly prevalent skeletal disease that frequently entails vertebral fractures. Areal bone mineral density (BMD) derived from dual-energy X-ray absorptiometry (DXA) is the reference standard, but has well-known limitations. Texture analysis can provide surrogate markers of tissue microstructure based on computed tomography (CT) or magnetic resonance imaging (MRI) data of the spine, thus potentially improving fracture risk estimation beyond areal BMD. However, it is largely unknown whether MRI-derived texture analysis can predict volumetric BMD (vBMD), or whether a model incorporating texture analysis based on CT and MRI may be capable of differentiating between patients with and without osteoporotic vertebral fractures.

Materials and Methods: Twenty-six patients (15 females, median age: 73 years, 11 patients showing at least one osteoporotic vertebral fracture) who had CT and 3-Tesla chemical shift encoding-based water-fat MRI (CSE-MRI) available were analyzed. In total, 171 vertebral bodies of the thoracolumbar spine were segmented using an automatic convolutional neural network (CNN)-based framework, followed by extraction of integral and trabecular vBMD using CT data. For CSE-MRI, manual segmentation of vertebral bodies and consecutive extraction of the mean proton density fat fraction (PDFF) and T2* was performed. First-order, second-order, and higher-order texture features were derived from texture analysis using CT and CSE-MRI data. Stepwise multivariate linear regression models were computed using integral vBMD and fracture status as dependent variables.

OPEN ACCESS

Edited by:
Jason Horton,
Upstate Medical University,
United States

Reviewed by:
Erica L. Scheller,
Washington University in St. Louis,
United States
Jiang Du,
University of California, San Diego,
United States

***Correspondence:**
Nico Sollmann
nico.sollmann@tum.de

†These authors have contributed equally to this work

Specialty section:
This article was submitted to Bone Research, a section of the journal Frontiers in Endocrinology

Received: 17 September 2021
Accepted: 06 December 2021
Published: 04 January 2022

Citation:
Sollmann N, Becherucci EA, Boehm C, Husseini ME, Ruschke S, Burian E, Kirschke JS, Link TM, Subburaj K, Karampinos DC, Krug R, Baum T and Dieckmeyer M (2022) Texture Analysis Using CT and Chemical Shift Encoding-Based Water-Fat MRI Can Improve Differentiation Between Patients With and Without Osteoporotic Vertebral Fractures. Front. Endocrinol. 12:778537. doi: 10.3389/fendo.2021.778537

Results: Patients with osteoporotic vertebral fractures showed significantly lower integral and trabecular vBMD when compared to patients without fractures ($p<0.001$). For the model with integral vBMD as the dependent variable, T2* combined with three PDFF-based texture features explained 40% of the variance (adjusted R^2 [R^2_a] = 0.40; $p<0.001$). Furthermore, regarding the differentiation between patients with and without osteoporotic vertebral fractures, a model including texture features from CT and CSE-MRI data showed better performance than a model based on integral vBMD and PDFF only (R^2_a = 0.47 vs. R^2_a = 0.81; included texture features in the final model: integral vBMD, CT_Short-run_emphasis, CT_Varianceglobal, and PDFF_Variance).

Conclusion: Using texture analysis for spine CT and CSE-MRI can facilitate the differentiation between patients with and without osteoporotic vertebral fractures, implicating that future fracture prediction in osteoporosis may be improved.

Keywords: bone mineral density, convolutional neural network, opportunistic imaging, osteoporosis, proton density fat fraction, texture analysis, vertebral fracture

INTRODUCTION

In clinical routine, assessment of areal bone mineral density (BMD) and the individual risk of bone fracture is commonly obtained using dual-energy X-ray absorptiometry (DXA) (1–4). Fractures due to low bone mass and microarchitectural deterioration are characteristic for osteoporosis, a systemic skeletal disease with very high prevalence worldwide (1, 4–7). Osteoporotic fragility fractures can severely impair the health-related quality of life and have been linked to premature mortality (1, 8–10). Among osteoporotic fragility fractures, vertebral fractures are particularly prevalent, with an estimated 12.6-fold increase in the risk of future additional vertebral fractures (1, 11–13). A major clinical issue of these fractures is that they occur frequently but can remain asymptomatic for a long time (13, 14). This can delay diagnosis, timely treatment initiation, and subsequent approaches to avoid future additional osteoporotic vertebral fractures (13, 14).

Clinical management requires a reliable assessment of the individual fracture risk in each patient, but DXA is known to have inherent limitations including inaccuracy in differentiating patients with and without prevalent vertebral fractures, in predicting new vertebral fractures, and for treatment monitoring in osteoporosis (15–17). Hence, imaging alternatives to DXA are needed to improve patient care, which include computed tomography (CT) and magnetic resonance imaging (MRI) (18–21). Using CT opportunistically for the assessment of volumetric BMD (vBMD) has become increasingly popular (i.e., extraction of the vBMD from routine CT data acquired for other purposes than osteoporosis screening, such as staging in oncologic patients), using conversion equations for translation of Hounsfield units (HU) into vBMD, showing overall good correlations with DXA measurements and sufficient reproducibility (18, 22–25). Regarding MRI, particularly chemical shift encoding-based water-fat MRI (CSE-MRI) has developed into a valuable tool to determine a vertebral body's proton density fat fraction (PDFF), which is considered a surrogate biomarker of bone health (19, 21). As such, the PDFF from CSE-MRI represents a quantitative, accurate, and robust marker of a tissue's relative fat content (26–30). The PDFF is defined as the ratio of density of mobile protons from fat (triglycerides) and the total density of protons from mobile triglycerides and mobile water and is a fundamental property of tissue (29). Osteoporosis has been linked to increased fat content of bone marrow, given that with aging, the composition of bone marrow shifts to favor the presence of adipocytes, while osteoclast activity increases and osteoblast function declines, leading to osteoporosis (31). Thus, increased PDFF can be observed in relation to osteoporosis, and inverse correlations with DXA- and CT-derived BMD have been reported (19, 32–34). However, a patient's susceptibility to fragility fractures is not solely explained by decreased BMD or alterations in fat content of bone marrow. Importantly, bone strength and resistance to fracture are also determined by other factors, including bone geometry and microstructural architecture (35).

Texture analysis has been applied as an advanced image analysis technique to provide a spatially resolved evaluation of osseous structures like the vertebral body in osteoporosis (18, 19, 36). In essence, texture analysis provides spatial and heterogeneity information of gray-level values in images, representing an objective and quantitative approach to analyze the distribution and relationship of pixel or voxel gray levels (37–39). In spine imaging, commonly used texture features include first-order, second-order, and higher-order features, and their

Abbreviations: 3D, Three-dimensional; AUC, Area under the curve; BMD, Bone mineral density; CI, Confidence interval; CNN, Convolutional neural network; CSE-MRI, Chemical shift encoding-based water-fat MRI; CT, Computed tomography; DXA, Dual-energy X-ray absorptiometry; GLCM, Gray-level co-occurrence matrix; GLRLM, Gray-level run-length matrix; HU, Hounsfield units; MRI, Magnetic resonance imaging; PACS, Picture Archiving and Communication System; PDFF, Proton density fat fraction; R^2_a, Adjusted R^2; ROI, Region of interest; TE, Echo time; TR, Repetition time; UTE, Ultra-short echo-time; vBMD, Volumetric BMD.

extraction has been achieved for sagittal reformations with up to 3 mm slice thickness for routine multi-detector CT, and, more recently, also for CSE-MRI (40, 41). Yet, it is largely unknown whether CSE-MRI-derived texture analysis can predict vBMD, or whether a model incorporating texture analysis based on both CT and CSE-MRI in the same patients may lead to improved capability for differentiating patients with and without osteoporotic vertebral fractures.

Against this background, the main purposes of this study were to apply texture analysis to CSE-MRI data of the thoracolumbar spine to predict vBMD, and to facilitate discrimination between patients with and without osteoporotic vertebral fractures by implementing texture analysis. We hypothesize that combining CT- and CSE-MRI-based texture analysis may result in improved differentiation between patients with and without osteoporotic vertebral fractures compared to vBMD and PDFF alone.

MATERIAL AND METHODS

Study Inclusion and Patient Cohort

This retrospective study was approved by the local institutional review board and was conducted in accordance with the Declaration of Helsinki. The requirement for written informed consent was waived due to the study's retrospective character.

Eligible patients underwent CT and MRI scans covering the thoracolumbar spine and were identified in our institution's digital Picture Archiving and Communication System (PACS). Inclusion criteria were as follows: 1) age of at least 18 years, 2) acquisition of routine CT and CSE-MRI within a maximum of six months, and 3) overlap in spatial coverage between CT and CSE-MRI of at least two consecutive vertebral bodies. The exclusion criteria were as follows: 1) malignant bone lesions (e.g., vertebral bone metastases), 2) hematological or metabolic bone disorders aside from osteoporosis, and 3) motion artifacts in imaging data. Patients who had undergone previous surgery at the spine and showed spinal instrumentation were included, but vertebral bodies with foreign material were excluded from the analyses (due to metal-related artifacts in imaging data). Both CT and CSE-MRI were acquired for standard routine clinical indications (e.g., lumbar back pain, screening for vertebral fractures).

Overall, 26 patients fulfilled the eligibility criteria and underwent imaging at the same institution between July 2018 and September 2019. **Figure 1** provides an overview of the data processing pipeline.

Computed Tomography

Image Acquisition

Scanning was performed with five different CT scanners (Philips iQon, iCT 256, Ingenuity, Ingenuity Core, Philips Healthcare, Best, The Netherlands; Somatom Definition AS+, Siemens Healthineers, Erlangen, Germany). Scans in five of the included patients were performed after administration of either both oral (Barilux Scan, Sanochemia Diagnostics) and intravenous (Iomeron 400, Bracco) contrast media, or only after administration of an intravenous contrast medium. The contrast-enhanced scans were acquired either in the arterial or portal venous phase, triggered by a threshold of CT attenuation surpassed in a region of interest (ROI) placed in the aorta or after a delay of 70 s, respectively, which was dependent on the distinct clinical indication for imaging.

Image data were acquired with all scanners in helical mode (using asynchronous calibration), a slice thickness of 0.9 to 1 mm, and adaptive tube load. The median tube voltage was 120 kV (range: 120 – 140 kV), the median tube current amounted to 316 mA (range: 118 – 363 mA). Sagittal reformations of the spine using a bone kernel were either available with a slice thickness of 2 mm (18 patients) or 3 mm (8 patients). The presence of vertebral fractures was determined in sagittal reformations of the spine with a bone kernel by a board-certified radiologist with eleven years of experience (T.B.), using the classification system described by Genant et al. (42).

Image Processing and Segmentation

From PACS, images were transferred to our in-house developed, convolutional neural network (CNN)-based framework (https://anduin.bonescreen.de) (**Figures 1** and **2**) (43–45). This tool identifies and labels each vertebra in an automated process, followed by creating corresponding segmentation masks for each vertebra as well as its subregions. Furthermore, it adjusts for the used scanner, scanning parameters, and contrast media (if administered during imaging) to asynchronously convert measured HU into vBMD (43–45).

For this study, we used segmentation masks of the trabecular and cortical compartment of the vertebral body, respectively. By combining the trabecular and cortical compartment, the entire vertebral body was enclosed. The generated labels and segmentation masks of all vertebrae were checked visually by a radiologist (two years of experience in spine imaging, M.D.), and were manually corrected if necessary (e.g., in case of labeling or segmentation errors due to Schmorl nodes, fused vertebral bodies, or thoracolumbar or lumbosacral transitional anatomy). Then, the segmentation masks of the entire vertebral bodies were used for level-wise extraction of integral vBMD, and subregion masks of the trabecular compartment were used for sampling of trabecular vBMD. All thoracolumbar vertebral bodies without foreign material (e.g., due to spinal instrumentation), severe degenerative changes (e.g, Modic type 3 endplate changes), or vertebral fractures were considered for integral and trabecular vBMD extractions.

Magnetic Resonance Imaging

Image Acquisition

All patients were scanned using the same 3-Tesla MRI system (Ingenia, Philips Healthcare, Best, The Netherlands). The pulse sequence protocol was individually determined based on the clinical indication for imaging, but included a sagittal six-echo time (TE)-interleaved three-dimensional (3D) spoiled gradient echo sequence for CSE-MRI (46).

Imaging was performed in supine position using the built-in-the-table posterior coil elements (12-channel array). The six echoes of the CSE-MRI sequence were acquired in two

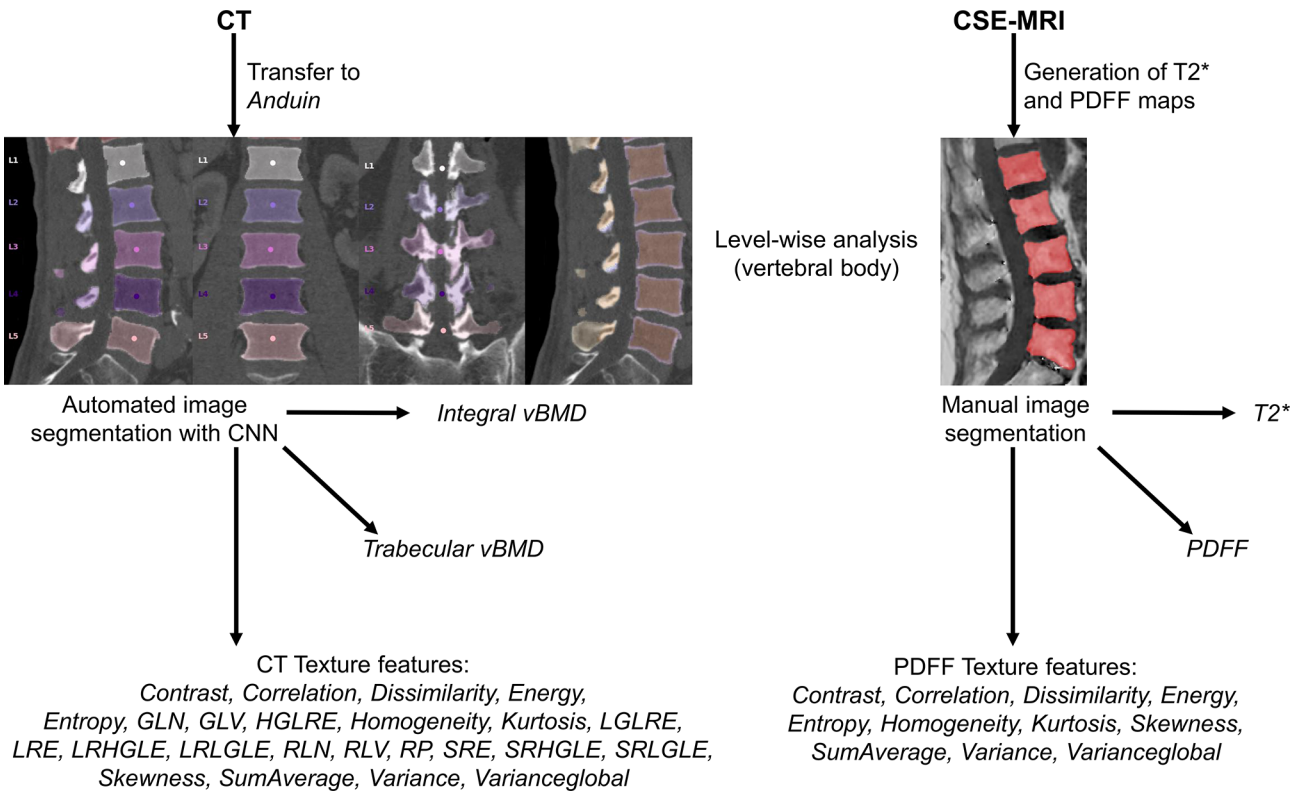

FIGURE 1 | Overview of the study setup. In this study, texture analysis to extract different texture features was achieved based on computed tomography (CT) and chemical shift encoding-based water-fat magnetic resonance imaging (CSE-MRI) data. For labeling and segmentation of vertebral bodies from CT data, a convolutional neural network (CNN)-based framework was used (https://anduin.bonescreen.de). After generation of proton density fat fraction (PDFF) and T2* maps, vertebral bodies were segmented manually on the PDFF maps. In addition to different texture features, integral and trabecular volumetric bone mineral density (vBMD) were extracted from segmented CT data, and mean PDFF and T2* values were extracted level-wise from segmented CSE-MRI data.

interleaves acquiring 3 echoes per repetition time (TR), using flyback (monopolar) read-out gradients and the following imaging parameters: TR/TE1/effective ΔTE = 8.3/1.32/1.0 ms, acquisition matrix size = 124 × 122 x 69, acquisition voxel size = 1.80 mm × 1.80 mm × 1.80 mm, receiver bandwidth = 1,083 Hz/pixel, frequency direction = anterior-posterior, 1 average, approximate scan time = 3 min 38 s. A flip angle of 3° was used to minimize T1-bias effects (47, 48).

Image Processing and Segmentation

Reconstruction of raw data, fat quantification, and T2* mapping were performed offline. The MATLAB-based Reconstruction Library (MRecon/ReconFrame, version 4.3.3; https://www.gyrotools.com/gt/index.php/products/reconframe with MATLAB, version R2021a; MathWorks Inc., Natick, MA, USA) was used for raw data reconstruction. Water-fat separation was performed using a graph-cut algorithm, employing a multi-peak fat model specific to bone marrow and a single T2* decay model (49, 50). The PDFF maps were computed as the ratio of the fat signal over the sum of fat and water signals (29, 51, 52). T2* maps were extracted in addition to PDFF maps.

The vertebral bodies were manually segmented using sagittal images. In the reconstructed maps, manual polygonal ROIs were carefully placed to enclose the vertebral body using MITK ([http://mitk.org/wiki/The_Medical_Imaging_Interaction_Toolkit_(MITK)]; German Cancer Research Center, Division of Medical and Biological Informatics, Medical Imaging Interaction Toolkit, Heidelberg, Germany; **Figures 1** and **3**) (51, 52). The segmentations did not include the posterior elements and were performed by the same radiologist who had also performed visual inspection of the results of the CNN-based algorithm for CT data processing (two years of experience in spine imaging, M.D.). Level-wise PDFF and T2* values were then extracted from the segmentation masks for those vertebral bodies that were also depicted and considered during CT data analyses.

Texture Analysis

On the basis of the distribution of gray-level values, texture analysis was used to characterize structural image properties of predefined regions by quantifying different texture features (37–39). Texture analysis was performed using the segmentation masks derived from CT and CSE-MRI enclosing single vertebral bodies, and different first-order statistical moments from global

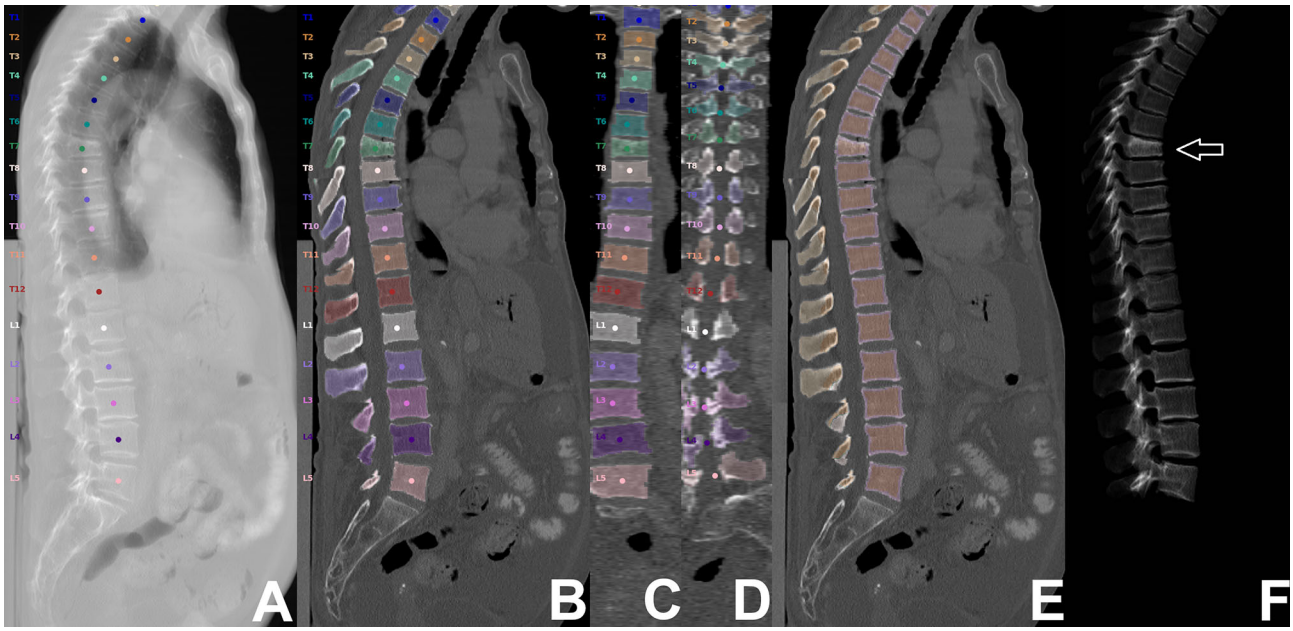

FIGURE 2 | Segmentation of computed tomography (CT) data. CT scan of a 63-year-old woman visualized as virtual radiograph-like images in lateral projection **(A, F)** and as planar reconstructions in lateral and coronal views **(B–E)**, covering the thoracolumbar spine (T1-L5). Labeling and segmentation of single vertebrae and vertebral subregions was achieved automatically using a convolutional neural network (CNN)-based framework. Segmentation masks were used to extract integral volumetric bone mineral density (vBMD), trabecular vBMD, and texture features following texture analysis. However, this patient showed a vertebral fracture at level T7 (white arrow); thus, extraction of these parameters was not performed for this vertebral body.

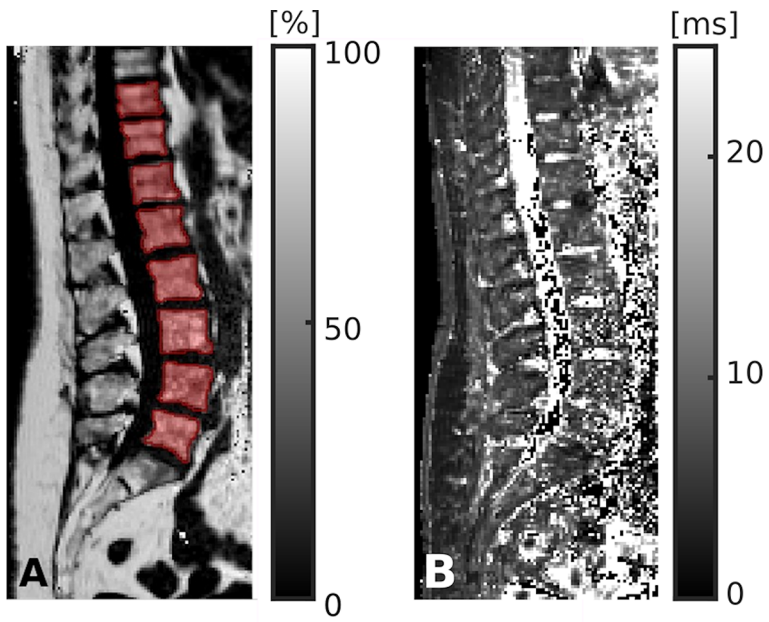

FIGURE 3 | Segmentation of chemical shift encoding-based water-fat magnetic resonance imaging (CSE-MRI) data. CSE-MRI scan of a 74-year-old woman: proton density fat fraction (PDFF) map [%] with manually prescribed segmentation masks **(A)** and T2* map [ms] **(B)** covering the lower thoracic and lumbar vertebral bodies (T10-L5). Segmentation masks were used to extract PDFF, T2*, and texture features following texture analysis.

gray-level histograms, second-order features based on the gray-level co-occurrence matrix (GLCM), and higher-order features based on the gray-level run-length matrix (GLRLM) were extracted (**Figure 1** and **Table 1**) (40, 41, 51, 53–55).

The GLCM reflects how often pairs of voxels with a given gray-level value and offset occur in an image. The entries of the GLCMs at different angular directions θ = (0°, 45°, 90°, and 135°) were generated by computing the joint probability of two adjacent voxel intensities at a given offset d = (dx, dy, dz) and given θ, with dx, dy, and dz denoting the displacement along the x-, y-, and z-axis, respectively. 3D GLCM analysis was achieved by computation of the co-occurrence probabilities of voxel intensities from the 26 neighbors aligned in 13 directions. Averaging over the 13 directions ensures rotation invariance. Furthermore, a gray-level run is defined as a set of successive voxels with identical gray-level values that are arranged collinearly in a certain direction, and the run-length represents the number of voxels in it. The GLRLM features are calculated based on the occurrence and distribution of such runs within the GLCM and measure directional changes in the GLCM. Analogously, 3D GLRLM was computed by simultaneously adding up all possible run-lengths in the 13 directions of the 3D space. For GLCM and GLRLM analysis, direction-dependent discretization length differences were taken into account when measurements were combined by averaging or summation. All steps of the texture analysis were performed with MATLAB (version R2021a; MathWorks Inc., Natick, MA, USA) using a radiomics toolbox (https://github.com/mvallieres/radiomics).

Statistical Analysis

For statistical analyses, SPSS (version 26.0; IBM SPSS Statistics for Windows, IBM Corp., Armonk, NY, USA) and GraphPad Prism (version 6.0; GraphPad Software Inc., San Diego, CA, USA) were used. A p-value of < 0.05 (two-sided) was considered statistically significant.

Descriptive statistics were calculated for integral and trabecular vBMD, PDFF, T2*, and the different texture features extracted from CT and CSE-MRI data, respectively. Shapiro-Wilk normality tests indicated non-Gaussian distribution for the majority of these parameters. Integral and trabecular vBMD were compared between patients with and without osteoporotic vertebral fractures using Mann-Whitney tests. Furthermore, age and sex

TABLE 1 | Texture features derived from computed tomography (CT) and chemical shift encoding-based water-fat magnetic resonance imaging (CSE-MRI).

Category	Texture Feature	Description	Included in CT-Based Texture Analysis	Included in CSE-MRI-Based Texture Analysis
Global	Varianceglobal	Spread of gray-level distribution	x	x
	Skewness	Shape of gray-level distribution	x	x
	Kurtosis	Flatness of gray-level distribution	x	x
Second-order (GLCM)	Energy	Uniformity	x	x
	Contrast	Local intensity variation	x	x
	Entropy	Randomness	x	x
	Homogeneity	Homogeneous scene	x	x
	Correlation	Linear spatial relationships between texture elements	x	x
	SumAverage	Spread of the mean voxel co-occurrence distribution	x	x
	Variance	Voxel co-occurrence distribution	x	x
	Dissimilarity	Heterogeneity	x	x
Higher-order (GLRLM)	SRE	Short-run emphasis	x	
	LRE	Long-run distribution	x	
	GLN	Similarities of gray-levels	x	
	RLN	Similarity in length of runs	x	
	RP	Distribution and homogeneity of runs with a specific direction	x	
	LGLRE	Distribution of low gray-level values	x	
	HGLRE	Distribution of high gray-level values	x	
	SRLGLE	Joint distribution of short runs and low gray-level values	x	
	SRHGLE	Joint distribution of short runs and high gray-level values	x	
	LRLGLE	Joint distribution of long runs and low gray-level values	x	
	LRHGLE	Joint distribution of long runs and high gray-level values	x	
	GLV	Weighted variances of gray-level values	x	
	RLV	Weighted variances of gray-level runs	x	

Global (histogram-based), gray-level co-occurrence matrix (GLCM)-based, and gray-level run-length matrix (GLRLM)-based texture features and their descriptions. The table provides information about which texture features were considered for texture analysis based on computed tomography (CT) and chemical shift encoding-based water-fat magnetic resonance imaging (CSE-MRI) data. SRE, short-run emphasis; LRE, long-run emphasis; GLN, gray-level non-uniformity; RLN, run-length non-uniformity; RP, run percentage; LGLRE, low gray-level run emphasis; HGLRE, high gray-level run emphasis; SRLGLE, short-run low gray-level emphasis; SRHGLE, short-run high gray-level emphasis; LRLGLE, long-run low gray-level emphasis; LRHGLE, long-run high gray-level emphasis; GLV, gray-level variance; RLV, run-length variance.

distributions were compared between the subgroups of patients with and without osteoporotic vertebral fractures using Mann-Whitney and Chi-squared tests, respectively.

For vertebral level-wise analyses, data from each vertebral body were considered as a separate data point. One stepwise linear regression model using integral vBMD as the dependent and PDFF, T2*, and all CSE-MRI-derived texture features as independent variables was calculated. Furthermore, two additional linear regression models with a stepwise approach were generated, using the binary fracture status (at least one osteoporotic vertebral fracture present/no osteoporotic vertebral fracture present) as the dependent and 1) integral vBMD, PDFF, and T2*, or 2) integral vBMD, PDFF, T2*, and all CT-derived as well as the CSE-MRI-derived texture features as independent variables. Patient age, sex, the number of independent variables, and the vertebral level (T1-L5) were considered for adjustment of these regression models.

Furthermore, integral and trabecular vBMD, PDFF, T2*, and texture features derived from CT and CSE-MRI were averaged over the included vertebral bodies to provide one value per parameter in each patient, respectively. Using these mean values, two additional linear regression models with a stepwise approach were computed, using again the binary fracture status (at least one osteoporotic vertebral fracture present/no osteoporotic vertebral fracture present) as the dependent and 1) integral vBMD, PDFF, and T2*, or 2) integral vBMD, PDFF, T2*, and all CT-derived as well as the CSE-MRI-derived texture features as independent variables. Patient age, sex, and the number of independent variables were used for adjustment of these regression models.

Independent variables were included stepwise in the linear regression models based on a p-value threshold of < 0.05. Per model, the adjusted R^2 (R^2_a) is reported with related β coefficients and 95%-confidence intervals (CIs), and F-tests were performed to assess statistical significance of the final models after stepwise inclusion of variables.

RESULTS

Patient Characteristics

Analyses included 171 vertebral bodies of the thoracolumbar spine, which were derived from 26 patients (15 females, 11 males, median age: 73 years, age range: 29 – 86 years). Eight of the included patients had imaging by CT and CSE-MRI on the same day, the median interval between CT and CSE-MRI acquisitions was four days.

Eleven of the included patients (42.3%) showed at least one osteoporotic vertebral fracture according to CT image reading (only Genant grade 1 fractures: 2 patients, only Genant grade 2 fractures: 2 patients, combination of fracture grades including Genant grade 3 fractures: 7 patients). Patients with and without vertebral fractures did not statistically significantly differ in age (patients with fractures: median age: 75.1 years, age range: 59 – 86 years, patients without fractures: median age: 71.5 years, age range: 29 – 78 years; $p = 0.097$) or sex distributions (patients with fractures: 3 males & 8 females, patients without fractures: 8 males & 7 females; $p = 0.184$).

Regarding the analyzed thoracic vertebrae (89 thoracic vertebral bodies in total), T1 was considered in five patients, T2, T3, and T4 in six patients, T5, T6, T10, and T11 in seven patients, T7, T8, and T9 in eight patients, and T12 in 14 patients, respectively. Furthermore, for the lumbar spine (82 lumbar vertebral bodies in total), L1 and L4 were included from 18 patients each, while L2 was considered in 17 patients, L3 in 14 patients, and L5 in 15 patients, respectively.

Volumetric Bone Mineral Density

Patients with osteoporotic vertebral fractures had statistically significantly lower integral and trabecular vBMD as compared to patients without osteoporotic vertebral fractures regarding all included vertebrae (integral vBMD: 153.1 ± 46.5 mg/cm^3 vs. 218.5 ± 45.4 mg/cm^3; $p < 0.001$; trabecular vBMD: 77.7 ± 30.3 mg/cm^3 vs. 130.8 ± 34.8 mg/cm^3; $p < 0.001$). The minimum value measured for a vertebral body in patients with an osteoporotic vertebral fracture was 82.6 mg/cm^3 for integral vBMD and 21.6 mg/cm^3 for trabecular vBMD, compared to 132.4 mg/cm^3 for integral vBMD and 71.8 mg/cm^3 for trabecular vBMD in patients without osteoporotic vertebral fractures.

Prediction of Volumetric Bone Mineral Density and Differentiation Between Patients According to Fracture Status

For the model with integral vBMD as the dependent variable (independent variables: PDFF, T2*, and texture features derived from CSE-MRI), R^2_a amounted to 0.40 ($F(7, 163) = 17.5$, $p < 0.001$), with the following variables being kept in the final model after the stepwise approach: T2*, PDFF_Kurtosis (global texture feature, representing the flatness of gray-level distribution), PDFF_Variance (second-order texture feature, representing the voxel co-occurrence distribution), and PDFF_Energy (second-order texture feature, representing uniformity).

For vertebral level-wise analyses with the fracture status as the dependent variable (independent variables: integral vBMD, PDFF, and T2*), R^2_a of 0.44 was obtained ($F(5, 165) = 27.4$, $p < 0.001$; variables included in the final model: vBMD and PDFF). Including the texture features in the model (independent variables: integral vBMD, PDFF, T2*, texture features derived from CT and CSE-MRI) resulted in a statistically significant model with an improved R^2_a of 0.66 ($F(10, 160) = 34.7$, $p < 0.001$; **Table 2**). Specifically, the variables included in the final model were CT_Correlation (second-order texture feature, representing the linear spatial relationships between texture elements), CT_SRLGLE (higher-order texture feature, representing the joint distribution of short runs and low gray-level values), PDFF_SumAverage (second-order texture feature, representing the spread of the mean voxel co-occurrence distribution), CT_Varianceglobal (global texture feature, representing the spread of gray-level distribution), CT_LRHGLE (higher-order texture feature, representing the joint distribution of long runs and high gray-level values), CT_Contrast (second-order texture feature, representing the local intensity variation), and PDFF_Energy (second-order texture feature, representing uniformity).

TABLE 2 | Differentiation between patients with and without osteoporotic vertebral fractures including texture analysis – analysis on vertebral level.

Term	Description	β coefficient	95%-CI	p-value
CT_Correlation	Second-order texture feature, representing the linear spatial relationships between texture elements	-0.639	-1.308;-0.938	<0.001
CT_SRLGLE	Higher-order texture feature, representing the joint distribution of short runs and low gray-level values	0.173	-44.109;2028.023	0.060
PDFF_SumAverage	Second-order texture feature, representing the spread of the mean voxel co-occurrence distribution	-0.183	-134.472;-30.952	0.002
CT_Varianceglobal	Global texture feature, representing the spread of gray-level distribution	-0.435	-0.020;-0.005	0.001
CT_LRHGLE	Higher-order texture feature, representing the joint distribution of long runs and high gray-level values	-0.724	0.000;0.000	<0.001
CT_Contrast	Second-order texture feature, representing the local intensity variation	0.551	0.000;0.000	<0.001
PDFF_Energy	Second-order texture feature, representing uniformity	-0.201	-227.524;-36.375	0.007

This table shows the variables kept in the final linear regression model (adjusted R^2 [R^2_a] = 0.66, (F(10, 160) = 34.7, p < 0.001) after a stepwise approach using the binary fracture status (at least one osteoporotic vertebral fracture present/no osteoporotic vertebral fracture present) as the dependent variable (vertebral level-wise analyses). Specifically, it included the texture features CT_Correlation, CT_SRLGLE, PDFF_SumAverage, CT_Varianceglobal, CT_LRHGLE, CT_Contrast, and PDFF_Energy (β coefficients, 95%-confidence intervals [CIs], and p-values shown per texture feature). Patient age, sex, the number of independent variables, and the vertebral level (T1-L5) were considered for adjustment. For vertebral level-wise analyses, the data from each vertebral body were considered as a separate data point.

On a patient level, using the fracture status as the dependent variable (independent variables: integral vBMD, PDFF, and T2*) resulted in R^2_a of 0.47 (F(4, 21) = 6.5, p = 0.001; variables included in final model: vBMD and PDFF). Comparable to the level-wise analyses, including texture analysis in the model (independent variables: integral vBMD, PDFF, T2*, texture features derived from CT and CSE-MRI) resulted in a statistically significant model with an improved R^2_a of 0.81 (F(6, 19) = 19.2, p < 0.001, **Table 3**). The variables included in the final model were integral vBMD, CT_SRE (higher-order texture feature, representing the short-run emphasis), CT_Varianceglobal (global texture feature, representing the spread of gray-level distribution), and PDFF_Variance (second-order texture feature, representing the voxel co-occurrence distribution).

DISCUSSION

In this study, we used texture analysis on CT and CSE-MRI data covering the thoracolumbar spine in patients with and without osteoporotic vertebral fractures to predict vBMD, and to discriminate between patients with and without osteoporotic vertebral fractures based on models including vBMD, PDFF, T2*, and texture features. The main findings are as follow: first, a model including T2* combined with three PDFF-based texture features explained 40% of the variance in integral vBMD; second, a model consisting of integral vBMD and three texture features (CT_SRE, CT_Varianceglobal, and PDFF_Variance) explained 81% of the variance regarding the osteoporotic vertebral fracture status, compared to 47% when the model was based on integral vBMD and PDFF only.

Main complications of osteoporosis are vertebral fractures as a result of decreased bone strength, which is determined by a multitude of factors such as bone geometry, cortical thickness and porosity, trabecular bone morphology, and intrinsic properties of bony tissue (35). Of note, DXA as the reference standard for measuring the areal BMD and assessing individual fracture risk cannot fully capture many of those factors, thus harboring well-known limitations for predicting new osteoporotic vertebral fractures or differentiating between patients with and without prevalent vertebral fractures, as well as for treatment monitoring (15–17). In this regard, it is estimated that DXA-based areal BMD values only account for about 60 to 70% of the variation in bone strength (35). Yet, texture analysis based on CT or MRI data can provide spatially resolved assessments of vertebral body composition, thus supplementing conventional vBMD measurements with parameters potentially valuable for improving image-based osteoporosis diagnostics and fracture prediction. Specifically, it has been demonstrated that texture analysis with a support vector machine can be performed opportunistically on routine CT data of the spine, potentially enabling to discriminate between patients depending on their fracture status (considering the texture features Energy, Entropy, and Homogeneity) (40). The support vector machine classifier operated with linear, polynomial, and radial basis function kernels to discriminate between healthy subjects and patients with fractures, while the radial basis function kernel revealed the best performance (sensitivity of 93.33%, specificity of 79.33%, and

TABLE 3 | Differentiation between patients with and without osteoporotic vertebral fractures including texture analysis – analysis on patient level.

Term	Description	β coefficient	95%-CI	p-value
Integral vBMD	–	-0.669	-0.010;-0.005	<0.001
CT_SRE	Higher-order texture feature, representing the short-run emphasis	0.721	154.622;287.516	<0.001
CT_Varianceglobal	Global texture feature, representing the spread of gray-level distribution	-0.519	-0.021;-0.008	<0.001
PDFF_Variance	Second-order texture feature, representing the voxel co-occurrence distribution	0.351	5.390;36.408	0.011

This table shows the variables kept in the final linear regression model (adjusted R^2 [R^2_a] = 0.81 (F(6, 19) = 19.2, p < 0.001) after a stepwise approach using the binary fracture status (at least one osteoporotic vertebral fracture present/no osteoporotic vertebral fracture present) as the dependent variable (analyses on patient level). Specifically, it included integral volumetric bone mineral density (vBMD) and the texture features CT_SRE, CT_Varianceglobal, and PDFF_Variance (β coefficients, 95%-confidence intervals [CIs], and p-values shown per texture feature). Patient age, sex, and the number of independent variables were considered for adjustment. For analyses on patient level, integral and trabecular vBMD, PDFF, T2, and texture features were averaged over the included vertebral bodies to provide one value per parameter in each patient, respectively.*

accuracy of 83% among different kernel functions) (40). Another study demonstrated that an improved classification of patients with and without prevalent vertebral fractures is possible by combining texture features with regional vBMD [area under the curve (AUC) = 0.88)], with global vBMD showing inferior performance (AUC = 0.64) (56). Likewise, a set of texture features derived from routine CT exams in a machine-learning approach identified patients who would suffer from vertebral fractures with high accuracy (AUC = 0.97) (57).

Recently, the feasibility of texture analysis based on CSE-MRI has been demonstrated, which could principally provide insights into bone health beyond mean PDFF of vertebral bodies (41, 51). Leveraging CSE-MRI by additionally using texture analysis has revealed that vertebral bone marrow heterogeneity is dependent on sex and age, and is increased in postmenopausal women, which is a patient cohort at particular risk for osteoporosis and related vertebral fractures (41, 51). Results of the present study show that a model incorporating T2* and three texture features based on CSE-MRI predicted the variation in integral vBMD by a proportion of 40%, while PDFF alone was no significant predictor in the model. This may be regarded as evidence for the need for more advanced analyses of CSE-MRI data beyond mere PDFF. However, further improvement in explanatory power for vBMD variance based on CSE-MRI-derived parameters may not be feasible, given that primarily mineralized tissue (trabecular and cortical bone) contributes to the vBMD, while PDFF primarily captures the vertebral bone marrow located in the cavities of trabecular bone (18, 19, 31). Increased PDFF in osteoporosis and inverse correlations with DXA- or CT-derived BMD have been previously reported, though (19, 32–34). Moreover, T2* was kept in the model, which can be considered an MRI-based parameter related to bone microstructure and density (58–60). Specifically, it has been demonstrated that T2* correlates with the density and orientation of trabecular bone (59). Thus, explanation to a certain degree of the variance in vBMD by a model including T2* seems reasonable. In this regard, recent work presented a 3D adiabatic inversion recovery prepared ultra-short echo-time (UTE) Cones sequence for direct volumetric imaging of trabecular bone of the human spine that is robust in suppressing both water and fat, and can provide high image contrast for short T2 trabecular bone (61). While previous work has mostly focused on UTE imaging for cortical bone, this method may be used to also distinctly visualize trabecular bone, together with T2* quantification of trabecular bone (61). Hence, the role of T2* as an MRI-derived marker in osteoporosis may possibly become more important when UTE imaging using such a sequence is increasingly available.

An additive approach using quantification from CT and CSE-MRI may have higher potential for osteoporosis imaging since the two modalities provide different measures for distinct aspects of bone health, thus exploiting measures from two separate techniques as complementary information. Indeed, integrating texture analysis by adding texture features from both CT and CSE-MRI to the model with integral vBMD and PDFF increased the proportion of the explained variance for differentiating between patients with and without osteoporotic vertebral fractures from 47% to 81% according to the results of this study. Thus, when only relying on integral vBMD and PDFF as the standard measures derived from CT and CSE-MRI, a considerably larger proportion of unexplained variance may be assumed. The final model also included SRE for CT, a complex higher-order texture feature, and previous work has indicated that some GLRLM-based features that are defined over information of consecutive pixels of the same value in a given direction could be negatively associated with trabecular bone volume as measured by bone histo-morphometric evaluations (62, 63). One second-order texture feature of the final model was Variance, which is derived from GLCM and could capture image intensities and their differences of directly neighboring voxels and thereby reflect how orderly a certain microarchitecture is preserved (55). Thus, it seems reasonable that these variables were kept in the model for differentiating between patients with and without osteoporotic vertebral fractures.

To the best of our knowledge, the present study is the first to combine texture analysis for CT and CSE-MRI data to differentiate between patients with and without osteoporotic vertebral fractures. Although vertebral body segmentation as well as texture analysis are not part of the clinical routine, approaches are feasible without considerable computational efforts. In detail, CT image segmentation and vBMD extraction are already established, automated, computationally optimized, and their computational effort can therefore be considered negligible in comparison to the remaining tasks (when implementing a pipeline such as the herein used CNN-based framework for vertebral body labeling and segmentation with parameter extraction) (43–45). Details on the computational efficiency of the water-fat separation for generating PDFF and T2* maps have been reported previously for a similar workflow (49). On average, manual segmentation in PDFF maps required approximately 3 min per vertebral body, and the parallelized computation of texture features required approximately 25.5 s per vertebra for CT images and approximately 8.5 s per vertebra for PDFF maps, using a machine with 2.0 GHz CPU (Intel Core i7-8550U, 4 cores) and 16 GB RAM. However, there are limitations to this study that need to be acknowledged. First, the cohort size is small, but overall 171 vertebral bodies were included for analyses. Given our inclusion criteria that required both CT and CSE-MRI of the thoracolumbar spine within a certain period of image acquisition, eligibility was restricted to a rather small number of patients. However, we are confident that prioritizing quality and comparability of CT and MRI data over data quantity from high patient numbers is a justified approach for the purpose of this study. Second, we did not solely consider the lumbar spine (particularly L1-L3) as the site for measurements, although it is the common location for BMD assessments in clinical routine. As a consequence, we are not able to provide evidence for the common reference site for measurements exclusively. However, previous work on CT-based texture analysis has shown that improved classification of patients with and without prevalent vertebral fractures is possible by combining texture features with regional vBMD, while, importantly, all thoracolumbar levels contributed significantly to the classification (56). Third, an automatic, CNN-based approach was used for labeling and segmentation of vertebral bodies in CT images,

while a manual approach was used for CSE-MRI data. According to the authors' knowledge, accurate transfer of segmentation masks between modalities has not been achieved or made available yet, which may be related to several issues including different patient positioning during CT and MRI acquisitions, and a field of view that exhibits only a partial overlap between the two modalities in our cohort. Yet, automatic segmentation of vertebral bodies in CSE-MRI data that could be used for PDFF extraction has been described recently (64). Future work may explore applications for transfer and accurate co-registration of segmentation masks between modalities to further automatize, standardize, and accelerate medical image analyses.

CONCLUSION

This study used texture analysis for CSE-MRI data of the thoracolumbar spine to predict vBMD, and to facilitate discrimination between patients with and without osteoporotic vertebral fractures. A regression model including T2* combined with three PDFF-based texture features explained 40% of the variance in integral vBMD. Further, a regression model consisting of integral vBMD and several texture features for CT and CSE-MRI data was able to predict 81% of the variance regarding the osteoporotic vertebral fracture status, compared to 47% when the model was based on integral vBMD and PDFF only. Thus, texture analysis used for advanced processing of routine CT and CSE-MRI data may improve differentiation of patients according to their fracture status when compared to vBMD and PDFF alone, which could improve prediction of the individual fracture risk in the future. Improved fracture risk prediction by using texture analysis could have important clinical implications for timely treatment initiation and prevention strategies in osteoporosis.

DATA AVAILABILITY STATEMENT

The raw data supporting the conclusions of this article will be made available by the authors, without undue reservation.

ETHICS STATEMENT

The studies involving human participants were reviewed and approved by the Ethikkommission der Technischen Universität München. Written informed consent for participation was not required for this study in accordance with the national legislation and the institutional requirements.

AUTHOR CONTRIBUTIONS

Conceptualization, NS, CB, ME, SR, KS, DK, RK, TB, and MD. Methodology, NS, EAB, CB, ME, SR, EB, JK, TL, KS, DK, RK, TB, and MD. Software, NS, EAB, CB, ME, SR, and MD. Validation, NS, TB, and MD. Formal analysis, NS, EAB, CB, TB, and MD. Investigation, NS, EAB, CB, ME, SR, EB, JK, DK, TB, and MD. Resources, NS, EAB, CB, ME, SR, EB, JK, TL, KS, DK, RK, TB, and MD. Data curation, NS, CB, ME, SR, and MD. Writing—original draft preparation, NS, TB, and MD. Writing—review and editing, EAB, CB, ME, SR, EB, JK, TL, KS, DK, and RK. Visualization, NS, CB, and MD. Supervision, NS, JK, KS, DK, RK, TB, and MD. Project administration, NS, TB, and M.D. Funding acquisition, NS, JK, TL, DK, RK, TB, and MD. All authors have read and agreed to the published version of the manuscript.

FUNDING

The present work was supported by the European Research Council (grant agreement No. 677661 – ProFatMRI, DK and grant agreement No. 637164 – iBack, JK), the German Research Foundation (Deutsche Forschungsgemeinschaft, DFG, project 432290010, JK and TB), the German Society of Musculoskeletal Radiology (Deutsche Gesellschaft für Muskuloskelettale Radiologie, DGMSR, NS and MD), the B. Braun Foundation (project BBST-D-19-00106, NS), and the German Academic Exchange Service (Deutscher Akademischer Austauschdienst, DAAD, NS).

REFERENCES

1. NIH Consensus Development Panel on Osteoporosis Prevention Diagnosis and Therapy. Osteoporosis Prevention, Diagnosis, and Therapy. *JAMA* (2001) 285(6):785–95. doi: 10.1001/jama.285.6.785
2. Jain RK, Vokes T. Dual-Energy X-Ray Absorptiometry. *J Clin Densitom* (2017) 20(3):291–303. doi: 10.1016/j.jocd.2017.06.014
3. Blake GM, Fogelman I. An Update on Dual-Energy X-Ray Absorptiometry. *Semin Nucl Med* (2010) 40(1):62–73. doi: 10.1053/j.semnuclmed.2009.08.001
4. Sambrook P, Cooper C. Osteoporosis. *Lancet* (2006) 367(9527):2010–8. doi: 10.1016/S0140-6736(06)68891-0
5. Reginster JY, Burlet N. Osteoporosis: A Still Increasing Prevalence. *Bone* (2006) 38(2 Suppl 1):S4–9. doi: 10.1016/j.bone.2005.11.024
6. Cole ZA, Dennison EM, Cooper C. Osteoporosis Epidemiology Update. *Curr Rheumatol Rep* (2008) 10(2):92–6. doi: 10.1007/s11926-008-0017-6
7. Sanchez-Riera L, Wilson N, Kamalaraj N, Nolla JM, Kok C, Li Y, et al. Osteoporosis and Fragility Fractures. *Best Pract Res Clin Rheumatol* (2010) 24 (6):793–810. doi: 10.1016/j.berh.2010.10.003
8. Hallberg I, Bachrach-Lindstrom M, Hammerby S, Toss G, Ek AC. Health-Related Quality of Life After Vertebral or Hip Fracture: A Seven-Year Follow-Up Study. *BMC Musculoskelet Disord* (2009) 10:135. doi: 10.1186/1471-2474-10-135
9. Bliuc D, Nguyen ND, Milch VE, Nguyen TV, Eisman JA, Center JR. Mortality Risk Associated With Low-Trauma Osteoporotic Fracture and Subsequent Fracture in Men and Women. *JAMA* (2009) 301(5):513–21. doi: 10.1001/jama.2009.50
10. Center JR, Nguyen TV, Schneider D, Sambrook PN, Eisman JA. Mortality After All Major Types of Osteoporotic Fracture in Men and Women: An Observational Study. *Lancet* (1999) 353(9156):878–82. doi: 10.1016/S0140-6736(98)09075-8
11. Cummings SR, Melton LJ. Epidemiology and Outcomes of Osteoporotic Fractures. *Lancet* (2002) 359(9319):1761–7. doi: 10.1016/S0140-6736(02)08657-9
12. Schousboe JT. Epidemiology of Vertebral Fractures. *J Clin Densitom* (2016) 19 (1):8–22. doi: 10.1016/j.jocd.2015.08.004
13. Melton LJ3rd, Atkinson EJ, Cooper C, O'Fallon WM, Riggs BL. Vertebral Fractures Predict Subsequent Fractures. *Osteoporos Int* (1999) 10(3):214–21. doi: 10.1007/s001980050218

14. Haczynski J, Jakimiuk A. Vertebral Fractures: A Hidden Problem of Osteoporosis. *Med Sci Monit* (2001) 7(5):1108–17.
15. Arabi A, Baddoura R, Awada H, Khoury N, Haddad S, Ayoub G, et al. Discriminative Ability of Dual-Energy X-Ray Absorptiometry Site Selection in Identifying Patients With Osteoporotic Fractures. *Bone* (2007) 40(4):1060–5. doi: 10.1016/j.bone.2006.11.017
16. Maricic M. Use of DXA-Based Technology for Detection and Assessment of Risk of Vertebral Fracture in Rheumatology Practice. *Curr Rheumatol Rep* (2014) 16(8):436. doi: 10.1007/s11926-014-0436-5
17. Siris ES, Chen YT, Abbott TA, Barrett-Connor E, Miller PD, Wehren LE, et al. Bone Mineral Density Thresholds for Pharmacological Intervention to Prevent Fractures. *Arch Internal Med* (2004) 164(10):1108–12. doi: 10.1001/archinte.164.10.1108
18. Loffler MT, Sollmann N, Mei K, Valentinitsch A, Noel PB, Kirschke JS, et al. X-Ray-Based Quantitative Osteoporosis Imaging at the Spine. *Osteoporos Int* (2020) 31(2):233–50. doi: 10.1007/s00198-019-05212-2
19. Sollmann N, Loffler MT, Kronthaler S, Bohm C, Dieckmeyer M, Ruschke S, et al. MRI-Based Quantitative Osteoporosis Imaging at the Spine and Femur. *J Magn Reson Imaging* (2021) 54(1):12–35. doi: 10.1002/jmri.27260
20. Link TM, Kazakia G. Update on Imaging-Based Measurement of Bone Mineral Density and Quality. *Curr Rheumatol Rep* (2020) 22(5):13. doi: 10.1007/s11926-020-00892-w
21. Karampinos DC, Ruschke S, Dieckmeyer M, Diefenbach M, Franz D, Gersing AS, et al. Quantitative MRI and Spectroscopy of Bone Marrow. *J Magn Reson Imaging: JMRI* (2018) 47(2):332–53. doi: 10.1002/jmri.25769
22. Schreiber JJ, Anderson PA, Rosas HG, Buchholz AL, Au AG. Hounsfield Units for Assessing Bone Mineral Density and Strength: A Tool for Osteoporosis Management. *J Bone Joint Surg Am* (2011) 93(11):1057–63. doi: 10.2106/JBJS.J.00160
23. Burns JE, Yao J, Summers RM. Vertebral Body Compression Fractures and Bone Density: Automated Detection and Classification on CT Images. *Radiology* (2017) 284(3):788–97. doi: 10.1148/radiol.2017162100
24. Baum T, Muller D, Dobritz M, Rummeny EJ, Link TM, Bauer JS. BMD Measurements of the Spine Derived From Sagittal Reformations of Contrast-Enhanced MDCT Without Dedicated Software. *Eur J Radiol* (2011) 80(2):e140–5. doi: 10.1016/j.ejrad.2010.08.034
25. Baum T, Muller D, Dobritz M, Wolf P, Rummeny EJ, Link TM, et al. Converted Lumbar BMD Values Derived From Sagittal Reformations of Contrast-Enhanced MDCT Predict Incidental Osteoporotic Vertebral Fractures. *Calcif Tissue Int* (2012) 90(6):481–7. doi: 10.1007/s00223-012-9596-3
26. Dixon WT. Simple Proton Spectroscopic Imaging. *Radiology* (1984) 153(1):189–94. doi: 10.1148/radiology.153.1.6089263
27. Glover GH, Schneider E. Three-Point Dixon Technique for True Water/Fat Decomposition With B0 Inhomogeneity Correction. *Magnetic Reson Med: Off J Soc Magnetic Reson Medicine/Society Magnetic Reson Med* (1991) 18(2):371–83. doi: 10.1002/mrm.1910180211
28. Reeder SB, Pineda AR, Wen Z, Shimakawa A, Yu H, Brittain JH, et al. Iterative Decomposition of Water and Fat With Echo Asymmetry and Least-Squares Estimation (IDEAL): Application With Fast Spin-Echo Imaging. *Magnetic Reson Med: Off J Soc Magnetic Reson Medicine/Society Magnetic Reson Med* (2005) 54(3):636–44. doi: 10.1002/mrm.20624
29. Reeder SB, Hu HH, Sirlin CB. Proton Density Fat-Fraction: A Standardized MR-Based Biomarker of Tissue Fat Concentration. *J Magn Reson Imaging: JMRI* (2012) 36(5):1011–4. doi: 10.1002/jmri.23741
30. Ma J. Dixon Techniques for Water and Fat Imaging. *J Magn Reson Imaging: JMRI* (2008) 28(3):543–58. doi: 10.1002/jmri.21492
31. Rosen CJ, Bouxsein ML. Mechanisms of Disease: Is Osteoporosis the Obesity of Bone? *Nat Clin Pract Rheumatol* (2006) 2(1):35–43. doi: 10.1038/ncprheum0070
32. Kuhn JP, Hernando D, Meffert PJ, Reeder S, Hosten N, Laqua R, et al. Proton-Density Fat Fraction and Simultaneous R2* Estimation as an MRI Tool for Assessment of Osteoporosis. *Eur Radiol* (2013) 23(12):3432–9. doi: 10.1007/s00330-013-2950-7
33. Zhao Y, Huang M, Ding J, Zhang X, Spuhler K, Hu S, et al. Prediction of Abnormal Bone Density and Osteoporosis From Lumbar Spine MR Using Modified Dixon Quant in 257 Subjects With Quantitative Computed Tomography as Reference. *J Magn Reson Imaging: JMRI* (2019) 49(2):390–9. doi: 10.1002/jmri.26233
34. Li G, Xu Z, Gu H, Li X, Yuan W, Chang S, et al. Comparison of Chemical Shift-Encoded Water-Fat MRI and MR Spectroscopy in Quantification of Marrow Fat in Postmenopausal Females. *J Magn Reson Imaging: JMRI* (2017) 45(1):66–73. doi: 10.1002/jmri.25351
35. Ammann P, Rizzoli R. Bone Strength and Its Determinants. *Osteoporos Int* (2003) 14 Suppl 3:S13–8. doi: 10.1007/s00198-002-1345-4
36. Waldt S, Meier N, Renger B, Lenzen H, Fiebich M, Rummeny EJ, et al. The Texture-Analysis of High-Resolution Computed Tomograms as an Additional Procedure in Osteoporosis Diagnosis: *In-Vitro* Studies on Vertebral Segments. *Rofo* (1999) 171(2):136–42. doi: 10.1055/s-1999-242
37. Lubner MG, Smith AD, Sandrasegaran K, Sahani DV, Pickhardt PJ. CT Texture Analysis: Definitions, Applications, Biologic Correlates, and Challenges. *Radiographics* (2017) 37(5):1483–503. doi: 10.1148/rg.2017170056
38. Castellano G, Bonilha L, Li LM, Cendes F. Texture Analysis of Medical Images. *Clin Radiol* (2004) 59(12):1061–9. doi: 10.1016/j.crad.2004.07.008
39. Varghese BA, Cen SY, Hwang DH, Duddalwar VA. Texture Analysis of Imaging: What Radiologists Need to Know. *AJR Am J Roentgenology* (2019) 212(3):520–8. doi: 10.2214/AJR.18.20624
40. Mookiah MRK, Rohrmeier A, Dieckmeyer M, Mei K, Kopp FK, Noel PB, et al. Feasibility of Opportunistic Osteoporosis Screening in Routine Contrast-Enhanced Multi Detector Computed Tomography (MDCT) Using Texture Analysis. *Osteoporos Int* (2018) 29(4):825–35. doi: 10.1007/s00198-017-4342-3
41. Burian E, Subburaj K, Mookiah MRK, Rohrmeier A, Hedderich DM, Dieckmeyer M, et al. Texture Analysis of Vertebral Bone Marrow Using Chemical Shift Encoding-Based Water-Fat MRI: A Feasibility Study. *Osteoporos Int* (2019) 30(6):1265–74. doi: 10.1007/s00198-019-04924-9
42. Genant HK, Wu CY, van Kuijk C, Nevitt MC. Vertebral Fracture Assessment Using a Semiquantitative Technique. *J Bone Miner Res* (1993) 8(9):1137–48. doi: 10.1002/jbmr.5650080915
43. Loffler MT, Jacob A, Scharr A, Sollmann N, Burian E, El Husseini M, et al. Automatic Opportunistic Osteoporosis Screening in Routine CT: Improved Prediction of Patients With Prevalent Vertebral Fractures Compared to DXA. *Eur Radiol* (2021) 31(8):6069–77. doi: 10.1007/s00330-020-07655-2
44. Loffler MT, Sollmann N, Burian E, Bayat A, Aftahy K, Baum T, et al. Opportunistic Osteoporosis Screening Reveals Low Bone Density in Patients With Screw Loosening After Lumbar Semi-Rigid Instrumentation: A Case-Control Study. *Front Endocrinol (Lausanne)* (2020) 11:552719. doi: 10.3389/fendo.2020.552719
45. Sekuboyina A, Husseini ME, Bayat A, Loffler M, Liebl H, Li H, et al. VerSe: A Vertebrae Labelling and Segmentation Benchmark for Multi-Detector CT Images. *Med Image Anal* (2021) 73:102166. doi: 10.1016/j.media.2021.102166
46. Ruschke S, Eggers H, Kooijman H, Diefenbach MN, Baum T, Haase A, et al. Correction of Phase Errors in Quantitative Water-Fat Imaging Using a Monopolar Time-Interleaved Multi-Echo Gradient Echo Sequence. *Magnetic Reson Med: Off J Soc Magnetic Reson Medicine/Society Magnetic Reson Med* (2017) 78(3):984–96. doi: 10.1002/mrm.26485
47. Karampinos DC, Yu H, Shimakawa A, Link TM, Majumdar S. T(1)-Corrected Fat Quantification Using Chemical Shift-Based Water/Fat Separation: Application to Skeletal Muscle. *Magnetic Reson Med: Off J Soc Magnetic Reson Medicine/Society Magnetic Reson Med* (2011) 66(5):1312–26. doi: 10.1002/mrm.22925
48. Liu CY, McKenzie CA, Yu H, Brittain JH, Reeder SB. Fat Quantification With IDEAL Gradient Echo Imaging: Correction of Bias From T(1) and Noise. *Magnetic Reson Med: Off J Soc Magnetic Reson Medicine/Society Magnetic Reson Med* (2007) 58(2):354–64. doi: 10.1002/mrm.21301
49. Boehm C, Diefenbach MN, Makowski MR, Karampinos DC. Improved Body Quantitative Susceptibility Mapping by Using a Variable-Layer Single-Min-Cut Graph-Cut for Field-Mapping. *Magnetic Reson Med: Off J Soc Magnetic Reson Medicine/Society Magnetic Reson Med* (2021) 85(3):1697–712. doi: 10.1002/mrm.28515
50. Ren J, Dimitrov I, Sherry AD, Malloy CR. Composition of Adipose Tissue and Marrow Fat in Humans by 1H NMR at 7 Tesla. *J Lipid Res* (2008) 49(9):2055–62. doi: 10.1194/jlr.D800010-JLR200
51. Dieckmeyer M, Junker D, Ruschke S, Mookiah MRK, Subburaj K, Burian E, et al. Vertebral Bone Marrow Heterogeneity Using Texture Analysis of Chemical Shift Encoding-Based MRI: Variations in Age, Sex, and

Anatomical Location. *Front Endocrinol (Lausanne)* (2020) 11:555931. doi: 10.3389/fendo.2020.555931
52. Sollmann N, Dieckmeyer M, Schlaeger S, Rohrmeier A, Syvaeri J, Diefenbach MN, et al. Associations Between Lumbar Vertebral Bone Marrow and Paraspinal Muscle Fat Compositions-An Investigation by Chemical Shift Encoding-Based Water-Fat MRI. *Front Endocrinol (Lausanne)* (2018) 9:563. doi: 10.3389/fendo.2018.00563
53. Dieckmeyer M, Rayudu NM, Yeung LY, Loffler M, Sekuboyina A, Burian E, et al. Prediction of Incident Vertebral Fractures in Routine MDCT: Comparison of Global Texture Features, 3D Finite Element Parameters and Volumetric BMD. *Eur J Radiol* (2021) 141:109827. doi: 10.1016/j.ejrad.2021.109827
54. Sollmann N, Rayudu NM, Lim JJS, Dieckmeyer M, Burian E, Loffler MT, et al. Multi-Detector Computed Tomography (MDCT) Imaging: Association of Bone Texture Parameters With Finite Element Analysis (FEA)-Based Failure Load of Single Vertebrae and Functional Spinal Units. *Quant Imaging Med Surg* (2021) 11(7):2955–67. doi: 10.21037/qims-20-1156
55. Haralick RM, Shanmugam K, Dinstein I. Textural Features for Image Classification. *IEEE Trans Systems Man Cybernetics* (1973) SMC-3(6):610–21. doi: 10.1109/TSMC.1973.4309314
56. Valentinitsch A, Trebeschi S, Kaesmacher J, Lorenz C, Loffler MT, Zimmer C, et al. Opportunistic Osteoporosis Screening in Multi-Detector CT Images *via* Local Classification of Textures. *Osteoporos Int* (2019) 30(6):1275–85. doi: 10.1007/s00198-019-04910-1
57. Muehlematter UJ, Mannil M, Becker AS, Vokinger KN, Finkenstaedt T, Osterhoff G, et al. Vertebral Body Insufficiency Fractures: Detection of Vertebrae at Risk on Standard CT Images Using Texture Analysis and Machine Learning. *Eur Radiol* (2019) 29(5):2207–17. doi: 10.1007/s00330-018-5846-8
58. Wehrli FW, Ford JC, Attie M, Kressel HY, Kaplan FS. Trabecular Structure: Preliminary Application of MR Interferometry. *Radiology* (1991) 179(3):615–21. doi: 10.1148/radiology.179.3.2027962
59. Wehrli FW, Song HK, Saha PK, Wright AC. Quantitative MRI for the Assessment of Bone Structure and Function. *NMR Biomed* (2006) 19 (7):731–64. doi: 10.1002/nbm.1066
60. Majumdar S, Thomasson D, Shimakawa A, Genant HK. Quantitation of the Susceptibility Difference Between Trabecular Bone and Bone Marrow: Experimental Studies. *Magnetic Reson Med: Off J Soc Magnetic Reson Medicine/Society Magnetic Reson Med* (1991) 22(1):111–27. doi: 10.1002/mrm.1910220112
61. Ma YJ, Chen Y, Li L, Cai Z, Wei Z, Jerban S, et al. Trabecular Bone Imaging Using a 3D Adiabatic Inversion Recovery Prepared Ultrashort TE Cones Sequence at 3T. *Magnetic Reson Med: Off J Soc Magnetic Reson Medicine/Society Magnetic Reson Med* (2020) 83(5):1640–51. doi: 10.1002/mrm.28027
62. Chappard D, Guggenbuhl P, Legrand E, Basle MF, Audran M. Texture Analysis of X-Ray Radiographs Is Correlated With Bone Histomorphometry. *J Bone Miner Metab* (2005) 23(1):24–9. doi: 10.1007/s00774-004-0536-9
63. Kimmel DB, Recker RR, Gallagher JC, Vaswani AS. Aloia JF. A Comparison of Iliac Bone Histomorphometric Data in Post-Menopausal Osteoporotic and Normal Subjects. *Bone Miner* (1990) 11(2):217–35. doi: 10.1016/0169-6009(90)90061-j
64. Zhou J, Damasceno PF, Chachad R, Cheung JR, Ballatori A, Lotz JC, et al. Automatic Vertebral Body Segmentation Based on Deep Learning of Dixon Images for Bone Marrow Fat Fraction Quantification. *Front Endocrinol (Lausanne)* (2020) 11:612. doi: 10.3389/fendo.2020.00612

Conflict of Interest: The authors declare that the research was conducted in the absence of any commercial or financial relationships that could be construed as a potential conflict of interest.

Publisher's Note: All claims expressed in this article are solely those of the authors and do not necessarily represent those of their affiliated organizations, or those of the publisher, the editors and the reviewers. Any product that may be evaluated in this article, or claim that may be made by its manufacturer, is not guaranteed or endorsed by the publisher.

frontiers in Endocrinology

MINI REVIEW
published: 11 March 2022
doi: 10.3389/fendo.2022.853765

The Implications of Bone Marrow Adipose Tissue on Inflammaging

Nicole Aaron[1,2†], *Samantha Costa*[3,4†], *Clifford J. Rosen*[3,4*] *and Li Qiang*[1,5*]

[1] Naomi Berrie Diabetes Center, Columbia University, New York, NY, United States, [2] Department of Pharmacology, Columbia University, New York, NY, United States, [3] Center for Clinical and Translational Research, Maine Medical Center Research Institute, Scarborough, ME, United States, [4] Graduate School of Biomedical Science and Engineering, University of Maine, Orono, ME, United States, [5] Department of Pathology, Columbia University, New York, NY, United States

Once considered an inert filler of the bone cavity, bone marrow adipose tissue (BMAT) is now regarded as a metabolically active organ that plays versatile roles in endocrine function, hematopoiesis, bone homeostasis and metabolism, and, potentially, energy conservation. While the regulation of BMAT is inadequately understood, it is recognized as a unique and dynamic fat depot that is distinct from peripheral fat. As we age, bone marrow adipocytes (BMAds) accumulate throughout the bone marrow (BM) milieu to influence the microenvironment. This process is conceivably signaled by the secretion of adipocyte-derived factors including pro-inflammatory cytokines and adipokines. Adipokines participate in the development of a chronic state of low-grade systemic inflammation (inflammaging), which trigger changes in the immune system that are characterized by declining fidelity and efficiency and cause an imbalance between pro-inflammatory and anti-inflammatory networks. In this review, we discuss the local effects of BMAT on bone homeostasis and the hematopoietic niche, age-related inflammatory changes associated with BMAT accrual, and the downstream effect on endocrine function, energy expenditure, and metabolism. Furthermore, we address therapeutic strategies to prevent BMAT accumulation and associated dysfunction during aging. In sum, BMAT is emerging as a critical player in aging and its explicit characterization still requires further research.

Keywords: inflammation, bone marrow adipocytes, inflammaging, aging, bone marrow adipose tissue (BMAT)

OPEN ACCESS

Edited by:
Jason Horton, Upstate Medical University, United States

Reviewed by:
Michael Dieckmeyer, Technical University of Munich, Germany

***Correspondence:**
Clifford J. Rosen
rosenc@mmc.org
Li Qiang
lq2123@cumc.columbia.edu

[†]These authors have contributed equally to this work and share first authorship

Specialty section:
This article was submitted to Bone Research, a section of the journal Frontiers in Endocrinology

Received: *13 January 2022*
Accepted: *16 February 2022*
Published: *11 March 2022*

Citation:
Aaron N, Costa S, Rosen CJ and Qiang L (2022) The Implications of Bone Marrow Adipose Tissue on Inflammaging. Front. Endocrinol. 13:853765. doi: 10.3389/fendo.2022.853765

INTRODUCTION

All tissues are affected by aging, but diseases that weaken the skeleton constitute the most prevalent chronic impairments in the United States (1–3). Skeletal diseases and related conditions are of grave concern among the aging population as they have the potential to significantly compromise systemic and local functions and diminish quality of life. The increase in bone marrow adiposity (BMA) over a lifetime is thought to be a major contributor to age-associated chronic conditions such as osteoporosis, osteoarthritis, and cancer (4–7). Qualitative studies have reported changes in the bone marrow (BM) of humans since 1882 when Ernest Neumann recognized aging resulted in trabecular bone loss and most of the BM consisted of adipose tissue (8). Since then, studies in both rodents and humans have validated that aging is associated with a significant increase in bone marrow adipose tissue (BMAT) (9, 10) with a concurrent decline in bone mineral density (11). Over

the years, considerable advancements have been made related to BM imaging and BMAT quantification in humans and rodents. In humans, quantitative magnetic resonance imaging (MRI) and spectroscopy (MRS) allows for noninvasive monitoring of BMAT development and expansion (12–15). This compares to osmium tetroxide and contrast enhanced computed tomography, considered the gold standard in rodents, which provides both volumetric and spatial quantification of BMAT (16). Notwithstanding the advances in methodologies, BMAT represents an understudied aspect of adipocyte biology. Distinct from peripheral adipose tissue, BMAT displays a unique response to physiological changes (i.e., aging, exercise, cold exposure, nutritional variations like high-fat diet and fasting) (17–20). Furthermore, given its unique location, BMAT directly influences mechanisms of bone remodeling, hematopoiesis, and inflammation within the BM microenvironment (21, 22).

In general, aging is associated with impaired tissue regeneration that is congruent with increased BMA and an inflammaging phenotype. Inflammaging is characterized by unresolved and uncontrolled inflammation and a dysfunctional immune response that exacerbate the aging process and age-related chronic diseases (23, 24). Furthermore, this process is believed to exacerbate the decline in the regenerative capacity of the skeleton (25) by affecting bone marrow stromal cell (BMSC) proliferation, frequency, and fate determination (25). With recent evidence supporting BMAT as an endocrine and paracrine organ capable of local regulation of the BM microenvironment, it is important to further understand the relationship between bone marrow adipocytes (BMAds) and the observed inflammaging phenotype in aging.

THE EFFECTS OF BMA ON BONE MARROW STROMAL CELLS AND HEMATOPOIETIC STEM CELLS

BMA and BMSC Potential

As we age, our capacity for tissue repair and regeneration in response to injury declines (**Figure 1**). Accordingly, bone repair is delayed and impaired as well. BMSCs are the foundation of bone regeneration by serving as the progenitor cells of osteoblasts as well as of adipocytes (26, 27). In addition, BMSCs support proliferation and differentiation of hematopoietic stem cells (HSCs), promote HSC engraftment in animal models, and can decrease inflammation under normal conditions (28). However, aging affects BMSCs through intrinsic and extrinsic factors. Intrinsically, BMSCs accumulate DNA damage, reactive oxygen species (ROS), and damaged proteins that may promote aging (29). Extrinsically, the composition of the BM niche and the growth factors and cytokines that are secreted into the local environment change with age (29) (**Table 1**). In particular, the increase in BMAds may disrupt the microenvironment structure and alter the fate of BMSCs. Age-related bone loss has thought to be driven in part by a decline in BMSC proliferation and function as well as

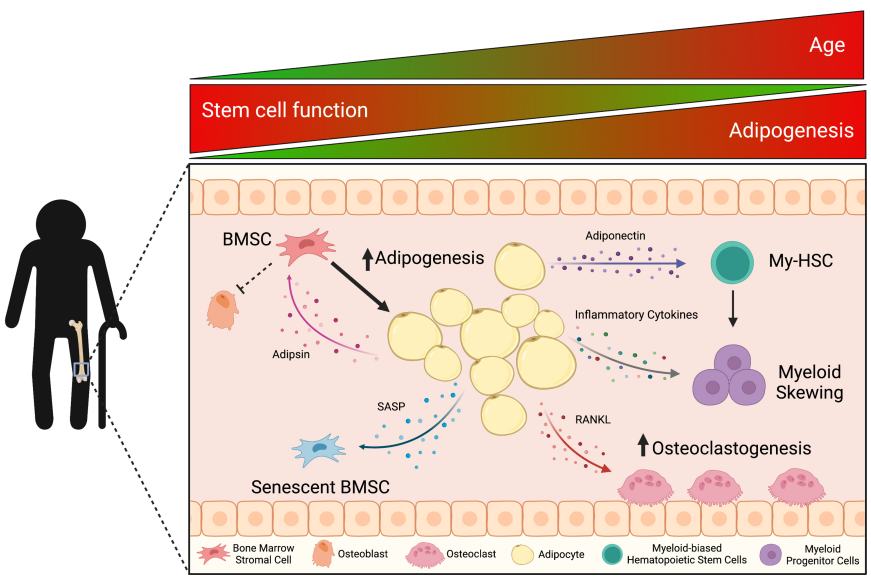

FIGURE 1 | With age, the accumulation of bone marrow adipocyte (BMAd)-derived factors influences mechanisms of bone remodeling, hematopoiesis, and inflammation, which triggers a cascade effect within the bone marrow (BM) microenvironment. Aging is associated with increased bone marrow adiposity (BMA) and decreased bone mineral density. These classic characteristics of aging result from adipsin priming bone marrow stromal cells (BMSCs) towards adipogenesis and adipocytes (including pre-adipocytes in aged mice) secreting the pro-osteoclastic factor, RANKL. Adipocytes also secrete adiponectin and pro-inflammatory cytokines that skew hematopoietic stem cell differentiation towards the myeloid lineage, which is observed in the chronic inflammatory state of aging (inflammaging). In the BM, this pro-inflammatory microenvironment leads to senescence-associated secretory phenotype (SASP) factors decreasing BMSC potential and functionality. *This figure was created using BioRender.com*.

TABLE 1 | BMAT-derived factors and the age-associated phenotype.

Age-Related Mechanism	Secreted Factors	Associated Effect	References
BMSC Potential	IL-1α TNF-α RELA	↓ skeletal stem/progenitor cell number and function ↓ osteoblastogenesis	Josephson (25)
Bone Loss	PPARγ	↑ adipogenesis	Fazeli (9)
	RANKL,	↓ osteoblastogenesis	Goto 2011 (55), Hardouin (30)
	Leptin, Resistin, Chemerin	↑ osteoclastogenesis	Hamrick (31), Thommesen (32), Han (33)
	Adipsin	-pro-inflammatory; regulates adipogenesis -prime BMSC differentiation towards adipogenesis	Aaron (19)
Hematopoietic Cells	Adiponectin	-prevents progenitor expansion ↑ myeloid skewing of HSCs ↓ BM cellularity	DiMascio (34), Naveiras (35) Pang (36), Ogawa (37)
Decreased Immune Fidelity	IL-6	-can alter immune response and hematopoiesis	Tanaka (38), Udagawa (39)
	IL-1, NLRP3	-inhibits B lymphopoiesis	Kennedy (40)
	CCL2/MCP-1 COX-2	-induces the differentiation of immunoregulatory cells like regulatory T-cells and MDSCs -induces macrophage migration	Wang (41), Sinha (42), Mahic (43), Obermajer (44)
Cellular Senescence	NF-kB (pro-inflammatory gene)	↑ pro-inflammatory cytokines	Miggitsch (45), Pangrazzi (23)
	IL-1α, IL-1β, TGF-β (pro-inflammatory cytokines)	↑ ROS	da Silva (46)
	p21, p16 (tumor suppressing genes)	↓ proliferative and differentiation capacities of surrounding cells	Josephson (25),
	CXCL1/2, CCL2/MCP-1 (chemokines)	↓ stem/progenitor cell number and functionality	Kovtonyuk (47)

↓ = *down-regulates/decreases;* ↑ = *up-regulates/increases.*

increased commitment of BMSCs to adipogenic lineages (48). At the cellular level, the BMSC pool in the BM niche shows a biased differentiation towards adipogenesis at the cost of osteoblastogenesis in aging (48). Despite their regenerative capabilities, BMSCs were shown to have decreased differentiation potential when exposed to inflammatory environments (49). Josephson et al. revealed that skeletal stem/progenitor cell (SSPC) frequency significantly declined with increased age, and this directly correlated to a longer fracture healing time in a human cohort (25). Using *in vivo* and *in vitro* models, the authors recapitulated reduced bone healing commonly associated with advanced aging. SSPCs cultured with 52-week-old serum began to express pro-inflammatory cytokines (elevated IL-1a, TNF-a, RELA expression), illustrating the declined SSPC number and function were negatively affected by the cytokine milieu associated with age (25). The expansion of BMAT, which is known to actively produce pro-inflammatory factors, likely exacerbates this effect (45).

Adipogenesis and Bone Loss

Aging studies have shown increased BMAT coincides with decreased bone mass, suggestive of a link between bone formation and BMA. The general understanding is a common progenitor cell undergoes adipogenesis at the expense of osteogenesis (27, 48, 50, 51). For example, it has been shown that upregulation of PPARγ promotes the differentiation of BMSCs into adipocytes while repressing osteoblast differentiation. In aging, the increased expression of PPARγ in the BM leads to enhanced adipogenesis and reduced osteogenesis (9). In addition to expression, post-translational modification of PPARγ, particularly acetylation, is also critical to this lineage determination (19, 52) thus, PPARγ is appreciated as a critical lineage-switching regulator. However, this bifurcated differentiation path between adipocytes and osteoblasts has remained poorly understood, despite the elucidation of PPARγ expression in the BM. Recent studies have delineated mesenchymal progenitors to their bi-lineage differentiation stages and characterized non-proliferative, adiponectin-expressing BMAd precursors, termed MALPs (marrow adipogenic lineage precursor) (53). These are thought to secrete a number of factors that can drive bone loss such as RANKL. Upon maturation, BMAT is responsible for the release of adipokines and free fatty acids that potentially interfere with bone formation (19, 52). For example, adipsin is among the group of adipokines released by BMAT expansion that has been shown to retroactively affect BMSC differentiation by priming these cells toward adipogenesis (19).

Coinciding with the increase in BMA, often an age-related decline in trabecular bone volume, but not in cortical bone, is observed (9). The impaired skeletal health with aging is accounted for not only by defective bone formation capabilities but also by accelerated bone resorption through increased osteoclast number and/or activity (54). In contrast to the repressive function on osteoblasts, BMAds play a favorable role on osteoclasts. Primary human femoral BMAds were shown to express the pro-osteoclastogenic factor, RANKL, and through direct cell contact mediate the differentiation of osteoclast precursors (30, 55, 56). In murine studies, an age-dependent increase in osteoclastogenesis was observed (57). Additionally, RANKL expression was shown to be associated with BMAd differentiation and with pre-adipocytes in the BM of aged mice

(30, 58). This creates a self-reinforcing cycle of osteoclastogenesis and adipogenesis which leads to increased deleterious effects on the bone architecture and increases the incidences of fractures within the elderly (54). Furthermore, osteoblasts in aged mice (16 months old) were found to exhibit markedly impaired adhesion to the bone surface and significantly reduced mineralization (59). Thus, the age-associated decline in bone mass is an integrative pathology of BMAds filling the BM cavity and their crosstalk to bone remodeling cells.

BMA and Hematopoietic Cells

While BMAds have a defined function as regulators of bone turnover, evidence also suggests BMAT impacts hematopoietic activity (45, 48). Human BMAds were reported to support differentiation of $CD34^+$ HSCs into myeloid and lymphoid immune cells (60). Accordingly, myelopoiesis was shown to positively correlate with increased adipogenesis and reduced osteoblastogenesis in the senescence-accelerated mouse prone 6 (SAMP6) mouse model, representative of advanced aging (61). In diet-induced obese mice an enhancement in hematopoietic and lymphopoietic BM cell populations were correlated with increased marrow adiposity (62). In contrast, lipid-laden BMAds were linked to the suppression of growth and differentiation of HSCs (35, 63) and were considered negative regulators of the hematopoietic niche (64, 65). This suppressive activity was primarily attributed to reduced production of granulocyte-macrophage colony-stimulating factor (GM-CSF) and granulocyte colony-stimulating factor (G-CSF) as well as increased secretion of neuropilin and lipocalin-2 (35, 66, 67). Of note, BMAds are a significant source of plasma adiponectin in mice during calorie restriction and in cancer patients receiving radiotherapy or chemotherapy (20). Moreover, increased BMA during aging has been negatively correlated to hematopoietic cell function during aging through the secretion of adiponectin (20). Adiponectin appears to positively affect multipotent stem cells proliferation, but not more committed progenitor cells (34), a phenomenon suspected in preserving the HSC pool while preventing progenitor expansion (35). This ultimately highlights the anti-inflammatory properties of adiponectin (68) and the dynamic relationship between BMAds and the hematopoietic niche. Overall, aging in humans and mice, a process associated with increased BMA (69–71), induces myeloid skewing in HSCs (36), while promoting an overall decrease in BM cellularity (37).

AGE-RELATED BMAT EXPANSION RESULTS IN DECREASED IMMUNE FIDELITY AND CELLULAR SENESCENCE

Decreased Immune Fidelity

With aging, inflammaging is thought to be a major contributor to the decline in fidelity and efficiency of the immune system. The immune system waxes and wanes in response to stimuli. A decline in immunocompetency or the capacity for a normal functioning immune system with aging can increase susceptibility to infections, decrease the number of T- and B-cells as myelopoiesis occurs (the process in which innate immune cells develop from myeloid progenitor cells), and increase the prevalence of autoimmune diseases (47). Gasparrini et al. analyzed cytokines produced by BMAT and found 53 proteins upregulated in aging (72), one of which they identified as IL-6, a well-known pro-inflammatory protein that can affect immune response, hematopoiesis, and suppress bone formation (38, 39). *In vitro* cultures of BMAds were shown to secrete adipocyte-derived soluble factors that inhibit B lymphopoiesis, particularly at the earliest progenitor stage in which differentiation into pre-pro B-cells occurs, while simultaneously promoting the differentiation and subsequent proliferation of HSCs towards the myeloid lineage (73). In humans and mice (74–76), B lymphopoiesis wanes in mid (77) and late stages of life (73, 78, 79). In mice, the decline in B lymphopoiesis has been attributed to BMAds altering the BM stroma and/or by direct action on hematopoietic progenitors (77–79). Kennedy et al. revealed that BMAds induce myeloid-derived suppressor cells (MDSCs), particularly in mononuclear cells ($CD11b^+Ly6C^+Ly6G^-$), which inhibit B lymphopoiesis by producing IL-1 (80). Additionally, BMAds can also activate inflammasomes, such as the nod-like receptor 3 (NLRP3), which directly inhibit B lymphopoiesis (40). Activation of inflammasomes can stimulate thymic degeneration (81, 82) and exert a negative effect on T-cell proliferation (83), likely contributing to systemic inflammatory conditions associated with advanced age.

There is growing evidence to support the involvement of chemokines such as C-motif chemokine ligand 2/monocyte chemoattractant protein 1 (CCL2/MCP-1) and cyclooxygenase-2 (COX-2) in regulation of the BM microenvironment (84). During inflammatory events, high expression of COX-2 is often coupled with CCL2/MCP-1 upregulation (85–87). The major COX-2 metabolite, prostaglandin E2 (PGE2), is known to induce differentiation of immunoregulatory cells like regulatory T-cells and MDSCs (41–44). Cox-2 inhibitors prevent CCL2/MCP-1 production by activated macrophages (88, 89). Under normal physiological conditions, COX-2 expression in macrophages is low but is increased in response to pro-inflammatory stimuli (90). In fact, the COX-2 expression and PGE2 release by macrophages were shown to be stimulated by CCL2/MCP-1 and to be important for macrophage migration (91–93). *In vitro* studies using conditioned media from BMAds demonstrated that macrophages are highly stimulated by BMAd-derived factors and that invasiveness increases with age (94). Obesity phenocopies aging with increased BMA, which has been shown to induce CCL2/MCP-1 and COX-2 within the BM (94), emphasizing a close relationship between immune response and BMA.

Cellular Senescence

Aging studies have consistently shown a strong correlation between increased BMA and pro-inflammatory factors (18). It has been suggested that a sustained pro-inflammatory state may negatively impact the proliferative and differentiation capacities of surrounding cells. This effect is referred to as the "bystander effect" and most notably contributes to the accumulation of

senescent cells in the BM, a process that naturally occurs with aging (46). Despite studies finding relatively low percentages (10–20%) of senescent cells in aged BMSCs, the bystander effect greatly impairs osteogenic capacities of non-senescent BMSCs, likely through senescence-associated secretory phenotype (SASP) factors (IL-1α, IL-1β, NF-κB, CXCL1/2, TGF-β, p21, p16, CCL2/MCP-1) and the resulting inflammation (95, 96).

BMAT expansion induces pro-inflammatory cytokines, which perpetuates the damaging effects on neighboring cells (46). In this pro-inflammatory microenvironment, BMSCs become senescent, resulting in decreased stem/progenitor cell number and decreased functionality (25, 47). In addition, the increased levels of pro-inflammatory cytokines promote ROS within the BM, further contributing to cellular senescence (23, 45). Flow cytometry analysis by Miggitsch et al. highlighted BMAds as a major contributor of ROS by determining higher ROS levels within femoral BMAds compared to subcutaneous white adipose tissue (WAT) from the thigh (45). Treatment of both tissues with ROS scavengers, N-acetylcysteine (NAC) and vitamin C, significantly reduced ROS levels within the BMAT compared to the WAT (45). The role of ROS in hematopoiesis has been well documented, thus these results demonstrate that BMAds limit the capacity of BMSCs to support the hematopoietic niche (97, 98).

Mimicking the potential effect of increased BMAT, Lo et al. showed that in conditions of elevated glucose *in vitro*, β-galactosidase activity and adipogenic differentiation markers (*Pparγ* and *Fas*) were notably increased while osteogeneic markers (*Runx2* and *Col1a1*) were decreased in BMSCs, indicative of altered differentiation potential (99). This hyperglycemic condition induces inflammation and senescence through oxidant-mediated autophagy, ultimately contributing to dysfunction of bone development and hematopoiesis in the BM microenvironment (100). BMP-2, an established pro-osteoblastogenic protein, can stimulate bone production in healthy, non-senescent BMSCs. However, in senescent cells recombinant BMP-2 upregulates pathways of inflammation, adipogenesis, and cell apoptosis (101). In mouse models, FOXP1, a regulator of the pro-adipogenic CEBPβ/δ complex in BMAT, has been shown to attenuate senescence through repressing $p16^{INK4A}$ (encoded by *CDKN2A*), a cell cycle repressor that functions by inducing a G1 phase arrest (102). Collectively, BMAds play a critical role in inducing senescence of BMSCs, thereby determining the microenvironmental status in the BM compartment during aging.

POTENTIAL TARGETS FOR AGE-RELATED BONE CONDITIONS

Senolytics

Senolytics are a class of drugs that selectively induce apoptosis in senescent cells. Studies have shown reductions in age-related chronic inflammation led to functional restoration of bone regeneration through decreased senescence, increased stem/progenitor cell number, and increased osteogenic gene expression (25). In a pharmacological rescue experiment, Zhou et al. showed that BMSCs from aged mice (27 months old) had lower proliferation rates (30%) than young, 3-month-old mice (45%) (95). Twenty-four-hour treatment with dasatinib (generic chemotherapy; tyrosine kinase inhibitor) and quercetin (flavonol; antioxidant and chelating abilities) increased proliferation rates of the old BMSCs to 40% but did not affect the proliferative rates of the young BMSCs (95, 103, 104). Furthermore, dasatinib and quercetin treatments have been shown to improve osteogenic capacity in the aged BMSCs and reduce their expression of several senescence-related and inflammation markers including p21, $p16^{INK4A}$, IL-6, CXCL1 and MCP-1 (95) in multiple aged tissues (105, 106). Therefore, clearance of senescent cells by senolytics shows promise in improving osteogenesis of aged BMSCs and ameliorating BM inflammation.

miRNAs

In the past few decades, microRNAs (miRNAs) have emerged as key regulators of different aspects in development, homeostasis, and function. However, only a handful of miRNAs have been identified as capable of mediating adipocyte differentiation and function (107, 108). Multiple studies have implicated a potential role for miRNAs on post-transcriptional regulation of BMSC differentiation and aging (109, 110). For example, mice lacking miR-188, an age-associated miRNA found in the BM, showed substantial protection from bone loss and BMAT accumulation over time (109). In comparison, BMSCs transfected with miR-183-5p mimicked reduced cell proliferation and osteogenic differentiation and demonstrated increased cellular senescence (111). Therefore, miRNAs represent a unique class of therapeutic targets of bone inflammaging, given that their specific roles in the BM during aging become elucidated.

Antioxidants

Given the positive effect of low-glucose conditions on senescent BMSCs, methods for glucose reduction have the potential to improve BM health through increasing mitochondrial respiration (99). Studies have shown that restricted glucose conditions increase the presence of antioxidant enzymes and decrease superoxide production, highlighting a therapeutic role for antioxidant defenses (99). An antioxidant and free radical scavenger, apocynin, was used to establish potential inhibition of cellular senescence, even in a senescence-accelerated mouse model, while concurrently improving osteogenesis (112). Similarly, treatment of aged rats with the aforementioned ROS scavenger, NAC, displayed an improved bone phenotype (113). Natural antioxidants have the potential to ameliorate concerns of age-related BMAT expansion. For example, phloretin, a flavonoid commonly found in apples, activates osteogenic gene OPG while promoting BMAd apoptosis to promote osteoblast differentiation, even in aged BMSCs (114). Given what we know about the link between inflammation and aging, it is not surprising to note that in addition to antioxidants, nonsteroidal anti-inflammatory drugs such as aspirin have been shown to counteract the effects of BMSCs senescence by improving cell proliferation and osteogenic differentiation (115, 116).

Adipokines

Adipokines have the potential to regulate physiological functions including satiety, glucose homeostasis, energy expenditure (117), and inflammation (118). As a major regulator of the bone marrow niche with changes during inflammation and aging, adipokines are of great potential for future therapeutics. Numerous cytokines such as CCL2/MCP-1 (94), IL-6, and TNF-α (119) have elucidated roles in linking BMA with bone loss through inflammation. Of note, existing anti-TNF-α therapy infliximab and other TNF-α inhibitors have been shown to prevent age-related bone loss in various conditions (120, 121). In addition, pro-inflammatory adipokines shown to drive decline in bone health include leptin (31), resistin (32), chemerin (33), and adipsin (19). Among them, adipsin provides a straightforward relationship that might be of interest therapeutically by being produced abundantly in the BM and directly priming BMSCs. Furthermore, adipsin is involved in the alternative pathway (AP) of the complement system, a known activator of inflammation in the bone marrow further contributing to bone loss conditions (122–125). In human studies, patients with bone-related conditions such as post-menopausal bone loss and osteoarthritis displayed an increase in serum adipsin levels positively associated with other pro-inflammatory cytokines (126, 127). As such, current pharmacological advancements including the synthesis and pre-clinical characterization of adipsin inhibitors targeting the AP may be of interest in addressing inflammaging and bone loss (128).

CONCLUSION

The development of BMAT is a normal physiological process and is arguably of importance in regulating BM microenvironment, skeletal homeostasis, hematopoiesis, endocrine function, and energy expenditure, and metabolism. However, extensive BMAT accumulation that occurs with aging and in clinical conditions such as obesity, calorie restriction/anorexia (20, 129), and in response to chemotherapy and irradiation treatments (130–132), suggests that aberrant BMAT formation has pathological implications. The increased adiposity within the BM exacerbates age-related inflammation and contributes to reduced bone health through physical changes in the bone matrix and defects in the BM stroma and HSCs. Ultimately, the age-associated shift of BMSCs toward adipogenesis promotes increased ROS, reduced HSC potential, dysfunctional immune cell response through increased myelopoiesis, and cellular senescence. As such, therapeutic interventions to maintain BMAT in appropriate quantity and quality may improve overall bone health, inflammaging, and senescence, further contributing to increases in life expectancy and quality of life for the elderly population.

AUTHOR CONTRIBUTIONS

NA and SC have contributed equally to this work and share first authorship. NA and SC wrote the manuscript. LQ and CR advised and edited the manuscript. All authors contributed to manuscript revision and approved the submitted version.

FUNDING

Funding was supplied by the NIH/NIDDK R24 DK092759-06 (CR), NIH U19AG060917 (CR), NIH/NIDDK R01 DK112943-05 (LQ), R01 DK128848 (LQ), and NIH/NIDDK F31 DK124926 (NA).

ACKNOWLEDGMENTS

The authors would like to acknowledge Samantha Costa and Clifford Rosen (Maine Medical Center Research Institute) for the publication and licensing rights to use BioRender.com.

REFERENCES

1. Burge R, Dawson-Hughes B, Solomon DH, Wong JB, King A, Tosteson A. Incidence and Economic Burden of Osteoporosis-Related Fractures in the United States, 2005-2025. *J Bone Miner Res* (2007) 22:465–75. doi: 10.1359/jbmr.061113
2. Williams SA, Daigle SG, Weiss R, Wang Y, Arora T, Curtis JR. Economic Burden of Osteoporosis-Related Fractures in the US Medicare Population. *Ann Pharmacother* (2021) 55:821–9. doi: 10.1177/1060028020970518
3. Williams SA, Chastek B, Sundquist K, Barrera-Sierra S, Leader D, Weiss RJ, et al. Economic Burden of Osteoporotic Fractures in US Managed Care Enrollees. *Am J Manage Care* (2020) 26:E142–9. doi: 10.37765/ajmc.2020.43156
4. Ganguly P, El-Jawhari JJ, Giannoudis PV, Burska AN, Ponchel F, Jones EA. Age-Related Changes in Bone Marrow Mesenchymal Stromal Cells: A Potential Impact on Osteoporosis and Osteoarthritis Development. *Cell Transplant* (2017) 26:1520–9. doi: 10.1177/0963689717721201
5. Sanghani-Kerai A, Osagie-Clouard L, Blunn G, Coathup M. The Influence of Age and Osteoporosis on Bone Marrow Stem Cells From Rats. *Bone Jt Res* (2018) 7:289–97. doi: 10.1302/2046-3758.74.BJR-2017-0302.R1
6. Jaul E, Barron J. Age-Related Diseases and Clinical and Public Health Implications for the 85 Years Old and Over Population. *Front Public Heal* (2017) 5:335. doi: 10.3389/fpubh.2017.00335
7. Luo G, He Y, Yu X. Bone Marrow Adipocyte: An Intimate Partner With Tumor Cells in Bone Metastasis. *Front Endocrinol (Lausanne)* (2018) 9:339. doi: 10.3389/fendo.2018.00339
8. Nehlin JO, Jafari A, Tencerova M, Kassem M. Aging and Lineage Allocation Changes of Bone Marrow Skeletal (Stromal)Stem Cells. *Bone* (2019) 123:265–73. doi: 10.1016/j.bone.2019.03.041
9. Fazeli PK, Horowitz MC, MacDougald OA, Scheller EL, Rodeheffer MS, Rosen CJ, et al. Marrow Fat and Bone-New Perspectives. *J Clin Endocrinol Metab* (2013) 98:935–45. doi: 10.1210/jc.2012-3634
10. Justesen J, Stenderup K, Ebbesen EN, Mosekilde L, Steiniche T, Kassem M. Adipocyte Tissue Volume in Bone Marrow is Increased With Aging and in Patients With Osteoporosis. *Biogerontology* (2001) 2:165–71. doi: 10.1023/A:1011513223894
11. Shen W, Chen J, Punyanitya M, Shapses S, Heshka S, Heymsfield SB. MRI-Measured Bone Marrow Adipose Tissue is Inversely Related to DXA-Measured Bone Mineral in Caucasian Women. *Osteoporos Int* (2007) 18:641–7. doi: 10.1007/s00198-006-0285-9

12. Ruschke S, Pokorney A, Baum T, Eggers H, Miller JH, Hu HH, et al. Measurement of Vertebral Bone Marrow Proton Density Fat Fraction in Children Using Quantitative Water-Fat MRI. *MAGMA* (2017) 30:449–60. doi: 10.1007/S10334-017-0617-0
13. Karampinos DC, Ruschke S, Dieckmeyer M, Diefenbach M, Franz D, Gersing AS, et al. And Spectroscopy of Bone Marrow. *J Magn Reson Imaging* (2018) 47:332–53. doi: 10.1002/JMRI.25769
14. Baum T, Rohrmeier A, Syväri J, Diefenbach MN, Franz D, Dieckmeyer M, et al. Anatomical Variation of Age-Related Changes in Vertebral Bone Marrow Composition Using Chemical Shift Encoding-Based Water-Fat Magnetic Resonance Imaging. *Front Endocrinol (Lausanne)* (2018) 9:141. doi: 10.3389/FENDO.2018.00141
15. Singhal V, Bredella MA. Marrow Adipose Tissue Imaging in Humans. *Bone* (2019) 118:69–76. doi: 10.1016/j.bone.2018.01.009
16. Scheller EL, Troiano N, Vanhoutan JN, Bouxsein MA, Fretz JA, Xi Y, et al. Use of Osmium Tetroxide Staining With Microcomputerized Tomography to Visualize and Quantify Bone Marrow Adipose Tissue *In Vivo*, in: Methods Enzymol. *Methods Enzymol* (2014) 537:123–39. doi: 10.1016/B978-0-12-411619-1.00007-0
17. Suchacki KJ, Tavares AAS, Mattiucci D, Scheller EL, Papanastasiou G, Gray C, et al. Bone Marrow Adipose Tissue is a Unique Adipose Subtype With Distinct Roles in Glucose Homeostasis. *Nat Commun* (2020) 11:3097. doi: 10.1038/s41467-020-16878-2
18. Mancuso P, Bouchard B. The Impact of Aging on Adipose Function and Adipokine Synthesis. *Front Endocrinol (Lausanne)* (2019) 10:137. doi: 10.3389/fendo.2019.00137
19. Aaron N, Kraakman MJ, Zhou Q, Liu Q, Costa S, Yang J, et al. Adipsin Promotes Bone Marrow Adiposity by Priming Mesenchymal Stem Cells. *Elife* (2021) 10:e69209. doi: 10.7554/eLife.69209
20. Cawthorn WP, Scheller EL, Learman BS, Parlee SD, Simon BR, Mori H, et al. Bone Marrow Adipose Tissue is an Endocrine Organ That Contributes to Increased Circulating Adiponectin During Caloric Restriction. *Cell Metab* (2014) 20:368–75. doi: 10.1016/j.cmet.2014.06.003
21. Ferland-McCollough D, Maselli D, Spinetti G, Sambataro M, Sullivan N, Blom A, et al. MCP-1 Feedback Loop Between Adipocytes and Mesenchymal Stromal Cells Causes Fat Accumulation and Contributes to Hematopoietic Stem Cell Rarefaction in the Bone Marrow of Patients With Diabetes. *Diabetes* (2018) 67:1380–94. doi: 10.2337/db18-0044
22. Veldhuis-Vlug AG, Rosen CJ. Clinical Implications of Bone Marrow Adiposity. *J Intern Med* (2018) 283:121–39. doi: 10.1111/joim.12718
23. Pangrazzi L, Meryk A, Naismith E, Koziel R, Lair J, Krismer M, et al. "Inflamm-Aging" Influences Immune Cell Survival Factors in Human Bone Marrow. *Eur J Immunol* (2017) 47:481–92. doi: 10.1002/eji.201646570
24. Chung HY, Kim DH, Lee EK, Chung KW, Chung S, Lee B, et al. Redefining Chronic Inflammation in Aging and Age-Related Diseases: Proposal of the Senoinflammation Concept. *Aging Dis* (2019) 10:367–82. doi: 10.14336/AD.2018.0324
25. Josephson AM, Bradaschia-Correa V, Lee S, Leclerc K, Patel KS, Lopez EM, et al. Age-Related Inflammation Triggers Skeletal Stem/Progenitor Cell Dysfunction. *Proc Natl Acad Sci U S A* (2019) 116:6995–7004. doi: 10.1073/pnas.1810692116
26. Owen M, Friedenstein AJ. Stromal Stem Cells: Marrow-Derived Osteogenic Precursors. *Ciba Found Symp* (1988) 136:42–60. doi: 10.1002/9780470513637.ch4
27. Tencerova M, Kassem M. The Bone Marrow-Derived Stromal Cells: Commitment and Regulation of Adipogenesis. *Front Endocrinol (Lausanne)* (2016) 7:127. doi: 10.3389/fendo.2016.00127
28. Noort WA, Kruisselbrink AB, In't Anker PS, Kruger M, Van Bezooijen RL, De Paus RA, et al. Mesenchymal Stem Cells Promote Engraftment of Human Umbilical Cord Blood-Derived CD34+ Cells in NOD/SCID Mice. *Exp Hematol* (2002) 30:870–8. doi: 10.1016/S0301-472X(02)00820-2
29. Liu H, Xia X, Li B. Mesenchymal Stem Cell Aging: Mechanisms and Influences on Skeletal and non-Skeletal Tissues. *Exp Biol Med* (2015) 240:1099–106. doi: 10.1177/1535370215591828
30. Hardouin P, Rharass T, Lucas S. Bone Marrow Adipose Tissue: To Be or Not To Be a Typical Adipose Tissue? *Front Endocrinol (Lausanne)* (2016) 7:85. doi: 10.3389/fendo.2016.00085
31. Hamrick MW, Pennington C, Newton D, Xie D, Isales C. Leptin Deficiency Produces Contrasting Phenotypes in Bones of the Limb and Spine. *Bone* (2004) 34:376–83. doi: 10.1016/j.bone.2003.11.020
32. Thommesen L, Stunes AK, Monjo M, Grøsvik K, Tamburstuen MV, Kjøbli E, et al. Expression and Regulation of Resistin in Osteoblasts and Osteoclasts Indicate a Role in Bone Metabolism. *J Cell Biochem* (2006) 99:824–34. doi: 10.1002/JCB.20915
33. Han L, Zhang Y, Wan S, Wei Q, Shang W, Huang G, et al. Loss of Chemerin Triggers Bone Remodeling *In Vivo* and *In Vitro*. *Mol Metab* (2021) 53:101322. doi: 10.1016/j.molmet.2021.101322
34. DiMascio L, Voermans C, Uqoezwa M, Duncan A, Lu D, Wu J, et al. Identification of Adiponectin as a Novel Hemopoietic Stem Cell Growth Factor. *J Immunol* (2007) 178:3511–20. doi: 10.4049/jimmunol.178.6.3511
35. Naveiras O, Nardi V, Wenzel PL, Hauschka PV, Fahey F, Daley GQ. Bone-Marrow Adipocytes as Negative Regulators of the Haematopoietic Microenvironment. *Nature* (2009) 460:259–63. doi: 10.1038/nature08099
36. Pang WW, Price EA, Sahoo D, Beerman I, Maloney WJ, Rossi DJ, et al. Human Bone Marrow Hematopoietic Stem Cells are Increased in Frequency and Myeloid-Biased With Age. *Proc Natl Acad Sci U S A* (2011) 108:20012–7. doi: 10.1073/pnas.1116110108
37. Ogawa T, Kitagawa M, Hirokawa K. Age-Related Changes of Human Bone Marrow: A Histometric Estimation of Proliferative Cells, Apoptotic Cells, T Cells, B Cells and Macrophages. *Mech Ageing Dev* (2000) 117:57–68. doi: 10.1016/S0047-6374(00)00137-8
38. Tanaka T, Narazaki M, Kishimoto T. Il-6 in Inflammation, Immunity, And Disease. *Cold Spring Harb Perspect Biol* (2014) 6:a016295. doi: 10.1101/cshperspect.a016295
39. Udagawa N, Takahashi N, Katagiri T, Tamura T, Wada S, Findlay DM, et al. Interleukin (IL)-6 Induction of Osteoclast Differentiation Depends on IL-6 Receptors Expressed on Osteoblastic Cells But Not on Osteoclast Progenitors. *J Exp Med* (1995) 182:1461–8. doi: 10.1084/jem.182.5.1461
40. Kennedy DE, Knight KL. Inflammatory Changes in Bone Marrow Microenvironment Associated With Declining B Lymphopoiesis. *J Immunol* (2017) 198:3471–9. doi: 10.4049/jimmunol.1601643
41. Wang D, Dubois RN. Eicosanoids and Cancer. *Nat Rev Cancer* (2010) 10:181–93. doi: 10.1038/nrc2809
42. Sinha P, Clements VK, Fulton AM, Ostrand-Rosenberg S. Prostaglandin E2 Promotes Tumor Progression by Inducing Myeloid-Derived Suppressor Cells. *Cancer Res* (2007) 67:4507–13. doi: 10.1158/0008-5472.CAN-06-4174
43. Mahic M, Yaqub S, Johansson CC, Taskén K, Aandahl EM. FOXP3+CD4+CD25+ Adaptive Regulatory T Cells Express Cyclooxygenase-2 and Suppress Effector T Cells by a Prostaglandin E2-Dependent Mechanism. *J Immunol* (2006) 177:246–54. doi: 10.4049/jimmunol.177.1.246
44. Obermajer N, Muthuswamy R, Lesnock J, Edwards RP, Kalinski P. Positive Feedback Between PGE2 and COX2 Redirects the Differentiation of Human Dendritic Cells Toward Stable Myeloid-Derived Suppressor Cells. *Blood* (2011) 118:5498–505. doi: 10.1182/blood-2011-07-365825
45. Miggitsch C, Meryk A, Naismith E, Pangrazzi L, Ejaz A, Jenewein B, et al. Human Bone Marrow Adipocytes Display Distinct Immune Regulatory Properties. *EBioMedicine* (2019) 46:387–98. doi: 10.1016/j.ebiom.2019.07.023
46. da Silva PFL, Ogrodnik M, Kucheryavenko O, Glibert J, Miwa S, Cameron K, et al. The Bystander Effect Contributes to the Accumulation of Senescent Cells In Vivo. *Aging Cell* (2019) 18:e12848. doi: 10.1111/acel.12848
47. Kovtonyuk LV, Fritsch K, Feng X, Manz MG, Takizawa H. Inflamm-Aging of Hematopoiesis, Hematopoietic Stem Cells, and the Bone Marrow Microenvironment. *Front Immunol* (2016) 7:502. doi: 10.3389/fimmu.2016.00502
48. Infante A, Rodríguez CI. Osteogenesis and Aging: Lessons From Mesenchymal Stem Cells. *Stem Cell Res Ther* (2018) 9:244. doi: 10.1186/s13287-018-0995-x
49. Planat-Benard V, Varin A, Casteilla L. MSCs and Inflammatory Cells Crosstalk in Regenerative Medicine: Concerted Actions for Optimized Resolution Driven by Energy Metabolism. *Front Immunol* (2021) 12:626755. doi: 10.3389/fimmu.2021.626755
50. Cawthorn WP, Scheller EL. Editorial: Bone Marrow Adipose Tissue: Formation, Function, and Impact on Health and Disease. *Front Endocrinol (Lausanne)* (2017) 8:112. doi: 10.3389/fendo.2017.00112

51. Jacobs FA, Sadie-Van Gijsen H, van de Vyver M, Ferris WF. Vanadate Impedes Adipogenesis in Mesenchymal Stem Cells Derived From Different Depots Within Bone. *Front Endocrinol (Lausanne)* (2016) 7:108. doi: 10.3389/fendo.2016.00108
52. Kraakman MJ, Liu Q, Postigo-Fernandez J, Ji R, Kon N, Larrea D, et al. PPAR? Deacetylation Dissociates Thiazolidinedione's Metabolic Benefits From its Adverse Effects. *J Clin Invest* (2018) 128:2600–12. doi: 10.1172/JCI98709
53. Zhong L, Yao L, Tower RJ, Wei Y, Miao Z, Park J, et al. Single Cell Transcriptomics Identifies a Unique Adipose Lineage Cell Population That Regulates Bone Marrow Environment. *Elife* (2020) 9:e54695. doi: 10.7554/eLife.54695
54. Corrado A, Cici D, Rotondo C, Maruotti N, Cantatore FP. Molecular Basis of Bone Aging. *Int J Mol Sci* (2020) 21:3679. doi: 10.3390/ijms21103679
55. Goto H, Osaki M, Fukushima T, Sakamoto K, Hozumi A, Baba H, et al. Human Bone Marrow Adipocytes Support Dexamethasone-Induced Osteoclast Differentiation and Function Through RANKL Expression. *Biomed Res* (2011) 32:37–44. doi: 10.2220/biomedres.32.37
56. Goto H, Hozumi A, Osaki M, Fukushima T, Sakamoto K, Yonekura A, et al. Primary Human Bone Marrow Adipocytes Support TNF-α-Induced Osteoclast Differentiation and Function Through RANKL Expression. *Cytokine* (2011) 56:662–8. doi: 10.1016/j.cyto.2011.09.005
57. Cao JJ, Wronski TJ, Iwaniec U, Phleger L, Kurimoto P, Boudignon B, et al. Aging Increases Stromal/Osteoblastic Cell-Induced Osteoclastogenesis and Alters the Osteoclast Precursor Pool in the Mouse. *J Bone Miner Res* (2005) 20:1659–68. doi: 10.1359/JBMR.050503
58. Takeshita S, Fumoto T, Naoe Y, Ikeda K. Age-Related Marrow Adipogenesis is Linked to Increased Expression of RANKL. *J Biol Chem* (2014) 289:16699–710. doi: 10.1074/jbc.M114.547919
59. Lai P, Song Q, Yang C, Li Z, Liu S, Liu B, et al. Loss of Rictor With Aging in Osteoblasts Promotes Age-Related Bone Loss. *Cell Death Dis* (2016) 7: e2408–8. doi: 10.1038/cddis.2016.249
60. Corre J, Planat-Benard V, Corberand JX, Pénicaud L, Casteilla L, Laharrague P. Human Bone Marrow Adipocytes Support Complete Myeloid and Lymphoid Differentiation From Human CD34+ Cells. *Br J Haematol* (2004) 127:344–7. doi: 10.1111/j.1365-2141.2004.05198.x
61. Jilka RL. Osteoblast Progenitor Fate and Age-Related Bone Loss. *J Musculoskelet Neuronal Interact* (2002) 2:581–3.
62. Trottier MD, Naaz A, Li Y, Fraker PJ. Enhancement of Hematopoiesis and Lymphopoiesis in Diet-Induced Obese Mice. *Proc Natl Acad Sci U S A* (2012) 109:7622–9. doi: 10.1073/pnas.1205129109
63. Gimble JM, Nuttall ME. The Relationship Between Adipose Tissue and Bone Metabolism. *Clin Biochem* (2012) 45:874–9. doi: 10.1016/j.clinbiochem.2012.03.006
64. Lecka-Czernik B. Marrow Fat Metabolism is Linked to the Systemic Energy Metabolism. *Bone* (2012) 50:534–9. doi: 10.1016/j.bone.2011.06.032
65. Omatsu Y, Sugiyama T, Kohara H, Kondoh G, Fujii N, Kohno K, et al. The Essential Functions of Adipo-Osteogenic Progenitors as the Hematopoietic Stem and Progenitor Cell Niche. *Immunity* (2010) 33:387–99. doi: 10.1016/j.immuni.2010.08.017
66. Miharada K, Hiroyama T, Sudo K, Danjo I, Nagasawa T, Nakamura Y. Lipocalin 2-Mediated Growth Suppression is Evident in Human Erythroid and Monocyte/Macrophage Lineage Cells. *J Cell Physiol* (2008) 215:526–37. doi: 10.1002/jcp.21334
67. Belaid-Choucair Z, Lepelletier Y, Poncin G, Thiry A, Humblet C, Maachi M, et al. Human Bone Marrow Adipocytes Block Granulopoiesis Through Neuropilin-1-Induced Granulocyte Colony-Stimulating Factor Inhibition. *Stem Cells* (2008) 26:1556–64. doi: 10.1634/stemcells.2008-0068
68. Ouchi N, Walsh K. Adiponectin as an Anti-Inflammatory Factor. *Clin Chim Acta* (2007) 380:24–30. doi: 10.1016/j.cca.2007.01.026
69. Gimble JM, Nuttall ME. Bone and Fat: Old Questions, New Insights. *Endocrine* (2004) 23:183–8. doi: 10.1385/ENDO:23:2-3:183
70. Rosen CJ, Ackert-Bicknell C, Rodriguez JP, Pino AM. Marrow Fat and the Bone Microenvironment: Developmental, Functional, and Pathological Implications. *Crit Rev Eukaryot Gene Expr* (2009) 19:109–24. doi: 10.1615/CritRevEukarGeneExpr.v19.i2.20
71. Kawai M, de Paula FJA, Rosen CJ. New Insights Into Osteoporosis: The Bone-Fat Connection. *J Intern Med* (2012) 272:317–29. doi: 10.1111/j.1365-2796.2012.02564.x
72. Gasparrini M, Rivas D, Elbaz A, Duque G. Differential Expression of Cytokines in Subcutaneous and Marrow Fat of Aging C57BL/6J Mice. *Exp Gerontol* (2009) 44:613–8. doi: 10.1016/j.exger.2009.05.009
73. Bilwani FA, Knight KL. Adipocyte-Derived Soluble Factor(s) Inhibits Early Stages of B Lymphopoiesis. *J Immunol* (2012) 189:4379–86. doi: 10.4049/jimmunol.1201176
74. Rossi MID, Yokota T, Medina KL, Garrett KP, Comp PC, Schipul AH, et al. B Lymphopoiesis is Active Throughout Human Life, But There are Developmental Age-Related Changes. *Blood* (2003) 101:576–84. doi: 10.1182/blood-2002-03-0896
75. McKenna RW, Washington LBT, Aquino DB, Picker LJ, Kroft SH. Immunophenotypic Analysis of Hematogones (B-Lymphocyte Precursors) in 662 Consecutive Bone Marrow Specimens by 4-Color Flow Cytometry. *Blood* (2001) 98:2498–507. doi: 10.1182/blood.V98.8.2498
76. Nuñez C, Nishimoto N, Gartland GL, Billips LG, Burrows PD, Kubagawa H, et al. B Cells are Generated Throughout Life in Humans. *J Immunol* (1996) 156:866–72.
77. Johnson KM, Owen K, Witte PL. Aging and Developmental Transitions in the B Cell Lineage. *Int Immunol* (2002) 14:1313–23. doi: 10.1093/intimm/dxf092
78. Stephan RP, Reilly CR, Witte PL. Impaired Ability of Bone Marrow Stromal Cells to Support B-Lymphopoiesis With Age. *Blood* (1998) 91:75–88. doi: 10.1182/blood.v91.1.75
79. Frasca D, Blomberg BB. Effects of Aging on B Cell Function. *Curr Opin Immunol* (2009) 21:425–30. doi: 10.1016/j.coi.2009.06.001
80. Kennedy DE, Knight KL. Inhibition of B Lymphopoiesis by Adipocytes and IL-1–Producing Myeloid-Derived Suppressor Cells. *J Immunol* (2015) 195:2666–74. doi: 10.4049/jimmunol.1500957
81. Salminen A, Kaarniranta K, Kauppinen A. Inflammaging: Disturbed Interplay Between Autophagy and Inflammasomes. *Aging (Albany NY)* (2012) 4:166–75. doi: 10.18632/aging.100444
82. Vandanmagsar B, Youm YH, Ravussin A, Galgani JE, Stadler K, Mynatt RL, et al. The NLRP3 Inflammasome Instigates Obesity-Induced Inflammation and Insulin Resistance. *Nat Med* (2011) 17:179–89. doi: 10.1038/nm.2279
83. Wang H, Leng Y, Gong Y. Bone Marrow Fat and Hematopoiesis. *Front Endocrinol (Lausanne)* (2018) 9:694. doi: 10.3389/fendo.2018.00694
84. Craig MJ, Loberg RD. CCL2 (Monocyte Chemoattractant Protein-1) in Cancer Bone Metastases. *Cancer Metastasis Rev* (2006) 25:611–9. doi: 10.1007/s10555-006-9027-x
85. Chen YC, Sosnoski DM, Gandhi UH, Novinger LJ, Prabhu KS, Mastro AM. Selenium Modifies the Osteoblast Inflammatory Stress Response to Bone Metastatic Breast Cancer. *Carcinogenesis* (2009) 30:1941–8. doi: 10.1093/carcin/bgp227
86. Hsieh PS, Lu KC, Chiang CF, Chen CH. Suppressive Effect of COX2 Inhibitor on the Progression of Adipose Inflammation in High-Fat-Induced Obese Rats. *Eur J Clin Invest* (2010) 40:164–71. doi: 10.1111/j.1365-2362.2009.02239.x
87. Anderson GD, Hauser SD, McGarity KL, Bremer ME, Isakson PC, Gregory SA. Selective Inhibition of Cyclooxygenase (COX)-2 Reverses Inflammation and Expression of COX-2 and Interleukin 6 in Rat Adjuvant Arthritis. *J Clin Invest* (1996) 97:2672–9. doi: 10.1172/JCI118717
88. Muta M, Matsumoto G, Nakashima E, Toi M. Mechanical Analysis of Tumor Growth Regression by the Cyclooxygenase-2 Inhibitor, DFU, in a Walker256 Rat Tumor Model: Importance of Monocyte Chemoattractant Protein-1 Modulation. *Clin Cancer Res* (2006) 12:264–72. doi: 10.1158/1078-0432.CCR-05-1052
89. Fujita M, Kohanbash G, Fellows-Mayle W, Hamilton RL, Komohara Y, Decker SA, et al. COX-2 Blockade Suppresses Gliomagenesis by Inhibiting Myeloid-Derived Suppressor Cells. *Cancer Res* (2011) 71:2664–74. doi: 10.1158/0008-5472.CAN-10-3055
90. Eliopoulos AG, Dumitru CD, Wang CC, Cho J, Tsichlis PN. Induction of COX-2 by LPS in Macrophages is Regulated by Tpl2-Dependent CREB Activation Signals. *EMBO J* (2002) 21:4831–40. doi: 10.1093/emboj/cdf478
91. Nakao S, Kuwano T, Tsutsumi-Miyahara C, Ueda SI, Kimura YN, Hamano S, et al. Infiltration of COX-2-Expressing Macrophages is a Prerequisite for IL-1β-Induced Neovascularization and Tumor Growth. *J Clin Invest* (2005) 115:2979–91. doi: 10.1172/JCI23298

92. Tanaka S, Tatsuguchi A, Futagami S, Gudis K, Wada K, Seo T, et al. Monocyte Chemoattractant Protein 1 and Macrophage Cyclooxygenase 2 Expression in Colonic Adenoma. *Gut* (2006) 55:54–61. doi: 10.1136/gut.2004.059824
93. Tajima T, Murata T, Aritake K, Urade Y, Hirai H, Nakamura M, et al. Lipopolysaccharide Induces Macrophage Migration *via* Prostaglandin D 2 and Prostaglandin E2. *J Pharmacol Exp Ther* (2008) 326:493–501. doi: 10.1124/jpet.108.137992
94. Hardaway AL, Herroon MK, Rajagurubandara E, Podgorski I. Bone Marrow Fat: Linking Adipocyte-Induced Inflammation With Skeletal Metastases. *Cancer Metastasis Rev* (2014) 33:527–43. doi: 10.1007/s10555-013-9484-y
95. Zhou Y, Xin X, Wang L, Wang B, Chen L, Liu O, et al. Senolytics Improve Bone Forming Potential of Bone Marrow Mesenchymal Stem Cells From Aged Mice. *NPJ Regen Med* (2021) 6:34. doi: 10.1038/s41536-021-00145-z
96. Khosla S, Farr JN, Kirkland JL. Inhibiting Cellular Senescence: A New Therapeutic Paradigm for Age-Related Osteoporosis. *J Clin Endocrinol Metab* (2018) 103:1282–90. doi: 10.1210/jc.2017-02694
97. Zhu H, Kwak H-J, Liu P, Bajrami B, Xu Y, Park S-Y, et al. Reactive Oxygen Species–Producing Myeloid Cells Act as a Bone Marrow Niche for Sterile Inflammation–Induced Reactive Granulopoiesis. *J Immunol* (2017) 198:2854–64. doi: 10.4049/jimmunol.1602006
98. Khatri R, Krishnan S, Roy S, Chattopadhyay S, Kumar V, Mukhopadhyay A. Reactive Oxygen Species Limit the Ability of Bone Marrow Stromal Cells to Support Hematopoietic Reconstitution in Aging Mice. *Stem Cells Dev* (2016) 25:948–58. doi: 10.1089/scd.2015.0391
99. Lo T, Ho JH, Yang MH, Lee OK. Glucose Reduction Prevents Replicative Senescence and Increases Mitochondrial Respiration in Human Mesenchymal Stem Cells. *Cell Transplant* (2011) 20:813–25. doi: 10.3727/096368910X539100
100. Chang TC, Hsu MF, Wu KK. High Glucose Induces Bone Marrow-Derived Mesenchymal Stem Cell Senescence by Upregulating Autophagy. *PloS One* (2015) 10:e0126537. doi: 10.1371/journal.pone.0126537
101. Cho JH, Lee JH, Lee KM, Lee CK, Shin DM. BMP-2 Induced Signaling Pathways and Phenotypes: Comparisons Between Senescent and Non-Senescent Bone Marrow Mesenchymal Stem Cells. *Calcif Tissue Int* (2021) 1–15. doi: 10.1007/s00223-021-00923-3
102. Li H, Liu P, Xu S, Li Y, Dekker JD, Li B, et al. FOXP1 Controls Mesenchymal Stem Cell Commitment and Senescence During Skeletal Aging. *J Clin Invest* (2017) 127:1241–53. doi: 10.1172/JCI89511
103. Heim KE, Tagliaferro AR, Bobilya DJ. Flavonoid Antioxidants: Chemistry, Metabolism and Structure-Activity Relationships. *J Nutr Biochem* (2002) 13:572–84. doi: 10.1016/S0955-2863(02)00208-5
104. Lindauer M, Hochhaus A. Dasatinib, in: Recent Results Cancer Res. *Recent Results Cancer Res* (2018) 212:29–68. doi: 10.1007/978-3-319-91439-8_2
105. Xu M, Pirtskhalava T, Farr JN, Weigand BM, Palmer AK, Weivoda MM, et al. Senolytics Improve Physical Function and Increase Lifespan in Old Age. *Nat Med* (2018) 24:1246–56. doi: 10.1038/s41591-018-0092-9
106. Farr JN, Xu M, Weivoda MM, Monroe DG, Fraser DG, Onken JL, et al. Targeting Cellular Senescence Prevents Age-Related Bone Loss in Mice. *Nat Med* (2017) 23:1072–9. doi: 10.1038/nm.4385
107. Arner P, Kulyté A. MicroRNA Regulatory Networks in Human Adipose Tissue and Obesity. *Nat Rev Endocrinol* (2015) 11:276–88. doi: 10.1038/nrendo.2015.25
108. Brandão BB, Guerra BA, Mori MA. Shortcuts to a Functional Adipose Tissue: The Role of Small non-Coding RNAs. *Redox Biol* (2017) 12:82–102. doi: 10.1016/j.redox.2017.01.020
109. Li CJ, Cheng P, Liang MK, Chen YS, Lu Q, Wang JY, et al. MicroRNA-188 Regulates Age-Related Switch Between Osteoblast and Adipocyte Differentiation. *J Clin Invest* (2015) 125:1509–22. doi: 10.1172/JCI77716
110. Xu J, Huang Z, Lin L, Fu M, Song Y, Shen Y, et al. MiRNA-130b is Required for the ERK/FOXM1 Pathway Activation-Mediated Protective Effects of Isosorbide Dinitrate Against Mesenchymal Stem Cell Senescence Induced by High Glucose. *Int J Mol Med* (2015) 35:59–71. doi: 10.3892/ijmm.2014.1985
111. Davis C, Dukes A, Drewry M, Helwa I, Johnson MH, Isales CM, et al. MicroRNA-183-5p Increases With Age in Bone-Derived Extracellular Vesicles, Suppresses Bone Marrow Stromal (Stem) Cell Proliferation, and Induces Stem Cell Senescence. *Tissue Eng - Part A* (2017) 23:1231–40. doi: 10.1089/ten.tea.2016.0525
112. Sun J, Ming L, Shang F, Shen L, Chen J, Jin Y. Apocynin Suppression of NADPH Oxidase Reverses the Aging Process in Mesenchymal Stem Cells to Promote Osteogenesis and Increase Bone Mass. *Sci Rep* (2015) 5:1–11. doi: 10.1038/srep18572
113. Geißler S, Textor M, Schmidt-Bleek K, Klein O, Thiele M, Ellinghaus A, et al. In Serum Veritas-in Serum Sanitas? Cell non-Autonomous Aging Compromises Differentiation and Survival of Mesenchymal Stromal Cells *via* the Oxidative Stress Pathway. *Cell Death Dis* (2013) 4:e970–e970. doi: 10.1038/cddis.2013.501
114. Casado-díaz A, Rodríguez-ramos Á, Torrecillas-baena B, Dorado G, Quesada-gómez JM, Gálvez-moreno MÁ. Flavonoid Phloretin Inhibits Adipogenesis and Increases Opg Expression in Adipocytes Derived From Human Bone-Marrow Mesenchymal Stromal-Cells. *Nutrients* (2021) 13:4185. doi: 10.3390/nu13114185
115. Yamaza T, Miura Y, Bi Y, Liu Y, Akiyama K, Sonoyama W, et al. Pharmacologic Stem Cell Based Intervention as a New Approach to Osteoporosis Treatment in Rodents. *PloS One* (2008) 3:e2615. doi: 10.1371/journal.pone.0002615
116. Wang L, Zhao Y, Liu Y, Akiyama K, Chen C, Qu C, et al. IFN-γ and TNF-α Synergistically Induce Mesenchymal Stem Cell Impairment and Tumorigenesis *via* Nfκb Signaling. *Stem Cells* (2013) 31:1383–95. doi: 10.1002/stem.1388
117. Fasshauer M, Blüher M. Adipokines in Health and Disease. *Trends Pharmacol Sci* (2015) 36:461–70. doi: 10.1016/j.tips.2015.04.014
118. Blüher M. Clinical Relevance of Adipokines. *Diabetes Metab J* (2012) 36:317–27. doi: 10.4093/dmj.2012.36.5.317
119. Walsh NC, Gravallese EM. Bone Loss in Inflammatory Arthritis: Mechanisms and Treatment Strategies. *Curr Opin Rheumatol* (2004) 16:419–27. doi: 10.1097/01.bor.0000127824.42507.68
120. Poutoglidou F, Pourzitaki C, Manthou ME, Samoladas E, Saitis A, Malliou F, et al. Infliximab Prevents Systemic Bone Loss and Suppresses Tendon Inflammation in a Collagen-Induced Arthritis Rat Model. *Inflammopharmacology* (2021) 29:661–72. doi: 10.1007/s10787-021-00815-w
121. Nigil Haroon N, Sriganthan J, Al Ghanim N, Inman RD, Cheung AM. Effect of TNF-Alpha Inhibitor Treatment on Bone Mineral Density in Patients With Ankylosing Spondylitis: A Systematic Review and Meta-Analysis. *Semin Arthritis Rheum* (2014) 44:155–61. doi: 10.1016/j.semarthrit.2014.05.008
122. Roche-Molina M, Sanz-Rosa D, Cruz FM, García-Prieto J, López S, Abia R, et al. Induction of Sustained Hypercholesterolemia by Single Adeno-Associated Virus-Mediated Gene Transfer of Mutant Hpcsk9. *Arterioscler Thromb Vasc Biol* (2015) 35:50–9. doi: 10.1161/ATVBAHA.114.303617
123. Szulc P, Naylor K, Hoyle NR, Eastell R, Leary ET. Use of CTX-I and PINP as Bone Turnover Markers: National Bone Health Alliance Recommendations to Standardize Sample Handling and Patient Preparation to Reduce Pre-Analytical Variability. *Osteoporos Int* (2017) 28:2541–56. doi: 10.1007/s00198-017-4082-4
124. Ehrnthaller C, Huber-Lang M, Nilsson P, Bindl R, Redeker S, Recknagel S, et al. Complement C3 and C5 Deficiency Affects Fracture Healing. *PloS One* (2013) 8:e81341. doi: 10.1371/journal.pone.0081341
125. Bloom AC, Collins FL, van't Hof RJ, Ryan ES, Jones E, Hughes TR, et al. Deletion of the Membrane Complement Inhibitor CD59a Drives Age and Gender-Dependent Alterations to Bone Phenotype in Mice. *Bone* (2016) 84:253–61. doi: 10.1016/j.bone.2015.12.014
126. Azizieh FY, Shehab D, Al Jarallah K, Mojiminiyi O, Gupta R, Raghupathy R. Circulatory Pattern of Cytokines, Adipokines and Bone Markers in Postmenopausal Women With Low BMD. *J Inflamm Res* (2019) 12:99–108. doi: 10.2147/JIR.S203590
127. Zhu J, Ruan G, Cen H, Meng T, Zheng S, Wang Y, et al. Association of Serum Levels of Inflammatory Markers and Adipokines With Joint Symptoms and Structures in Participants With Knee Osteoarthritis. *Rheumatology* (2021) 0:1–9. doi: 10.1093/rheumatology/keab479
128. Karki RG, Powers J, Mainolfi N, Anderson K, Belanger DB, Liu D, et al. Design, Synthesis, and Preclinical Characterization of Selective Factor D Inhibitors Targeting the Alternative Complement Pathway. *J Med Chem* (2019) 62:4656–68. doi: 10.1021/acs.jmedchem.9b00271
129. Devlin MJ, Cloutier AM, Thomas NA, Panus DA, Lotinun S, Pinz I, et al. Caloric Restriction Leads to High Marrow Adiposity and Low Bone Mass in Growing Mice. *J Bone Miner Res* (2010) 25:2078–88. doi: 10.1002/JBMR.82
130. Bolan PJ, Arentsen L, Sueblinvong T, Zhang Y, Moeller S, Carter JS, et al. Water-Fat MRI for Assessing Changes in Bone Marrow Composition Due to Radiation and Chemotherapy in Gynecologic Cancer Patients. *J Magn Reson Imaging* (2013) 38:1578–84. doi: 10.1002/JMRI.24071

131. Carmona R, Pritz J, Bydder M, Gulaya S, Zhu H, Williamson CW, et al. Fat Composition Changes in Bone Marrow During Chemotherapy and Radiation Therapy. *Int J Radiat Oncol Biol Phys* (2014) 90:155–63. doi: 10.1016/J.IJROBP.2014.05.041
132. Hui SK, Arentsen L, Sueblinvong T, Brown K, Bolan P, Ghebre RG, et al. A Phase I Feasibility Study of Multi-Modality Imaging Assessing Rapid Expansion of Marrow Fat and Decreased Bone Mineral Density in Cancer Patients. *Bone* (2015) 73:90–7. doi: 10.1016/J.BONE.2014.12.014

Conflict of Interest: The authors declare that the research was conducted in the absence of any commercial or financial relationships that could be construed as a potential conflict of interest.

Publisher's Note: All claims expressed in this article are solely those of the authors and do not necessarily represent those of their affiliated organizations, or those of the publisher, the editors and the reviewers. Any product that may be evaluated in this article, or claim that may be made by its manufacturer, is not guaranteed or endorsed by the publisher.

frontiers | Frontiers in Endocrinology

POLICY AND PRACTICE REVIEWS
published: 13 April 2022
doi: 10.3389/fendo.2022.879588

Next Generation Bone Marrow Adiposity Researchers: Report From the 1st BMAS Summer School 2021

Rossella Labella[1†], Sarah Little-Letsinger[2†], Viktorjia Avilkina[3], Rita Sarkis[4,5], Michaela Tencerova[6], Annegreet Vlug[7] and Biagio Palmisano[8]*

[1] Department of Physiology and Cellular Biophysics, Columbia University Medical Center, New York, NY, United States, [2] Department of Evolutionary Anthropology, Duke University, Durham, NC, United States, [3] Marrow Adiposity and Bone Lab (MAB Lab) ULR4490, Univ Littoral Côte d'Opale, Boulogne-sur-Mer, France, [4] Laboratory of Regenerative Hematopoiesis, Institute of Bioengineering, Ecole Polytechnique Fédérale de Lausanne, Lausanne, Switzerland, [5] Department of Biomedical Sciences, University of Lausanne, Lausanne, Switzerland, [6] Molecular Physiology of Bone, Institute of Physiology of the Czech Academy of Sciences, Prague 4, Czechia, [7] Section of Endocrinology, Department of Internal Medicine, Center for Bone Quality, Leiden University Medical Center, Leiden, Netherlands, [8] Department of Molecular Medicine, Sapienza University of Rome, Rome, Italy

OPEN ACCESS

Edited by:
Andre Van Wijnen, University of Vermont, United States

Reviewed by:
Michaela Ruth Reagan, Maine Medical Center Research Institute, United States
Meghan E McGee-Lawrence, Augusta University, United States

***Correspondence:**
Biagio Palmisano
biagio.palmisano@uniroma1.it

†These authors have contributed equally to this work and share first authorship

Specialty section:
This article was submitted to Bone Research, a section of the journal Frontiers in Endocrinology

Received: *19 February 2022*
Accepted: *21 March 2022*
Published: *13 April 2022*

Citation:
Labella R, Little-Letsinger S, Avilkina V, Sarkis R, Tencerova M, Vlug A and Palmisano B (2022) Next Generation Bone Marrow Adiposity Researchers: Report From the 1st BMAS Summer School 2021. Front. Endocrinol. 13:879588. doi: 10.3389/fendo.2022.879588

The first International Summer School on Bone Marrow Adiposity was organized by members of Bone Marrow Adiposity Society and held virtually on September 6-8 2021. The goal of this meeting was to bring together young scientists interested in learning about bone marrow adipose tissue biology and pathology. Fifty-two researchers from different backgrounds and fields, ranging from bone physiopathology to adipose tissue biology and hematology, participated in the summer school. The meeting featured three keynote lectures on the fundamentals of bone marrow adiposity, three scientific workshops on technical considerations in studying bone marrow adiposity, and six motivational and career development lectures, spanning from scientific writing to academic career progression. Moreover, twenty-one participants presented their work in the form of posters. In this report we highlight key moments and lessons learned from the event.

Keywords: bone marrow adipose tissue (BMAT), bone marrow adiposity, bone marrow adipocytes, metabolism, imaging technique, BMSC – bone marrow stromal cells, histology, career development

BACKGROUND

The growing interest in bone marrow adipose tissue (BMAT) is evident from the increase in articles published yearly by researchers all over the world (**Figure 1**). The credit for bringing this field to international attention is given to Dr. Mehdi Tavassoli with his works in the early 70's (1), although observations of the transformation of red marrow into yellow marrow have been published since the 1800's (2, 3). In the last twenty years, the study of BMAT has emerged as an important field in bone and bone marrow biology.

Beginning in 2015, international meetings on Bone Marrow Adiposity (BMA) have been organized with the aim to bring together scientists working on or interested in BMAT (4–8). Later in 2017, a group of BMA scientists founded the BMA Society (BMAS) (http://bma-society.org/) with Dr. Pierre Hardouin as the founding president. The aims of the newly established society were to advance the knowledge of BMA by facilitating interdisciplinary exchanges, developing research strategies, and

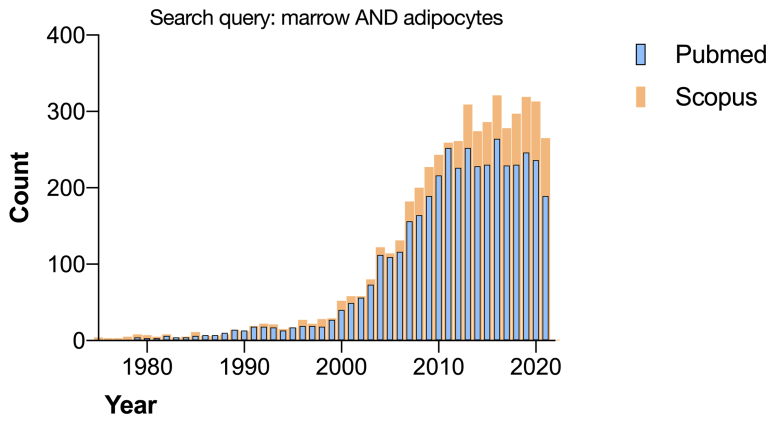

FIGURE 1 | Search results for "marrow AND adipocytes" on Pubmed and Scopus performed in November 2021.

standardizing nomenclature and methods to study BMAT. Thus far, the society has produced and published three consensus articles (9–11).

One of BMAS's key goals is to promote BMAT research by training and supporting young scientists interested in this field. Therefore, a group of young scientists from Europe and the United States envisioned the first BMAS Summer School, which was held as a virtual meeting on September 6-8, 2021. The goal of the event was to foster general knowledge of BMAT research to young researchers from all fields in order to provide fundamentals about how BMAT originates, develops, and interacts with other organs, as well as how to study BMA and what methods to use in both clinical and basic research. Moreover, the event program contained career development workshops with the aim to provide tips on how to face difficulties and overcome obstacles in the academic life, which alternative paths exist outside academia, and how to write a good manuscript and how to understand where to publish. Fifty-two participants from all over the world (**Figure 2**) attended the meeting, with active participation, live discussion, and incredible enthusiasm.

The three-day event consisted of a daily keynote lecture on BMA, followed by a scientific workshop on how to study BMA and two motivational and career development workshops with a total of twelve presentations from invited speakers. Moreover, twenty-one abstracts were selected and presented as posters with a live discussion; these abstracts have been published and are available elsewhere (12).

FIGURE 2 | Word cloud performed with the countries of origin of the attendees at the 1st BMAS Summer School. The number of attendees from each country correlates with the word size in the cloud. The higher the number of attendees, the bigger the word. The analysis was carried out with WordCloud package in R.

LECTURES ON BONE MARROW ADIPOSITY

BMAT: Origin, Multicellularity, Regulation of Lineage Commitment, and Functional Implications

Dr. Moustapha Kassem (University of Southern Denmark) opened the three-day event with a lecture entitled "BMAT: origin, multicellularity, regulation of lineage commitment, and functional implications". In his talk, Dr. Kassem described a historical roadmap from the first correlations with bone diseases, such as osteoporosis, to the most recent studies on the regulation of bone marrow stromal cell differentiation potential towards osteoblasts or bone marrow adipocytes. This session was moderated by Dr. Gustavo Duque (University of Melbourne). Dr. Kassem gave an overview of the major findings and discoveries on BMA in relation to bone health and homeostasis and its relevance to clinical outcomes. His talk pointed out the concept of cellular heterogeneity of bone marrow stromal cells (BMSCs) and presence

of committed adipogenic and osteogenic progenitors besides multipotent BMSCs, which contribute to the interaction between bone and fat mass and cellular changes in the bone marrow microenvironment (13). In order to understand the mechanisms underlying age- and osteoporosis-related changes in bone formation, his laboratory discovered several secreted factors derived from BMSCs [e.g., Delta Like Non-Canonical Notch Ligand 1(DLK1), Legumain (LGMN), Cell Migration Inducing Hyaluronidase 1(KIAA1199)], which play a key role in stem cell differentiation and provide a link between bone biology and whole body energy metabolism (14–17). At the end of his talk, Dr. Kassem presented data on human BMSCs isolated from obese subjects demonstrating a hypermetabolic and accelerated senescent phenotype in comparison to lean-derived BMSCs. Dr. Kassem's work provides important insights into metabolic changes occurring in the bone marrow microenvironment and its relation to higher bone fragility in metabolic diseases (18, 19). These data will contribute to the explanation of the obesity paradox in bone biology, as obese subjects are characterized with unchanged or increased bone mass but high rates of bone fragility.

BMAT and Bone/Bone Marrow Diseases

The second keynote lecture was given by Dr. Mara Riminucci (Sapienza University of Rome) and moderated by Dr. Ling Qin (University of Pennsylvania). The main focus of this talk was the role played by BMAT in bone and disease. She started by defining bone marrow adipocytes (BMAds), referring to Tavassoli's definition, as recognized large cells with a single lipid droplet (20) and positive for markers such as Perilipin-1 and Adiponectin. She emphasized that both morphology and marker expression are crucial to recognizing BMAds. In terms of origin, BMAds appear in perinatal/post-natal life. The development of the "yellow marrow" (to distinguish from the hematopoietic "red marrow") is a complex phenomenon tightly regulated by multiple genetic, developmental, and functional factors (2). *Ex vivo* transplantation studies have revealed a common progenitor for both BMAds and osteogenic cells that resides in the bone marrow stromal compartment (21–24). The fate choice of this common progenitor plays a crucial role in bone physiology and health. Functionally, one of the roles of BMAT is to fill the marrow space: after birth in fact, hematopoietic bone marrow becomes progressively filled with adipocytes among hematopoietic cells. However, BMA is highly flexible and reversible. Besides the space filling function, BMAT contributes to systemic metabolism (25), supports hematopoiesis (26), and modulates cell differentiation within the bone marrow stroma (27). Moreover, based on their localization as perivascular cells, BMAds regulate the sinusoid caliber and distribution of marrow blood flow (28).

The second part of the lecture focused on the role of BMAT in the context of human pathology. BMAT is, in fact, involved in different pathologies of the bone and bone marrow, including osteoporosis, bone fragility, hematological tumors, bone cancer metastasis, and some genetic disorders involving the skeleton (29, 30). On the other hand, BMAT may have its own tissue-specific pathology such as lipoma and hibernoma (31, 32).

Metabolic Function of Bone Marrow Adipose Tissue

The third keynote lecture was provided by Dr. William Cawthorn (University of Edinburgh) and moderated by Dr. William Ferris (Stellenbosch University). The presentation focused mainly on BMAT's impact on metabolic and skeletal homeostasis within bone marrow. Dr. Cawthorn began his lecture by introducing subtypes of adipose tissue, their location, and structure. As extensive research has been done to characterize white adipose tissue (WAT) and brown adipose tissue (BAT), the talk focused on their metabolic functions, covering the processes of energy storage and energy release within WAT, as well as thermogenesis in BAT. In contrast with WAT and BAT, little is known about BMAT metabolic characteristics and its systemic function. As a leading expert in the study of BMAT, Dr Cawthorn, presented a detailed description of lipid content properties and metabolism (e.g., lipogenesis and lipolysis) in BMAT from different skeletal sites. Furthermore, his research group conducted transcriptional characterization comparing BMAT and WAT using microarray analysis. The results demonstrated that BMAT is less responsive to insulin compared to WAT (33). These findings were tested by PET/CT scan, which showed a lack of insulin-stimulated glucose uptake in BMAT (distal tibia), concluding that BMAT is insulin resistant (33). Additionally, Dr Cawthorn's group demonstrated that BMAT is not cold responsive, as it does not increase glucose uptake during cold exposure (33, 34). Another finding, suggested that BMAT glucose uptake is able to influence systemic glucose homeostasis (33, 35). This lecture concluded with the statement that BMAT is a metabolically distinct fat depot with importance in numerous clinical conditions.

WORKSHOPS ON BONE MARROW ADIPOSITY

Standard Nomenclature, Abbreviation, and Units for the Analysis of Bone Marrow Adiposity

The first workshop entitled "Standard nomenclature, abbreviations and units for the analysis of bone marrow adipose tissue" was given by Dr. Nathalie Bravenboer (University Medical Center) and moderated by Dr. Stefanie Lucas (Université du Littoral Côte d'Opale). Dr. Bravenboer started with some historical data of the discovery of the bone marrow space and role in red blood cell development (36). The first part of her talk can be summarized with the mission of the nomenclature working group: "Our purpose is not to encourage or discourage the use of abbreviations and symbols but to ensure that the same ones are used by everybody" (10). Dr. Bravenboer listed some consensus notes: first, BMAd is the adopted abbreviation for the bone marrow adipocytes; second, BMA can be considered as a tissue, and third, anatomical location is important to give reference due to documented differences in sub-depots (e.g., proximal versus distal in the mouse tibia). The last part of this workshop was dedicated to a description of the

methodologies for the analysis of BMAT including histomorphometry, Magnetic Resonance Imaging (MRI), Magnetic Resonance Spectroscopy (MRS), and Computed Tomography (CT) analysis, along with a full list of the parameters adopted to define BMAT while using each of those techniques. A detailed list of all the nomenclature and methodologies recommendations can be found in the two consensus papers published in 2021 (9, 10).

Skill Development on Histology

The second skill development workshop featured an invited talk by Dr. Erica Scheller (Washington University in St. Louis) covering histology of BMAT and was moderated by Dr. Michaela Tencerova (Institute of Physiology of the Czech Academy of Sciences). Dr. Scheller began the session outlining the potential uses of histology to study BMAds, including cell number, size, localization, molecular analyses, and lineage tracing, with a focus on the importance of technical considerations decided *a priori*. While the necessary considerations vary across specific histologic techniques, some factors of notable importance were generally applicable. Consistency in region of interest (ROI), analysis of a large and representative ROI, sufficient sample size (*e.g.*, 100-300 adipocytes per sample), and the use of controls are critical to successful and reproducible histology. Hematoxylin and eosin staining of formalin-fixed paraffin-embedded tissue is ideal for investigating cell number and size (9, 37, 38). Investigation of localization or co-localization requires the usage of immunostaining methods, including both immunohistochemistry, utilizing a single antibody, and immunofluorescence, enabling multi-antibody staining (39, 40). Antibodies must be validated and optimized through positive and negative controls, including omission of the secondary antibody and tissue from genetic knockouts (41). Molecular analyses and BMAd-specific protein expression can be difficult to assess using immunostaining alone and may require lineage tracing or reporter lines (42). Despite its limitations, histology is a powerful tool for the study of BMAds and can be highly informative when care is taken to ensure rigor and reproducibility through the employment of appropriate controls and technical considerations. In summary, this workshop was an excellent introduction to the histology of BMAds for students and researchers new to the technique and will enable the usage of histological best practices.

Standard Imaging Methods in the Assessment of Bone Marrow Adipose Tissue

Dr. Dimitrios Karampinos (Technical University of Munich) delivered the third BMAT workshop: "Standard imaging methods in the assessment of bone marrow adipose tissue" that was moderated by Dr. Greet Kerckhofs (Katholieke Universiteit Leuven). Dr. Karampinos provided an extensive overview of the imaging techniques in use to assess both BMAT and bone properties, outlining the difficulties to explore both with the same imaging technique. He explained the concept of Magnetic Resonance (MR) contrast mechanisms to study fat, the T1-weighted imaging and chemical shift encoding resulting in a proton density fat fraction (PDFF). The PDFF has been used to demonstrate the fat fraction increases with aging (43, 44) and is higher in patients with osteoporosis (45). To explore in more depth the composition of fatty acids in BMAT, unsaturated and saturated fat can be measured. Data shows that saturated fats are lower in patients with fractures and/or diabetes (46), although this remains a challenging measurement especially in regions with more hematopoietic marrow (47). Finally, the newest development in BMAT imaging, i.e. measuring lipid droplet size using MRI techniques, was discussed (48). This talk was extremely useful to improve the understanding of *in vivo* measurement of BMAT.

CAREER DEVELOPMENT WORKSHOPS

From Scientific Writing to Getting Your Paper Published

The first Career Development Workshop was given by Dr. Jonathan Tobias (University of Bristol) and moderated by Dr. Claire Edwards (University of Oxford). As a Specialty Chief Editor of the Bone Research Section in Frontiers in Endocrinology, Dr. Tobias focused on aspects of writing a scientific paper and going through the publication process. This talk covered the basic paper and journal types, reviewed the paper preparation process (e.g., paper structure and content), and the process of choosing appropriate journals for submission. Moreover, Dr. Tobias discussed the peer review process, covered the types of peer review and emphasized the importance of this process to improve the quality of publication. He also provided guidelines for responding to reviewers and tips on "Surviving the Peer Review" process, which was highly useful and informative for young researchers who are currently undergoing these processes with their first publications.

Academic Career Progression

The academic career progression talk was given by Dr. Michaela Reagan (Maine Medical Center Research/Tufts University and was moderated by Dr. Annegreet Veldhuis (Leiden University Medical Center). During the Academic Career Progression workshop, Dr. Reagan first took us with her on her academic journey and highlighted the importance of giving talks and meeting people during conferences to obtain new positions and advance your career. She shared her motivation to pursue an academic career and her keys to success, including diversification, finding a good mentor, considering work life balance, and personal traits like resiliency, open-mindedness, and most importantly, enjoying your work! Common mistakes were also discussed, such as being too optimistic, perfectionism, never saying no, and imposter syndrome. She explained the different academic career paths (tenure track, non- tenure track, or adjunct faculty) and highlighted useful grant options in the USA (e.g., NIH F31, F99/K00, NIH F32, DoD Postdoc Fellowship, or other Foundations and society). All in all, this workshop helped to gain more insight into the academic career progression and get some very useful advice.

How I Write a Grant

The career development workshop titled "How I write a grant" was given by Dr. Christopher Hernandez (Cornell University)

and moderated by Dr. Julien Paccou (Lille University Hospital). Dr. Hernandez began the session detailing the importance of writing clarity in not only increasing the chances of being awarded the grant, but also in receiving feedback that will make the next grant better in the event it is not awarded. To this end, providing a strong framework, directly stating answers to review criteria, and using definitive verbiage (e.g., determine, establish, etc.) in your specific aims can improve the likelihood of receiving funding. Another key aspect of writing a grant is striking a balance between the big picture and technical details. Consideration of varying backgrounds of potential reviewers and the circumstances the grant will be read in (e.g., after hours, weekends), as well as developing skills in science communication can be extremely helpful. Numerous resources are available for additional help, including seminars, workshops, and published workbooks (49).

How to Start a Collaboration

This career development workshop continued with an invited talk by Dr. Stavroula Kousteni (Columbia University Irving Medical Center) on how to start a collaboration and was moderated by Dr. Bram van der Eerden (Erasmus University Rotterdam). This workshop was led in a very interactive format. Dr. Kousteni began by directly asking the participants what are the main aspects/points that you look for in a new collaborator (e.g., expertise, new methodology, clinical samples, animal models) as it can help to refine your search for the best collaborator. She also mentioned it is important to set up the rules of the collaboration at the beginning in order to avoid any miscommunication and delay progress of the project. Another trick to establishing successful collaborations is to find a collaborator with a similar personality. In addition, this workshop summarized several positive and negative aspects of starting new collaborations and left us with several tips on what is crucial in this important part of our scientific work.

A Path to the Science of the HeART

The career development talk entitled "A path to the science of the HeART" was given by Dr. Ana Silva and was moderated by Dr. Rossella Labella (Columbia University). Dr. Silva shared her personal transition from postdoc in academia to a freelancer position as a scientific illustrator. Like the majority of early-stage investigators in academia, she was considering becoming a Principal Investigator as her first choice. She was excluding other career options for three main reasons: ego, expectation, and fear. With the help of the MIND (Making Informed Career Decisions) program at the Gladstone Institute she decided to mix her two passions, science and illustration, and to pursue an alternative career path as a scientific illustrator. This led to the opening of her own business in Portugal. She concluded the workshop with several pros and cons of being a freelancer worker.

Learning from Failure in Life and Research

The last talk of the BMAS Summer School 2021, was given by Dr. Jennifer Heemstra (Emory University) and moderated by Dr. Erica Scheller (Washington University in St. Louis). The main goal of this talk was to share the tremendous lessons that Dr. Heemstra has learned from her scientific and life experiences. She first invited the audience to reflect on their own challenges and lessons in their career path. She began with a first lesson: your success is determined by what you do when everything is going wrong; and added that our life is the most interesting experiment that we get to run. She reminded the audience that there will be times in research and in life where things do not go as planned. It is true that these challenges and failures are frustrating, but they can also be an opportunity for us to learn and grow. She shared the many challenges she has faced in her career, including being advised not to pursue a scientific career by one of her high school academic advisors, her participation in Science Olympiad, challenging herself with the organic course chemistry where she discovered her passion for chemistry, losing her father and one of her best friends, becoming pregnant during her first week of postdoctoral training, and not passing the tenure votes. Dr. Heemstra reflected on not receiving tenure as one of the worst times of her life because she felt that she disappointed both her family and lab members. Through all of these challenges she discovered that she is stronger than she thought.

Finally, we should learn to enjoy what we are doing and do it with passion. Discovering the passion is essential and fulfilling. However, we should develop our passion rather than follow it. Dr. Heemstra ended the talk by encouraging the audience to take a step out of their comfort zone every day to challenge our capabilities. One lesson we learned from this talk: what might be your biggest failure can empower you to the most life-changing experience in your whole life.

Poster Sessions

Poster sessions consisted of a combination of pre-recorded 3-minute video presentations and a live discussion over Zoom in individual rooms. Abstracts covered a wide range of topics (**Figure 3**) and were divided into three categories, one per day of the summer school: 1) BMAT and stem cells, 2) BMAT, aging and cancer, and 3) BMAT and metabolic diseases. A detailed list of poster presenters and abstract titles is available in **Table 1**, while abstracts with consent for publication are available online (12).

Awards

All the abstracts were evaluated from the scientific board of the BMAS in a blinded mode, each abstract was evaluated by three scientific board members and the final score was the sum of the three different evaluations. For abstract evaluation, the following criteria were considered: effectiveness of background and hypothesis, novelty of the data, clearness of communication, and overall quality of writing. The abstract that got the highest score was entitled *Glucocorticoid receptor in bone marrow adipocytes is not required for expansion during calorie restriction* and presented by Dr. Rebecca L. Schill from University of Michigan, USA.

In addition, the organizing committee of the summer school gave awards for the best poster presentation and for the most active participant. The former was assigned to Laura Trainor from Medical Research Institute, Adelaide, Australia and the latter to Husam Bensreti from Augusta University, Georgia, USA.

FIGURE 3 | Word cloud of the abstract keywords. The keyword size correlates with the number of times that keyword was used in the abstracts. The analysis was carried out with WordCloud package in R.

TABLE 1 | List of the presenters and titles of the three poster sessions.

Presenter	Poster Title
1) BMAT and stem cells	
Viktorija Avilkina	How the severity level and duration of energy deficit in mice model affects the bone phenotype, bone marrow adiposity and bone marrow stromal cells differentiation capacity?
Federica Quacquarelli	Ex vivo human cellular models to study adipocyte-induced trans differentiation of osteoblasts.
Drenka Trivanović	Human bone marrow adipose tissue niche supports mesenchymal progenitors with unique metabolic and stem cell features.
Amélie Paquet	Bone Marrow Adipocytes differentiated *in vitro* express the mRNA of the human cathelicidin antimicrobial peptide (hCAMP).
Thomas H. Ambrosi	Distinct lineage fates of diverse skeletal stem cell types orchestrate long bone physiology.
George Soultoukis	Physiological And Nutrition-related Effects on Bone Marrow Adipocyte Formation.
Vagelis Rinotas	Investigating the effects of Denosumab treatment and discontinuation in bone marrow adiposity through analysis of Tg/RANKL osteoporotic mice
2) BMAT, aging and cancer	
Laura Trainor	Bone marrow adipocyte phenotype is altered early in progression to multiple myeloma.
Stefan Ruschke	Variation of the human vertebral bone marrow water T2 relaxation time assessed by *in vivo* single-voxel magnetic resonance spectroscopy.
Michele Dello Spedale Venti	Morphologic and phenotypic changes of human bone marrow adipocytes in marrow metastasis and chronic myeloid neoplasia.
Charlotte Rinne	The Effects of Nutrients on Stem Cell Function and Regeneration in Bone Tissue in Response to Ectopic Adipogenesis.
Wangjie Liu	Deciphering the hierarchy of human bone marrow stromal cells.
Laimar C Garmo	Effects of Per- and Polyfluoroalkyl Substances on Bone Marrow Adipose Environment: Potential Implications for Bone Metastatic Cancers.
Katelyn Greene	Assessing Bone Marrow Adipose Tissue in Older Adult Lumbar Vertebrae.
3) BMAT and metabolic diseases	
Husam Bensreti	Orchiectomy sensitizes the skeleton of male mice to the deleterious effects of kynurenine.
Dalia Ali	High Fat Diet (HFD)-Induced Obesity Augments the Deleterious Effects of Estrogen Deficiency in Bone. Evidence from ovariectomized Mice.
Rebecca L. Schill	Glucocorticoid Receptor in Bone Marrow Adipocytes is not Required for Expansion During Calorie Restriction.
Katja Wegener	Hyaluronan matrix in bone marrow adipose tissue: implications for the development and progression of insulin resistance.
Andrea Benova	The effect of novel thiazolidinedione analog on bone and metabolic parameters in animal model of diet induced obesity.
Jacob M. Bond	The role of Nox4-ROS in driving obesogenic bone marrow mesenchymal stem cell phenotype in mice.
Not shown	*Poster 14*

CONCLUDING REMARKS AND PERSPECTIVES

Our understanding of BMA's role and function in health and disease has grown considerably in the last years. Since 2015, an annual meeting on BMA has been organized with the aim to help collaborative research in the field and promote knowledge, which was accomplished with growing number of BMAS members and experts. In 2021, BMAS launched the first edition of the BMAS Summer School, an event organized by young scientists and addressed to trainees and junior investigators interested in the BMA field. Many biological questions remain to be addressed about the origin, development, and physiopathology of BMA, supporting the need to raise a young generation of scientists to the study of BMA. For instance, do BMAds share a common progenitor with osteoblasts? Why does BMAT develop? Do BMAds have only a filling function in bone marrow? Why do BMAds increase in conditions such as osteoporosis? Why do BMAds decrease with metastatic invasion of the bone marrow? Are there transcription factors and/or cell surface markers that are specific to BMAds and not other adipocytes? Will we be able to routinely measure BMAT in patients? Will it be possible in future to use BMAT assessment as diagnostic or prognostic tool?

BMAS Summer School 2021 was a success not only for the productive discussion coming from the insightful lectures of the speakers and the vibrant community of attendees, but also for bringing in scientists from fields other than BMA, and for the creation of a young investigator working group, the Next Generation BMAS. The main aim of the group will be to organize the biannual summer school, and other events like virtual happy hours, data discussion series, and "meet the professor" events, that will be included in the BMA meetings.

AUTHOR CONTRIBUTIONS

RL and BP served as co-chairs of the BMAS SS 2021 meeting, and S-LL, VA, RS, MT, and AV as members of the organizing committee. BP collected and analyzed metadata. RL, S-LL, VA, RS, MT, AV, and BP wrote and revised the manuscript. All authors approved the submitted version.

ACKNOWLEDGMENTS

BMAS Summer School 2021 was supported by Frontiers and the BMAS. Technical support was provided by Joey Daoud from NewTerritory Media. The organizers would like to thank all the invited speakers and the attendees.

REFERENCES

1. Tavassoli M. Ultrastructural Development of Bone Marrow Adipose Cell. *Cells Tissues Organs* (1976) 94(1):65–77. doi: 10.1159/000144545
2. Neumann E. The Law of Distribution of Yellow and Red Marrow in the Bones of the Extremities. *Cent J Med Sci* (1882) 20:321–3.
3. Piney A. The Anatomy of the Bone Marrow: With Special Reference to the Distribution of the Red Marrow. *Br Med J* (1922) 2(3226):792–5.
4. Hardouin P, Marie PJ, Rosen CJ. New Insights Into Bone Marrow Adipocytes: Report From the First European Meeting on Bone Marrow Adiposity (BMA 2015). *Bone* (2016) 93:212–5. doi: 10.1016/j.bone.2015.11.013
5. van der Eerden B, van Wijnen A. Meeting Report of the 2016 Bone Marrow Adiposity Meeting. *Adipocyte* (2017) 6(4):304–13. doi: 10.1080/21623945.2017.1313374
6. Corsi A, Palmisano B, Tratwal J, Riminucci M, Naveiras O. Brief Report From the 3rd International Meeting on Bone Marrow Adiposity (BMA 2017). *Front Endocrinol (Lausanne)* (2019) 10. doi: 10.3389/fendo.2019.00336
7. Penel G, Kerckhofs G, Chauveau C. Brief Report From the 4th International Meeting on Bone Marrow Adiposity (BMA2018). *Front Endocrinol (Lausanne)* (2019) 10:691. doi: 10.3389/fendo.2019.00691
8. Scheller EL, McGee-Lawrence ME, Lecka-Czernik B. Report From the 6th International Meeting on Bone Marrow Adiposity (BMA2020). *Front Endocrinol (Lausanne)* (2021) 12:712088. doi: 10.3389/fendo.2021.712088
9. Tratwal J, Labella R, Bravenboer N, Kerckhofs G, Douni E, Scheller EL, et al. Reporting Guidelines, Review of Methodological Standards, and Challenges Toward Harmonization in Bone Marrow Adiposity Research. Report of the Methodologies Working Group of the International Bone Marrow Adiposity Society. *Front Endocrinol (Lausanne)* (2020) 11. doi: 10.3389/fendo.2020.00065
10. Bravenboer N, Bredella MA, Chauveau C, Corsi A, Douni E, Ferris WF, et al. Standardised Nomenclature, Abbreviations, and Units for the Study of Bone Marrow Adiposity: Report of the Nomenclature Working Group of the International Bone Marrow Adiposity Society. *Front Endocrinol (Lausanne)* (2020) 10. doi: 10.3389/fendo.2019.00923
11. Lucas S, Tencerova M, von der Weid B, Andersen TL, Attané C, Behler-Janbeck F, et al. Guidelines for Biobanking of Bone Marrow Adipose Tissue and Related Cell Types: Report of the Biobanking Working Group of the International Bone Marrow Adiposity Society. *Front Endocrinol (Lausanne)* (2021) 12. doi: 10.3389/fendo.2021.744527
12. Palmisano B, Labella R, Avilkina V, Little S, Sarkis R, Tencerova M, et al. *1st Bone Marrow Adiposity Society (Bmas) Summer School*. Frontiers Media SA (2021).
13. Post S, Abdallah BM, Bentzon JF, Kassem M. Demonstration of the Presence of Independent Pre-Osteoblastic and Pre-Adipocytic Cell Populations in Bone Marrow-Derived Mesenchymal Stem Cells. *Bone* (2008) 43(1):32–9. doi: 10.1016/j.bone.2008.03.011
14. Kristensen LP, Chen L, Nielsen MO, Qanie DW, Kratchmarova I, Kassem M, et al. Temporal Profiling and Pulsed SILAC Labeling Identify Novel Secreted Proteins During Ex Vivo Osteoblast Differentiation of Human Stromal Stem Cells. *Mol Cell Proteomics* (2012) 11(10):989–1007. doi: 10.1074/mcp.M111.012138
15. Abdallah BM, Ditzel N, Laborda J, Karsenty G, Kassem M. DLK1 Regulates Whole-Body Glucose Metabolism: A Negative Feedback Regulation of the Osteocalcin-Insulin Loop. *Diabetes* (2015) 64(9):3069–80. doi: 10.2337/db14-1642
16. Jafari A, Qanie D, Andersen TL, Zhang Y, Chen L, Postert B, et al. Legumain Regulates Differentiation Fate of Human Bone Marrow Stromal Cells and is Altered in Postmenopausal Osteoporosis. *Stem Cell Rep* (2017) 8(2):373–86. doi: 10.1016/j.stemcr.2017.01.003
17. Tencerova M, Kassem M. The Bone Marrow-Derived Stromal Cells: Commitment and Regulation of Adipogenesis. *Front Endocrinol (Lausanne)* (2016) 7:127. doi: 10.3389/fendo.2016.00127
18. Tencerova M, Frost M, Figeac F, Nielsen TK, Ali D, Lauterlein J-JL, et al. Obesity-Associated Hypermetabolism and Accelerated Senescence of Bone Marrow Stromal Stem Cells Suggest a Potential Mechanism for Bone Fragility. *Cell Rep* (2019) 27(7):2050–2062.e6. doi: 10.1016/j.celrep.2019.04.066
19. Tencerova M, Okla M, Kassem M. Insulin Signaling in Bone Marrow Adipocytes. *Curr Osteoporos Rep* (2019) 17(6):446–54. doi: 10.1007/s11914-019-00552-8
20. Cohen L. Bone Marrow: Structure and Function by Mehdi Tavassoli and Joseph Mendel Yoffey. *Perspect Biol Med* (1985) 28(3):479–81. doi: 10.1353/pbm.1985.0032
21. Chan CKF, Gulati GS, Sinha R, Weissman IL, Chang HY, Longaker MT, et al. Identification of the Human Skeletal Stem Cell Article Identification of the Human Skeletal Stem Cell. *Cell* (2018) 175(1):43–56.e21. doi: 10.1016/j.cell.2018.07.029

22. Pinho S, Frenette PS. Haematopoietic Stem Cell Activity and Interactions With the Niche. *Nat Rev Mol Cell Biol* (2019) 20(5):303–20. doi: 10.1038/s41580-019-0103-9
23. Sacchetti B, Funari A, Michienzi S, Di Cesare S, Piersanti S, Saggio I, et al. Self-Renewing Osteoprogenitors in Bone Marrow Sinusoids can Organize a Hematopoietic Microenvironment. *Cell* (2007) 131(2):324–36. doi: 10.1016/j.cell.2007.08.025
24. Donsante S, Palmisano B, Serafini M, Robey PG, Corsi A, Riminucci M. From Stem Cells to Bone-Forming Cells. *Int J Mol Sci* (2021) 22(8). doi: 10.3390/ijms22083989
25. Cawthorn WP, Scheller EL, Learman BS, Parlee SD, Simon BR, Mori H, et al. Bone Marrow Adipose Tissue is an Endocrine Organ That Contributes. *Cell Metab* (2015) 20(2):368–75. doi: 10.1016/j.cmet.2014.06.003
26. Valet C, Batut A, Vauclard A, Dortignac A, Bellio M, Payrastre B, et al. Adipocyte Fatty Acid Transfer Supports Megakaryocyte Maturation. *Cell Rep* (2020) 32(1):107875. doi: 10.1016/j.celrep.2020.107875
27. Duan D-Y, Tang J, Tian H-T, Shi Y-Y, Jia J. Adipocyte-Secreted Microvesicle-Derived Mir-148a Regulates Adipogenic and Osteogenic Differentiation by Targeting Wnt5a/Ror2 Pathway. *Life Sci* (2021) 278:119548. doi: 10.1016/j.lfs.2021.119548
28. Bianco P. Bone and the Hematopoietic Niche: A Tale of Two Stem Cells. *Blood* (2011) 117(20):5281–8. doi: 10.1182/blood-2011-01-315069
29. Nehlin JO, Jafari A, Tencerova M, Kassem M. Aging and Lineage Allocation Changes of Bone Marrow Skeletal (Stromal) Stem Cells. *Bone* (2019) 123:265–73. doi: 10.1016/j.bone.2019.03.041
30. Reagan MR, Fairfield H, Rosen CJ. Bone Marrow Adipocytes: A Link Between Obesity and Bone Cancer. *Cancers (Basel)* (2021) 13(3):364. doi: 10.3390/cancers13030364
31. Eyzaguirre E, Liqiang W, Karla GM, Rajendra K, Alberto A, Gatalica Z. Intraosseous Lipoma. A Clinical, Radiologic, and Pathologic Study of 5 Cases. *Ann Diagn Pathol* (2007) 11(5):320–5. doi: 10.1016/j.anndiagpath.2006.09.006
32. Thorns C, Schardt C, Katenkamp D, Kähler C, Merz H, Feller AC. Hibernoma-Like Brown Fat in the Bone Marrow: Report of a Unique Case. *Virchows Arch* (2008) 452(3):343–5. doi: 10.1007/s00428-007-0559-4
33. Suchacki KJ, Tavares AAS, Mattiucci D, Scheller EL, Papanastasiou G, Gray C, et al. Bone Marrow Adipose Tissue is a Unique Adipose Subtype With Distinct Roles in Glucose Homeostasis. *Nat Commun* (2020) 11(1):3097. doi: 10.1038/s41467-020-16878-2
34. Pham TT, Ivaska KK, Hannukainen JC, Virtanen KA, Lidell ME, Enerbäck S, et al. Human Bone Marrow Adipose Tissue is a Metabolically Active and Insulin-Sensitive Distinct Fat Depot. *J Clin Endocrinol Metab* (2020) 105(7):2300–10. doi: 10.1210/clinem/dgaa216
35. Ermetici F, Briganti S, Delnevo A, Cannaò P, Di LG, Benedini S, et al. Bone Marrow Fat Contributes to Insulin Sensitivity and Adiponectin Secretion in Premenopausal Women. *Endocrine* (2018) 59(2):410–8. doi: 10.1007/s12020-017-1349-7
36. Cooper B. The Origins of Bone Marrow as the Seedbed of Our Blood: From Antiquity to the Time of Osler. *Baylor Univ Med Cent Proc* (2011) 24(2):115–8. doi: 10.1080/08998280.2011.11928697
37. Beeve AT, Shen I, Zhang X, Magee K, Yan Y, MacEwan MR, et al. Neuroskeletal Effects of Chronic Bioelectric Nerve Stimulation in Health and Diabetes. *Front Neurosci* (2021) 15. doi: 10.3389/fnins.2021.632768
38. Parlee SD, Lentz SI, Mori H, MacDougald OA. Quantifying Size and Number of Adipocytes in Adipose Tissue. *Methods Enzymol* (2014) 537:93–122. doi: 10.1016/B978-0-12-411619-1.00006-9
39. Lorenz MR, Brazill JM, Beeve AT, Shen I, Scheller EL. A Neuroskeletal Atlas: Spatial Mapping and Contextualization of Axon Subtypes Innervating the Long Bones of C3H and B6 Mice. *J Bone Miner Res* (2021) 36(5):1012–25. doi: 10.1002/jbmr.4273
40. Idleburg C, Lorenz MR, DeLassus EN, Scheller EL, Veis DJ. Immunostaining of Skeletal Tissues. *Methods Mol Biol* (2021) 2021:261–73. doi: 10.1007/978-1-0716-0989-7_15
41. Pontén F, Schwenk JM, Asplund A, Edqvist P-HD. The Human Protein Atlas as a Proteomic Resource for Biomarker Discovery. *J Intern Med* (2011) 270(5):428–46. doi: 10.1111/j.1365-2796.2011.02427.x
42. Craft CS, Robles H, Lorenz MR, Hilker ED, Magee KL, Andersen TL, et al. Bone Marrow Adipose Tissue Does Not Express UCP1 During Development or Adrenergic-Induced Remodeling. *Sci Rep* (2019) 9(1):17427. doi: 10.1038/s41598-019-54036-x
43. Griffith JF, Yeung DKW, Ma HT, Leung JCS, Kwok TCY, Leung PC. Bone Marrow Fat Content in the Elderly: A Reversal of Sex Difference Seen in Younger Subjects. *J Magn Reson Imaging* (2012) 36(1):225–30. doi: 10.1002/jmri.23619
44. Baum T, Rohrmeier A, Syväri J, Diefenbach MN, Franz D, Dieckmeyer M, et al. Anatomical Variation of Age-Related Changes in Vertebral Bone Marrow Composition Using Chemical Shift Encoding-Based Water–Fat Magnetic Resonance Imaging. *Front Endocrinol (Lausanne)* (2018) 9. doi: 10.3389/fendo.2018.00141
45. Karampinos DC, Ruschke S, Dieckmeyer M, Diefenbach M, Franz D, Gersing AS, et al. Quantitative MRI and Spectroscopy of Bone Marrow. *J Magn Reson Imaging* (2018) 47(2):332–53. doi: 10.1002/jmri.25769
46. Patsch JM, Li X, Baum T, Yap SP, Karampinos DC, Schwartz AV, et al. Bone Marrow Fat Composition as a Novel Imaging Biomarker in Postmenopausal Women With Prevalent Fragility Fractures. *J Bone Miner Res* (2013) 28(8):1721–8. doi: 10.1002/jbmr.1950
47. Syväri J, Ruschke S, Dieckmeyer M, Hauner HH, Junker D, Makowski MR, et al. Estimating Vertebral Bone Marrow Fat Unsaturation Based on Short-TE STEAM MRS. *Magn Reson Med* (2021) 85(2):615–26. doi: 10.1002/mrm.28453
48. Weidlich D, Honecker J, Boehm C, Ruschke S, Junker D, Van AT, et al. Lipid Droplet–Size Mapping in Human Adipose Tissue Using a Clinical 3T System. *Magn Reson Med* (2021) 86(3):1256–70. doi: 10.1002/mrm.28755
49. Robertson JD RSMD. *The Grant Application Writer's Workbook: National Institutes of Health Version*. Grant Writ Semin Work LLC (2018), 2018.

Conflict of Interest: The authors declare that the research was conducted in the absence of any commercial or financial relationships that could be construed as a potential conflict of interest.

frontiers | Frontiers in Endocrinology

REVIEW
published: 22 April 2022
doi: 10.3389/fendo.2022.882297

Toward Marrow Adipocytes: Adipogenic Trajectory of the Bone Marrow Stromal Cell Lineage

Yuki Matsushita, Wanida Ono and Noriaki Ono *

University of Texas Health Science Center at Houston School of Dentistry, Houston, TX, United States

Bone marrow contains precursor cells for osteoblasts and adipocytes in the stromal compartment. Bone marrow adipose tissue (BMAT) is an important constituent of the bone marrow that is particularly abundant in adults. BMAT is composed of the proximal "regulated" BMAT containing individual adipocytes interspersed within actively hematopoietic marrow, and the distal "constitutive" BMAT containing large adipocytes in the area of low hematopoiesis. Historically, bone marrow adipocytes were regarded as one of the terminal states of skeletal stem cells, which stand at the pinnacle of the lineage and possess trilineage differentiation potential into osteoblasts, chondrocytes and adipocytes. Recent single-cell RNA-sequencing studies uncover a discrete group of preadipocyte-like cells among bone marrow stromal cells (BMSCs), and recent mouse genetic lineage-tracing studies reveal that these adipocyte precursor cells possess diverse functions in homeostasis and regeneration. These adipogenic subsets of BMSCs are abundant in the central marrow space and can directly convert not only into lipid-laden adipocytes but also into skeletal stem cell-like cells and osteoblasts under regenerative conditions. It remains determined whether there are distinct adipocyte precursor cell types contributing to two types of BMATs. In this short review, we discuss the functions of the recently identified subsets of BMSCs and their trajectory toward marrow adipocytes, which is influenced by multiple modes of cell-autonomous and non-cell autonomous regulations.

Keywords: single-cell RNA sequencing (scRNAseq), skeletal stem cells (SSCs), *in vivo* lineage-tracing experiments, bone marrow stromal cell (BMSC), bone marrow adipose tissue (BMAT)

OPEN ACCESS

Edited by:
Jason Horton,
Upstate Medical University,
United States

Reviewed by:
Ormond A. MacDougald,
University of Michigan, United States
Kenneth Lewis,
University of Michigan, United States in collaboration with reviewer OM
Elizabeth Rendina-Ruedy,
Vanderbilt University Medical Center,
United States

***Correspondence:**
Noriaki Ono
noriaki.ono@uth.tmc.edu

Specialty section:
This article was submitted to Bone Research, a section of the journal Frontiers in Endocrinology

Received: *23 February 2022*
Accepted: *24 March 2022*
Published: *22 April 2022*

Citation:
Matsushita Y, Ono W and Ono N (2022) Toward Marrow Adipocytes: Adipogenic Trajectory of the Bone Marrow Stromal Cell Lineage. Front. Endocrinol. 13:882297. doi: 10.3389/fendo.2022.882297

INTRODUCTION

Bone marrow houses diverse classes of cells, including cells in the skeletal (or mesenchymal), the hematopoietic (blood) and the endothelial (vascular) lineages. Bone marrow contains precursor cells for bone-making osteoblasts and lipid-accumulating adipocytes in the stromal compartment, both of which are considered to play important roles in bone homeostasis and regeneration, as well as in hematopoiesis by providing a microenvironment. Classically, skeletal stem cells with self-renewability and multipotency are considered to stand at the top of the lineage, and their descendants fall through a hierarchical model, differentiating first into progenitors then into terminally differentiated cells such as

osteoblasts or adipocytes (1). However, it remains largely undefined whether skeletal stem/progenitor cells can be defined as discrete cell populations within the continuous spectrum of the bone marrow stromal cell lineage, and how their relationships with osteoblasts and adipocytes develop in a complex bone marrow microenvironment.

Recent single-cell RNA-sequencing (scRNA-seq) studies reveal profound cellular heterogeneity within bone marrow stromal cells (BMSCs) that are isolated by fluorescence-activated cell sorting (FACS) (2–9). These studies consistently found discrete preadipocyte-like cells populations expressing *leptin receptor* (*Lepr*) and *C-X-C motif chemokine ligand 12* (*Cxcl12*) within BMSCs. These cells highly express classical adipocyte markers such as *adiponectin* (*Adipoq*) and adipogenic transcription factors such as *peroxisome proliferator activated receptor gamma* (*Pparg*). These adipogenic cell populations encompass newly defined subsets of Adipo-CXCL12 abundant reticular cells (Adipo-CAR cells) (10, 11) and marrow adipogenic lineage precursors (MALPs) (12), which mainly exist as non-proliferative pericytes and perivascular stromal cells. Recent mouse genetic studies highlight the diverse functions of bone marrow adipocyte precursor cells that not only contribute to the formation of bone marrow adipose tissues (BMATs) but also regulate the formation of the trabecular and cortical bones (for more detailed reviews, see (13, 14)).

In this short review, we discuss the functions of bone marrow adipocyte precursor cells in homeostasis and regeneration, and potentially diverse cellular sources of bone marrow adipocytes.

BONE MARROW ADIPOSE TISSUE (BMAT) AND ITS FUNCTION

Functionally, bone marrow adipocyte precursor cells are poised to differentiate into lipid-laden adipocytes that generate bone marrow adipose tissues (BMATs). Marrow adiposity increases under various physiological and pathological conditions such as aging, osteoporosis, radiation, chemotherapy (15). BMAT represents a unique form of adipose tissues that constitutes over 10% of the total fat mass in lean and healthy human adults (16). BMAT is composed of regulated and constitutive BMATs (rBMAT and cBMAT, respectively) with distinct functionality (17). rBMAT is mainly located in the proximal skeletal components and contains individual adipocytes interspersed within the areas of active hematopoiesis. In contrast, cBMAT is mainly located in the distal portion and contains large adipocytes that develop in the areas of low hematopoiesis; the latter cBMAT develops earlier and remains preserved upon systemic challenges (17–19).

Historically, the two types of bone marrow, "red marrow" and "yellow marrow", have been recognized for several decades (20). The "red marrow" consists of blood-forming cells with scattered adipocytes, whereas the "yellow marrow" is filled almost entirely with adipocytes (21, 22). The cBMAT starts to form in the distal area at prenatal to neonatal stages, followed by rapid expansion early in life (17). In contrast, rBMAT develops later and expands with age, generally in areas of active hematopoiesis (17). BMAT acts as an endocrine organ and energy storage depot that can contribute to bone homeostasis, metabolism, hematopoiesis, and cancers (23), and associates with the pathophysiology of bone diseases such as osteoporosis (24). For example, osteoporosis is commonly associated with increased BMAT (25), and adipocyte-derived factors from BMAT can suppress osteoblast differentiation of skeletal stem cells and regulate bone remodeling (26). Interestingly, lipid metabolism of BMAT is distinct from that of subcutaneous adipocytes, as bone marrow adipocytes show diminished lipolytic activities and exhibit cholesterol-directed metabolism (27, 28). BMAT also has distinct roles in glucose homeostasis (29, 30). Moreover, bone marrow adipocytes regulate hematopoiesis through direct contact and cytokine secretion. In fact, marrow adipogenesis is associated with impaired hematopoiesis (31). Bone marrow adipocytes also regulate the progression of hematological diseases (32) and hematopoietic microenvironment (HME) regeneration (33), and promote proliferation and bone metastasis of cancer cells including prostate and breast cancers and melanoma (34–37). Therefore, BMAT has important regulatory functions in bone metabolism, hematopoiesis and bone metastasis.

Despite unique metabolic status and functions, whether rBMAT and cBMAT are supported by distinct populations of precursor cells remains unknown. Subcutaneous and marrow adipocytes are derived from different precursor cell populations and possess different metabolic patterns. It is important to characterize marrow adipocyte precursor cells further to unravel molecular mechanisms supporting the unique functions of distinct classes of BMATs.

THE BONE MARROW STROMAL CELL LINEAGE AND ITS TRAJECTORY TOWARD MARROW ADIPOCYTES

Understanding the landscape of the bone marrow stromal cell lineage is essential to identifying potential cellular origins of BMATs. Cells constituting the bone marrow stromal cell lineage have been at least partly revealed by recent large-scale scRNA-seq studies of BMSCs that are isolated by cell sorting (2–5, 11). The major limitation of these single-cell approaches is that bone marrow adipocytes are large-sized (~150μm) and fragile, therefore cannot be captured through conventional cell sorting or encapsulated in oil droplets in microfluidic devices. Nonetheless, these scRNA-seq studies successfully have identified discrete clusters of adipocyte precursor cells (preadipocyte-like cells) that abundantly express *Lepr*, in addition to cell clusters that might correspond to skeletal stem and progenitor cells, preosteoblasts and other stromal cell types.

These studies further infer the potential lineage relationship among identified bone marrow stromal cell types using computational approaches, such as RNA velocity (3, 4, 11). These studies identify putative skeletal stem cell populations,

such as *Lepr*$^+$ (encoding LepR) (3), *Cspg4*$^+$ (encoding NG2) (11) or *Nt5e*$^+$ (encoding CD73) (4), which are predicted to provide a cellular source of adipocyte precursor cells. Importantly, these studies place osteoblasts and preadipocytes at the opposite ends of the inferred lineage trajectory, while simultaneously identifying a number of transitional cell types among putative terminal states, highlighting the contiguous nature of the bone marrow stromal cell lineage that spans over osteoblasts and marrow adipocytes.

Therefore, recent scRNA-seq studies corroborate with the well-established ideas that preadipocyte-like cells represent a distinct state from osteoblasts and their precursors among BMSCs. However, the identities of putative skeletal stem/progenitor cell populations are variable among studies, therefore remain largely ambiguous. Further studies are required to delineate the identities of these stem cells and their relationships with more abundant preadipocyte-like stromal cells.

ADIPOGENIC SUBSET OF CXCL12$^+$LEPR$^+$ CELLS (ADIPO-CAR CELLS) AND THEIR OSTEOGENIC FUNCTIONS

As mentioned above, cells abundantly expressing adipocyte-related markers such as *Lepr* and *Adipoq* constitute major cellular subsets of BMSCs (5, 11). *Lepr* encodes leptin receptor (LepR) that is a cognate receptor for the circulating adipokine, leptin. LepR$^+$ stromal cells overlap substantially with CXCL12-abundant reticular (CAR) cells, as cells marked by Cxcl12-GFP coincide (approximately 90%) with cells marked by *Lepr-cre* (10, 38). LepR$^+$ stromal cells provide a major source of adipocytes in adult bone marrow (38), which is further supported by more recent lineage-tracing studies using *Lepr-creER* (39). Functionally, LepR promotes marrow adipogenesis, as conditional deletion of LepR in BMSCs using *Prrx1-cre* increases osteogenesis and decreases adipogenesis in bone marrow (40).

CAR cells have been originally described as adipo-osteogenic progenitors that form a component of the hematopoietic stem cell niche (41). CAR cells can be uniformly marked by *Ebf3-creER* in the adult stage (Ebf3$^+$ CAR cells), and contribute to both osteoblasts and adipocytes (42), supporting that LepR$^+$ and CXCL12$^+$ cells have similar cell fates. Importantly, CXCL12 is most abundantly expressed by reticular stromal cells in the central marrow space, and plays important roles in maintaining hematopoietic stem and progenitor cells (43–49). In fact, CXCL12 deletion in BMSCs causes reduction in hematopoietic cells in bone marrow (50, 51).

CAR cells have been recently reclassified into two classes of Osteo-CAR and Adipo-CAR cells (11), instead of a uniform entity as adipo-osteogenic progenitors (**Figure 1**). Osteo-CAR cells express both *Cxcl12* and *Alpl* (encoding alkaline phosphatase, a preosteoblast marker), but not *Lepr*. These Osteo-CAR cells are localized to arterioles and in proximity to the bone surface, which are poised to differentiate into osteoblasts. In contrast, Adipo-CAR cells with pre-adipocyte-like properties are localized to the areas around sinusoidal vessels located in the center of the marrow space, which are poised to differentiate into adipocytes. Adipo-CAR cells abundantly express classical adipocyte markers (*Adipoq*, *Lepr*) as well as hematopoiesis-supporting cytokines (*Kitl* and *Cxcl12*), but do not express osteogenic markers and cytokines such as *Alpl*, *Sp7* and *Clec11a* at the same level. It is intriguing to speculate that the adipocyte precursor identity may confer these Adipo-CAR cell with some metabolic advantages to secrete large amounts of cytokines, such as Kit ligand (SCF), CXCL12 and Adiponectin.

The next important question is, what are the *in vivo* cell fates and functions of preadipocyte-like BMSCs including Adipo-CAR cells? The answer to this question has been partly contributed by mouse genetic lineage-tracing studies using a *Cxcl12-creER* line (10). Interestingly, the *Cxcl12-creER* bacterial artificial chromosome (BAC) transgenic line can almost exclusively mark a preadipocyte-like subset of CAR cells, which may correspond to Adipo-CAR cells, upon tamoxifen injection. These cells are quiescent and dormant with little colony-forming activities in physiological conditions. These Cxcl12-creER$^+$ preadipocyte-like cells readily become marrow adipocytes, but do not become cortical bone osteoblasts in normal conditions. However, these Cxcl12-creER$^+$ cells can rapidly convert their identity into a skeletal stem cell-like state in response to injury, associated with upregulation of osteoblast-signature genes and activation of canonical Wnt signaling components. As a result, these cells further differentiate into cortical bone osteoblasts to repair bone defects.

Therefore, Adipo-CAR cells, which are broadly distributed throughout the central marrow space, may maintain the potential to dedifferentiate into skeletal stem cell-like cells under regenerative conditions, supporting the theory that dormant adipocyte-like marrow stromal cells can support the remarkable regenerative capacity of bones through cellular plasticity. These findings also suggest that skeletal stem cells that are actively involved in regenerative conditions may be at least in part contributed through cellular plasticity in adults (**Figure 2A**) (10, 52).

Additionally, another preadipocyte-like subset of BMSCs termed marrow adipogenic lineage precursor (MALP) cells, which are marked by "adipocyte-specific" lines such as *Adipoq-cre* and *Adipoq-creER*, regulates bone formation within marrow space (12). MALP cells form a vast three-dimensional network surrounding sinusoidal blood vessels, and ablation of these cells using a diphtheria toxin fragment A (DTA) allele causes a massive increase of trabecular bones throughout marrow space, especially in female mice (12, 53). This is considered to arise from loss of MALP cell-derived factors that locally inhibit differentiation of skeletal stem/progenitor cells. Therefore, MALP cells can regulate osteogenesis in a cell non-autonomous manner.

Therefore, multiple adipocyte-related cell types have been described to date in the bone marrow, and these adipogenic subsets of BMSCs possess unexpectedly diverse functions beyond formation of marrow adipose tissues, particularly in the context of cortical and trabecular bone formation and regeneration. The important remaining question is whether these thus-far identified adipogenic BMSC subsets represent separate or overlapping entities, or reside in distinct bone marrow

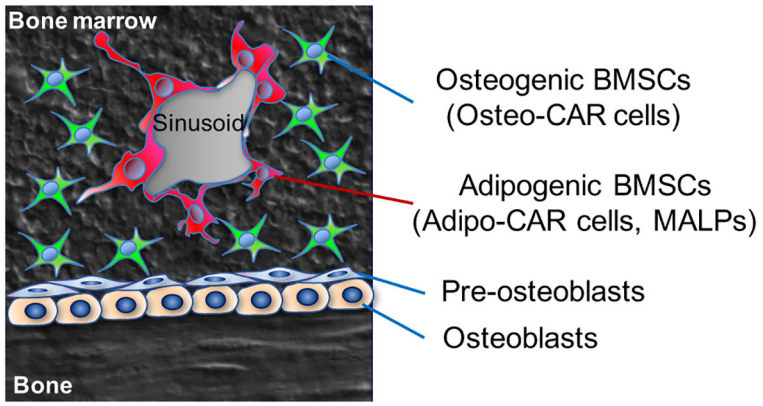

FIGURE 1 | Two major subsets of bone marrow stromal cells (BMSCs). Adipogenic BMSCs (Adipo-CAR cells) with pre-adipocyte-like properties are localized to the areas around sinusoidal vessels located in the center of the marrow space, which are poised to differentiate into adipocytes.

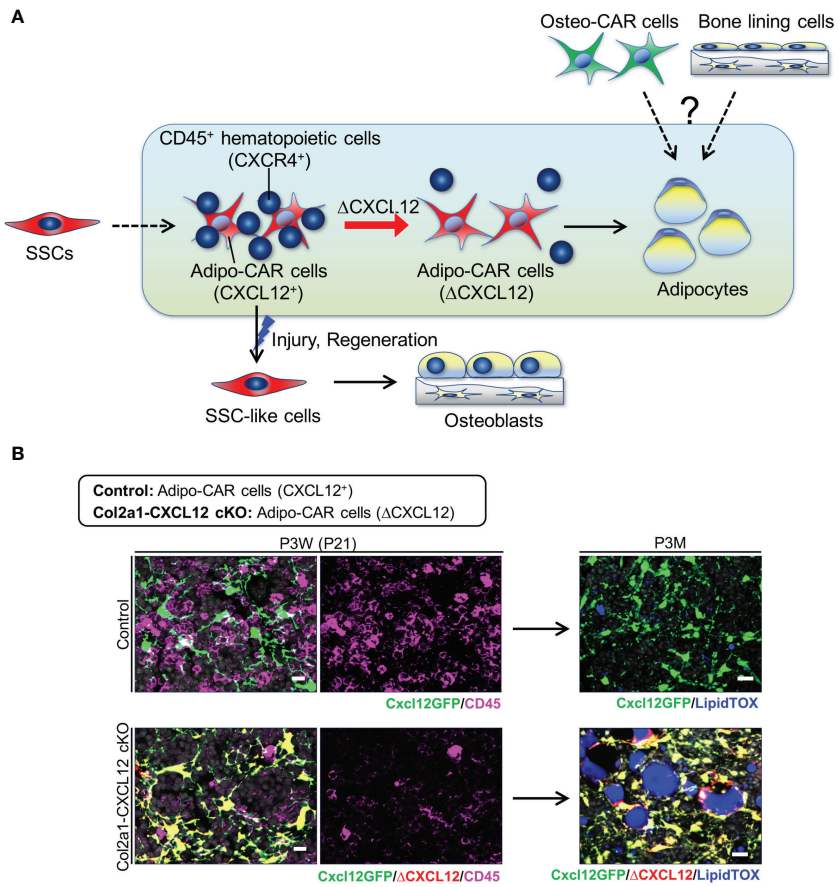

FIGURE 2 | Adipogenic trajectory of the bone marrow stromal cell lineage. **(A)** In physiological condition, dormant Adipo-CAR cells can become marrow adipocytes. Hematopoietic cells may regulate marrow adipogenesis in a manner dependent on CXCL 12-mediated physical coupling. CXCL 12 deletion leads to a reduction of stromal-hematopoietic coupling and accelerates marrow adipogenesis. In contrast, Adipo-CAR cells convert into skeletal stem cell-like cells in response to injury, and redifferentiate into osteoblasts through cellular plasticity to support cortical bone regeneration. **(B)** Central bone marrow of control (*Cxcl12*$^{GFP/+}$) and Col2a1-CXCL12 cKO (*Col2a1-cre; Cxcl12*$^{GFP/fl}$) mice stained for CD45 and lipid TOX, at 3W (left) and 3M (right).

microenvironments in a way consistent with two different classes of BMATs. Delineating adipogenic BMSC subsets further will facilitate our understanding of diverse functions of bone marrow adipocytes and their precursor cells.

CXCL12-MEDIATED CELL NON-AUTONOMOUS MECHANISMS DIRECT BONE MARROW ADIPOGENESIS

The prevailing notion is that bone marrow adiposity is induced by an aberrant cell fate shift of bone marrow skeletal stem cell populations due to cell-intrinsic changes. For example, loss of Wnt/β-catenin signaling (54), intracrine VEGF signaling (55) or PTH/PTHrP receptor signaling (56) and its downstream Gsα signaling (57), has been shown to induce a bias in cell differentiation toward adipocytes. However, because there are a large number of preadipocyte-like cells within the stromal compartment throughout the marrow space and these cells have not yet accumulated intracellular lipid, marrow adiposity may be more promptly regulated at the transition between these precursor cells to fully lipid-laden marrow adipocytes. In other words, the rate-limiting step for marrow adiposity may be at the level of precursor cells, but not at the level of stem cells.

CXCL12 has well-documented roles in hematopoiesis. Additionally, CXCL12 released by BMSCs regulates osteogenesis and adipogenesis; while osteogenesis is controlled by a cell-autonomous mechanism mediated by the CXCL12-CXCR4 signaling pathway, adipogenesis is regulated by a cell-non-autonomous mechanism involving an unidentified cell type (50). The Lai group demonstrates that conditional deletion of *Cxcl12* using *Prrx1-cre* or *Osx-cre* leads to marrow adiposity and reduced trabecular bones, whereas conditional deletion of *Cxcr4* using *Prrx1-cre* causes reduced trabecular bones without marrow adiposity. Interestingly, marrow adiposity in these *Cxcl12*-deficient mice occurs in the metaphyseal region starting from neonatal stages (50). These premature bone marrow adipose tissues in the mutant mice resemble rBMAT, indicating that rBMAT formation may be at least in part regulated by non-cell autonomous mechanisms.

The next important question is, what are the potential cell non-autonomous mechanisms that regulate premature marrow adiposity associated with CXCL12-deficient BMSCs? More recent studies demonstrate that many CXCL12$^+$ preadipocyte-like cells (Cxcl12-creER$^+$, Adipo-CAR cells) are physically coupled with hematopoietic cells, particularly with B-cell precursors, monocytes and granulocytes, in a protease-sensitive manner, possibly through CXCL12-CXCR4 interactions (51). Further, CXCL12 deletion in BMSCs using *Col2a1-cre* leads to a reduction of stromal-hematopoietic coupling and extensive marrow adipogenesis specifically in adult bone marrow (**Figure 2B**). Interestingly, unlike other CXCL12-deficient models, marrow adiposity does not occur in younger stages in these *Col2a1-cre*-driven *Cxcl12* mutant mice, with Adipo-CAR cells appearing to directly convert into lipid-laden adipocytes without involving cell-intrinsic defects in skeletal stem/progenitor cell fates.

Therefore, these studies indicate that there may be a potential link between CXCL12-dependent stromal-hematopoietic coupling and marrow adipogenesis, as the adipogenic subset of CXCL12$^+$ BMSCs are highly interactive with hematopoietic cells. One possible mechanism is that physically-coupled hematopoietic cells provide some types of microenvironmental cues to prevent premature differentiation of pre-adipocyte-like stromal cells into fully lipid-laden marrow adipocytes (50, 51). It is intriguing to think that hematopoietic cells may directly or indirectly regulate marrow adipogenesis in a manner dependent on CXCL12-mediated physical coupling, although details need to be clarified by further experimentation (**Figure 2**). This may serve as one of the important mechanisms that dictate age and disease-related increase in marrow adiposity commonly observed in humans.

BONE-SPECIFIC SECONDARY ADIPOGENESIS PATHWAY: FROM OSTEO-CAR TO MARROW ADIPOCYTES?

Interestingly, recent studies demonstrate that there might be an alternative bone-specific adipogenic pathway that bypasses classical adiponectin-expressing preadipocyte-like cells. This unique adipogenic pathway has been discovered in fat-free (FF) mice, in which essentially all adiponectin-expressing adipocytes and their precursor cells are ablated using *Adipoq-cre* and inducible DTA expression (58). This genetic model mimics Berardinelli-Seip congenital generalized lipodystrophy, which is associated with increased bone mass and diabetic conditions. Interestingly, in these lipodystrophic FF mice, bone marrow adipocytes still develop within regions of bone marrow that are normally devoted to hematopoiesis under aging and states of metabolic stresses. These bone marrow adipocytes are recruited from adiponectin-negative stromal cells and specialized for lipid storage with compromised lipid mobilization and cytokine expression.

What is the identity of adiponectin-negative stromal cells that can give rise to special bone marrow adipocytes under lipodystrophic conditions? One possibility is that bone marrow adipocytes can originate alternatively from alternative preosteoblast-like subsets of BMSCs, such as Osteo-CAR cells that localize to the peripheral arterioles and endocortical surfaces, or bone-lining cells that are marked by a pulse-chase protocol using *Dmp1-creER* (59) (**Figure 2A**), although neither of these studies (53, 59) provided direct evidence based on rigorous *in vivo* lineage-tracing approaches that can directly target these cells. These potentially diverse cellular sources of bone marrow adipocytes highlight the adaptability of BMATs, particularly "regulated" rBMAT in bone marrow, which can promptly respond to systemic and local health and disease conditions (17). In fact, these ectopic lipodystrophic marrow adipocytes develop in the regions that normally develop rBMATs, indicating an association between adiponectin-negative adipocyte precursor cells and rBMAT formation. It remains to be determined if preosteoblast-like subsets of BMSCs (such as Osteo-CAR cells) can be directly converted to bone marrow adipocytes in rBMAT under physiological conditions.

LIMITATIONS OF CURRENT STUDIES AND FUTURE DIRECTIONS

It is evident that bone marrow adipocytes constituting the two types of BMATs originate from BMSC subsets. Therefore, the unique metabolic and functional features of bone marrow adipocytes are likely to be conferred by their precursor cell populations. Single-cell RNA-seq studies reveal that preadipocyte-like BMSCs do not represent a single homogenous entity, but are instead constituted by a spectrum of heterogeneous cell types spanning over preosteoblasts and lipid-laden adipocytes. The reasonable hypothesis is that the two distinct classes of BMATs are formed by different types of bone marrow adipocyte precursor cells. However, detailed characteristics of these adipocyte precursor cell subtypes have not been successfully revealed.

Despite tremendous progress in the field in recent years, in-depth functional analyses of bone marrow adipocytes have been hampered due to critical technical limitations. First, bone marrow adipocytes are extremely fragile and large-sized, therefore there is no reliable method to isolate these cells for single-cell analyses or culture them *in vitro*. Second, no transgenic tool is available yet to target only adipocytes and their precursors in bone marrow, but not those in subcutaneous tissues or elsewhere. Because of these technical hurdles, the functional significance of bone marrow adipocytes in bone metabolism and hematopoiesis has not been fully uncovered. Third, an inducible genetic tool that can specifically mark preosteoblast-like subsets of BMSCs, such as Osteo-CAR cells, is not yet available. Therefore, whether an alternative bone-specific adipogenesis pathway truly exists has not been formally demonstrated.

Technical breakthroughs are needed to unravel intercellular interactions among bone marrow adipocytes and their surrounding cells at a single-cell level in their native environment. Bone marrow adipocytes constitute a part of the stromal-reticular network, residing in an intricate microenvironment (60) and abundantly secreting a large variety of cytokines including SCF and CXCL12. More sophisticated approaches will be needed to fully define the functions of different types of bone marrow adipocytes and their precursor cells *in vivo*, and eventually define how they regulate bone metabolism and hematopoiesis through both cell-autonomous and cell-non-autonomous mechanisms.

CONCLUSION

In this review, we discussed the current understanding of the bone marrow stromal cell lineage, which is largely contributed by recent scRNA-seq and *in vivo* lineage-tracing studies. These studies have substantially refined our idea on bone marrow adipocytes and their precursor cells, particularly highlighting important functions of the adipogenic subsets of bone marrow stromal cells in marrow adiposity and bone homeostasis.

It has been generally considered that skeletal stem cells have pivotal roles as a cellular origin of bone marrow adipocytes. While this concept still holds true, the emerging notion is that the important regulatory step may lie downstream at the level of adipocyte precursor cells; this is facilitated by the discovery of a discrete preadipocyte-like population of $CXCL12^{+}LepR^{+}$ BMSCs that exist in a large number throughout the marrow space. Functionally important subsets of adipogenic BMSCs include recently described populations of Adipo-CAR cells and MALPs that have substantial regulatory functions in osteogenesis. Prompt increase in marrow adiposity in aging and other disease conditions may be induced by virtue of the inherent capacity of adipogenic BMSCs that can easily convert to lipid-laden bone marrow adipocytes.

The trajectory to bone marrow adipocytes is now becoming clearer. The remaining task is to clarify if there are discrete precursor cell populations that contribute to two types of BMATs. It is possible that bone marrow adipocytes of "regulated" rBMAT are also contributed to by an alternative bone-specific pathway originating from preosteoblasts, although this pathway has been demonstrated so far only in extreme adipocyte scarcity in lipodystrophic fat-free mice. Clarifying further cellular origins of bone marrow adipocytes of cBMAT and rBMAT will give us the opportunity to clarify the formation and the disappearance of marrow adipocytes in normal development, pathological conditions and therapeutic responses. These future endeavors will lead to a more detailed understanding of the function of bone marrow adipocytes that have incredibly diverse functions through local and systemic regulations.

AUTHOR CONTRIBUTIONS

YM and NO drafted the manuscript and generated the figure. YM conducted literature search. WO critically revised the manuscript. All approved the final version of the manuscript.

FUNDING

This research was supported by National Institute of Health grants R01DE026666 and R01DE030630 (to NO) and R01DE029181 (to WO)

REFERENCES

1. Matsushita Y, Ono W, Ono N. Skeletal Stem Cells for Bone Development and Repair: Diversity Matters. *Curr Osteoporos Rep* (2020) 18(3):189–98. doi: 10.1007/s11914-020-00572-9
2. Tikhonova AN, Dolgalev I, Hu H, Sivaraj KK, Hoxha E, Cuesta-Domínguez Á, et al. The Bone Marrow Microenvironment at Single-Cell Resolution. *Nature* (2019) 569(7755):222–8. doi: 10.1038/s41586-019-1104-8
3. Baryawno N, Przybylski D, Kowalczyk MS, Kfoury Y, Severe N, Gustafsson K, et al. A Cellular Taxonomy of the Bone Marrow Stroma in Homeostasis and Leukemia. *Cell* (2019) 177(7):1915–32.e16. doi: 10.1016/j.cell.2019.04.040
4. Wolock SL, Krishnan I, Tenen DE, Matkins V, Camacho V, Patel S, et al. Mapping Distinct Bone Marrow Niche Populations and Their Differentiation Paths. *Cell Rep* (2019) 28(2):302–11.e5. doi: 10.1016/j.celrep.2019.06.031

5. Dolgalev I, Tikhonova AN. Connecting the Dots: Resolving the Bone Marrow Niche Heterogeneity. *Front Cell Dev Biol* (2021) 9:622519. doi: 10.3389/fcell.2021.622519
6. Boulais PE, Mizoguchi T, Zimmerman S, Nakahara F, Vivié J, Mar JC, et al. The Majority of CD45. *Immunity* (2018) 49(4):627–39.e6. doi: 10.1016/j.immuni.2018.08.019
7. Méndez-Ferrer S, Michurina TV, Ferraro F, Mazloom AR, Macarthur BD, Lira SA, et al. Mesenchymal and Haematopoietic Stem Cells Form a Unique Bone Marrow Niche. *Nature* (2010) 466(7308):829–34. doi: 10.1038/nature09262
8. Morikawa S, Mabuchi Y, Kubota Y, Nagai Y, Niibe K, Hiratsu E, et al. Prospective Identification, Isolation, and Systemic Transplantation of Multipotent Mesenchymal Stem Cells in Murine Bone Marrow. *J Exp Med* (2009) 206(11):2483–96. doi: 10.1084/jem.20091046
9. Matsushita Y, Ono W, Ono N. Flow Cytometry-Based Analysis of the Mouse Bone Marrow Stromal and Perivascular Compartment. *Methods Mol Biol* (2021) 2308:83–94. doi: 10.1007/978-1-0716-1425-9_7
10. Matsushita Y, Nagata M, Kozloff KM, Welch JD, Mizuhashi K, Tokavanich N, et al. A Wnt-Mediated Transformation of the Bone Marrow Stromal Cell Identity Orchestrates Skeletal Regeneration. *Nat Commun* (2020) 11(1):332. doi: 10.1038/s41467-019-14029-w
11. Baccin C, Al-Sabah J, Velten L, Helbling PM, Grünschläger F, Hernández-Malmierca P, et al. Combined Single-Cell and Spatial Transcriptomics Reveal the Molecular, Cellular and Spatial Bone Marrow Niche Organization. *Nat Cell Biol* (2020) 22(1):38–48. doi: 10.1038/s41556-019-0439-6
12. Zhong L, Yao L, Tower RJ, Wei Y, Miao Z, Park J, et al. Single Cell Transcriptomics Identifies a Unique Adipose Lineage Cell Population That Regulates Bone Marrow Environment. *Elife* (2020) 9:e54695. doi: 10.7554/eLife.54695
13. Zhong L, Yao L, Seale P, Qin L. Marrow Adipogenic Lineage Precursor: A New Cellular Component of Marrow Adipose Tissue. *Best Pract Res Clin Endocrinol Metab* (2021) 35(4):101518. doi: 10.1016/j.beem.2021.101518
14. Wang L, Zhang H, Wang S, Chen X, Su J. Bone Marrow Adipocytes: A Critical Player in the Bone Marrow Microenvironment. *Front Cell Dev Biol* (2021) 9:770705. doi: 10.3389/fcell.2021.770705
15. Devlin MJ, Rosen CJ. The Bone-Fat Interface: Basic and Clinical Implications of Marrow Adiposity. *Lancet Diabetes Endocrinol* (2015) 3(2):141–7. doi: 10.1016/S2213-8587(14)70007-5
16. Cawthorn WP, Scheller EL, Learman BS, Parlee SD, Simon BR, Mori H, et al. Bone Marrow Adipose Tissue is an Endocrine Organ That Contributes to Increased Circulating Adiponectin During Caloric Restriction. *Cell Metab* (2014) 20(2):368–75. doi: 10.1016/j.cmet.2014.06.003
17. Scheller EL, Doucette CR, Learman BS, Cawthorn WP, Khandaker S, Schell B, et al. Region-Specific Variation in the Properties of Skeletal Adipocytes Reveals Regulated and Constitutive Marrow Adipose Tissues. *Nat Commun* (2015) 6:7808. doi: 10.1038/ncomms8808
18. Scheller EL, McGee-Lawrence ME, Lecka-Czernik B. Report From the 6. *Front Endocrinol (Lausanne)* (2021) 12:712088. doi: 10.3389/fendo.2021.712088
19. Mori H, Dugan CE, Nishii A, Benchamana A, Li Z, Cadenhead TS, et al. The Molecular and Metabolic Program by Which White Adipocytes Adapt to Cool Physiologic Temperatures. *PloS Biol* (2021) 19(5):e3000988. doi: 10.1371/journal.pbio.3000988
20. Tavassoli M. Marrow Adipose Cells. Histochemical Identification of Labile and Stable Components. *Arch Pathol Lab Med* (1976) 100(1):16–8.
21. Cawthorn WP, Scheller EL. Editorial: Bone Marrow Adipose Tissue: Formation, Function, and Impact on Health and Disease. *Front Endocrinol (Lausanne)* (2017) 8:112. doi: 10.3389/fendo.2017.00112
22. Bravenboer N, Bredella MA, Chauveau C, Corsi A, Douni E, Ferris WF, et al. Standardised Nomenclature, Abbreviations, and Units for the Study of Bone Marrow Adiposity: Report of the Nomenclature Working Group of the International Bone Marrow Adiposity Society. *Front Endocrinol (Lausanne)* (2019) 10:923. doi: 10.3389/fendo.2019.00923
23. Scheller EL, Burr AA, MacDougald OA, Cawthorn WP. Inside Out: Bone Marrow Adipose Tissue as a Source of Circulating Adiponectin. *Adipocyte* (2016) 5(3):251–69. doi: 10.1080/21623945.2016.1149269
24. Pino AM, Miranda M, Figueroa C, Rodríguez JP, Rosen CJ. Qualitative Aspects of Bone Marrow Adiposity in Osteoporosis. *Front Endocrinol (Lausanne)* (2016) 7:139. doi: 10.3389/fendo.2016.00139
25. Muruganandan S, Govindarajan R, Sinal CJ. Bone Marrow Adipose Tissue and Skeletal Health. *Curr Osteoporos Rep* (2018) 16(4):434–42. doi: 10.1007/s11914-018-0451-y
26. Abdallah BM. Marrow Adipocytes Inhibit the Differentiation of Mesenchymal Stem Cells Into Osteoblasts *via* Suppressing BMP-Signaling. *J BioMed Sci* (2017) 24(1):11. doi: 10.1186/s12929-017-0321-4
27. Attané C, Estève D, Chaoui K, Iacovoni JS, Corre J, Moutahir M, et al. Human Bone Marrow Is Comprised of Adipocytes With Specific Lipid Metabolism. *Cell Rep* (2020) 30(4):949–58.e6. doi: 10.1016/j.celrep.2019.12.089
28. Scheller EL, Khandaker S, Learman BS, Cawthorn WP, Anderson LM, Pham HA, et al. Bone Marrow Adipocytes Resist Lipolysis and Remodeling in Response to β-Adrenergic Stimulation. *Bone* (2019), 118:32–41. doi: 10.1016/j.bone.2018.01.016
29. Suchacki KJ, Tavares AAS, Mattiucci D, Scheller EL, Papanastasiou G, Gray C, et al. Bone Marrow Adipose Tissue is a Unique Adipose Subtype With Distinct Roles in Glucose Homeostasis. *Nat Commun* (2020) 11(1):3097. doi: 10.1038/s41467-020-16878-2
30. Li Y, Meng Y, Yu X. The Unique Metabolic Characteristics of Bone Marrow Adipose Tissue. *Front Endocrinol (Lausanne)* (2019) 10:69. doi: 10.3389/fendo.2019.00069
31. Naveiras O, Nardi V, Wenzel PL, Hauschka PV, Fahey F, Daley GQ. Bone-Marrow Adipocytes as Negative Regulators of the Haematopoietic Microenvironment. *Nature* (2009) 460(7252):259–63. doi: 10.1038/nature08099
32. Wang H, Leng Y, Gong Y. Bone Marrow Fat and Hematopoiesis. *Front Endocrinol (Lausanne)* (2018) 9:694. doi: 10.3389/fendo.2018.00694
33. Ambrosi TH, Scialdone A, Graja A, Gohlke S, Jank AM, Bocian C, et al. Adipocyte Accumulation in the Bone Marrow During Obesity and Aging Impairs Stem Cell-Based Hematopoietic and Bone Regeneration. *Cell Stem Cell* (2017) 20(6):771–84.e6. doi: 10.1016/j.stem.2017.02.009
34. Morris EV, Edwards CM. Bone Marrow Adipose Tissue: A New Player in Cancer Metastasis to Bone. *Front Endocrinol (Lausanne)* (2016) 7:90. doi: 10.3389/fendo.2016.00090
35. Herroon MK, Rajagurubandara E, Hardaway AL, Powell K, Turchick A, Feldmann D, et al. Bone Marrow Adipocytes Promote Tumor Growth in Bone *via* FABP4-Dependent Mechanisms. *Oncotarget* (2013) 4(11):2108–23. doi: 10.18632/oncotarget.1482
36. Templeton ZS, Lie WR, Wang W, Rosenberg-Hasson Y, Alluri RV, Tamaresis JS, et al. Breast Cancer Cell Colonization of the Human Bone Marrow Adipose Tissue Niche. *Neoplasia* (2015) 17(12):849–61. doi: 10.1016/j.neo.2015.11.005
37. Chen GL, Luo Y, Eriksson D, Meng X, Qian C, Bäuerle T, et al. High Fat Diet Increases Melanoma Cell Growth in the Bone Marrow by Inducing Osteopontin and Interleukin 6. *Oncotarget* (2016) 7(18):26653–69. doi: 10.18632/oncotarget.8474
38. Zhou BO, Yue R, Murphy MM, Peyer JG, Morrison SJ. Leptin-Receptor-Expressing Mesenchymal Stromal Cells Represent the Main Source of Bone Formed by Adult Bone Marrow. *Cell Stem Cell* (2014) 15(2):154–68. doi: 10.1016/j.stem.2014.06.008
39. Shu HS, Liu YL, Tang XT, Zhang XS, Zhou B, Zou W, et al. Tracing the Skeletal Progenitor Transition During Postnatal Bone Formation. *Cell Stem Cell* (2021) 28(12):2122–2136.e3. doi: 10.1016/j.stem.2021.08.010
40. Yue R, Zhou BO, Shimada IS, Zhao Z, Morrison SJ. Leptin Receptor Promotes Adipogenesis and Reduces Osteogenesis by Regulating Mesenchymal Stromal Cells in Adult Bone Marrow. *Cell Stem Cell* (2016) 18(6):782–96. doi: 10.1016/j.stem.2016.02.015
41. Omatsu Y, Sugiyama T, Kohara H, Kondoh G, Fujii N, Kohno K, et al. The Essential Functions of Adipo-Osteogenic Progenitors as the Hematopoietic Stem and Progenitor Cell Niche. *Immunity* (2010) 33(3):387–99. doi: 10.1016/j.immuni.2010.08.017
42. Seike M, Omatsu Y, Watanabe H, Kondoh G, Nagasawa T. Stem Cell Niche-Specific Ebf3 Maintains the Bone Marrow Cavity. *Genes Dev* (2018) 32(5-6):359–72. doi: 10.1101/gad.311068.117
43. Ding L, Saunders TL, Enikolopov G, Morrison SJ. Endothelial and Perivascular Cells Maintain Haematopoietic Stem Cells. *Nature* (2012) 481 (7382):457–62. doi: 10.1038/nature10783
44. Ding L, Morrison SJ. Haematopoietic Stem Cells and Early Lymphoid Progenitors Occupy Distinct Bone Marrow Niches. *Nature* (2013) 495 (7440):231–5. doi: 10.1038/nature11885
45. Sugiyama T, Kohara H, Noda M, Nagasawa T. Maintenance of the Hematopoietic Stem Cell Pool by CXCL12-CXCR4 Chemokine Signaling in

Bone Marrow Stromal Cell Niches. *Immunity* (2006) 25(6):977–88. doi: 10.1016/j.immuni.2006.10.016
46. Nagasawa T, Hirota S, Tachibana K, Takakura N, Nishikawa S, Kitamura Y, et al. Defects of B-Cell Lymphopoiesis and Bone-Marrow Myelopoiesis in Mice Lacking the CXC Chemokine PBSF/SDF-1. *Nature* (1996) 382 (6592):635–8. doi: 10.1038/382635a0
47. Greenbaum A, Hsu YM, Day RB, Schuettpelz LG, Christopher MJ, Borgerding JN, et al. CXCL12 in Early Mesenchymal Progenitors Is Required for Haematopoietic Stem-Cell Maintenance. *Nature* (2013) 495(7440):227–30. doi: 10.1038/nature11926
48. Tzeng YS, Li H, Kang YL, Chen WC, Cheng WC, Lai DM. Loss of Cxcl12/Sdf-1 in Adult Mice Decreases the Quiescent State of Hematopoietic Stem/Progenitor Cells and Alters the Pattern of Hematopoietic Regeneration After Myelosuppression. *Blood* (2011) 117(2):429–39. doi: 10.1182/blood-2010-01-266833
49. Asada N, Kunisaki Y, Pierce H, Wang Z, Fernandez NF, Birbrair A, et al. Differential Cytokine Contributions of Perivascular Haematopoietic Stem Cell Niches. *Nat Cell Biol* (2017) 19(3):214–23. doi: 10.1038/ncb3475
50. Tzeng YS, Chung NC, Chen YR, Huang HY, Chuang WP, Lai DM. Imbalanced Osteogenesis and Adipogenesis in Mice Deficient in the Chemokine Cxcl12/Sdf1 in the Bone Mesenchymal Stem/Progenitor Cells. *J Bone Miner Res* (2018) 33(4):679–90. doi: 10.1002/jbmr.3340
51. Matsushita Y, Chu AKY, Ono W, Welch JD, Ono N. Intercellular Interactions of an Adipogenic CXCL12-Expressing Stromal Cell Subset in Murine Bone Marrow. *J Bone Miner Res* (2021) 36(6):1145–58. doi: 10.1002/jbmr.4282
52. Matsushita Y, Ono W, Ono N. Bone Regeneration *via* Skeletal Cell Lineage Plasticity: All Hands Mobilized for Emergencies: Quiescent Mature Skeletal Cells Can be Activated in Response to Injury and Robustly Participate in Bone Regeneration Through Cellular Plasticity. *Bioessays* (2021) 43(1):e2000202. doi: 10.1002/bies.202000202
53. Zhang X, Robles H, Magee KL, Lorenz MR, Wang Z, Harris CA, et al. A Bone-Specific Adipogenesis Pathway in Fat-Free Mice Defines Key Origins and Adaptations of Bone Marrow Adipocytes with Age and Disease. *Elife* (2021) 10:e66275. doi: 10.7554/eLife.66275
54. Song L, Liu M, Ono N, Bringhurst FR, Kronenberg HM, Guo J. Loss of Wnt/β-Catenin Signaling Causes Cell Fate Shift of Preosteoblasts From Osteoblasts to Adipocytes. *J Bone Miner Res* (2012) 27(11):2344–58. doi: 10.1002/jbmr.1694
55. Liu Y, Berendsen AD, Jia S, Lotinun S, Baron R, Ferrara N, et al. Intracellular VEGF Regulates the Balance Between Osteoblast and Adipocyte Differentiation. *J Clin Invest* (2012) 122(9):3101–13. doi: 10.1172/JCI61209
56. Fan Y, Hanai JI, Le PT, Bi R, Maridas D, DeMambro V, et al. Parathyroid Hormone Directs Bone Marrow Mesenchymal Cell Fate. *Cell Metab* (2017) 25 (3):661–72. doi: 10.1016/j.cmet.2017.01.001
57. Sinha P, Aarnisalo P, Chubb R, Ono N, Fulzele K, Selig M, et al. Loss of Gsα Early in the Osteoblast Lineage Favors Adipogenic Differentiation of Mesenchymal Progenitors and Committed Osteoblast Precursors. *J Bone Miner Res* (2014) 11):2414–26. doi: 10.1002/jbmr.2270
58. Zou W, Rohatgi N, Brestoff JR, Li Y, Barve RA, Tycksen E, et al. Ablation of Fat Cells in Adult Mice Induces Massive Bone Gain. *Cell Metab* (2020) 32 (5):801–813.e6. doi: 10.1016/j.cmet.2020.09.011
59. Lee JY, Yang JY, Kim SW. Bone Lining Cells Could Be Sources of Bone Marrow Adipocytes. *Front Endocrinol (Lausanne)* (2021) 12:766254. doi: 10.3389/fendo.2021.766254
60. Robles H, Park S, Joens MS, Fitzpatrick JAJ, Craft CS, Scheller EL. Characterization of the Bone Marrow Adipocyte Niche With Three-Dimensional Electron Microscopy. *Bone* (2019) 118:89–98. doi: 10.1016/j.bone.2018.01.020

Conflict of Interest: The authors declare that the research was conducted in the absence of any commercial or financial relationships that could be construed as a potential conflict of interest.

Publisher's Note: All claims expressed in this article are solely those of the authors and do not necessarily represent those of their affiliated organizations, or those of the publisher, the editors and the reviewers. Any product that may be evaluated in this article, or claim that may be made by its manufacturer, is not guaranteed or endorsed by the publisher.

frontiers | Frontiers in Endocrinology

ORIGINAL RESEARCH
published: 06 June 2022
doi: 10.3389/fendo.2022.880503

Severity Level and Duration of Energy Deficit in Mice Affect Bone Phenotype and Bone Marrow Stromal Cell Differentiation Capacity

Viktorija Avilkina[1], Damien Leterme[1], Guillaume Falgayrac[2], Jérôme Delattre[2], Flore Miellot[1], Véronique Gauthier[1], Christophe Chauveau[1] and Olfa Ghali Mhenni[1]**

[1] MAB Lab ULR4490, Univ Littoral Côte d'Opale, Boulogne-sur-Mer, France, [2] MAB Lab ULR4490, Univ Lille Nord de France, Lille, France

OPEN ACCESS

Edited by:
Sarah Beck-Cormier,
U1229 Médecine Régénératrice et Squelette (RMeS) (INSERM), France

Reviewed by:
William Peter Cawthorn,
University of Edinburgh, United Kingdom
Noriaki Ono,
University of Texas Health Science Center at Houston, United States

***Correspondence:**
Christophe Chauveau
christophe.chauveau@univ-littoral.fr
Olfa Ghali Mhenni
olfa.ghali@univ-littoral.fr

Specialty section:
This article was submitted to Bone Research, a section of the journal Frontiers in Endocrinology

Received: 21 February 2022
Accepted: 25 April 2022
Published: 06 June 2022

Citation:
Avilkina V, Leterme D, Falgayrac G, Delattre J, Miellot F, Gauthier V, Chauveau C and Ghali Mhenni O (2022) Severity Level and Duration of Energy Deficit in Mice Affect Bone Phenotype and Bone Marrow Stromal Cell Differentiation Capacity. Front. Endocrinol. 13:880503. doi: 10.3389/fendo.2022.880503

Anorexia nervosa is known to induce changes in bone parameters and an increase in bone marrow adiposity (BMA) that depend on the duration and seriousness of the disease. Previous studies have found that bone loss is associated with BMA accumulation. Sirtuin of type 1 (Sirt1), a histone deacetylase that is partly regulated by energy balance, was shown to have pro-osteoblastogenic and anti-adipogenic effects. To study the effects of the severity and duration of energy deficits related to bone loss, a mouse model of separation-based anorexia (SBA) was established. We recently demonstrated that moderate body weight loss (18%) 8-week SBA protocol in mice resulted in an increase in BMA, bone loss, and a significant reduction in Sirt1 expression in bone marrow stromal cells (BMSCs) extracted from SBA mice. We hypothesised that Sirt1 deficit in BMSCs is associated with bone and BMA alterations and could potentially depend on the severity of weight loss and the length of SBA protocol. We studied bone parameters, BMA, BMSC differentiation capacity, and Sirt1 expression after induction of 4 different levels of body weight loss (0%,12%,18%,24%), after 4 or 10 weeks of the SBA protocol. Our results demonstrated that 10 week SBA protocols associated with body weight loss (12%, 18%, 24%) induced a significant decrease in bone parameters without any increase in BMA. BMSCs extracted from 12% and 18% SBA groups showed a significant decrease in Sirt1 mRNA levels before and after co-differentiation. For these two groups, decrease in Sirt1 was associated with a significant increase in the mRNA level of adipogenic markers and a reduction of osteoblastogenesis. Inducing an 18% body weight loss, we tested a short SBA protocol (4-week). We demonstrated that a 4-week SBA protocol caused a significant decrease in Tb.Th only, without change in other bone parameters, BMA, Sirt1 expression, or differentiation capacity of BMSCs. In conclusion, this study showed, for the first time, that the duration and severity of energy deficits are critical for changes in bone parameters, BMSC differentiation, and Sirt1 expression. Furthermore, we showed that in this context, Sirt1 expression could impact BMSC differentiation with further effects on bone phenotype.

Keywords: energy deficit, bone, bone marrow adiposity, sirtuin type 1 (SIRT1), bone marrow stromal cell (BMSC), differentiation

INTRODUCTION

Anorexia nervosa (AN) is a disorder with psychiatric origins characterized by inadequate dietary intake resulting in low body weight. Many studies have demonstrated that a higher volume of bone marrow adipose tissue (BMAT) is present in anorexic patients than in normal-weight controls (1–3). This high level of BMAT is often associated with a decline in bone mass, resulting in increased fracture risk (4, 5). Recently, a negative correlation was shown between the fraction of fat in the bone marrow cavity and the bone mineral density (BMD) at the femoral neck and at the hip of anorexic patients in multiple anatomical subregions, even after weight recovery (6).

Marrow adipocytes originate from skeletal stem cells (SSCs) that also function as precursors to muscle, cartilage, and bone-forming osteoblasts (7–9). Moreover, it has been shown that the accumulation of marrow adipocytes, which is observed in bone loss situations, is potentially caused by a shift in the commitment of SSCs from the osteogenic pathway to the adipogenic pathway (10). This finding suggested the existence of a competitive relationship between these two pathways. Furthermore, bone marrow stromal cells (BMSCs), which include SSCs from aged mice express more adipocytic transcripts and fewer osteoblastic transcripts than BMSCs extracted from young animals (11).

The differentiation of SSCs towards the adipocytic or osteoblastic pathway could be influenced by many modulators of signalling pathways, such as glucocorticoids, Wnts, and bone morphogenetic proteins (12–14). Moreover, the histone deacetylase (HDAC) family was also shown to influence the fate of differentiating mesenchymal progenitor cells by removing acetyl groups from lysine residues in histones and other proteins, thus, altering chromatin structure, gene expression, and protein activity (15, 16).

Sirtuin type 1 (Sirt1) is classified as a class III HDAC and is known to be involved in the extension of lifespan in mammals and other organisms and in protection against age-associated diseases (such as diabetes and obesity) (17). Additionally, Sirt1 is involved in the regulation of BMSC differentiation into either osteoblasts or adipocytes. Indeed, several studies have demonstrated that activation of Sirt1 promotes osteoblastic differentiation (18–21), while a decrease in Sirt1 expression induces adipocytic differentiation (22, 23). Interestingly, caloric restriction (CR) has been shown to stimulate the expression and activity of Sirt1 in various mammalian tissues, such as liver and white adipose tissue. Also, CR has been shown to induce a decrease in the level of Sirt1 mRNA in the cerebellum and midbrain (24, 25).

Recently, we demonstrated that 8 weeks of a separation-based anorexia (SBA) protocol, inducing medium weight loss (18%) vs day 0 of experiment in mice, is associated with an increase in bone marrow adiposity (BMA), bone loss, and a significant reduction in Sirt1 expression in BMSCs extracted from SBA mice (26). We hypothesised that Sirt1 deficit in BMSCs is involved in bone and BMA alterations and could potentially depend on the severity of weight loss and the length of SBA protocol. To verify these hypotheses, we characterized bone and BMA, and determined BMSC differentiation capacity and Sirt1 expression after a 10-week induction of 4 different levels of body weight changes (0%, -12%, -18% and -24%) relative to mice at Day 0. The same parameters were also analyzed after a 4-week SBA protocol with 18% weight loss.

MATERIALS AND METHODS

Animals

Seven-week-old female C57BL/6J mice purchased from Charles River Laboratories (St Germain sur l'Abresle, France) were used for the separation-based anorexia (SBA) model (27). This particular mouse strain was chosen because of its use in various studies related to calorie restriction-induced bone alterations. Additionally, C57BL/6J mice exhibit a medium level of BMA, which allows us to detect any change in this parameter.

Mice were housed 6 per cage in a controlled room temperature (22°C+/- 1°C) under a 12-hour dark/light cycle (lights off at 10 a.m.) and with free access to water. Before induction of the SBA protocol, mice were acclimatized for one week. The SBA protocol was generated for ten weeks and aimed to induce 4 different weight loss conditions in randomly allocated mice – no weight loss (SBA 0%), a light 12% weight loss (SBA 12%) (achieved 12.97%), a moderate body weight loss of 18% (SBA 18%) (achieved 17.27%) and severe weight loss of 24% (SBA 24%) (achieved 23.17%), relative to Day 0 (D0). A time restricted-feeding was used to induce weight loss in mice, a food access time was gradually reduced from 6 h to 2 h per day during the protocol, depending on the desired weight loss to achieve. Mice allocated to severe, moderate, and light weight loss groups had reduced food availability and time dependent on the progression of weight loss. For no weight loss group the time of the feeding was not decreased dramatically, in order to maintain the initial mice weight. Furthermore, throughout the protocol mice of SBA groups were kept in the separate sections of the cage with free access to water and this encouraged the increased energy expenditure by thermogenesis. The SBA mice were gathered together in regular cages for the periods of feeding. The CT group was housed in standard conditions in collective cages with water and food provided *ad libitum*. This study was specifically approved by the Committee on the Ethics of Animal Experiments (CEEA) of Nord-Pas de Calais, France (permit number: CEEA#2016070717275082).

Additionally, a 4-week SBA protocol was performed using seven-week-old female C57BL/6J mice, similar to the 10-week protocol. After one week of acclimatization, the SBA protocol was generated for 4 weeks to achieve moderate weight loss of 18% (SBA 18%) (achieved 18.75%) in mice relative to their weight at D0. This study was specifically approved by the Committee on the Ethics of Animal Experiments (CEEA) of Nord-Pas de Calais, France (permit number: CEEA#2016070717275082).

Dual Energy X-Ray Absorptiometry (DEXA) Analysis

The fat mass, lean mass, and bone mineral content (BMC) of mice were analyzed using the Lunar PIXImus Mouse Densitometer (GE Healthcare, Madison, WI) according to a previously described protocol (27).

Mineralized Bone Micro-CT Analysis

Tibiae extracted from CT and SBA mice were scanned using a Skyscan 1172 microCT device (Bruker MicroCT, Kontich, Belgium). The software suite provided by the manufacturer was used for image acquisition, reconstruction, analysis, and 3D visualisation (Skyscan 1172©, NRecon©, Dataviewer, CTAn©, CTVox™). Analysis of the tibia trabecular bone volume/tissue volume (BV/TV) ratio, cortical thickness (Cort.Th), trabecular thickness (Tb.Th), trabecular number (Tb.N) and trabecular spacing (Tb.Sp) of all animals were determined in a 0.5mm region beginning 250µm proximal to the proximal growth plate. More detailed description for the quantification of 3D microarchitecture of trabecular bone has been previously presented (28).

Bone Marrow Adipose Tissue Content - Micro-CT Analysis

The BMAT and bone parameters analyzed by micro-CT of all mice were quantified using a previously published protocol (29) in the proximal tibia. To quantify the BMAT content, the same region of interest (ROI) was used as in the analysis of mineralized bone. After the first micro-CT scan, tibiae were decalcified in 4% formic acid/10% NBF (1:1), pH 7.4, for 48 h. Then bones were rinsed in distilled water and stained in the fume hood for 48 h in the aqueous staining solution (1% osmium tetroxide solution stabilized in a 2.5% dichromate potassium) at room temperature. Then, bones were rinsed for 48 h at room temperature in PBS with regular renewal of the solution. Osmium-stained bones were then stored at 4°C in PBS until the second micro-CT acquisition. The study focused on quantifying the percentage of the ratio of adipocyte volume to marrow volume (%, Ad.V/Ma.V). The data are presented in the form of the percentage of BMAT volume in marrow volume.

Primary Bone Marrow Cell Cultures

Primary bone marrow cells were harvested from the tibiae and femurs of CT and SBA mice and grown for 7-10 days in αMEM media (PAN BIOTECH; P04-21050) with 15% fetal bovine serum (PAN BIOTECH; P30-3306), 1% penicillin/streptomycin (PAN BIOTECH; P04-85100) and 1% stable glutamine (PAN BIOTECH; P06-07100). After reaching full confluency, the plated BMSC population was differentiated into both osteoblasts and adipocytes according to the co-differentiation protocol described in a previously published article (30). The media containing co-differentiation inducers was replaced every two days during the 14 days of the co-differentiation experiment. This culture duration was chosen because of its brevity, which allowed for minimizing the time for cells to change after leaving the *in vivo* state.

Raman Microspectroscopy

Cells were plated on calcium fluoride (CaF2) substrate, which is adapted to Raman analysis. The Raman microspectrometer was a LabRAM HR800 (Jobin-Yvon, France) instrument equipped with an XYZ motorized stage and a diode laser λ=785 nm. The Raman spectrometer was coupled with a microscope (BX40, Olympus). Raman acquisitions were performed with a water objective 100x lens (Nikon, numerical aperture = 1.1 Japan). The water immersion objective focused the laser on the cell within the micrometre scale on the centre of individual lipid droplets, where one spectrum corresponds to one adipocyte lipid droplet. A total of 1,252 lipid droplets were acquired over 109 adipocytes (**Table 1**), representing an average of 83.4 lipid droplets analyzed per well and an average of 7.2 adipocytes analyzed per well. Spectral acquisition was performed in the 400-1800 cm^{-1} range. The Raman signal was collected by a multichannel CCD detector (1024×256 pixels). The acquisition time was set at 60 s averaged 2 times per spectrum (total acquisition time = 120 sec). Raman spectra were processed using Labspec software (HORIBA, Jobin-Yvon, France). A Savitzky–Golay smoothing filter was applied to all Raman spectra. The band areas were integrated over defined Raman shift regions in the spectrum using a sum filter. The filter calculates the areas within the chosen borders and the background is subtracted by taking the baseline from the first to the second border. The band area was estimated at 1441 cm^{-1} (peak-ROI 1400-1500 cm^{-1}) and 1654 cm^{-1} (peak-ROI 1620-1694 cm^{-1}). The Raman bands at 1441 cm^{-1} and 1654 cm^{-1} are assigned to vibrations CH2 and C=C, respectively (31). The unsaturation ratio was calculated as the ratio of band areas 1654 cm^{-1}/1441 cm^{-1} (31).

Mineralization Quantification

The sample mineralization level was quantified using the same protocol previously described (30). Briefly, cells were harvested in a solution of PBS 1X/Triton 0.2%/HCl 6 M and disrupted by sonication. After, 5 µl of HCl 6 M was added to 95 µl of each sample and incubated overnight at 4°C. Following by centrifugation at 1500 × g for 5 min, the protein content was determined using the DC protein assay kit BioRad. The mineralization content was quantified.

RNA Extraction, Reverse Transcription and Real-Time PCR

Total RNA was extracted from BMSC cultures by the previously described protocol (30). Reverse transcription and RT–PCR were performed as previously described (32). The sequences of the primers (TibMolBiol, Berlin, Germany), annealing temperature, product length, and GenBank reference for each of the analyzed genes are shown in **Table 2**.

TABLE 1 | Details of lipid droplets studied in each condition of the 10-week and 4-week protocols.

Condition	Number of lipid droplets = number spectra over 3 wells	Number of adipocytes analysed over 3 wells per condition
10-week		
CT	519	41
SBA24%	111	13
SBA18%	299	30
SBA12%	134	10
SBA0%	189	15
Total	1252	109
4-week		
CT	45	18
SBA18%	109	25
Total	154	43

Statistical Analysis

The 10-week study was performed with 6 samples per condition, except for the mineralization experiment, which had 4 replicated per group. The 4-week study was performed with 5 samples per condition. The median and interquartile range were calculated for the groups. Due to the low number of replicates, the normality of the data could not be tested. In 10-week study, we performed Kruskal-Wallis One-Way ANOVA test to show the significance between all the conditions. Additionally, we conducted Dunn's test in order to see the relationships between specific pairs of conditions. For the 4-week studies we performed Mann–Whitney's test to see the statistically significant relationship between the two particular conditions. All tests were performed using GraphPad Prism software. Differences with $p<0.05$ were considered statistically significant.

RESULTS

The 10-Week SBA Protocols Induced a Significant Decrease in Mouse Body Weight (12%, 18%, 24%) and Were Shown to Cause Changes Not Only in Fat Mass But Also in Lean Mass and Bone Mineral Composition

To study the effect of energy deficit severity on bone and BMSCs, we performed four different SBA protocols on female mice. We induced 0%, 12%, 18%, and 24% weight loss from the initial mouse weight over 10 weeks. Prior to the study, mice were randomized into five experimental groups that did not display significant differences in body weight at Day 0. Mice from the control group (*ad libitum* and not separated) displayed a significant body weight increase (+22.42% vs. D0) after 10 weeks (**Figure 1A**). In the SBA 0% group, no significant weight change (+4.39% vs. D0) was observed, as this condition did not imply weight change (**Figure 1A**). In all other SBA groups, we observed a significant decrease in weight after 2 weeks of protocol and this decrease was maintained until the end of the 10 weeks (SBA 12% (-12.97%) vs. D0; SBA 18% (-17.27%) vs. D0; and SBA 24% (-23.17%) vs. D0) ($p<0.005$ vs. D0). The results of DEXA analysis showed a significant decrease in total body bone mineral content (BMC) only in light (12%) and moderate (18%) weight loss conditions (SBA 12% -17% vs. CT; SBA 18% -15% vs. CT) (**Figure 1B**). The study of the BMC at specific sites, revealed that all three weigh loss conditions induced a significant decrease in femur BMC - SBA 12% (-27% vs. CT), 18% (-29% vs. CT) and 24% (-30% vs. CT) (**Figure 1C**). However, only the SBA 18% group showed a significant decrease in the BMC of lumbar vertebrae (L3-L5) (SBA 18% -23% vs. CT) (**Figure 1D**). The BMC decrease was potentially associated with a decrease in lean absolute mass in mice from the SBA groups 12% (-19% vs. CT) and 24% (-22% vs. CT). This parameter was significantly reduced only in weight loss conditions, while in the SBA 18% group, lean absolute mass just showed a tendency to decrease without statistically significant change (**Figure 1E**). However, study of lean percentage (%) of total mouse mass, showed a significant increase in all three weigh loss conditions (SBA 12%. 18% and 24%). This was due to a significant decrease in fat mass in same conditions (on average -53% vs. CT). Fat absolute mass in weight loss conditions exhibited a great decrease (59-64%, p 0.0001 vs. CT) (**Figure 1F**). These data highlight that absolute lean mass and fat mass parameters can be associated with BMD under weight loss conditions, as a significant decrease in whole-body

TABLE 2 | Primer sequences and conditions of quantitative RT–PCR.

Gene	Primer Sequences	Annealing temperature	Product length	GenBank
18S	F: ATTCCGATAACGAACGAGAC R: GCTTATGACCCGCACTTACT	60°C	297 bp	X03205
Gapdh	F: GGCATTGCTCTCAATGACAA R: TGTGAGGGAGATGCTCAGTG	62°C	200 bp	NM_008084
Pparg2	F: TCGCTGATGCACTGCCTATG R: GAGAGGTCCACAGAGCTGATT	60°C	103 bp	NM_011146
Adipoq	F: TGTTCCTCTTAATCCTGCCCA R: CCAACCTGCACAAGTTCCCTT	60°C	104 bp	NM_009605
Lep	F: GAGACCCCTGTGTCGGTTC R: CTGCGTGTGTGAAATGTCATTG	60°C	139 bp	NM_008493
Plin1	F: CACCATCTCTACCCGCCTTC R: GGGTGTTGGCGGCATATTC	58°C	149 bp	NM_001113471.1
Glut4	F: ACTCTTGCCACACAGGCTCT R: AATGGAGACTGATGCGCTCT	62°C	174 bp	NM_009204
Runx2	F: GCCGGGAATGATGAGAACTA R: GGACCGTCCACTGTCACTTT	62°C	200 bp	NM_001146038.2
Bglap	F: AAGCAGGAGGGCAATAAGGT R: CGTTTGTAGGCGGTCTTCA	60°C	364 bp	L24431
Sp7	F: ATGGCGTCCTCTCTGCTTG R: TGAAAGGTCAGCGTATGGCTT	54°C	237 bp	NM_130458
Col1a1	F: GGTGAGCCTGGTCAAACGG R: ACTGTGTCCTTTCACGCCTTT	60°C	189 bp	NM_007743
Sirt1	F: TAGGGAACCTTTGCCTCATC R: GGCATATTCACCACCTAGCC	51°C	100 bp	NM_019812.2

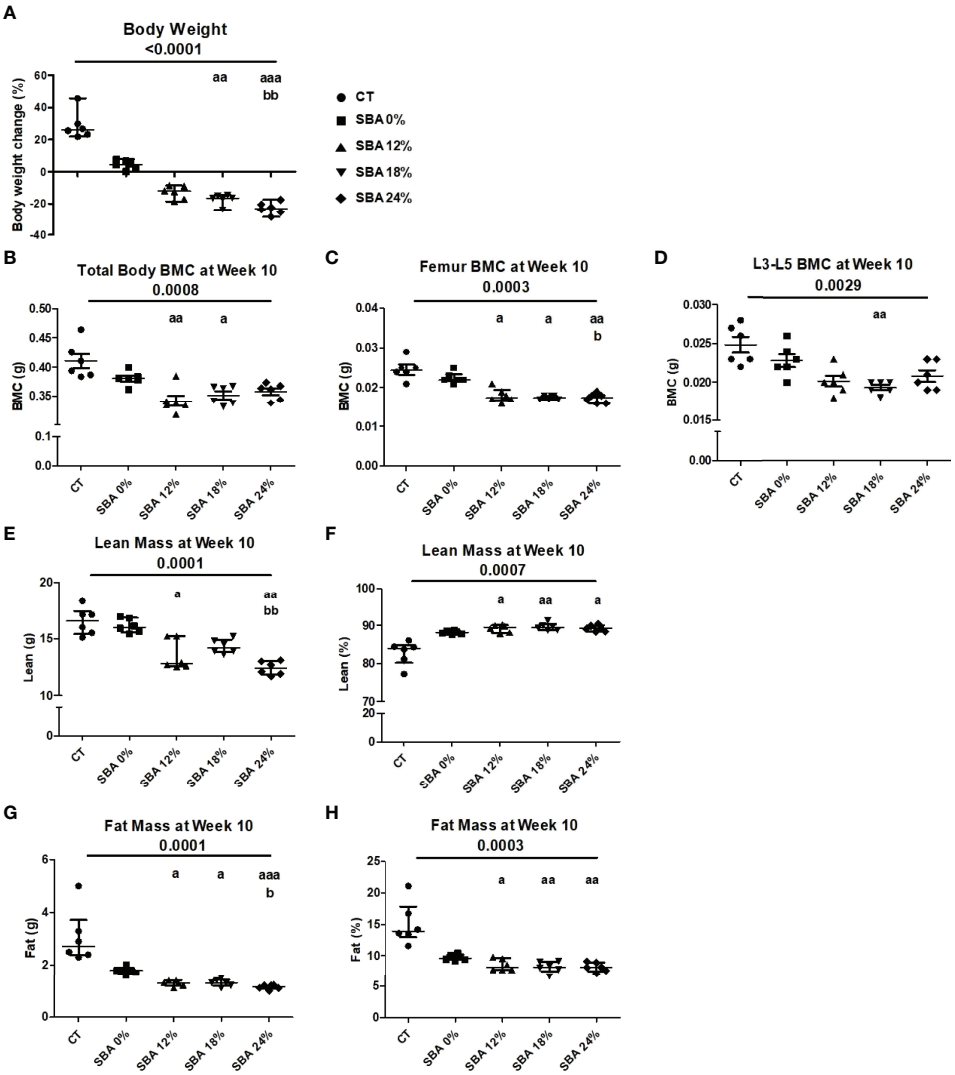

FIGURE 1 | Body mass, BMC, fat and lean mass in mice after 10 weeks of SBA protocols of different severity. The body weight and composition analysis were performed on standard condition (CT), constant weight group (SBA 0%) and three weight loss groups with different severity levels (SBA 12%, 18% and 24%). **(A)** Graph represents a percentage body weight loss on mice between day 0 and 10 weeks of SBA protocol; **(B-D)** Study of total mouse body mineral content (BMC), femur BMC and vertebra (L3-L5) BMC, respectively, were evaluated for each animal and each condition after 10 weeks of SBA protocol.; **(E, F)** Lean mass content presented in grams and % of total mass, respectively was evaluated for each mouse and condition after 4 weeks of SBA protocol; **(G, H)** Fat mass content presented in grams and % of total mass, respectively was evaluated for each mouse and condition after 4 weeks of SBA protocol. Data represent median and interquartile range; n = 6. Statistical analysis was performed using Kruskal-Wallis One-Way ANOVA test and Dunn's test; a - $p < 0.05$, aa - $p < 0.005$ and aaa - $p < 0.0005$ when compared to the CT group (b – when compared to the SBA 0% group).

BMC or femoral/vertebral BMC together with lean and fat mass was observed only in the weight loss mice.

The 18% and 24% SBA Protocols Resulted in a Significant Decrease in Trabecular and Cortical Thickness, Without Any Increase in Bone Marrow Adiposity

To determine the effect of SBA severity on bone microarchitecture, we conducted proximal tibia micro-CT analysis. Bone volume fraction (BV/TV) showing the relative volume of mineralized trabecular bone was not affected by the SBA protocols (**Figure 2A**). Trabecular thickness (Tb.Th) was significantly decreased only under severe weight loss conditions (SBA 24%: -29% vs. CT) (**Figure 2B**). In contrast with the thickness of the trabecular bone, the trabecular number (Tb.N) and trabecular spacing (Tb.Sp) were not significantly affected, even for the 24% group (**Figures 2C, D**). One of the bone fragility parameters was assessed through the study of cortical thickness (Cort.Th), which is affected by the SBA protocol. Indeed, the SBA 18% and 24% caused 16% and 17% decreases in this parameter, respectively (p 0.0001 vs. CT) (**Figure 2E**), demonstrating the potential link between moderate and severe energy deficit and

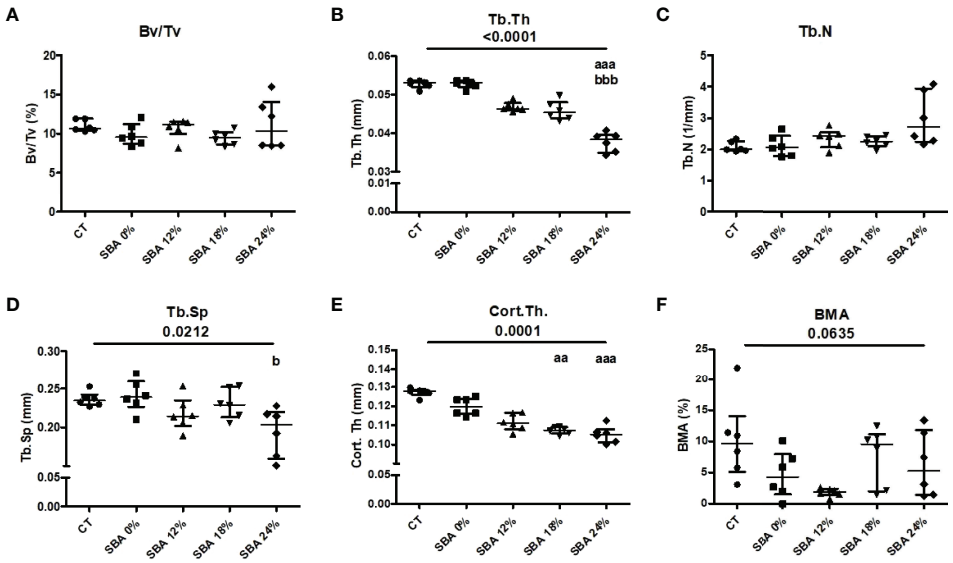

FIGURE 2 | The results of micro-CT analysis of tibia, showing different bone parameters after exposure to 10 weeks of SBA protocols at different levels of severity. **(A)** Bone volume fraction (BV/TV) was expressed as a percentage on mineralized tissue in each condition after 10 weeks; **(B–E)** Trabecular thickness (Tb.Th), trabecular number (Tb.N) and trabecular spacing (Tb.Sp), and cortical thickness (Cort.Th), respectively, were evaluated for each animal and each condition after 10 weeks of SBA protocol (expressed in millimetres); **(F)** Bone marrow adiposity (BMA) was calculated as a percentage of BMAT volume in marrow volume. Data represent median and interquartile range; n = 6. Statistical analysis was performed using Kruskal-Wallis One-Way ANOVA test and Dunn's test; a - $p < 0.05$, aa - $p < 0.005$ and aaa - $p < 0.0005$ when compared to the CT group (b – when compared to the SBA 0% group).

decrease in Cort.Th. The results of bone marrow adiposity (BMA) showed a high heterogeneity of the samples in each group. Only the SBA 12% group exhibited a tendency of BMA decrease by 82% ($p<0.1$, **Figure 2F**).

SBA Protocol Resulted in Rapid Adipogenesis of BMSCs and Weight Loss Conditions Were Associated With a Decrease in Lipid Unsaturation Levels

Throughout the co-differentiation experiment, cells extracted from SBA and control mice were observed under light microscopy. BMSCs extracted from CT mice started to form lipid droplets after the 7th day of co-differentiation. Cells extracted from SBA mice (0%, 12%, 18%, and 24%) showed the first appearance of lipid droplets much faster, after the 3rd day of co-differentiation (**Figure 3**). This finding suggests that the SBA protocol induces *in vivo* changes in BMSC commitment and that these cells are potentially committed to differentiating into adipocytes. After qualitative study (microscopic observations) of adipocytes on Day 10 of differentiation, BMSCs extracted from the SBA 12%, 18%, and 24% groups globally seemed to generate more numerous and larger adipocytes compared to the CT or SBA 0% groups

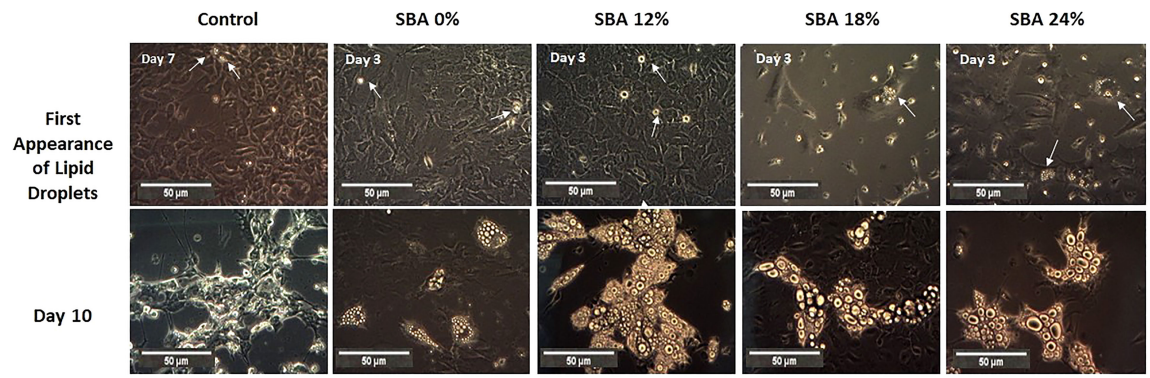

FIGURE 3 | Overview of adipocyte first appearance and size. A. Light microscope images of cells from each condition were taken on different points of differentiation showing the first appearance of lipid droplets and adipocytes at day 10.

(**Figure 3**). Additionally, Raman spectroscopy analysis was performed to characterize more of the adipocytes from different groups. The lipid unsaturation levels in the SBA 12%, 18%, and 24% groups were significantly lower than those in the SBA 0% group, showing that the severity of energy deficit can lead to a decrease in lipid unsaturation levels (**Supplementary Figure 1**).

Only SBA 18% and 24% Protocols Resulted in an Increase in Adipogenesis and Subsequent Decrease in Osteoblastogenesis

To confirm the commitment of BMSCs to the adipocyte lineage, the mRNA levels of adipocytic markers in the SBA and CT groups were analyzed. The marker gene relative mRNA level was measured 48 hours after plating (adherent cells) and at day 14 of co-differentiation. This culture duration was chosen because of its brevity, which minimized the time for cells to change after leaving the *in vivo* state. Interestingly, after 48 hours of adhesion in a standard medium, the unstimulated BMSCs from mice of SBA 24% protocols already exhibited high levels of peroxisome proliferator-activated receptor gamma 2 (*Pparg2*) mRNA (+125% vs CT) (**Figure 4A**), showing a potential commitment to adipogenic differentiation prior to co-differentiation stimulation and thus probably *in vivo*. The SBA 0% group showed similar expression level of *Pparg2* to CT and SBA 12% and 24% conditions, also showed significant increase in *Pparg2* relative mRNA level vs. SBA 0%. Furthermore, *Pparg2* mRNA levels were similarly enhanced after 14 days of co-differentiation in severe weight loss group (SBA 24%: +236% vs. CT) (**Figure 4B**). Additionally, the SBA 18% group demonstrated the highest upregulation of *Pparg2* (+ 285%vs. CT and vs. SBA 0%) (**Figure 4B**). Other marker genes characterizing cell commitment to adipogenic differentiation (leptin (*Lep)* and facilitated glucose transporter member 4 (*Glut4)*) exhibited an increase in the moderate and severe weight loss groups (SBA 18% - *Lep* +1292% vs CT, *Glut4* +807% vs. CT; SBA 24% - *Lep* +1864% vs. CT) (**Figures 4C, E**). The adiponectin (*Adipoq)* mRNA level was found to be upregulated only in the SBA 18% group (+53% vs. SBA 0%) (**Figure 4D**). However, the 12% weight loss condition displayed the lowest mRNA level of *Adipoq* (**Figure 4D**).

In our study, we wanted to determine whether the severity of SBA causes an imbalance in BMSC lineage commitment and whether upregulation of adipogenesis is achieved at the expense of osteoblastogenesis. Thus, after 14 days of co-differentiation, the mineralization level of CT and SBA cells was studied by quantifying the calcium to protein ratio. The results demonstrated a strong alteration of mineralization capabilities in moderate and severe weight loss SBA conditions (18% and 24%, on average -82% vs. CT) (**Figure 5A**). However, this trend was not significant. Only 18% weigh loss condition exhibited significant decrease in mineralization vs. SBA 0%. The mRNA level analysis showed that the early marker of osteoblastogenesis [runt-related transcription factor 2 (*Runx2)*] was significantly

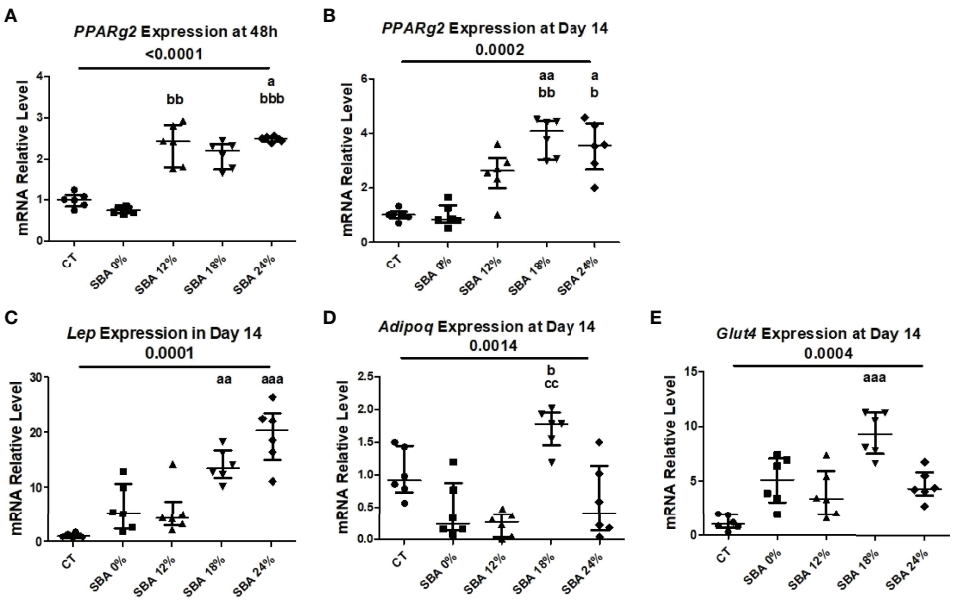

FIGURE 4 | 10-week SBA protocol induced an increase in adipogenesis. **(A, B)** Relative mRNA expression level of early adipogenic marker gene (*Pparg2*) in CT and SBA groups (0%, 12%, 18%, 24%), cells were cultured for 48 hours in standard growth media and for 14 days were exposed to co-differentiation media, respectively; **(C-E)** Relative mRNA expression level of other adipogenic marker genes (*Lep, Adipoq*, and *Glut4*, respectively) in CT and SBA groups (0%, 12%, 18%, 24%) after exposure to co-differentiation media during 14 days. Data represent median and interquartile range; n=6. Statistical analysis was performed using Kruskal-Wallis One-Way ANOVA test and Dunn's test; a - $p < 0.05$, aa - $p < 0.005$ and aaa - $p < 0.0005$ when compared to the CT group (b – when compared to the SBA 0% group; c – when compared to SBA 12% group). Peroxisome proliferator-activated receptor gamma 2 (*Pparg2*), leptin (*Lep*), adiponectin (*Adipoq*), facilitated glucose transporter member 4 (*Glut4*).

reduced in severe weight loss condition (SBA 24% -55% vs. CT) 48 hours after cell plating in standard media and after 14 days in co-differentiation medium both moderate and severe conditions induced changes in *Runx2* mRNA level (SBA 18% -75% vs. CT; SBA 24% -70% vs. CT) (**Figures 5B, C**). Interestingly, further study of other markers of osteoblastogenesis [collagen1A1 (*Col1a1*), osteocalcin (*Bglap*) and osterix (*Sp7*)] at the end of co-differentiation revealed a reduction in mRNA levels only in the moderate and severe weight loss groups (*Col1a1* - SBA 18% -77% vs SBA 0%, SBA 24% -83% vs. SBA 12%; *Bglap* - SBA 18% -73%, SBA 24% -72% vs. CT; *Sp7* - SBA 18% -81%, SBA 24% -77% vs. CT) (**Figures 5D–F**). Moreover, the results suggest that an increase in adipogenesis occurs at the expense of osteoblastogenesis and that BMSCs extracted from SBA mice are apparently more committed to adipogenic lineage.

Recently, we demonstrated that the 18% SBA protocol favors BMSC lineage commitment towards adipogenesis and a decrease in *Sirt1* level and activity, a potential regulator of BMSC differentiation (26). In the present study, we examined the impact of weight loss severity on the expression level of *Sirt1* mRNA. The results of the SBA 18% protocol showed a 67% decrease (vs. CT) in *Sirt1* mRNA in BMSCs after 48 hours of adhesion in growth media and a 75% decrease (vs. CT) after 14 days of co-differentiation (**Figure 6**). This finding confirmed our previously published data. Additionally, the *Sirt1* mRNA level was significantly altered in the 24% groups (-60% vs. CT) after 48 hours of adhesion and after 14 days of co-differentiation (-68% vs. CT) (**Figure 6**). So, decrease in *Sirt1* mRNA levels under moderate and severe weight loss conditions could be associated with an increase in adipogenic mRNA markers and a subsequent downregulation of osteoblastogenesis in BMSCs.

The 4-Week SBA Protocol Induced a Significant Decrease in Mouse Body Weight (18%) and Was Shown to Cause Changes Only in Fat Mass and Trabecular Thickness

Long-term SBA protocols (10-week duration) have been shown to induce changes in mouse BMSC differentiation capacity; however, we were interested in the duration of energy deficit affecting the mouse bone composition and BMSC differentiation capacity. Therefore, we conducted a 4-week SBA protocol. In the 10-week study detailed above, the SBA 18% group exhibited alterations in bone parameters and in BMSC differentiation capacity, confirming the hypothesis that adipogenesis is upregulated in these cells at the expense of osteoblastogenesis. Based on these findings, we compared CT mice with 18% weight loss mice after exposure to the SBA protocol for 4 weeks.

The mouse body weight showed a significant decrease in percentage body weight loss in the SBA 18% group vs. CT (**Figure 7A**). After the study of body composition, it was concluded that the 4-week SBA protocol induced alterations in

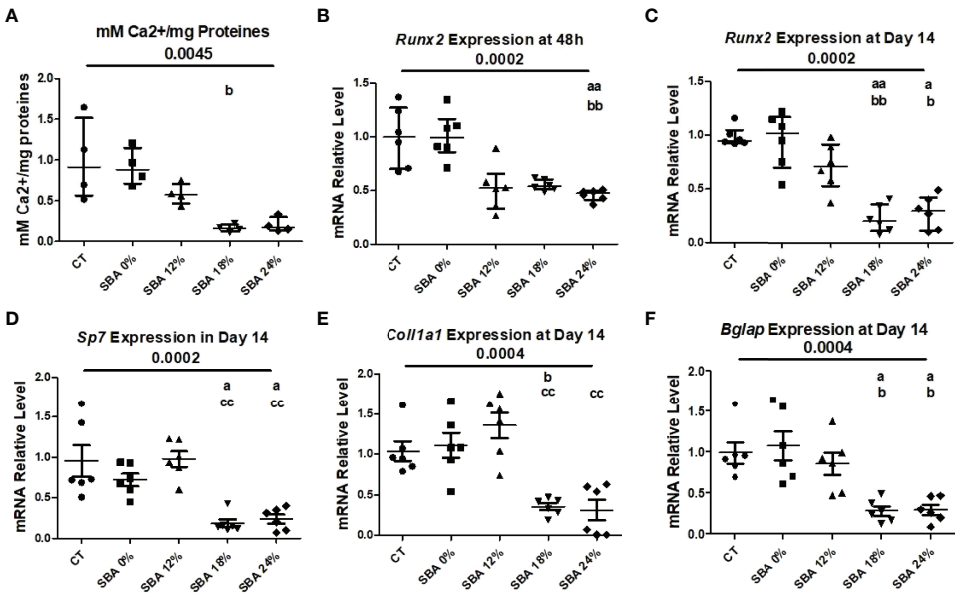

FIGURE 5 | 10-week SBA protocol induced a decrease in osteoblastogenesis. **(A)** Mineralization level of CT and SBA groups (0%, 12%, 18%, 24%) quantified by measuring the calcium to protein ratio; **(B, C)** Relative mRNA expression level of early osteoblastogenic marker gene (*Runx2*) in CT and SBA groups (0%, 12%, 18%, 24%), cells were cultured for 48 hours in standard growth media and for 14 days were exposed to co-differentiation media, respectively; **(D-F)** Relative mRNA expression level of other osteoblastogenic marker genes (*Sp7, Col1a1*, and *Bglap*, respectively) in CT and SBA groups (0%, 12%, 18%, 24%) after exposure to co-differentiation media for 14 days. Data represent median and interquartile range; Mineralisation study n = 4, qPCR n = 6. Statistical analysis was performed using Kruskal-Wallis One-Way ANOVA test and Dunn's test; a - $p < 0.05$, aa - $p < 0.005$ when compared to the CT group (b – when compared to the SBA 0% group; c – when compared to SBA 12% group). Runt-related transcription factor 2 (*Runx2*), osterix (*Sp7*), collagen1a1 (*Col1a1*), osteocalcin (*Bglap*). *Sirt1 is sustainably decreased in BMSCs from SBA mice (18% and 24%).*

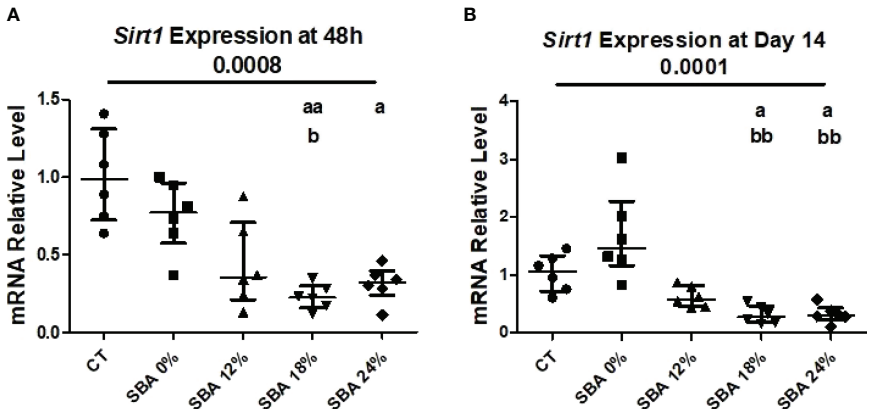

FIGURE 6 | 10-week SBA protocol induced a suppression of SIRT1 mRNA level. **(A, B)** Relative mRNA expression level of sirtuin type 1 (*Sirt1*) in CT and SBA groups (0%, 12%, 18%, 24%), cells were cultured for 48 hours in standard growth media and for 14 days were exposed to co-differentiation media, respectively. Data represent median and interquartile range; n = 6. Statistical analysis was performed using Kruskal-Wallis One-Way ANOVA test and Dunn's test; a - $p < 0.05$, aa - $p < 0.005$ when compared to the CT group (b – when compared to the SBA 0% group).

mouse fat absolute mass (-50% vs. CT), with no change in BMC or lean absolute mass (**Figure 7**). However, the significant decrease in fat % of total mouse weight was accompanied with significant increase in lean % mass (**Figures 7C, E**).

Furthermore, the bone microarchitecture results showed that the short SBA protocol induced changes in Tb.Th (-16% vs. CT) (**Figure 7B**) to a similar extent as the 10-week 18% weight loss protocol (**Figure 2B**). The 4-week SBA protocol also had no effect on BV/TV, Tb.N and Tb.Sp (**Figures 8A, B, D**), similar to SBA 18% group in 10-week protocol (**Figure 2**). However, in contrast with 10-week protocol, short duration of SBA had no effect on Cort.Th (**Figure 8E**). Additionally, bone marrow adiposity was not affected by the 4-week SBA protocol (**Figure 8F**). Thus, the 4-week protocol was not enough to induce changes in cortical bone microarchitecture, unlike the 10-week protocol.

Reduced Length of SBA Protocol Did Not Result in Alterations of BMSC Differentiation Capacity or Changes in Sirt1 Expression

After BMSCs were extracted from bone marrow and co-differentiation was induced, the cells were studied under a light microscope. Images showed that the first appearance of lipid droplets took place on the 7th day of co-differentiation in both the CT and SBA 18% groups (**Figure 9A**). Additionally, after 10 days of differentiation, there was no difference observed in the accumulation of adipocytes in SBA 18% vs. CT (**Figure 9A**). Therefore, the 4-week SBA protocol did not induce a shift of BMSCs towards adipocyte differentiation, as suggested by the results of the 10-week experiments. Similarly, it did not induce changes in lipid accumulation capacities. Raman spectroscopy showed no difference in lipid unsaturation levels between the control and SBA 18% groups (**Supplementary Figure 2**). Similar to the 10-week SBA study, we analyzed the relative mRNA levels of adipogenic/osteoblastogenic genes in extracted BMSCs. The results of the early adipogenic marker gene (*Pparg2*) showed that after 48 hours of proliferation in standard growth media, BMSCs extracted from SBA 18% mice had significantly increased expression levels (+350% vs. CT) (**Figure 9B**). However, this upregulation of *Pparg2* expression was not long term and after 14 days of co-differentiation, there was no significant difference observed between the two conditions (**Figure 9C**). The analysis of late adipogenic marker genes (*Lep*, *Adipoq*, *Plin1*) demonstrated no change in the SBA 18% group compared to the CT group after 14 days of co-differentiation (**Figures 9D–F**).

The next step was to determine the expression level of osteoblastic marker genes in the CT and SBA 18% groups. The early osteoblastogenic marker (*Runx2*) was not affected by 4 weeks of CR after 48 hours of incubation in proliferation media or after 14 days of exposure to co-differentiation media (**Figures 10A, B**). Moreover, other osteoblastogenic marker genes (*Col1a1*, *Sp7* and *Bglap*) were also not altered by the short-term SBA protocol (**Figures 10C–E**). The results of this study suggest that the 4-week protocol does not induce alterations in BMSC differentiation capacity.

To confirm the association between *Sirt1* expression and BMSC lineage commitment, we examined relative mRNA levels in the 4-week SBA 18% group vs. the CT group. The findings showed that the expression of *Sirt1* was not affected by the short SBA protocol, further suggesting its involvement in BMSC fate decisions (**Figure 11**).

DISCUSSION

Ten Weeks of 18% and 24% Body Weight Loss Induce an Alteration of Bone Mineral Content Without Increase in Bone Marrow Adiposity

We recently demonstrated that a long-term energy deficit characterized by a moderate weight loss (18%) in mice is

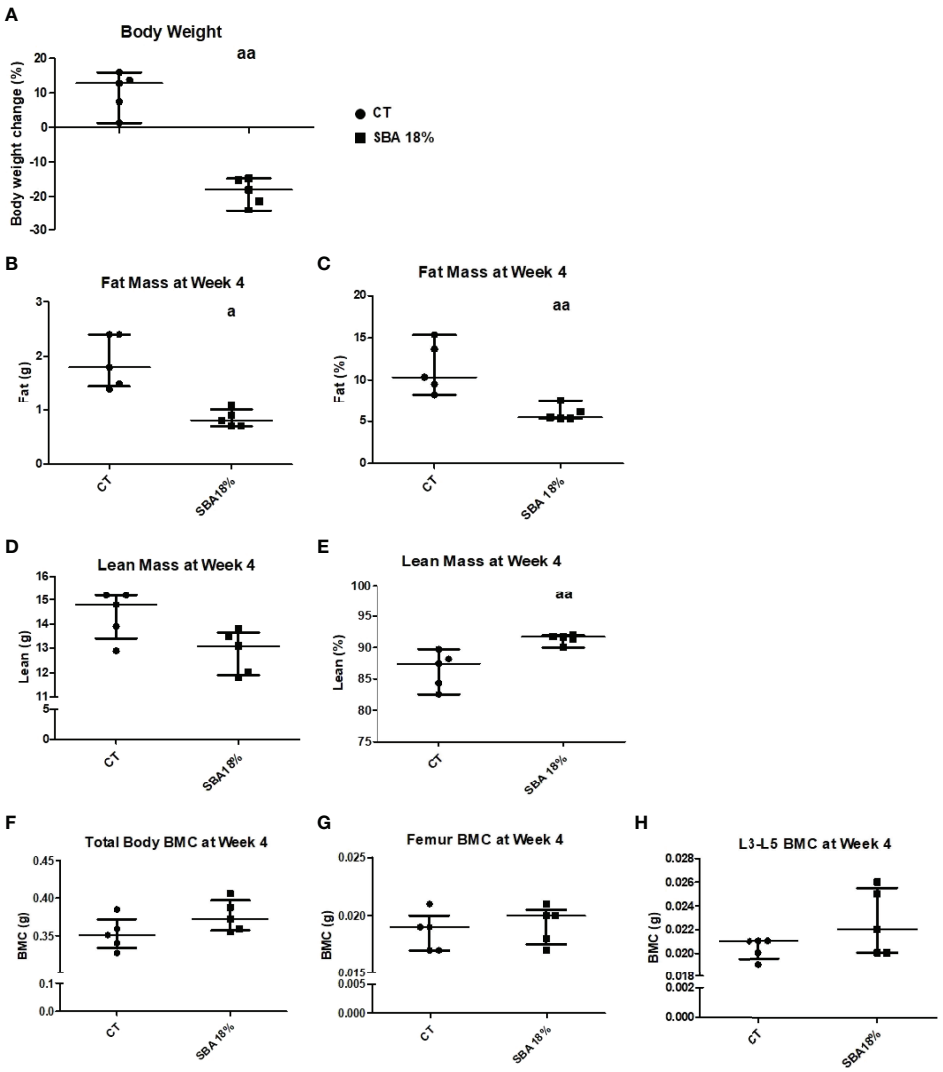

FIGURE 7 | Body mass, BMC, fat and lean mass in mice after 4 weeks of SBA protocol. The body weight and composition analysis were performed on standard condition (CT) and weight loss group (SBA 18%). **(A)** Graph represents a percentage body weight loss on mice between day 0 and 4 weeks of SBA protocol; **(B, C)** Fat mass content presented in grams and % of total mass, respectively was evaluated for each mouse and condition after 4 weeks of SBA protocol; **(D, E)** Lean mass content presented in grams and % of total mass, respectively was evaluated for each mouse and condition after 4 weeks of SBA protocol; **(F-H)** Study of total mouse body mineral content (BMC), femur BMC and vertebra (L3-L5) BMC, respectively, evaluated for each animal and each condition after 4 weeks of SBA protocol. Data represent median and interquartile range; n = 5. Statistical analysis was performed using Mann–Whitney's test; a - $p < 0.05$, aa - $p < 0.005$, when compared to the CT group.

associated with bone loss and an increase in BMA (26). In this study, we sought to determine the impact of a different degree of severity on bone architecture, BMA, and then to identify the potential molecular mechanisms involved in BMA regulation in this context. The mice were exposed for 10 weeks to a separation-induced increase in energy expenditure and a time-restricted feeding that prevented compensatory feeding and resulted in significant weight loss (SBA) (27). Results of mice body parameters showed similar fat mass decrease in all SBA groups compared to the control group. The 12%, 18%, and 24% groups displayed a decrease in BMC at least in femur. These results suggest that a significant weight loss over a long period of time (10 weeks) is required to induce changes in mineralized bone (**Figure 1**). Moreover, these bone changes are not directly related to fat mass because they are not shown in the 0% group. This was already shown in adult male mice by Mitchell et al. (33). They demonstrated that different levels of CR 10%, 20%, 30%, and 40% in male mice induced body weight losses of around 0%, 11%, 22%, and 28%, respectively after 12 weeks (33). These weight changes were associated to fat mass decrease of approximately 12% for 10% CR and 30 to 35% for the other groups. In this study, no significant changes in BMC, trabecular bone microarchitecture, and cortical bone were detected. Unfortunately, BMA was not determined. The conflicting

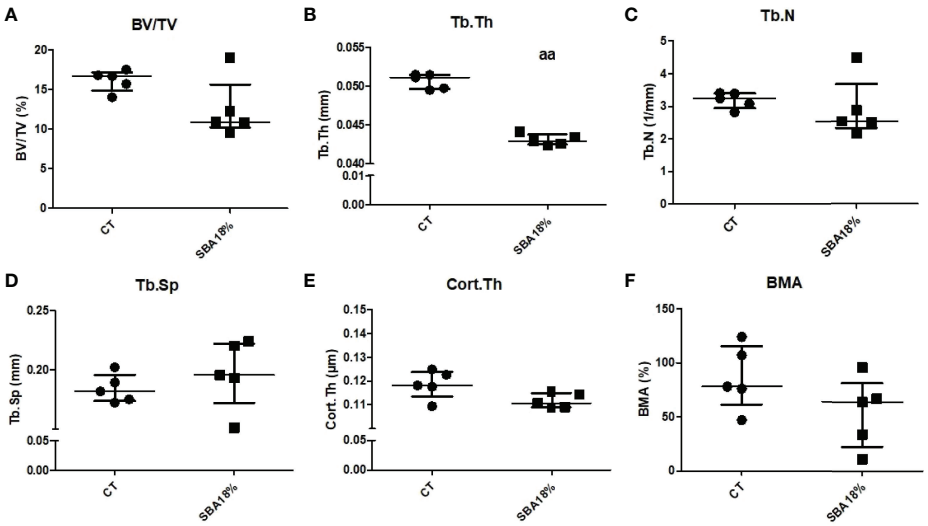

FIGURE 8 | The results of micro-CT analysis of tibia, showing different bone parameters after exposure to 4 weeks of SBA protocol. **(A)** Bone volume fraction (BV/TV) was expressed as a percentage on mineralized tissue in each condition after 4 weeks; **(B-E)** Trabecular thickness (Tb.Th), trabecular number (Tb.N) and trabecular spacing (Tb.Sp), and cortical thickness (Cort.Th), respectively, were evaluated for each animal and each condition after 4 weeks of SBA protocol (expressed in millimetres); **(F)** Bone marrow adiposity (BMA) was calculated as a percentage of BMAT in marrow volume. Data represent median and interquartile range; n = 5. Statistical analysis was performed using Mann–Whitney's test. In C, aa - $p < 0.005$ when compared to CT group.

results on bone in the present study and that of Mitchell could be due to sex, age, and protocol differences. Furthermore, Mitchell's study also showed the lack of relationship between fat mass decrease and bone in energy deficit experiment.

Previously, we showed that the SBA protocol of 18% weight loss results in an increase in BMA (26). Interestingly, in the current study, BMA appeared to be altered only in one weight loss condition. BMA displayed a decrease (not significant) in SBA mice with a light weight loss (12%) (**Figure 2F**). Firstly, the apparent discrepancy between the two studies could be explained by the fact that we observed a high heterogeneity in BMA among mice of the same group. Secondly, in the first study, BMA was assessed using histological (2D) approaches with slices focused on a specific area of the proximal tibia and with a specific orientation, while this study used 3D assessment on a larger volume including the area analyzed in the previous study. So, the increase observed in a specific area and the lack of significant changes observed on the large volume suggest that very localized changes could occur in the density of adipocytes in the marrow. Various studies demonstrated an increase in BMA associated with bone alteration in anorexic patients (9, 10, 13). In rodent, models of food or calorie restriction demonstrated that 9 weeks of a 30% restriction on food in 3-week-old male mice induced low BV/TV (-11%), Cort.Th (-27%), and body weight (-40%), which were accompanied with high BMA (700%) compared to CT mice (34). Also, it has been shown that 6 weeks of a 30% calorie-restricted diet in 9-week-old female mice induced an increase in tibia BMA (700%) compared to that in the *ad libitum* group (35). Interestingly, in these two studies, the high increase in BMA was associated with a body weight increase of 80% vs. day 0 (34) or a final body weight similar to that of day 0 of the experiment (35). The difference in our BMA results compared to these two studies (34, 35) may be explained by the fact that we used young adult female mice, while the first one investigated growing male mice (34) and by the difference in body weight loss relative to that on day 0 (33, 34). In addition, it is reported that an extensive CR in rabbits can cause a loss of BMAT (34). A similar finding has been observed with severe anorexic patients (36). Thus, the sex of animals and level of body weight loss may strongly affect BMA. In contrast, a calorie restriction protocol (low carbohydrate feeding) for 12 weeks on 6-month-old Sprague–Dawley female rats, demonstrated that restricted rats displayed body weight loss (20% vs. day 0 and 25% vs. CT rats), a low volumetric BMD at the proximal tibia (-14%) and only a two-fold increase in BMA measured at the distal femur (37). More recently, male Sprague–Dawley rats (8 months old) exposed to 40% calorie restriction during 12 months, displayed 40% body weight loss vs. CT rats, which resulted in a decrease in the bone mineral index (30% vs. CT rats) and an increase in BMA at the proximal tibia (20% vs. CT rats) (38). Conversely, 10 weeks of CR in 14-week-old male mice led to a body weight loss of 30% (relative to CT mice) and a total disappearance of bone marrow adipocytes in the distal femur (34). Altogether, these data suggest that restriction-induced changes in BMA and bone quality may be modulated by severity of protocol, body weight loss, age, sex, and duration of restriction.

Ten Weeks of 18% and 24% Body Weight Loss Induce an Imbalance Between Osteoblastogenesis and Adipogenesis

Due to the fact that, in the current study, bone alterations were not associated to a high BMA, we hypothesised that the

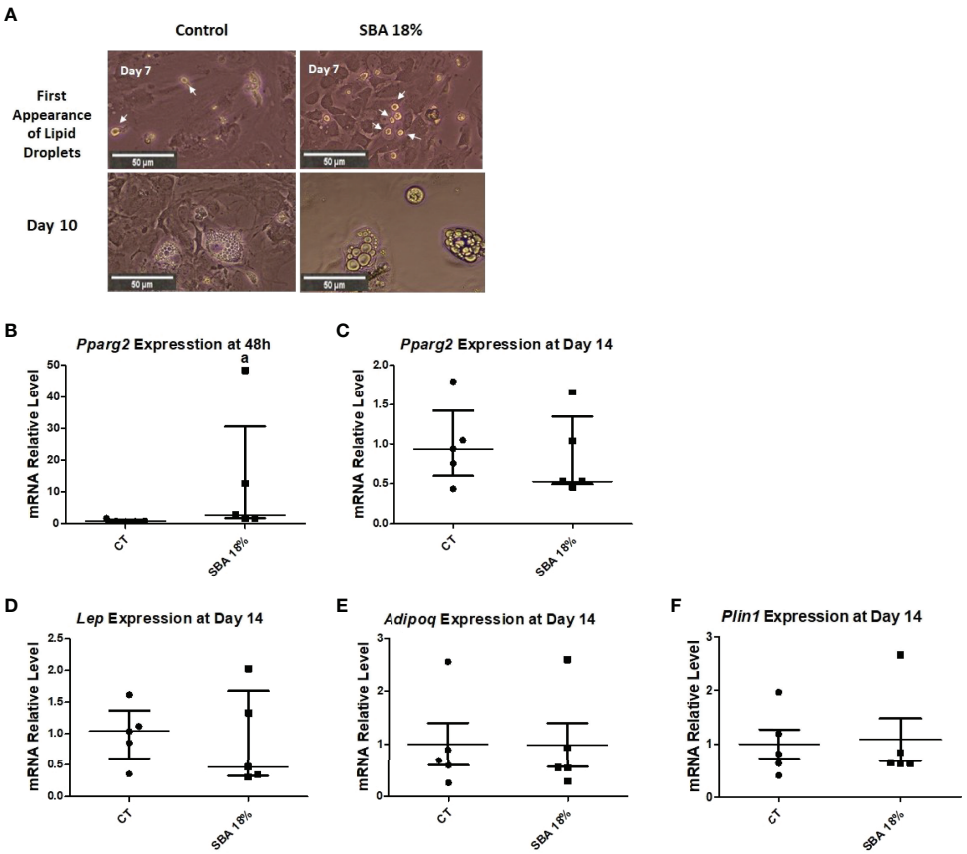

FIGURE 9 | Study of adipocyte first appearance, size and adipogenic gene expression in BMSCs. **(A)** Light microscopic images of cells from each condition were taken at different time points of co-differentiation showing the first appearance of lipid droplets (day 7) and adipocytes at Day 10; **(B, C)** Relative mRNA expression level of early adipogenic marker gene (*Pparg2*) in CT and SBA (18%) groups, cells were cultured for 48 hours in standard growth media and for 14 days were exposed to co-differentiation media, respectively; **(D–F)** Relative mRNA expression level of other adipogenic marker genes (leptin, adiponectin, and perilipin, respectively) in CT and SBA groups (18%) after exposure to co-differentiation media for 14 days. Data represents median and interquartile range; n = 5. Statistical analysis was performed using Mann–Whitney's test. In **(B)**, a - $p < 0.05$ when compared to CT group. Peroxisome proliferator-activated receptor gamma 2 (*Pparg2*), leptin (*Lep*), adiponectin (*Adipoq*), perilipin (*Plin1*).

commitment of BMSCs towards the adipogenic pathway could impact bone mass even if adipocytes are not able to reach a mature state. Therefore, it was important to study BMSC differentiation to obtain a more precise understanding of the cell commitment towards the adipogenic or osteoblastogenic pathway.

Given that osteoblasts and adipocytes are derived from a common mesenchymal progenitor, skeletal stem cells (39, 40), we tested the hypothesis that the degree of severity of body weight loss could impact the differentiation capacity of BMSCs extracted from SBA mice. After just 48 hours of adhesion in a standard proliferative medium, the unstimulated BMSCs from SBA mice with body weight loss (12%, 18%, and 24%) exhibited high levels of *Pparg2* mRNA even if not significantly for the 18% group (**Figure 4A**). This finding suggests that extracted BMSCs display commitment to the adipocytic lineage. As shown in **Figures 3** and **4**, SBA weight loss protocols enhance BMSC adipogenesis *in vitro*, especially for SBA 18% and 24% groups. The mRNA level of adiponectin was dramatically decreased in SBA mice with light weight loss (12%) and this finding could be associated with a significant decrease in BMA under the same weight loss conditions. Significant loss of mature adipocytes *in vivo* could potentially affect the level of adiponectin production and *Adipoq* mRNA levels (41). Raman spectroscopy analysis (**Supplementary Figure 1**) further revealed that SBA protocol results in a decrease of unsaturated lipids ratio in BMSC-derived adipocytes. This suggests that energy deficit induces a long-lasting alteration of lipid quality regardless the level of body weight loss. Our analysis of osteoblastogenesis in BMSCs (**Figure 5**) suggests that only 18% and 24% weight loss groups induce significant and long-lasting changes in osteoblastogenesis *in vitro*.

Findings above led us to conclude that there potentially exists a preferential commitment of BMSCs extracted from SBA mice to the adipogenic pathway. Results show that adipogenesis and osteoblastogenesis seem to be affected by the severity of energy deficit and that at least an 18% weight loss is required to observe these alterations.

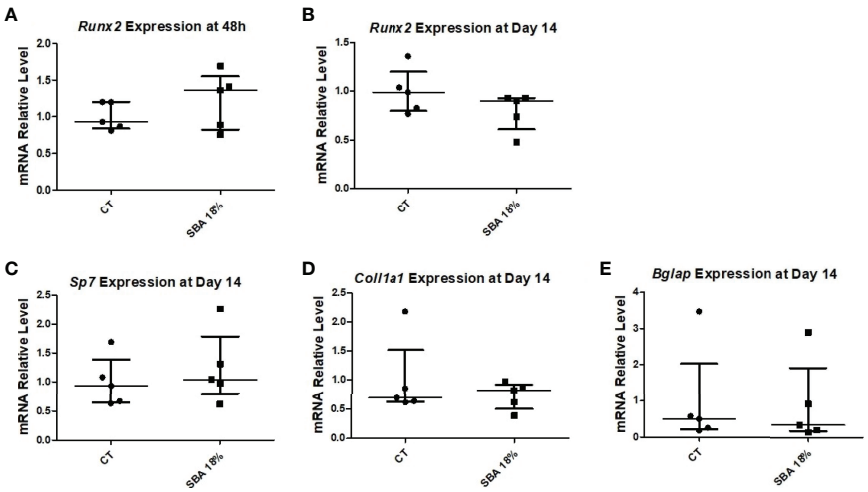

FIGURE 10 | 4-week SBA protocol did not induce changes in osteoblastogenesis. **(A, B)** Relative mRNA expression level of early osteoblastogenic marker gene (RUNX2) in CT and SBA groups (18%), respectively, cells were cultured for 48 hours in standard growth media and for 14 days were exposed to co-differentiation media, respectively; **(C-E)** Relative mRNA expression level of other osteoblastogenic marker genes (osterix, collagen1, and osteocalcin, respectively) in CT and SBA (18%) groups after exposure to co-differentiation media for 14 days. Data represent median and interquartile range; n = 5. Statistical analysis was performed using Mann–Whitney's test. Runt-related transcription factor 2 (*Runx2*), osterix (*Sp7*), collagen1a1 (*Col1a1*), osteocalcin (*Bglap*).

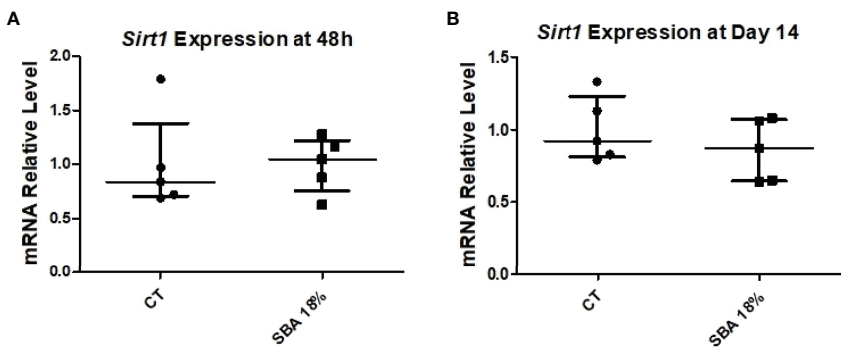

FIGURE 11 | 4-week SBA protocol induced no change in *Sirt1* expression. **(A, B)** Relative mRNA expression level of sirtuin type 1 (*Sirt1*) in CT and SBA groups (18%), cells were cultured for 48 hours in standard growth media and for 14 days were exposed to co-differentiation media, respectively. Data represent median and interquartile range; n = 5. Statistical analysis was performed using Mann–Whitney's test.

Sirt1 Is Sustainably Altered in BMSCs From 18% and 24% Groups at 10 Weeks

To determine the potential molecular mechanism involved in the regulation of BMSC differentiation in SBA mice, the relative mRNA level of *Sirt1* was measured. Indeed, we recently demonstrated that 18% weight loss in mice is associated with the downregulation of the expression and activity of *Sirt1* and further, possibly leads to an increase in adipogenesis at the expense of osteoblastogenesis (26). In the current study, we hypothesised that *Sirt1* could be altered by the degree of severity of energy deficit, leading to an imbalance between osteoblastogenesis and adipogenesis. It is important to note that *Sirt1* is widely known for its pro-osteoblastic and anti-adipogenic effects (18–23). Indeed, *in vivo* activation of *Sirt1* restores bone mass, structure, and biomechanical properties in ovariectomised female mice (42) and it protects against age-associated bone loss in male mice (43). *In vitro* studies demonstrated that activation of *Sirt1* promotes osteoblastogenic differentiation at the expense of adipogenesis (18–21). Interestingly, our results demonstrated that BMSCs from SBA mice with moderate and severe weight loss (18% and 24%) presented a substantial low *Sirt1* mRNA level after 48 hours of culture and after 14 days of co-differentiation (**Figure 6**). These findings suggest that the decrease in *Sirt1* expression could be responsible for the observed increase in adipogenesis at the expense of osteoblastogenesis in these two groups.

Other studies have shown that CR can stimulate the expression and activity of *Sirt1* in various mammalian tissues, such as the liver or white adipose tissue (24, 25). It was also shown that CR decreases the mRNA level of *Sirt1* in the cerebellum and midbrain (44),

suggesting tissue-dependent regulation of the expression. More recently, in contrast to our study, it was demonstrated that 12 months of 40% calorie restriction of male Sprague–Dawley rats (8 months old) induced an upregulation in protein expression of *Sirt1* in bone marrow fat compared to that in *ad libitum* animals (38). This discrepancy between our results and others from Cohen et al. (24) and (38) could be explained by changes in calorie or food restriction protocols, mouse strain or species, age, and sex. Indeed, twelve-month-old male rats were used in Cohen et al. studies and calorie restriction involved a daily food allotment of 60% of that eaten by the *ad libitum* animals immediately after weaning (24). In our study, eight-week-old female C57BL/6J mice were submitted to the 10-week SBA protocol. Furthermore, the weight loss of mice in each protocol of calorie restriction could also explain this discrepancy. Indeed, contrary to our protocol, which induces 12%, 18%, and 24% weight loss in mice, there is no information on weight loss in the study by Cohen et al. (24) and there was a 40% lower weight (vs CT) in the study by Duque et al. (38). Thus, the loss of Sirt1 seems to be closely associated to bone and BMSCs alterations and could explain the strong and long-lasting commitment of BMSCs towards the adipogenic pathway in SBA mice.

In our study, 18% is considered moderate weight loss, which is associated with a decrease in all parameters of body composition (low fat mass, tendency to low lean mass, low total body BMC, low femur and lumbar spine BMC) and cortical bone thickness. Furthermore, only in this weight loss category we found an upregulation of most of the adipocyte markers analyzed (*Pparg2, Lep*, and *Glut4*) and a downregulation of most of the osteoblast markers analyzed (*Runx2, Sp7*, and *Bglap*). In addition, this weight loss group displayed a strong decrease in *Sirt1* mRNA level. Considering these results, the rest of the study was dedicated to focusing on SBA 18% and investigating the effect of a short duration of SBA protocol (4 weeks) on body composition, bone architecture, BMA, BMSC differentiation and *Sirt1* expression.

A Short Duration of Moderate Weight Loss Did Not Affect Bone Architecture, BMA, BMSC Differentiation or Sirt1 Expression

Four weeks of the SBA protocol induced only a decrease in fat mass (**Figure 7B**) and Tb.Th (**Figure 8B**) without affecting the other parameters of bone architecture and BMA (**Figure 8**). Selective change in Tb.Th does not seem to be associated with an overall bone alteration. Moreover, this short duration did not impact BMSC differentiation towards adipogenic lineage or osteoblastogenic lineage nor did it affect the unsaturation ratio of lipid droplets (**Figures 9**–**11**, **Supplementary Figure 2**). Interestingly, this lack of effects on bone and BMSCs differentiation is associated with a lack of effects on Sirt1 mRNA level. This strengthens the hypothesis of a direct involvement of Sirt1 alteration on BMSCs fate decision and bone. Altogether, these results suggest that in addition to the degree of severity, the duration of energy deficit could play an important role in regulating bone architecture, BMA, and BMSC differentiation, which requires long-term protocols to be altered. This line of inquiry will be required in the future to determine when the first alterations in bone, BMA, and *Sirt1* expression can occur in our SBA model.

CONCLUSION

The present study demonstrated, for the first time, the impact of severity and length of energy deficit on bone and BMSCs differentiation capacity. The data from two groups (moderate and severe weight loss) support the hypothesis that there is a link between decrease in Sirt1 mRNA levels and alterations in bone and BMSCs differentiation capacity. A comparison of the 10-week SBA protocol to the 4-week SBA protocol strengthen this hypothesis. Finally, bone alterations appear to be totally disconnected from BMA changes in this model, probably because the increase in the number of BM pre-adipocytes, which takes place at the expense of osteoblastogenesis and does not result in an increase in mature adipocytes.

In vivo changes in BMSCs engagement in the adipogenic pathway remain to be specified using FACS analysis. Furthermore, the molecular mechanisms responsible for Sirt1 long lasting downregulation will be explored through the RNA sequencing approach.

DATA AVAILABILITY STATEMENT

The original contributions presented in the study are included in the article/**Supplementary Material**. Further inquiries can be directed to the corresponding authors.

ETHICS STATEMENT

The animal study was reviewed and approved by the Committee on the Ethics of Animal Experiments (CEEA) of Nord-Pas de Calais, France (permit number: CEEA#2016070717275082).

AUTHOR CONTRIBUTIONS

CC, OG, and VA contributed to the conception and design of the work. VA carried out all the cell cultures experiments, qPCR and their analysis. DL and VG contributed to sample collection during mice sacrifice. JD and FM contributed to acquisition and analysis of the microCT data. GF performed the Raman analysis. VA, OG, and CC contributed to statistical analysis. VA and OG wrote the manuscript. CC and OG contributed to the review and editing the manuscript. All authors contributed to the article and approved the submitted version.

FUNDING

VA is supported by Université du Littoral Côte d'Opale and Région Hauts-de-France.

SUPPLEMENTARY MATERIAL

The Supplementary Material for this article can be found online at: https://www.frontiersin.org/articles/10.3389/fendo.2022.880503/full#supplementary-material

REFERENCES

1. Bredella MA, Fazeli PK, Miller KK, Misra M, Torriani M, Thomas BJ, et al. Increased Bone Marrow Fat in Anorexia Nervosa. *J Clin Endocrinol Metab* (2009) 94(6):2129–36. doi: 10.1210/jc.2008-2532
2. Ecklund K, Vajapeyam S, Feldman HA, Buzney CD, Mulkern RV, Kleinman PK, et al. Bone Marrow Changes in Adolescent Girls With Anorexia Nervosa. *J Bone Mineral Res* (2010) 25(2):298–304. doi: 10.1359/jbmr.090805
3. Mayo-Smith W, Rosenthal DI, Goodsitt MM, Klibanski A. Intravertebral Fat Measurement With Quantitative CT in Patients With Cushing Disease and Anorexia Nervosa. *Radiology* (1989) 170(3):835–8. doi: 10.1148/radiology.170.3.2916039
4. Miller KK, Grinspoon SK, Ciampa J, Hier J, Herzog D, Klibanski A. Medical Findings in Outpatients With Anorexia Nervosa. *Arch Internal Med* (2005) 165(5):561–6. doi: 10.1001/archinte.165.5.561
5. Grinspoon S, Thomas E, Pitts S, Gross E, Mickley D, Miller K, et al. Prevalence and Predictive Factors for Regional Osteopenia in Women With Anorexia Nervosa. *Ann Intern Med* (2000) 133(10):790–4. doi: 10.7326/0003-4819-133-10-200011210-00011
6. Badr S, Legroux-Gérot I, Vignau J, Chauveau C, Ruschke S, Karampinos DC, et al. Comparison of Regional Bone Marrow Adiposity Characteristics at the Hip of Underweight and Weight-Recovered Women With Anorexia Nervosa Using Magnetic Resonance Spectroscopy. *Bone* (2019) 127:135–45. doi: 10.1016/j.bone.2019.05.033
7. OWEN M. Marrow Stromal Stem Cells. *J Cell Sci* (1988) 1988 (Supplement_10):63–76. doi: 10.1242/jcs.1988.Supplement_10.5
8. Nishimura R, Hata K, Ikeda F, Ichida F, Shimoyama A, Matsubara T, et al. Signal Transduction and Transcriptional Regulation During Mesenchymal Cell Differentiation. *J Bone Mineral Metab* (2008) 26(3):203. doi: 10.1007/s00774-007-0824-2
9. Pittenger Mark F, Mackay Alastair M, Beck Stephen C, Jaiswal Rama K, Douglas R, Mosca Joseph D, et al. Multilineage Potential of Adult Human Mesenchymal Stem Cells. *Science* (1999) 284(5411):143–7. doi: 10.1126/science.284.5411.143
10. Beresford JN, Bennett JH, Devlin C, Leboy PS, Owen ME. Evidence for an Inverse Relationship Between the Differentiation of Adipocytic and Osteogenic Cells in Rat Marrow Stromal Cell Cultures. *J Cell Sci* (1992) 102 (2):341. doi: 10.1242/jcs.102.2.341
11. Moerman EJ, Teng K, Lipschitz DA, Lecka-Czernik B. Aging Activates Adipogenic and Suppresses Osteogenic Programs in Mesenchymal Marrow Stroma/Stem Cells: The Role of PPAR-Gamma2 Transcription Factor and TGF-Beta/BMP Signaling Pathways. *Aging Cell* (2004) 3(6):379–89. doi: 10.1111/j.1474-9728.2004.00127.x
12. Li J, Zhang N, Huang X, Xu J, Fernandes JC, Dai K, et al. Dexamethasone Shifts Bone Marrow Stromal Cells From Osteoblasts to Adipocytes by C/EBPalpha Promoter Methylation. *Cell Death Disease* (2013) 4(10):e832–2. doi: 10.1038/cddis.2013.348
13. Song L, Liu M, Ono N, Bringhurst FR, Kronenberg HM, Guo J. Loss of Wnt/β-Catenin Signaling Causes Cell Fate Shift of Preosteoblasts From Osteoblasts to Adipocytes. *J Bone Miner Res* (2012) 27(11):2344–58. doi: 10.1002/jbmr.1694
14. Skillington J, Choy L, Derynck R. Bone Morphogenetic Protein and Retinoic Acid Signaling Cooperate to Induce Osteoblast Differentiation of Preadipocytes. *J Cell Biol* (2002) 159(1):135–46. doi: 10.1083/jcb.200204060
15. Bradley EW, McGee-Lawrence ME, Westendorf JJ. Hdac-Mediated Control of Endochondral and Intramembranous Ossification. *Crit Rev Eukaryot Gene Expr* (2011) 21(2):101–13. doi: 10.1615/critreveukargeneexpr.v2
16. McGee-Lawrence ME, Carpio LR, Schulze RJ, Pierce JL, McNiven MA, Farr JN, et al. Hdac3 Deficiency Increases Marrow Adiposity and Induces Lipid Storage and Glucocorticoid Metabolism in Osteochondroprogenitor Cells. *J Bone Miner Res* (2016) 31(1):116–28. doi: 10.1002/jbmr.2602
17. Bordone L, Cohen D, Robinson A, Motta MC, Van Veen E, Czopik A, et al. SIRT1 Transgenic Mice Show Phenotypes Resembling Calorie Restriction. *Aging Cell* (2007) 6(6):759–67. doi: 10.1111/j.1474-9726.2007.00335.x
18. Bäckesjö C-M, Li Y, Lindgren U, Haldosén L-A. Activation of Sirt1 Decreases Adipocyte Formation During Osteoblast Differentiation of Mesenchymal Stem Cells. *J Bone Mineral Res* (2006) 21(7):993–1002. doi: 10.1359/jbmr.060415
19. Simic P, Zainabadi K, Bell E, Sykes DB, Saez B, Lotinun S, et al. SIRT1 Regulates Differentiation of Mesenchymal Stem Cells by Deacetylating β-Catenin. *EMBO Mol Med* (2013) 5(3):430–40. doi: 10.1002/emmm.201201606
20. Shakibaei M, Shayan P, Busch F, Aldinger C, Buhrmann C, Lueders C, et al. Resveratrol Mediated Modulation of Sirt-1/Runx2 Promotes Osteogenic Differentiation of Mesenchymal Stem Cells: Potential Role of Runx2 Deacetylation. *PloS One* (2012) 7(4):e35712–2. doi: 10.1371/journal.pone.0035712
21. Tseng P-C, Hou S-M, Chen R-J, Peng H-W, Hsieh C-F, Kuo M-L, et al. Resveratrol Promotes Osteogenesis of Human Mesenchymal Stem Cells by Upregulating RUNX2 Gene Expression *via* the SIRT1/FOXO3A Axis. *J Bone Mineral Res* (2011) 26(10):2552–63. doi: 10.1002/jbmr.460
22. Chiara B, Ilaria C, Antonietta C, Francesca C, Marco M, Lucia A, et al. SIRT1 Inhibition Affects Angiogenic Properties of Human MSCs. *BioMed Res Int* (2014) 2014:783459. doi: 10.1155/2014/783459
23. Orecchia A, Scarponi C, Di Felice F, Cesarini E, Avitabile S, Mai A, et al. Sirtinol Treatment Reduces Inflammation in Human Dermal Microvascular Endothelial Cells. *PloS One* (2011) 6(9):e24307. doi: 10.1371/journal.pone.0024307
24. Cohen HY, Miller C, Bitterman KJ, Wall NR, Hekking B, Kessler B, et al. Calorie Restriction Promotes Mammalian Cell Survival by Inducing the SIRT1 Deacetylase. *Science* (2004) 305(5682):390. doi: 10.1126/science.1099196
25. Zainabadi K, Liu CJ, Caldwell ALM, Guarente L. SIRT1 is a Positive Regulator of *In Vivo* Bone Mass and a Therapeutic Target for Osteoporosis. *PloS One* (2017) 12(9):e0185236–e0185236. doi: 10.1371/journal.pone.0185236
26. Louvet L, Leterme D, Delplace S, Miellot F, Marchandise P, Gauthier V, et al. Sirtuin 1 Deficiency Decreases Bone Mass and Increases Bone Marrow Adiposity in a Mouse Model of Chronic Energy Deficiency. *Bone* (2020) 136:115361. doi: 10.1016/j.bone.2020.115361
27. Zgheib S, Méquinion M, Lucas S, Leterme D, Ghali O, Tolle V, et al. Long-Term Physiological Alterations and Recovery in a Mouse Model of Separation Associated With Time-Restricted Feeding: A Tool to Study Anorexia Nervosa Related Consequences. *PloS One* (2014) 9(8):e103775. doi: 10.1371/journal.pone.0103775
28. Coutel X, Olejnik C, Marchandise P, Delattre J, Béhal H, Kerckhofs G, et al. A Novel microCT Method for Bone and Marrow Adipose Tissue Alignment Identifies Key Differences Between Mandible and Tibia in Rats. *Calcified Tissue Int* (2018) 103(2):189–97. doi: 10.1007/s00223-018-0397-1
29. Coutel X, Delattre J, Marchandise P, Falgayrac G, Béhal H, Kerckhofs G, et al. Mandibular Bone is Protected Against Microarchitectural Alterations and Bone Marrow Adipose Conversion in Ovariectomized Rats. *Bone* (2019) 127:343–52. doi: 10.1016/j.bone.2019.06.031
30. Ghali O, Broux O, Falgayrac G, Haren N, van Leeuwen JPTM, Penel G, et al. Dexamethasone in Osteogenic Medium Strongly Induces Adipocyte Differentiation of Mouse Bone Marrow Stromal Cells and Increases Osteoblast Differentiation. *BMC Cell Biol* (2015) 16:9–9. doi: 10.1186/s12860-015-0056-6
31. Czamara K, Majzner K, Pacia MZ, Kochan K, Kaczor A, Baranska M. Raman Spectroscopy of Lipids: A Review. *J Raman Spectroscopy* (2015) 46(1):4–20. doi: 10.1002/jrs.4607
32. Ghali O, Chauveau C, Hardouin P, Broux O, Devedjian J-C. TNF-α's Effects on Proliferation and Apoptosis in Human Mesenchymal Stem Cells Depend on RUNX2 Expression. *J Bone Mineral Res* (2010) 25(7):1616–26. doi: 10.1002/jbmr.52
33. Mitchell SE, Tang Z, Kerbois C, Delville C, Konstantopedos P, Bruel A, et al. The Effects of Graded Levels of Calorie Restriction: I. Impact of Short Term Calorie and Protein Restriction on Body Composition in the C57BL/6 Mouse. *Oncotarget* (2015) 6(18):15902–30. doi: 10.18632/oncotarget.4142
34. Devlin MJ, Cloutier AM, Thomas NA, Panus DA, Lotinun S, Pinz I, et al. Caloric Restriction Leads to High Marrow Adiposity and Low Bone Mass in Growing Mice. *J Bone Miner Res* (2010) 25(9):2078–88. doi: 10.1002/jbmr.82
35. Cawthorn WP, Scheller EL, Parlee SD, Pham HA, Learman BS, Redshaw CMH, et al. Expansion of Bone Marrow Adipose Tissue During Caloric Restriction Is Associated With Increased Circulating Glucocorticoids and Not With Hypoleptinemia. *Endocrinology* (2016) 157(2):508–21. doi: 10.1210/en.2015-1477
36. Abella E, Feliu E, Granada I, Millá F, Oriol A, Ribera JM, et al. Bone Marrow Changes in Anorexia Nervosa Are Correlated With the Amount of Weight

Loss and Not With Other Clinical Findings. *Am J Clin Pathol* (2002) 118 (4):582–8. doi: 10.1309/2Y7X-YDXK-006B-XLT2
37. Baek K, Bloomfield SA. Blocking β-Adrenergic Signaling Attenuates Reductions in Circulating Leptin, Cancellous Bone Mass, and Marrow Adiposity Seen With Dietary Energy Restriction. *J Appl Physiol* (2012) 113 (11):1792–801. doi: 10.1152/japplphysiol.00187.2012
38. Duque G, Al Saedi A, Rivas D, Miard S, Ferland G, Picard F, et al. Differential Effects of Long-Term Caloric Restriction and Dietary Protein Source on Bone and Marrow Fat of the Aging Rat. *J Gerontol A Biol Sci Med Sci* (2020) 75 (11):2031–6. doi: 10.1093/gerona/glaa093
39. Bianco P, Robey PG, Saggio I, Riminucci M. 'Mesenchymal' Stem Cells in Human Bone Marrow (Skeletal Stem Cells): A Critical Discussion of Their Nature, Identity, and Significance in Incurable Skeletal Disease. *Hum Gene Ther* (2010) 21(9):1057–66. doi: 10.1089/hum.2010.136
40. Vashi AV, Keramidaris E, Abberton KM, Morrison WA, Wilson JL, O'Connor AJ, et al. Adipose Differentiation of Bone Marrow-Derived Mesenchymal Stem Cells Using Pluronic F-127 Hydrogel *In Vitro*. *Biomaterials* (2008) 29(5):573–9. doi: 10.1016/j.biomaterials.2007.10.017
41. Cawthorn WP, Scheller EL, Learman BS, Parlee SD, Simon BR, Mori H, et al. Bone Marrow Adipose Tissue Is an Endocrine Organ That Contributes to Increased Circulating Adiponectin During Caloric Restriction. *Cell Metab* (2014) 20(2):368–75. doi: 10.1016/j.cmet.2014.06.003
42. Artsi H, Cohen-Kfir E, Gurt I, Shahar R, Bajayo A, Kalish N, et al. The Sirtuin1 Activator SRT3025 Down-Regulates Sclerostin and Rescues Ovariectomy-Induced Bone Loss and Biomechanical Deterioration in Female Mice. *Endocrinology* (2014) 155(9):3508–15. doi: 10.1210/en.2014-1334
43. Herranz D, Muñoz-Martin M, Cañamero M, Mulero F, Martinez-Pastor B, Fernandez-Capetillo O, et al. Sirt1 Improves Healthy Ageing and Protects From Metabolic Syndrome-Associated Cancer. *Nat Commun* (2010) 1(1):3. doi: 10.1038/ncomms1001
44. Chen D, Steele AD, Hutter G, Bruno J, Govindarajan A, Easlon E, et al. The Role of Calorie Restriction and SIRT1 in Prion-Mediated Neurodegeneration. *Exp Gerontol* (2008) 43(12):1086–93. doi: 10.1016/j.exger.2008.08.050

Conflict of Interest: The authors declare that the research was conducted in the absence of any commercial or financial relationships that could be construed as a potential conflict of interest.

Publisher's Note: All claims expressed in this article are solely those of the authors and do not necessarily represent those of their affiliated organizations, or those of the publisher, the editors and the reviewers. Any product that may be evaluated in this article, or claim that may be made by its manufacturer, is not guaranteed or endorsed by the publisher.

frontiers | Frontiers in Endocrinology

ORIGINAL RESEARCH
published: 08 June 2022
doi: 10.3389/fendo.2022.882379

Morphological and Immunophenotypical Changes of Human Bone Marrow Adipocytes in Marrow Metastasis and Myelofibrosis

Michele Dello Spedale Venti[1], *Biagio Palmisano*[1], *Samantha Donsante*[1], *Giorgia Farinacci*[1], *Flavia Adotti*[1], *Ilenia Coletta*[1], *Marta Serafini*[2], *Alessandro Corsi*[1] *and Mara Riminucci*[1]*

[1] Department of Molecular Medicine, Sapienza University of Rome, Rome, Italy, [2] Centro Ricerca M. Tettamanti, Department of Pediatrics, University of Milano-Bicocca, Monza, Italy

OPEN ACCESS

Edited by:
Jason Horton,
Upstate Medical University,
United States

Reviewed by:
Noriaki Ono,
University of Texas Health Science Center at Houston, United States
Meghan E. McGee-Lawrence,
Augusta University, United States

***Correspondence:**
Mara Riminucci
mara.riminucci@uniroma1.it

Specialty section:
This article was submitted to Bone Research, a section of the journal Frontiers in Endocrinology

Received: 23 February 2022
Accepted: 19 April 2022
Published: 08 June 2022

Citation:
Dello Spedale Venti M, Palmisano B, Donsante S, Farinacci G, Adotti F, Coletta I, Serafini M, Corsi A and Riminucci M (2022) Morphological and Immunophenotypical Changes of Human Bone Marrow Adipocytes in Marrow Metastasis and Myelofibrosis. Front. Endocrinol. 13:882379. doi: 10.3389/fendo.2022.882379

The bone marrow adipose tissue constitutes more than two-thirds of the bone marrow volume in adult life and is known to have unique metabolic and functional properties. In neoplastic disorders, bone marrow adipocytes (BMAds) contribute to create a favorable microenvironment to survival and proliferation of cancer cells. Many studies explored the molecular crosstalk between BMAds and neoplastic cells, predominantly in *ex-vivo* experimental systems or in animal models. However, little is known on the features of BMAds in the human neoplastic marrow. The aim of our study was to analyze the *in situ* changes in morphology and immunophenotype of BMAds in two different types of neoplastic marrow conditions. We selected a series of archival iliac crest and vertebral bone biopsies from patients with bone marrow metastasis (MET), patients with myeloproliferative neoplasia with grade-3 myelofibrosis (MPN-MF) and age-matched controls (CTR). We observed a significant reduction in the number of BMAds in MET and MPN-MF compared to CTR. Accordingly, in the same groups, we also detected a significant reduction in the mean cell diameter and area. Immunolocalization of different adipocyte markers showed that, compared to CTR, in both MET and MPN-MF the percentages of adiponectin- and phosphorylated hormone sensitive lipase-positive BMAds were significantly reduced and increased respectively. No statistically significant difference was found between MET and MPN-MF. Interestingly, in one MET sample, "remodeled" BMAds containing a large lipid vacuole and multiple, smaller and polarized lipid droplets were identified. In conclusion, our data show that in different types of marrow cancers, BMAds undergo significant quantitative and qualitative changes, which need to be further investigated in future studies.

Keywords: bone marrow, marrow metastasis, myeloproliferative neoplasia, myelofibrosis, bone marrow adipose tissue, bone marrow adipocytes, histomorphometry, immunohistochemistry

INTRODUCTION

The bone marrow adipose tissue (BMAT) (1) constitutes more than two-thirds of the bone marrow (BM) volume in adult life (2, 3). It is comprised of cells, BM adipocytes (BMAds), that bear a single, large cytoplasmic lipid droplet and express adipose-lineage markers such as fatty acid binding proteins, leptin, adiponectin and others (4). BMAds appear at birth in the extravascular marrow space to contribute to the three-dimensional stromal cell network that holds hematopoietic cells, and progressively expand during skeletal growth in parallel with the centripetal retraction of the hematopoiesis (Neumann's law) (5). Based on this inverse relationship with the hematopoietic tissue, BMAds have long been thought as white fat cells with a simple supporting/filling function. However, it is now widely recognized that BMAds represent a distinct fat depot with metabolic and functional properties that are different from those of the other human fat tissues (6). In addition, it is now well known that BMAds participate in the regulation of skeletal homeostasis, in systemic metabolism and in the pathogenesis of different bone and BM diseases (4, 7).

Over the last years, the potential pathogenetic role of BMAds and its molecular bases have been intensively investigated in marrow neoplastic conditions such as hematological malignancies and cancer metastasis. Thus, it has been shown that BMAds are able to modulate the migration and aggressiveness of neoplastic cells (8), to sustain their growth (9) and, in some cases, to promote their survival during therapy (10, 11). These effects are achieved by multiple mechanisms such as the generation and transfer of fatty acids (9) and the secretion of different types of adipokines (4). On the other side, it has also been reported that tumor cells are able to harness the metabolic and biological functions of BMAds to generate a microenvironment that promotes their own growth. The tumor-dependent modifications of BMAds reported so far include the stimulation of a lipolytic state (9), the increased expression of lipid transporter genes (9) and the induction of a senescence-associated secretory phenotype (12). However, although these studies have significantly expanded the knowledge on the molecular crosstalk between BMAds and neoplastic cells, they have been performed predominantly in *ex-vivo* experimental systems or in animal models thus providing little, if any, information on the *in situ* features of BMAds in the human neoplastic BM.

In this study, we have analyzed the number, morphology and phenotype of BMAds in archival bone biopsies obtained from patients with marrow metastasis, either from epithelial and non-epithelial tumors, and myeloproliferative neoplasms featuring grade-3 myelofibrosis. We selected BM metastasis since *in situ* features of BMAds in this condition have never been investigated. The samples of chronic myeloproliferative neoplasms were chosen based on the absence of data on the *in situ* immunophenotype of BMAds in these haematological malignancies. In order to generate a homogenous experimental group, the latter samples were selected based on the presence of myelofibrosis, which is frequently found in patients with chronic myeloproliferative neoplasms. We report that BMAds in the neoplastic marrow samples were characterized by altered histomorphometric and immunophenotypic features that might reflect their tumor-promoting activity.

MATERIALS AND METHODS

Bone Biopsies

Human trephine BM biopsies with either BM metastasis (MET) or myeloproliferative neoplasms with grade-3 myelofibrosis (MPN-MF) performed between 2012 and 2020 were retrospectively identified in the archive of the Section of Pathology of the Policlinico Umberto I Hospital of Rome, Italy.

The MET group was composed of 8 patients (7 females and 1 male, median age 55 years, range 27-73 years), affected by breast carcinoma (four patients, two with infiltrating ductal carcinoma, one with infiltrating lobular carcinoma and one undefined), signet-ring cell carcinoma of the stomach (one patient), high-grade neuroendocrine carcinoma and undifferentiated carcinoma of unknown origin (one patient each) and malignant glioma (one patient). In the last patient the sample was obtained from vertebral BM. The quantitative data obtained from the analysis of this sample have been considered within the MET group as iliac crest and vertebrae are both axial hematopoietic (red) marrow sites (5). The MPN-MF group included 8 patients (6 females and 2 males, median age of 58.5 years, range 39-81 years). Iliac crest biopsies performed for lymphoproliferative disease staging in the same period of time in eight patients (6 females and 2 males, median age 52.5 years, range 41-68 years) with no evidence of BM involvement by either neoplasia or other pathologies were also selected in the same archive and used as control (CTR) group. The study was conducted according to the guidelines of the Declaration of Helsinki and approved by the Institutional Review Board (Department of Molecular Medicine, Sapienza University of Rome, Italy, 17/02/2022). Written informed consent was not deemed necessary owing to the retrospective nature of the study.

Histology and Immunohistochemistry

Biopsies were fixed in 4% phosphate-buffered formaldehyde and routinely processed for paraffin embedding after decalcification with ethylenediaminetetraacetic acid in disodium salt acid buffer (Osteodec, Bio-Optica, Milan, Italy). For diagnostic purpose, the slides were examined by two of the authors. For this study, 4μm thick tissue sections were re-cut from each paraffin block and used for haematoxylin-eosin (HE) stain and for immunohistochemistry. Immunohistochemical analysis was performed in a blinded fashion as described previously (13, 14). The following primary antibodies diluted in phosphate buffer were used: polyclonal anti-human perilipin-1 (PLIN1) (Abcam, Cambridge, UK, ab3526, 1:500); polyclonal anti-human fatty acid binding protein 4 (FABP4) (Abcam, ab13979, 1:200); monoclonal anti-human adiponectin (ADIPOQ) (InVitrogen, Carlsbad, CA, USA, MA1-054, 1:50); polyclonal anti-human phosphorylated-hormone sensitive lipase antibody (p-HSL)

(InVitrogen, PA5-38087, 1:100). Primary antibodies were omitted in negative technical controls. The color reaction was developed using 3,3'-diaminobenzidine tetrahydrochloride (DAB, Sigma, St- Louis, MO) as substrate.

Histomorphometry

Histomorphometric analysis was performed in a blinded fashion and according to the guidelines of the Bone Marrow Adiposity Society (1, 15). HE-stained and immunostained sections were scanned *via* Aperio Scan Scope CS (Leica Biosystem Imaging, Nußloch, Baden-Wurttemberg, Germany) and analyzed using ImageJ (16). For each scanned section, 10 snapshots were taken at 20x magnification from the central portion of the trephine biopsies. The region of interest (ROI) ranged from 1.35 mm^2 to 1.93 mm^2. Bone trabeculae, areas of hemorrhages, harvesting or processing tissue damage artifacts were excluded. Marrow area (Ma.Ar), number of BMAds per marrow area (N.Ad/Ma.Ar), maximum diameter (Ad.Dm) and area (Ad.Ar) of individual BMAds were measured on HE-stained sections. Immunostained pictures were used to calculate the fraction of immunoreactive BMAds on the total number of adipocytes by ImageJ plugin Cell Counter.

Statistical Analysis

Ordinary one-way ANOVA test with Tukey's multiple comparison test was performed by GraphPad Prism 8.0.2 software. A *p*-value less than 0.05 was considered statistically significant.

RESULTS

BMAd Number and Size Reduction in Marrow Metastasis and Myeloproliferative Neoplasia

The microscopic review of all bone biopsies confirmed the presence of normal haematopoiesis in the CTR group (**Figure 1A**); non-hematological neoplastic cells were observed in the MET group (**Figure 1B**), while atypical hematopoietic cells separated by fibrous bundles were present in the MPN-MF biopsies (**Figure 1C**).

The comparative analysis of the adipocyte number in the different groups revealed a significant reduction in the two neoplastic conditions compared to the control biopsies (CTR vs MET $p = 0.0004$; CTR vs MPN-MF $p = 0.001$) (**Figure 1D**). Moreover, histomorphometric analysis demonstrated a statistically significant reduction in the adipocyte diameter (CTR vs MET $p = 0.017$ and CTR vs MPN-MF $p = 0.013$) and area (CTR vs MET $p = 0.0003$, CTR vs MPN-MF $p = 0.0104$) in the neoplastic samples compared to the controls (**Figures 1E, F**). In contrast, no difference between the two neoplastic conditions was observed for adipocyte number, diameter and area (**Figures 1D–G**), although the frequency distribution of adipocyte area revealed a higher frequency of smaller adipocytes in the MET group (**Figures 1B, H**). These data indicate that marrow metastasis, from epithelial and non-epithelial tumors, and myeloproliferative neoplasms featuring

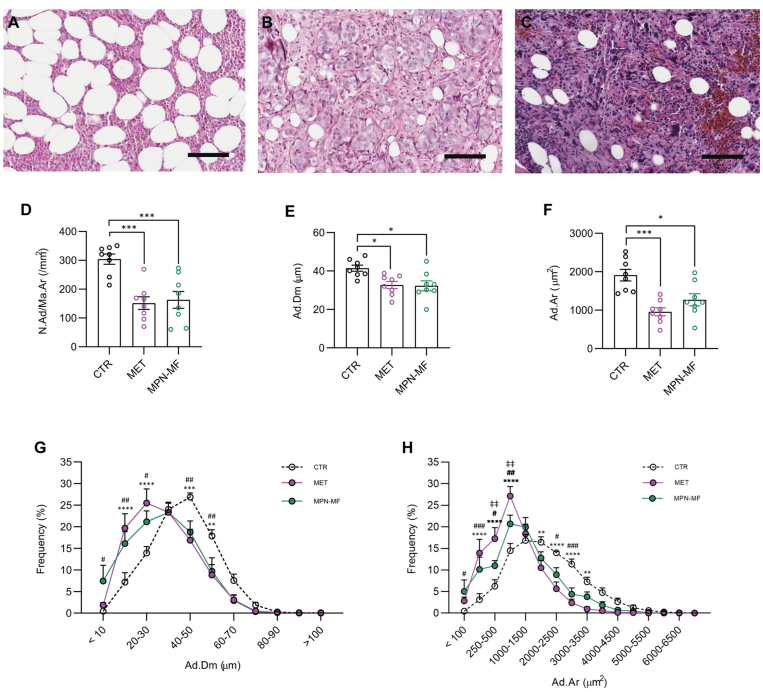

FIGURE 1 | Representative histologic images of CTR **(A)**, MET **(B)** and MPN-MF **(C)** bone biopsies. Histomorphometric analysis of BMAds number (**D**, N.Ad/Ma.Ar), diameter (**E**, Ad.Dm) and area (**F,** Ad.Ar). Frequency distribution curves of BMAds diameter and area are illustrated in **(G**, **H)**, respectively. Scale bar: 100 µm. In **(D–F)**: $^{*}p < 0.05$, $^{***}p < 0.001$; In **(G**, **H)**: CTR *vs* MET: $^{**}p < 0.01$, $^{***}p < 0.001$, $^{****}p < 0.0001$; CTR *vs* MPN-MF: $^{\#}p < 0.05$ and $^{\#\#}p < 0.01$, $^{\#\#\#}p < 0.001$; MET *vs* MPN-MF: $^{\ddagger\ddagger}p < 0.01$.

grade-3 myelofibrosis, are associated with a significant reduction in the number of adipocytes and with an increase in small adipocytes.

BMAd Immunophenotypic Changes in Marrow Metastasis and Myeloproliferative Neoplasia

We performed immunohistochemistry to compare the fractions of BMAds marked by the presence of PLIN1, FABP4, ADIPOQ and p-HSL in the different experimental groups.

The percentage of PLIN1-positive BMAds was not significantly different among the three groups (**Figures 2A–D, Q**). Similarly, the percentage of FABP4-positive BMAds was not significantly different among the three groups even though a trend towards reduction was observed in the neoplastic samples (CTR vs MET $p = 0.0903$; CTR vs MPN-MF $p = 0.0638$) (**Figures 2E–H, R**).

Interestingly, the number of BMAds expressing ADIPOQ was significantly reduced both in MET ($p = 0.0032$) and MPN-MF ($p = 0.0136$) compared to CTR (**Figures 2I–L, S**). Since AdipoQ has been reported to enhance adipocyte lipid storage (17, 18), this result may suggest a reduction of this process in BM involved by neoplasia. pHSL immunostaining revealed a higher number of positive adipocytes in neoplastic biopsies (**Figures 2M–P, T**), in which their number was higher by almost 50% compared to CTR (**Figure 2P**, CTR vs MET $p = 0.0006$; CTR vs MPN-MF $p = 0.0014$). No significant difference in the percentage of positive BMAds was detected between the two types of tumors (ADIPOQ: MET vs MPN-MF $p = 0.8087$; pHSL: MET vs MPN-MF $p = 0.9373$) (**Figures 2L, P**).

Interestingly, in the bone biopsy from the patient with metastasis of malignant glioma (**Figure 3A**), we observed an unusual morphology of BMAds characterized by the presence of a large vacuole associated with small lipid droplets that were clustered together beneath the plasma membrane, as better shown by ADIPOQ **Figure 3B**) and PLIN1 (**Figure 3C**) immunostaining.

DISCUSSION

The human BM is the site of origin of most haematological malignancies and a frequent site of metastasis of non-haematological tumors. In marrow neoplasia, the BMAT undergoes metabolic and molecular changes that help cancer cells to thrive at the expense of the other BM cell types. BMAds are known to secrete adipokines (e.g., adiponectin and leptin) and inflammatory factors (e.g., interleukin-6 and tumor necrosis factor-α) and are thought to be the energy source of tumor cells (e.g., through the release of free fatty acids), which, in turn, modulate their activities by releasing different types of molecules (e.g., cytokines and chemokines) (4, 8, 11, 19).

Previous work showed that in peripheral white adipose tissue (WAT), adipocytes located in close proximity of invasive cancer cells undergo morphological changes [i.e., loss of lipid content (delipidation) and acquisition of a fibroblast-like/pre-adipocyte phenotype (dedifferentiation)] and functional modifications (e.g., decreased expression of adipocyte-related genes and increased production of pro-inflammatory cytokines) (20). However, only a few studies investigated the *in situ*

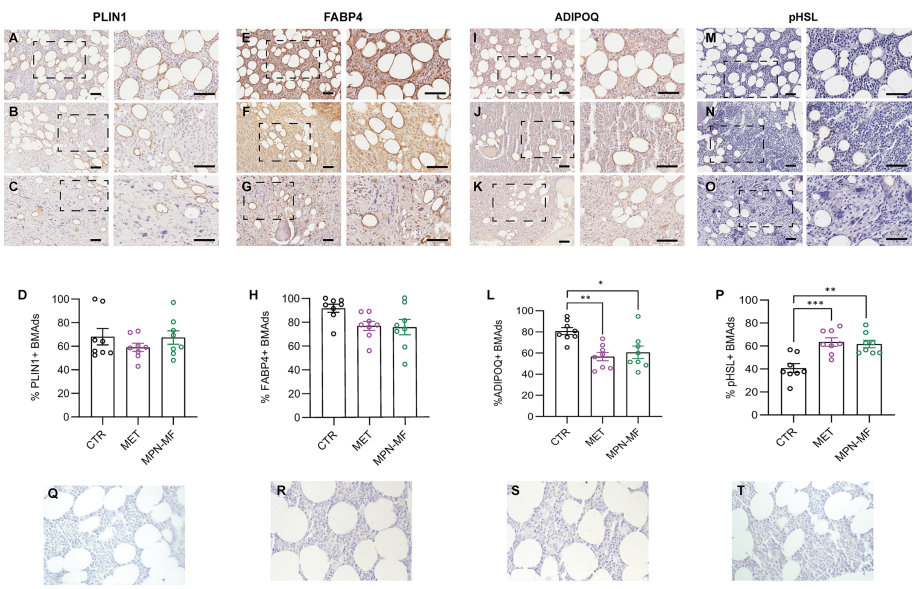

FIGURE 2 | Representative images of PLIN1-, FABP4-, ADIPOQ- and p-HSL-immunostained sections from CTR **(A, E, I, M)**, MET **(B, F, J, N)** and MPN-MF **(C, G, K, O)** bone biopsies. The right panels of each image illustrate the zoomed boxed area. Scale bars: 50 μm. Graphs in **(D, H, L, P)** represent the quantitative analysis of each immunostaining. Negative technical controls in which primary antibodies were omitted are shown in panels **(Q–T)**. $^{*}p < 0.05$, $^{**}p < 0.01$; $^{***}p < 0.001$.

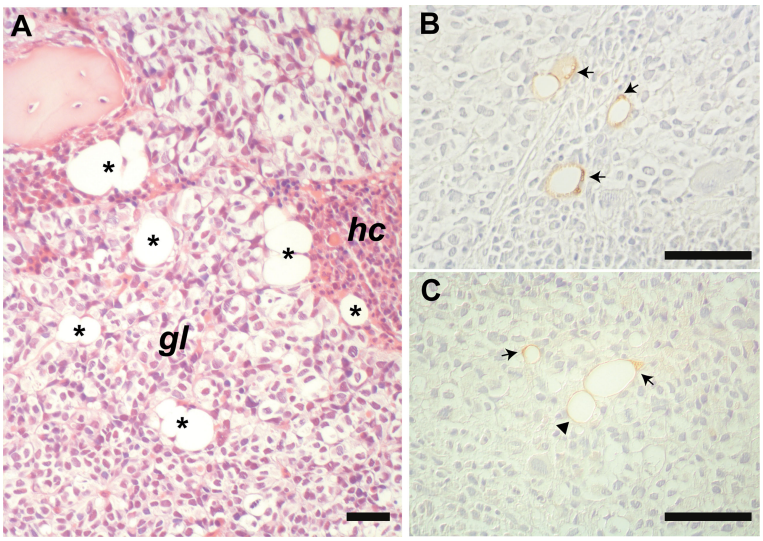

FIGURE 3 | Representative histological image of the marrow metastasis of glioma **(A)**. BMAds (asterisks) are intercalated among the neoplastic cells (*gl*) and the haematopoietic cells (*hc*). Immunostaining for PLIN1 **(B)** and ADIPOQ **(C)** highlights intra-tumoral "remodeled" BMAds containing very small intracytoplasmic lipid droplets clustered together and polarized beneath the plasma membrane (arrows), which are not observed in morphologically typical unilocular adipocyte (arrowhead). Panel **(A)**: HE stain. Scale bars: 50 μm.

morphology and phenotype of BMAT in the human neoplastic BM.

The analysis of BMAds neighboring marrow tumors may provide information of relevance for the pathogenesis and possibly for the diagnosis of marrow neoplastic diseases. For example, it may reveal changes of BMAds that occur at a specific time (e.g., early *vs* late stage of marrow cancer infiltration) and/or anatomical space (e.g., in subcortical *vs* perisinusoidal BMAT) during the progression of the disease. On the other side, it may assist in the diagnostic identification of neoplastic BM samples when cancer cells are very few and barely detectable. Currently available work on the *in situ* features of BMAds in the neoplastic BM consists essentially in a few histomorphometry studies performed exclusively on hematological tumors (21).

Here, we report the results of the quantitative and qualitative analyses of BMAds in bone biopsies from patients with different types of marrow cancer metastasis and with myeloproliferative neoplasia with grade-3 myelofibrosis. We provide the first data on the *in situ* immunophenotype of BMAds in haematological malignancies and the first analysis ever of their *in situ* quantitative and immunophenotypic features in BM cancer metastasis.

Our study revealed a significant decrease in the number of BMAds in affected bone biopsies, regardless of the type of neoplasia. The quantitative reduction of BMAds in the presence of tumors seems to be a recurrent finding and was previously observed in Multiple Myeloma (MM) (12), Acute Lymphoblastic Leukaemia (ALL) (22), Myelodysplasia (21, 23), Acute Myeloid Leukaemia (AML) (24) and MPN (21). The reason for the lowering of BMAds in marrow neoplastic conditions is currently under investigation. Some studies showed that it is unrelated to the amount of marrow cellularity and may not be explained solely by the physical pressure caused by tumor infiltration (12, 22). Other studies reported a compromised growth and differentiation of BMAd progenitor cells (22, 24, 25). BMAds derive from skeletal stem/progenitor cells that appear after birth in the marrow cavity (26) and are included within the fibroblast-like cell subset of the BM stroma (Bone marrow stromal cells, BMSCs) (27). Reduced adipogenic differentiation was shown in BMSCs isolated from AML patients, in which the defective generation of mature adipocytes was not reproduced in the extra-skeletal WAT depots (24), and from patients with MM (25). In addition, in ALL patients, Heydt et al. observed an altered growth of BMSCs with accumulation of adipocyte-primed cells and suggested that the differentiation of adipocyte progenitors was stalled by blast-dependent mechanisms (22). Interestingly, we previously observed that BM stromal progenitor cells isolated from patients with AML were characterized by an enhanced terminal adipogenic differentiation compared to controls when transplanted *in vivo* in the absence of leukemic blasts (28). The negative modulation of BM adipogenesis seems to be in contrast with the positive effect of BMAds on cancer growth. A plausible explanation for our results is that this positive effect is an early event no longer required in the established disease. However, it must be reminded that BMAds also support the maturation of the normal myeloid-erythroid lineages (24), which compete with the neoplastic cells for the same microenvironment. Thus, it is possible that the modulation of BMAd number in the neoplastic marrow reflects, at least in part, the need for the tumor to generate a supporting microenvironment while suppressing the normal haematopoiesis.

We also observed a reduced size of BMAds in all our samples, consistent with previous report on MM (29) and other lympho- and myelo-proliferative conditions (21). The change in the dimension of individual BMAds was previously related to the enhanced lipolysis induced by neoplastic cells (9, 30), although subsequent studies did not detect a lipolytic activity in BMAds (6). Regardless of the mechanism(s), the shrinking of BMAds may have multiple potential consequences on the neoplastic microenvironment that should not be overlooked. For example, since BMAds are in close contact with the marrow sinusoidal network (31), a pronounced modification of their dimension may affect the blood flow and, as a consequence, the amount of oxygen and nutrients for neoplastic cells. In addition, as previously reported in WAT, variations in the cell size within BMAT could be correlated with different chemokine and lipid secretory profiles and therefore with different modulatory effects on the tumor growth (32).

As major changes in the overall phenotype of BMAT, we detected a reduced number of ADIPOQ positive and an increased number of p-HSL positive BMAds in the neoplastic marrow compared to control biopsies. ADIPOQ is the most abundant molecule produced by the adipose tissue and in humans it is highly expressed in BMAT compared to WAT (33). Reduced levels of ADIPOQ, in parallel with an increase in the level of leptin, are associated with an enhanced risk of development of different tumors, including hematological neoplasia (34, 35). Indeed, ADIPOQ inhibits proliferation and promotes apoptosis in different types of cancer cells (36). Recently, it has been reported that the content of this adipokine in the marrow plasma is lower in patients with ALL compared to healthy subjects (22). In agreement with these data, we demonstrate here for the first time a reduction in the number of ADIPOQ positive BMAds in the presence of cancer metastasis and myeloproliferative neoplasia with grade-3 myelofibrosis, thus confirming that the modulation of the secretory activity of BMAT contributes to the changes in the marrow/serum levels of this adipokine in neoplastic conditions.

HSL is a lipase that is activated upon phosphorylation and is involved in the breakdown of triglycerides (37). Cancer cells may upregulate its expression and phosphorylation in WAT (38, 39). Although BMAds seem to have a specific lipid metabolism compared to WAT (6), HSL phosphorylation was reported to be induced in BMAds co-cultured with ALL blasts (9). In this study we have confirmed this effect *in situ* showing that, in the presence of neoplastic cells, the fraction of p-HSL positive BMAds was expanded. The metabolic implication of the increase of p-HSL and its significance in the context of BM cancer involvement remains to be clarified. However, it is interesting to note that in the marrow metastasis of glioma, we observed BMAds bearing a large lipid vacuole and a polarized cluster of small droplets beneath the plasma membrane. This finding is reminiscent of the remodeled BMAds previously detected in the mouse femur upon stimulation with a β3 adrenergic receptor agonist (40). Thus, it is possible that a remodeling phenomenon occurs in human BMAds too, at least in some specific rare conditions as the exposure to glioma cells. Of note, it is known in the literature that astrocytomas may cause lipodystrophy (41) and that lipolysis is increased in the glioma microenvironment (42).

In conclusion, although this study has important limitations (such as the reduced number of bone biopsies, the absence of correlation with patients' clinic and anthropometric data), it demonstrates for the first time that, in different types of marrow cancers, BMAds undergo significant quantitative and morpho-phenotypical changes, which need to be further investigated in future studies.

DATA AVAILABILITY STATEMENT

The raw data supporting the conclusions of this article will be made available by the authors, without undue reservation.

ETHICS STATEMENT

The studies involving human participants were reviewed and approved by Institutional Review Board, Department of Molecular Medicine, Sapienza University of Rome, Italy, 17/02/2022. Written informed consent was not deemed necessary owing to the retrospective nature of the study.

AUTHOR CONTRIBUTIONS

MDSV, BP, SD, GF, FA and IC performed morphometric analysis and immunohistochemical stains. MDSV, BP, MS, AC and MR analyzed the data. MDSV and BP performed statistical analysis and wrote the draft of the manuscript. MDSV, BP, MS, AC and MR edited the manuscript. All authors approved the final version of the manuscript.

FUNDING

Sapienza University to AC (RM118164289636F0) and MR (RM11916B839074A8 and RM120172B8BF5C15).

REFERENCES

1. Bravenboer N, Bredella MA, Chauveau C, Corsi A, Douni E, Ferris WF, et al. Standardised Nomenclature, Abbreviations, and Units for the Study of Bone Marrow Adiposity: Report of the Nomenclature Working Group of the International Bone Marrow Adiposity Society. *Front Endocrinol (Lausanne)* (2020) 10:923. doi: 10.3389/FENDO.2019.00923
2. Steiner RM, Mitchell DG, Rao VM, Murphy S, Rofkin M, Burk D, et al. Magnetic Resonance Imaging of Bone Marrow: Diagnostic Value in Diffuse Hematologic Disorders. *Magn Reson Q* (1990) 6(1):17–34.

3. Fazeli PK, Horowitz MC, MacDougald OA, Scheller EL, Rodeheffer M, Rosen C, et al. Marrow Fat and Bone-New Perspectives. *J Clin Endocrinol Metab* (2013) 98(3):935–45. doi: 10.1210/jc.2012-3634
4. Luo G, He Y, Yu X. Bone Marrow Adipocyte: An Intimate Partner With Tumor Cells in Bone Metastasis. *Front Endocrinol (Lausanne)* (2018) 9:339. doi: 10.3389/fendo.2018.00339
5. Neumann E. The Law of Distribution of Yellow and Red Marrow in the Bones of the Extremities. *Cent J Med Sci* (1882) 321:323. E N.
6. Attané C, Estève D, Chaoui K, Iacovoni JS, Corre J, Moutahir M, et al. Human Bone Marrow Is Comprised of Adipocytes With Specific Lipid Metabolism. *Cell Rep* (2020) 30(4):949–958.e6. doi: 10.1016/j.celrep.2019.12.089
7. Reagan MR, Fairfield H, Rosen CJ. Bone Marrow Adipocytes: A Link Between Obesity and Bone Cancer. *Cancers (Basel)* (2021) 13(3):1–14. doi: 10.3390/cancers13030364
8. Trotter TN, Gibson JT, Sherpa TL, Gowda PS, Peker D, Yang Y. Adipocyte-Lineage Cells Support Growth and Dissemination of Multiple Myeloma in Bone. *Am J Pathol* (2016) 186(11):3054–63. doi: 10.1016/j.ajpath.2016.07.012
9. Shafat MS, Oellerich T, Mohr S, Robinson S, Edwards D, Marlein C, et al. Leukemic Blasts Program Bone Marrow Adipocytes to Generate a Protumoral Microenvironment. *Blood* (2017) 129(10):1320–32. doi: 10.1182/blood-2016-08-734798
10. Jafari A, Fairfield H, Andersen TL, Reagan MR. Myeloma-Bone Marrow Adipocyte Axis in Tumour Survival and Treatment Response. *Br J Cancer* (2021) 125(6): 775–777. doi: 10.1038/s41416-021-01371-4
11. Tabe Y, Konopleva M. Leukemia Stem Cells Microenvironment. *Adv Exp Med Biol* (2017) 1041:19–32. doi: 10.1007/978-3-319-69194-7_3
12. Fairfield H, Dudakovic A, Khatib CM, Costa S, Falank C, Hinge M, et al. Myeloma-Modified Adipocytes Exhibit Metabolic Dysfunction and a Senescence-Associated Secretory Phenotype. *Cancer Res* (2021) 81(3):634–47. doi: 10.1158/0008-5472.CAN-20-1088
13. Palmisano B, Spica E, Remoli C, Labella R, di Filippo A, Donsante S, et al. RANKL Inhibition in Fibrous Dysplasia of Bone: A Preclinical Study in a Mouse Model of the Human Disease. *J Bone Miner Res* (2019) 34(12):2171–82. doi: 10.1002/JBMR.3828
14. Corsi A, Cherman N, Donaldson DL, Robey PG, Collins MT, Riminucci M. Neonatal McCune-Albright Syndrome: A Unique Syndromic Profile With an Unfavorable Outcome. *JBMR plus* (2019) 3(8). doi: 10.1002/JBM4.10134
15. Tratwal J, Labella R, Bravenboer N, Kerckhofs G, Douni E, Scheller EL, et al. Reporting Guidelines, Review of Methodological Standards, and Challenges Toward Harmonization in Bone Marrow Adiposity Research. Report of the Methodologies Working Group of the International Bone Marrow Adiposity Society. *Front Endocrinol (Lausanne)* (2020) 11:65. doi: 10.3389/FENDO.2020.00065
16. Schindelin J, Arganda-Carreras I, Frise E, Kaynig V, Longair M, Pietzsch T, et al. Fiji: An Open-Source Platform for Biological-Image Analysis. *Nat Methods* (2012) 9(7):676–82. doi: 10.1038/NMETH.2019
17. Fu Y, Luo N, Klein RL, Timothy Garvey W. Adiponectin Promotes Adipocyte Differentiation, Insulin Sensitivity, and Lipid Accumulation. *J Lipid Res* (2005) 46(7):1369–79. doi: 10.1194/jlr.M400373-JLR200
18. Stern JH, Rutkowski JM, Scherer PE. Adiponectin, Leptin, and Fatty Acids in the Maintenance of Metabolic Homeostasis Through Adipose Tissue Crosstalk. *Cell Metab* (2016) 23(5):770–84. doi: 10.1016/j.cmet.2016.04.011
19. Falank C, Fairfield H, Reagan MR. Reflections on Cancer in the Bone Marrow: Adverse Roles of Adipocytes. *Curr Mol Biol Rep* (2017) 3(4):254–62. doi: 10.1007/s40610-017-0074-6
20. Morris EV, Edwards CM. Bone Marrow Adipose Tissue: A New Player in Cancer Metastasis to Bone. *Front Endocrinol (Lausanne)* (2016) 7:90. doi: 10.3389/fendo.2016.00090
21. Frączak E, Olbromski M, Piotrowska A, Glatzel-Plucińska E, Dzięgiel P, Dybko J, et al. Bone Marrow Adipocytes in Haematological Malignancies. *Acta Histochem* (2018) 120(1):22–7. doi: 10.1016/J.ACTHIS.2017.10.010
22. Heydt Q, Xintaropoulou C, Clear A, Austin M, Pislariu I, Miraki-Moud F, et al. Adipocytes Disrupt the Translational Programme of Acute Lymphoblastic Leukaemia to Favour Tumour Survival and Persistence. *Nat Commun* (2021) 12(1):5507. doi: 10.1038/S41467-021-25540-4
23. Rozman C, Reverter JC, Feliu E, Berga L, Rozman M, Climent C. Variations of Fat Tissue Fraction in Abnormal Human Bone Marrow Depend Both on Size and Number of Adipocytes: A Stereologic Study. *Blood* (1990) 76(5):892–5. doi: 10.1182/blood.v76.5.892.bloodjournal765892
24. Boyd AL, Reid JC, Salci KR, Aslostovar L, Benoit YD, Shapovalova Z, et al. Acute Myeloid Leukaemia Disrupts Endogenous Myelo-Erythropoiesis by Compromising the Adipocyte Bone Marrow Niche. *Nat Cell Biol* (2017) 19(11):1336–47. doi: 10.1038/ncb3625
25. Mehdi SJ, Johnson SK, Epstein J, Zangari M, Qu P, Hoering A, et al. Mesenchymal Stem Cells Gene Signature in High-Risk Myeloma Bone Marrow Linked to Suppression of Distinct IGFBP2-Expressing Small Adipocytes. *Br J Haematol* (2019) 184(4):578–93. doi: 10.1111/BJH.15669
26. Donsante S, Palmisano B, Serafini M, Robey PG, Corsi A, Riminucci M. From Stem Cells to Bone-Forming Cells. *Int J Mol Sci* (2021) 22(8):3989. doi: 10.3390/IJMS22083989
27. Robey PG, Kuznetsov SA, Bianco P, Riminucci M. Bone Marrow Stromal Cell Assays: *In Vitro* and *In Vivo*. *Methods Mol Biol* (2021) 2230:379–96. doi: 10.1007/978-1-0716-1028-2_23
28. Pievani A, Donsante S, Tomasoni C, Corsi A, Dazzi F, Biondi A, et al. Acute Myeloid Leukemia Shapes the Bone Marrow Stromal Niche *In Vivo*. *Haematologica* (2021) 106(3):865–70. doi: 10.3324/HAEMATOL.2020.247205
29. Lu W, Wan Y, Li Z, Zhu B, Yin C, Liu H, et al. Growth Differentiation Factor 15 Contributes to Marrow Adipocyte Remodeling in Response to the Growth of Leukemic Cells. *J Exp Clin Cancer Res* (2018) 37(1):1–10. doi: 10.1186/s13046-018-0738-y
30. Lu W, Weng W, Zhu Q, Zhai Y, Wan Y, Liu H, et al. Small Bone Marrow Adipocytes Predict Poor Prognosis in Acute Myeloid Leukemia. *Hematologica* (2018) 103(1):e21–e24. doi: 10.3324/haematol.2017.173492
31. Bianco P. Bone and the Hematopoietic Niche: A Tale of Two Stem Cells. *Blood* (2011) 117(20):5281–9. doi: 10.1182/blood-2011-01-315069
32. Skurk T, Alberti-Huber C, Herder C, Hauner H. Relationship Between Adipocyte Size and Adipokine Expression and Secretion. *J Clin Endocrinol Metab* (2007) 92(3):1023–33. doi: 10.1210/JC.2006-1055
33. Cawthorn WP, Scheller EL, Learman BS, Parlee SD, Simon BR, Mori H, et al. Bone Marrow Adipose Tissue Is an Endocrine Organ That Contributes to Increased Circulating Adiponectin During Caloric Restriction. *Cell Metab* (2014) 20(2):368–75. doi: 10.1016/j.cmet.2014.06.003
34. Kelesidis I, Kelesidis T, Mantzoros CS. Adiponectin and Cancer: A Systematic Review. *Br J Cancer* (2006) 94(9):1221–5. doi: 10.1038/SJ.BJC.6603051
35. Dalamaga M, Karmaniolas K, Panagiotou A, Hsi A, Chamberland J, Dimas C, et al. Low Circulating Adiponectin and Resistin, But Not Leptin, Levels Are Associated With Multiple Myeloma Risk: A Case-Control Study. *Cancer Causes Control* (2009) 20(2):193–9. doi: 10.1007/S10552-008-9233-7
36. Dalamaga M, Diakopoulos KN, Mantzoros CS. The Role of Adiponectin in Cancer: A Review of Current Evidence. *Endocr Rev* (2012) 33(4):547–94. doi: 10.1210/er.2011-1015
37. Kraemer FB, Shen WJ. Hormone-Sensitive Lipase: Control of Intracellular Tri-(Di-)Acylglycerol and Cholesteryl Ester Hydrolysis. *J Lipid Res* (2002) 43(10):1585–94. doi: 10.1194/JLR.R200009-JLR200
38. Lengyel E, Makowski L, DiGiovanni J, Kolonin MG. Cancer as a Matter of Fat: The Crosstalk Between Adipose Tissue and Tumors. *Trends Cancer* (2018) 4(5):374–84. doi: 10.1016/J.TRECAN.2018.03.004
39. Sagar G, Sah RP, Javeed N, Dutta SK, Smyrk TC, Lau JS, et al. Pathogenesis of Pancreatic Cancer Exosome-Induced Lipolysis in Adipose Tissue. *Gut* (2016) 65(7):1165–74. doi: 10.1136/GUTJNL-2014-308350
40. Scheller EL, Khandaker S, Learman BS, Cawthorn WP, Anderson LM, An Pham H, et al. Bone Marrow Adipocytes Resist Lipolysis and Remodeling in Response to β-Adrenergic Stimulation. *Bone* (2019) 118:32–41. doi: 10.1016/J.BONE.2018.01.016
41. Patni N, Alves C, Von Schnurbein J, Wabitsch M, Tannin MG, Rakheja D, et al. A Novel Syndrome of Generalized Lipodystrophy Associated With Pilocytic Astrocytoma. *J Clin Endocrinol Metab* (2015) 100(10):3603–6. doi: 10.1210/JC.2015-2476

42. Hu X, Matsumoto K, Jung RS, Weston TA, Heizer PJ, He C, et al. GPIHBP1 Expression in Gliomas Promotes Utilization of Lipoprotein-Derived Nutrients. *Elife* (2019) 8:e47178. doi: 10.7554/ELIFE.47178

Conflict of Interest: The authors declare that the research was conducted in the absence of any commercial or financial relationships that could be construed as a potential conflict of interest.

Publisher's Note: All claims expressed in this article are solely those of the authors and do not necessarily represent those of their affiliated organizations, or those of the publisher, the editors and the reviewers. Any product that may be evaluated in this article, or claim that may be made by its manufacturer, is not guaranteed or endorsed by the publisher.

frontiers | Frontiers in Endocrinology

ORIGINAL RESEARCH
published: 06 July 2022
doi: 10.3389/fendo.2022.881699

Stimulatory Effect of Tofacitinib on Bone Marrow Adipocytes Differentiation

*Jean-Guillaume Letarouilly[1], Julien Paccou[1], Sammy Badr[2], Christophe Chauveau[3], Odile Broux[3] and Aline Clabaut[3]**

[1] Université de Lille, Centre Hospitalier Universitaire CHU CENTRE HOSPITALIER UNIVERSITAIRE (CHU) Lille, MABLab ULR 4490, Service de Rhumatologie, Lille, France, [2] Université de Lille, Centre Hospitalier Universitaire (CHU) Lille, MABLab ULR 4490, Service de Radiologie et Imagerie Musculosquelettique, Lille, France, [3] Université Littoral Côte d'Opale, MABLab ULR 4490, Boulogne-sur-Mer, France

Background: Systemic inflammation is the main factor underlying secondary osteoporosis in patients with rheumatoid arthritis (RA). Janus kinase inhibitors (JAKi), such as tofacitinib (Tofa), can control systemic inflammation and may have beneficial effects on bone in various models. This might be due to direct effects on the bone microenvironment and not exclusively based on their anti-inflammatory function. Bone marrow adipocytes (BMAds) are abundant in the bone microenvironment. The effect of JAKi on BMAds is unknown, but evidence suggests that there is competition between human bone marrow-derived stromal cell (hBMSC) differentiation routes towards BMAds and osteoblasts (Ob) in osteoporosis.

Objectives: The aims of the study are to determine whether Tofa influences BMAds and Ob derived from hBMSCs and to investigate the potential effects of Tofa on bone marrow adiposity in RA patients.

Methods: To determine the effect of Tofa on cellular commitment, hBMSCs were differentiated to BMAds or OBs for 3 days together with Tofa at 200, 400, or 800 nM and TNFα. This study was also conducted using differentiated BMAds. The impact of Tofa was determined by gene and protein expression analysis and cell density monitoring. In parallel, in a pilot study of 9 RA patients treated with Tofa 5 mg twice a day (NCT04175886), the proton density fat fraction (PDFF) was measured using MRI at the lumbar spine at baseline and at 6 months.

Results: In non-inflammatory conditions, the gene expression of Runx2 and Dlx5 decreased in Ob treated with Tofa ($p < 0.05$). The gene expression of PPARγ2, C/EBPα, and Perilipin 1 were increased compared to controls ($p < 0.05$) in BMAds treated with Tofa. Under inflammatory conditions, Tofa did not change the expression profiles of Ob compared to TNFα controls. In contrast, Tofa limited the negative effect of TNFα on BMAd differentiation ($p < 0.05$). An increase in the density of differentiated BMAds treated

OPEN ACCESS

Edited by:
Jason Horton,
Upstate Medical University,
United States

Reviewed by:
Silke Frey,
University Hospital Erlangen, Germany
Kaisa K. Ivaska,
University of Turku, Finland

***Correspondence:**
Aline Clabaut
aline.clabaut@univ-littoral.fr

Specialty section:
This article was submitted to Bone Research, a section of the journal Frontiers in Endocrinology

Received: *22 February 2022*
Accepted: *12 May 2022*
Published: *06 July 2022*

Citation:
Letarouilly J-G, Paccou J, Badr S, Chauveau C, Broux O and Clabaut A (2022) Stimulatory Effect of Tofacitinib on Bone Marrow Adipocytes Differentiation. Front. Endocrinol. 13:881699. doi: 10.3389/fendo.2022.881699

with Tofa under TNFα was noted (p <0.001). These findings were consolidated by an increase in PDFF at 6 months of treatment with Tofa in RA patients (46.3 ± 7.0% versus 53.2 ± 9.2% p <0.01).

Conclusion: Together, these results suggest a stimulatory effect of Tofa on BMAd commitment and differentiation, which does not support a positive effect of Tofa on bone.

Keywords: tofacitinib, rheumatoid arthritis, human bone marrow-derived stromal cells, bone marrow adipocytes, osteoblasts, differentiation

1 INTRODUCTION

Rheumatoid arthritis (RA) is a systemic, immune-mediated disease characterized by synovitis and/or inflammation of periarticular structures and systemic inflammation with a prevalence in the range of 0.5–1.0% in Western countries (1, 2). Osteoporosis is a common feature in patients with RA and leads to an increased risk of fractures (3). In a meta-analysis, patients with RA had a significantly higher risk of fractures than patients without RA (relative risk = 2.25, 95% CI [1.76–2.87]) (4).

Systemic inflammation is the main factor underlying this secondary osteoporosis in RA patients. Cytokines such as tumor necrosis factor alpha (TNFα) and interleukin 6 (IL-6) directly stimulate the maturation of osteoclasts and inhibit the differentiation of osteoblasts (Ob), leading to an imbalance in bone resorption and bone formation (5).

Twenty years ago, RA often led to joint destruction and considerable disability. Since then, scientific progress has prompted major advances in the treatment of the disease (2). Janus Kinase inhibitors (JAKi), which inhibit the JAK/STAT (signal transducer and activator of transcription) pathway can control the disease activity and thus prevent joint destruction (6–8). Moreover, JAKi, such as tofacitinib (Tofa), can control systemic inflammation and may have beneficial effects on bone. Tofa inhibits several STATs such as STAT1, STAT3, and STAT5 (9, 10). Two *in vitro* studies showed that Tofa may enhance osteogenic differentiation (11, 12). One study showed an increase in osteocalcin (OC) expression in murine bone marrow-derived stromal cells treated with Tofa 1 day after osteogenic induction. In contrast, the expression of runt-related transcription factor 2 (Runx2), the key transcription factor in osteogenesis, was not affected by Tofa (11). In the other study, Runx2 expression only increased under hypoxic conditions in human bone marrow-derived stromal cells (hBMSCs) treated with Tofa 7 days after osteogenic induction (12).

In a one-year pilot study, no changes in bone mineral density (BMD) by dual-energy X-ray absorptiometry (DXA) were observed in RA patients under Tofa (n = 26) whereas C-terminal collagen crosslinks (CTX) significantly decreased (13). Furthermore, Vidal et al. analyzed how treatment intervention with Tofa prevents the early disturbances of bone structure and mechanics in a rat model of adjuvant-induced arthritis (14). Tofa could control the inflammatory activity and, to increase cortical bone and trabecular hardness measured by nanoindentation, but did not reverse the effects of arthritis on the cortical and trabecular bone structure and on mechanical properties (14).

More studies are needed to understand the impact of Tofa on bone, as previous studies used different models and conditions.

This impact might be due to direct effects on the bone microenvironment and not exclusively based on its anti-inflammatory function. Bone marrow adipocytes (BMAds) are abundant in the bone microenvironment (15) and have been historically viewed as passive 'fillers' of bone marrow space that are metabolically inert (16). An increasing number of studies have shown that there is an association between decreased bone mass and the accumulation of bone marrow adipose tissue, suggesting a competition between hBMSCs differentiation routes toward BMAds and Ob in osteoporosis (15)

The study aimed to determine whether Tofa influences the cells of the bone microenvironment, such as BMAds and Ob derived from hBMSCs, under inflammatory and noninflammatory conditions. Then, in a prospective pilot study, we investigated the potential effects of Tofa on bone marrow adiposity and bone parameters in patients with RA.

Abbreviations: bDMARDs, Biological Disease-Modifying Antirheumatic Drugs; BMAds, Bone Marrow Adipocytes; BMD, Bone Mineral Adiposity; C/EBPα, CCAAT/enhancer-binding protein alpha; CRP, C Reactive Protein; csDMARDs, Conventional Synthetic Disease-Modifying Antirheumatic Drugs; CTX, C-terminal collagen crosslinks; Dlx5, Distal-less homeobox 5; DMEM, Dulbecco's Modified Eagle Medium; DXA, Dual-energy X-ray Absorptiometry; FCS, Fetal Calf Serum; hBMSC, human bone marrow-derived stromal cell; IL, interleukin; IPAQ-SF, International Physical Activity Questionnaire—Short Form; JAK, Janus Kinase; JAKi, JAK inhibitors; MRI, Magnetic Resonance Imaging; Ob, Osteoblast; PBS, Phosphate Buffered Saline; PCR, Polymerase Chain Reaction; PDFF, Proton Density Fat Fraction; PLIN, Perilipin; PPARγ2, Peroxisome Proliferator-activated Receptor gamma 2; RA, Rheumatoid Arthritis; RNA, Ribonucleic Acid; Runx2, Runt-related transcription factor 2; STAT, Signal Transducer and Activator of Transcription; TNFα, Tumor Necrosis Factor alpha; Tofa, Tofacitinib; WST-1, Water Soluble Tetrazolium Salts-1; Ywhaz, tyrosine 3-monooxygenase/tryptophan 5-monooxygenase activation protein.

2 MATERIALS AND METHODS

2.1 Cell Culture Experiments

2.1.1 Cell Culture and Induction of Osteogenic and Adipogenic Differentiation

Purified hBMSCs from 3 donors (1 female, 20 years; 2 males, 25 and 22 years) were purchased from RoosterBio (Frederick, MD, USA). Cells were specified as >90% positive for CD73, CD90, and

CD105, and <10% negative for CD14, CD34, and CD45 surface marker expression.

Differentiation experiments were started when hBMSCs reached confluence (D0). To induce osteogenesis, hBMSCs were cultured in DMEM (Pan Biotech, Aidenbach, Germany) with 10% FCS (Pan Biotech, Aidenbach, Germany) supplemented with osteogenic inductors (50 µM ascorbic acid, 10 mM β-glycerophosphate, and 10^{-8} M vitamin D3 (Sigma-Aldrich)). For adipogenic differentiation, hBMSCs were cultured in DMEM with 10% FCS supplemented with adipogenic inductors (0.5 µM dexamethasone, 0.5 mM isobutyl-1methylxanthine, and 50 µM indomethacin (Sigma-Aldrich)). hBMSCs were cultured with 1 ng/ml TNFα (Gibco, Carlsbad, CA, USA) to mimic the inflammatory conditions in RA. The differentiation protocols were previously validated, as presented in **Supplementary Figure 1**.

To determine the impact of Tofa at an early commitment, hBMSCs were differentiated into Ob or BMAds in appropriate media for 3 days with TNFα and Tofa. To evaluate the effect of Tofa on fully differentiated BMAds, a similar treatment was applied for 6 days after 14 days of differentiation (**Figure 1**).

2.1.2 Test Reagents

Tofa was graciously provided by Pfizer (New York, NY, USA), dissolved in sterile water and stored at −20 °C after sonication. Recombinant human TNFα was purchased from Gibco (Carlsbad, CA, USA), dissolved in sterile water and stored at −20 °C. Three concentrations of Tofa were used: 200, 400, and 800 nM. According to Pfizer, Tofa at 400 nM was considered as equivalent of the therapeutic dosage of Tofa used in RA (5 mg twice a day).

2.1.3 Cell Viability Assay

In 96-well plates, Ob and BMAds were incubated with Tofa and TNF-α before being treated with 10 µl of WST-1 (Cell Proliferation Reagent WST-1; Roche, Mannheim, Germany). The mixture was then incubated for 4 h at 37 °C, after which the absorbance was measured at 450 nm. The reference wavelength was measured at 690 nm.

2.1.4 Oil Red O Staining

After 20 days, differentiated BMAds were fixed in 2% paraformaldehyde for 15 min, washed in water, incubated with 60% isopropanol for 5 min, and stained with newly filtered Oil Red O solution for 10 min at room temperature. After staining, the cells were rinsed with water before counterstaining with hematoxylin solution, Gill no. 3 (Sigma Aldrich, St. Louis, MO, USA) for 5 min at room temperature.

2.1.5 BMAd Density, BMAd Droplet Surface, and BMAd Surface

After 20 days, differentiated BMAds were fixed in 2% paraformaldehyde for 15 min, washed in water. BMAd density was assessed by counting the number of BMAds and the total number of cells in 12 images (6 per donor) for each condition. The BMAd droplet surface was assessed in 60 BMAds (30 per donor), and the BMAd surface was assessed in 100 BMAds (50 per donor) using ImageJ software (version 1.45).

2.1.6 RNA Expression Measurement

2.1.6.1 RNA Isolation

Total RNA was extracted from Ob and BMAd using an RNeasy® Micro Kit including a DNase I digestion step (Qiagen, Hilden, Germany), according to the instructions of the manufacturer, and quantified by Nanodrop at 260 nm wavelength.

2.1.6.2 mRNA Expression Analysis

Total RNA was reverse transcribed using a Maxima First-Strand cDNA Synthesis kit (Thermo Fisher Scientific, Waltham, MA, USA) and subjected to quantitative real-time PCR on the StepOnePlus® system (Applied Biosystems, Foster City, CA,

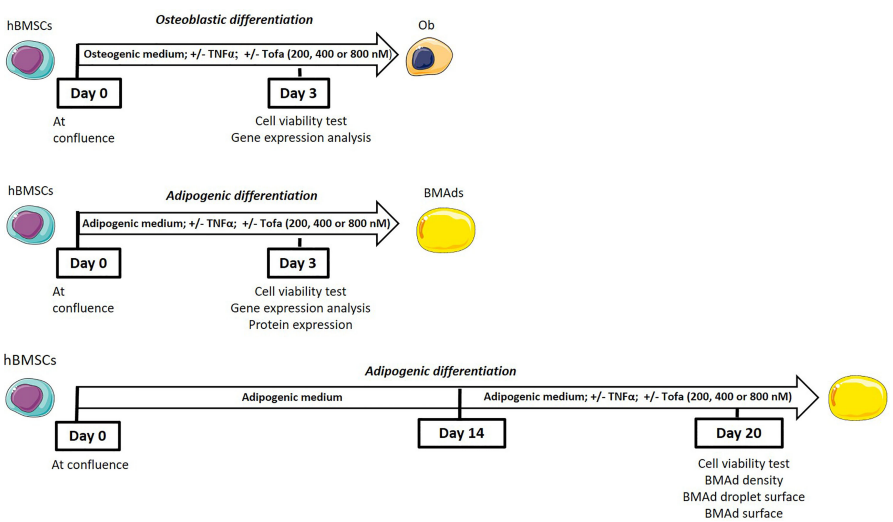

FIGURE 1 | General scheme of the experiments.

TABLE 1 | Primer sequences and conditions of PCR.

cDNA	GenBank	Forward and reverse primers	Ta (°C)	Product (pb)
RNAPol2	NM_000937	F: 5'-CCAAGCAGGACGTAATAGAGG-3' R: 5'-GCGGTCTAGCAACTCGTTCT-3'	55	193
PPIA	NM_021130	F: 5'-ACCGTGTTCTTCGACATTGC-3' R: 5'-CAGGACCCGTATGCTTTAGGA-3'	55	274
PPARγ2	NM_015869	F: 5'-CAAACCCCTATTCCATGCTGTT-3' R: 5'-AATGGCATCTCTGTGTCAACC-3'	53	135
C/EBPα	NM_004364	F: 5'-ACTGGGACCCTCAGCCTTG-3' R: 5'-TGGACTGATCGTGCTTCGTG-3'	55	75
IL6	NM_000600	F: 5'-CAATGAGGAGACTTGCCTGG-3' R: 5'-GCACAGCTCTGGCTTGTTCC-3'	53	113
PLIN 1	NM_002666	F: 5'-GAGACACTGCGGAATTTGC-3' R: 5'-ATCGAGAGAGGGTGTTGGTC-3'	58,2	222
Ywhaz	NM_145690	F: 5'-GGTCATCTTGGAGGGTCGTC-3' R: 5'-GTCATCACCAGCGGCAAC-3'	55	245
Runx2	AF001450	F: 5'-GCTGTTATGAAAAACCAAGT-3' R: 5'-GGGAGGATTTGTGAAGAC-3'	60	108
OC	NM_199173	F: 5'-ATGAGAGCCCTCACACTCCTC-3' R: 5'-GCCGTAGAAGCGCCGATAGGC-3'	55	293
Dlx5	BC006226	F: 5'-CCAGAGAAAGAAGTGACCGA-3' R: 5'-CCTGTGTTTGTGTCAATCCC-3'	55	190

The primer sequences, annealing temperatures (Ta), lengths of the corresponding PCR products and GenBank accession numbers are shown. F, Forward; R, Reverse. IL6, Interleukin 6; PLIN 1, Perilipin 1; C/EBPα, CCAAT/enhancer-binding protein alpha; PPARγ2, Peroxisome proliferator-activated receptor gamma 2; PPIA, peptidylpropyl isomerase; Runx2, Runt-related transcription factor 2; Ywhaz, Tyrosine 3-monooxygenase/tryptophan 5-monooxygenase activation protein; OC, Osteocalcin; Dlx5, Distal-less homeobox 5.

USA) using POWER SYBR® Green PCR Master Mix (Thermo Fisher Scientific, Waltham, MA USA) and specific primers designed using Oligo 6 software (MedProbe), or Taqman Universal Master Mix II (Applied Biosystems, Foster City, CA, USA) and specific probes (**Table 1**). Relative gene expression levels were normalized to YWHAZ (tyrosine 3-monooxygenase/tryptophan 5-monooxygenase activation protein) and PPIA (peptidylprolyl isomerase A) for Ob and RNAPol2 (RNA polymerase II) and YWAZ transcripts for BMAds and determined using the $2^{-\Delta\Delta Ct}$ method.

2.1.7 Protein Sampling, Quantification, and Western Blot Analysis

For sampling, BMAds were washed in ice-cold PBS (Pan Biotech, Aidenbach, Germany) and lysed in lysis buffer [HEPES, MgCl2, Glycerol, KCl, EDTA, DTT] supplemented with Halt Protease Inhibitor Single-Use Cocktail (Thermo Fisher Scientific, Waltham, MA, USA) and sodium orthovanadate. Cellular debris was discarded by centrifugation after cell lysis. To adjust the protein concentration, extracts were quantified using the DC Protein Assay Kit (Bio-Rad, Hercules, CA, USA) according to the instructions of the manufacturer and denatured in 4× Laemmli Sample Buffer (Bio-Rad, Hercules, CA, USA). Protein extracts were separated on 8% SDS–polyacrylamide gels and transferred onto 0.2 µm nitrocellulose membranes (Bio-Rad, Hercules, CA, USA) using a Trans-Blot Turbo System (semidry transfer) (Bio-Rad, Hercules, CA, USA). The membranes were blocked in 5% bovine serum albumin (Sigma Aldrich, St. Louis, MO, USA) for phosphorylated proteins or with 5% skimmed milk for the other proteins in Tris-buffered saline solution with 0.05% Tween 20 (Acros Organics, Morris Plains, NJ, USA) for 1 h. Blots were probed with antibodies against the following targets overnight: anti-phospho-STAT3 (Tyr705; Cell Signaling Technology, Danvers, MA, USA), anti-STAT 3 (D3Z2G; Cell Signaling Technology, Danvers, MA, USA), anti-Actin (A2066, Sigma Aldrich, St. Louis, MO, USA) and anti-Perilipin (D1D8; Cell Signaling Technology, Danvers, MA, USA). Horseradish peroxidase–conjugated immunoglobulin G (Santa Cruz Biotechnology, Dallas, TX, USA) was used as secondary antibody. Blots were developed using Amersham ECL Prime Western Blotting Detection Reagent substrate (GE Healthcare, Chicago, IL, USA) in a chemiluminescence imager (Amersham Imager 600, GE Healthcare, Chicago, IL, USA). Band intensities were measured using ImageQuant TL (GE Healthcare, Chicago, IL, USA). Band intensity was semiquantified using ImageJ software (version 1.45). Actin was used as an internal control for normalization.

2.2 Clinical Research

2.2.1 Study Design and Patients

The TOFAT study was an open, prospective 6-month follow-up study (NCT04175886) assessing the impact of Tofa on bone marrow adiposity, BMD, and body composition in RA patients 18 years and older. Key inclusion criteria include 2010 RA ACR/EULAR classification criteria (17), and an indication for Tofa. Key exclusion criteria included oral corticosteroids >10 mg prednisone/day; patients on or considering a restrictive diet during the study period; patients undertaking or planning to undertake an intense exercise program; history of treatment with bone active substances such as bisphosphonates; weight >160 kg; and any MRI contraindication. In patients who were receiving Biological Disease-Modifying Antirheumatic Drugs (bDMARDs), a five-half-life washout period was required between bDMARD interruption and inclusion in the study.

2.2.2 Study Approval

The study protocol was approved by the local Institutional Review Board (2019–001159–37), and the study procedures

complied with the ethical standards of the relevant institutional and national Human Experimentation Ethics Committees (reference CPP 40/19). All patients provided written informed consent. The study was designed to include 38 patients but was prematurely stopped due to the results of the safety Phase IV randomized clinical trial (18). Only 10 patients were included, and one participant was excluded at follow-up due to discontinuation of Tofa before 6 months.

2.2.3 Clinical Assessment

Demographic and clinical characteristics were recorded, particularly the 28-joint Disease Activity Score (DAS28), adjusted for C Reactive Protein (CRP) levels, current use of conventional synthetic disease-modifying antirheumatic drugs (csDMARDs) and corticosteroids, and physical activity using the International Physical Activity Questionnaire-Short Form (IPAQ-SF) and the handgrip test. Past use of bDMARDs was also recorded.

2.2.4 Bone Mineral Density and Body Composition Measurements Using DXA Scan

Bone mineral density (BMD) in RA patients was measured at the lumbar spine (L1–L4) and at the nondominant hip using a DXA scan (HOLOGIC Horizon W S/N 300869M).

All RA patients underwent total body DXA scanning (HOLOGIC Horizon W S/N 300869M). Fat, lean, and bone mass for the total body and per region (arms, legs, and trunk) were measured and analyzed using validated software from the manufacturer (version 13.6.0.5). Body fat percentage (BFP, %) was calculated as the proportion of total fat mass (TFM) to total mass. Appendicular lean mass (kg) was computed as the sum of the tissue compartment (lean) of both arms and legs. Visceral adipose tissue (VAT, cm^2) was recorded.

2.2.5 Laboratory Variables

Fasting (at least 8 h) blood samples were obtained. Serum cross-laps (CTX) were measured by a chemiluminescence assay using the IDS-iSYS Multi-Discipline Automated Analyzer (Immunodiagnostic Systems, Inc., Fountain Hills, AZ). Plasma concentrations of leptin were measured by ELISA using the E07 kit provided by Mediagnost (Reutlinger, Germany).

2.2.6 Bone Marrow Adiposity Measurement by MRI

2.2.6.1 Imaging Acquisition

All subjects underwent an MRI examination on a 3 Tesla system (Ingenia; Philips Healthcare, Best, Netherlands) using the built-in 12-channel posterior body coil and a 16-channel anterior coil, under the supervision of a senior musculoskeletal radiologist. Patients were positioned head-first in the supine position. A conventional imaging protocol was performed first, including T1- and T2-weighted 2-point Dixon turbo-spin echo (TSE) acquisitions in the sagittal plane, followed by an optional T2-weighted acquisition in the axial plane based on clinical history and the decision of the radiologist.

Immediately after this clinical exploration, bone marrow adiposity quantification (proton density fat fraction, PDFF) was achieved using a six-echo three-dimensional gradient echo sequence (mDixon-Quant; Philips Healthcare, Best, Netherlands), permitting a chemical shift encoding-based water-fat separation at the lumbar spine (sagittal). Imaging parameters were repetition time (TR)/echo time (TE)/ΔTE: 11/1.43/1.1 ms; field of view (FOV): 220 × 220 mm; voxel size: 1.8 × 1.8 mm; slice thickness: 3 mm; number of excitations: 1; no SENSE acceleration; fold-over direction: foot-head; bandwidth: 1,563 Hz and scan time: 1 min 41 s. In both situations, a low flip angle of 3° was used to minimize T1-bias (19).

2.2.6.2 Bone Marrow Adiposity Quantification

A senior musculoskeletal radiologist (SB) reviewed all examinations on a dedicated workstation (IntelliSpace Porta; Phillips Healthcare, Best, the Netherlands). A systematic morphological assessment was conducted first, looking for lumbosacral transitional vertebrae, degenerative changes, and bone marrow replacement lesions. Based on the 3 most sagittal slices acquired using the mDixon-Quant sequence, polygonal regions of interest (polygonal ROI) were drawn in the vertebral body of L1 to L4, avoiding subchondral bone, replacing lesions, severe degenerative changes, and the basivertebral vein. For each subject, a mean proton density fat fraction (PDFF) was calculated as an average of all measured values in the lumbar spine, from L1 to L4.

2.3 Statistical Analysis

Categorical variables are expressed as numbers (percentage), and continuous variables are expressed as the means (standard deviation, SD, or standard error of the mean, SEM). The normality of model residuals was assessed graphically and using a D'Agostino's K-squared test. Changes were examined during treatment by comparing baseline and 6-month values using a paired t-test or a Wilcoxon signed-rank test, depending on the normality of intra-patient differences. In the *in vitro* study, all experiments were repeated at least three times, and the Mann–Whitney U test and Student's t-test were used according to the distribution of the data. Statistical testing was performed at the two-tailed α level of 0.05. Data were analyzed using the GraphPad Prism software package, release 5.04 (GraphPad Software, San Diego, CA, USA).

3 RESULTS

3.1 Tofa Does Not Inhibit Survival of hBMSCs During Ob or BMAd Differentiation

Cytotoxicity tests were performed to assess whether cell survival is influenced by Tofa concentrations at 200, 400, and 800 nM (**Figure 2**).

We observed no changes during BMAd differentiation (BMAds at 3 days) regarding proinflammatory or noninflammatory conditions or the doses of Tofa tested. In Ob differentiated at 3 days, Tofa did not impact cellular viability but rather seemed to improve it when the cells were in the presence of TNFα. In fact, the significant decrease in cellular viability observed in Ob TNFα compared to the control was not observed in Ob TNFα + Tofa.

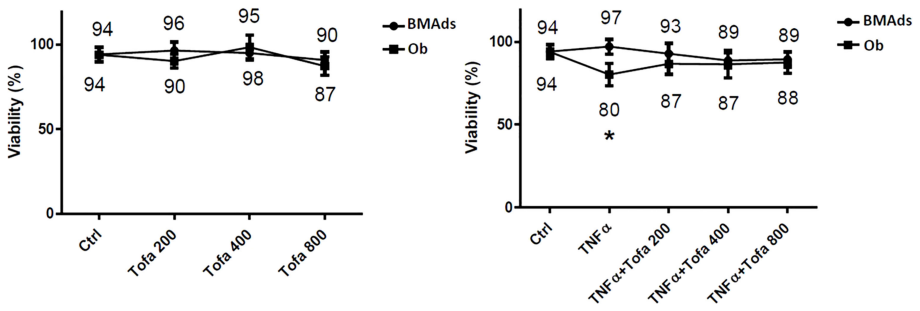

FIGURE 2 | Effect of Tofa and TNFα on the cellular viability of hBMSCs. Ob and BMAds were differentiated from hBMSCs for 3 days and treated with Tofa (200, 400, and 800 nM) and TNFα (1 ng/ml). Cell viability was assessed using the WST-1 method, and the percentage of viability is shown above and below the symbols. Data represent the mean ± SD of four independent experiments. ∗p <0.05 versus control (untreated group) by Mann–Whitney U test.

3.2 Tofa Treatment Has Little Effect on Ob Differentiation But Increases BMAds Differentiation Under Noninflammatory Conditions

To determine the impact of Tofa on cellular commitment, gene expression analysis was performed on specific markers related to Ob and BMAds differentiation. The results of quantitative real-time RT-PCR are displayed as the relative expression of mRNA levels in the Tofa-treated group compared to the control (untreated group).

Under noninflammatory conditions, we showed that Tofa significantly decreased expression levels of Runx2 at 400 nM and at 800 nM and Dlx5 (Distal-less homeobox 5, another key transcription factor of Ob differentiation) for all concentrations compared with the Ob control ($p < 0.05$) (**Figure 3A**). No effect of Tofa on osteocalcin gene expression levels was observed (**Figure 3A**).

Conversely, BMAds treated with Tofa exhibited a significant increase in the gene expression of PPARγ2, C/EBPα (two key transcription factors of BMAds differentiation) and Perilipin 1 (PLIN 1), the most specific marker associated with lipid droplet) compared with BMAds controls ($p < 0.05$). An increase was observed from 200-nM Tofa for each marker (**Figure 3B**).

The increase in expression of PLIN was also confirmed at the protein level in BMAds cultivated for 9 days in adipogenic medium, whatever the Tofa concentration applied (**Figure 3C**).

3.3 Tofa Limits the Negative Effect of TNFα During Differentiation But Only in an Adipocytic Context

As expected, the addition of TNFα stimulated proinflammatory cytokine expression in both cultures, as demonstrated here by the increase in IL6 gene expression up to 300-fold higher in BMAds TNFα and 9-fold in Ob TNFα compared to the controls, which were untreated BMAds and Ob (**Figure 4A**).

TNFα also impacted Ob and BMAd differentiation, marked by a significant decrease in Runx2 (40%), Dlx5 (58%), OC (62%) (**Figure 4B**), PPARγ2 (83.5%), C/EBPα (80%), and PLIN 1 (97%) (**Figure 4C**).

The addition of Tofa to TNFα did not change the expression profiles of Ob compared to TNFα controls (**Figure 4B**). In contrast, analysis of PPARγ2 gene expression revealed that the addition of Tofa limited the negative effect of TNFα on BMAd differentiation (**Figure 4C**). Expression levels of PPARγ2 were increased by an average of 4, 2.5, and 1.3 times, in response to Tofa 200, 400, and 800 nM, compared to TNFα-treated cells.

3.4 A Positive Effect of Tofa on BMAds Under Inflammatory Condition Was Also Observed at a Later Stage of Maturation

Given our results above, we chose to further evaluate the action of Tofa on BMAds after 14 days of differentiation followed by 6 days of TNFα + Tofa treatment. Previously, the effect of TNFα + Tofa on the cellular viability of differentiated BMAds was assessed and no change was observed compared to the control, BMAds + TNFα (**Figure 5A**).

To evaluate the effect of Tofa, optical images of BMAds treated with TNFα + Tofa at 200, 400, and 800 nM were analyzed and BMAd density was determined (number of BMAds/number of total cells). First, we observed a phenotype change and a decrease in BMAd density in response to TNFα treatment. In fact, TNFα induced a phenotypic conversion of BMAds toward a fibroblastic phenotype with a drastic decrease in BMAd surface ($p < 0.001$) and droplet surface compared to controls ($p < 0.001$) (**Figure 5B**).

The addition of Tofa to the culture media limited the phenotypic conversion and maintained a BMAd density close to that of the control (untreated cells) with a dose–response effect (**Figure 5C**). The surface of BMAds was affected at 200 nM ($p < 0.01$), but not at 400 or 800-nM Tofa (**Figure 5D**).

3.5 Tofa Inhibits pSTAT3 in BMAds

Although TOFA is a specific inhibitor of JAK1/3 and inhibits STAT1/3 phosphorylation, we were preferentially interested in the phosphorylation profile of STAT3 (pSTAT3) after 3 days of hBMSC differentiation. Indeed, the JAK3/STAT3 signaling pathway was upregulated during adipocyte differentiation and associated with an upregulation of pSTAT3 expression profile (**Figure 6A**). For JAK1/STAT1, the expression levels were stable during differentiation and were similar to those found in hBMSCs (data not shown). In response to Tofa, pSTAT3

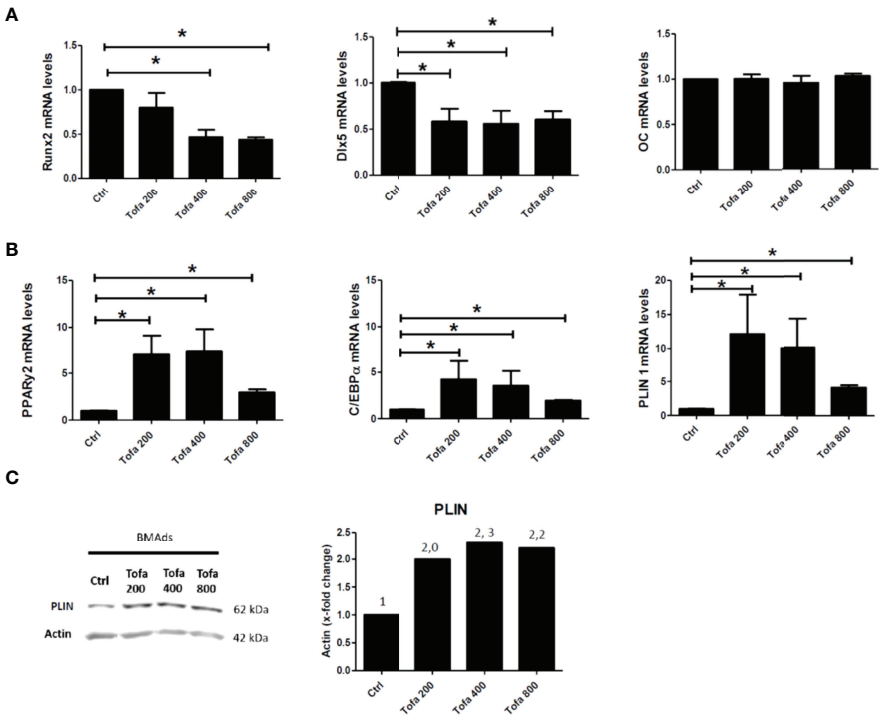

FIGURE 3 | Effect of Tofa on Ob and BMAds differentiation under noninflammatory conditions. Ob and BMAds were differentiated from hBMSCs and treated with Tofa (200, 400, and 800 nM) for 3 days. Ctrl: Ob or BMAds untreated **(A, B)** Quantitative RT-PCR analysis of osteoblast **(A)** and adipocyte-specific genes on day 3 **(B)**. Data are expressed as means ± SEM. Statistical significance was calculated using the Mann–Whitney U test (*p <0.05). **(C)** Western blot analysis of hBMSCs cultivated 9 days in adipogenic medium with Tofa 200, 400, and 800 nM. Representative western blots for PLIN with actin as a loading control and corresponding quantification of protein quantity (PLIN/Actin).

markedly decreased in BMAds compared to controls (untreated cells), suggesting a potential role for STAT3 in the expansion of bone marrow adipose tissue (**Figure 6B**).

3.6 Bone Marrow Adiposity is Increased in RA Patients Treated With Tofa

3.6.1 Baseline Characteristics of Patients

Age and disease duration (mean (SD)) were 58.0 (10.1) years and 7.3 (8.3) years, respectively. DAS28-CRP was 3.81 (1.2). Five patients were currently receiving corticosteroids (prednisone) at a dosage of less than 10 mg per day (6.8 (2.9) mg per day). Two patients had previously received at least one anti-TNFα treatment.

3.6.2 Clinical, Physical and Body Composition Changes in RA Patients During Treatment With Tofa

One participant was excluded at follow-up due to discontinuation of Tofa before 6 months. No significant change in disease activity was noted (DAS 28 CRP: 3.81 (1.19) vs 3.00 (1.06), p = 0.16). After 6 months of Tofa, a significant increase in the handgrip test was noted, whereas no change in BMI was observed (**Table 2**).

Changes in body composition, BMD, and lumbar spine PDFF are presented in **Table 2**. After 6 months of Tofa, a significant increase in the lumbar spine PDFF was noted (46.3% (7.0) vs 53.2% (9.2), p = 0.008) (**Figure 7**), whereas no changes in BMD or body composition were observed.

No significant changes in CTX (3,503 (1,830) pmol/L vs. 2,712 (2,196) pmol/L, p = 0.91), or leptin (14.9 (19.7) ng/L vs. 19.4 (24.9) ng/L, p = 0.30) levels were observed at 6 months.

4 DISCUSSION

Studies have reported an increased risk of bone loss and fracture in RA patients (20). Tofa may have beneficial effects on bone, which might be due to direct effects on the bone microenvironment and not exclusively based on its anti-inflammatory function. As common progenitor cells of BMAds and Ob, hBMSCs are delicately balanced in their differentiation commitment (21, 22). In osteoporosis, numerous *in vitro* and clinical investigations have demonstrated the ability of hBMSCs to differentiate in a preferential way toward BMAds (23–28). In this study, the ability of Tofa to counteract this imbalance was investigated. For that, the effects of Tofa on the viability and Ob and BMAd differentiation of hBMSCs were assessed.

First, the lack of data on this subject led us to explore the influence of Tofa under noninflammatory conditions. The results

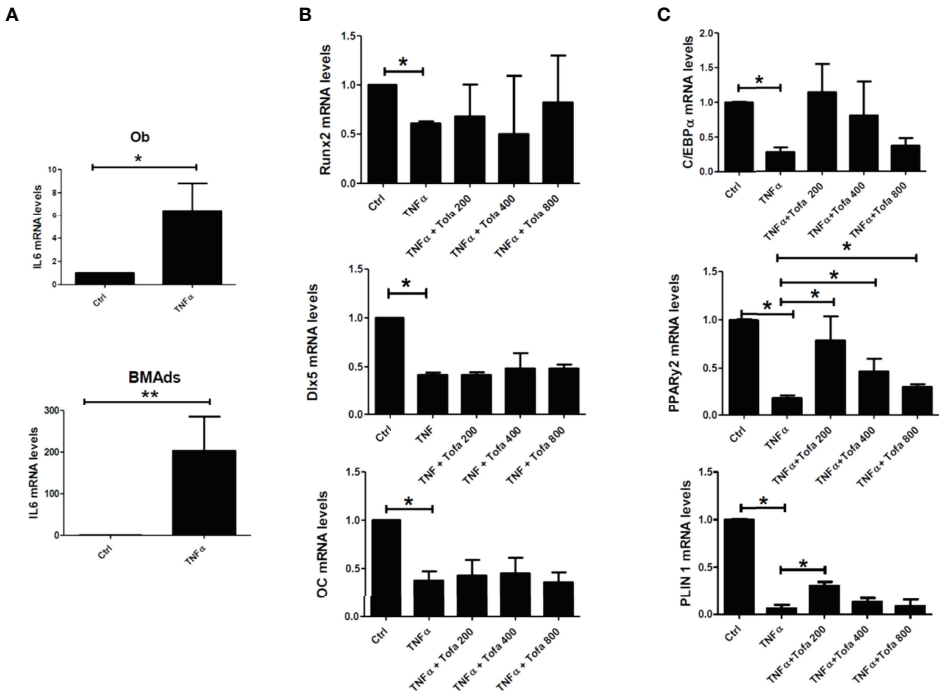

FIGURE 4 | Effect of Tofa on Ob and BMAd differentiation under inflammatory conditions. Ob and BMAds were differentiated from hBMSCs and treated with Tofa (200, 400, and 800 nM) and TNFα (1 ng/ml) for 3 days. Ctrl: Ob or BMAds untreated **(A–C)** Quantitative RT-PCR analysis of IL-6 **(A)**, osteoblast **(B)**, and adipocyte-specific genes on day 3 **(C)**. Data are expressed as the means ± SEM. Statistical significance was calculated using the Mann–Whitney U test (*p <0.05, **p <0.01).

at the cellular and molecular levels revealed that Tofa promoted adipocyte differentiation, even at low concentrations, but decreased the Ob differentiation after 3 days of treatment. Tofa has a fast onset of action, as the impact of Tofa on adipocytes and Ob differentiation has already been observed after only 3 days of treatment.

Concomitantly to our work, a stimulating effect of Tofa on differentiated adipocytes has also been reported on primary human bone marrow cells isolated from patients undergoing orthopedic surgery (29). In this study, Russell et al. reported an increase in the number of adipocytes for cells differentiated and treated by Tofa for 14 or 21 days.

Considering those results, we investigated the origin of the expansion of the adipose tissue treated with Tofa. Adipose tissue expansion results either from an increase in the size of differentiated adipocytes (adipocyte hypertrophy) and/or an increase in the formation of new adipocytes (adipocyte hyperplasia). This question was also raised by Russell et al. and was answered through the experiments conducted in our study. Indeed, measurements of the BMAd surface did not show an increase in the surface under Tofa, but the number of adipocytes was increased for the highest concentrations of Tofa (400 and 800 nM). These new findings confirm that Tofa participates in the expansion of adipose tissue by recruiting more preadipocytes and activating their differentiation. Consequently, we can also conclude that the increase in PLIN protein expression observed by western-blotting is therefore related to the appearance of new adipocytes rather than to the increase in the number of lipid droplets in the adipocytes already formed. This impact could be mediated through STAT3 inactivation. However, it has been shown in different studies that STAT3 is a rather pro-adipogenic factor (29, 30). Furthermore, in another *in vitro* model, Tofa treatment also resulted in off-target activation, leading to great complexity in its signaling (31, 32). Therefore, further studies are therefore needed to understand the mechanism that induces increased adipogenesis under Tofa.

Second, to get as close as possible to the inflammatory conditions of pathology, we treated the cultures with TNFα in addition to Tofa. Numerous studies have focused on the effect of TNFα on Ob and have shown the deleterious effect of this molecule on differentiation, characterized by a drastic decrease in Ob factors such as Runx2 or Dlx5 (33). However, even when gene expression levels of Runx2/Dlx5 were lowered by the effect of TNFα, tofacitinib was unable to counteract the action of TNFα and to stimulate Runx2 or Dlx5 as in noninflammatory conditions. These results support the latest published results and oppose the osteoanabolic effect previously described in the literature (11, 12). Russell et al. observed that Tofa did not affect the Ob differentiation at 14 days, as assessed by ALP activity and accumulation of calcium (34). Similarly, Gaber's experiments did not reveal any changes in the gene expression of osteoblastic markers in hBMSCs treated with Tofa 7 days after osteogenic induction, grown under standard conditions. An increase in Runx2 expression was observed only under hypoxic conditions (12).

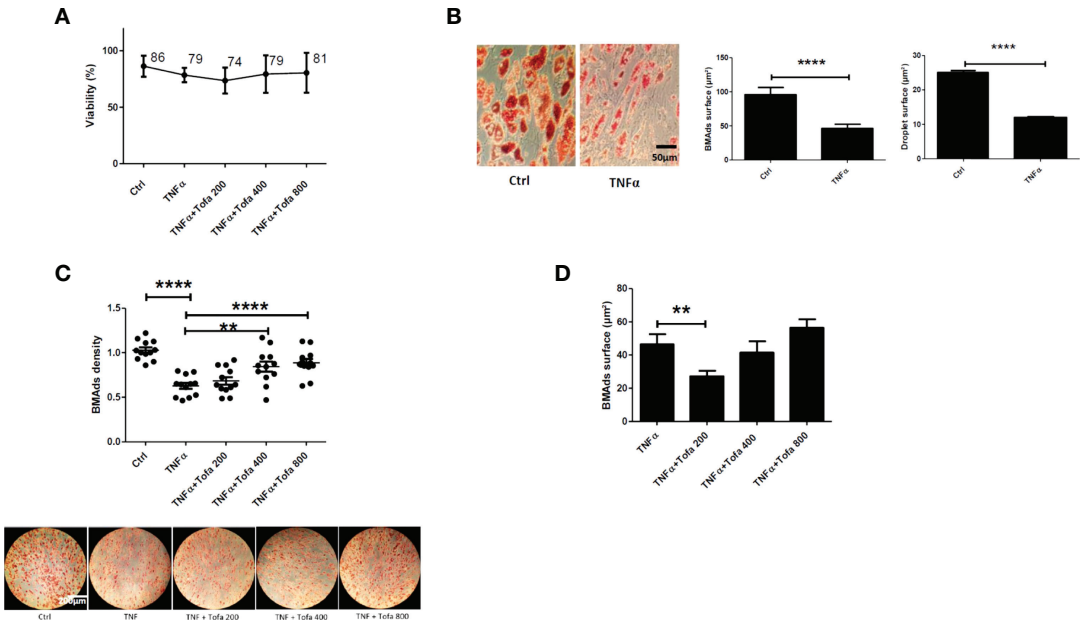

FIGURE 5 | Effect of Tofa on differentiated BMAds under inflammatory condition. BMAds were differentiated from hBMSCs for 14 days and then cultured in the presence or absence of Tofa and TNFα for 6 days. **(A)** Cell viability was assessed using the WST-1 method, and the percentage of viability is shown above and below the symbols. Data represent the mean ± SD of four independent experiments. **(B)** Representative image showing the effect of TNFα treatment on adipogenesis, visualized by the uptake of oil red into lipid vacuoles (red). Quantification of BMAd surface and droplet surface (μm^2) after TNFα treatment. **(C)** Quantification of the number of BMAds (number of BMAds/number of total cells) and **(D)** BMAd surface, after TNFα and Tofa treatment. **(B–D)** Data are expressed as the means ± SEM (n = 2). Statistical significance was calculated using Mann–Whitney U test for non-parametric variables and Student's t-test (**p <0.01, ****p <0.0001).

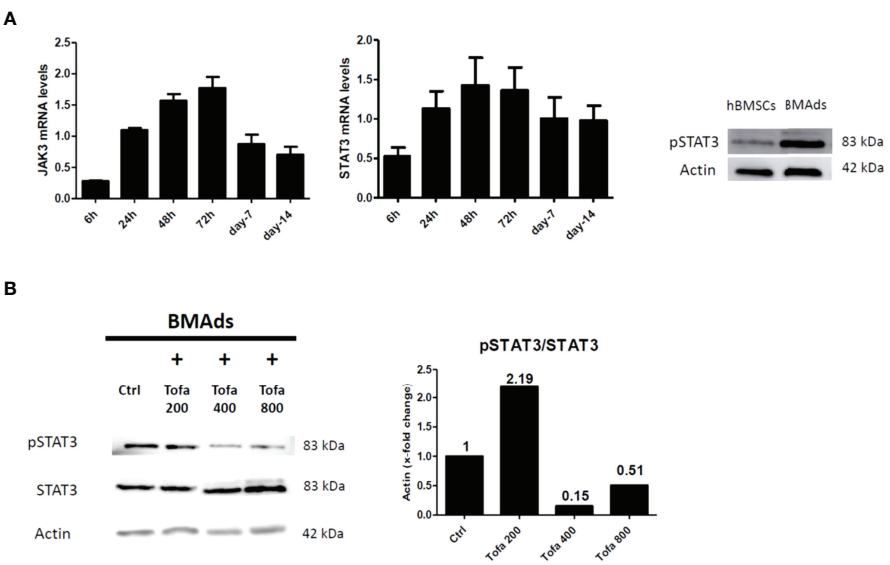

FIGURE 6 | Analysis of pSTAT3 profile in BMAds. Quantitative RT-PCR analysis of JAK3 and STAT3 **(A)** during adipocyte differentiation compared to day 0 (hBMSCs confluents). STAT3 activity (pSTAT3) during adipocyte differentiation was demonstrated by western blot analysis. BMAds were differentiated 48 h in adipogenic medium and compared to hBMSCs. **(B)** Western blot analysis was used to determine relative pSTAT3/STAT3 expression in BMAds after 48 h of differentiation and treated 3 days with Tofa (200, 400, and 800 nM). Actin was used as a loading control. Data are representative of three independent experiments.

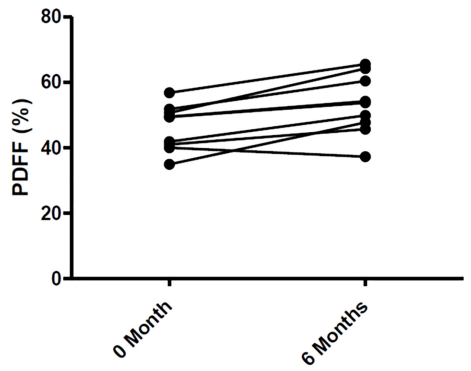

FIGURE 7 | Changes of Bone Marrow Fat in 9 RA patients treated with Tofa. Bone marrow fat was assessed by MRI at lumbar spine in the 9 patients treated with Tofa during 6 months. PDFF, Proton Density Fat Fraction.

In contrast, Tofa appears to attenuate the deleterious effect of TNFα on the cellular viability of hBMSCs placed in osteogenic medium. In a recent study and in a different context, the protective effect of Tofa on cellular viability has also been reported (35). The authors used an oxygen-glucose deprivation/reoxygenation (OGD/R)-induced normal rat small intestinal epithelial cell model to simulate the physiological environment of intestinal I/R injury, treated or not with Tofa. The results showed that Tofa exerted protective effects on oxidative stress and inflammation in these cells but also on apoptosis during OGD/R. This effect could be mediated through the inhibition of the JAK/STAT3 pathway since the use of an agonist of this pathway partially abrogated the beneficial effect of Tofa.

In humans, the effects of Tofa on bone marrow adiposity in RA patients have never been evaluated. We have now conducted a prospective pilot study in 9 patients with RA, in which Tofa increased lumbar spine PDFF and resulted in no changes in BMD or body composition over 6 months. These clinical findings reinforce the *in vitro* results on the stimulatory effect of Tofa on BMAd differentiation, even if several limitations are to be underlined in this study. The hBMSCs used were obtained from healthy donors and treated with TNFα, which only partially reflected the pathology. It would be interesting to validate these results using hBMSCs collected from RA patients, especially since the clinical data obtained predicts a similar positive effect of Tofa on adipocyte differentiation. Clinically, we acknowledge that 6 months of follow-up is a short period to evaluate the BMD and body composition in patients treated with Tofa, and that 9 patients is a small population, but despite that, we were able to observe an increase in lumbar spine PDFF.

In conclusion, *in vitro* and clinical results suggest a stimulatory effect of Tofa on BMAd commitment and differentiation, which does not seem to support the beneficial effects of Tofa on the bone microenvironment. Studies on the impact of the other JAKi on bone marrow adiposity are needed to determine whether the stimulatory effect on bone marrow adiposity is a class effect or is specific to Tofa.

DATA AVAILABILITY STATEMENT

The original contributions presented in the study are included in the article/**Supplementary Material**. Further inquiries can be directed to the corresponding author.

ETHICS STATEMENT

The studies involving human participants were reviewed and approved by the Institutional Review Board of CHU de Lille (2019–001159–37) and the National Human Experimentation Ethics Committees (reference CPP 40/19). The patients/participants provided their written informed consent to participate in this study.

AUTHOR CONTRIBUTIONS

J-GL and AC performed the experiments. J-GL, JP, and AC wrote the manuscript. All authors listed have made a substantial, direct, and intellectual contribution to the work and approved it for publication.

TABLE 2 | Changes in rheumatoid arthritis patients treated with Tofacitinib for 6 months.

Patients	M0N = 9	M6N = 9	Absolute difference	P-value
Body mass index, kg/m²	25.9 (3.4)	26.1 (6.3)	+0.2	0.64
Handgrip test, kg	**22.5 (8.9)**	**27.9 (14.0)**	**+5.4**	**0.01**
IPAQ-SF, MET-min/week	6,203 (8,461)	7,110 (4,111)	+907	0.49
Body Fat Percentage, %	3939.4 (8.5)	39.4 (9.0)	0	0.46
Appendicular lean mass, kg	16.6 (4.5)	16.7 (4.9)	+0.1	0.50
Visceral Adipose Tissue, cm²	150 (81)	173 (88)	+23	0.18
Lumbar spine BMD, g/cm²	1.011 (0.142)	0.996 (0.146)	–0.015	0.058
Femoral neck BMD, g/cm²	0.728 (0.108)	0.713 (0.095)	–0.015	0.30
Total hip BMD, g/cm²	0.902 (0.130)	0.891 (0.105)	–0.011	0.82
Lumbar spine PDFF (%)	**46.3 (7.0)**	**53.2 (9.2)**	**+6.9**	**0.008**
CTX, pmol/L	3,503 (1,830)	2,712 (2,196)	–791	0.91
Leptine, ng/L	14.9 (19.7)	19.4 (24.9)	+4.5	0.30

Data reported as mean (Standard Deviation) unless otherwise indicated. CTX , Cross laps; DAS, Disease Activity Score; IPAQ-SF, International Physical Activity Questionnaire—Short Form; MET, Metabolic Equivalent of Task; PDFF, Proton Density Fat Fraction. Bold values mean statistically significant.

FUNDING

JGL was supported by a PhD grant from Société Française de Rhumatologie and from ISite-ULNE. The TOFAT study received funding from Pfizer. The funder was not involved in the study design, collection, analysis, interpretation of data, the writing of this article or the decision to submit it for publication. All authors declare no other competing interests.

ACKNOWLEDGMENTS

Tofacitinib (Tofa) was graciously provided by Pfizer. TOFAT was sponsored by Pfizer with an unrestricted grant.

SUPPLEMENTARY MATERIAL

The Supplementary Material for this article can be found online at: https://www.frontiersin.org/articles/10.3389/fendo.2022.881699/full#supplementary-material

Supplementary Figure 1 | Adipogenic differentiation of hBMSCs was confirmed **(A)** by using Q-PCR analysis of mRNA levels of adipogenic markers (PPARγ, C/EBPα, PLIN 1) performed over a 14 days period of induction from day 0 (control hBMSCs) and Oil Red O staining. Osteogenic differentiation of hBMSCs was confirmed **(B)** by using Q-PCR analysis of mRNA levels of osteogenic markers (RUNX2, OC) performed over a 14 days period of induction from day 0 (control hBMSCs), ALP activity and Alizarin Red Staining at 21 days of differentiation. The data are representative of three independent experiments.

REFERENCES

1. Oude Voshaar MAH, Das Gupta Z, Bijlsma JWJ, Boonen A, Chau J, Courvoisier DS, et al. International Consortium for Health Outcome Measurement Set of Outcomes That Matter to People Living With Inflammatory Arthritis: Consensus From an International Working Group. *Arthritis Care Res (Hoboken)* (2019) 71:1556–65. doi: 10.1002/acr.23799
2. Smolen JS, Aletaha D, Barton A, Burmester GR, Emery P, Firestein GS, et al. Rheumatoid Arthritis. *Nat Rev Dis Primers* (2018) 4:18001. doi: 10.1038/nrdp.2018.1
3. Tanaka Y. Managing Osteoporosis and Joint Damage in Patients With Rheumatoid Arthritis: An Overview. *J Clin Med* (2021) 10:1241. doi: 10.3390/jcm10061241
4. Xue AL, Wu SY, Jiang L, Feng AM, Guo HF, Zhao P. Bone Fracture Risk in Patients With Rheumatoid Arthritis: A Meta-Analysis. *Med (Baltimore)* (2017) 96:e6983. doi: 10.1097/MD.0000000000006983
5. Tanaka Y. Clinical Immunity in Bone and Joints. *J Bone Miner Metab* (2019) 37:2–8. doi: 10.1007/s00774-018-0965-5
6. Lee EB, Fleischmann R, Hall S, Wilkinson B, Bradley JD, Gruben D, et al. Tofacitinib Versus Methotrexate in Rheumatoid Arthritis. *N Engl J Med* (2014) 370:2377–86. doi: 10.1056/NEJMoa1310476
7. Genovese MC, Kremer J, Zamani O, Ludivico C, Krogulec M, Xie L, et al. Baricitinib in Patients With Refractory Rheumatoid Arthritis. *N Engl J Med* (2016) 374:1243–52. doi: 10.1056/NEJMoa1507247
8. Flanagan ME, Blumenkopf TA, Brissette WH, Brown MF, Casavant JM, Shang-Poa C, et al. Discovery of CP-690,550: A Potent and Selective Janus Kinase (JAK) Inhibitor for the Treatment of Autoimmune Diseases and Organ Transplant Rejection. *J Med Chem* (2010) 53:8468–84. doi: 10.1021/jm1004286
9. Gao W, McGarry T, Orr C, McCormick J, Veale DJ, Fearon U. Tofacitinib Regulates Synovial Inflammation in Psoriatic Arthritis, Inhibiting STAT Activation and Induction of Negative Feedback Inhibitors. *Ann Rheum Dis* (2016) 75:311–5. doi: 10.1136/annrheumdis-2014-207201
10. Migita K, Miyashita T, Izumi Y, Koga T, Komori A, Maeda Y, et al. Inhibitory Effects of the JAK Inhibitor CP690,550 on Human CD4(+) T Lymphocyte Cytokine Production. *BMC Immunol* (2011) 12:51. doi: 10.1186/1471-2172-12-51
11. Adam S, Simon N, Steffen U, Andes FT, Scholtysek C, Müller DIH, et al. JAK Inhibition Increases Bone Mass in Steady-State Conditions and Ameliorates Pathological Bone Loss by Stimulating Osteoblast Function. *Sci Transl Med* (2020) 12:5867. doi: 10.1126/scitranslmed.aay4447
12. Gaber T, Brinkman ACK, Pienczikowski J, Diesing K, Damerau A, Pfeiffenberger M, et al. Impact of Janus Kinase Inhibition With Tofacitinib on Fundamental Processes of Bone Healing. *Int J Mol Sci* (2020) 21.:865. doi: 10.3390/ijms21030865
13. Hamar A, Szekanecz Z, Pusztai A, Czókolyová M, Végh E, Pethő Z, et al. Effects of One-Year Tofacitinib Therapy on Bone Metabolism in Rheumatoid Arthritis. *Osteoporos Int* (2021) 32:1621–9. doi: 10.1007/s00198-021-05871-0
14. Vidal B, Cascão R, Finnilä MAJ, Lopes IP, da Glória VG, Saarakkala S, et al. Effects of Tofacitinib in Early Arthritis-Induced Bone Loss in an Adjuvant-Induced Arthritis Rat Model. *Rheumatol (Oxford)* (2018) 57:1461–71. doi: 10.1093/rheumatology/kex258
15. Paccou J, Penel G, Chauveau C, Cortet B, Hardouin P. Marrow Adiposity and Bone: Review of Clinical Implications. *Bone* (2019) 118:8–15. doi: 10.1016/j.bone.2018.02.008
16. Li J, Chen X, Lu L, Yu X. The Relationship Between Bone Marrow Adipose Tissue and Bone Metabolism in Postmenopausal Osteoporosis. *Cytokine Growth Factor Rev* (2020) 52:88–98. doi: 10.1016/j.cytogfr.2020.02.003
17. Aletaha D, Neogi T, Silman AJ, Funovits J, Felson DT, Bingham CO, et al. Rheumatoid Arthritis Classification Criteria: An American College of Rheumatology/European League Against Rheumatism Collaborative Initiative. *Ann Rheum Dis* (2010) 62(9):2569–81. doi: 10.1002/art.27584.
18. Ytterberg SR, Bhatt DL, Mikuls TR, Koch GG, Fleischmann R, Rivas JL, et al. Cardiovascular and Cancer Risk With Tofacitinib in Rheumatoid Arthritis. *New Engl J Med* (2022) 386:316–26. doi: 10.1056/NEJMoa2109927
19. Karampinos DC, Yu H, Shimakawa A, Link TM, Majumdar S. T_1-Corrected Fat Quantification Using Chemical Shift-Based Water/Fat Separation: Application to Skeletal Muscle. *Magn Reson Med* (2011) 66:1312–26. doi: 10.1002/mrm.22925.
20. Baillet A, Gossec L, Carmona L, de Wit M, van Eijk-Hustings Y, Bertheussen H, et al. Points to Consider for Reporting, Screening for and Preventing Selected Comorbidities in Chronic Inflammatory Rheumatic Diseases in Daily Practice: A EULAR Initiative. *Ann Rheumatol Dis* (2016) 75:965–73. doi: 10.1136/annrheumdis-2016-209233
21. Pittenger MF, Mackay AM, Beck SC, Jaiswal RK, Douglas R, Mosca JD, et al. Multilineage Potential of Adult Human Mesenchymal Stem Cells. *Science* (1999) 284:143–7. doi: 10.1126/science.284.5411.143
22. Owen M. Marrow Stromal Stem Cells. *J Cell Sci Suppl* (1988) 10:63–76. doi: 10.1242/jcs.1988.Supplement_10.5
23. Hardouin P, Pansini V, Cortet B. Bone Marrow Fat. *Joint Bone Spine* (2014) 81:313–9. doi: 10.1016/j.jbspin.2014.02.013
24. Justesen J, Stenderup K, Ebbesen EN, Mosekilde L, Steiniche T, Kassem M. Adipocyte Tissue Volume in Bone Marrow is Increased With Aging and in Patients With Osteoporosis. *Biogerontology* (2001) 2:165–71. doi: 10.1023/a:1011513223894
25. Duque G. Bone and Fat Connection in Aging Bone. *Curr Opin Rheumatol* (2008) 20:429–34. doi: 10.1097/BOR.0b013e3283025e9c
26. Gimble JM, Zvonic S, Floyd ZE, Kassem M, Nuttall ME. Playing With Bone and Fat. *J Cell Biochem* (2006) 98:251–66. doi: 10.1002/jcb.20777
27. Li Y, Meng Y, Yu X. The Unique Metabolic Characteristics of Bone Marrow Adipose Tissue. *Front Endocrinol (Lausanne)* (2019) 10:69. doi: 10.3389/fendo.2019.00069
28. Rosen CJ, Bouxsein ML. Mechanisms of Disease: Is Osteoporosis the Obesity of Bone? *Nat Clin Pract Rheumatol* (2006) 2:35–43. doi: 10.1038/ncprheum0070
29. Zhang K, Guo W, Yang Y, Wu J. JAK2/STAT3 Pathway is Involved in the Early Stage of Adipogenesis Through Regulating C/Ebpβ Transcription. *J Cell Biochem* (2011) 112:488–97. doi: 10.1002/jcb.22936
30. Deng J, Hua K, Lesser SS, Harp JB. Activation of Signal Transducer and Activator of Transcription-3 During Proliferative Phases of 3T3-L1

Adipogenesis. *Endocrinology* (2000) 141:2370–6. doi: 10.1210/endo.141.7.7551
31. Ostrovskyi D, Rumpf T, Eib J, Lumbroso A, Slynko I, Klaeger S, et al. Tofacitinib and Analogs as Inhibitors of the Histone Kinase PRK1 (Pkn1). *Future Med Chem* (2016) 8:1537–51. doi: 10.4155/fmc-2016-0132
32. Eberl HC, Werner T, Reinhard FB, Lehmann S, Thomson D, Chen P, et al. Chemical Proteomics Reveals Target Selectivity of Clinical Jak Inhibitors in Human Primary Cells. *Sci Rep* (2019) 9:14159. doi: 10.1038/s41598-019-50335-5
33. Zhao B. TNF Bone Remodeling. *Curr Osteoporos Rep* (2017) 15:126–34. doi: 10.1007/s11914-017-0358-z
34. Russell T, Rowe H, Bridgewood C, Cuthbert RJ, Watad A, Newton D, et al. Tofacitinib Blocks Entheseal Lymphocyte Activation and Modulates MSC Adipogenesis, But Does Not Directly Affect Chondro- and Osteogenesis. *Immuno* (2021) 1:545–57. doi: 10.3390/immuno1040038
35. Yang J, Xie X. Tofacitinib Protects Intestinal Epithelial Cells Against Oxygen-Glucose Deprivation/Reoxygenation Injury by Inhibiting the JAK/STAT3 Signaling Pathway. *Exp Ther Med* (2021) 22:1108. doi: 10.3892/etm.2021.10542

Conflict of Interest: The authors declare that the research was conducted in the absence of any commercial or financial relationships that could be construed as a potential conflict of interest.

frontiers | Frontiers in Endocrinology

TYPE Review
PUBLISHED 15 September 2022
DOI 10.3389/fendo.2022.981487

OPEN ACCESS

EDITED BY
Jason Horton,
Upstate Medical University,
United States

REVIEWED BY
Elizabeth Rendina-Ruedy,
Vanderbilt University Medical Center,
United States
Drenka Trivanović,
University Hospital Würzburg,
Germany

*CORRESPONDENCE
Dalia Ali
dayesh@health.sdu.dk
Abbas Jafari
ajafari@sund.ku.dk

SPECIALTY SECTION
This article was submitted to Bone Research, a section of the journal Frontiers in Endocrinology

RECEIVED 29 June 2022
ACCEPTED 29 August 2022
PUBLISHED 15 September 2022

CITATION
Ali D, Tencerova M, Figeac F, Kassem M and Jafari A (2022) The pathophysiology of osteoporosis in obesity and type 2 diabetes in aging women and men: The mechanisms and roles of increased bone marrow adiposity.
Front. Endocrinol. 13:981487.
doi: 10.3389/fendo.2022.981487

The pathophysiology of osteoporosis in obesity and type 2 diabetes in aging women and men: The mechanisms and roles of increased bone marrow adiposity

Dalia Ali[1]*, Michaela Tencerova[2], Florence Figeac[1], Moustapha Kassem[1] and Abbas Jafari[3]*

[1]Department of Molecular Endocrinology, KMEB, University of Southern Denmark and Odense University Hospital, Odense, Denmark, [2]Laboratory of Molecular Physiology of Bone, Institute of Physiology of the Czech Academy of Sciences, Prague, Czechia, [3]Department of Cellular and Molecular Medicine, University of Copenhagen, Copenhagen, Denmark

Osteoporosis is defined as a systemic skeletal disease characterized by decreased bone mass and micro-architectural deterioration leading to increased fracture risk. Osteoporosis incidence increases with age in both post-menopausal women and aging men. Among other important contributing factors to bone fragility observed in osteoporosis, that also affect the elderly population, are metabolic disturbances observed in obesity and Type 2 Diabetes (T2D). These metabolic complications are associated with impaired bone homeostasis and a higher fracture risk. Expansion of the Bone Marrow Adipose Tissue (BMAT), at the expense of decreased bone formation, is thought to be one of the key pathogenic mechanisms underlying osteoporosis and bone fragility in obesity and T2D. Our review provides a summary of mechanisms behind increased Bone Marrow Adiposity (BMA) during aging and highlights the pre-clinical and clinical studies connecting obesity and T2D, to BMA and bone fragility in aging osteoporotic women and men.

KEYWORDS

aging, osteoporosis, bone marrow adiposity, bone fragility, type 2 diabetes (T2D), obesity

Abbreviations: BM, Bone Marrow; BMA, Bone marrow adiposity; BMAT, Bone marrow adipose tissue; BMD, Bone mineral density; BMSCS, Bone Marrow Stromal Stem Cells; BMPs, Bone morphogenic proteins; DEXA, Dual energy X-ray absorptiometry; HFD, High fat diet; IGF-1, Insulin like growth factor-1; IL-6, Interleukin 6; OVX, Ovariectomy; P1NP, Procollagen 1Intact N-Terminal Propeptide; PPARγ, Peroxisome proliferation-activated receptor gamma; RANKL, Receptor activator of nuclear factor kappa β ligand; RUNX2, Runt related transcription factor 2; SASP, Senescence associated secretory phenotype markers; TNFα, Tumor necrosis factor alpha.

Osteoporosis

Osteoporosis is a chronic-skeletal disorder characterized by low bone mass, and deterioration in the microarchitecture of the bone tissue that results in bone fragility and increased fracture risk (1). It is the most common bone disease worldwide, affecting more than 200 million people and causing more than 9 million fractures in the year 2000 (2). In 2016, a European study estimated that 6.6% of men and 22.1% of women over the age of 50 years were diagnosed with osteoporosis, and around 3.5 million with fragility fractures. Osteoporosis causes vertebral and hip fractures, as well as chronic pain, that in many cases, are associated with disability and reduced life quality. Fractures, due to osteoporosis, require hospitalization and increase risk of mortality by 20%, and in 50% of the cases, result in chronic disability (3). The World Health Organization (WHO) has defined osteoporosis as a disease of low bone mass as measured by Dual-Energy X-ray Absorptiometry (DEXA) with Bone Mineral Density (BMD) equal or less than -2.5 standard deviations of the average value for young healthy persons (known as (T-score≤-2.5) (4, 5).

Pathophysiology of bone loss in age-related osteoporosis

Osteoporosis is primarily attributed to aging and sex-steroid deficiency, which at the cellular level leads to increased bone resorption by osteoclasts and decreased bone formation by osteoblasts (6, 7). A number of underlying pathogenic mechanisms of osteoporosis have been proposed, such as estrogen deficiency-associated Bone Marrow (BM) inflammation (8) or decreased levels of anabolic hormones (9, 10). However, increasing evidence has suggested a possible role of Bone Marrow Adiposity (BMA) in pathogenesis of bone loss in osteoporosis.

BMA and bone loss in age-related osteoporosis

Aging is defined as a gradual loss of normal tissue homeostasis and progressive deterioration of the organ functions, due to accumulation of cellular/DNA damage and senescence throughout aging (11). Aging is associated with significant bone loss and structural bone damage, due to accelerated trabecular thinning and disconnection, cortical thinning, and porosity (12), leading to increased fracture risk. Thus, osteoporosis is an exaggerated expression of aging process in the bone tissue (13). One of the key underlying mechanisms of bone loss in age-related osteoporosis is the altered lineage allocation of Bone Marrow Stromal Cells (BMSCs), associated with enhanced differentiation towards adipocyte lineage, leading to expansion of the Bone Marrow Adipose Tissue (BMAT), at the expense of compromised osteoblast differentiation and bone formation (13). Comprehensive characterization of the epigenomic and transcriptional changes associated with osteoblast and adipocyte differentiation of BMSCs has shown that the inverse correlation between fate specification of BMSCs into osteoblast versus adipocyte lineages is regulated by a large and diverse network of transcription factors (14).

Expansion of BMAT is caused by the increase in adipocyte size and/or number and is defined as the proportion of the BM cavity occupied by the adipocytes (15). The expansion of BMAT in aging can lead to space limitation for other cells that are required for normal skeletal homeostasis, such as BMSCs, osteoblastic, or hematopoietic cells (16). In addition, factors that are secreted by Bone Marrow Adipocytes (BMAds) can also contribute to altered skeletal homeostasis after BMAT expansion, such as adipokines, RANKL, immune-regulatory and pro-inflammatory cytokines. Examples of BMAd-secreted factors that can regulate bone cell function include RANKL, adiponectin, leptin, legumain, and chemerin (17–19).

Age-related expansion of BMAT and osteoporotic bone loss are mediated through intrinsic and extrinsic mechanisms, such as cellular senescence within the bone microenvironment or age-related endocrine dysfunction.

Intrinsic mechanisms

Accumulation of senescent cells

Aging is associated with accumulation of senescent cells, due to diverse stress stimuli (e.g. shortening of telomeres, oncogenic or metabolic insults), causing the cell to enter a state of irreversible growth arrest (20). Senescence is also associated with different cellular alterations including changes in chromatin organization, gene expression (e.g. increased expression of cell cycle regulators/tumor suppressors such as $p16^{Ink4a}$ and p53), mitochondrial dysfunction, and resistance to apoptosis, reviewed in (21, 22). In addition, a key feature of senescent cells is development of a distinctive secretome, known as Senescence-Associated Secretory Phenotype (SASP), characterized by secreting high levels of pro-inflammatory cytokines, immune modulators, growth factors, and proteases, that can spread throughout the tissue, and further exacerbate the senescence and tissue dysfunction (23–29).

Murine studies using the SAMP6 model had shown that accelerated senescence is associated with enhanced adipogenesis and inhibited osteoblastogenesis within the bone

microenvironment, leading to compromised bone formation and decreased bone mass (30). Analysis of human bone specimens had shown presence of senescence microenvironment in the bone tissue obtained from old individuals compared to young control subjects, evidenced by increased expression of $p16^{Ink4a}$ and p21 (31). Furthermore genetic depletion of senescent cells, using the inducible INK-ATTAC 'suicide' transgene that eliminates the $p16^{Ink4a}$ expressing cells, in a murine pre-clinical model of age-related osteoporosis, exhibited anti-resorptive and anabolic impact on bone, leading to decreased BMAT and increased bone mass (32).

Aging is also accompanied with increased levels of Reactive Oxygen Species (ROS) and oxidative stress in the bone microenvironment, leading to impaired osteoblast differentiation and function, and enhanced adipocyte differentiation (33). It was shown that presence of the antioxidant agent Resveratrol in the cultures of human BMSCs obtained from old individuals enhances differentiation and function of osteoblasts and inhibits formation of BMAds (34). In addition, *in vivo* murine studies using irradiation or physiological aging models, in which increased levels of ROS within the bone microenvironment are associated with expansion of BMAT and compromised skeletal homeostasis, indicated that antioxidant agents Dasatinib and Quercetin reduced BMAT and enhanced bone formation, by decreasing the ROS levels and senescent cells (35). These studies provide strong evidence for use of antioxidants as a promising approach for preventing age-related bone loss and osteoporosis.

Few studies have reported that senescence can be regulated *via* transcription factors (36, 37). Forkhead box rotein P1 (FOXP1) is involved in transcriptional control of BMSC senescence, and its expression levels had been shown to decline with aging, and inversely correlate with $p16^{Ink4a}$ expression. Mouse genetic studies had shown that conditional depletion of Foxp1 in BMSCs leads to premature aging, bone loss, and increased BMA *via* Foxp1 interactions with different members of C/EBP family proteins, such as C/EBP β/δ, which are key modulators of adipogenesis (38). Another study in aged mice revealed that senescence is associated with down regulation of expression of osteoblast transcription factors such as Runx2 and Dlx5, leading to impaired osteoblastogenesis and enhanced adipogenesis of BMSCs *via* up-regulation of adipocyte-specific transcription factor PPAR-γ (39). Furthermore, an *in vivo* study using murine irradiation model indicated the increased burden of senescence in bone cells from day 1 to day 7 after irradiation (evidenced by increased expression of p21), followed by expansion of BMAT starting at day 7 and continuing until day 42 post irradiation (35). This study also indicated a direct correlation between the increased senescence burden in the bone tissue and up-regulation of mir-27a, which is known to be involved in obesity and regulation of adipose-tissue related transcription factors (40). These studies provide strong evidence for role of senescent microenvironment in expansion of BMAT.

DNA damage

DNA damage can be caused by exogenous factors such as Ionizing Radiation (IR), chemotherapeutic agents, and Ultraviolet (UV) light exposure, as well as endogenous factors such as ROS that are generated by mitochondria in the process of ATP production (41). These factors have been shown to cause impairment of osteoblastogenesis, and enhanced adipogenesis within the bone microenvironment. Pre-clinical and clinical studies have shown that cancer treatment using IR or chemotherapy leads to significant expansion of BMAT, which may contribute to the progressive bone loss in cancer survivors (42–44). In addition, it is shown that aging is associated with an intrinsic defect in osteoblasts, due to accumulation of DNA damage, leading to decreased osteoblast number, compromised osteoblast function, and induction of osteoclast formation (45). This study employed young (6 months) and old (20-24months) Osx1-Cre; TdRFP-mice and showed that the number of TdRFP-Osx1 cells are decreased by 50% in the BM of old male and female mice as compared to young mice. The TdRFP-Osx1 cells obtained from old mice also exhibited increased levels of DNA damage and senescence markers, such as formation of γ-H2AX foci, phosphorylation of p53, and G1 cell cycle arrest. BMSCs obtained from old mice also exhibited increased expression of SASP markers, leading to increased osteoclast formation, as well as increased expression of the adipogenic transcription factor PPAR-γ (45).

Murine studies using radiation-induced osteoporosis had indicated that accumulation of DNA damage leads to significant increase in the percentage of adipocytes within the BM. In addition, proteosome inhibitors or sclerostin neutralizing antibody reduced the BMA and prevented the trabecular bone structural deterioration post-radiation, *via* induction of DNA-repair (at least partially) (46, 47).

Although these studies provide evidence for the role of DNA damage in expansion of BMAT, the exact underlying mechanisms are not fully understood. However, induction of senescence (35) and the altered expression of genes involved in regulating the fate specification of BMSCs toward osteoblast and adipocyte lineages are among possible mechanisms. In addition, these studies suggest that mitigation of DNA damage can be employed as an approach for reducing BMA and improving the bone architecture post radiation.

Extrinsic mechanisms involved in age-related bone loss and BMAT expansion

Extrinsic factors such as disrupted hormonal status, malnutrition, and reduced physical activity, have an important role in disturbed skeletal homeostasis in aging,

leading to inhibited bone formation and enhanced bone resorption (48).

Endocrine Aging

Bone growth and maintenance of the skeleton is regulated *via* different endocrine factors (hormones) such as estrogens and androgens (49, 50). Fuller Albright proposed 70 years ago, that osteoporosis in women was caused by estrogen deficiency (51) and that bone loss induced *via* ovariectomy in women can be reversed by estrogen therapy (52). Estrogen is involved in molecular signaling in bone and regulation of BMAds (53–55) as estrogen is a positive regulator of osteogenesis through activation of estrogen receptor (ER)-dependent cytoplasmic kinases, BMPs and Wnt signaling (56, 57).

Testosterone exhibits an anabolic impact on bone formation in the periosteal surface in mice (58), and that oral administration of testosterone reduces the accelerated bone loss in orchiectomized mice (59). Gradual reduction in the testosterone levels in aging men are associated with reduction in bone mass (60, 61), and osteoblast dysfunction (62). In a clinical study of 350 men between the ages of 20-90 years, the levels of bioavailable testosterone were decreased by 64%, and bioavailable estrogen by 47% in old versus young individuals. This study also indicated that age-related bone loss in men is associated with decline in testosterone as well as estrogen (63). Another human study investigated the impact of endogenous estrogen and testosterone production on bone, using 59 elderly men and demonstrated that estrogen is the dominant sex-steroid hormone protecting men from age-related bone resorption, whereas both hormones of estrogen and testosterone are critical for bone formation (64).

Several mechanisms have been proposed to be involved in mediating the direct/indirect roles of estrogen deficiency in accelerated bone loss. Estrogen deficiency is involved in increased expression of pro-inflammatory cytokines in the bone microenvironment such as TNFα, IL1, IL-6 and receptor activator of RANKL/OPG/RANK system that regulates osteoclast differentiation (65–67). Estrogen deficiency also leads to decreased production of endogenous antioxidants (68, 69), which together with the elevated ROS production and the senescence microenvironment observed during aging or in obese mice and human, can lead to significantly increased levels of oxidative stress in the bone microenvironment (70, 71).

Studies using ovariectomized rats and postmenopausal women revealed increased bone turnover in response to estrogen deficiency, i.e. increased bone resorption and bone formation, manifested by increased number of osteoblast precursors, osteoblast proliferation and increased osteoblast number (72, 73). However, the increased bone formation levels are not enough to account for the bone loss due to elevated bone resorption, thereby leading to bone loss.

An interesting question that has been raised is whether the biological sex has an impact on the expansion of BMAT during aging? Griffith et al, investigated BMD and BMAT in the lumbar spine of 259 healthy subjects (145 females, 114 males; age range: 62-90 years) using MR spectroscopy of L3 vertebral body, and revealed that in males, BMAT increases gradually throughout life, whereas in females, BMAT increased between 55 and 65 years (74). BMAT in the vertebral bones in females with the age of more than 60 years increased by nearly 10% higher compared to age-matched males, indicating the positive impact of estrogen deficiency on BMAT expansion. In addition, human studies have shown that aging and loss of steroid hormones make women more vulnerable to the negative impacts of BMAT on loss of trabecular bone at the spine and femoral neck, and greater loss of spine strength (75), while in men vertebral BMAT is significantly increased with osteoporosis (76). Table 1 provides a summary of several clinical and preclinical studies related to association of endocrine aging and BMAT.

Another question that has been raised recently is whether gender-affirming interventions have an impact on bone microstructure and BMA?

Gender-affirming interventions using hormone therapy or surgery aim to align the physical characteristics with an individual's gender identity (85). Bretherton et al. recently employed high-resolution peripheral quantitative computed tomography of the distal radial and tibial microarchitecture and showed that trans men have normal bone microarchitecture as compared to cis female controls, whereas trans women had deteriorated bone microarchitecture compared to cis male controls (86). In addition, Nasomyont et al. showed lower bone mass acquisition and greater increases in BMAT indices in Transgender and Gender Non-Conforming (TGNC) youth after 12 months of pubertal suppression with gonadotropin-releasing hormone agonists (87). Additional investigations are required to establish the impacts of gender-affirming interventions on bone and BMA, and the related underlying mechanisms, also in the context of aging, obesity, and diabetes.

Obesity and diabetes

Bone fragility and microstructural changes in BM associated with T2D

Aging, osteoporosis and metabolic diseases such as obesity and diabetes robustly affect microstructural changes in the BM and contribute to impairment of bone homeostasis, which leads to higher risk of bone fractures (88, 89). The altered cellular landscape and molecular networks within the bone microenvironment in obesity and diabetes induce changes in trabecular and cortical bone volume or increased amount of

TABLE 1 Summary of several clinical and preclinical studies related to investigating the association of endocrine aging and BMAT expansion .

Study	Design	Outcome	Reference
The Effect of Roux-en-Y Gastric Bypass on Bone Marrow Adipose Tissue and Bone Mineral Density in Postmenopausal, Nondiabetic Women	14 postmenopausal, nondiabetic obese women were scheduled for laparoscopic Roux-en-Y gastric bypass surgery (RYGB).	Decrease in BMAT at the level of the L3-L5 vertebrae, 12 months post-surgery measured by quantitative chemical shift imaging (QCSI) with magnetic resonance imaging (MRI), as well as decrease in vertebral volumetric BMD (vBMD).	(77)
Short-Term Effect of Estrogen on Human Bone Marrow Fat.	Measured vertebral bone marrow fat fraction every week for 6 consecutive weeks in 6 postmenopausal women before, during, and after 2 weeks of oral 17-β estradiol treatment (2 mg/day).	17-β estradiol rapidly reduced the marrow fat fraction, suggesting that 17-β estradiol regulates bone marrow fat independent of bone mass.	(78)
Effects of estrogen therapy on bone marrow adipocytes in postmenopausal osteoporotic women	bone biopsies from a randomized, placebo-controlled trial involving 56 postmenopausal osteoporotic women (mean age, 64 years) treated either with placebo (PL, n = 27) or transdermal estradiol (0.1 mg/d, n = 29) for 1 year.	AV/TV and BMAd number increased in the PL group but were unchanged (BMAd) or decreased in the E group. E treatment also prevented increases in mean adipocyte size over 1 year. Increased bone loss and bone marrow adipocyte number and size in postmenopausal osteoporotic women may be due estrogen deficiency.	(79)
Association of vertebral bone marrow fat a with trabecular BMD and vertebral fracture in older adults	257 participants, mean age was 79 years,	Vertebral BMA was associated with lower BMD and vertebral fractures in older women.	(80)
Correlation of vertebral bone marrow fat content with abdominal adipose tissue, lumbar spine, bone mineral density, and blood biomarkers in women with type 2 diabetes mellitus	Thirteen postmenopausal women with T2D	There is a correlation between BMA and subcutaneous adipose tissue in women with and without T2D and with visceral adipose in women with T2D.	(81)
Bone Marrow Adiposity and prediction ofBone Loss in Older Women	women (n = 148) and mean age (80.9 ± 4.2) years	BMA is associated with higher loss of trabecular bone at the spine area and femoral neck, and greater loss of spine strength	(75)
Changes in BMA during aging in males and females	145 females, 114 males; age range (62-90) years.	Marrow fat content increases significantly in female subjects of age range (55 and 65) years of age while male subjects increase in marrow fat at a steady rate. Females aged older than 60 years have a higher marrow fat content than males.	(74)
Effects of risedronate on bone marrow adipocytes in postmenopausal women	Transiliac bone biopsies from a randomized, placebo-controlled clinical trial in women with postmenopausal osteoporosis (n=14 per group)	Risedronate reduced age-dependent expansion of BMAT, compared to placebo.	(82)
Analysis of vertebral bone mineral density, marrow perfusion, and fat content in healthy men and men with osteoporosis using dynamic contrast-enhanced MR imaging and MR spectroscopy	MR imaging of the lumbar spine in 90 men (mean age, 73 years; range, 67-101 years)	Increased BMA in osteoporotic patients compared to osteopenic subjects. Increased BMA in osteopenic subjects compared to healthy control individuals.	(76)
Effect of estrogens on bone marrow adipogenesis and Sirt1 in aging C57BL/6J mice	Young skeletally mature (5 months) and old (22–24 months) female C57BL/6J mice were either gonadally intact, OVX or OVX +E2	Significant decreasing effect of E2 on BMAT in both young and old mice.	(83)
Analysis of bone marrow fat content in relation to bone remodeling and serum chemistry in intact and ovariectomized dogs	Beagle dogs (6 control, 9 ovariectomized)	BMAT was expanded (11 months post ovariectomy) together with reduced hematopoietic volume fraction, associated with decrease in estrogen levels.	(84)

BMAT, leading to a detrimental effect on bone quality and strength.

Osteoporosis and aging are characterized with decreased BMD, along with increased BMAT and accompanied by increased resorption activity in the BM in mice and humans (90, 91). Metabolic complications associated with impairment of glucose homeostasis have been shown to contribute to higher risk of bone fractures and accelerate the manifestation of bone fragility and osteoporosis. Previous studies in mice and humans under High Fat Diet (HFD) condition have reported increased BMAT formation evaluated by measurement of BMAT volume, BMAd size and number (70, 92–98), which was correlated with increased, unchanged, or decreased BMD in mice depending on the employed diabetic model (T1D or T2D) (70, 71, 94, 95, 99), but associated with a higher risk of fractures. Therefore, recent studies have focused on the design of experiments to include measurement of BMAT parameters in relation to bone fragility. Indeed, our recent study using T2D diabetic animal model (HFD in combination with streptozotocin) confirmed the expansion of BMAT in T2D mice along with decreased bone volume, which

contributed to the delayed bone healing in monocortical fracture model (100).

Interestingly in humans, obesity is associated with increased BMD in children and adults (89, 101, 102). Along with this finding, several clinical studies including ours have noted reduced bone turnover in patients with metabolic diseases (71, 103). Paradoxically, there are also clinical studies suggesting that women and men with high BMI and T2D may be protected from osteoporosis, due to increased BMD (104–109). These clinical studies are summarized in Table 2. The mechanisms underlying the higher bone mass but reduced bone turnover in patients with obesity and T2D were partially explained by our clinical study in obese subjects that revealed hypermetabolic status of BMSCs and accelerated senescent BM microenvironment contributing to the bone fragility (71). These changes lead to impairment of the bone material properties and increased cortical porosity in T2D (126). However, further follow up studies are needed to collect more clinical data on bone microstructural parameters along with BMAT volume in relation to bone quality in specific target groups of patients, to better predict the fracture risk.

Human studies had shown that expansion of visceral fat is associated with enhanced adipocyte formation in the BM microenvironment in osteoporotic obese women (97). Furthermore, BMAT was shown to be expanded in the bone biopsies from overweight and obese subjects compared to healthy age-matched individuals (127). Similarly, BMSCs obtained from obese men exhibited enhanced adipocyte differentiation and accelerated senescence phenotype that would contribute to the skeletal fragility in obesity (71). T2D is another risk factor in skeletal fragility and osteoporosis in aging men and postmenopausal women (128–130), despite the increase in BMD or independent of BMD (131, 132). The combination of obesity and T2D were shown to exhibit higher serum insulin levels and BMA at the lumbar spine and femoral metaphysis compared to the subjects without T2D. In addition, it is shown that lumbar spine BMD is inversely associated with the lumbar adiposity in adults with morbid obesity, and that morbid obesity and T2D exhibits a higher BMA than non-diabetic controls of similar weight (98). In agreement with these observations, Sheu et al. reported that in 38 old diabetic men there was a higher vertebral BMA, spine and hip BMD and a higher fracture risk when compared to control men without diabetes (133).

Fazeli et al. examined how human BMAT responds to acute nutrient changes by employing 10 days of high calorie protocol followed by 10 days fasting protocol. This study indicated a significant increase in vertebral BMAT after high calorie feeding and fasting, and that high calorie feeding up-regulated the inflammatory marker TNFα in BMAds, which was decreased upon fasting (134).

Kim et al., reported that BMAT levels were reduced after bariatric surgery in obese T2D patients compared to the obese non-diabetic individuals, and that there was an inverse correlation between the changes in BMAT in lumbar spine and femoral neck and spine BMD (135). In addition, 6 weeks of low calorie diet was reported to induce weight loss in obese T2D subjects (19 women and 10 men) together with decrease in vertebral BMA (136).

Pre-clinical studies using murine models have also provided evidence for impact of obesity and diabetes on BMAT and bone mass. HFD-induced-obesity using C57Bl/6J male mice, was reported to lead to enhanced adipocyte differentiation of BMSCs, associated with increased *in vivo* BMAT volume and decreased trabecular and cortical bone mass (70). Another *in vivo* study in male C57Bl/6J mice reported that HFD-induced obesity and T2D compromised the skeletal macro- and micro-architecture of the bone (137). In addition, increased bone resorption is also shown to contribute to the reduced bone mass and strength in a pre-clinical obese-diabetic mouse model (138).

Transition of metabolic status from obesity to insulin resistance and T2D is accompanied with changes in glucose, insulin and circulating lipid levels, as well as changes in inflammatory pathways and hormonal alterations. The relative contribution of each of these factors to the expansion of BMAT, compromised bone quality, and skeletal fragility remain unclear. In addition, the length of exposure to obesogenic and diabetic conditions has an impact on the effect of these conditions on the bone microstructure in mice and humans. Therefore, it is important to include more longitudinal studies to investigate the changes of bone and BMAT parameters measured at several timepoints, in order to better understand the impact of different elements of obesity and T2D on the bone quality and strength and to determine the parameters that can be employed for predicting the risk of fracture.

Role of BMSC dysfunction and BMAds in pathogenesis of increased bone fragility in obesity and T2D

Although different mechanisms have been proposed to be involved in pathogenesis of bone fragility in obesity and T2D, the underlying cellular and molecular events are not yet fully understood. Impaired BMSC function and differentiation is one of the key mechanisms that is suggested to have role in expansion of BMAT and decreased bone mass and quality in obesity and T2D, thereby leading to increased skeletal fragility during aging.

Increased levels of oxidative stress and senescence within the bone microenvironment in obesity and T2D are among factors that can contribute to BMSC dysfunction, and a shift in BMSC differentiation phenotype, favoring adipogenesis than osteogenesis (139–142).

BMSCs from obese subjects are shown to exhibit a hypermetabolic state and a shift of molecular phenotype

TABLE 2 Clinical studies investigating effect of obesity and diabetes on bone in men & women.

Study	Type of study	Participants	Main outcome	Reference
Relation between body size and bone mineral density in elderly men and women	Cross-sectional	1492 ambulatory white adults, 55–84 years	High BMI was positively related with high BMD. the mechanical effect of weight increased BMD.	(110)
Are general obesity and visceral adiposity in men linked to reduced bone mineral content resulting from normal ageing? A population-based study	RCT	Polish men (272 men, 20–60 years)	Visceral adiposity (assessed by waist/hip ratio) was associated with reduced bone mass in men.	(111)
Associations between components of the metabolic syndrome versus bone mineral density and vertebral fractures in patients with type 2 diabetes	RCT	187 men (28–83 years) and 125 postmenopausal women (46–82 years) with type 2 diabetes	Obesity and diabetes were associated with increased femoral neck bone mineral density. Effects on fracture risk were site dependant.	(112)
Is obesity protective for osteoporosis? Evaluation of bone mineral density in individuals with high body mass index	RCT	398 patients (291 women, 107 men, age 44.1 + 14.2 years, BMI 35.8 + 5.9 kg/m^2	Obesity had a negative impact on lumbar BMD than expected for that age.	(113)
Bone mineral density of the spine in normal Japanese subjects using dual-energy X-ray absorptiometry: effect of obesity and menopausal status	RCT	N= (1,048 women, age 40-49 and >50) Menopause N= (248 men, age 20-29 and >50)	Bone mineral density measurements at the lumbar spine using DEXA-scan revealed that bone loss starts at early menopause stage and concluded a positive correlation between obesity and BMD, particularly in postmenopausal women.	(114)
Determinants of total body and regional bone mineral density in normal postmenopausal women–a key role for fat mass	RCT	N= (140 post-menopausal women) (age= 45-71 years, mean 58years)	Total body BMD was positively related to fat mass, and similar relationships were found in other body regions as in the lumbar spine and proximal femur.	(115)
Obesity and Postmenopausal Bone Loss: The Influence of Obesity on Vertebral Density and Bone Turnover in Postmenopausal Women.	Cross-sectional	N= (176 women aged 45-71 years). (49 perimenopausal) (28 obese peri-menopausal) (49 obese post-menopausal) Mean age was the same yet there was significant change in the weight.	In non-obese post-menopausal women, BMD was lower, and higher serum osteocalcin (OC) and fasting urinary calcium to creatinine (Ca : Cr). Obesity may be protective in post-menopause state.	(106)
Influence of obesity on bone density in postmenopausal women	Case-control	N= (588 women) Age = (41 to 60 years) Group 1: (1-6 years since menopause) Group 2: (6-10 years since menopause)	Positive influence of obesity at increasing BMD at lumbar spine, femoral neck (FN), and trochanter (TR) between the groups, yet the role of obesity is demolished by the impact of estrogen deficiency and aging.	(116)
Cigarette Smoking, Obesity, and Bone Mass	Case-control	N= (84 healthy, peri- and postmenopausal women) were studied prospectively over 3.5 years.	Menopause combined with obesity led to bone loss, independent of smoking.	(117)
Plasma Leptin Values in Relation to Bone Mass and Density and to Dynamic Biochemical Markers of Bone Resorption and Formation in Postmenopausal Women	Case-control	N= (54 post-menopausal women)	Positive correlation of leptin plasma levels with body weight, fat mass and BMD yet no correlation with biochemical markers of either osteoclastic or osteoblastic activity.	(118)
Calcium Supplementation Suppresses Bone Turnover During Weight Reduction in Postmenopausal Women	Randomized-double blind placebo control	N= (43 post-menopause women) Subject to take calcium citrate 1gm/day (N= 21), subjects to take placebo (N=22).	Obesity in postmenopausal women tend to increase MD and that weight loss in postmenopausal women should consume calcium supplement (1500 mg/day) to prevent a high rate of bone turnover and loss in BMD.	(119)
Factors affecting bone mineral density in postmenopausal women	Cross-sectional	N= (537 women) Age (of 67.9 ± 6.7 years and mean menopause duration (MD) of 15.8 ± 5.1 years)	Obesity may protect again osteoporosis as its associated with higher BMD also significant positive association between osteoporosis and menopausal duration.	(120)
Influence of obesity on vertebral fracture prevalence and vitamin D status in postmenopausal women	RCT	N= (429 post-menopausal women (mean age, weight and BMI of 59.5 ± 8.3 (50 to 83) years, 75.8 ± 13.3 (35 to 165) kgs and 29.9 ± 5.2 (14.6 to 50.8) kg/m^2)	Obesity was correlated with increased BMD yet vertebral fractures were related to duration of menopause, low vitamin D intake and increased osteoporosis.	(121)

(Continued)

TABLE 2 Continued

Study	Type of study	Participants	Main outcome	Reference
Relationship between body composition, body mass index and bone mineral density in a large population of normal, osteopenic and osteoporotic women	RCT	N= (6,249 Italian women, aged 30–80 years)	Obesity was increased with age yet is believed to be protective against osteoporosis as BMD is increased, yet obesity did not decrease the risk of osteopenia, with aging above 50years, the risk of osteopenia and osteoporosis is increased, respectively.	(122)
Evaluation of bone loss in diabetic postmenopausal women	Cross-sectional	N= (200 diabetic postmenopausal women with 400 non-diabetic postmenopausal women) Age (65.23 ± 4.80 non-diabetic vs. 66.91 ± 5.78 years in diabetic)	Diabetes increases the risk of osteopenia and osteoporosis when comparing postmenopausal diabetic and no-diabetic women.	(123)
Influence of obesity on bone mineral density in postmenopausal asthma patients undergoing treatment with inhaled corticosteroids	Case-control	N= (46 patients with asthma taking inhalations of **corticosteroids**, age 62.5 ± 10.6 and 60 healthy female controls, age 63.0 ± 6.1) all post-menopaused.	Obesity in asthmatic patient is positively correlated with decreased osteoporosis yet this effect is overcome by aging and years since menopause.	(124)
Obesity Is Not Protective against Fracture in Postmenopausal Women: GLOW	RCT	N= (60,393 women aged >55 years) menopause women.	Obesity is not protective against fracture risk in ankle and upper leg was significantly higher in obese than in nonobese women.	(125)

towards adipocyte progenitors, together with altered expression of genes involved in metabolic regulation, such as glycolysis and oxidoreductase activity. The hyper-metabolic state of BMSCs in obesity is associated with increased abundance of leptin receptor and insulin receptor positive cells and an accelerated senescence phenotype and increased ROS production (71). Leptin and leptin receptor signaling promotes adipogenesis in the BM, in response to HFD (143). In addition, insulin receptor signaling is reported to be increased under oxidative stress condition, associated with cellular senescence phenotype (144).

The above-mentioned studies provide evidence for the role of cell autonomous defects in BMSCs in pathogenesis of bone fragility in obesity and T2D. However, Devlin et al. employed the male TALLYHO/JngJ murine model of T2D and indicated that in the context of early onset T2D, impaired bone formation and the consequent skeletal deficits are due to the altered bone microenvironment, but not the cell autonomous defects in BMSCs (145).

Increasing evidence has shown that BMAds may also play an important role in altered bone microenvironment in obesity and T2D (146–148). BMAds secrete a number of adipokines and cytokines that affect bone cell functions directly or indirectly, e.g. through modulation of inflammation within the bone microenvironment (149).

IL-6 is one of the cytokines that is secreted by BMAds and increases osteoclast formation and bone resorption, thereby leading to decreased BMD in men and women (150, 151). IL-6 enhances osteoclastogenesis by stimulating the expression of RANKL on stromal/osteoblastic cells (152), and also by direct support of osteoclast formation through RANKL-independent mechanisms (153).In addition, Li et al. revealed that IL-6 KO mice are protected against HFD-induced trabecular bone loss, and the associated BMSC senescence and BMAT expansion (154). BMAd-derived factors that can affect skeletal homeostasis are reviewed by Aaron et al. (155).

Can the deleterious effects of obesity and T2D on the skeleton be accelerated by postmenopausal estrogen deficiency?

In post-menopausal women, obesity is another accompanying complication besides estrogen deficiency that affects energy homeostasis and metabolism of bone and adipose tissue (156). Menopause is associated with shift in BMSCs phenotype towards adipogenesis, reduced osteogenesis, increase in the osteoporotic bone phenotype and fracture risk (157–160). Possible mechanisms of deleterious effects of estrogen deficiency on bone metabolism is discussed above (Endocrine aging and Table 1). Combination of estrogen deficiency and obesity includes a chain of pathologic events, leadingto disturbed skeletal homeostasis that further contribute to the accelerated aging of BMSCs and compromised bone regeneration and increased fracture risk (161). Several clinical studies in postmenopausal women (presented in Table 2) have however shown that obese postmenopausal women exhibit increased BMD, that is paradoxically associated with increased bone fragility and fracture risk, whereas the status of BMA is not evaluated in these studies (116, 162).

Interventions to reduce BMA, enhance bone mass, and reduce bone fragility

To reverse the detrimental effects of metabolic complications on bone fragility, various interventions have been applied including diet, exercise, or pharmacological treatment. However, in many of these studies there is limited information on BMAT changes in relation to bone and energy metabolism, especially in human studies, as the evaluation of BMAT (fat content in BM) is not a common clinical practice.

Nutritional intervention

A "Bone Healthy Diet" should contain the nutritional components that are required for normal skeletal homeostasis, such as calcium, vitamin D, vitamin C, vitamin K, vitamin A, protein, and phytoestrogens, that help enhancing BMD and reduce bone loss (163).

1,25 dihydroxy vitamin D is the active form of vitamin D, and its main function in bone is to modulate osteoblast proliferation, differentiation, and providing suitable microenvironment for bone mineralization. Presence of calcitriol in aging osteoblast cultures revealed enhanced osteoblastic function (164). Different mechanisms of action have been proposed for the effect of vitamin D on osteoblast differentiation and bone formation (165, 166). Many studies have revealed the significance of Vitamin D deficiency in inducing bone loss, osteoporosis, and affecting the function of skeletal muscle. It is shown that vitamin D restricted diet (for 28 days) leads to decreased bone mineral content and muscle mass in ovariectomized rats challenged with HFD (167). Vitamin D deficiency in the elderly people causes secondary hyperparathyroidism and increased risk of hip fracture (168), as low circulating levels of vitamin D increases parathyroid hormone (PTH) levels, which induce bone resorption and bone loss in elderly subjects (169–171). Vitamin D combined with calcium is also used to prevent osteoporosis (172).

Is there a connection between vitamin D and BMA regulation?

Calcitriol has shown anti-adipogenic effects in cultures of 3T3-L1 cells (173, 174) as it inhibits the transactivation capacity of PPARγ, through Vitamin D Receptor (VDR) signaling. VDR could inhibit PPARγ transactivation activity, by competing for binding to their common heterodimer partner RXR (175). In VDR null mice, the BMSCs exhibited high expression of PPARγ, along with higher expression of DKK1 and SFRP2, that are inhibitors of the pro-osteogenic canonical Wnt signaling pathway, and the expression of these Wnt inhibitors was downregulated by calcitriol in wild-type BMSCs, in the absence or presence of adipogenic inducers (176). Similar results were observed in human BMSCs (177).

Anti-adipogenic effect of vitamin D is also observed in femur-derived mouse BMSCs and is mediated through inhibiting the expression of aP2 and adipsin (178). Vitamin D3 supplementation is recommended upon aging (179) and leads to increasing the circulating IGF-1 levels (180). Increasing the levels of circulating IGF-1 may help in counteracting the age associated BMAT expansion (181, 182). Thus, these *in vitro* and *in vivo* studies suggest that vitamin D signaling may contribute to the regulation of BMA. However, more clinical investigations are required to directly examine the effect of vitamin D supplementation on BMA in human, and to assess the correlation between vitamin D levels, BMAT volume, and fracture risk.

Lifestyle factors

Creating awareness and understanding of the lifestyle factors that may delay the aging bone phenotype is crucial. One of the most important lifestyle factors is the physical activity (114). Physical activity leads to strengthening of the hip and spine due to skeletal loading and inducing bone formation at the stressed skeletal sites (183).

Styner et al. employed a murine model (4 weeks old female C57BL/6 mice) to investigate the impact of running exercise on the obesity associated BMAT and whether this is associated with increased bone quantity and quality (184). The study showed that BMAT was increased by 44% in diet-induced obesity measured by osmium-μCT, whereas exercise was associated with reduced BMAT (−48%), as well as increased trabecular bone volume (+19%), and higher bone stiffness in obese mice

The anti-diabetic drug, rosiglitazone, which is a PPARγ-agonist, is known to significantly increase BMA and fracture risk. It is shown that physical exercise significantly lowers BMA in rosiglitazone-treated male C57Bl/6J mice (185).

A randomized clinical trial investigated the effect of exercise on BMA in forty patients with chronic non-specific low back pain, and revealed that lumbar vertebral fat fraction was lower post exercise in these patients compared to the baseline (186). Chronic alcohol consumption is another risk factor in osteoporotic-bone loss associated with increased BMA (187). It is shown that 3 months of chronic alcohol consumption in the diet of 4-week-old male Sprague-Dawley rats leads to skeletal abnormalities together with increased BMA.

Pharmacological treatment

Several drugs have been developed to improve bone parameters in metabolic bone diseases. Additional challenge in treatment of bone diseases is now to reduce BMAT volume,

which may lead to increased bone mass and strength, together with decreased risk of bone fracture.

Several antidiabetic drugs have been tested in clinical settings for treatment of metabolic bone disease, including insulin-sensitizers such metformin, modified TZD analogs (PPARγ-independent), inhibitors of inflammatory molecules such as DPP4 (dipeptidyl peptidase-4). Ambrosi et al. has reported that DDP4 inhibition (secreted from adipocytes and increased with obesity in bones) in mouse model of obesity improved bone parameters and decreased BMAT (146). Similar results have been demonstrated in OVX female mice treated with DPP4 inhibitor (188). Clinical studies using DDP4 inhibitor, sitagliptin, showed improvement of bone turnover markers and decreased fracture risk in diabetic patients (189, 190).

Studies using metformin treatment in rodents and humans showed positive results or no changes in bone parameters suggesting that metformin might have a positive effect on bone metabolism in diabetic conditions, depending on the other medical complications associated with diabetes and length of disease manifestation. However, BMAT parameters were not evaluated in these conditions (191). Human studies of the Rochester cohort suggest that metformin decreases fracture risk in T2D patients (hazard ratio 0.7) (192). Although the ADOPT studies did not demonstrate beneficial effects of metformin on fracture risk (193), they showed decreased levels of bone resorption marker CTX and, contrary to the animal studies, decreased levels of bone formation marker P1NP (194). In a large case-control study metformin utilization was also associated with a reduction in the risk of fractures (195). In contrast, there are case control studies in which no association was observed between treatment with the insulin-sensitizing drug metformin and incidence of bone fractures in T2D patients (196).

In order to decrease the negative side effects of TZDs, novel TZD analogs with PPARγ independent effect on glucose metabolism have been developed. Stechschulte et al., reported that post-translational modifications of PPARγ at S112 and S273, which influence PPARγ pro-adipocytic and insulin sensitizing activities, improved bone parameters and decreased BMAT in lean and obese mice (197). Blocking PPARγ only at S273 by SR10171 had a beneficial effect on trabecular and cortical bone while maintaining its metabolic effect on glucose metabolism.

Another TZD analogue, with PPARγ independent affinity, MSDC-0602 has been reported to have a beneficial effect on bone parameters by decreasing osteoclast activation and BMAT formation in lean aged mice, while keeping its insulin sensitizing features (198). This drug is in clinical trial 2b (199).

Another category of pharmacological treatment used as anti-aging drugs has been tested to improve bone parameters and decreased bone fragility (e.g. resveratrol). Our recent study showed that resveratrol has anti-adipogenic effect along with decreased senescence in primary BMSCs isolated from patients with osteoporosis (34), which was also confirmed in animal studies with OVX rats (200, 201). However, the clinical relevance of these findings has not yet been investigated.

Sclerostin (SOST), osteocyte-secreted biomolecule with a negative impact on bone homeostasis (as it is an inhibitor of Wnt signaling), has become a potential drug target for anabolic treatment of diverse bone loss states (202). SOST circulating levels are increased with obesity, aging, and osteoporosis (203). Thus, neutralizing antibodies against sclerostin (SostAb) have been developed for testing its potential in clinical use to decrease bone fragility in osteoporosis and obesity. Using SostAb in animals showed improvement in fracture healing in diabetic mice (204) and OVX rats (205, 206). SostAb treatment in T2D rat models has also been shown to improve bone mass and strength (207). Clinical trials with SostAb have shown promising results with improvement of bone density and bone strength in postmenopausal women (208–210) Therefore, SostAb seems to be a promising osteoanabolic drug for treatment of skeletal fragility observed in osteoporosis, obesity and T2D (211). However, these clinical studies did not evaluate the effects of SostAb on BMAT. Recent studies in animal models suggest that SostAb may revert negative effect of rosiglitazone-induced increased BMAT in BM (212) and thus confirms its impact on adipogenesis of BMSCs (213).

Antiresorptive treatments

Several antiresorptive agents including bisphosphonates, or RANKL antagonist, denosumab have been proven to safely reduce fracture risk in various high-risk populations (214, 215). They are recommended as first-line therapy for patients with osteoporosis. However, using antiresorptive drugs in treatment of osteoporosis in T2D patients might not be the perfect choice as patients with metabolic diseases (obesity, insulin resistance or T2D) have decreased bone turnover and their use would just further diminish the bone homeostasis. In addition, a recent clinical study showed that denosumab-treated patients had improved HbA1c similar to the effect of other anti-diabetic drugs, suggesting its possible insulin sensitizing effect (216). Clinical and animal studies have indicated beneficial effect of denosumab on insulin sensitivity, bone formation and muscle strength (217). However, its impact on BMAT volume has not been evaluated yet and more clinical investigations are needed to include this parameter to measure in their outcomes.

Conclusion and future perspectives

Increased accumulation of BMAT in bones has been recognized as a feature of aging bones associated with increased fracture risk. However, endocrine, and metabolic disturbances in organism such as hormone deficiency, obesity, and T2D can accelerate the detrimental changes in bone homeostasis and contribute to the early onset of osteoporosis and microstructural changes that compromise the bone strength (Figure 1.). Several mechanisms underlie these symptoms including transcription

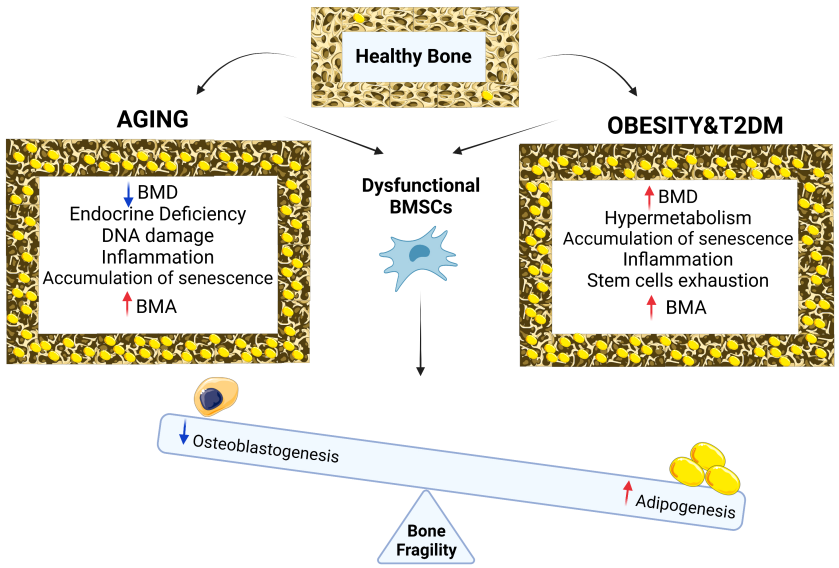

FIGURE 1
Chronological aging in bone is associated with reduction in BMD, endocrine deficiency, DNA damage, inflammation, accumulation of senescence, BMA and osteoporotic bone phenotype while with metabolic diseases such as obesity and type 2 diabetes, bone phenotype is associated with increased in BMD, cellular hypermetabolism, stem cell exhaustion, accumulation of senescence, inflammation, BMA and osteoporotic bone phenotype. Both conditions (aging vs metabolic diseases of obesity and T2D) result in BMSCs dysfunction leading to differentiation imbalance decreasing osteogenesis, increasing adipogenesis, BMA and bone fragility.

factors, DNA damage, ROS production, accumulation of senescent cells in BM microenvironment and secretion of bioactive molecules regulating function of BMSCs directing their fate towards BMAds. Using different animal models of osteoporosis and metabolic disorders, it has been shown that targeting senescent cells and regulation of hormonal levels can modulate the negative impact of expanded BMAT on bone loss fragility. More importantly, recent clinical interventions including patients with a broad range of age and complications reported that lifestyle modifications such as a special diet, caloric restriction, and physical activity may modulate BMAand improve bone parameters. However, more follow up studies are needed to evaluate the changes on bone structure and cellular modifications in real time at different timepoints, to establish the impact of such interventions on bone remodeling. Finally, including more imaging methods to evaluate bone and BMAT parameters in future clinical studies can facilitate further examination of the BMAT and its roles in skeletal fragility in the context of obesity and T2D in aging population, thereby providing novel therapeutic possibilities and also possibly, development of better approaches for estimation of fracture risk.

Authors contributions

DA, MT, FF and AJ researched data, wrote and reviewed the manuscript. MK contributed to the conceptual framing of the manuscript. DA and AJ edited the manuscript. All authors contributed to the article and approved the submitted version

Funding

(MT) START UP Research Program from IPHYS, the Czech Science Foundation GACR 20-03586S, GACR 22-12243S, EFSD/NovoNordisk foundation Future leaders award (NNF20SA0066174). (AJ, MK) Olav Thon Foundation (2019).

Conflict of interest

The authors declare that the research was conducted in the absence of any commercial or financial relationships that could be construed as a potential conflict of interest.

Publisher's note

All claims expressed in this article are solely those of the authors and do not necessarily represent those of their affiliated organizations, or those of the publisher, the editors and the reviewers. Any product that may be evaluated in this article, or claim that may be made by its manufacturer, is not guaranteed or endorsed by the publisher.

References

1. Armas LA, Recker RR. Pathophysiology of osteoporosis: New mechanistic insights. *Endocrinol Metab Clin North Am* (2012) 41:475–86. doi: 10.1016/j.ecl.2012.04.006

2. Johnell O, Kanis JA. An estimate of the worldwide prevalence and disability associated with osteoporotic fractures. *Osteoporos Int* (2006) 17:1726–33. doi: 10.1007/s00198-006-0172-4

3. Liu J, Curtis EM, Cooper C, Harvey NC. State of the art in osteoporosis risk assessment and treatment. *J Endocrinol Invest* (2019) 42:1149–64. doi: 10.1007/s40618-019-01041-6

4. Kanis JA. Assessment of fracture risk and its application to screening for postmenopausal osteoporosis: synopsis of a WHO report. *WHO Study Group Osteoporos Int* (1994) 4:368–81. doi: 10.1007/BF01622200

5. Kanis JA, Melton LJ 3rd, Christiansen C, Johnston CC, Khaltaev N. The diagnosis of osteoporosis. *J Bone Miner Res* (1994) 9:1137–41. doi: 10.1002/jbmr.5650090802

6. Kassem M, Marie PJ. Senescence-associated intrinsic mechanisms of osteoblast dysfunctions. *Aging Cell* (2011) 10:191–7. doi: 10.1111/j.1474-9726.2011.00669.x

7. Marie PJ, Kassem M. Osteoblasts in osteoporosis: Past, emerging, and future anabolic targets. *Eur J Endocrinol* (2011) 165:1–10. doi: 10.1530/EJE-11-0132

8. Charatcharoenwitthaya N, Khosla S, Atkinson EJ, McCready LK, Riggs BL. Effect of blockade of TNF-alpha and interleukin-1 action on bone resorption in early postmenopausal women. *J Bone Miner Res* (2007) 22:724–9. doi: 10.1359/jbmr.070207

9. Boonen S, Mohan S, Dequeker J, Aerssens J, Vanderschueren D, Verbeke G, et al. Down-regulation of the serum stimulatory components of the insulin-like growth factor (IGF) system (IGF-I, IGF-II, IGF binding protein [BP]-3, and IGFBP-5) in age-related (type II) femoral neck osteoporosis. *J Bone Miner Res* (1999) 14:2150–8. doi: 10.1359/jbmr.1999.14.12.2150

10. Locatelli V, Bianchi VE. Effect of GH/IGF-1 on Bone Metabolism and Osteoporsosis. *Int J Endocrinol* (2014) 2014:235060. doi: 10.1155/2014/235060

11. Lopez-Otin C, Blasco MA, Partridge L, Serrano M, Kroemer G. The hallmarks of aging. *Cell* (2013) 153:1194–217. doi: 10.1016/j.cell.2013.05.039

12. Seeman E. Pathogenesis of bone fragility in women and men. *Lancet* (2002) 359:1841–50. doi: 10.1016/S0140-6736(02)08706-8

13. Khosla S, Riggs BL. Pathophysiology of age-related bone loss and osteoporosis. *Endocrinol Metab Clin North Am* (2005) 34:1015–30. doi: 10.1016/j.ecl.2005.07.009

14. Rauch A, Haakonsson AK, Madsen JGS, Larsen M, Forss I, Madsen MR, et al. Osteogenesis depends on commissioning of a network of stem cell transcription factors that act as repressors of adipogenesis. *Nat Genet* (2019) 51:716–27. doi: 10.1038/s41588-019-0359-1

15. Rozman C, Feliu E, Berga L, Reverter JC, Climent C, Ferran MJ. Age-related variations of fat tissue fraction in normal human bone marrow depend both on size and number of adipocytes: a stereological study. *Exp Hematol* (1989) 17:34–7.

16. Reinisch A, Etchart N, Thomas D, Hofmann NA, Fruehwirth M, Sinha S, et al. Epigenetic and *in vivo* comparison of diverse MSC sources reveals an endochondral signature for human hematopoietic niche formation. *Blood* (2015) 125:249–60. doi: 10.1182/blood-2014-04-572255

17. Han L, Zhang Y, Wan S, Wei Q, Shang W, Huang G, et al. Loss of chemerin triggers bone remodeling *in vivo* and in vitro. *Mol Metab* (2021) 53:101322. doi: 10.1016/j.molmet.2021.101322

18. Herrmann M. Marrow Fat-Secreted Factors as Biomarkers for Osteoporosis. *Curr Osteoporos Rep* (2019) 17:429–37. doi: 10.1007/s11914-019-00550-w

19. Jafari A, Qanie D, Andersen TL, Zhang Y, Chen L, Postert B, et al. Legumain Regulates Differentiation Fate of Human Bone Marrow Stromal Cells and Is Altered in Postmenopausal Osteoporosis. *Stem Cell Rep* (2017) 8:373–86. doi: 10.1016/j.stemcr.2017.01.003

20. de Magalhães JP, Passos JF. Stress, cell senescence and organismal ageing. *Mech Ageing Dev* (2018) 170:2–9. doi: 10.1016/j.mad.2017.07.001

21. Roger L, Tomas F, Gire V. Mechanisms and regulation of cellular senescence. *Int J Mol Sci* (2021) 22. doi: 10.3390/ijms222313173

22. Zhu X, Chen Z, Shen W, Huang G, Sedivy JM, Wang H, et al. Inflammation, epigenetics, and metabolism converge to cell senescence and ageing: the regulation and intervention. *Signal Transduct Target Ther* (2021) 6:245. doi: 10.1038/s41392-021-00646-9

23. Childs BG, Durik M, Baker DJ, van Deursen JM. Cellular senescence in aging and age-related disease: from mechanisms to therapy. *Nat Med* (2015) 21:1424–35. doi: 10.1038/nm.4000

24. Coppe JP, Desprez PY, Krtolica A, Campisi J. The senescence-associated secretory phenotype: the dark side of tumor suppression. *Annu Rev Pathol* (2010) 5:99–118. doi: 10.1146/annurev-pathol-121808-102144

25. Coppe JP, Patil CK, Rodier F, Sun Y, Munoz DP, Goldstein J, et al. Senescence-associated secretory phenotypes reveal cell-nonautonomous functions of oncogenic RAS and the p53 tumor suppressor. *PloS Biol* (2008) 6:2853–68. doi: 10.1371/journal.pbio.0060301

26. Swanson EC, Manning B, Zhang H, Lawrence JB. Higher-order unfolding of satellite heterochromatin is a consistent and early event in cell senescence. *J Cell Biol* (2013) 203:929–42. doi: 10.1083/jcb.201306073

27. Tchkonia T, Zhu Y, van Deursen J, Campisi J, Kirkland JL. Cellular senescence and the senescent secretory phenotype: therapeutic opportunities. *J Clin Invest* (2013) 123:966–72. doi: 10.1172/JCI64098

28. von Zglinicki T, Saretzki G, Ladhoff J, d'Adda di Fagagna F, Jackson SP. Human cell senescence as a DNA damage response. *Mech Ageing Dev* (2005) 126:111–7. doi: 10.1016/j.mad.2004.09.034

29. Ziegler DV, Wiley CD, Velarde MC. Mitochondrial effectors of cellular senescence: beyond the free radical theory of aging. *Aging Cell* (2015) 14:1–7. doi: 10.1111/acel.12287

30. Kajkenova O, Lecka-Czernik B, Gubrij I, Hauser SP, Takahashi K, Parfitt AM, et al. Increased adipogenesis and myelopoiesis in the bone marrow of SAMP6, a murine model of defective osteoblastogenesis and low turnover osteopenia. *J Bone Miner Res* (1997) 12:1772–9. doi: 10.1359/jbmr.1997.12.11.1772

31. Farr JN, Fraser DG, Wang H, Jaehn K, Ogrodnik MB, Weivoda MM, et al. Identification of Senescent Cells in the Bone Microenvironment. *J Bone Miner Res* (2016) 31:1920–9. doi: 10.1002/jbmr.2892

32. Farr JN, Xu M, Weivoda MM, Monroe DG, Fraser DG, Onken JL, et al. Targeting cellular senescence prevents age-related bone loss in mice. *Nat Med* (2017) 23:1072–9. doi: 10.1038/nm.4385

33. Atashi F, Modarressi A, Pepper MS. The role of reactive oxygen species in mesenchymal stem cell adipogenic and osteogenic differentiation: A review. *Stem Cells Dev* (2015) 24:1150–63. doi: 10.1089/scd.2014.0484

34. Ali D, Chen L, Kowal JM, Okla M, Manikandan M, AlShehri M, et al. Resveratrol inhibits adipocyte differentiation and cellular senescence of human bone marrow stromal stem cells. *Bone* (2020) 133:115252. doi: 10.1016/j.bone.2020.115252

35. Chandra A, Lagnado AB, Farr JN, Schleusner M, Monroe DG, Saul D, et al. Bone Marrow Adiposity in Models of Radiation- and Aging-Related Bone Loss Is Dependent on Cellular Senescence. *J Bone Miner Res* (2022) 37:997–1011. doi: 10.1002/jbmr.4537

36. Dimri GP, Itahana K, Acosta M, Campisi J. Regulation of a senescence checkpoint response by the E2F1 transcription factor and p14(ARF) tumor suppressor. *Mol Cell Biol* (2000) 20:273–85. doi: 10.1128/MCB.20.1.273-285.2000

37. Zhou X, Sen I, Lin XX, Riedel CG. Regulation of age-related decline by transcription factors and their crosstalk with the epigenome. *Curr Genomics* (2018) 19:464–82. doi: 10.2174/1389202919666180503125850

38. Li H, Liu P, Xu S, Li Y, Dekker JD, Li B, et al. FOXP1 controls mesenchymal stem cell commitment and senescence during skeletal aging. *J Clin Invest* (2017) 127:1241–53. doi: 10.1172/JCI89511

39. Moerman EJ, Teng K, Lipschitz DA, Lecka-Czernik B. Aging activates adipogenic and suppresses osteogenic programs in mesenchymal marrow stroma/stem cells: the role of PPAR-gamma2 transcription factor and TGF-beta/BMP signaling pathways. *Aging Cell* (2004) 3:379–89. doi: 10.1111/j.1474-9728.2004.00127.x

40. Lin Q, Gao Z, Alarcon RM, Ye J, Yun Z. A role of miR-27 in the regulation of adipogenesis. *FEBS J* (2009) 276:2348–58. doi: 10.1111/j.1742-4658.2009.06967.x

41. Peterson CL, Cote J. Cellular machineries for chromosomal DNA repair. *Genes Dev* (2004) 18:602–16. doi: 10.1101/gad.1182704

42. Masamoto Y, Arai S, Sato T, Kubota N, Takamoto I, Kadowaki T, et al. Adiponectin Enhances Quiescence Exit of Murine Hematopoietic Stem Cells and Hematopoietic Recovery Through mTORC1 Potentiation. *Stem Cells* (2017) 35:1835–48. doi: 10.1002/stem.2640

43. Zhou BO, Yu H, Yue R, Zhao Z, Rios JJ, Naveiras O, et al. Bone marrow adipocytes promote the regeneration of stem cells and haematopoiesis by secreting SCF. *Nat Cell Biol* (2017) 19:891–903. doi: 10.1038/ncb3570

44. Bolan PJ, Arentsen L, Sueblinvong T, Zhang Y, Moeller S, Carter JS, et al. Water-fat MRI for assessing changes in bone marrow composition due to radiation and chemotherapy in gynecologic cancer patients. *J Magn Reson Imaging* (2013) 38:1578–84. doi: 10.1002/jmri.24071

45. Kim HN, Chang J, Shao L, Han L, Iyer S, Manolagas SC, et al. DNA damage and senescence in osteoprogenitors expressing Osx1 may cause their decrease with age. *Aging Cell* (2017) 16:693–703. doi: 10.1111/acel.12597

46. Chandra A, Wang L, Young T, Zhong L, Tseng WJ, Levine MA, et al. Proteasome inhibitor bortezomib is a novel therapeutic agent for focal radiation-induced osteoporosis. *FASEB J* (2018) 32:52–62. doi: 10.1096/fj.201700375R

47. Chandra A, Lin T, Young T, Tong W, Ma X, Tseng WJ, et al. Suppression of Sclerostin Alleviates Radiation-Induced Bone Loss by Protecting Bone-Forming Cells and Their Progenitors Through Distinct Mechanisms. *J Bone Miner Res* (2017) 32:360–72. doi: 10.1002/jbmr.2996

48. Marie PJ, Kassem M. Extrinsic mechanisms involved in age-related defective bone formation. *J Clin Endocrinol Metab* (2011) 96:600–9. doi: 10.1210/jc.2010-2113

49. Vanderschueren D, Vandenput L, Boonen S, Lindberg MK, Bouillon R, Ohlsson C. Androgens and bone. *Endocr Rev* (2004) 25:389–425. doi: 10.1210/er.2003-0003

50. Khosla S, Melton LJ3rd, Riggs BL. Clinical review 144: Estrogen and the male skeleton. *J Clin Endocrinol Metab* (2002) 87:1443–50. doi: 10.1210/jcem.87.4.8417

51. Forbes AP, Albright F. His concept of postmenopausal osteoporosis and what came of it. *Clin Orthop Relat Res* (1991), 128–41.

52. Lindsay R, Hart DM, Aitken JM, MacDonald EB, Anderson JB, Clarke AC. Long-term prevention of postmenopausal osteoporosis by oestrogenEvidence for an increased bone mass after delayed onset of oestrogen treatment. *Lancet* (1976) 1:1038–41. doi: 10.1016/s0140-6736(76)92217-0

53. Abdallah BM, Bay-Jensen AC, Srinivasan B, Tabassi NC, Garnero P, Delaisse JM, et al. Estrogen inhibits Dlk1/FA1 production: A potential mechanism for estrogen effects on bone turnover. *J Bone Miner Res* (2011) 26:2548–51. doi: 10.1002/jbmr.444

54. Abdallah BM, Ditzel N, Mahmood A, Isa A, Traustadottir GA, Schilling AF, et al. DLK1 is a novel regulator of bone mass that mediates estrogen deficiency-induced bone loss in mice. *J Bone Miner Res* (2011) 26:1457–71. doi: 10.1002/jbmr.346

55. Jacobsen BK, Bonaa KH. The reproducibility of dietary data from a self-administered questionnaire. The Tromso Study. *Int J Epidemiol* (1990) 19:349–53. doi: 10.1093/ije/19.2.349

56. Almeida M, Martin-Millan M, Ambrogini E, Bradsher R3rd, Han L, Chen XD, et al. Estrogens attenuate oxidative stress and the differentiation and apoptosis of osteoblasts by DNA-binding-independent actions of the ERalpha. *J Bone Miner Res* (2010) 25:769–81. doi: 10.1359/jbmr.091017

57. Kousteni S, Almeida M, Han L, Bellido T, Jilka RL, Manolagas SC. Induction of osteoblast differentiation by selective activation of kinase-mediated actions of the estrogen receptor. *Mol Cell Biol* (2007) 27:1516–30. doi: 10.1128/MCB.01550-06

58. Wiren KM, Semirale AA, Zhang XW, Woo A, Tommasini SM, Price C, et al. Targeting of androgen receptor in bone reveals a lack of androgen anabolic action and inhibition of osteogenesis: a model for compartment-specific androgen action in the skeleton. *Bone* (2008) 43:440–51. doi: 10.1016/j.bone.2008.04.026

59. Prakasam G, Yeh JK, Chen MM, Castro-Magana M, Liang CT, Aloia JF. Effects of growth hormone and testosterone on cortical bone formation and bone density in aged orchiectomized rats. *Bone* (1999) 24:491–7. doi: 10.1016/s8756-3282(99)00018-6

60. Orwoll ES. Androgens as anabolic agents for bone. *Trends Endocrinol Metab* (1996) 7:77–84. doi: 10.1016/1043-2760(96)00024-0

61. Ebeling PR. Clinical practice. Osteoporosis in men. *N Engl J Med* (2008) 358:1474–82. doi: 10.1056/NEJMcp0707217

62. Marie PJ, de Vernejoul MC, Connes D, Hott M. Decreased DNA synthesis by cultured osteoblastic cells in eugonadal osteoporotic men with defective bone formation. *J Clin Invest* (1991) 88:1167–72. doi: 10.1172/JCI115418

63. Khosla S, Melton LJ3rd, Atkinson EJ, O'Fallon WM, Klee GG, Riggs BL. Relationship of serum sex steroid levels and bone turnover markers with bone mineral density in men and women: a key role for bioavailable estrogen. *J Clin Endocrinol Metab* (1998) 83:2266–74. doi: 10.1210/jcem.83.7.4924

64. Falahati-Nini A, Riggs BL, Atkinson EJ, O'Fallon WM, Eastell R, Khosla S. Relative contributions of testosterone and estrogen in regulating bone resorption and formation in normal elderly men. *J Clin Invest* (2000) 106:1553–60. doi: 10.1172/JCI10942

65. Kearns AE, Khosla S, Kostenuik PJ. Receptor activator of nuclear factor kappaB ligand and osteoprotegerin regulation of bone remodeling in health and disease. *Endocr Rev* (2008) 29:155–92. doi: 10.1210/er.2007-0014

66. Pacifici R. Cytokines, estrogen, and postmenopausal osteoporosis–the second decade. *Endocrinology* (1998) 139:2659–61. doi: 10.1210/endo.139.6.6087

67. Zallone A. Direct and indirect estrogen actions on osteoblasts and osteoclasts. *Ann N Y Acad Sci* (2006) 1068:173–9. doi: 10.1196/annals.1346.019

68. Ha H, Kwak HB, Lee SW, Jin HM, Kim HM, Kim HH, et al. Reactive oxygen species mediate RANK signaling in osteoclasts. *Exp Cell Res* (2004) 301:119–27. doi: 10.1016/j.yexcr.2004.07.035

69. Lean JM, Davies JT, Fuller K, Jagger CJ, Kirstein B, Partington GA, et al. A crucial role for thiol antioxidants in estrogen-deficiency bone loss. *J Clin Invest* (2003) 112:915–23. doi: 10.1172/JCI18859

70. Tencerova M, Figeac F, Ditzel N, Taipaleenmaki H, Nielsen TK, Kassem M. High-fat diet-induced obesity promotes expansion of bone marrow adipose tissue and impairs skeletal stem cell functions in mice. *J Bone Miner Res* (2018) 33:1154–65. doi: 10.1002/jbmr.3408

71. Tencerova M, Frost M, Figeac F, Nielsen TK, Ali D, Lauterlein JL, et al. Obesity-associated hypermetabolism and accelerated senescence of bone marrow stromal stem cells suggest a potential mechanism for bone fragility. *Cell Rep* (2019) 27:2050–2062.e6. doi: 10.1016/j.celrep.2019.04.066

72. Marie PJ, Sabbagh A, de Vernejoul MC, Lomri A. Osteocalcin and deoxyribonucleic acid synthesis *in vitro* and histomorphometric indices of bone formation in postmenopausal osteoporosis. *J Clin Endocrinol Metab* (1989) 69:272–9. doi: 10.1210/jcem-69-2-272

73. Modrowski D, Miravet L, Feuga M, Marie PJ. Increased proliferation of osteoblast precursor cells in estrogen-deficient rats. *Am J Physiol* (1993) 264:E190–6. doi: 10.1152/ajpendo.1993.264.2.E190

74. Griffith JF, Yeung DK, Ma HT, Leung JC, Kwok TC, Leung PC. Bone marrow fat content in the elderly: A reversal of sex difference seen in younger subjects. *J Magn Reson Imaging* (2012) 36:225–30. doi: 10.1002/jmri.23619

75. Woods GN, Ewing SK, Sigurdsson S, Kado DM, Eiriksdottir G, Gudnason V, et al. Greater bone marrow adiposity predicts bone loss in older women. *J Bone Miner Res* (2020) 35:326–32. doi: 10.1002/jbmr.3895

76. Griffith JF, Yeung DK, Antonio GE, Lee FK, Hong AW, Wong SY, et al. Vertebral bone mineral density, marrow perfusion, and fat content in healthy men and men with osteoporosis: Dynamic contrast-enhanced MR imaging and MR spectroscopy. *Radiology* (2005) 236:945–51. doi: 10.1148/radiol.2363041425

77. Rothman MS, Iwamoto SJ. Bone Health in the Transgender Population. *Clin Rev Bone Mineral Metab* (2019) 17:77–85. doi: 10.1007/s12018-019-09261-3

78. Bretherton I, Ghasem-Zadeh A, Leemaqz SY, Seeman E, Wang X, McFarlane T, et al. Bone microarchitecture in transgender adults: A cross-sectional study. *J Bone Miner Res* (2022) 37:643–8. doi: 10.1002/jbmr.4497

79. Nasomyont N, Meisman AR, Ecklund K, Vajapeyam S, Cecil KM, Tkach JA, et al. Changes in bone marrow adipose tissue in transgender and gender non-conforming youth undergoing pubertal suppression: A pilot study. *J Clin Densitometry* (2022). doi: 10.1016/j.jocd.2022.06.006

80. Khosla S, Samakkarnthai P, Monroe DG, Farr JN. Update on the pathogenesis and treatment of skeletal fragility in type 2 diabetes mellitus. *Nat Rev Endocrinol* (2021) 17:685–97. doi: 10.1038/s41574-021-00555-5

81. Napoli N, Chandran M, Pierroz DD, Abrahamsen B, Schwartz AV, Ferrari SL, et al. Mechanisms of diabetes mellitus-induced bone fragility. *Nat Rev Endocrinol* (2017) 13:208–19. doi: 10.1038/nrendo.2016.153

82. Morris JA, Kemp JP, Youlten SE, Laurent L, Logan JG, Chai RC, et al. An atlas of genetic influences on osteoporosis in humans and mice. *Nat Genet* (2019) 51:258–66. doi: 10.1038/s41588-018-0302-x

83. Riggs BL, Wahner HW, Seeman E, Offord KP, Dunn WL, Mazess RB, et al. Changes in bone mineral density of the proximal femur and spine with aging. Differences between the postmenopausal and senile osteoporosis syndromes. *J Clin Invest* (1982) 70:716–23. doi: 10.1172/jci110667

84. Lecka-Czernik B, Stechschulte LA, Czernik PJ, Dowling AR. High bone mass in adult mice with diet-induced obesity results from a combination of initial increase in bone mass followed by attenuation in bone formation; implications for high bone mass and decreased bone quality in obesity. *Mol Cell Endocrinol* (2015) 410:35–41. doi: 10.1016/j.mce.2015.01.001

85. Halade GV, Rahman MM, Williams PJ, Fernandes G. High fat diet-induced animal model of age-associated obesity and osteoporosis. *J Nutr Biochem* (2010) 21:1162–9. doi: 10.1016/j.jnutbio.2009.10.002

86. Doucette CR, Horowitz MC, Berry R, MacDougald OA, Anunciado-Koza R, Koza RA, et al. A high fat diet increases bone marrow adipose tissue (mat) but does not alter trabecular or cortical bone mass in c57bl/6j mice. *J Cell Physiol* (2015) 230:2032–7. doi: 10.1002/jcp.24954

87. Scheller EL, Khoury B, Moller KL, Wee NK, Khandaker S, Kozloff KM, et al. Changes in skeletal integrity and marrow adiposity during high-fat diet and after weight loss. *Front Endocrinol (Lausanne)* (2016) 7:102. doi: 10.3389/fendo.2016.00102

88. Bredella MA, Gill CM, Keating LK, Torriani M, Anderson EJ, Punyanitya M, et al. Assessment of abdominal fat compartments using DXA in premenopausal women from anorexia nervosa to morbid obesity. *Obes (Silver Spring)* (2013) 21:2458–64. doi: 10.1002/oby.20424

89. Bredella MA, Torriani M, Ghomi RH, Thomas BJ, Brick DJ, Gerweck AV, et al. Vertebral bone marrow fat is positively associated with visceral fat and inversely associated with IGF-1 in obese women. *Obes (Silver Spring)* (2011) 19:49–53. doi: 10.1038/oby.2010.106

90. Yu EW, Greenblatt L, Eajazi A, Torriani M, Bredella MA. Marrow adipose tissue composition in adults with morbid obesity. *Bone* (2017) 97:38–42. doi: 10.1016/j.bone.2016.12.018

91. Bilha SC, Leustean L, Preda C, Branisteanu DD, Mihalache L, Ungureanu MC. Bone mineral density predictors in long-standing type 1 and type 2 diabetes mellitus. *BMC Endocr Disord* (2021) 21:156. doi: 10.1186/s12902-021-00815-5

92. Figeac F, Tencerova M, Ali D, Andersen TL, Appadoo DRC, Kerckhofs G, et al. Impaired Bone Fracture Healing in Type 2 Diabetes Is Caused by Defective Functions of Skeletal Progenitor Cells. *Stem Cells* (2022) 40:149–64. doi: 10.1093/stmcls/sxab011

93. Fintini D, Cianfarani S, Cofini M, Andreoletti A, Ubertini GM, Cappa M, et al. The Bones of Children With Obesity. *Front Endocrinol (Lausanne)* (2020) 11:200. doi: 10.3389/fendo.2020.00200

94. Walsh JS, Vilaca T. Obesity, Type 2 Diabetes and Bone in Adults. *Calcif Tissue Int* (2017) 100:528–35. doi: 10.1007/s00223-016-0229-0

95. Tonks KT, White CP, Center JR, Samocha-Bonet D, Greenfield JR. Bone Turnover Is Suppressed in Insulin Resistance, Independent of Adiposity. *J Clin Endocrinol Metab* (2017) 102:1112–21. doi: 10.1210/jc.2016-3282

96. Migliaccio S, Greco EA, Fornari R, Donini LM, Lenzi A. Is obesity in women protective against osteoporosis? *Diabetes Metab Syndr Obes* (2011) 4:273–82. doi: 10.2147/DMSO.S11920

97. Kin K, Kushida K, Yamazaki K, Okamoto S, Inoue T. Bone mineral density of the spine in normal Japanese subjects using dual-energy X-ray absorptiometry: effect of obesity and menopausal status. *Calcif Tissue Int* (1991) 49:101–6. doi: 10.1007/BF02565129

98. Ribot C, Tremollieres F, Pouilles JM, Bonneu M, Germain F, Louvet JP. Obesity and postmenopausal bone loss: The influence of obesity on vertebral density and bone turnover in postmenopausal women. *Bone* (1987) 8:327–31. doi: 10.1016/8756-3282(87)90062-7

99. Jang M, Kim H, Lea S, Oh S, Kim JS, Oh B. Effect of duration of diabetes on bone mineral density: A population study on East Asian males. *BMC Endocr Disord* (2018) 18:61. doi: 10.1186/s12902-018-0290-y

100. Bonds DE, Larson JC, Schwartz AV, Strotmeyer ES, Robbins J, Rodriguez BL, et al. Risk of fracture in women with type 2 diabetes: The Women's Health Initiative Observational Study. *J Clin Endocrinol Metab* (2006) 91:3404–10. doi: 10.1210/jc.2006-0614

101. Schwartz AV, Vittinghoff E, Bauer DC, Hillier TA, Strotmeyer ES, Ensrud KE, et al. Association of BMD and FRAX score with risk of fracture in older adults with type 2 diabetes. *JAMA* (2011) 305:2184–92. doi: 10.1001/jama.2011.715

102. Farr JN, Drake MT, Amin S, Melton LJ3rd, McCready LK, Khosla S. *In vivo* assessment of bone quality in postmenopausal women with type 2 diabetes. *J Bone Miner Res* (2014) 29:787–95. doi: 10.1002/jbmr.2106

103. Cohen A, Dempster DW, Recker RR, Lappe JM, Zhou H, Zwahlen A, et al. Abdominal fat is associated with lower bone formation and inferior bone quality in healthy premenopausal women: A transiliac bone biopsy study. *J Clin Endocrinol Metab* (2013) 98:2562–72. doi: 10.1210/jc.2013-1047

104. Carnevale V, Romagnoli E, D'Erasmo L, D'Erasmo E. Bone damage in type 2 diabetes mellitus. *Nutr Metab Cardiovasc Dis* (2014) 24:1151–7. doi: 10.1016/j.numecd.2014.06.013

105. Lee RH, Sloane R, Pieper C, Lyles KW, Adler RA, Van Houtven C, et al. Glycemic control and insulin treatment alter fracture risk in older men with type 2 diabetes mellitus. *J Bone Miner Res* (2019) 34:2045–51. doi: 10.1002/jbmr.3826

106. Vestergaard P. Diabetes and bone fracture: risk factors for old and young. *Diabetologia* (2014) 57:2007–8. doi: 10.1007/s00125-014-3338-1

107. Janghorbani M, Van Dam RM, Willett WC, Hu FB. Systematic review of type 1 and type 2 diabetes mellitus and risk of fracture. *Am J Epidemiol* (2007) 166:495–505. doi: 10.1093/aje/kwm106

108. Schwartz AV, Sellmeyer DE, Ensrud KE, Cauley JA, Tabor HK, Schreiner PJ, et al. Older women with diabetes have an increased risk of fracture: a prospective study. *J Clin Endocrinol Metab* (2001) 86:32–8. doi: 10.1210/jcem.86.1.7139

109. Sheu Y, Amati F, Schwartz AV, Danielson ME, Li X, Boudreau R, et al. Vertebral bone marrow fat, bone mineral density and diabetes: The Osteoporotic Fractures in Men (MrOS) study. *Bone* (2017) 97:299–305. doi: 10.1016/j.bone.2017.02.001

110. Fazeli PK, Bredella MA, Pachon-Peña G, Zhao W, Zhang X, Faje AT, et al. The dynamics of human bone marrow adipose tissue in response to feeding and fasting. *JCI Insight* (2021) 6. doi: 10.1172/jci.insight.138636

111. Kim TY, Schwartz AV, Li X, Xu K, Black DM, Petrenko DM, et al. Bone marrow fat changes after gastric bypass surgery are associated with loss of bone mass. *J Bone Miner Res* (2017) 32:2239–47. doi: 10.1002/jbmr.3212

112. Vogt LJ, Steveling A, Meffert PJ, Kromrey ML, Kessler R, Hosten N, et al. Magnetic resonance imaging of changes in abdominal compartments in obese diabetics during a low-calorie weight-loss program. *PloS One* (2016) 11:e0153595. doi: 10.1371/journal.pone.0153595

113. Kerckhofs G, Durand M, Vangoitsenhoven R, Marin C, van der Schueren B, Carmeliet G, et al. Changes in bone macro- and microstructure in diabetic obese mice revealed by high resolution microfocus X-ray computed tomography. *Sci Rep* (2016) 6:35517. doi: 10.1038/srep35517

114. Tanaka H, Yamashita T, Yoneda M, Takagi S, Miura T. Characteristics of bone strength and metabolism in type 2 diabetic model Tsumura, Suzuki, Obese Diabetes mice. *Bone Rep* (2018) 9:74–83. doi: 10.1016/j.bonr.2018.07.004

115. Wellen KE, Hotamisligil GS. Obesity-induced inflammatory changes in adipose tissue. *J Clin Invest* (2003) 112:1785–8. doi: 10.1172/JCI20514

116. Mundy GR. Osteoporosis and inflammation. *Nutr Rev* (2007) 65:S147–51. doi: 10.1111/j.1753-4887.2007.tb00353.x

117. Wright EJr., Scism-Bacon JL, Glass LC. Oxidative stress in type 2 diabetes: The role of fasting and postprandial glycaemia. *Int J Clin Pract* (2006) 60:308–14. doi: 10.1111/j.1368-5031.2006.00825.x

118. Dos Santos JM, Tewari S, Mendes RH. The role of oxidative stress in the development of diabetes mellitus and its complications. *J Diabetes Res* (2019) 2019:4189813. doi: 10.1155/2019/4189813

119. Yue R, Zhou BO, Shimada IS, Zhao Z, Morrison SJ. Leptin receptor promotes adipogenesis and reduces osteogenesis by regulating mesenchymal stromal cells in adult bone marrow. *Cell Stem Cell* (2016) 18:782–96. doi: 10.1016/j.stem.2016.02.015

120. Droge W. Oxidative aging and insulin receptor signaling. *J Gerontol A Biol Sci Med Sci* (2005) 60:1378–85. doi: 10.1093/gerona/60.11.1378

121. Devlin MJ, Van Vliet M, Motyl K, Karim L, Brooks DJ, Louis L, et al. Early-onset type 2 diabetes impairs skeletal acquisition in the male TALLYHO/JngJ mouse. *Endocrinology* (2014) 155:3806–16. doi: 10.1210/en.2014-1041

122. Ambrosi TH, Scialdone A, Graja A, Gohlke S, Jank AM, Bocian C, et al. Adipocyte accumulation in the bone marrow during obesity and aging impairs stem cell-based hematopoietic and bone regeneration. *Cell Stem Cell* (2017) 20:771–784.e6. doi: 10.1016/j.stem.2017.02.009

123. Boskey AL, Imbert L. Bone quality changes associated with aging and disease: a review. *Ann N Y Acad Sci* (2017) 1410:93–106. doi: 10.1111/nyas.13572

124. Naveiras O, Nardi V, Wenzel PL, Hauschka PV, Fahey F, Daley GQ. Bone-marrow adipocytes as negative regulators of the haematopoietic microenvironment. *Nature* (2009) 460:259–63.

125. Fantuzzi G, tissue A. adipokines, and inflammation. *J Allergy Clin Immunol* (2005) 115:911–9. doi: 10.1016/j.jaci.2005.02.023

126. Barbour KE, Zmuda JM, Boudreau R, Strotmeyer ES, Horwitz MJ, Evans RW, et al. The effects of adiponectin and leptin on changes in bone mineral density. *Osteoporos Int* (2012) 23:1699–710. doi: 10.1007/s00198-011-1768-x

127. Basurto L, Galvan R, Cordova N, Saucedo R, Vargas C, Campos S, et al. Adiponectin is associated with low bone mineral density in elderly men. *Eur J Endocrinol* (2009) 160:289–93. doi: 10.1530/EJE-08-0569

128. O'Brien CA, Gubrij I, Lin SC, Saylors RL, Manolagas SC. STAT3 activation in stromal/osteoblastic cells is required for induction of the receptor activator of NF-kappaB ligand and stimulation of osteoclastogenesis by gp130-utilizing cytokines or interleukin-1 but not 1,25-dihydroxyvitamin D3 or parathyroid hormone. *J Biol Chem* (1999) 274:19301–8. doi: 10.1074/jbc.274.27.19301

129. Kudo O, Sabokbar A, Pocock A, Itonaga I, Fujikawa Y, Athanasou NA. Interleukin-6 and interleukin-11 support human osteoclast formation by a RANKL-independent mechanism. *Bone* (2003) 32:1–7. doi: 10.1016/s8756-3282(02)00915-8

130. Li Y, Lu L, Xie Y, Chen X, Tian L, Liang Y, et al. Interleukin-6 Knockout Inhibits Senescence of Bone Mesenchymal Stem Cells in High-Fat Diet-Induced Bone Loss. *Front Endocrinol (Lausanne)* (2020) 11:622950. doi: 10.3389/fendo.2020.622950

131. Aaron N, Costa S, Rosen CJ, Qiang L. The Implications of Bone Marrow Adipose Tissue on Inflammaging. *Front Endocrinol (Lausanne)* (2022) 13:853765. doi: 10.3389/fendo.2022.853765

132. Kozakowski J, Gietka-Czernel M, Leszczynska D, Majos A. Obesity in menopause - our negligence or an unfortunate inevitability? *Prz Menopauzalny* (2017) 16:61–5. doi: 10.5114/pm.2017.68594

133. Justesen J, Stenderup K, Ebbesen EN, Mosekilde L, Steiniche T, Kassem M. Adipocyte tissue volume in bone marrow is increased with aging and in patients with osteoporosis. *Biogerontology* (2001) 2:165–71. doi: 10.1023/a:1011513223894

134. Li G, Xu Z, Fan J, Yuan W, Zhang L, Hou L, et al. To assess differential features of marrow adiposity between postmenopausal women with osteoarthritis

and osteoporosis using water/fat MRI. *Menopause* (2017) 24:105–11. doi: 10.1097/GME.0000000000000732

135. Milisic L, Vegar-Zubovic S, Valjevac A. Bone marrow adiposity is inversely associated with bone mineral density in postmenopausal females. *Med Glas (Zenica)* (2020) 17:15–21. doi: 10.17392/1053-20

136. Sekiya I, Larson BL, Vuoristo JT, Cui JG, Prockop DJ. Adipogenic differentiation of human adult stem cells from bone marrow stroma (MSCs). *J Bone Miner Res* (2004) 19:256–64. doi: 10.1359/JBMR.0301220

137. Nehlin JO, Jafari A, Tencerova M, Kassem M. Aging and lineage allocation changes of bone marrow skeletal (stromal) stem cells. *Bone* (2019) 123:265–73. doi: 10.1016/j.bone.2019.03.041

138. Salamat MR, Salamat AH, Janghorbani M. Association between obesity and bone mineral density by gender and menopausal status. *Endocrinol Metab (Seoul)* (2016) 31:547–58. doi: 10.3803/EnM.2016.31.4.547

139. Silva HG, Mendonca LM, Conceicao FL, Zahar SE, Farias ML. Influence of obesity on bone density in postmenopausal women. *Arq Bras Endocrinol Metabol* (2007) 51:943–9. doi: 10.1590/s0004-27302007000600008

140. Bonjour JP. Dietary protein: An essential nutrient for bone health. *J Am Coll Nutr* (2005) 24:526S–36S. doi: 10.1080/07315724.2005.10719501

141. Kveiborg M, Rattan SI, Clark BF, Eriksen EF, Kassem M. Treatment with 1,25-dihydroxyvitamin D3 reduces impairment of human osteoblast functions during cellular aging in culture. *J Cell Physiol* (2001) 186:298–306. doi: 10.1002/1097-4652(200002)186:2<298::AID-JCP1030>3.0.CO;2-H

142. Fretz JA, Zella LA, Kim S, Shevde NK, Pike JW. 1,25-Dihydroxyvitamin D3 regulates the expression of low-density lipoprotein receptor-related protein 5 *via* deoxyribonucleic acid sequence elements located downstream of the start site of transcription. *Mol Endocrinol* (2006) 20:2215–30. doi: 10.1210/me.2006-0102

143. van Driel M, van Leeuwen JP. Vitamin D endocrine system and osteoblasts. *Bonekey Rep* (2014) 3:493. doi: 10.1038/bonekey.2013.227

144. Nakaoka K, Yamada A, Noda S, Goseki-Sone M. Influence of dietary vitamin D deficiency on bone strength, body composition, and muscle in ovariectomized rats fed a high-fat diet. *Nutrition* (2019) 60:87–93. doi: 10.1016/j.nut.2018.09.001

145. Lips P. Vitamin D deficiency and secondary hyperparathyroidism in the elderly: consequences for bone loss and fractures and therapeutic implications. *Endocr Rev* (2001) 22:477–501. doi: 10.1210/edrv.22.4.0437

146. Boonen S, Lips P, Bouillon R, Bischoff-Ferrari HA, Vanderschueren D, Haentjens P. Need for additional calcium to reduce the risk of hip fracture with vitamin d supplementation: Evidence from a comparative metaanalysis of randomized controlled trials. *J Clin Endocrinol Metab* (2007) 92:1415–23. doi: 10.1210/jc.2006-1404

147. Chapuy MC, Pamphile R, Paris E, Kempf C, Schlichting M, Arnaud S, et al. Combined calcium and vitamin D3 supplementation in elderly women: confirmation of reversal of secondary hyperparathyroidism and hip fracture risk: the Decalyos II study. *Osteoporos Int* (2002) 13:257–64. doi: 10.1007/s001980200023

148. Sahota O, Mundey MK, San P, Godber IM, Lawson N, Hosking DJ. The relationship between vitamin D and parathyroid hormone: Calcium homeostasis, bone turnover, and bone mineral density in postmenopausal women with established osteoporosis. *Bone* (2004) 35:312–9. doi: 10.1016/j.bone.2004.02.003

149. Tang BM, Eslick GD, Nowson C, Smith C, Bensoussan A. Use of calcium or calcium in combination with vitamin D supplementation to prevent fractures and bone loss in people aged 50 years and older: A meta-analysis. *Lancet* (2007) 370:657–66. doi: 10.1016/S0140-6736(07)61342-7

150. Ding J, Nagai K, Woo JT. Insulin-dependent adipogenesis in stromal ST2 cells derived from murine bone marrow. *Biosci Biotechnol Biochem* (2003) 67:314–21. doi: 10.1271/bbb.67.314

151. Kong J, Li YC. Molecular mechanism of 1,25-dihydroxyvitamin D3 inhibition of adipogenesis in 3T3-L1 cells. *Am J Physiol Endocrinol Metab* (2006) 290:E916–24. doi: 10.1152/ajpendo.00410.2005

152. Whitfield GK, Hsieh JC, Nakajima S, MacDonald PN, Thompson PD, Jurutka PW, et al. A highly conserved region in the hormone-binding domain of the human vitamin D receptor contains residues vital for heterodimerization with retinoid X receptor and for transcriptional activation. *Mol Endocrinol* (1995) 9:1166–79. doi: 10.1210/mend.9.9.7491109

153. Cianferotti L, Demay MB. VDR-mediated inhibition of DKK1 and SFRP2 suppresses adipogenic differentiation of murine bone marrow stromal cells. *J Cell Biochem* (2007) 101:80–8. doi: 10.1002/jcb.21151

154. Duque G, Rivas D. Alendronate has an anabolic effect on bone through the differentiation of mesenchymal stem cells. *J Bone Miner Res* (2007) 22:1603–11. doi: 10.1359/jbmr.070701

155. Kelly KA, Gimble JM. 1,25-Dihydroxy vitamin D3 inhibits adipocyte differentiation and gene expression in murine bone marrow stromal cell clones and primary cultures. *Endocrinology* (1998) 139:2622–8. doi: 10.1210/endo.139.5.5970

156. Meehan M, Penckofer S. The role of vitamin d in the aging adult. *J Aging Gerontol* (2014) 2:60–71. doi: 10.12974/2309-6128.2014.02.02.1

157. Ameri P, Giusti A, Boschetti M, Bovio M, Teti C, Leoncini G, et al. Vitamin D increases circulating IGF1 in adults: Potential implication for the treatment of GH deficiency. *Eur J Endocrinol* (2013) 169:767–72. doi: 10.1530/EJE-13-0510

158. Gomez JM. The role of insulin-like growth factor I components in the regulation of vitamin D. *Curr Pharm Biotechnol* (2006) 7:125–32. doi: 10.2174/138920106776597621

159. Sadie-Van Gijsen H, Crowther NJ, Hough FS, Ferris WF. The interrelationship between bone and fat: From cellular see-saw to endocrine reciprocity. *Cell Mol Life Sci* (2013) 70:2331–49. doi: 10.1007/s00018-012-1211-2

160. Baxter-Jones AD, Kontulainen SA, Faulkner RA, Bailey DA. A longitudinal study of the relationship of physical activity to bone mineral accrual from adolescence to young adulthood. *Bone* (2008) 43:1101–7. doi: 10.1016/j.bone.2008.07.245

161. Carter MI, Hinton PS. Physical activity and bone health. *Mo Med* (2014) 111:59–64.

162. Styner M, Pagnotti GM, McGrath C, Wu X, Sen B, Uzer G, et al. Exercise decreases marrow adipose tissue through ss-oxidation in obese running mice. *J Bone Miner Res* (2017) 32:1692–702. doi: 10.1002/jbmr.3159

163. Pagnotti GM, Styner M. Exercise Regulation of Marrow Adipose Tissue. *Front Endocrinol (Lausanne)* (2016) 7:94. doi: 10.3389/fendo.2016.00094

164. Belavy DL, Miller CT, Owen PJ, Rantalainen T, Connell D, Hahne AJ, et al. Exercise may impact on lumbar vertebrae marrow adipose tissue: Randomised controlled trial. *Bone* (2022) 157:116338. doi: 10.1016/j.bone.2022.116338

165. Maddalozzo GF, Turner RT, Edwards CH, Howe KS, Widrick JJ, Rosen CJ, et al. Alcohol alters whole body composition, inhibits bone formation, and increases bone marrow adiposity in rats. *Osteoporos Int* (2009) 20:1529–38. doi: 10.1007/s00198-009-0836-y

166. Kyle KA, Willett TL, Baggio LL, Drucker DJ, Grynpas MD. Differential effects of PPAR-{gamma} activation versus chemical or genetic reduction of DPP-4 activity on bone quality in mice. *Endocrinology* (2011) 152:457–67. doi: 10.1210/en.2010-1098

167. Dombrowski S, Kostev K, Jacob L. Use of dipeptidyl peptidase-4 inhibitors and risk of bone fracture in patients with type 2 diabetes in Germany-A retrospective analysis of real-world data. *Osteoporos Int* (2017) 28:2421–8. doi: 10.1007/s00198-017-4051-y

168. Monami M, Dicembrini I, Antenore A, Mannucci E. Dipeptidyl peptidase-4 inhibitors and bone fractures: A meta-analysis of randomized clinical trials. *Diabetes Care* (2011) 34:2474–6. doi: 10.2337/dc11-1099

169. Sedlinsky C, Molinuevo MS, Cortizo AM, Tolosa MJ, Felice JI, Sbaraglini ML, et al. Metformin prevents anti-osteogenic *in vivo* and *ex vivo* effects of rosiglitazone in rats. *Eur J Pharmacol* (2011) 668:477–85. doi: 10.1016/j.ejphar.2011.07.033

170. Melton LJ3rd, Leibson CL, Achenbach SJ, Therneau TM, Khosla S. Fracture risk in type 2 diabetes: Update of a population-based study. *J Bone Miner Res* (2008) 23:1334–42. doi: 10.1359/jbmr.080323

171. Kahn SE, Zinman B, Lachin JM, Haffner SM, Herman WH, Holman RR, et al. Rosiglitazone-associated fractures in type 2 diabetes: An Analysis from A Diabetes Outcome Progression Trial (ADOPT). *Diabetes Care* (2008) 31:845–51. doi: 10.2337/dc07-2270

172. Zinman B, Haffner SM, Herman WH, Holman RR, Lachin JM, Kravitz BG, et al. Effect of rosiglitazone, metformin, and glyburide on bone biomarkers in patients with type 2 diabetes. *J Clin Endocrinol Metab* (2010) 95:134–42. doi: 10.1210/jc.2009-0572

173. Vestergaard P, Rejnmark L, Mosekilde L. Relative fracture risk in patients with diabetes mellitus, and the impact of insulin and oral antidiabetic medication on relative fracture risk. *Diabetologia* (2005) 48:1292–9. doi: 10.1007/s00125-005-1786-3

174. Monami M, Cresci B, Colombini A, Pala L, Balzi D, Gori F, et al. Bone fractures and hypoglycemic treatment in type 2 diabetic patients: A case-control study. *Diabetes Care* (2008) 31:199–203. doi: 10.2337/dc07-1736

175. Stechschulte LA, Czernik PJ, Rotter ZC, Tausif FN, Corzo CA, Marciano DP, et al. PPARG post-translational modifications regulate bone formation and bone resorption. *EBioMedicine* (2016) 10:174–84. doi: 10.1016/j.ebiom.2016.06.040

176. Fukunaga T, Zou W, Rohatgi N, Colca JR, Teitelbaum SL, thiazolidinedione Ani-s. which minimally activates PPARgamma, does not cause bone loss. *J Bone Miner Res* (2015) 30:481–8. doi: 10.1002/jbmr.2364

177. Harrison SA, Alkhouri N, Davison BA, Sanyal A, Edwards C, Colca JR, et al. Insulin sensitizer MSDC-0602K in non-alcoholic steatohepatitis: A

randomized, double-blind, placebo-controlled phase IIb study. *J Hepatol* (2020) 72:613–26. doi: 10.1016/j.jhep.2019.10.023

178. Lin Q, Huang YM, Xiao BX, Ren GF. Effects of resveratrol on bone mineral density in ovarectomized rats. *Int J BioMed Sci* (2005) 1:76–81.

179. Yang X, Jiang T, Wang Y, Guo L. The role and mechanism of sirt1 in resveratrol-regulated osteoblast autophagy in osteoporosis rats. *Sci Rep* (2019) 9:18424. doi: 10.1038/s41598-019-44766-3

180. Rios H, Koushik SV, Wang H, Wang J, Zhou HM, Lindsley A, et al. periostin null mice exhibit dwarfism, incisor enamel defects, and an early-onset periodontal disease-like phenotype. *Mol.Cell Biol* (2005) 25:11131–44.

181. Suen PK, Qin L. Sclerostin, an emerging therapeutic target for treating osteoporosis and osteoporotic fracture: A general review. *J Orthop Translat* (2016) 4:1–13. doi: 10.1016/j.jot.2015.08.004

182. Yee CS, Xie L, Hatsell S, Hum N, Murugesh D, Economides AN, et al. Sclerostin antibody treatment improves fracture outcomes in a Type I diabetic mouse model. *Bone* (2016) 82:122–34. doi: 10.1016/j.bone.2015.04.048

183. McDonald MM, Morse A, Mikulec K, Peacock L, Yu N, Baldock PA, et al. Inhibition of sclerostin by systemic treatment with sclerostin antibody enhances healing of proximal tibial defects in ovariectomized rats. *J Orthop Res* (2012) 30:1541–8. doi: 10.1002/jor.22109

184. Suen PK, He YX, Chow DH, Huang L, Li C, Ke HZ, et al. Sclerostin monoclonal antibody enhanced bone fracture healing in an open osteotomy model in rats. *J Orthop Res* (2014) 32:997–1005. doi: 10.1002/jor.22636

185. Hamann C, Rauner M, Hohna Y, Bernhardt R, Mettelsiefen J, Goettsch C, et al. Sclerostin antibody treatment improves bone mass, bone strength, and bone defect regeneration in rats with type 2 diabetes mellitus. *J Bone Miner Res* (2013) 28:627–38. doi: 10.1002/jbmr.1803

186. McColm J, Hu L, Womack T, Tang CC, Chiang AY. Single- and multiple-dose randomized studies of blosozumab, a monoclonal antibody against sclerostin, in healthy postmenopausal women. *J Bone Miner Res* (2014) 29:935–43. doi: 10.1002/jbmr.2092

187. Recker RR, Benson CT, Matsumoto T, Bolognese MA, Robins DA, Alam J, et al. A randomized, double-blind phase 2 clinical trial of blosozumab, a sclerostin antibody, in postmenopausal women with low bone mineral density. *J Bone Miner Res* (2015) 30:216–24. doi: 10.1002/jbmr.2351

188. Recknor CP, Recker RR, Benson CT, Robins DA, Chiang AY, Alam J, et al. The effect of discontinuing treatment with blosozumab: follow-up results of a phase 2 randomized clinical trial in postmenopausal women with low bone mineral density. *J Bone Miner Res* (2015) 30:1717–25. doi: 10.1002/jbmr.2489

189. Rauner M, Taipaleenmaki H, Tsourdi E, Winter EM. Osteoporosis treatment with anti-sclerostin antibodies-mechanisms of action and clinical application. *J Clin Med* (2021) 10. doi: 10.3390/jcm10040787

190. Farrell M, Fairfield H, Costa S, D'Amico A, Falank C, Brooks DJ, et al. Sclerostin-neutralizing antibody treatment rescues negative effects of rosiglitazone on mouse bone parameters. *J Bone Miner Res* (2021) 36:158–69. doi: 10.1002/jbmr.4170

191. Fairfield H, Falank C, Harris E, Demambro V, McDonald M, Pettitt JA, et al. The skeletal cell-derived molecule sclerostin drives bone marrow adipogenesis. *J Cell Physiol* (2018) 233:1156–67. doi: 10.1002/jcp.25976

192. Jackuliak P, Kuzma M, Payer J. Effect of antidiabetic treatment on bone. *Physiol Res* (2019) 68:S107–20. doi: 10.33549/physiolres.934297

193. Chen JS, Sambrook PN. Antiresorptive therapies for osteoporosis: a clinical overview. *Nat Rev Endocrinol* (2011) 8:81–91. doi: 10.1038/nrendo.2011.146

194. Weivoda MM, Chew CK, Monroe DG, Farr JN, Atkinson EJ, Geske JR, et al. Identification of osteoclast-osteoblast coupling factors in humans reveals links between bone and energy metabolism. *Nat Commun* (2020) 11:87. doi: 10.1038/s41467-019-14003-6

195. Bonnet N, Bourgoin L, Biver E, Douni E, Ferrari S. RANKL inhibition improves muscle strength and insulin sensitivity and restores bone mass. *J Clin Invest* (2019) 129:3214–23. doi: 10.1172/JCI125915

196. Beekman KM, Akkerman EM, Streekstra GJ, Veldhuis-Vlug AG, Acherman Y, Gerdes VE, et al. The effect of roux-en-y gastric bypass on bone marrow adipose tissue and bone mineral density in postmenopausal, nondiabetic women. *Obes (Silver Spring)* (2021) 29:1120–7. doi: 10.1002/oby.23171

197. Limonard EJ, Veldhuis-Vlug AG, van Dussen L, Runge JH, Tanck MW, Endert E, et al. Short-term effect of estrogen on human bone marrow fat. *J Bone Miner Res* (2015) 30:2058–66. doi: 10.1002/jbmr.2557

198. Syed FA, Oursler MJ, Hefferanm TE, Peterson JM, Riggs BL, Khosla S. Effects of estrogen therapy on bone marrow adipocytes in postmenopausal osteoporotic women. *Osteoporos Int* (2008) 19:1323–30. doi: 10.1007/s00198-008-0574-6

199. Schwartz AV, Sigurdsson S, Hue TF, Lang TF, Harris TB, Rosen CJ, et al. Vertebral bone marrow fat associated with lower trabecular BMD and prevalent vertebral fracture in older adults. *J Clin Endocrinol Metab* (2013) 98:2294–300. doi: 10.1210/jc.2012-3949

200. Baum T, Yap SP, Karampinos DC, Nardo L, Kuo D, Burghardt AJ, et al. Does vertebral bone marrow fat content correlate with abdominal adipose tissue, lumbar spine bone mineral density, and blood biomarkers in women with type 2 diabetes mellitus? *J Magn Reson Imaging* (2012) 35:117–24. doi: 10.1002/jmri.22757

201. Duque G, Li W, Adams M, Xu S, Phipps R. Effects of risedronate on bone marrow adipocytes in postmenopausal women. *Osteoporos Int* (2011) 22:1547–53. doi: 10.1007/s00198-010-1353-8

202. Elbaz A, Rivas D, Duque G. Effect of estrogens on bone marrow adipogenesis and Sirt1 in aging C57BL/6J mice. *Biogerontology* (2009) 10:747–55. doi: 10.1007/s10522-009-9221-7

203. Martin RB, Chow BD, Lucas PA. Bone marrow fat content in relation to bone remodeling and serum chemistry in intact and ovariectomized dogs. *Calcif Tissue Int* (1990) 46:189–94. doi: 10.1007/BF02555043

204. Edelstein SL, Barrett-Connor E. Relation between body size and bone mineral density in elderly men and women. *Am J Epidemiol* (1993) 138:160–9. doi: 10.1093/oxfordjournals.aje.a116842

205. Jankowska EA, Rogucka E, Medras M. Are general obesity and visceral adiposity in men linked to reduced bone mineral content resulting from normal ageing? A population-based study. *Andrologia* (2001) 33:384–9. doi: 10.1046/j.1439-0272.2001.00469.x

206. Yamaguchi T, Kanazawa I, Yamamoto M, Kurioka S, Yamauchi M, Yano S, et al. Associations between components of the metabolic syndrome versus bone mineral density and vertebral fractures in patients with type 2 diabetes. *Bone* (2009) 45:174–9. doi: 10.1016/j.bone.2009.05.003

207. Greco EA, Fornari R, Rossi F, Santiemma V, Prossomariti G, Annoscia C, et al. Is obesity protective for osteoporosis? Evaluation of bone mineral density in individuals with high body mass index. *Int J Clin Pract* (2010) 64:817–20. doi: 10.1111/j.1742-1241.2009.02301.x

208. Reid IR, Ames R, Evans MC, Sharpe S, Gamble G, France JT, et al. Determinants of total body and regional bone mineral density in normal postmenopausal women–a key role for fat mass. *J Clin Endocrinol Metab* (1992) 75:45–51. doi: 10.1210/jcem.75.1.1619030

209. Slemenda CW, Hui SL, Longcope C, Johnston CC Jr. Cigarette smoking, obesity, and bone mass. *J Bone Miner Res* (1989) 4:737–41. doi: 10.1002/jbmr.5650040513

210. Goulding A, Taylor RW. Plasma leptin values in relation to bone mass and density and to dynamic biochemical markers of bone resorption and formation in postmenopausal women. *Calcif Tissue Int* (1998) 63:456–8. doi: 10.1007/s002239900557

211. Ricci TA, Chowdhury HA, Heymsfield SB, Stahl T, Pierson RNJr., Shapses SA. Calcium supplementation suppresses bone turnover during weight reduction in postmenopausal women. *J Bone Miner Res* (1998) 13:1045–50. doi: 10.1359/jbmr.1998.13.6.1045

212. Heidari B, Hosseini R, Javadian Y, Bijani A, Sateri MH, Nouroddini HG. Factors affecting bone mineral density in postmenopausal women. *Arch Osteoporos* (2015) 10:15. doi: 10.1007/s11657-015-0217-4

213. El Maghraoui A, Sadni S, El Maataoui A, Majjad A, Rezqi A, Ouzzif Z, et al. Influence of obesity on vertebral fracture prevalence and vitamin D status in postmenopausal women. *Nutr Metab (Lond)* (2015) 12:44. doi: 10.1186/s12986-015-0041-2

214. Andreoli A, Bazzocchi A, Celi M, Lauro D, Sorge R, Tarantino U, et al. Relationship between body composition, body mass index and bone mineral density in a large population of normal, osteopenic and osteoporotic women. *Radiol Med* (2011) 116:1115–23. doi: 10.1007/s11547-011-0689-2

215. Karimifar M, Pasha MA, Salari A, Zamani A, Salesi M, Motaghi P. Evaluation of bone loss in diabetic postmenopausal women. *J Res Med Sci* (2012) 17:1033–8.

216. Yanik B, Ayrim A, Ozol D, Koktener A, Gokmen D. Influence of obesity on bone mineral density in postmenopausal asthma patients undergoing treatment with inhaled corticosteroids. *Clinics (Sao Paulo)* (2009) 64:313–8. doi: 10.1590/s1807-59322009000400008

217. Compston JE, Watts NB, Chapurlat R, Cooper C, Boonen S, Greenspan S, et al. Obesity is not protective against fracture in postmenopausal women: GLOW. *Am J Med* (2011) 124:1043–50. doi: 10.1016/j.amjmed.2011.06.013

frontiers | Frontiers in Endocrinology

TYPE Original Research
PUBLISHED 06 October 2022
DOI 10.3389/fendo.2022.959743

OPEN ACCESS

EDITED BY
Sarah Beck-Cormier,
INSERM U1229 Médecine Régénératrice et Squelette (RMeS), France

REVIEWED BY
Christophe Chauveau,
Université du Littoral Côte d'Opale, France
Xiao Zhang,
Washington University in St. Louis, United States

*CORRESPONDENCE
Urszula T. Iwaniec
urszula.iwaniec@oregonstate.edu

SPECIALTY SECTION
This article was submitted to Bone Research, a section of the journal Frontiers in Endocrinology

RECEIVED 02 June 2022
ACCEPTED 15 September 2022
PUBLISHED 06 October 2022

CITATION
Turner RT, Nesser KL, Philbrick KA, Wong CP, Olson DA, Branscum AJ and Iwaniec UT (2022) Leptin and environmental temperature as determinants of bone marrow adiposity in female mice. *Front. Endocrinol.* 13:959743. doi: 10.3389/fendo.2022.959743

Leptin and environmental temperature as determinants of bone marrow adiposity in female mice

Russell T. Turner[1,2], Kira L. Nesser[1], Kenneth A. Philbrick[1], Carmen P. Wong[1], Dawn A. Olson[1], Adam J. Branscum[3] and Urszula T. Iwaniec[1,2]*

[1]Skeletal Biology Laboratory, School of Biological and Population Health Sciences, Oregon State University, Corvallis, OR, United States, [2]Center for Healthy Aging Research, Oregon State University, Corvallis, OR, United States, [3]Biostatistics Program, School of Biological and Population Health Sciences, Oregon State University, Corvallis, OR, United States

Bone marrow adipose tissue (BMAT) levels are higher in distal femur metaphysis of female mice housed at thermoneutral (32°C) than in mice housed at 22°C, as are abdominal white adipose tissue (WAT) mass, and serum leptin levels. We performed two experiments to explore the role of increased leptin in temperature-enhanced accrual of BMAT. First, we supplemented 6-week-old female C57BL/6J (B6) mice with leptin for 2 weeks at 10 µg/d using a subcutaneously implanted osmotic pump. Controls consisted of *ad libitum* (*ad lib*) fed mice and mice pair fed to match food intake of leptin-supplemented mice. The mice were maintained at 32°C for the duration of treatment. At necropsy, serum leptin in leptin-supplemented mice did not differ from *ad lib* mice, suggesting suppression of endogenous leptin production. In support, *Ucp1* expression in BAT, percent body fat, and abdominal WAT mass were lower in leptin-supplemented mice. Leptin-supplemented mice also had lower BMAT and higher bone formation in distal femur metaphysis compared to the *ad lib* group, changes not replicated by pair-feeding. In the second experiment, BMAT response was evaluated in 6-week-old female B6 wild type (WT), leptin-deficient *ob/ob* and leptin-treated (0.3 µg/d) *ob/ob* mice housed at 32°C for the 2-week duration of the treatment. Compared to mice sacrificed at baseline (22°C), BMAT increased in *ob/ob* mice as well as WT mice, indicating a leptin independent response to increased temperature. However, infusion of *ob/ob* mice with leptin, at a dose rate having negligible effects on either energy metabolism or serum leptin levels, attenuated the increase in BMAT. In summary, increased housing temperature and increased leptin have independent but opposing effects on BMAT in mice.

KEYWORDS

leptin, BMAT, thermoneutral, room temperature, marrow adipose tissue, histomorphometry

Introduction

Bone marrow adipose tissue (BMAT) is a fat depot spatially confined within the skeleton. The resident adipocytes are derived primarily from bone marrow mesenchymal stem cells. As reviewed (1–4), BMAT differs from other adipose depots in that the density and spatial distribution of adipocytes can vary dramatically within and among bones and adipocytes are interspersed among many other cell populations, including hematopoietic lineage cells. The function and regulation of BMAT is incompletely understood but has received considerable recent attention, particularly in regard to its role as a potential regulator of bone metabolism (5, 6). In rodents, conditions such as diet-induced obesity, chronic heavy alcohol consumption, severe caloric restriction and microgravity have been reported to result in increased BMAT. Notably, the same conditions are often associated with decreased osteoblast differentiation and/or activity, and bone loss (7–10). Mechanistically, some investigators have hypothesized that differentiation to adipocytes at the expense of osteoblasts and/or production of adipocyte-derived adipokines lead to a negative bone turnover balance (11, 12). However, a negative relationship between BMAT levels and osteoblasts is far from universal (6, 13–15) and, when the relationship occurs, causality has not been established. In total, the experimental evidence to date does not strongly support a deterministic model where reducing BMAT will invariably lead to increased bone mass (1).

Mice are commonly used as a mammalian model organism, in part because of their diminutive size, relatively short lifespan and ease of genetic manipulation. However, skeletal adaptations do not scale linearly with body size (16). In addition to being physically small, mice are daily facultative heterotherms and have a thermoneutral zone that is much higher than in humans (17). One outcome of this difference in thermoregulation is that mice housed at room temperature (~22°C) experience cold stress. Adaptation to chronic cold stress is recognized to have profound physiological effects that influence disease processes (18, 19). In contrast to larger rodents and humans, male and female mice lose cancellous bone in femur and lumbar vertebra well before growth has ceased (20). We have shown that cold stress induced by room temperature housing contributes to, and may be fully responsible for, premature cancellous bone loss in mice. Additionally, cold stress in growing mice results in compartment-specific reductions in bone accrual, reduced leptin levels, and decreased accrual of BMAT (21, 22).

There is strong circumstantial evidence that the adipokine leptin is an important negative regulator of BMAT in mice (23). Compared to C57BL/6J (B6) wild type (WT) mice, bone growth and turnover are lower and BMAT higher in long bones of leptin-deficient ob/ob mice (24–28). Furthermore, treatment of ob/ob mice with leptin by either intracerebroventricular or subcutaneous delivery normalizes bone growth and turnover and reduces BMAT levels (23, 25, 29, 30). On the other hand, there are circumstances where elevated leptin is associated with increased BMAT. For example, compared to mice housed at 22°C, housing B6 female mice at 32°C results in increases in serum leptin and BMAT (31). Additionally, high blood leptin levels in obese rodents are associated with increased BMAT (32). These discrepant findings, where higher levels of leptin can be associated with either increases or decreases in BMAT, suggest that environmental temperature has actions on BMAT that do not require leptin.

To better understand the role of leptin as a potential mediator of the response of BMAT to changes in environmental temperature, we performed 2 experiments where we measured BMAT 2 weeks following transfer of mice housed at room temperature (22°C) to near thermoneutral (32°C) housing. It is challenging to house mice at true thermoneutral because the thermoneutral point differs by several degrees between the dark and light photo periods (33). However, a constant temperature of 30-32°C approximates the midrange of thermoneutrality and was shown to prevent cold stress-induced cancellous bone loss in male and female mice as well as result in increased BMAT in female mice (21).

In the first experiment, we supplemented 6-week-old female B6 WT mice with leptin, administered for 2 weeks using a subcutaneously implanted osmotic pump, at 10 μg/d. Controls consisted of ad libitum (ad lib) fed mice and mice pair fed to match food consumption of leptin-supplemented mice. In the second experiment, BMAT response was evaluated in 6-week-old female B6 WT, leptin-deficient ob/ob and leptin-treated (0.3 μg/d) ob/ob mice housed at 32°C for the 2-week duration of treatment.

Materials and methods

The experimental protocols were approved by the Institutional Animal Care and Use Committee at Oregon State University in accordance with the NIH Guide for the Care and Use of Laboratory Animals.

Experiment 1: Effects of leptin supplementation on food intake, body composition, bone and bone marrow adiposity in female B6 mice

Six-week-old female B6 mice were purchased from Jackson Laboratory (Bar Harbor, ME, USA). We chose 6-week-old mice because this age corresponds to near peak cancellous bone volume fraction in femur in the B6 female (20). The animals were placed at 32°C upon arrival and maintained individually housed on a 12 h light:12 h dark cycle. Near thermoneutral housing was used

10.3389/fendo.2022.959743

to prevent cold stress associated with subthermoneutral housing (e.g., standard room temperature, ~22°C) (31, 34). The mice were randomized by weight into one of 3 treatment groups: (1) ad lib (n=16), (2) leptin-supplemented (leptin) (n=9), or (3) vehicle-treated and pair-fed to leptin (pair-fed) (n=10) (Figure 1). Mouse leptin (10 µg/d, equivalent to 400 ng/h; 498-OB-05M, R&D Systems, Minneapolis, MN) or vehicle (20 mM Tris-HCL, Invitrogen, Carlsbad, CA) were delivered via subcutaneously implanted osmotic pumps (Alzet Model 1002, Durect Corporation, Cupertino, CA) to leptin and pair-fed mice, respectively as described (35). Food (Teklad 8604, Harlen Laboratories, Indianapolis, IN) and water were provided ad libitum to the ad lib and leptin-supplemented mice. The pair-fed mice were calorically restricted to match food intake of the leptin-supplemented mice. These mice also served as vehicle-treated surgery controls. We did not include B6 mice housed at 22°C as an additional control because a pilot study (data not shown) revealed no change in BMAT. Food intake was recorded daily for the 2-week duration of treatment. Body weight was recorded 2 days prior to implant surgery, on day of implant surgery (only mice undergoing surgery were weighed), and on days 4, 11, and 14 (necropsy) post-surgery. Calcein was administered at 4 and 1 d prior to necropsy to label mineralizing bone. Mice were fasted overnight and dual energy x-ray absorptiometry (DXA) was performed prior to necropsy. For tissue collection death was induced by cardiac exsanguination. Abdominal white adipose tissue (WAT) – perigonadal, mesenteric, perirenal, retroperitoneal – was excised and weighed. Samples of perigonadal WAT were stored in RNAlater for evaluation of gene expression. Interscapular brown adipose tissue (BAT) was also excised and stored in RNAlater for evaluation of gene expression. Femora were removed, fixed for 24h in 10% buffered formalin and stored in 70% ethanol for histomorphometric analysis. Tibiae were frozen in liquid nitrogen and stored at −80°C for analysis of gene expression.

Experiment 2: Effects of leptin on body composition and bone marrow adiposity in leptin-deficient ob/ob female mice

Six-week-old female B6 WT mice and ob/ob mice on a B6 background were purchased from Jackson Laboratory (Bar Harbor, ME, USA). Following arrival, the B6 WT mice were randomized by weight into one of 2 groups: (1) baseline (n=8) and (2) no treatment control (n=9) (Figure 1). The ob/ob mice were randomized by weight into 3 groups: (1) baseline (n=7), (2) vehicle (n=8), or (3) leptin-treated (n=8). The baseline groups were sacrificed at the start of the experiment and treatment mice placed at 32°C. Mouse leptin (0.3 µg/d, equivalent to 12 ng/h; 498-OB-05M, R&D Systems, Minneapolis, MN) or vehicle (20 mM Tris-HCL, Invitrogen, Carlsbad, CA) were delivered via subcutaneously implanted osmotic pumps (Alzet Model 1002, Durect Corporation, Cupertino, CA) to leptin and vehicle mice, respectively. Infusion of leptin at 0.3 µg/d was shown to increase longitudinal bone growth and bone formation with minimal effects on hypothalamic gene expression in ob/ob mice (35). Food (Teklad 8604, Harlen Laboratories, Indianapolis, IN) and water were provided ad libitum to all groups. We did not include mice housed at 22°C as an additional control because a pilot study (data not shown) did not reveal a change in BMAT. As in Experiment 1, percent body fat (DXA) and abdominal WAT mass (perigonadal, mesenteric, perirenal, retroperitoneal) were recorded at necropsy. In addition, interscapular BAT was removed and stored in RNA later for evaluation of gene expression and femora were removed, fixed for 24h in 10%

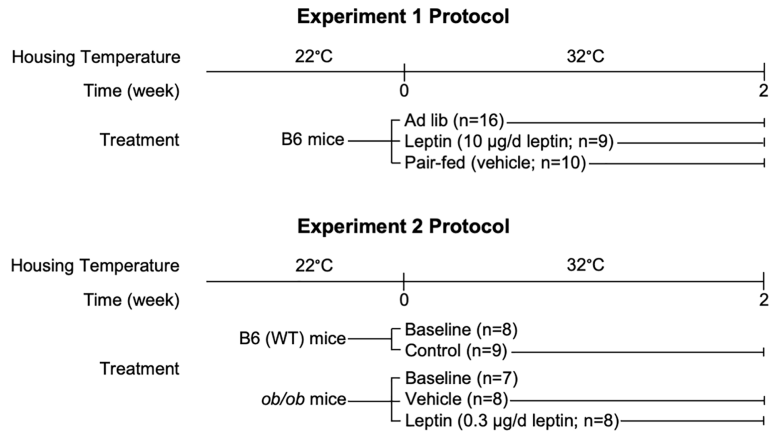

FIGURE 1
Experimental design.

buffered formalin, and stored in 70% ethanol for histomorphometric analysis of bone marrow adiposity.

Dual energy absorptiometry

Total body bone mineral content (g), bone area (cm^2), bone mineral density (g/cm^2) and percent body fat were determined using DXA (PIXImus2, Lunar, Madison, WI) under isoflurane anesthesia immediately prior to necropsy.

Blood measurements

Serum leptin was measured using Mouse Leptin Quantikine ELISA Kit (R&D Systems, Minneapolis, MN), serum osteocalcin was measured using Mouse Gla-Osteocalcin High Sensitive EIA Kit (Clontech, Mountain View, CA), and serum Mouse C terminal telopeptides of type I collagen (CTX-1) was measured using ELISA kit (Life Sciences Advanced Technologies, St. Petersburg, FL) according to the respective manufacturer's protocol. Intra-assay coefficient of variation (CV) for all ELISA assays were within the manufactures' reported CVs of ≤ 5%.

Histomorphometry

The methods used to measure static and dynamic bone histomorphometry have been described, with modifications for mice (36). In brief, distal femora were dehydrated in a graded series of ethanol and xylene, and embedded undecalcified in modified methyl methacrylate. Longitudinal sections (4 μm thick) were cut with a vertical bed microtome (Leica 2065) and affixed to slides precoated with 1% gelatin solution. One section/animal was mounted unstained for measurement of fluorochrome labels and marrow adipocytes using ultraviolet illumination. All data were collected using the OsteoMeasure System (OsteoMetrics, Inc., Atlanta, GA) in the distal femur metaphysis (10x) and distal femur diaphysis (6.7x) (Supplemental Figure 1). The sampling site for the distal femoral metaphysis was located 0.25 – 1.1 mm proximal to the growth plate, averaged 0.92 mm^2 in area, and excluded primary spongiosa and cortical bone. The sampling site for the distal femoral diaphysis was located 2.0 – 2.7 mm proximal to the growth plate, averaged 0.63 mm^2 in area, and excluded cortical bone. Proper depth was identified by a characteristic v-shaped growth plate and parallel diaphyseal cortices approximately equal in width (Supplemental Figure 1).

Fluorochrome-based measurements of bone formation included mineralizing perimeter (mineralizing perimeter/bone perimeter: cancellous bone perimeter covered with double plus half single label normalized to bone perimeter, %), 2) mineral apposition rate (the distance between two fluorochrome markers that comprise a double label divided by the 3-day interlabel interval, μm/d), and 3) bone formation rate (bone formation rate/bone perimeter: calculated by multiplying mineralizing perimeter by mineral apposition rate normalized to bone perimeter, $\mu m^2/\mu m/y$). All bone histomorphometric data are reported using standard 2-dimensional referents and nomenclature (37). Cell-based BMAT measurements included adipocyte area fraction (adipocyte area/tissue area, %), adipocyte number ($\#/mm^2$) and adipocyte size (μm^2). Adipocytes were identified as large circular, oval or ellipsoid-shaped cells bordered by a prominent cell membrane; adipocytes are easily detected because ultraviolet absorption by lipid storage droplets is negligible due to alcohol extraction of intracellular lipids during processing. These cells can be appreciated as black 'ghosts' surrounded by a membrane in Supplemental Figure 1B. The size of each adipocyte was determined by outlining the cell perimeter; the OsteoMeasure software was used to calculate cell area. On average, we counted 55 adipocytes/mouse in the ROI in distal femur metaphysis and 17 adipocytes/mouse in the ROI in distal femur diaphysis.

Gene expression

Total RNA from BAT, WAT and tibia was isolated from 8 mice/group and individually analyzed. Whereas histomorphometry focused on a defined region of interest in femur, evaluation of gene expression included the entire tibia. Tibiae were pulverized with a mortar and pestle in liquid nitrogen and further homogenized in Trizol (Life Technologies, Grand Island, NY). BAT and WAT were directly homogenized in Trizol. Total RNA was isolated according to the manufacturer's protocol, and mRNA was reverse transcribed into cDNA using SuperScript III First-Strand Synthesis SuperMix for qRT-PCR (Life Technologies). All quantitative polymerase chain (qPCR) reactions were done using Fast SYBR Green Master Mix (ThermoFisher), and relative quantification was determined using the ΔΔCt method.

qPCR for BAT Ucp1 gene expression was done using primers specific for mouse Ucp1 (For: GTGAAGGTCAGAATGCAAGC, Rev: AGGGCCCCCTTCATGAGGTC) and mouse 18S ribosomal RNA (Rn18s) (For: CCGCAGCTAGGAATAATGGAAT, Rev: CGAACCTCCGACTTTCGTTCT). Data represent average fold change normalized to Rn18S.

Expression levels for genes related to adipogenesis were determined for WAT and tibia using the Mouse Adipogenesis RT2 Profiler PCR Array (Qiagen). Gene expression was normalized using the averaged expression of Gapdh, Gusb, and Hsp90ab1 housekeeping genes, and relative quantification (ΔΔCt method) was determined using RT2 Profiler PCR Array Data Analysis software (Qiagen).

Statistical analysis

Experiment 1

Numerical outcome variables collected in female B6 mice that were supplemented with leptin or served as controls (ad lib-fed mice and mice pair-fed to match food consumption by leptin-supplemented mice) were compared using parametric one-factor analysis of variance or nonparametric Kruskal-Wallis tests. Group mean comparisons were made using the fitted analysis of variance linear model, Welch's two-sample t-test, or Wilcoxon-Mann-Whitney tests.

Experiment 2

Linear models with 5 groups (untreated B6 WT or ob/ob mice housed at 22°C, untreated B6 WT mice housed at thermoneutral temperature, and ob/ob mice receiving leptin at 0.3μg/day or a vehicle control housed at thermoneutral temperature) were used to evaluate the effects of housing temperature and leptin supplementation on BMAT.

Experiments 1 and 2

Residual analysis and Levene's test were used to assess homogeneity of variance and normality. Adjustment for multiple comparisons was made by setting the maximum false discovery rate equal to 5% (38). Differences were considered significant at false discovery rate adjusted p-value ≤ 0.05. All data are presented as mean ± SD. Data analysis was performed using R version 4.1.2.

Results

Experiment 1: Effects of leptin supplementation on food intake, body composition, bone, and bone marrow adiposity in female B6 mice

The effects of leptin supplementation and pair feeding on food intake, body composition, serum leptin, and Ucp1 gene expression in BAT are shown in Figure 2. Food intake (panel A) decreased over time in all groups; leptin-supplemented and pair-fed mice consumed less food/day than ad lib-fed mice until day 7, after which food consumption did not differ among groups. Cumulative food intake (panel B) was lower in leptin-supplemented and pair-fed mice compared to ad lib mice. Body mass did not differ among treatment groups at any time point evaluated, including at termination of treatment (panel C). However, body mass change over the 14 days of treatment (panel D) was lower in leptin-supplemented and pair-fed mice compared to ad lib mice and tended ($p = 0.06$) to be lower in leptin-supplemented compared to pair-fed mice. Normalized body mass relative to baseline body mass was lower in leptin-supplemented and pair-fed mice compared to ad lib mice at all time points evaluated (panel E and F). Percent body fat (panel G) and WAT mass (panel H) were lower in leptin-supplemented mice than in ad lib or pair-fed mice. Significant differences in percent body fat or WAT mass were not detected between ad lib and pair-fed mice. Serum leptin levels (panel I) did not differ among treatment groups. Ucp1 expression in BAT (panel J) was lower in leptin-supplemented mice compared to ab lib and pair-fed mice. Significant differences in Ucp1 expression were not detected between ab lib and pair-fed mice.

The effects of leptin supplementation and pair feeding on total body bone area, mass and density, and on serum markers of global bone turnover are shown in Figure 3. Bone area (panel A) was higher in leptin-supplemented mice compared to both ad lib and pair-fed mice. Bone mineral content (panel B) was also higher in leptin-supplemented mice than in pair-fed mice. Significant differences in bone area or bone mineral content were not detected between ad lib and pair-fed mice. In addition, significant differences in bone mineral density (panel C) were not detected with treatment. Serum CTX (panel D) was lower in leptin-supplemented and pair-fed mice compared to ad lib mice but leptin-supplemented mice did not differ from pair-fed mice. Serum osteocalcin levels (panel E) did not differ among groups.

The effects of leptin supplementation and pair feeding on bone, bone formation and marrow adiposity in distal femur metaphysis and on marrow adiposity in distal femur diaphysis are shown in Figure 4. Significant differences in bone area/tissue area in the distal femur metaphysis (panel A) were not detected with treatment. However, mineralizing perimeter (panel B) was lower in pair-fed mice compared to ad lib mice and leptin-supplemented mice, and mineral apposition rate (panel C) was higher in leptin-supplemented mice than in ad lib mice and pair-fed mice. Bone formation rate (panel D) tended ($p = 0.053$) to be higher in leptin-supplemented mice compared to ad lib and was higher compared to pair-fed mice. Bone formation rate was lower in pair-fed mice compared to ad lib mice. Adipocyte area fraction (panel E) and adipocyte density (panel F) were lower in leptin-supplemented mice compared to ad lib and pair-fed mice whereas adipocyte size (panel G) did not differ between ad lib and leptin-supplemented mice but was higher in pair-fed mice compared to both ad lib and leptin-supplemented mice. The differences in BMAT among the treatment groups in the distal femur metaphysis can be readily appreciated in panel H. Treatment effects on BMAT were likewise observed in the distal femur diaphysis. Adipocyte area fraction (panel I), density (panel J) and size (panel K) were lower or tended to be lower in leptin-supplemented mice compared to ad lib and pair-fed mice. However, differences in marrow adiposity were not detected between ad lib and pair-fed mice.

The effects of leptin supplementation on differential expression of genes related to adipogenesis in abdominal WAT and tibia are shown in Figures 5, 6, respectively. In abdominal

10.3389/fendo.2022.959743

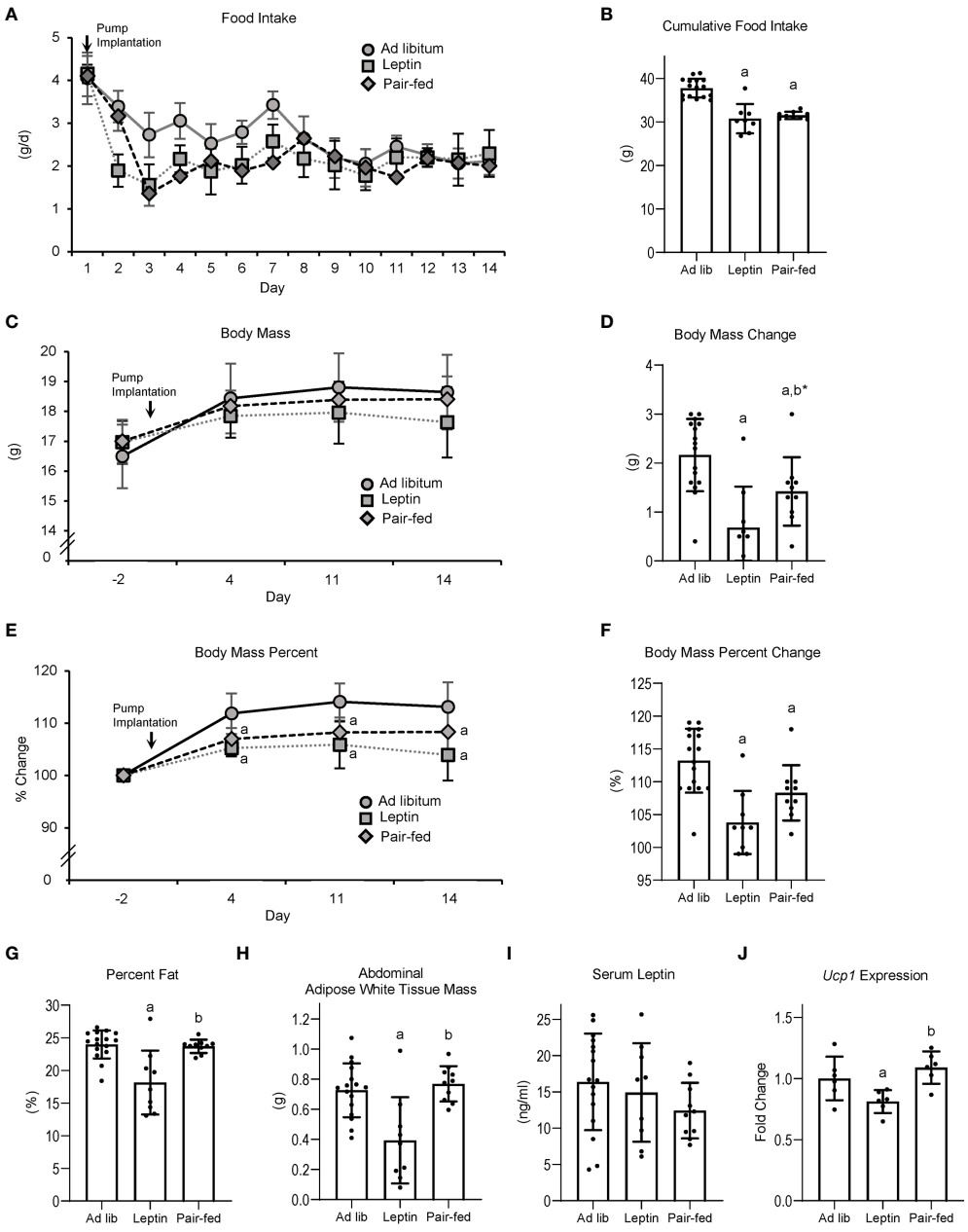

FIGURE 2
Effects of leptin supplementation and pair feeding on food intake over duration of treatment **(A)**, cumulative food intake **(B)**, body mass **(C)**, body mass change over duration of treatment **(D)**, percent change in body mass relative to baseline mass **(E)**, cumulative percent change in body mass relative to baseline mass **(F)**, percent body fat **(G)**, abdominal white adipose tissue mass **(H)**, serum leptin **(I)**, and brown adipose tissue *Ucp1* gene expression **(J)** in C57BL/6J female mice. Data are mean ± SD with individual data points shown as dots. N = 9-16/group for panels **(A–G)** and n = 8/group for panel **(H)** Analysis of variance followed by appropriate posthoc tests was used to assess differences among groups. [a]Different from *ad lib*, FDR-adjusted $P < 0.05$. [b]Different from leptin, FDR-adjusted $P<0.05$; [b]*$P<0.1$.

WAT, 8/84 genes were differentially expressed in leptin-supplemented mice compared to ad lib mice, 3/84 genes were differentially expressed in pair-fed mice compared to ad lib mice, and 7/84 genes were differentially expressed in leptin-supplemented mice compared to pair-fed mice. In tibia, 14/84 genes were differentially expressed in leptin-supplemented mice compared to ad lib mice, 32/84 genes were differentially expressed in pair-fed mice compared to ad lib mice, and 17/84 genes were differentially expressed in leptin-supplemented mice compared to pair-fed mice.

10.3389/fendo.2022.959743

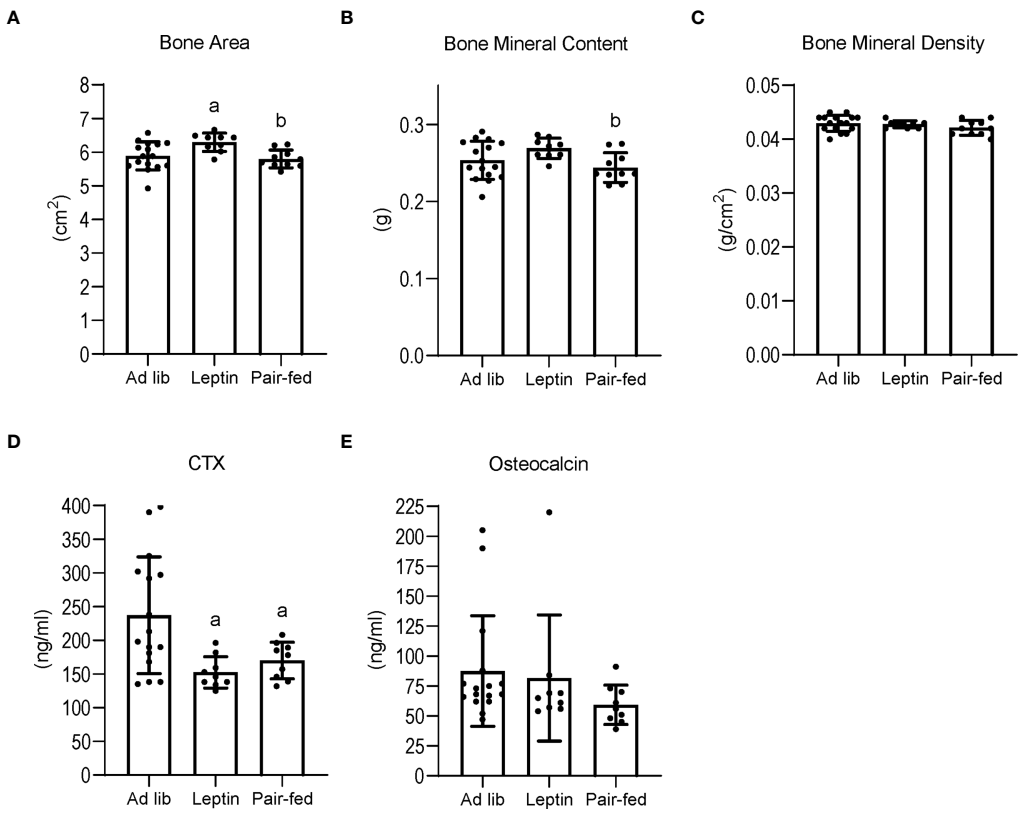

FIGURE 3
Effects of leptin supplementation and pair feeding on total body bone area **(A)**, bone mineral content **(B)**, and bone mineral density **(C)**, and on serum CTX, an index of global bone resorption **(D)** and osteocalcin, an index of global bone formation **(E)** in C57BL/6J female mice. Data are mean ± SD with individual data points shown as dots. N = 9-16/group for panels **(A–E)** Analysis of variance followed by appropriate posthoc tests was used to assess differences among groups. [a]Different from *ad lib*, FDR-adjusted P<0.05. [b]Different from leptin, FDR-adjusted P<0.05.

Experiment 2: Effects of leptin on body composition and bone marrow adiposity in leptin-deficient ob/ob female mice

The effects (1) of increasing housing temperature on body composition and BMAT in WT and ob/ob mice and (2) of leptin treatment on body composition and BMAT in ob/ob mice housed at 32°C are shown in Figure 7. Percent body fat (panel A) and abdominal WAT mass (panel B) increased in WT mice and increased (percent fat) or tended (p = 0.064) to increase (abdominal WAT) in ob/ob mice following transfer from room temperature (baseline, 22°C) to thermoneutral housing (32°C). Leptin treatment in ob/ob mice resulted in lower percent body fat but had no effect on abdominal WAT mass. As expected, Ucp1 expression in BAT (panel C) decreased in WT mice following transfer to thermoneutral housing while thermoneutral housing had no effect on Ucp1 expression in the ob/ob mice. Administration of leptin to ob/ob mice resulted in higher Ucp1 expression compared to administration of vehicle. Adipocyte area fraction (panel D), adipocyte density (panel E) and adipocyte size (panel F) increased in both WT and ob/ob mice following transfer to thermoneutral housing. Leptin treatment in ob/ob mice resulted in lower adipocyte area fraction and adipocyte density compared to vehicle. Significant differences in adipocyte size were not detected with leptin treatment in the ob/ob mice.

Discussion

Food consumption decreased in B6 mice following transfer from room temperature to thermoneutral housing in this and prior studies (21, 22). The time course for reduced food consumption was advanced (i.e., occurred earlier) but the magnitude of the decrease was not influenced by leptin supplementation. Compared to ad lib mice, supplementation of B6 mice with leptin had no effect on serum leptin levels measured at necropsy but resulted in lower BAT Ucp1 expression, lower serum CTX, lower abdominal WAT and lower BMAT in metaphysis and diaphysis of the distal femur,

10.3389/fendo.2022.959743

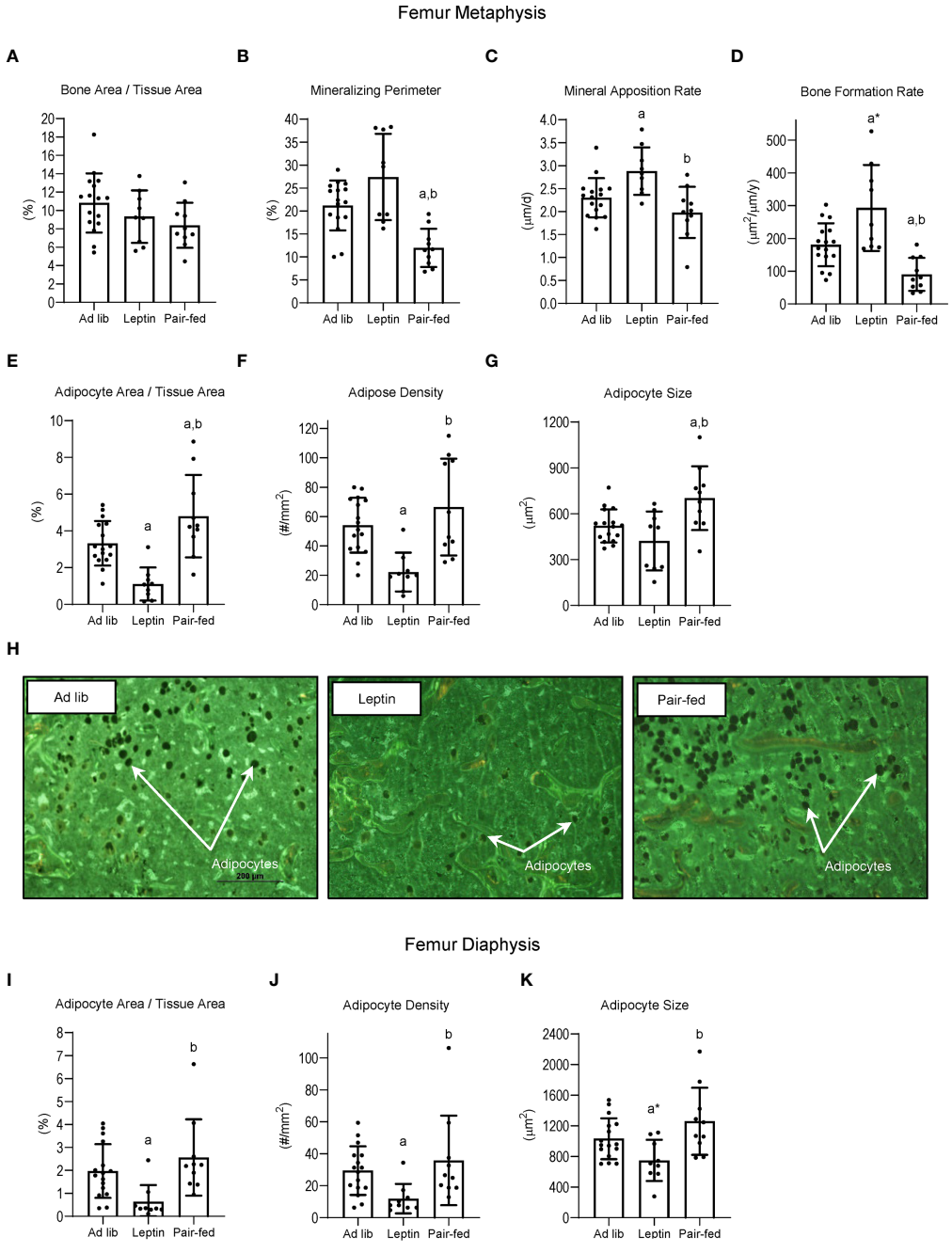

FIGURE 4
Effects of leptin supplementation and pair feeding on bone area and indices of bone formation, bone resorption, and bone marrow adiposity in distal femur metaphysis and on indices of bone marrow adiposity in distal femur diaphysis: bone area fraction (bone area/tissue area) **(A)**, mineralizing perimeter **(B)**, mineral apposition rate **(C)**, bone formation rate **(D)**, adipocyte area fraction **(E)**, adipocyte density **(F)**, and adipocyte size **(G)** in distal femur metaphysis and adipocyte area fraction **(I)**, adipocyte density **(J)**, and adipocyte size **(K)** in distal femur diaphysis in C57BL/6J female mice. Representative images of the bone marrow adiposity in femur metaphysis in each treatment group are shown in panel **(H)** Data are mean ± SD with individual data points shown as dots. N = 9-16/group. Analysis of variance followed by appropriate posthoc tests was used to assess differences among groups. [a]Different from *ad lib*, FDR-adjusted P < 0.05; [a]*P < 0.1. [b]Different from leptin, FDR-adjusted P < 0.05.

10.3389/fendo.2022.959743

	Leptin versus *Ad libitum*		Pair-fed versus *Ad libitum*		Leptin versus Pair-fed	
Symbol	Fold Change	p-value	Fold Change	p-value	Fold Change	p-value
Acacb	**2.7**	**0.030**	1.8	0.071	1.5	0.174
Adig	**1.8**	**0.049**	1.0	0.937	1.7	0.051
Adipoq	-1.0	0.828	-1.3	0.470	1.3	0.549
Adrb2	-1.1	0.358	-1.0	0.713	-1.1	0.324
Agt	1.1	0.573	-1.4	0.960	1.5	0.670
Angpt2	-1.2	0.205	-1.5	0.289	1.2	0.857
Axin1	-1.1	0.423	1.2	0.263	-1.4	0.119
Bmp2	-1.3	0.545	1.4	0.314	-1.8	0.228
Bmp4	-1.2	0.232	1.3	0.305	-1.5	0.144
Bmp7	-1.2	0.654	2.0	0.265	-2.4	0.249
Ccnd1	-1.3	0.130	1.3	0.222	**-1.7**	**0.035**
Cdk4	-1.3	0.585	1.0	0.804	-1.3	0.695
Cdkn1a	1.1	0.306	-1.2	0.905	1.3	0.324
Cdkn1b	-1.1	0.784	1.3	0.490	-1.4	0.321
Cebpa	1.5	0.115	1.7	0.112	-1.1	0.527
Cebpb	1.2	0.387	-1.1	0.769	1.4	0.353
Cebpd	-1.1	0.473	1.0	0.958	-1.1	0.420
Cfd	1.7	0.213	-1.5	0.288	**2.6**	**0.018**
Creb1	1.2	0.999	1.3	0.405	-1.1	0.311
Ddit3	1.2	0.054	-1.1	0.531	-1.2	0.106
Dio2	-1.1	0.404	1.9	0.346	-2.1	0.217
Dkk1	-1.6	0.461	-1.1	0.652	-1.5	0.640
Dlk1	-1.7	0.055	-1.3	0.338	-1.3	0.286
E2f1	-1.0	0.739	-1.3	0.767	1.3	0.915
Egr2	**-1.8**	**0.008**	**-1.5**	**0.018**	-1.2	0.240
Fabp4	1.3	0.512	1.1	0.906	1.2	0.561
Fasn	**3.8**	**0.003**	**2.4**	**0.019**	1.6	0.076
Fgf1	-1.2	0.246	-1.4	0.215	1.2	0.732
Fgf10	1.3	0.765	-1.1	0.722	1.3	0.420
Fgf2	-1.0	0.662	1.3	0.492	-1.4	0.274
Foxc2	-1.1	0.597	1.3	0.538	-1.4	0.172
Foxo1	1.0	0.841	1.1	0.559	-1.1	0.461
Gata2	-1.0	0.521	2.2	0.053	**-2.2**	**0.035**
Gata3	1.1	0.886	1.9	0.341	-1.8	0.345
Hes1	-1.3	0.248	1.1	0.480	-1.3	0.337
Insr	1.3	0.205	1.6	0.093	-1.3	0.202
Irs1	-1.0	0.854	1.2	0.327	-1.2	0.286
Irs2	-1.1	0.655	1.4	0.125	-1.5	0.070
Jun	**-1.6**	**0.021**	-1.2	0.220	**-1.4**	**0.039**
Klf15	1.2	0.263	1.2	0.216	-1.0	0.855
Klf2	-1.2	0.316	1.0	0.995	-1.3	0.273
Klf3	-1.0	0.485	1.5	0.143	**-1.5**	**0.041**
Klf4	-1.2	0.282	1.2	0.839	-1.4	0.077
Lep	-1.2	0.620	1.5	0.463	-1.7	0.221
Lipe	1.6	0.135	1.5	0.172	1.0	0.574
Lmna	-1.1	0.312	1.1	0.422	-1.3	0.166
Lpl	1.5	0.367	1.4	0.649	1.1	0.650
Lrp5	-1.1	0.591	1.2	0.342	-1.2	0.196
Mapk14	1.0	0.698	-1.0	0.835	1.1	0.532
Ncoa2	1.1	0.947	1.3	0.355	-1.2	0.289
Ncor2	-1.2	0.142	1.3	0.171	**-1.5**	**0.044**
Nr0b2	-1.2	0.465	-2.6	0.654	2.2	0.515
Nr1h3	1.3	0.246	1.1	0.616	1.2	0.563
Nrf1	-1.1	0.671	1.2	0.248	-1.3	0.183
Ppara	-1.2	0.339	1.2	0.666	-1.5	0.114
Ppard	1.1	0.798	1.1	0.562	-1.0	0.681
Pparg	1.3	0.552	1.1	0.815	1.2	0.321
Ppargc1a	1.3	0.870	1.4	0.542	-1.2	0.415
Ppargc1b	1.2	0.907	1.5	0.428	-1.3	0.323
Prdm16	1.0	0.826	1.4	0.159	-1.4	0.107
Rb1	1.6	0.214	1.3	0.514	1.3	0.704
Retn	**1.7**	**0.038**	1.1	0.736	1.5	0.082
Runx1t1	1.2	0.627	1.5	0.234	-1.2	0.420
Rxra	1.3	0.255	**1.6**	**0.037**	-1.3	0.108
Sfrp1	-1.7	0.208	-1.1	0.724	-1.6	0.301
Sfrp5	-1.5	0.320	1.1	0.937	-1.7	0.397
Shh	1.3	0.389	2.2	0.336	-1.7	0.344
Sirt1	1.2	0.715	1.1	0.641	1.1	0.886
Sirt2	-1.1	0.481	-1.0	0.882	-1.1	0.398
Sirt3	-1.1	0.476	-1.0	0.985	-1.1	0.595
Slc2a4	**1.8**	**0.023**	1.6	0.064	1.1	0.675
Src	-1.2	0.581	1.7	0.155	-2.1	0.102
Srebf1	**2.2**	**0.044**	1.3	0.501	1.6	0.060
Taz	-1.1	0.473	1.0	0.623	-1.1	0.323
Tcf7l2	-1.1	0.282	1.1	0.697	-1.2	0.204
Tsc22d3	1.1	0.747	1.0	0.854	1.1	0.615
Twist1	1.1	0.711	-1.0	0.956	1.1	0.677
Ucp1	-1.1	0.425	-1.0	0.861	-1.1	0.403
Vdr	-1.5	0.263	1.2	0.545	-1.8	0.079
Wnt1	-1.7	0.337	-1.0	0.565	-1.6	0.583
Wnt10b	1.2	0.694	-1.2	0.461	1.4	0.323
Wnt3a	-1.4	0.649	1.4	0.531	-2.0	0.270
Wnt5a	-1.1	0.483	1.8	0.060	**-1.9**	**0.022**
Wnt5b	-1.4	0.185	1.2	0.561	-1.7	0.065

FIGURE 5
Differentially expressed genes in abdominal white adipose tissue in (1) leptin-supplemented versus *ad libitum* control mice, (2) pair-fed versus *ad libitum* control mice, and (3) leptin-supplemented versus pair-fed mice.

	Leptin versus *Ad libitum*		Pair-fed versus *Ad libitum*		Leptin versus Pair-fed	
Symbol	Fold Change	p-value	Fold Change	p-value	Fold Change	p-value
Acacb	1.1	0.734	1.1	0.917	1.1	0.455
Adig	-1.1	0.867	1.1	0.389	-1.2	0.378
Adipoq	-1.2	0.196	-1.1	0.389	-1.1	0.665
Adrb2	-1.0	0.831	-1.1	0.239	1.1	0.217
Agt	**-1.3**	**0.034**	**-1.3**	**0.022**	-1.0	0.787
Angpt2	**1.2**	**0.044**	1.2	0.083	1.0	0.679
Axin1	1.0	0.936	-1.1	0.475	1.1	0.365
Bmp2	-1.1	0.281	**-1.2**	**0.037**	1.0	0.900
Bmp4	-1.1	0.340	-1.2	0.059	1.0	0.675
Bmp7	-1.2	0.111	**-1.4**	**0.005**	1.1	0.562
Ccnd1	-1.1	0.163	**-1.2**	**0.004**	1.0	0.704
Cdk4	-1.1	0.517	-1.1	0.365	-1.0	0.846
Cdkn1a	-1.1	0.326	**-1.7**	**0.000**	1.3	0.100
Cdkn1b	1.1	0.494	**-1.2**	**0.039**	**1.2**	**0.001**
Cebpa	1.2	0.054	1.2	0.074	1.1	0.305
Cebpb	1.1	0.107	-1.0	0.660	**1.2**	**0.006**
Cebpd	**1.3**	**0.029**	1.1	0.352	**1.2**	**0.020**
Cfd	-1.1	0.533	1.0	0.986	-1.1	0.461
Creb1	-1.0	0.631	-1.1	0.166	1.1	0.540
Ddit3	-1.0	0.535	-1.1	0.199	1.0	0.986
Dio2	-1.1	0.664	**-1.4**	**0.001**	**1.3**	**0.016**
Dkk1	**-1.6**	**0.001**	**-1.9**	**0.000**	1.0	0.782
Dlk1	-1.3	0.283	**-1.5**	**0.006**	1.1	0.431
E2f1	1.0	0.989	**1.5**	**0.027**	**-1.3**	**0.037**
Egr2	-1.4	0.052	-1.0	0.994	-1.4	0.091
Fabp4	-1.0	0.661	**1.2**	**0.037**	**-1.3**	**0.019**
Fasn	1.0	0.962	-1.0	0.702	1.1	0.537
Fgf1	-1.2	0.117	-1.2	0.168	-1.1	0.351
Fgf10	**-1.4**	**0.014**	1.2	0.270	**-1.6**	**0.006**
Fgf2	-1.1	0.532	**-1.3**	**0.014**	1.2	0.131
Foxc2	-1.1	0.492	-1.2	0.087	1.1	0.524
Foxo1	1.0	0.662	**-1.3**	**0.015**	**1.2**	**0.048**
Gata2	-1.1	0.530	-1.1	0.266	1.1	0.518
Gata3	-1.2	0.132	1.1	0.629	-1.2	0.087
Hes1	-1.1	0.221	**-1.4**	**0.001**	1.2	0.162
Insr	**1.2**	**0.040**	-1.1	0.500	**1.3**	**0.000**
Irs1	-1.1	0.489	**-1.3**	**0.003**	1.2	0.135
Irs2	1.1	0.209	1.1	0.481	1.1	0.302
Jun	-1.0	0.890	**-1.4**	**0.000**	**1.3**	**0.010**
Klf15	1.1	0.627	-1.1	0.478	1.1	0.289
Klf2	**1.2**	**0.034**	-1.1	0.669	**1.3**	**0.006**
Klf3	1.1	0.208	-1.0	0.545	1.1	0.059
Klf4	-1.0	0.689	**-1.2**	**0.007**	**1.2**	**0.026**
Lep	-1.5	0.093	1.1	0.584	**-1.6**	**0.023**
Lipe	1.1	0.547	1.1	0.484	1.0	0.628
Lmna	-1.0	0.622	-1.1	0.264	1.0	0.862
Lpl	-1.3	0.081	**-1.4**	**0.006**	1.0	0.915
Lrp5	**-1.1**	**0.042**	**-1.3**	**0.004**	1.1	0.276
Mapk14	1.0	0.750	-1.0	0.515	1.1	0.120
Ncoa2	1.1	0.192	-1.1	0.319	**1.2**	**0.004**
Ncor2	1.1	0.318	-1.0	0.866	1.2	0.060
Nr0b2	**2.4**	**0.004**	**5.0**	**0.009**	-1.5	0.162
Nr1h3	-1.1	0.396	-1.1	0.169	-1.0	0.984
Nrf1	1.1	0.509	1.0	0.608	1.0	0.759
Ppara	-1.2	0.626	-1.0	0.814	-1.2	0.559
Ppard	-1.1	0.314	**-1.2**	**0.047**	**1.1**	**0.035**
Pparg	**-1.2**	**0.027**	**-1.1**	**0.007**	-1.1	0.238
Ppargc1a	1.0	0.799	1.0	0.796	1.0	0.909
Ppargc1b	-1.1	0.226	-1.2	0.086	1.0	0.622
Prdm16	-1.1	0.461	1.1	0.196	-1.1	0.209
Rb1	1.1	0.500	1.1	0.560	1.0	0.783
Retn	-1.2	0.290	1.6	0.100	-1.8	0.057
Runx1t1	-1.0	0.724	-1.1	0.211	1.1	0.377
Rxra	-1.1	0.230	-1.0	0.736	-1.1	0.270
Sfrp1	-1.0	0.853	**-1.2**	**0.032**	1.2	0.062
Sfrp5	-1.3	0.098	**-1.5**	**0.004**	1.0	0.792
Shh	-1.3	0.183	1.0	0.866	-1.4	0.144
Sirt1	1.1	0.331	1.1	0.227	1.0	0.987
Sirt2	-1.0	0.567	**-1.2**	**0.005**	**1.1**	**0.048**
Sirt3	-1.0	0.749	-1.0	0.600	-1.0	0.971
Slc2a4	1.0	0.926	1.2	0.342	-1.1	0.702
Src	-1.2	0.088	-1.1	0.217	-1.1	0.327
Srebf1	-1.2	0.080	**-1.2**	**0.043**	-1.0	0.894
Taz	1.1	0.305	1.0	0.797	1.1	0.242
Tcf7l2	-1.1	0.434	-1.1	0.400	-1.1	0.517
Tsc22d3	1.1	0.621	-1.1	0.292	1.1	0.298
Twist1	-1.2	0.161	**-1.7**	**0.003**	1.3	0.254
Ucp1	**-1.5**	**0.045**	1.0	0.894	**-1.5**	**0.049**
Vdr	-1.1	0.400	**-1.6**	**0.006**	1.3	0.190
Wnt1	**-1.5**	**0.033**	**-1.4**	**0.033**	-1.2	0.405
Wnt10b	-1.2	0.225	**-1.5**	**0.001**	1.1	0.514
Wnt3a	**-2.0**	**0.031**	-1.2	0.571	-1.8	0.084
Wnt5a	-1.2	0.155	**-1.6**	**0.000**	1.2	0.208
Wnt5b	**-1.3**	**0.007**	**-1.7**	**0.000**	1.2	0.342

FIGURE 6
Differentially expressed genes in tibia in (1) leptin-supplemented versus ad libitum control mice, (2) pair-fed versus *ad libitum* control mice, and (3) leptin-supplemented versus pair-fed mice.

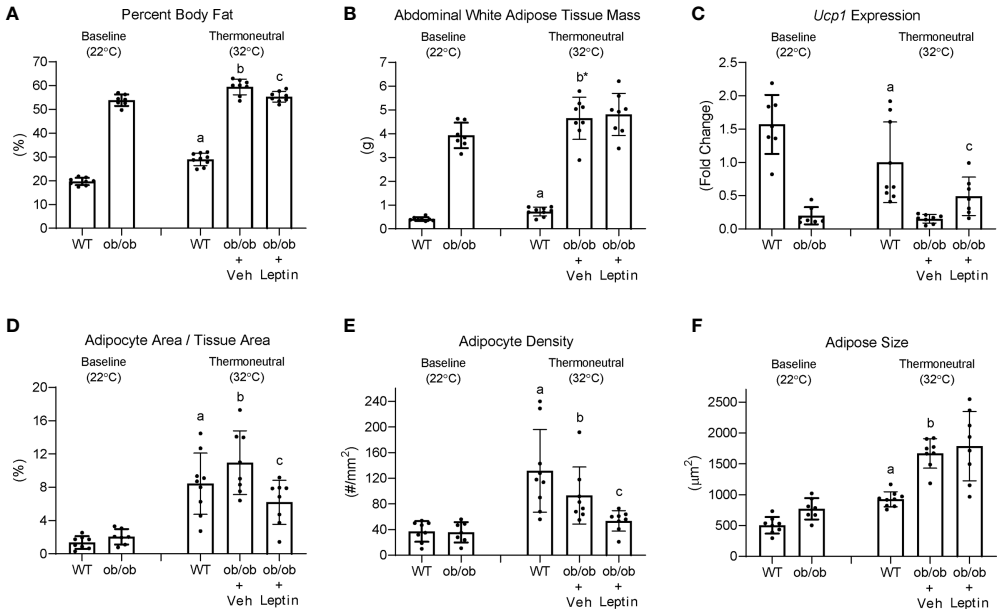

FIGURE 7
Effects of temperature and leptin administration on percent body fat **(A)**, abdominal white adipose tissue mass **(B)**, brown adipose tissue *Ucp1* gene expression **(C)** and on adipocyte area fraction **(D)**, adipocyte density **(E)**, and adipocyte size **(F)** in distal femur metaphysis in *ob/ob* female mice. Data are mean ± SD with individual data points shown as dots. N = 7-9/group. Analysis of variance followed by appropriate posthoc tests was used to assess differences among groups. [a]WT control (32°C) different from WT baseline (22°C), FDR-adjusted P < 0.05. [b]*ob/ob* + vehicle control (32°C) different from *ob/ob* baseline (22°C), FDR-adjusted P<0.05; [b]* FDR-adjusted P < 0.1. [c]*ob/ob* + leptin different from *ob/ob* + vehicle control, FDR-adjusted P < 0.05.

and higher bone formation rate in distal femur metaphysis. Pair feeding did not closely replicate the effects of leptin supplementation on B6 mice housed at thermoneutral. Transfer of ob/ob mice from room temperature to thermoneutral resulted in higher abdominal WAT and higher BMAT in distal femur. Finally, treatment of ob/ob mice with low dose leptin reduced the increase in BMAT in distal femur following transfer to thermoneutral housing but did not impact abdominal WAT weight.

In the present study, we observed a reciprocal relationship between bone formation rate (increased) and BMAT levels (decreased) in distal femur of B6 mice following leptin supplementation. We and others noted inverse relationships between bone formation and BMAT at various skeletal sites during aging and in response to hypophysectomy, spaceflight, ionizing radiation, high fat diets and chronic heavy alcohol consumption (7–10, 14, 23, 39–42). However, as mentioned in the Introduction, a causal association between changes in BMAT levels and bone formation rate has not been demonstrated and there are numerous exceptions to this reciprocal relationship. For example, ovariectomy (ovx) in rats results in increases in osteoblast-lined bone perimeter as well as BMAT, as does increasing housing temperature of mice from room temperature to the thermoneutral range (43). Furthermore, BMAT was increased and bone formation unchanged in ovx rats following a 14-day spaceflight (39). Finally, treatment with the bone anabolic hormones fibroblast growth factor or parathyroid hormone increased bone formation in rodents without reducing BMAT (14, 44).

It remains uncertain as to whether BMAT alters the skeletal response to regulatory factors such as hormones and mechanical loads. Compared to B6 WT mice, adult ob/ob mice have higher BMAT levels. However, hindlimb unloading resulted in cancellous bone loss and changes in bone turnover in ob/ob mice indistinguishable from the skeletal response in B6 WT mice (45). Female mice housed at thermoneutral have higher BMAT and cancellous bone mass than female mice housed at room temperature but antagonizing accrual of BMAT by treatment with the nonspecific β-adrenergic receptor antagonist propranolol had minimal effect on bone mass, microarchitecture and turnover (31). Additionally, in spite of differences in BMAT, inflammation-induced bone loss was similar in distal femur metaphysis of female mice housed at room temperature and at thermoneutral (46).

The receptor tyrosine kinase cKit is required for fat storage in long bones and lumbar vertebra of mice (47, 48). Therefore, attenuation of cKit signaling provides a novel approach for investigating the regulation and function of BMAT. Results of studies performed in cKit-deficient Kit^{W/W^v} mice do not exclude

the possibility that BMAT influences bone metabolism but do demonstrate that mature bone marrow adipocytes are not required for a negative bone turnover balance following ovx or during simulated microgravity (43, 49). Indeed, having normal BMAT levels appeared to attenuate bone loss in distal femur induced by simulated microgravity (49). A limitation of $Kit^{W/Wv}$ mice is that they have hereditary macrocytic anemia, which could independently influence bone metabolism or alternatively modify the effects of BMAT (50, 51). However, adoptive transfer of purified WT (WBB6F1/J) hematopoietic stem cells into $Kit^{W/Wv}$ mice (WT→ $Kit^{W/Wv}$) normalized bone marrow Kit expression (52). Hindlimb unloading resulted in reduced cancellous bone in WT→ $Kit^{W/Wv}$ mice verifying that the BMAT-deficient mice are not protected against hindlimb unloading-induced cancellous bone loss (49). Taken together, factors such as ckit signaling, mechanical loading, leptin status, sex hormones and aging clearly influence BMAT levels but strong evidence that BMAT is an obligatory regulator of bone turnover balance is largely absent. These null results do not imply that BMAT is unimportant; there is compelling evidence that BMAT plays a role in regulated hematopoiesis (1, 53–55). Also, marrow adipocytes produce hormones, adipokines and cytokines capable of positive as well as negative effects on bone metabolism (1, 56–60). In the present study, leptin and pair feeding influenced expression of genes for adipokines (Lep), hormones and growth factors (Fgf2, Fgf10, Agt, Angpt2, Bmp2, Bmp7, Dlk1), cell cycle regulators (Ccnd1, Cdkn1a, Cdkn1b), nuclear hormone receptors (Ppard, Pparg), transcription factors (Jun, Nrob2, Twist1, E2f1, Hes1, Srebf1), and signaling pathways (Sfrp1, Sfrp5, Vdr, Wnt10b, Dkk1, Wnt3a, Wnt5a, Wnt5b, Kfl2, Insr, Irs1). These changes in gene expression in bone marrow may lead to local, systemic or neuronal actions to influence bone metabolism, but definitive evidence for this is lacking.

Leptin supplementation (Experiment 1) did not result in an increase in serum leptin levels in B6 mice, when measured at necropsy. We interpret this as evidence that supplemental leptin resulted in a compensatory reduction in endogenous hormone production and an increase in leptin sensitivity. Our conclusion is supported by the observed lower abdominal WAT weight and BAT Ucp1 expression in leptin-supplemented mice compared to ad lib or pair-fed mice and lower BMAT in leptin-supplemented B6 WT as well as leptin-treated ob/ob mice. Down regulation of Lep expression in adipocytes is a potential alternative mechanism to decrease serum leptin levels and there is evidence that this mechanism is induced by hypothalamic leptin gene therapy (61). However, this alternative mechanism is unlikely because reduced abdominal WAT in the present study was not accompanied by a reduction in Lep expression. It is notable that the reduction in BMAT accrual in leptin-treated ob/ob mice was not accompanied by a parallel decrease in abdominal WAT. This suggests that leptin inhibits BMAT accrual at much lower levels than is required to inhibit WAT accrual, a conclusion supported by dose-response studies where leptin was administered to ob/ob mice (35). Indeed, administration of leptin at a dose rate of 0.3 μg/d did not increase serum leptin levels above the detection limit of 0.5 μg/ml.

Food consumption was lower in leptin-supplemented mice compared to ad lib-fed mice for several days following osmotic pump insertion, but afterwards there was no difference in food intake among treatment groups. We interpret this as further evidence that growing mice fed a normal diet are highly leptin sensitive. In support, partially leptin-deficient heterozygote ob/+ mice adapt to partial leptin deficiency by increasing adipose tissue mass until achieving leptin levels similar to B6 WT mice (62). Treatment of ob/ob mice with leptin resulted in dose-dependent decreases in appetite (35, 63). This finding contrasts with B6 mice fed a high fat diet; when treated with leptin, obese mice exhibit an attenuated response, attributable to leptin resistance (64).

Sympathetic signaling is a positive regulator of non-shivering thermogenesis and the β-adrenergic receptor antagonist propranolol blunted thermoneutral-associated increases in BMAT and WAT (65). Thus, leptin and environmental temperature may influence BMAT levels by regulating overlapping pathways. However, it is likely that the actions of leptin on BMAT differ from the adipokine's positive central nervous system-mediated regulatory effects on non-shivering thermogenesis. It is well established that adipocytes express leptin receptors (54, 66). Additionally, treatment with leptin at a dose rate with minimal actions on energy metabolism decreased BMAT and increased bone formation in ob/ob mice (35). In contrast, mild caloric restriction by pair feeding was associated with an increase in BMAT levels. Taken together, our results strongly suggest that leptin signaling and environmental temperature independently regulate BMAT levels.

Thermoneutral housing alters many, but not all, metabolic responses (67–70). Regarding bone, compared to room temperature, thermoneutral housing prevents premature cancellous bone loss, attenuates risperidone-induced trabecular bone loss, has modest effects on cortical response to mechanical loading, and does not impact polyethylene-particle induced osteolysis (46, 71, 72). We have shown that increasing environmental temperature from room temperature to thermoneutral impacts gene expression in WAT and bone (65). In the present study, performed at thermoneutral, leptin supplementation, but not pair feeding, increased expression of genes important to fat synthesis and turnover in WAT; Acacb (Acetyl-CoA acetyltransferase), Adig (adipogenin), Retn (resistin), Slc2a4 (facilitated glucose transporter member 4, GLUT4), and Srebf1 (Sterol regulatory element-binding transcription factor 1). The findings are consistent with fat mobilization in response to leptin supplementation. Leptin supplementation and pair feeding also altered gene expression in whole tibia. However, there was no overlap in genes differentially expressed in WAT and tibia. In general agreement with treatment-associated differences in bone

histomorphometry, there were differences in gene expression between leptin-treated mice and pair-fed or ad lib controls. Taken together, the results suggest that these two leptin target tissues respond differently to the hormone.

The present studies were performed in growing female mice and evaluated (1) distal femur metaphysis (histomorphometry), a skeletal site where BMAT is closely associated with cancellous bone undergoing rapid turnover, and (2) whole tibia (gene expression). The present studies do not include controls for age-related changes in BMAT that may have occurred during the 2-week intervention. However, we have previously reported higher levels of BMAT in female mice housed at thermoneutral compared to age-matched controls housed at room temperature and pilot studies revealed no change during the evaluated age range (31, 34). Our evaluation of one sex is a study limitation because there are sex differences in bone growth and BMAT accrual (21). Additionally, adipocyte number differs with skeletal site, suggesting possible differences in regulation and function. Future studies should evaluate the effects of environmental temperature and leptin on BMAT at multiple locations in skeletally mature and aging male and female mice. Furthermore, because energy balance and thermoregulation in mice differs markedly from humans it would be enlightening to investigate the response of BMAT to environmental temperatures in additional model organisms.

Our analyses were performed at 4 levels; quantitative histomorphometry, gene expression, serum biomarkers (indices of whole-body bone turnover and fat stores) and organ mass/density. Histomorphometry examined the relationships between bone turnover and BMAT at one cancellous bone site (distal femur metaphysis) in response to treatment. Evaluation of differential expression of a panel of genes related to adipogenesis was used to compare the response to leptin in WAT and whole tibia. The tibia, in addition to adipose tissue (regulated and constitutive BMAT), contains compartment-specific distributions of bone (e.g., cortical and cancellous), cartilage, hematopoietic tissue and other tissues. Differences between our skeletal site in femur and whole tibia preclude direct comparisons between these two long bones. This being said, changes identified in a long bone are generally representative of the appendicular skeleton (1, 31, 35, 43, 47, 49, 52, 62, 65). Serum biomarkers and whole organ measurements were performed as indices of macro changes in response to treatment.

In summary, increasing environmental temperature from room temperature to thermoneutral in growing female B6 and ob/ob mice has major effects on body composition, including an increase in BMAT in the distal femur metaphysis in both genotypes and an increase in leptin levels in B6 mice. Administration of leptin lowered BMAT levels in both B6 WT and leptin-deficient ob/ob mice. Based on these findings, we conclude that increases in leptin signaling in leptin-sensitive mice and environmental temperature in normal and leptin-deficient mice have independent but opposite effects on BMAT levels. Specifically, alleviation of cold stress by housing mice at thermoneutral increases BMAT compared to room temperature housing, whereas increasing leptin signaling decreases BMAT.

Data availability statement

The original contributions presented in the study are included in the article/Supplementary Materials. Further inquiries can be directed to the corresponding author.

Ethics statement

The animal study was reviewed and approved by Institutional Animal Care and Use Committee at Oregon State University.

Author contributions

Study conceptualization, RT, UI, KP, and AB; Study execution, KP; Data collection, KN, KP, CW, DO, and RT; Data analysis, AB; Manuscript draft, RT; Figure preparation, UI; UI takes responsibility for the integrity of the data. All authors contributed to the article and approved the submitted version.

Funding

This work was supported by National Institutes of Health (AR060913) and National Aeronautics and Space Administration (80NSSC19K0430).

Conflict of interest

The authors declare that the research was conducted in the absence of any commercial or financial relationships that could be construed as a potential conflict of interest.

Publisher's note

Supplementary material

The Supplementary Material for this article can be found online at: https://www.frontiersin.org/articles/10.3389/fendo.2022.959743/full#supplementary-material

References

1. Turner RT, Martin SA, Iwaniec UT. Metabolic coupling between bone marrow adipose tissue and hematopoiesis. *Curr Osteoporos Rep* (2018) 16(2):95–104. doi: 10.1007/s11914-018-0422-3

2. Lecka-Czernik B. Marrow fat metabolism is linked to the systemic energy metabolism. *Bone* (2012) 50(2):534–9. doi: 10.1016/j.bone.2011.06.032

3. Sulston RJ, Cawthorn WP. Bone marrow adipose tissue as an endocrine organ: Close to the bone? *Horm Mol Biol Clin Investig* (2016) 28(1):21–38. doi: 10.1515/hmbci-2016-0012

4. Li Z, Hardij J, Bagchi DP, Scheller EL, MacDougald OA. Development, regulation, metabolism and function of bone marrow adipose tissues. *Bone* (2018) 110:134–40. doi: 10.1016/j.bone.2018.01.008

5. Beresford JN, Bennett JH, Devlin C, Leboy PS, Owen ME. Evidence for an inverse relationship between the differentiation of adipocytic and osteogenic cells in rat marrow stromal cell cultures. *J Cell Sci* (1992) 102(Pt 2):341–51. doi: 10.1242/jcs.102.2.341

6. Pei L, Tontonoz P. Fat's loss is bone's gain. *J Clin Invest* (2004) 113(6):805–6. doi: 10.1172/JCI21311

7. Alund AW, Mercer KE, Pulliam CF, Suva LJ, Chen JR, Badger TM, et al. Partial protection by dietary antioxidants against ethanol-induced osteopenia and changes in bone morphology in female mice. *Alcohol Clin Exp Res* (2017) 41(1):46–56. doi: 10.1111/acer.13284

8. Gevers EF, Loveridge N, Robinson IC. Bone marrow adipocytes: A neglected target tissue for growth hormone. *Endocrinology* (2002) 143(10):4065–73. doi: 10.1210/en.2002-220428

9. Jee WS, Wronski TJ, Morey ER, Kimmel DB. Effects of spaceflight on trabecular bone in rats. *Am J Physiol* (1983) 244(3):R310–4. doi: 10.1152/ajpregu.1983.244.3.R310

10. Yarrow JF, Toklu HZ, Balaez A, Phillips EG, Otzel DM, Chen C, et al. Fructose consumption does not worsen bone deficits resulting from high-fat feeding in young male rats. *Bone* (2016) 85:99–106. doi: 10.1016/j.bone.2016.02.004

11. Muruganandan S, Sinal CJ. The impact of bone marrow adipocytes on osteoblast and osteoclast differentiation. *IUBMB Life* (2014) 66(3):147–55. doi: 10.1002/iub.1254

12. Verma S, Rajaratnam JH, Denton J, Hoyland JA, Byers RJ. Adipocytic proportion of bone marrow is inversely related to bone formation in osteoporosis. *J Clin Pathol* (2002) 55(9):693–8. doi: 10.1136/jcp.55.9.693

13. Akune T, Ohba S, Kamekura S, Yamaguchi M, Chung UI, Kubota N, et al. PPARgamma insufficiency enhances osteogenesis through osteoblast formation from bone marrow progenitors. *J Clin Invest* (2004) 113(6):846–55. doi: 10.1172/JCI200419900

14. Menagh PJ, Turner RT, Jump DB, Wong CP, Lowry MB, Yakar S, et al. Growth hormone regulates the balance between bone formation and bone marrow adiposity. *J Bone Miner Res* (2010) 25(4):757–68. doi: 10.1359/jbmr.091015

15. Turner RT, Iwaniec UT. Low dose parathyroid hormone maintains normal bone formation in adult male rats during rapid weight loss. *Bone* (2011) 48(4):726–32. doi: 10.1016/j.bone.2010.12.034

16. Galileo G. *Discorsi e dimostrazioni matematiche intorno a due nuove scienze*. Dialogues Concerning Two New Sciences. Macmillan. (1638).

17. Swoap SJ, Gutilla MJ. Cardiovascular changes during daily torpor in the laboratory mouse. *Am J Physiol Regul Integr Comp Physiol* (2009) 297(3):R769–74. doi: 10.1152/ajpregu.00131.2009

18. Karp CL. Unstressing intemperate models: How cold stress undermines mouse modeling. *J Exp Med* (2012) 209(6):1069–74. doi: 10.1084/jem.20120988

19. Vialard F, Olivier M. Thermoneutrality and immunity: How does cold stress affect disease? *Front Immunol* (2020) 11:588387. doi: 10.3389/fimmu.2020.588387

20. Glatt V, Canalis E, Stadmeyer L, Bouxsein ML. Age-related changes in trabecular architecture differ in female and male C57BL/6J mice. *J Bone Miner Res* (2007) 22(8):1197–207. doi: 10.1359/jbmr.070507

21. Martin SA, Philbrick KA, Wong CP, Olson DA, Branscum AJ, Jump DB, et al. Thermoneutral housing attenuates premature cancellous bone loss in male C57BL/6J mice. *Endocr Connect.* (2019) 8(11):1455–67. doi: 10.1530/EC-19-0359

22. Robbins A, Tom C, Cosman MN, Moursi C, Shipp L, Spencer TM, et al. Low temperature decreases bone mass in mice: Implications for humans. *Am J Phys Anthropol* (2018) 167(3):557–68. doi: 10.1002/ajpa.23684

23. Lindenmaier LB, Philbrick KA, Branscum AJ, Kalra SP, Turner RT, Iwaniec UT. Hypothalamic leptin gene therapy reduces bone marrow adiposity in ob/ob mice fed regular and high-fat diets. *Front Endocrinol (Lausanne).* (2016) 7:110. doi: 10.3389/fendo.2016.00110

24. Turner RT, Philbrick KA, Kuah AF, Branscum AJ, Iwaniec UT. Role of estrogen receptor signaling in skeletal response to leptin in female ob/ob mice. *J Endocrinol* (2017) 233(3):357–67. doi: 10.1530/JOE-17-0103

25. Bartell SM, Rayalam S, Ambati S, Gaddam DR, Hartzell DL, Hamrick M, et al. Central (ICV) leptin injection increases bone formation, bone mineral density, muscle mass, serum IGF-1, and the expression of osteogenic genes in leptin-deficient ob/ob mice. *J Bone Miner Res* (2011) 26(8):1710–20. doi: 10.1002/jbmr.406

26. Gat-Yablonski G, Phillip M. Leptin and regulation of linear growth. *Curr Opin Clin Nutr Metab Care* (2008) 11(3):303–8. doi: 10.1097/MCO.0b013e3282f795cf

27. McCabe IC, Fedorko A, Myers MGJr., Leinninger G, Scheller E, McCabe LR. Novel leptin receptor signaling mutants identify location and sex-dependent modulation of bone density, adiposity, and growth. *J Cell Biochem* (2019) 120(3):4398–408. doi: 10.1002/jcb.27726

28. Steppan CM, Crawford DT, Chidsey-Frink KL, Ke H, Swick AG. Leptin is a potent stimulator of bone growth in ob/ob mice. *Regul Pept* (2000) 92(1-3):73–8. doi: 10.1016/S0167-0115(00)00152-X

29. Hamrick MW, Della-Fera MA, Choi YH, Pennington C, Hartzell D, Baile CA. Leptin treatment induces loss of bone marrow adipocytes and increases bone formation in leptin-deficient ob/ob mice. *J Bone Miner Res* (2005) 20(6):994–1001. doi: 10.1359/JBMR.050103

30. Li S, Jiang H, Wang B, Gu M, Zhang N, Liang W, et al. Effect of leptin on marrow adiposity in ovariectomized rabbits assessed by proton magnetic resonance spectroscopy. *J Comput Assist Tomogr* (2018) 42(4):588–93. doi: 10.1097/RCT.0000000000000725

31. Iwaniec UT, Philbrick KA, Wong CP, Gordon JL, Kahler-Quesada AM, Olson DA, et al. Room temperature housing results in premature cancellous bone loss in growing female mice: implications for the mouse as a preclinical model for age-related bone loss. *Osteoporos Int* (2016) 27(10):3091–101. doi: 10.1007/s00198-016-3634-3

32. Piotrowska K, Tarnowski M. Bone marrow adipocytes-role in physiology and various nutritional conditions in human and animal models. *Nutrients* (2021) 13(5):1412. doi: 10.3390/nu13051412

33. Skop V, Guo J, Liu N, Xiao C, Hall KD, Gavrilova O, et al. Mouse thermoregulation: Introducing the concept of the thermoneutral point. *Cell Rep* (2020) 31(2):107501. doi: 10.1096/fasebj.2020.34.s1.05797

34. Kokolus KM, Capitano ML, Lee CT, Eng JW, Waight JD, Hylander BL, et al. Baseline tumor growth and immune control in laboratory mice are significantly influenced by subthermoneutral housing temperature. *Proc Natl Acad Sci U S A* (2013) 110(50):20176–81. doi: 10.1073/pnas.1304291110

35. Philbrick KA, Wong CP, Branscum AJ, Turner RT, Iwaniec UT. Leptin stimulates bone formation in ob/ob mice at doses having minimal impact on energy metabolism. *J Endocrinol* (2017) 232(3):461–74. doi: 10.1530/JOE-16-0484

36. Iwaniec UT, Wronski TJ, Turner RT. Histological analysis of bone. *Methods Mol Biol* (2008) 447:325–41. doi: 10.1007/978-1-59745-242-7_21

37. Dempster DW, Compston JE, Drezner MK, Glorieux FH, Kanis JA, Malluche H, et al. Standardized nomenclature, symbols, and units for bone histomorphometry: A 2012 update of the report of the ASBMR histomorphometry nomenclature committee. *J Bone Miner Res* (2013) 28(1):2–17. doi: 10.1002/jbmr.1805

38. Benjamini Y, Hochberg Y. Controlling the false dicovery rate: a practical and powerful approach to multiple testing. *J R Stat Soc Ser B* (1995) 57(1):289–300. doi: 10.1111/j.2517-6161.1995.tb02031.x

39. Keune JA, Philbrick KA, Branscum AJ, Iwaniec UT, Turner RT. Spaceflight-induced vertebral bone loss in ovariectomized rats is associated with increased bone marrow adiposity and no change in bone formation. *NPJ Microgravity* (2016) 2:16016. doi: 10.1038/npjmgrav.2016.16

40. Maddalozzo GF, Turner RT, Edwards CH, Howe KS, Widrick JJ, Rosen CJ, et al. Alcohol alters whole body composition, inhibits bone formation, and increases bone marrow adiposity in rats. *Osteoporos Int* (2009) 20(9):1529–38. doi: 10.1007/s00198-009-0836-y

41. Hui SK, Sharkey L, Kidder LS, Zhang Y, Fairchild G, Coghill K, et al. The influence of therapeutic radiation on the patterns of bone marrow in ovary-intact and ovariectomized mice. *PLoS One* (2012) 7(8):e42668. doi: 10.1371/journal.pone.0042668

42. Turner RT, Iwaniec UT, Wong CP, Lindenmaier LB, Wagner LA, Branscum AJ, et al. Acute exposure to high dose gamma-radiation results in transient activation of bone lining cells. *Bone* (2013) 57(1):164–73. doi: 10.1016/j.bone.2013.08.002

43. Iwaniec UT, Turner RT. Failure to generate bone marrow adipocytes does not protect mice from ovariectomy-induced osteopenia. *Bone* (2013) 53(1):145–53. doi: 10.1016/j.bone.2012.11.034

44. Aguirre JI, Leal ME, Rivera MF, Vanegas SM, Jorgensen M, Wronski TJ. Effects of basic fibroblast growth factor and a prostaglandin E2 receptor subtype 4 agonist on osteoblastogenesis and adipogenesis in aged ovariectomized rats. *J Bone Miner Res* (2007) 22(6):877–88. doi: 10.1359/jbmr.070313

45. Keune JA, Branscum AJ, Wong CP, Iwaniec UT, Turner RT. Effect of leptin deficiency on the skeletal response to hindlimb unloading in adult male mice. *Sci Rep* (2019) 9(1):9336. doi: 10.1038/s41598-019-45587-0

46. Philbrick KA, Wong CP, Kahler-Quesada AM, Olson DA, Branscum AJ, Turner RT, et al. Polyethylene particles inserted over calvarium induce cancellous bone loss in femur in female mice. *Bone Rep* (2018) 9:84–92. doi: 10.1016/j.bonr.2018.07.001

47. Turner RT, Wong CP, Iwaniec UT. Effect of reduced c-kit signaling on bone marrow adiposity. *Anat Rec (Hoboken).* (2011) 294(7):1126–34. doi: 10.1002/ar.21409

48. Potter JE, Wright EG. Bone marrow lipids in normal and anemic mice. *Am J Hematol* (1980) 8(4):361–7. doi: 10.1002/ajh.2830080404

49. Keune JA, Wong CP, Branscum AJ, Iwaniec UT, Turner RT. Bone marrow adipose tissue deficiency increases disuse-induced bone loss in male mice. *Sci Rep* (2017) 7:46325. doi: 10.1038/srep46325

50. Gowen J GE. Physiological factors necessary to alleviate genetic lethal anemia in mice. *Am Naturalist* (1932) 66(705):289–300. doi: 10.1086/280437

51. Lewis JP, O'Grady LF, Bernstein SE, Russell EE, Trobaugh FEJr. Growth and differentiation of transplanted W/Wv marrow. *Blood* (1967) 30(5):601–16. doi: 10.1182/blood.V30.5.601.601

52. Deyhle RTJr., Wong CP, Martin SA, McDougall MQ, Olson DA, Branscum AJ, et al. Maintenance of near normal bone mass and architecture in lethally irradiated female mice following adoptive transfer with as few as 750 purified hematopoietic stem cells. *Radiat Res* (2019) 191(5):413–27. doi: 10.1667/RR15164.1

53. Li Z, Bowers E, Zhu J, Yu H, Hardij J, Bagchi DP, et al. Lipolysis of bone marrow adipocytes is required to fuel bone and the marrow niche during energy deficits. *Elife* (2022) 11:e78496. doi: 10.7554/eLife.78496.sa2

54. Tratwal J, Rojas-Sutterlin S, Bataclan C, Blum S, Naveiras O. Bone marrow adiposity and the hematopoietic niche: A historical perspective of reciprocity, heterogeneity, and lineage commitment. *Best Pract Res Clin Endocrinol Metab* (2021) 35(4):101564. doi: 10.1016/j.beem.2021.101564

55. Zhang Z, Huang Z, Ong B, Sahu C, Zeng H, Ruan HB. Bone marrow adipose tissue-derived stem cell factor mediates metabolic regulation of hematopoiesis. *Haematologica* (2019) 104(9):1731–43. doi: 10.3324/haematol.2018.205856

56. Clabaut A, Delplace S, Chauveau C, Hardouin P, Broux O. Human osteoblasts derived from mesenchymal stem cells express adipogenic markers upon coculture with bone marrow adipocytes. *Differentiation.* (2010) 80(1):40–5. doi: 10.1016/j.diff.2010.04.004

57. Liu LF, Shen WJ, Ueno M, Patel S, Kraemer FB. Characterization of age-related gene expression profiling in bone marrow and epididymal adipocytes. *BMC Genomics* (2011) 12:212. doi: 10.1186/1471-2164-12-212

58. Taipaleenmaki H, Abdallah BM, AlDahmash A, Saamanen AM, Kassem M. Wnt signalling mediates the cross-talk between bone marrow derived pre-adipocytic and pre-osteoblastic cell populations. *Exp Cell Res* (2011) 317(6):745–56. doi: 10.1016/j.yexcr.2010.12.015

59. Wang D, Haile A, Jones LC. Dexamethasone-induced lipolysis increases the adverse effect of adipocytes on osteoblasts using cells derived from human mesenchymal stem cells. *Bone* (2013) 53(2):520–30. doi: 10.1016/j.bone.2013.01.009

60. Goto H, Osaki M, Fukushima T, Sakamoto K, Hozumi A, Baba H, et al. Human bone marrow adipocytes support dexamethasone-induced osteoclast differentiation and function through RANKL expression. *BioMed Res* (2011) 32(1):37–44. doi: 10.2220/biomedres.32.37

61. Turner RT, Wong CP, Fosse KM, Branscum AJ, Iwaniec UT. Caloric restriction and hypothalamic leptin gene therapy have differential effects on energy partitioning in adult female rats. *Int J Mol Sci* (2021) 22(13):6789. doi: 10.3390/ijms22136789

62. Philbrick KA, Turner RT, Branscum AJ, Wong CP, Iwaniec UT. Paradoxical effects of partial leptin deficiency on bone in growing female mice. *Anat Rec (Hoboken).* (2015) 298(12):2018–29. doi: 10.1002/ar.23267

63. Halaas JL, Boozer C, Blair-West J, Fidahusein N, Denton DA, Friedman JM. Physiological response to long-term peripheral and central leptin infusion in lean and obese mice. *Proc Natl Acad Sci U S A* (1997) 94(16):8878–83. doi: 10.1073/pnas.94.16.8878

64. Van Heek M, Compton DS, France CF, Tedesco RP, Fawzi AB, Graziano MP, et al. Diet-induced obese mice develop peripheral, but not central, resistance to leptin. *J Clin Invest.* (1997) 99(3):385–90. doi: 10.1172/JCI119171

65. Turner RT, Philbrick KA, Wong CP, Gamboa AR, Branscum AJ, Iwaniec UT. Effects of propranolol on bone, white adipose tissue, and bone marrow adipose tissue in mice housed at room temperature or thermoneutral temperature. *Front Endocrinol (Lausanne).* (2020) 11:117. doi: 10.3389/fendo.2020.00117

66. Priego T, Sanchez J, Palou A, Pico C. Effect of high-fat diet feeding on leptin receptor expression in white adipose tissue in rats: depot- and sex-related differential response. *Genes Nutr* (2009) 4(2):151–6. doi: 10.1007/s12263-009-0114-9

67. Chen X, Bollinger E, Cunio T, Damilano F, Stansfield JC, Pinkus CA, et al. An assessment of thermoneutral housing conditions on murine cardiometabolic function. *Am J Physiol Heart Circ Physiol* (2022) 322(2):H234–H45. doi: 10.1152/ajpheart.00461.2021

68. Wee NKY, Nguyen AD, Enriquez RF, Zhang L, Herzog H, Baldock PA. Neuropeptide y regulation of energy partitioning and bone mass during cold exposure. *Calcif Tissue Int* (2020) 107(5):510–23. doi: 10.1007/s00223-020-00745-9

69. van der Stelt I, Hoevenaars F, Siroka J, de Ronde L, Friedecky D, Keijer J, et al. Metabolic response of visceral white adipose tissue of obese mice exposed for 5 days to human room temperature compared to mouse thermoneutrality. *Front Physiol* (2017) 8:179. doi: 10.3389/fphys.2017.00179

70. Povinelli BJ, Kokolus KM, Eng JW, Dougher CW, Curtin L, Capitano ML, et al. Standard sub-thermoneutral caging temperature influences radiosensitivity of hematopoietic stem and progenitor cells. *PLoS One* (2015) 10(3):e0120078. doi: 10.1371/journal.pone.0120078

71. Kunst RF, Langlais AL, Barlow D, Houseknecht KL, Motyl KJ. Housing temperature influences atypical antipsychotic drug-induced bone loss in female C57BL/6J mice. *JBMR Plus* (2021) 5(10):e10541. doi: 10.1002/jbm4.10541

72. Tastad CA, Kohler R, Wallace JM. Limited impacts of thermoneutral housing on bone morphology and mechanical properties in growing female mice exposed to external loading and raloxifene treatment. *Bone* (2021) 146:115889. doi: 10.1016/j.bone.2021.115889

frontiers | Frontiers in Endocrinology

TYPE Original Research
PUBLISHED 16 November 2022
DOI 10.3389/fendo.2022.921073

OPEN ACCESS

EDITED BY
Jonathan H Tobias,
University of Bristol, United Kingdom

REVIEWED BY
William Peter Cawthorn,
University of Edinburgh,
United Kingdom
Nicola J Lee,
The University of Sydney, Australia

*CORRESPONDENCE
Sarah Beck-Cormier
sarah.beck@univ-nantes.fr

†PRESENT ADDRESSES
Marie Guicheteau,
Nantes Université, CNRS, INSERM,
l'institut du thorax, Nantes, France
Laurent Beck,
Nantes Université, CNRS, INSERM,
l'institut du thorax, Nantes, France
Sarah Beck-Cormier,
Nantes Université, CNRS, INSERM,
l'institut du thorax, Nantes, France

SPECIALTY SECTION
This article was submitted to
Bone Research,
a section of the journal
Frontiers in Endocrinology

RECEIVED 15 April 2022
ACCEPTED 24 October 2022
PUBLISHED 16 November 2022

CITATION
Frangi G, Guicheteau M, Jacquot F, Pyka G, Kerckhofs G, Feyeux M, Veziers J, Guihard P, Halgand B, Sourice S, Guicheux J, Prieur X, Beck L and Beck-Cormier S (2022) PiT2 deficiency prevents increase of bone marrow adipose tissue during skeletal maturation but not in OVX-induced osteoporosis.
Front. Endocrinol. 13:921073.
doi: 10.3389/fendo.2022.921073

PiT2 deficiency prevents increase of bone marrow adipose tissue during skeletal maturation but not in OVX-induced osteoporosis

Giulia Frangi[1], Marie Guicheteau[1†], Frederic Jacquot[2], Grzegorz Pyka[3,4], Greet Kerckhofs[3,4,5,6], Magalie Feyeux[7], Joëlle Veziers[1], Pierre Guihard[1], Boris Halgand[1], Sophie Sourice[1], Jérôme Guicheux[1], Xavier Prieur[8], Laurent Beck[1†] and Sarah Beck-Cormier[1*†]

[1]Nantes Université, Oniris, CHU Nantes, Inserm, Regenerative Medicine and Skeleton, RMeS, UMR 1229, SFR Bonamy, Nantes, France, [2]Nantes Université, CHU Nantes, Inserm, CNRS, CRCI2NA, Nantes, France, [3]Biomechanics lab, Institute of Mechanics, Materials, and Civil Engineering, UC Louvain, Louvain-la-Neuve, Belgium, [4]Department of Materials Engineering, KU Leuven, Leuven, Belgium, [5]IREC, Institute of Experimental and Clinical Research, UC Louvain, Woluwé-Saint-Lambert, Belgium, [6]Prometheus, Division of Skeletal Tissue Engineering, KU Leuven, Leuven, Belgium, [7]Nantes Université, CHU Nantes, CNRS, Inserm, BioCore, US16, SFR Bonamy, Nantes, France, [8]Nantes Université, CNRS, Inserm, l'Institut du Thorax, Nantes, France

The common cellular origin between bone marrow adipocytes (BMAds) and osteoblasts contributes to the intimate link between bone marrow adipose tissue (BMAT) and skeletal health. An imbalance between the differentiation ability of BMSCs towards one of the two lineages occurs in conditions like aging or osteoporosis, where bone mass is decreased. Recently, we showed that the sodium-phosphate co-transporter PiT2/SLC20A2 is an important determinant for bone mineralization, strength and quality. Since bone mass is reduced in homozygous mutant mice, we investigated in this study whether the BMAT was also affected in *PiT2*$^{-/-}$ mice by assessing the effect of the absence of PiT2 on BMAT volume between 3 and 16 weeks, as well as in an ovariectomy-induced bone loss model. Here we show that the absence of PiT2 in juveniles leads to an increase in the BMAT that does not originate from an increased adipogenic differentiation of bone marrow stromal cells. We show that although *PiT2*$^{-/-}$ mice have higher BMAT volume than control *PiT2*$^{+/+}$ mice at 3 weeks of age, BMAT volume do not increase from 3 to 16 weeks of age, leading to a lower BMAT volume in 16-week-old *PiT2*$^{-/-}$ compared to *PiT2*$^{+/+}$ mice. In contrast, the absence of PiT2 does not prevent the increase in BMAT volume in a model of ovariectomy-induced bone loss. Our data identify *SLC20a2/PiT2* as a novel

10.3389/fendo.2022.921073

gene essential for the maintenance of the BMAd pool in adult mice, involving mechanisms of action that remain to be elucidated, but which appear to be independent of the balance between osteoblastic and adipogenic differentiation of BMSCs.

KEYWORDS

PiT2/Slc20a2, adipocytes, bone, post-menopausal osteoporotic mouse model, marrow

Introduction

Bone marrow adipose tissue (BMAT) is no longer considered a marrow space filler tissue as the increasing number of studies on its function in the past 20 years has highlighted its important roles in skeletal health or energetic metabolism. However, the underlying cellular and molecular mechanisms involved remain to be determined (1–3). In mice, bone marrow adipocytes (BMAds) first develop in the distal tibia at a very early postnatal age and then appear in the proximal tibia at around 3 months of age (3, 4). The volume of BMAT increases with age in humans and mice, turning the bone marrow from "red" to "yellow". The proximal and distal BMAT are two distinct tissues mainly because the size and the lipidic components of the adipocytes are different, and both are differentially regulated (5). The proximal BMAT is also referred to as regulated BMAT (rBMAT) due to the observation that its volume is regulated by several physiopathological conditions (caloric restriction, cold exposure…), whereas the distal one is referred to as constitutive BMAT (cBMAT) because volume variations of this tissue are less frequently observed.

A growing interest in BMAT and its intimate relationship with skeletal health has emerged in recent years. Inverse correlation between BMAT volume and bone mass has been described in many situations (5) and also in some genetic mouse models (6–11). However, this negative correlation is not always observed and may even be controversial, as in the ovariectomy-induced osteoporosis model (7, 11). In healthy populations, BMAT increases with age both in men and women, with men generally having more BMAT (12, 13), and an inverse correlation between BMAT volume and bone mineral density (BMD) has been described (14–17). Nevertheless, during puberty, the amount of marrow fat is positively associated with total bone mineral content in girls (18) and, although men have more BMAT mass compared to women, they also have more bone mass (19). These observations highlight a complex relationship between BMAT and bone, which probably cannot be described in all circumstances as a simple inverse correlation.

Nonetheless, the relationship between BMAT and bone is based at least on the fact that osteoblasts and BMAds are both derived from bone marrow stromal cells (BMSCs). The imbalance between the differentiation capacities of BMSCs towards one of the two lineages is at the origin of the increased bone marrow adiposity in conditions like aging, obesity and other pathologies where the bone mass is decreased (11, 20, 21) and a better knowledge of the underlying mechanisms would allow a better understanding of the balancing relationship between bone and BMAT.

PiT2 is a member of the Slc20 family of sodium (Na)-phosphate (Pi) co-transporters, encoded by the *Slc20a2* gene. In the last 10 years, numerous studies have revealed the multifunctionality of PiT1/SLC20A1 and PiT2/SLC20A2 in the regulation of cellular proliferation, differentiation or survival (22–30). In bone, our group and others have shown the involvement of PiT2 in bone quality, mineralization and strength (31, 32). Homozygous mutant mice were shown to exhibit severe reduction of bone mechanical properties (decreased yield load, maximum load, fracture load and stiffness), reduced bone mineral density and reduced bone mass (31, 32). Considering the deleterious effect of PiT2 deficiency in bone, we questioned whether the BMAT could also be affected in PiT2 knockout mice. In addition, we evaluated the effect of the absence of PiT2 on the regulation of bone and BMAT volumes between 3 and 16 weeks and in a model of ovariectomy-induced bone loss.

Materials & methods

Mice

C57BL/6NTac-Slc20a2tm11a (EUCOMM) Wtsi (*Slc20a2*$^{+/-}$, hereafter named *PiT2*$^{+/-}$) heterozygous mice were obtained from the European Mouse Mutant Archive (EMMA) and maintained and genotyped at Nantes Université. Experiments on mice were conducted according to the French and European regulations on care and protection of laboratory animals (EC Directive 86/609, French Law 2001-486 issued on June 6, 2001). This study complied with ARRIVE (Animal Research: Reporting of *In Vivo* Experiments) guidelines and was approved by the Animal Care

Committee of Pays de la Loire (APAFIS agreements 02286.02, 14835-2020-05-13 and 22178-2019092614593965 v7). Animal care and maintenance were provided through the Nantes Université accredited animal facility at the "Unité de Thérapeutique Expérimentale" (UTE). Mice were housed under specific pathogen-free conditions in open or individually ventilated cages, with wood shavings for bedding and nesting material, in groups of up to five. The mice had *ad libitum* access to tap water and standard rodent chow (A04-10; SAFE, France). Genotyping was performed by PCR as described (31). Wild-type ($PiT2^{+/+}$) and $PiT2^{-/-}$ littermate mice were analysed at 3 and 16 weeks. Three-week-old mice were used for *in vitro* experiments (adipogenic differentiation, flow cytometry). Ovariectomy (OVX) was performed under isoflurane anesthesia in 13-week-old female $PiT2^{+/+}$ and $PiT2^{-/-}$ littermate mice, which were euthanized 5 weeks later. $PiT2^{+/+}$and $PiT2^{-/-}$ mice were randomly allocated to two groups: an OVX group and a sham group (mice were similarly incised but the ovaries were not removed). Mice were anesthetized with ketamine/xylazine administered intraperitoneally and were perfused transcardially with Phosphate Buffered Saline (PBS) and then 4% Paraformaldehyde (PFA; Sigma Aldrich, USA). Uterine aplasia was observed, confirming the successful ovariectomy. Right tibiae were removed and fixed in 4% PFA for 24 hours at 4°C and stored in PBS at 4°C for the subsequent CE-CT analyses.

Contrast-enhanced high resolution microfocus computed tomography

Before polyoxometalate-staining (33), the distal end of the bones was removed to allow better diffusion of the contrast agent into the bone marrow compartment. Samples were incubated in the staining solution during 48 hours at 4°C while shaking gently.

CE-CT acquisition and image processing were performed as previously described (33, 34). Briefly, samples were imaged using a Phoenix Nanotom S (GE Measurement and Control Solutions, Germany) and analysed using DataViewer (Bruker MicroCT, Belgium) for the reorientation of the CE-CT datasets and CTAn (Bruker MicroCT) for the assessment of the fat volume in the proximal and distal tibiae Ad.V relative to Ma.V (bone marrow without trabecular and cortical bones) was determined at 2-µm resolution in a 2mm (proximal) or 4mm (distal) region beginning right underneath the growth plate. Segmentation and morphological assessment of adipocytes was performed as previously described (33).

For bone volume fraction (BV/TV %) and Cortical thickness (Ct.th. mm) analyses, we used an in-house developed semi-automated protocol. Volumes of interest around the trabecular bone region were drawn in the proximal metaphysis starting directly underneath growth plate and covering a height of 1.2mm distal to the growth plate. Cortical thickness was determined in a mid-diaphyseal volume of interest starting 1mm proximal of the tibio-fibular junction, extending 1mm in the proximal direction.

BMSCs culture

BMSCs were harvested from tibiae of 3-week-old $PiT2^{-/-}$ and $PiT2^{+/+}$ mice. After removing the epiphyses, bones were flushed to isolate total bone marrow cells and BMSCs were expanded in growth media consisting of α-MEM (Eurobio, France) supplemented with 15% fetal bovine serum (FBS), 100IU/mL penicillin, 100mg/mL streptomycin, 2mM glutamine. At confluence, BMSCs were cultured in adipogenic media consisting of α-MEM (Eurobio, France) supplemented with 15% FBS, 100IU/mL penicillin, 100mg/mL streptomycin, 2mM glutamine, 0.5µM 3-isobutyl-1-methylxanthine (IBMX), 0.5µM hydrocortisone and 60µM indomethacin (Sigma Aldrich).

Oil Red O staining and relative quantification

Cells were fixed in 2% PFA for 15min, washed with water, incubated with 60% isopropanol for 5min and stained with newly filtered Oil Red O solution for 10min at room temperature. To quantify staining, Oil Red O was extracted from the cells with isopropanol and absorbance of the solution was measured at a wavelength of 520nm to determine the relative amount of dye. Determination of the number of adipocytes (Oil Red O positive cells) and the number of total cells (Hoechst positive cells) was performed by using the High Content Screening Arrayscan (ThermoScientific). Image acquisitions (361 images per well) were performed using the Cellomics ArrayScan VTI/HCS Reader (ThermoScientific) using x5 magnification. Images analysis was performed with CellProfiler (35).

Flow cytometry

Flow cytometry was performed on a BD LSRFortessa™ (BD Biosciences), FACS data were collected using DIVA (Becton Dickinson) and analysed using FlowJo software (Tree Star). For flow cytometry analyses, BMSCs were isolated by flushing tibiae of P21 mice, flushed bones were crushed with a mortar and treated with collagenase for 20min at 37°C to retrieve any remaining BMSCs. The reaction was stopped by adding α-MEM complemented with 15% FBS and the cell suspension was passed through a 70µm cell strainer (BD Falcon, MA, USA)

10.3389/fendo.2022.921073

to remove bone fragments. The cells were then added to the previously flushed bone marrow with isolated BMSCs. Cells were centrifuged at 1200rpm for 5min at RT, the pellet was resuspended in Red Blood Cell Lysis Buffer (Sigma, Product No. R 7757) to eliminate red blood cells and centrifuged again at 1200rpm for 5min at RT. The pellet was resuspended and the cells were counted. Five million cells were stained with antibodies (Supporting Table S1) for 30min on ice. Compensation was performed using OneComp^{TM} eBeads Compensation Beads (ThermoFisher Scientific Inc.). BMSCs were analysed as Ter119$^-$ CD45$^-$ Sca1$^+$ CD44$^+$ CD105$^+$ (36, 37) and adipogenic progenitors as Ter119$^-$ CD45$^-$ CD31$^-$ Sca1$^+$ CD24$^-$ (38).

RNA isolation and RT-qPCR

Total RNA was prepared with TRIzol Reagent (ThermoFisher Scientific) according to the manufacturer's instructions. The RNA was reverse transcribed and analysed on a Bio-Rad CFX96 detection system using SYBR Select Master Mix (Applied Biosystems, Warrington, UK). mRNA levels were normalized relative to beta-glucuronidase (*GusB*) and Pinin (*Pnn*) expression and quantified using the ΔΔCT method (39). RT-qPCR primers were: Pinin Forward (Fw)-ACCTGG AAGGGGCAGTCAGTA and Reverse (Rv)-ATCATCGT CTTCTGGGTCGCT, GusB Fw-CTCTGGTGGCCTT ACCTGAT and Rv- CAGTTGTTGTCACCTTCACCTC, PiT1 Fw-TGTGGCAAATGGGCAGAAG and Rv-AGAAA GCAGCGGAGAGACGA, PiT2 Fw-CCATCGGCT TCTCACTCGT and Rv AAACCAGGAGGCGACAATCT, FABP4 Fw-GAATTCGATGAAATCACCGCA and Rv-CTCTTTATTGTGGTCGACTTTCCA, AdipoQ Fw- TCTCCT GTTCCTCTTAATCCTGCC and Rv-CATCTCCTTT CTCTCCCTTCTCTC.

Statistics

Statistical analyses were performed using the GraphPad 8.0 software. Data were analysed for normal distribution within each experimental group using the Shapiro–Wilk normality test. Normally distributed data were analysed by ANOVA or t tests, as appropriate. Where data were not normally distributed, non-parametric tests were used. When appropriate, p values were adjusted for multiple comparisons as indicated in the figure legends. A p value of less than 0.05 was considered statistically significant (exact n and p values are indicated in the figures or legends). Data are expressed as means ± S.E.M. Units and abbreviations are reported in accordance with recently published guidelines for research relating to BM adiposity (40).

Results

Proximal BMAT volume does not increase in *PiT2*$^{-/-}$ mice between 3 and 16 weeks

Bone marrow adipose tissue was investigated by using Hf-POM-based CE-CT analysis on tibiae from 3- and 16-week-old *PiT2*$^{+/+}$ and *PiT2*$^{-/-}$ littermate mice. The 3D visualization and quantification of the bone marrow adipocytes showed an increase in BMAT volume within the proximal tibia of 3-week-old *PiT2*$^{-/-}$ female (Figure 1A, Supplementary Figure 1) and male (Supplementary Figure 2A, Supplementary Figure 3) mice compared to *PiT2*$^{+/+}$ mice, which is consistent with the increased mRNA gene expression of *Adiponectin* (*AdipoQ*) and *FABP4* (Figure 1B, Supplementary Figure 2B), two markers of mature adipocytes. The absence of *PiT2* mRNA expression was confirmed in whole tibia from *PiT2*$^{-/-}$ mice by RT-qPCR (Figure 1B, Supplementary Figure 2B). Interestingly, no difference in the expression of the paralog *PiT1* mRNA expression was observed in *PiT2*$^{-/-}$ whole tibia, making a possible PiT1-driven compensatory mechanism unlikely (Figure 1B, Supplementary Figure 2B).

In contrast to *PiT2*$^{+/+}$ mice, CE-CT analyses showed that BMAT volumes did not increase between 3 and 16 weeks in the proximal tibia of *PiT2*$^{-/-}$ mice, both in females (Figure 1A), and males, (Supplementary Figure 2A), leading to a downward trend in BMAT volume at 16 weeks in *PiT2*$^{-/-}$ compared to wild-type mice. This illustrates the possibility that the absence of PiT2 blunts the age-induced BMAT increase that is normally observed in the proximal tibiae of wild-type mice. Interestingly, in contrast to proximal tibiae, the increase in distal BMAT between 3 and 16 weeks was not affected by the absence of PiT2 at least in female (Figure 1C, not determined in males), suggesting a specific role for PiT2 in the proximal BMAT.

Lack of PiT2 does not alter BMSCs adipogenic differentiation

BMAds originate from the adipogenic differentiation of bone marrow stromal cells. To investigate the ability of PiT2-deficient BMSC to differentiate into adipocytes, we first quantified the adipogenic progenitors and explored the adipogenic differentiation capacity of BMSCs. We quantified these cells as Ter119$^-$ CD45$^-$ Sca1$^+$ CD44$^+$ CD105$^+$ cells by flow cytometry. The results showed no difference in the proportion of BMSCs in 3-week-old *PiT2*$^{-/-}$ female samples compared to *PiT2*$^{+/+}$ mice (Figure 2A). Moreover, similar to BMSCs, analyses of adipogenic progenitors sorted as Ter119$^-$ CD45$^-$ CD31$^-$ Sca1$^+$ CD24$^-$ cells, showed that the proportion of adipogenic progenitors in *PiT2*$^{-/-}$ female mice was equal to that of *PiT2*$^{+/+}$ mice (Figure 2A).

10.3389/fendo.2022.921073

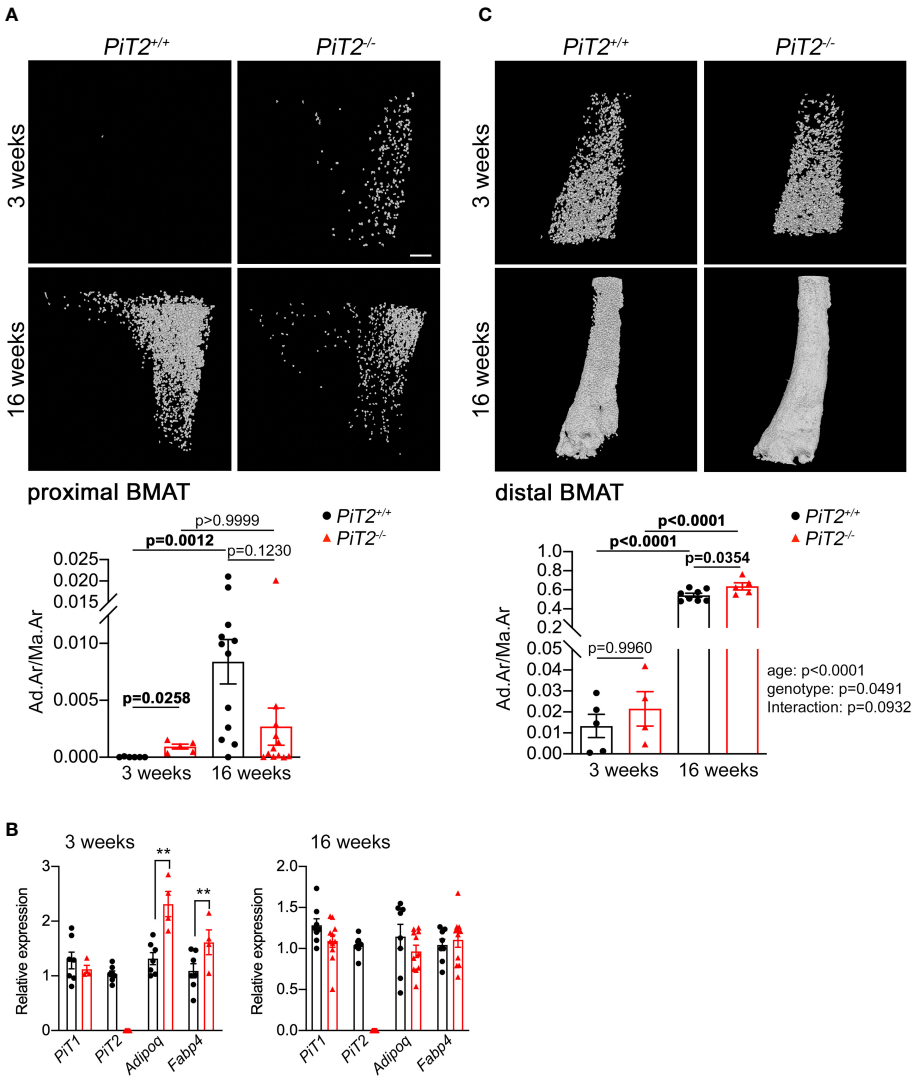

FIGURE 1
Deregulation of BMAT volume in *PiT2*$^{-/-}$ female mice. **(A)** *Upper* - Representative 3D visualization, using Hf-POM-based CE-CT, of the adipocytes in the bone marrow compartment of the proximal tibia of 3- and 16-week-old *PiT2*$^{+/+}$ and *PiT2*$^{-/-}$ female mice. Scale bar = 250µm. *Lower* - Graphs showing quantification of the volume fraction of the adipocytes in the VOI of the proximal tibia (Ad.Ar/Ma.Ar: Adipocyte area/Marrow Area) of 3- and 16-week-old *PiT2*$^{+/+}$ and *PiT2*$^{-/-}$ mice (n=6 and 12 per genotype, respectively). Data are means ± SEM, Bonferroni-corrected Mann-Whitney test. p values are indicated. **(B)** Relative *PiT1*, *PiT2*, *Adiponectin* and *FABP4* mRNA expression in the whole tibia from 3- (n=7 *PiT2*$^{+/+}$ and n=4-6 *PiT2*$^{-/-}$) and 16- (n=8 *PiT2*$^{+/+}$ and n=11 *PiT2*$^{-/-}$) week-old *PiT2*$^{+/+}$ and *PiT2*$^{-/-}$ female mice, as indicated. Data are means ± SEM, Mann-Whitney test, $^{**}p<0.01$. **(C)** *Upper* - Representative 3D visualization of the adipocytes in the bone marrow compartment of the distal tibia of 3- and 16-week-old *PiT2*$^{+/+}$ and *PiT2*$^{-/-}$ female mice. *Lower* - Graphs showing quantification of the volume fraction of the adipocytes in the VOI of the distal tibia of 3- and 16-week-old *PiT2*$^{+/+}$ and *PiT2*$^{-/-}$ mice (n=6 and 11 per genotype, respectively). Data are means ± SEM, the influence of age or genotype, and interactions between these, was determined by two-way ANOVA, with *p* values shown to the right of the graph. p values from multiple comparisons are indicated on the graph.

Adipogenic differentiation analyses of BMSCs isolated from tibiae of 3-week-old *PiT2*$^{-/-}$ and *PiT2*$^{+/+}$ mice did not show differences between mutant and *PiT2*$^{+/+}$ cells from female and male mice, neither by quantification of Oil Red O positive cells nor by *Adiponectin* and *FABP4* mRNA expression analyses (Figures 2B–D, Supplementary Figure 4). Similar to what is observed *in vivo*, *PiT1* mRNA expression showed no differences between *PiT2*$^{-/-}$ and *PiT2*$^{+/+}$ cells (Figure 2D and Supplementary Figure 4B). Altogether, these results revealed that lack of PiT2 expression did not alter BMSCs populations or adipogenic differentiation, despite aberrant regulation of proximal BMAT in mutant mice.

10.3389/fendo.2022.921073

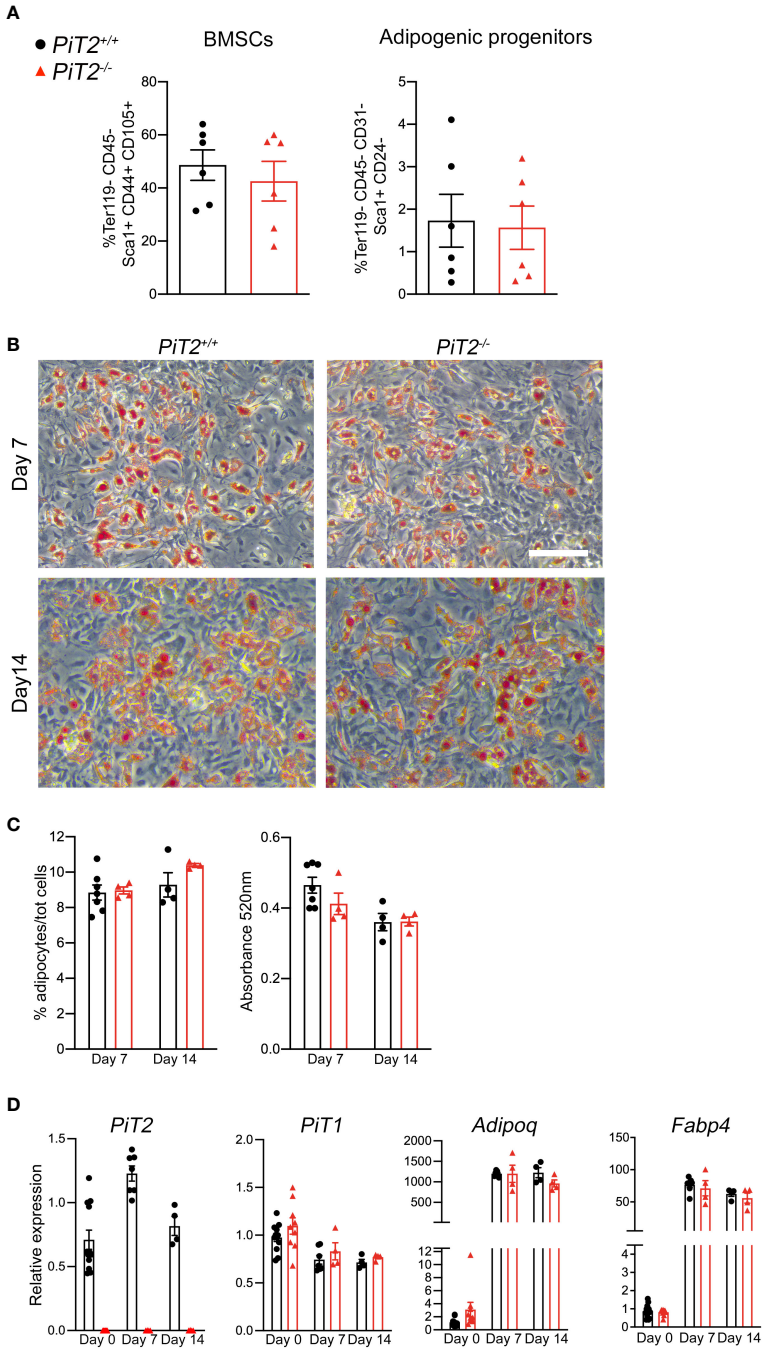

FIGURE 2
Characteristics of BMSCs in *PiT2*$^{-/-}$ mice. **(A)** FACS quantification of BMSCs (Ter119$^-$ CD45$^-$ Sca1$^+$ CD44$^+$ CD105$^+$) (*Left*) and adipogenic progenitors (Ter119$^-$ CD45$^-$ CD31$^-$ Sca1$^+$ CD24$^+$) (*Right*) in the bone marrow of tibiae from 3-week-old *PiT2*$^{+/+}$ and *PiT2*$^{-/-}$ female mice (n=6 per genotype). Data are means ± SEM, Mann-Whitney test. **(B)** Representative images of oil-red O (ORO) positive cells after adipogenic differentiation of *PiT2*$^{+/+}$ and *PiT2*$^{-/-}$ BMSCs. Scale bar = 100µm. **(C)** Quantitative analysis of ORO+ cells: *Left*, percentage of ORO+ cells related to the total number of Hoechst-positive cells; *right*, ORO absorbance at 520nm **(D)** Relative *PiT2*, *PiT1*, *Adiponectin* and *FABP4* mRNA expression at 0 (n=12 *PiT2*$^{+/+}$ and n=9 *PiT2*$^{-/-}$), 7 (n=7 *PiT2*$^{+/+}$ and n=4 *PiT2*$^{-/-}$) and 14 (n=4 *PiT2*$^{+/+}$ and n=4 *PiT2*$^{-/-}$) days of differentiation. N=3 independent experiments. Data are means ± SEM. Two-way ANOVA test.

Regulation of bone and BMAT volumes in *PiT2*$^{-/-}$ mice after ovariectomy (OVX)

To evaluate the regulation of bone and BMAT volumes, 13-week-old *PiT2*$^{-/-}$ female mice and their control littermate (*PiT2*$^{+/+}$) were subjected to OVX-induced osteoporosis. Five weeks after surgery, animals were analyzed for bone and BMAT volumes by CE-CT. Results show that sham-operated *PiT2*$^{-/-}$ female mice have similar trabecular BV/TV as *PiT2*$^{+/+}$ control mice, while cortical thickness was significantly reduced (Figure 3A), consistent with our previous study (31). In OVX mice, we showed a similar reduction in trabecular BV/TV and Ct.Th. in wild-type and *PiT2*$^{-/-}$ mice (Figure 3A). This reduction in bone volume parallels an increase in BMAT volume observed both in ovariectomized *PiT2*$^{+/+}$ and *PiT2*$^{-/-}$ mice compared with sham-operated controls (fold-change: 2.65 and 3.22, respectively; Figure 3B). Of note, sham-operated *PiT2*$^{-/-}$ mice showed a reduced BMAT volume compared with sham-operated *PiT2*$^{+/+}$ mice (Figure 3B), consistent with our observation in 16-week-old females (Figure 1A). These findings indicate that bone and BMAT volumes are inversely regulated in the model of ovariectomy-induced bone loss, and suggest that PiT2-deficient adipocytes retain the ability to be recruited after OVX.

Discussion

In the present study, we report for the first time a role for PiT2 in the maintenance of bone marrow adipose tissue volume.

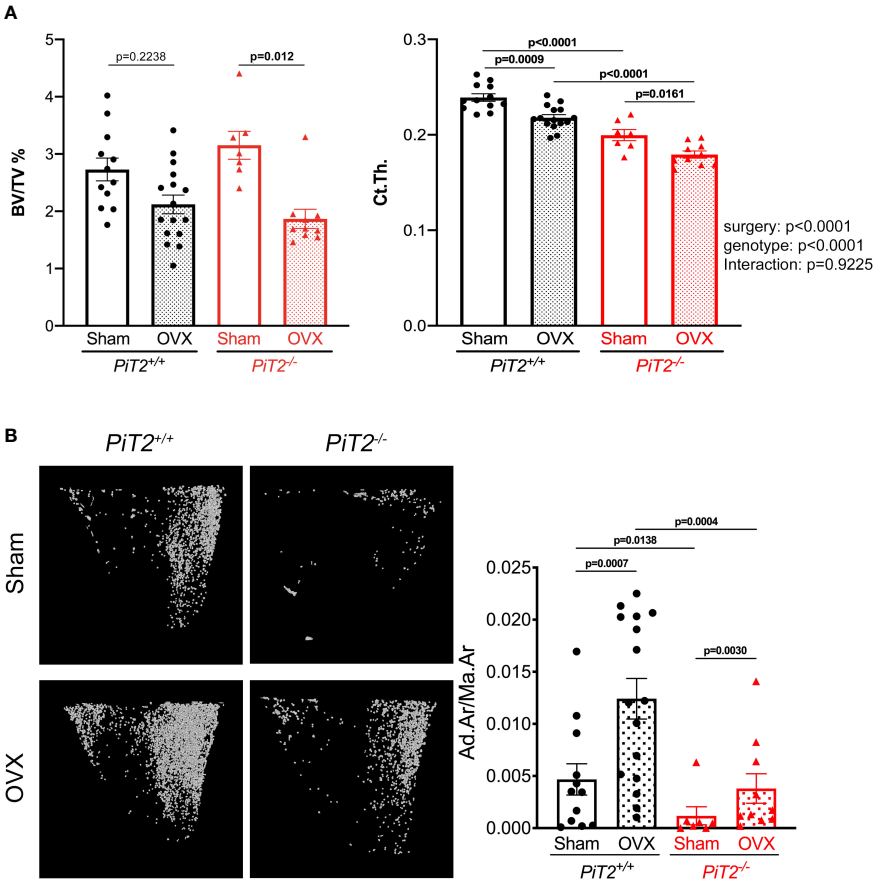

FIGURE 3
PiT2 deficiency does not prevent BMAT volume increase and bone mass loss after ovariectomy. **(A)** Bone volume/tissue volume (BV/TV, *left*) and cortical thickness (Ct.th., *right*) of tibia from shame operated mice (n=12 *PiT2*$^{+/+}$ and n=7 *PiT2*$^{-/-}$) or after ovariectomy (OVX, n=16 *PiT2*$^{+/+}$ and n=10 *PiT2*$^{-/-}$) quantified using CE-CT images. Data are means ± SEM, Bonferroni-corrected Mann-Whitney test (BV/TV) and two-way ANOVA test (Ct.Th.) For Ct.Th., the influence of surgery or genotype, and interactions between these, was determined by two-way ANOVA, with *p* values shown to the right of the graph. p values from multiple comparisons are indicated on the graphs **(B)** *Left:* representative 3D visualization, using Hf-POM-based CE-CT, of adipocytes in the bone marrow compartment of the proximal tibia (2mm height from the growth plate) of *PiT2*$^{+/+}$ and *PiT2*$^{-/-}$ female mice after ovariectomy (OVX). *Right*: graphs showing the quantification of the volume fraction of the adipocytes in the VOI of the proximal tibia (Ad.Ar/Ma.Ar: Adipocyte area/Marrow Area) in shamed operated mice (n=12 *PiT2*$^{+/+}$ and n=7 *PiT2*$^{-/-}$) or after ovariectomy (OVX, n=16 *PiT2*$^{+/+}$ and n=10 *PiT2*$^{-/-}$). Data are means ± SEM, Bonferroni-corrected Mann-Whitney test.

We also show that BMSCs with or without PiT2 are able to differentiate into adipocytes in an identical manner, suggesting that the regulation of proximal BMAT volume by PiT2 does not involve cell autonomous mechanisms.

Increased BMAT volume in young PiT2$^{-/-}$ mice

An increase in marrow adipocytes which inversely parallels a loss of bone volume is observed in numerous genetic models (6, 8, 10). This link between bone and BMAT volumes cross-regulation is based on either the balance between osteo-adipogenic differentiation of BMSC or the secreted factors from bone cells or BMAds which can act on the surrounding tissue (6, 8, 10, 41). Our previous work showed that bone mass in young (3-week-old) *PiT2*$^{-/-}$ mice was reduced compared to *PiT2*$^{+/+}$ mice (31), and we now show, conversely, that proximal BMAT volume is higher compared with wild-type mice. Although this is consistent with the expected inverse cross-regulation between bone and adipocyte volumes, we nevertheless show that adipogenic differentiation of PiT2-deficient BMSCs is not altered. However, the *in vitro* adipogenesis conditions used in our study may be so potent that they override any subtle differences in BMSC adipogenic potential that exist *in vivo*. In addition, the use of more sensitive technologies, such as single cell RNA sequencing, the use of other recently identified adipogenic progenitor markers could help to identify other *in vivo* stromal populations that modulate adipogenesis and whose expression may be abnormal in *PiT2*$^{-/-}$ mice (42–45). To date we have not identified which cellular or molecular mechanism affected by the loss of PiT2 deregulates adipocyte volume control. However, we interestingly observed that proximal BMAds can be detected at least from 16 days of age (not shown) in the *PiT2*$^{-/-}$ mice, which is very early compared to the appearance of proximal BMAT in wild-type mice that can only be observed from 4 weeks of age in C57Bl/6 (46). This may therefore suggest that PiT2 deletion affects cellular or molecular pathways that occur during development or very early after birth and may provide an invaluable study model to identify them.

No inverse correlation between BMAT and bone volumes in adult PiT2$^{-/-}$ mice

In adult *PiT2*$^{-/-}$ mice, the reduced bone mass is not associated with an increased BMAT volume compared to *PiT2*$^{+/+}$ mice. As we have shown previously, the bone defects in mutant mice are independent of osteoblast or osteoclast number or activity (31), supporting the hypothesis that BMAT and bone defects in the absence of PiT2 are not generated by a coupling imbalance between adipocytes and osteoblasts differentiation.

BMAT volume is known to be regulated by several hormones (*e.g.*, PTH, estrogen or FSH) (2, 3). However, we have previously shown that serum PTH levels were similar between *PiT2*$^{+/+}$ and *PiT2*$^{-/-}$ mice, excluding its role in the genesis of the phenotype (47). In post-menopausal women, BMAT volume is highly increased and ovariectomy is now a commonly used approach to increase BMAT volume in animal models (7, 10, 34, 48, 49). Estrogen, in addition to be a negative regulator of BMAds, is a positive regulator of the bone mass (48). These opposite effects of estrogen on bone and fat tissues may be explained by the imbalanced ability of BMSCs to differentiate into osteoblasts in favor of adipocytes, although no direct evidence has yet been obtained. In *PiT2*$^{-/-}$ mice, both bone and BMAT volumes are reduced and a similar phenotype is observed in males, ruling out the possibility that a defect in estrogen levels could explain the phenotype of these mutant mice. Hence, further studies will be needed to identify the possible systemic factor underlying the alterations in bone and marrow adipose tissues.

Bone and bone marrow adipose tissues are sensitive to estrogen depletion in PiT2$^{-/-}$ mice

The observation that BMAT volume does not increase between 3 and 16 weeks in *PiT2*$^{-/-}$ mice led us to question the regulation of bone and adipose tissue volumes in pathological conditions. In ovariectomized *PiT2*$^{-/-}$ mice, we showed that bone mass is decreased and that this is accompanied by BMAT accumulation similar to that in control mice. These results suggest that in the absence of PiT2 adipogenic differentiation is not affected and that the mechanisms that govern it are upstream of PiT2-dependent pathways. On the other hand, it is well documented that OVX-induced bone loss is primarily caused by induction of bone resorption. Here, we show that bone loss is similar in OVX- *PiT2*$^{+/+}$ mice and OVX-*PiT2*$^{-/-}$ mice, indicating that osteoclast formation and activity are not impaired, consistent with our previous findings that showed normal osteoclast activity in *PiT2*$^{-/-}$ mice (31). The lack of effect of PiT2 deletion on bone and fat phenotypes during ovariectomy is consistent with the fact that we do not observe differences in male and female mutant mice. As these results were obtained in adult mice, they may also support the idea that the role of PiT2 in the bone and BMAT phenotypic balance occurs earlier in the development or during the growth of the animal.

Could phosphate homeostasis explain the BMAT phenotype in PiT2$^{-/-}$ mice?

As one of the major cellular functions of PiT2 is to transport phosphate across the plasma membrane, it is reasonable to ask whether the observed phenotype of *PiT2*$^{-/-}$ mice may be phosphate-related. In the literature, a link between phosphate and adipose tissues is rarely reported, either in extra- or intra-

medullar adipose tissues. In humans, an inverse correlation between serum Pi levels and obesity has been observed, and an association between high phosphate diet and the suppression of lipogenesis in white adipose tissue has been described both in humans and rodents (50–57). Interestingly, acute phosphate restriction in mice decreases bone formation and results in an increase in BMAT due to defects in the commitment of BMSC preferentially towards the adipogenic lineage involving the Wnt signaling pathway (58, 59). It is therefore possible that a change in phosphate homeostasis may impact the balance between bone formation and BMAT. However, *PiT2*$^{-/-}$ mice show no differences in serum phosphate levels and key markers of phosphate homeostasis regulation (31, 32, 60, 61), precluding a role for serum phosphate in the BMAT defects observed in the absence of PiT2. However, as we hypothesize for the dental defects in the *PiT2*$^{-/-}$ mice (62), the local extracellular Pi level, rather than the serum Pi levels, may be responsible for the observed phenotype. Interestingly, invalidation of *Phospho1*, another phosphate-related gene, results in a reduction in bone volume and bone mineral density, along with an increase in BMAT volume (63, 64). Whether this phenotype is directly due to an abnormal local level of Pi within the skeleton or whether it is an indirect consequence of modified energy metabolism remains to be determined.

In summary, we have shown that loss of PiT2 leads to defects in bone and marrow adipose tissues, probably through a non-intrinsic defect of osteoblasts, osteoclasts and BMAds, leading to impaired bone quality and strength. Further identification is needed to decipher the underlying cellular mechanisms.

Data availability statement

The original contributions presented in the study are included in the article/Supplementary Materials. Further inquiries can be directed to the corresponding author.

Ethics statement

Experiments on mice were conducted according to the French and European regulations on care and protection of laboratory animals (EC Directive 86/609, French Law 2001-486 issued on June 6, 2001). This study complied with ARRIVE (Animal Research: Reporting of In Vivo Experiments) guidelines and was approved by the Animal Care Committee of Pays de la Loire (APAFIS agreements 02286.02, 14835-2020-05-13 and 22178-2019092614593965 v7).

Author contributions

Study design: GF, LB, and SB-C. Data collection: GF, MG, GP, PG, GK, MF, JV, BH, SS and SB-C. Data analysis and interpretation: GF, MG, GP, GK, MF, XP, LB and SBC. Drafting manuscript: GF, LB and SB-C. Revising manuscript content: GF, MG, JG, XP, LB and SB-C. Approving final version of manuscript: all authors. SBC takes responsibility for the integrity of the data analysis.

Funding

This work was supported by grants from Inserm, Region des Pays de la Loire (AdipOs) and Société Française de Rhumatologie (PITAMO and METABONE). GF and MG received a doctoral fellowship from Nantes Université.

Acknowledgments

The authors are grateful to the Experimental Health core facility (PES) and SC3M histology facility of the SFR Bonamy (Nantes, France) for their technical support, and MicroPiCell and Cytocell facilities (UMS BioCore, Inserm US16/CNRS UAR3556) for expert technical assistance. The authors gratefully acknowledge Carla Geeroms (Department of Materials Engineering, KU Leuven, Leuven, BELGIUM), Céline Menguy (Inserm U1087, Nantes, France) and Séverine Marionneau (Inserm U1232, Nantes) for technical help. The authors also gratefully acknowledge Dr Christophe Chauveau (MABLab, Boulogne-sur-mer, France) and Dr Céline Colnot (IMRB, Paris) for helpful discussions.

Conflict of interest

The authors declare that the research was conducted in the absence of any commercial or financial relationships that could be construed as a potential conflict of interest.

Publisher's note

Supplementary material

The Supplementary Material for this article can be found online at: https://www.frontiersin.org/articles/10.3389/fendo.2022.921073/full#supplementary-material

SUPPLEMENTARY FIGURE 1
Three-D visualization, using Hf-POM-based CE-CT, of the adipocytes in the bone marrow compartment of the proximal tibia of 3-week-old *PiT2*$^{+/+}$ and *PiT2*$^{-/-}$ female mice.

SUPPLEMENTARY FIGURE 2
Deregulation of BMAT volume in *PiT2*$^{-/-}$ male mice. **(A)** *Upper* - Representative 3D visualization, using Hf-POM-based CE-CT, of the adipocytes in the bone marrow compartment of the proximal tibia (2mm height from the growth plate) of 3- and 16-week-old *PiT2*$^{+/+}$ and *PiT2*$^{-/-}$ male mice. *Lower* - Graph showing quantification of the volume fraction of the adipocytes in the proximal tibia *PiT2*$^{+/+}$ and *PiT2*$^{-/-}$ mice at 3 weeks (n=5 and 3, respectively) and 16 weeks (n=6 and 5, respectively). Data are means ± SEM, Bonferroni-corrected Mann-Whitney test. (B) Relative *PiT1*, *PiT2*, *Adiponectin* and *FABP4* mRNA expression in the whole tibia from 3- (n=5 per genotype) and 16- (n= 7 *PiT2*$^{+/+}$ and n= 5 *PiT2*$^{-/-}$) week-old *PiT2*$^{+/+}$ and *PiT2*$^{-/-}$ male mice, as indicated. Data are means ± SEM, Mann-Whitney test, *$p<0.05$.

SUPPLEMENTARY FIGURE 3
Three-D visualization, using Hf-POM-based CE-CT, of the adipocytes in the bone marrow compartment of the proximal tibia of 3-week-old *PiT2*$^{+/+}$ and *PiT2*$^{-/-}$ male mice.

SUPPLEMENTARY FIGURE 4
Adipogenic differentiation of BMSCs from *PiT2*$^{-/-}$ males. **(A)** *Left* - Representative images of *PiT2*$^{+/+}$ and *PiT2*$^{-/-}$ BMSCs after adipogenic differentiation and ORO staining. Scale bar = 100µm. *Right* - Graphs showing the percentage of oil-red O (ORO) positive cells related to the total number of Hoechst-positive cells (left) and ORO absorbance at 520nm (right). **(B)** Relative *PiT1*, *Adiponectin* and *FABP4* mRNA expression at 0 and 7 days of differentiation, n are indicated on graph bars. Data are means ± SEM, Mann-Whitney test.

References

1. de Paula FJA, Rosen CJ. Marrow adipocytes: Origin, structure, and function. *Annu Rev Physiol* (2020) 82:461–84. doi: 10.1146/annurev-physiol-021119-034513

2. Li Z, Hardij J, Bagchi DP, Scheller EL, MacDougald OA. Development, regulation, metabolism and function of bone marrow adipose tissues. *Bone* (2018) 110:134–40. doi: 10.1016/j.bone.2018.01.008

3. Sebo ZL, Rendina-Ruedy E, Ables GP, Lindskog DM, Rodeheffer MS, Fazeli PK, et al. Bone marrow adiposity: Basic and clinical implications. *Endocr Rev* (2019) 40:1187–206. doi: 10.1210/er.2018-00138

4. Scheller EL, Cawthorn WP, Burr AA, Horowitz MC, MacDougald OA. Marrow adipose tissue: Trimming the fat. *Trends Endocrinol Metab* (2016) 27:392–403. doi: 10.1016/j.tem.2016.03.016

5. Tratwal J, Labella R, Bravenboer N, Kerckhofs G, Douni E, Scheller EL, et al. Reporting guidelines, review of methodological standards, and challenges toward harmonization in bone marrow adiposity research. report of the methodologies working group of the international bone marrow adiposity society. *Front Endocrinol (Lausanne)* (2020) 11:65. doi: 10.3389/fendo.2020.00065

6. Fan Y, Hanai JI, Le PT, Bi R, Maridas D, DeMambro V, et al. Parathyroid hormone directs bone marrow mesenchymal cell fate. *Cell Metab* (2017) 25:661–72. doi: 10.1016/j.cmet.2017.01.001

7. Iwaniec UT, Turner RT. Failure to generate bone marrow adipocytes does not protect mice from ovariectomy-induced osteopenia. *Bone* (2013) 53:145–53. doi: 10.1016/j.bone.2012.11.034

8. Matsumoto Y, La Rose J, Lim M, Adissu HA, Law N, Mao X, et al. Ubiquitin ligase RNF146 coordinates bone dynamics and energy metabolism. *J Clin Invest* (2017) 127:2612–25. doi: 10.1172/JCI92233

9. Xiao Z, Baudry J, Cao L, Huang J, Chen H, Yates CR, et al. Polycystin-1 interacts with TAZ to stimulate osteoblastogenesis and inhibit adipogenesis. *J Clin Invest* (2018) 128:157–74. doi: 10.1172/JCI93725

10. Yu B, Huo L, Liu Y, Deng P, Szymanski J, Li J, et al. PGC-1α controls skeletal stem cell fate and bone-fat balance in osteoporosis and skeletal aging by inducing TAZ. *Cell Stem Cell* (2018) 23:193–209.e5. doi: 10.1016/j.stem.2018.06.009

11. Zou W, Rohatgi N, Brestoff JR, Li Y, Barve RA, Tycksen E, et al. Ablation of fat cells in adult mice induces massive bone gain. *Cell Metab* (2020) 32:801–813.e6. doi: 10.1016/j.cmet.2020.09.011

12. Baum T, Rohrmeier A, Syväri J, Diefenbach MN, Franz D, Dieckmeyer M, et al. Anatomical variation of age-related changes in vertebral bone marrow composition using chemical shift encoding-based water-fat magnetic resonance imaging. *Front Endocrinol (Lausanne)* (2018) 9:141. doi: 10.3389/fendo.2018.00141

13. Justesen J, Stenderup K, Ebbesen EN, Mosekilde L, Steiniche T, Kassem M. Adipocyte tissue volume in bone marrow is increased with aging and in patients with osteoporosis. *Biogerontology* (2001) 2:165–71. doi: 10.1023/a:1011513223894

14. Di Iorgi N, Rosol M, Mittelman SD, Gilsanz V. Reciprocal relation between marrow adiposity and the amount of bone in the axial and appendicular skeleton of young adults. *J Clin Endocrinol Metab* (2008) 93:2281–6. doi: 10.1210/jc.2007-2691

15. Shen W, Chen J, Punyanitya M, Shapses S, Heshka S, Heymsfield SB. MRI-Measured bone marrow adipose tissue is inversely related to DXA-measured bone mineral in Caucasian women. *Osteoporos Int* (2007) 18:641–7. doi: 10.1007/s00198-006-0285-9

16. Shen W, Scherzer R, Gantz M, Chen J, Punyanitya M, Lewis CE, et al. Relationship between MRI-measured bone marrow adipose tissue and hip and spine bone mineral density in African-American and Caucasian participants: the CARDIA study. *J Clin Endocrinol Metab* (2012) 97:1337–46. doi: 10.1210/jc.2011-2605

17. Wren TA, Chung SA, Dorey FJ, Bluml S, Adams GB, Gilsanz V. Bone marrow fat is inversely related to cortical bone in young and old subjects. *J Clin Endocrinol Metab* (2011) 96:782–6. doi: 10.1210/jc.2010-1922

18. Newton AL, Hanks LJ, Davis M, Casazza K. The relationships among total body fat, bone mineral content and bone marrow adipose tissue in early-pubertal girls. *Bonekey Rep* (2013) 2:315. doi: 10.1038/bonekey.2013.49

19. Griffith JF, Yeung DK, Ma HT, Leung JC, Kwok TC, Leung PC. Bone marrow fat content in the elderly: a reversal of sex difference seen in younger subjects. *J Magn Reson Imaging* (2012) 36:225–30. doi: 10.1002/jmri.23619

20. Aaron N, Kraakman MJ, Zhou Q, Liu Q, Costa S, Yang J, et al. Adipsin promotes bone marrow adiposity by priming mesenchymal stem cells. *Elife* (2021) 10:e69209. doi: 10.7554/eLife.69209

21. Tencerova M, Figeac F, Ditzel N, Taipaleenmäki H, Nielsen TK, Kassem M. High-fat diet-induced obesity promotes expansion of bone marrow adipose tissue and impairs skeletal stem cell functions in mice. *J Bone Miner Res* (2018) 33:1154–65. doi: 10.1002/jbmr.3408

22. Beck L, Leroy C, Salaün C, Margall-Ducos G, Desdouets C, Friedlander G. Identification of a novel function of PiT1 critical for cell proliferation and independent of its phosphate transport activity. *J Biol Chem* (2009) 284:31363–74. doi: 10.1074/jbc.M109.053132

23. Beck L, Leroy C, Beck-Cormier S, Forand A, Salaün C, Paris N, et al. The phosphate transporter PiT1 (Slc20a1) revealed as a new essential gene for mouse liver development. *PloS One* (2010) 5:e9148. doi: 10.1371/journal.pone.0009148

24. Byskov K, Jensen N, Kongsfelt IB, Wielsøe M, Pedersen LE, Haldrup C, et al. Regulation of cell proliferation and cell density by the inorganic phosphate transporter PiT1. *Cell Div* (2012) 7:7. doi: 10.1186/1747-1028-7-7

25. Couasnay G, Bon N, Devignes CS, Sourice S, Bianchi A, Véziers J, et al. PiT1/Slc20a1 is required for endoplasmic reticulum homeostasis, chondrocyte survival, and skeletal development. *J Bone Miner Res* (2019) 34:387–98. doi: 10.1002/jbmr.3609

26. Forand A, Beck L, Leroy C, Rousseau A, Boitez V, Cohen I, et al. EKLF-driven PIT1 expression is critical for mouse erythroid maturation *in vivo* and *in vitro*. *Blood* (2013) 121:666–78. doi: 10.1182/blood-2012-05-427302

27. Kongsfelt IB, Byskov K, Pedersen LE, Pedersen L. High levels of the type III inorganic phosphate transporter PiT1 (SLC20A1) can confer faster cell adhesion. *Exp Cell Res* (2014) 326:57–67. doi: 10.1016/j.yexcr.2014.05.014

28. Liu L, Sánchez-Bonilla M, Crouthamel M, Giachelli C, Keel S. Mice lacking the sodium-dependent phosphate import protein, PiT1 (SLC20A1), have a severe defect in terminal erythroid differentiation and early b cell development. *Exp Hematol* (2013) 41:432–43.e7. doi: 10.1016/j.exphem.2013.01.004

29. Ma XX, Li X, Yi P, Wang C, Weng J, Zhang L, et al. PiT2 regulates neuronal outgrowth through interaction with microtubule-associated protein 1B. *Sci Rep* (2017) 7:17850. doi: 10.1038/s41598-017-17953-3

30. Salaün C, Leroy C, Rousseau A, Boitez V, Beck L, Friedlander G. Identification of a novel transport-independent function of PiT1/SLC20A1 in the regulation of TNF-induced apoptosis. *J Biol Chem* (2010) 285:34408–18. doi: 10.1074/jbc.M110.130989

31. Beck-Cormier S, Lelliott CJ, Logan JG, Lafont DT, Merametdjian L, Leitch VD, et al. Slc20a2, encoding the phosphate transporter PiT2, is an important genetic determinant of bone quality and strength. *J Bone Miner Res* (2019) 34:1101–14. doi: 10.1002/jbmr.3691

32. Yamada S, Wallingford MC, Borgeia S, Cox TC, Giachelli CM. Loss of PiT-2 results in abnormal bone development and decreased bone mineral density and length in mice. *Biochem Biophys Res Commun* (2018) 495:553–9. doi: 10.1016/j.bbrc.2017.11.071

33. Kerckhofs G, Stegen S, van Gastel N, Sap A, Falgayrac G, Penel G, et al. Simultaneous three-dimensional visualization of mineralized and soft skeletal tissues by a novel microCT contrast agent with polyoxometalate structure. *Biomaterials* (2018) 159:1–12. doi: 10.1016/j.biomaterials.2017.12.016

34. Beekman KM, Zwaagstra M, Veldhuis-Vlug AG, van Essen HW, den Heijer M, Maas M, et al. Ovariectomy increases RANKL protein expression in bone marrow adipocytes of C3H/HeJ mice. *Am J Physiol Endocrinol Metab* (2019) 317: E1050–4. doi: 10.1152/ajpendo.00142.2019

35. Carpenter AE, Jones TR, Lamprecht MR, Clarke C, Kang IH, Friman O, et al. CellProfiler: image analysis software for identifying and quantifying cell phenotypes. *Genome Biol* (2006) 7:R100. doi: 10.1186/gb-2006-7-10-r100

36. Boxall SA, Jones E. Markers for characterization of bone marrow multipotential stromal cells. *Stem Cells Int* (2012) 2012:975871. doi: 10.1155/2012/975871

37. Rostovskaya M, Anastassiadis K. Differential expression of surface markers in mouse bone marrow mesenchymal stromal cell subpopulations with distinct lineage commitment. *PloS One* (2012) 7:e51221. doi: 10.1371/journal.pone.0051221

38. Ambrosi TH, Scialdone A, Graja A, Gohlke S, Jank AM, Bocian C, et al. Adipocyte accumulation in the bone marrow during obesity and aging impairs stem cell-based hematopoietic and bone regeneration. *Cell Stem Cell* (2017) 20:771–784.e6. doi: 10.1016/j.stem.2017.02.009

39. Livak KJ, Schmittgen TD. Analysis of relative gene expression data using real-time quantitative PCR and the 2(-delta delta C(T)) method. *Methods* (2001) 25:402–8. doi: 10.1006/meth.2001.1262

40. Bravenboer N, Bredella MA, Chauveau C, Corsi A, Douni E, Ferris WF, et al. Standardised nomenclature, abbreviations, and units for the study of bone marrow adiposity: Report of the nomenclature working group of the international bone marrow adiposity society. *Front Endocrinol (Lausanne)* (2019) 10:923. doi: 10.3389/fendo.2019.00923

41. Sulston RJ, Cawthorn WP. Bone marrow adipose tissue as an endocrine organ: close to the bone. *Horm Mol Biol Clin Investig* (2016) 28:21–38. doi: 10.1515/hmbci-2016-0012

42. Baryawno N, Przybylski D, Kowalczyk MS, Kfoury Y, Severe N, Gustafsson K, et al. A cellular taxonomy of the bone marrow stroma in homeostasis and leukemia. *Cell* (2019) 177:1915–1932.e16. doi: 10.1016/j.cell.2019.04.040

43. Helbling PM, Piñeiro-Yáñez E, Gerosa R, Boettcher S, Al-Shahrour F, Manz MG, et al. Global transcriptomic profiling of the bone marrow stromal microenvironment during postnatal development, aging, and inflammation. *Cell Rep* (2019) 29:3313–3330.e4. doi: 10.1016/j.celrep.2019.11.004

44. Schwalie PC, Dong H, Zachara M, Russeil J, Alpern D, Akchiche N, et al. A stromal cell population that inhibits adipogenesis in mammalian fat depots. *Nature* (2018) 559:103–8. doi: 10.1038/s41586-018-0226-8

45. Tikhonova AN, Dolgalev I, Hu H, Sivaraj KK, Hoxha E, Cuesta-Domínguez Á, et al. The bone marrow microenvironment at single-cell resolution. *Nature* (2019) 569:222–8. doi: 10.1038/s41586-019-1104-8

46. Scheller EL, Doucette CR, Learman BS, Cawthorn WP, Khandaker S, Schell B, et al. Region-specific variation in the properties of skeletal adipocytes reveals regulated and constitutive marrow adipose tissues. *Nat Commun* (2015) 6:7808. doi: 10.1038/ncomms8808

47. Bon N, Frangi G, Sourice S, Guicheux J, Beck-Cormier S, Beck L. Phosphate-dependent FGF23 secretion is modulated by PiT2/Slc20a2. *Mol Metab* (2018) 11:197–204. doi: 10.1016/j.molmet.2018.02.007

48. Lecka-Czernik B, Stechschulte LA, Czernik PJ, Sherman SB, Huang S, Krings A. Marrow adipose tissue: Skeletal location, sexual dimorphism, and response to sex steroid deficiency. *Front Endocrinol (Lausanne)* (2017) 8:188. doi: 10.3389/fendo.2017.00188

49. Wu Y, Xie L, Wang M, Xiong Q, Guo Y, Liang Y, et al. Mettl3-mediated m^6A RNA methylation regulates the fate of bone marrow mesenchymal stem cells and osteoporosis. *Nat Commun* (2018) 9:4772. doi: 10.1038/s41467-018-06898-4

50. Abuduli M, Ohminami H, Otani T, Kubo H, Ueda H, Kawai Y, et al. Effects of dietary phosphate on glucose and lipid metabolism. *Am J Physiol Endocrinol Metab* (2016) 310:E526–38. doi: 10.1152/ajpendo.00234.2015

51. Ayoub JJ, Samra MJ, Hlais SA, Bassil MS, Obeid OA. Effect of phosphorus supplementation on weight gain and waist circumference of overweight/obese adults: a randomized clinical trial. *Nutr Diabetes* (2015) 5:e189. doi: 10.1038/nutd.2015.38

52. Bassil MS, Obeid OA. Phosphorus supplementation recovers the blunted diet-induced thermogenesis of overweight and obese adults: A pilot study. *Nutrients* (2016) 8:E801. doi: 10.3390/nu8120801

53. Billington EO, Gamble GD, Bristow S, Reid IR. Serum phosphate is related to adiposity in healthy adults. *Eur J Clin Invest* (2017) 47:486–93. doi: 10.1111/eci.12769

54. Eller P, Eller K, Kirsch AH, Patsch JJ, Wolf AM, Tagwerker A, et al. A murine model of phosphate nephropathy. *Am J Pathol* (2011) 178:1999–2006. doi: 10.1016/j.ajpath.2011.01.024

55. Imi Y, Yabiki N, Abuduli M, Masuda M, Yamanaka-Okumura H, Taketani Y. High phosphate diet suppresses lipogenesis in white adipose tissue. *J Clin Biochem Nutr* (2018) 63:181–91. doi: 10.3164/jcbn.17-141

56. Obeid OA. Low phosphorus status might contribute to the onset of obesity. *Obes Rev* (2013) 14:659–64. doi: 10.1111/obr.12039

57. Park W, Kim BS, Lee JE, Huh JK, Kim BJ, Sung KC, et al. Serum phosphate levels and the risk of cardiovascular disease and metabolic syndrome: a double-edged sword. *Diabetes Res Clin Pract* (2009) 83:119–25. doi: 10.1016/j.diabres.2008.08.018

58. Ko FC, Martins JS, Reddy P, Bragdon B, Hussein AI, Gerstenfeld LC, et al. Acute phosphate restriction impairs bone formation and increases marrow adipose tissue in growing mice. *J Bone Miner Res* (2016) 31:2204–14. doi: 10.1002/jbmr.2891

59. Ko FC, Kobelski MM, Zhang W, Grenga GM, Martins JS, Demay MB. Phosphate restriction impairs mTORC1 signaling leading to increased bone marrow adipose tissue and decreased bone in growing mice. *J Bone Miner Res* (2021) 36:1510–20. doi: 10.1002/jbmr.4312

60. Jensen N, Autzen JK, Pedersen L. Slc20a2 is critical for maintaining a physiologic inorganic phosphate level in cerebrospinal fluid. *Neurogenetics* (2016) 17:125–30. doi: 10.1007/s10048-015-0469-6

61. Wallingford MC, Gammill HS, Giachelli CM. Slc20a2 deficiency results in fetal growth restriction and placental calcification associated with thickened basement membranes and novel CD13 and lamininα1 expressing cells. *Reprod Biol* (2016) 16:13–26. doi: 10.1016/j.repbio.2015.12.004

62. Merametdjian L, Beck-Cormier S, Bon N, Couasnay G, Sourice S, Guicheux J, et al. Expression of phosphate transporters during dental mineralization. *J Dent Res* (2018) 97:209–17. doi: 10.1177/0022034517729811

63. Suchacki KJ, Morton NM, Vary C, Huesa C, Yadav MC, Thomas BJ, et al. PHOSPHO1 is a skeletal regulator of insulin resistance and obesity. *BMC Biol* (2020) 18:149. doi: 10.1186/s12915-020-00880-7

64. Yadav MC, Simão AM, Narisawa S, Huesa C, McKee MD, Farquharson C, et al. Loss of skeletal mineralization by the simultaneous ablation of PHOSPHO1 and alkaline phosphatase function: a unified model of the mechanisms of initiation of skeletal calcification. *J Bone Miner Res* (2011) 26:286–97. doi: 10.1002/jbmr.195

frontiers | Frontiers in Endocrinology

TYPE Original Research
PUBLISHED 23 November 2022
DOI 10.3389/fendo.2022.1001210

OPEN ACCESS

EDITED BY
Jason Horton,
Upstate Medical University,
United States

REVIEWED BY
Jeffrey Gimble,
Obatala Sciences, United States
Biagio Palmisano,
Department of Molecular Medicine,
Sapienza University of Rome, Italy
Shinsuke Shigeto,
Kwansei Gakuin University, Japan

*CORRESPONDENCE
Olaia Naveiras
olaia.naveiras@unil.ch

†These authors have contributed equally to this work and share first authorship

‡These authors have contributed equally to this work and share senior authorship

SPECIALTY SECTION
This article was submitted to Bone Research, a section of the journal Frontiers in Endocrinology

RECEIVED 23 July 2022
ACCEPTED 04 October 2022
PUBLISHED 23 November 2022

CITATION
Tratwal J, Falgayrac G, During A, Bertheaume N, Bataclan C, Tavakol DN, Campos V, Duponchel L, Daley GQ, Penel G, Chauveau C and Naveiras O (2022) Raman microspectroscopy reveals unsaturation heterogeneity at the lipid droplet level and validates an *in vitro* model of bone marrow adipocyte subtypes. *Front. Endocrinol.* 13:1001210. doi: 10.3389/fendo.2022.1001210

Raman microspectroscopy reveals unsaturation heterogeneity at the lipid droplet level and validates an *in vitro* model of bone marrow adipocyte subtypes

Josefine Tratwal[1†], Guillaume Falgayrac[2†], Alexandrine During[2], Nicolas Bertheaume[2], Charles Bataclan[1], Daniel N. Tavakol[1], Vasco Campos[1], Ludovic Duponchel[3], George Q. Daley[4], Guillaume Penel[2], Christophe Chauveau[2‡] and Olaia Naveiras[1,5,6*‡]

[1]Laboratory of Regenerative Hematopoiesis, Ecole Polytechnique Fédérale de Lausanne (EPFL) & Department of Biomedical Sciences, University of Lausanne (UNIL), Lausanne, Switzerland, [2]Univ. Lille, CHU Lille, Univ. Littoral Côte d'Opale, ULR 4490 - MABLab- Marrow Adiposity Laboratory, Lille, France, [3]Univ. Lille, CNRS, UMR 8516 - LASIRe - Laboratoire Avancé de Spectroscopie pour les Intéractions la Réactivité et l'Environnement, Lille, France, [4]Division of Hematology/Oncology, Boston Children's Hospital and Dana Farber Cancer Institute, Boston, Boston, MA, United States, [5]Service of Hematology, Department of Oncology, Lausanne University Hospital and University of Lausanne, Lausanne, Switzerland, [6]Service of Hematology, Department of Laboratory Medicine Oncology, Lausanne University Hospital and University of Lausanne, Lausanne, Switzerland

Bone marrow adipocytes (BMAds) constitute the most abundant stromal component of adult human bone marrow. Two subtypes of BMAds have been described, the more labile regulated adipocytes (rBMAds) and the more stable constitutive adipocytes (cBMAds), which develop earlier in life and are more resilient to environmental and metabolic disruptions. *In vivo*, rBMAds are enriched in saturated fatty acids, contain smaller lipid droplets (LDs) and more readily provide hematopoietic support than their cBMAd counterparts. Mouse models have been used for BMAds research, but isolation of primary BMAds presents many challenges, and thus *in vitro* models remain the current standard to study nuances of adipocyte differentiation. No *in vitro* model has yet been described for the study of rBMAds/cBMAds. Here, we present an *in vitro* model of BM adipogenesis with differential rBMAd and cBMAd-like characteristics. We used OP9 BM stromal cells derived from a (C57BL/6xC3H)F2-op/op mouse, which have been extensively characterized as feeder layer for hematopoiesis research. We observed similar canonical adipogenesis transcriptional signatures for spontaneously-differentiated (sOP9) and induced (iOP9) cultures, while fatty acid composition and desaturase expression of *Scd1* and *Fads2* differed at the population level. To resolve differences at the single adipocyte level we tested Raman microspectroscopy and show it constitutes a high-resolution method for studying adipogenesis *in vitro* in a label-free manner, with resolution to individual LDs. We found sOP9 adipocytes have

lower unsaturation ratios, smaller LDs and higher hematopoietic support than iOP9 adipocytes, thus functionally resembling rBMAds, while iOP9 more closely resembled cBMAds. Validation in human primary samples confirmed a higher unsaturation ratio for lipids extracted from stable cBMAd-rich sites (femoral head upon hip-replacement surgery) versus labile rBMAds (iliac crest after chemotherapy). As a result, the 16:1/16:0 fatty acid unsaturation ratio, which was already shown to discriminate BMAd subtypes in rabbit and rat marrow, was validated to discriminate cBMAds from rBMAd in both the OP9 model *in vitro* system and in human samples. We expect our model will be useful for cBMAd and rBMAd studies, particularly where isolation of primary BMAds is a limiting step.

KEYWORDS

fatty acid, unsaturation (fatty acid), OP9 cell, lipid droplet diameter, regulated bone marrow adiposity, constitutive bone marrow adiposity, stroma, bone marrow stromal cell (BMSC)

1 Introduction

Similar patterns of bone marrow adipocyte (BMAd) formation occur in vertebrate species including rodents, rabbits, and humans. Specifically, a decreasing rate of BMAd has been observed relative to the decreasing size and lifespan of the animal, with larger skeletons containing more BM adipose tissue (BMAT) which extends farther into the skeleton (1). The distal parts of the skeleton (ie. peripheral bones in human, the distal tibia, paws, and caudal vertebrae in mice) predominantly contain adipocytic marrow interspersed with some hematopoietic cells, comprising the more stable constitutive BMAds (cBMAds) that appear just around birth. The proximal locations of the skeleton (ie. thoracic vertebrae in human and mouse, as well as proximal tibia and other long bones in mouse) contain predominantly hematopoietic marrow interspersed with the more labile regulated BMAds (rBMAds) (1–3). The rBMAds are smaller in size and respond readily to either induction of bone marrow adipogenesis through nutritional challenge (high fat diet or caloric restriction) and hematopoietic failure, or to BMAd mass reduction in the context of cold exposure and increased hematological demand (e.g. phenylhydrazine). On the other hand, it is argued that cBMAds do not respond readily to environmental demands (1, 4–7). Stromal cells and BMAds are tightly linked to BM hematopoiesis. Various stromal populations in mouse and human have shown to promote hematopoietic support while more mature BMAds associate with reduced hematopoietic proliferation (8, 9) as reviewed in (10, 11). Meanwhile, adiponectin expressing cells within the BMAd lineage are beneficial to hematopoietic regeneration in most bones, but not the caudal vertebrae of mice (12, 13). These studies indicate the probability for population- and location-specific distinctions of BMAd maturation that specifically affect hematopoiesis and respond to hematopoietic demand [reviewed in (14)].

Isolation of BM stroma for differentiation and analyses of BMAds *in vitro* to study these processes in mouse models is challenging due to the limited amount of BMAd material obtained from each bone or bone segment. Moreover, this is compounded by the fact that the defining surface markers that would aid in purification of BMAd progenitor populations in homeostatic mice do not discriminate between the labile and stable BMAds (8). With such constraints, a promising alternative to the use of primary cells for *in vitro* studies are multipotent BM-derived stromal cell lines differentiated *in vitro*, especially when studies are possible at the single cell level to address heterogeneity (15). For this purpose, we developed a high-throughput image platform to monitor adipocytic differentiation though LD accumulation quantified by Digital Holographic Microscopy in live cells, which requires minimal handling to avoid perturbation of the culture (16). While not limited by end-point analysis or the introduction of handling or preparation biases, this technique cannot provide information on the molecular composition of the cells. Methods capable of combining manipulation-free, label-free, single-cell imaging with analysis of molecular composition are thus of great interest to the field of adipogenesis at large. Raman microspectroscopy is a non-invasive and label-free method that does not require specific sample preparation. With a sub-cellular resolution on the scale of ~1μm Raman microspectroscopy provides molecular composition with

spatial data where standard methods provide bulk information (e.g. mass spectroscopic and chromatographic methods) (17). We thus hypothesized that combining lipid profiling by Raman microspectroscopy with the inherently heterogenous *in vitro* stromal adipocytic differentiation model would serve as a powerful tool to aid in the understanding of BM adipogenesis.

LD formation (18) begins with fatty acids (FAs) that enter the cell either *via* fatty acid transport proteins or fatty acid translocase (19, 20), or which are synthesized through endogenous *de novo* lipogenesis (DNL). FAs then enter a bioactive pool to form fatty acyl-CoA to be used by glycerolipid synthesis enzymes in the endoplasmic reticulum (ER) to form neutral lipids such as triacylglycerols (TAGs) and eventually coalesce and form LDs (21). If attached to the ER, LDs may grow in size through diffusion of newly synthesized lipids to the LD, and if unattached, through local synthesis or fusion of smaller LDs to larger ones. LDs increase in size during adipocytic differentiation and perilipins (PLINs) bind to promote their stabilization (22). Lipases mobilize neutral lipids in LDs for metabolic energy by fatty acid oxidation, which is triggered through nutritional, hormonal, or inflammatory activation. Adipose triglyceride lipase (ATGL) catalyzes the initial step of intracellular TAG hydrolysis followed by hormone sensitive lipase (HSL) and monoacylglycerol lipase (MGL) into glycerol moieties (23, 24). FAs are necessary for energy production and lipid synthesis for cellular signaling and membrane formation. Despite their importance, increased concentrations of non-esterified FAs can be detrimental contributing to lipotoxicity, and thus TAG hydrolysis and FA cycling are carefully regulated (25, 26). As illustrated in Figure S1, the primary product of DNL is palmitic acid (16:0), in the family of saturated FAs that have cytotoxic effects and induce reactive oxygen species (ROS) (27). The monounsaturated FA (MUFA) oleic acid (18:1) may counteract this effect possibly by activating esterification of palmitic acid into TAGs and lipid droplet storage (28). Palmitic acid accumulation is therefore prevented by increased desaturation to palmitoleic acid (16:1n-7) or elongation to stearic acid (18:0) and further desaturation to oleic acid (18:1) (29). Notably, oleic acid inhibits palmitic-acid dependent osteoclastogenesis and palmitic acid is found to be increased in BM serum of osteoporotic women (30). Indeed, BMAT expansion throughout the red marrow (likely equating to rBMAd expansion) is associated with bone loss and increased fracture risk, while cBMAd formation is positively associated with bone accrual during early development through correlative and descriptive studies (31).

While concrete definitions and BMAd classification markers are being established (32), the oldest standard for classifying the two known subtypes of BMAds is by the composition of their lipid content (33, 34). The first reports by Mehdi Tavassoli showed that the adipocytic-rich yellow marrow -now denominated cBMAd- from the os calcis of rabbits was higher in the proportion of unsaturated FAs (palmitoleic -16:1n-7- and oleic -18:1n-9- acids), whereas fatty acid composition of BMAds from the adipocyte-poor red marrow of thoracic vertebrae (rBMAds) was richer in saturated FAs (palmitic -16:0- and stearic -18:0- acids) (35). In recent years, primary rat cBMAds from tail vertebrae and distal tibia were likewise shown to contain a higher proportion of unsaturated fatty acids in caudal vertebrae or distal tibia as compared to rat rBMAds isolated from either lumbar vertebrae or femur plus proximal tibia combined (1). Congruently magnetic resonance (MR) imaging, 1H-MR spectroscopy, and gas chromatographic data from human subjects consistently showed that BM adipose tissue (BMAT) from sites of red marrow contained highly saturated lipids, compared to the mostly unsaturated lipids detected at yellow marrow sites (1, 35–38). From murine samples, it is considerably more challenging to obtain sufficient BMAT for analysis due to the size of the animal as well as the limited amount of BMAT present in the bones (34). To our knowledge, the lipid composition of murine BMAds has not been described to date. However, between BMAT of red and yellow marrow there is a conservation of the differences in both the 16:1/16:0 and 18:0/18:1 fatty acid unsaturation ratios relative to total lipid content across species (summarized and compiled with our data in Table 1 and Figure S1, abbreviations and fatty acid nomenclature compiled in Table 2, 3).

In this study, we harness the inherent adipogenic potential of murine BM-derived OP9 stromal cells to further dissect intrinsic properties of BMAds using standard techniques for lipid profiling at the cell population-level, and Raman microspectroscopy for lipid profiling at the single-adipocyte level. We subjected OP9 cells to basal culture conditions or to a standard adipogenic cocktail, allowing the OP9 cells to differentiate spontaneously though serum exposure and confluency (sOP9) or through specific induction of the adipogenic differentiation program (iOP9). To test the hematopoietic supportive capacity of OP9 cells from these conditions, we assessed their interaction with hematopoietic stem and progenitor cells (HSPCs). We show that a full biochemical induction of the adipogenic differentiation program induces iOP9s to more closely resemble cBMAds in their lipid content, lipid droplet size and hematopoietic support than the sOP9 adipocytes that develop upon simple serum induction, which retain rBMAd-like properties. Furthermore, we validated the significance of the unsaturation ratio-driven cBMAd versus rBMAd definition. For this, we compared for the first time primary human samples from iliac crest samples drawn after hematological aplasia, which represent the most extreme case of rBMAd remodeling (3), to femoral specimens from hip replacement surgery, which represent one of the best characterized cBMAd depots (39, 40).

TABLE 1 Fatty acid unsaturation ratios in rat, rabbit, human, and OP9 cells from red and yellow BMAds.

Origin	BMAd type	16:1/16:0	c/r	18:1/18:0	c/r	Reference
Rat	constitutive regulated	0.25 0.09	2.8	1.18 0.81	1.5	Scheller et al., 2015
Rabbit	constitutive regulated	0.53 0.16	3.3	7.52 2.68	2.8	Tavassoli et al., 1977
Human	constitutive regulated	0.19 0.11	1.7	7.91 4.40	1.8	original data
OP9 cells	induced spontaneous	0.84 0.24	1.6	4.74 2.33	2.0	original data

The 16:1/16:0 and 18:1/18:0 unsaturation ratios were calculated from the proportion of total fatty acids. Rat BM data from Scheller et al., 2015 Supplementary Data 1 (regulated: femur and proximal tibia, constitutive: distal tibia). Rabbit BM data from Tavassoli 1977 Table 1 (regulated: vertebrae, constitutive: os calcis). Human original data from Figure 7 (regulated: iliac crest post-chemotherapy, constitutive: femoral head) and OP9 cell original data from Figure 6 (regulated: spontaneous, constitutive: induced) from HPLC analysis. Additional measurements in human BM have been made by MRI spectroscopy but cannot be compiled with these data due to the different methodology (37, 38). c, constitutive; r, regulated.

2 Methods

2.1 Cell culture

All stromal cells [MS5, C3H10T1/2, MC3T3-E1-4, MC3T3-E4-24 bone marrow stromal lines, AFT024 and BFC012 stromal lines from fetal liver (41) or embryonic stem cell-derived fibroblasts as in (42, 43)] were cultured in complete medium consisting of Minimum Essential Media alpha (MEMα) with GlutaMax™ (Gibco, catalog no. 32561) and 1% Penicillin/Streptomycin (P/S, Gibco, catalog no. 15140) supplemented 10% fetal bovine serum (FBS, Gibco, catalog no. 10270-106) at 37°C and 5% CO2 with media changed every 2-3 days, and differentiated as described below (44). For subsequent analysis, OP9 cells were plated in 24-well plates (Falcon) with CaF2 substrates (Crystran) for Raman microspectroscopy and RT-qPCR, or in 6-well plates (Falcon) for HPLC analysis, and in flat-bottom tissue culture-treated 96-well plates (Falcon) for co-culture assays. OP9 cells were either plated subconfluently at a density of 5,000 cells per cm2 (undifferentiated OP9 cells, uOP9) or plated at confluency of 20,000 cells per cm2 in complete medium (spontaneous OP9 cells, sOP9) for either 7 or 17 days, as specified in figure legends. Both OP9 cells and OP9-EGFP cells (16) were authenticated by the ATCC on June 24, 2021, by short tandem repeat (STR) analysis, indicating an exact match of the ATCC reference OP9 cell line (CRL-2749). OP9 cells are also directly available from the ATCC (CRL-2749), but this source has not been tested for adipogenesis or hematopoietic support in our laboratory.

2.1.1 *In vitro* differentiation and quantification

All stromal lines were plated at 20,000 per cm2 and cultured to confluency (uOP9) in 1% gelatin-coated plates (prepared overnight at 4°C), then allowed to spontaneously differentiate over time by confluency (sOP9) or induced toward adipocytic (iOP9) or osteogenic differentiation *via* a standard differentiation cocktail as in (15, 44). The adipogenic induction cocktail consisted of complete medium supplemented with 1μM dexamethasone (Sigma, catalog no. D4902), 5μg/ml insulin (Sigma, catalog no. I0516), and 0.5mM isobutyl-methylxanthine (IBMX, Sigma, catalog no. I5879). After four days, the adipogenic induction medium was changed to a maintenance medium consisting of complete medium with insulin and dexamethasone only. Media was changed every 3-4 days with aliquots prepared fresh from stock solutions (IBMX in DMSO, insulin in PBS, dexamethasone in ethanol) kept at -20°C in the dark. Short-term differentiation experiments were performed at day seven of adipocytic differentiation with minimal culture manipulation as in (16), and long-term experiments were carried out on day 17. Neutral lipids were stained with Oil Red O for quantification of adipogenesis in 96-well plates. First, cells were gently washed with phosphate buffered saline (PBS, Gibco, catalog no. 10010015) then fixed for 10min at room temperature with 4% paraformaldehyde (PFA) diluted in PBS from 32% stock solution, and gently washed three times with PBS. 100μl filtered Oil Red O solution freshly prepared from stock solution (Sigma, catalog no. 01391-250ML) diluted 3:2 with distilled water was added to the wells. Cells were incubated with Oil Red O at room temperature for 45min on a shaker, then washed gently with PBS three times and light transmission micrographs were obtained. 100μl isopropanol was then added to the wells and incubated at room temperature. After 10min, 70μl of the solution was transferred to a new 96 well plate and OD measurements read at 520nm with isopropanol as background. Osteogenic differentiation was performed by addition of dexamethasone 1μM, 2-phospho-L-ascorbic acid 50μg/ml (1000x stock in PBS), glycerophosphate 10mM (100x stock in PBS) and 1,25-hydroxyvitamine D3 0.01μM (stock 1000x in ethanol) for 28 days. Every 3-4 days differentiation media was changed. All media changes were made with fresh stock aliquots. Efficiency of osteoblastic differentiation was determined with Alizarin Red

stain (Sigma) in stromal cells fixed as described above for O Red Oil stains. Alizarin Red staining solution (alizarin red 2% in distilled water, filtered through 45-µm pore, pH adjusted to 4.0-4.3 with NH4OH and filtered again) was then added for 10-15 minutes until precipitates were visible. Alkaline Phosphatase development kits were purchased from Promega (S3771), and OP9 stains were performed according to manufacturer's instructions in lightly fixed cells (4%PFA for 1 minute at room temperature) by dilution of NBT in AP staining buffer (100mM Tris HCl pH9.5, 50mM MgCl2, 100mM NaCl and 0.1% Tween-20). Pictures were taken immediately after staining.

2.2 Raman microspectroscopy

Fixed 24-well plates were kept in PBS at 4°C and shipped to the University of Lille. Raman acquisitions were done on a LabRAM HR800 equipped with an immersion objective (Nikon, obj x100, numerical aperture = 1, Japan) and a diode laser λ=785 nm. The laser power at the sample was 30mW. The lateral resolution was 1-2µm. Spectral acquisition was made in the 400–1800cm^{-1}range and spectral resolution was 4cm^{-1}. The acquisition time was set at 60s per spectrum. Raman spectra were processed using Labspec software (HORIBA, Jobin-Yvon, France). The water immersion objective focused the laser on the center of individual lipid droplets where one spectrum corresponds to one adipocyte lipid droplet. In total 2944 spectra were measured over 120 sOP9-adipocytes (on average 24 spectra per adipocyte) and 2971 spectra over 138 iOP9-adipocytes (with an average of 21 spectra per adipocyte). The number of spectra per well was between 60 to 110. The unsaturation ratio was calculated as ratio of area under the curve of bands 1654cm^{-1}/1441cm^{-1}. The optical image of the adipocyte was saved for each acquisition. The diameter of LDs was evaluated from the optical image by using the software FIJI (45).

The instrument is also equipped with a XYZ motorized stage which allows the acquisition of Raman images. Raman images were acquired using the point-by-point imaging mode (Pt-Img). The laser beam was focused perpendicular to the sample surface. Acquisition time was set to 3sec (×2) for each spectrum. The laser beam was stepped in two dimensions (x and y), and a spectrum was recorded at each position (x,y). The step was set to 1 µm between 2 positions. The Pt-Img mode generated x×y spectra.

2.3 High-performance liquid chromatography

Cells were fixed with PFA as described above for adipocytic quantification. After washing, 500µl of PBS was left in the wells, plates were sealed with parafilm and stored at 4°C until processing for HPLC analysis. Cells were detached from the plate with 1mL (2 x 0.5ml) of PBS and lipids extracted with chloroform/methanol (2:1; v/v) under agitation for 30min at room temperature. The resulting lipid extract was then subjected to saponification, followed by fatty acid derivatization into naphthacyl esters as described previously (46). Fatty acid derivatives were applied into the HPLC Alliance system (2695 Separations Module, Waters, Saint-Quentin-en-Yvelines, France) equipped of an autosampler (200ml-loop sample), a photodiode array detector (model 2998), and the Empower software for data analyses. Fatty acid derivatives were eluted on a reverse phase YMC PRO C18 column (3mm, 4.6x150mm, 120Å) by using two solvent systems: a) methanol/acetonitrile/water (64:24:12; v/v/v) and, b) methanol/dichloromethane/water (65:28:7; v/v/v) under identical conditions reported previously (46). Fatty acid derivatives were detected at 246 nm and quantified by an external standard curve realized with the naphthacyl 19:0 derivative. Note that 19:0 was also used as internal standard to evaluate FA recoveries. Lipidomics LC-HRMS standards and solvents are provided in Table S1.

2.4 Real-time quantitative PCR

At day 7 or 17 of adipocytic differentiation, RNA was extracted with Trizol and cDNA was synthesized using Taq DNA polymerase (catalog no. 10342020, Life Technologies) according to manufacturer's instructions. Quantitative PCR was performed in technical triplicates using the Fast SYBR Green qPCR Mastermix with 250 µM of primer concentration (Applied Biosystems) on QuantStudio 6 (Life Technologies). Primers were pre-validated for high efficiency and housekeeping gene primers were internally tested not to vary upon OP9 differentiation. The geometric mean of housekeeping genes (RPL13 and YWHAZ) was used as reference to calculate the fold expression of each gene relative to the samples of undifferentiated OP9 cells as described for the delta-delta normalization method (47, 48). Primer sequences obtained from Microsynth are listed in Supplementary Table S2.

2.5 Bone marrow extraction and HSPC sorting

Total bone marrow was extracted from eight-week-old B6 ACTb-EGFP females housed in 12-hour day-night light cycles and provided ad-libitum sterile food and water as described previously, in accordance to Swiss law and ARRIVE guidelines, with the approval of cantonal authorities (Service Veterinaire de l'Etat de Vaud). Total bone marrow cells were extracted from femur, tibia and pelvis by crushing using a mortar and pestle in ice-cold PBS supplemented 1mM ethylenediaminetetraacetic acid (EDTA, catalog no. 15575020, Thermo Fisher Scientific).

The samples were dissociated and filtered through a 70μM cell strainer (catalog no. 352350, Falcon), lysed for 30sec at room temperature in red blood cell lysis buffer (Biolegend, catalog no. 420301), washed with ice-cold PBS-EDTA and centrifuged at 1300rpm for 10min at 4°C. For HSPC sorting prior to co-culture with OP9 stroma, the cell pellet was stained with 50μl biotinylated 'lineage' antibody cocktail (BD, catalog no. 558451) in 1ml PBS-EDTA per six bones for 15min on ice. The sample was washed with PBS-EDTA and stained with 50μl magnetic beads of the same kit in PBS-EDTA for 10min on ice. The samples were then washed and filtered through a 70μm cell strainer (catalog no. 352350, Falcon) prior to lineage depletion using the AutoMACS Pro (Miltenyi Biotec, USA). After depletion the negative fraction was resuspended in an antibody mix containing antibodies against Streptavidin-TxRed (1:200), cKit-PECy7 (1:200), Sca1-APC (1:100) and PI (1:1000). Cell sorting was performed on a FACSAria Fusion (Becton Dickinson, USA) cell sorter.

2.6 *In vitro* HSPC co-culture

OP9 cell seeding as detailed in Section 2.1, was followed by short-term *in vitro* adipocyte differentiation of OP9 cells, and then a gentle wash with PBS and pre-warmed Iscove's Modified Dulbecco's Medium (IMDM, catalog no. 12440053, Gibco) supplemented with 10% FBS and 1% Pen/Strep (P/S) was added. The washing was done using the Caliper Sciclone ALH 3000 (Caliper Life Sciences, USA) and consisted of four cycles of removing 140μl media and adding 140μl fresh IMDM media, to dilute the previous media so as to keep mature adipocyte detachment to a minimum. The wells were left with 100μl IMDM 10% FBS and 1% P/S. HSPCs extracted from B6 ACTb-EGFP mice were plated at a ratio of 1:10 initial OP9 cells (in volume of 100μl IMDM, totaling 200μl volume per well).

After seven days of co-culture, the 96-well plates were removed from the incubator and placed on ice. To count non-adherent cells, the cells in suspension were retrieved through repeated washes and stained with CD45-PacBlue at final concentration of 1:200, PI at 1:1000 and 5μl CountBright beads (catalog no. C36950, Invitrogen) directly added to the media. Without any further manipulation, the plates were analyzed using the High Throughput Sampler (HTS) module of a LSRII (Becton Dickinson, USA) flow cytometer. For accuracy, the settings were programmed to mix the wells thoroughly before sample uptake. To count adherent cells, a separate set of duplicate plates were taken from the incubator, the media manually removed, and wells washed once with 200μl PBS. 40μl of Trypsin EDTA (0.5%, catalog no. 25300-054, Gibco) was added to each well and incubated for five minutes at 37°C. 160μl of ice-cold PBS containing FBS (to neutralize the trypsin), CD45-APCCy7 (1:200), PI (1:1000) and 5μl CountBright beads were then added to the plates. The plates were stained on ice and directly analyzed by flow cytometry.

2.6.1 *In vitro* conditioned media preparation and culture

Conditioned media was prepared for four different conditions as follows. For the undifferentiated condition, undifferentiated OP9 cells were seeded in six-well plates at confluency (20,000 OP9 cells/cm2) in IMDM (catalog no. 12440053, Gibco) supplemented 10% FBS and 1% P/S (basal IMDM) and conditioned medium was harvested after two days in culture and stored at -20°C. For the spontaneous differentiation conditions, confluent OP9 cells were grown in MEMα as described for the short-term differentiation assays except that at day five media was changed to IMDM following three washes; conditioned medium was then harvested after two days and stored at -20°C. For the induced adipocytic conditions, confluent OP9 cells underwent the short (5 day) or long (17-day) DMI adipogenic induction protocols before changing media to basal IMDM for two additional days of culture; conditioned medium was then harvested and stored at -20°C. Subsequently 2000 live-sorted HSPCs were plated per well in 96-well round-bottom plates in the absence of stroma. Different ratios of conditioned-to-basal IMDM media were added. After two-day culture the cells were stained with Annexin V, Propidium Iodine (PI) and CD45 to select for live CD45+ hematopoietic cells *via* flow cytometric analysis with an LSRII cytometer (Becton Dickinson, USA). CountBright beads were added to count absolute cell numbers as described above.

2.6.2 Cobblestone formation assay

OP9 cells were plated at 20,000 cells/cm2 in gelatin-pre-coated 6-well plates and cultured with α-MEM media supplemented with 10%FBS and 1%P/S. The cells were induced to differentiate using the standard differentiation cocktail DMI, which was changed two times per week. After seven days of differentiation, the media was washed three times with PBS and changed to basal IMDM. On the same day, 200 sorted KLS cells were added into each well. After 7 days of co-culture the hematopoietic colonies were manually counted (49) and scored the following way: (i) shiny colonies (defined by majority of round and bright cells, as they float above the OP9 stromal layer, with no more than 10 cobblestone cells visible per colony; (ii) cobblestone colonies (defined as darker 'cobblestone'-like cells, because they are below the OP9 stromal layer) should not contain more than 20% of shiny cells; and (iii) mixed colonies that contain both shiny and cobblestone cells (50–52).

2.7 Clinical samples

This study complied with the Declaration of Helsinki and the local ethical authorities (CER-VD). All patients signed a specific consent for the reuse of biological samples in the context of our study. For HPLC, iliac crest BM aspirates from female and male patients undergoing treatment for acute myeloid leukemia (between ages 48 and 73, n=5) or surgical debris from patients undergoing hip replacement surgery (between ages 56 and 80, n=4) were received for analysis from the Lausanne University Hospital (Centre Hospitalier Universitaire Vaudois, CHUV). Floating adipose tissue, bone marrow serum, and oil fractions were isolated and processed for lipid extraction and processed as described for OP9 lipidomics.

2.8 Statistical analysis

Values are shown as mean plus or minus the standard deviation or standard error of the mean as indicated. Student's t-test was performed for all experiments when comparing two conditions only, or a Two-Way ANOVA when comparing multiple conditions, with P-values indicated for statistical significance.

Raman spectra were processed by using the PLS Toolbox and the MIA toolbox (v8.7 eigenvector Research, Inc., USA). The spectra were baseline corrected, normalized and mean centered. Two processes were done on Raman spectra. First, cluster analysis (CA) was performed using Ward's method. CA clustered individual Raman spectra into 3 categories (saturated-rich lipids, unsaturated-rich and mixture of saturated and unsaturated lipids). Second, principal component analysis (PCA) was used which highlighted the difference in spectral features between the spontaneous and induced conditions. All data are reported as mean ± standard deviation. All statistical analyses were performed using GraphPad Prism (version 8.0.0, GraphPad Software). Mean values were compared by Mann and Whitney test, or two-way analysis of variance (ANOVA) followed by Bonferroni's post hoc test. Statistical significance was accepted for $P<0.05$, and reported.

3 Results

3.1 Differential adipocyte lipidation and similar transcriptional signature upon adipogenic induction by confluency (spontaneous) versus DMI cocktail (induced).

We chose murine BM-derived OP9 stromal cells as a model for this study because of their propensity to differentiate into adipocytes while displaying both hematopoietic support and dual adipogenic and osteogenic differentiation capacities as compared to other commonly used murine stromal lines including BM-derived MS5 and C3H10T1/2 lines or MC3T3 subclones (Figures S2A-C and [44)]. Note retention of alkaline phosphatase (AP) activity in confluent and fully mature, lipidated OP9-derived O Red Oil positive adipocytes (Figure S2D), reminiscent of properties assigned to hematopoietic supportive AP+ reticular adventitial cells in the bone marrow (53) and possibly of AdipoCARs (54).

The non-clonal OP9 stromal cell line (55, 56) was originally derived from the calvaria of newborn osteopetrotic mice [(C57BL/6xC3H)F2-op/op] deficient in macrophage colony-stimulating factor (M-CSF), and were shown optimal for studies of hematopoietic cell development and differentiation sensitive to M-CSF (57, 58). OP9 cells have been described as preadipocytes with multilineage differentiation capacity which readily generate mature adipocytes, and express the transcriptional activators CCAAT/enhancer binding proteins (C/EBP) α and β, together with the master regulator of adipocyte differentiation peroxisome proliferator activated receptor-γ (PPARg), and perilipin (PLIN), a phosphoprotein associated with the surface of lipid droplets (LDs) (22, 56). Thanks to their multipotency, hematopoietic support, and adipocytic differentiation capacities, OP9 cells are thus ideal for *in vitro* studies on BM adipogenesis. Due to their non-clonal nature and inherent heterogeneity, they serve as a BM model for studying BMAd differentiation at the single cell level.

In vitro, the OP9 cell line spontaneously differentiates into adipocytes upon confluency in the presence of serum (spontaneous OP9 adipocytes, sOP9), a phenomenon that can be more robustly promoted by exposure to a classical adipocytic differentiation cocktail consisting of insulin, dexamethasone, and 3-isobutyl-1-methylxanthine (induced OP9 adipocytes, iOP9) (22, 55). After 17 days in culture, both sOP9 and iOP9 culture conditions contained numerous differentiated OP9-adipocytes (Figure 1) with a significantly greater prevalence of Oil Red O staining of lipids in the induced condition (iOP9) ($p<0.01$) as compared to control baseline undifferentiated OP9 cells plated at sub-confluency (uOP9) (Figure 1G). Spontaneous OP9-adipocytes formed under the minimal confluency condition (sOP9) and stained with Oil Red O at intermediate levels between undifferentiated uOP9 cells and induced iOP9 cultures (Figure 1G). No significant amount of mature adipocytes could be visualized in the uOP9 condition (Figures 1A, D). Adipocytes were defined as previously described, where cells containing at least four identifiable lipid droplets were accounted as mature adipocytes (59). Morphologically, both sOP9 and iOP9 adipocytes stained with Oil Red O at day 17, but iOP9 adipocytes constituted the majority of the cultures and often contained large lipid droplets, while sOP9 adipocytes were sparser and their lipid droplets seemed smaller.

Given the intermediate phenotype of sOP9 adipocytic cultures, containing a mixture of mature adipocytes and non

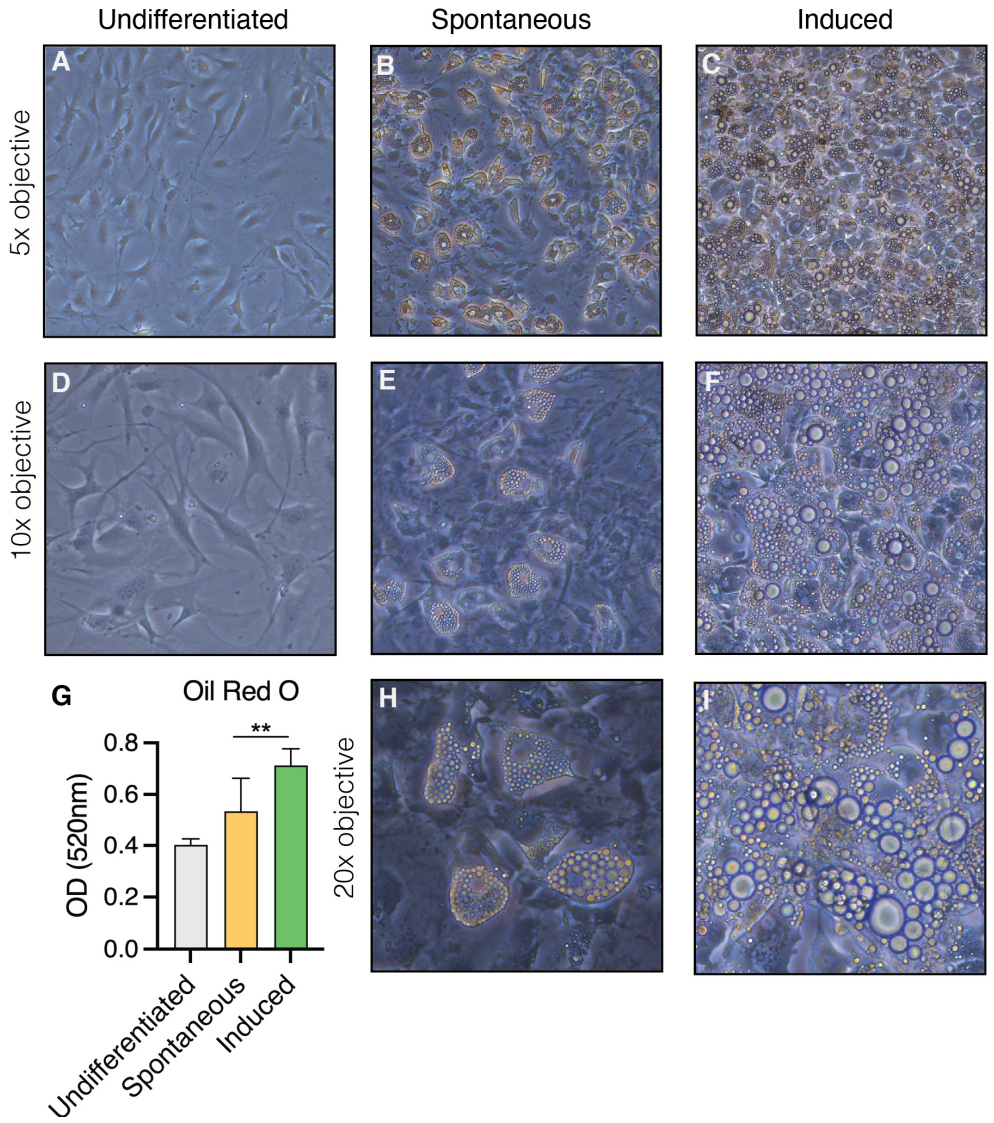

FIGURE 1
Heterogeneity in the formation of lipidated adipocytes upon induction of adipogenesis by confluency and serum exposure (spontaneous) versus DMI cocktail (induced). OP9 cells were **(A–D)** passaged subconfluently and remained undifferentiated on day 17 of culture, **(B, E, H)** differentiated spontaneously upon confluency in the presence of serum for 17 days, or **(E, F, I)** induced with a classical adipogenic differentiation cocktail in the same serum-containing conditions after confluent plating and 17 days in culture. **(G)** Oil red O measurements show the highest adipogenic differentiation in the induced condition at day 17 in culture. **P<0.01 by student's t-test. Error bars represent mean ± s.d. (n = 3 biological replicates). DMI: 1μM dexamethasone, 0.5mM isobutyl-methylxanthine, 5μg/ml insulin.

lipidated stromal cells likely including preadipocytes, we wished to determine whether the transcriptional profile and lipid composition of these cultures more resembled the undifferentiated uOP9 cultures or the highly lipidated iOP9 adipocytic cultures. We thus compared transcriptional adipocyte differentiation markers by RT-qPCR and the global fatty acid (FA) composition by high performance liquid chromatography (HPLC) for the three conditions.

RNA transcripts for the canonical adipocyte differentiation and maturation program (Fabp4, Adipoq, Cebpa, Pparg, Lpl, Pnpla2 -also known as Atgl-) in the sOP9 condition most resembled iOP9 adipocytic cultures, with average gene expression more than 10 times higher for the sOP9 and iOP9 conditions than for the control uOP9 condition (Figure 4A). These results were further validated in the OP9-EGFP cell line used in previous studies [Figures S3A, B (15)]. Further analysis of the desaturation and elongation pathway for fatty acid synthesis showed a similar pattern (Figure 4B), with overall higher expression for the sOP9 and iOP9 adipocytic conditions as compared to the uOP9 undifferentiated condition. Of note

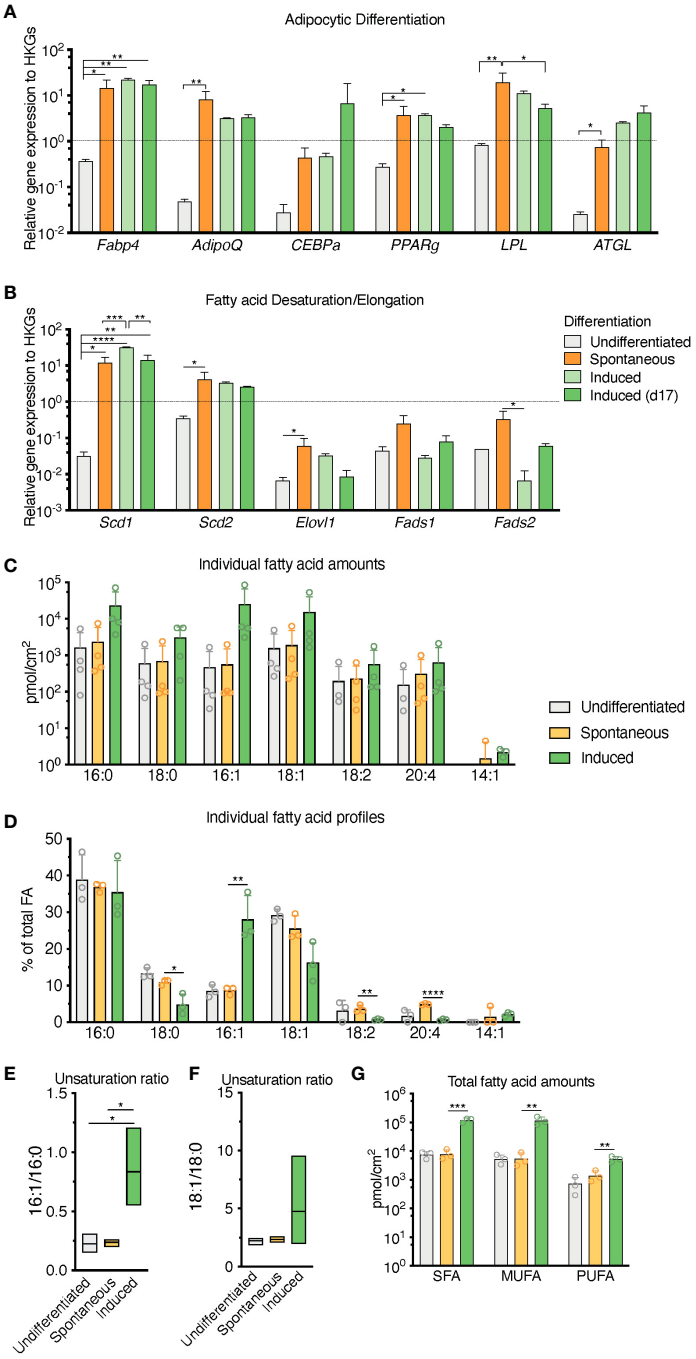

FIGURE 2
Population level differences in lipid composition are more marked than differences in the canonical adipocytic transcriptional signature for spontaneous versus induced cultures. **(A)** RT-qPCR markers of adipogenesis are increased in induced OP9-adipocytes. **(B)** Desaturase expression is highest in day 17 induced OP9-adipocytes while one of the elongases in fatty acid *de novo* synthesis is decreased. ****P < 0.0001, ***P < 0.001, **P < 0.01, *P < 0.05 by Bonferroni's multiple comparisons test. Error bars represent mean ± s.d. (n = 3 independent experiments). **(C–G)** HPLC analysis of spontaneously differentiated or induced OP9 adipocytes revealed **(C)** nuances of the most abundant saturated, mono-, and polyunsaturated lipid species, with **(D)** overall total higher unsaturation content in induced versus spontaneous conditions. **(E)** Percentage of individual fatty acid species reveals **(F)** a greater 16:1/16:0 unsaturation ratio in the induced condition. **(G)** Unsaturation ratios 18:1/18:0 were not significantly different. ****P < 0.0001, ***P < 0.001, **P < 0.01, *P < 0.05 by ANOVA test with Bonferroni's multiple comparisons adjustment. Error bars represent mean ± s.d. (n = 3 independent experiments). HKGs; housekeeping genes.

RNA transcripts for Sds1 and Fads2 were however significantly between sOP9 and iOP9 cultures. We thus conclude that, at the population level, expression of genes related to the adipocyte differentiation and fatty acid desaturation programs is similar for both sOP9 and iOP9 adipocytic conditions after 7 days of culture, suggesting that the transcriptional program is triggered in sOP9 cells prior to lipid droplet accumulation.

Conversely, total FA content and profiles were similar for control uOP9 cells and the sOP9 adipocytic condition as measured by HPLC analysis. Classical adipogenic induction of iOP9 cells resulted in a 16-fold increase of total FA content as compared with sOP9 cells or uOP9 cells (2.4x105 ± 2.2x104pmol/cm2 versus 1.5x104 ± 7.0x103pmol/cm2 and 17.4x104 ± 3.7x104pmol/cm2 respectively, Figure 2C). FA profiles revealed a preferential enrichment of MUFAs in iOP9 cells (47% MUFAs versus 38% in uOP9s and 36% in sOP9 cells), mostly to the detriment of PUFAs (only 2% in iOP9 cells versus 6% PUFAs in uOP9s and 10% in sOP9 cells, p<0.0001) (Figures 2D, G). In terms of individual FAs, the most striking finding was the marked high ratio of palmitoleic acid (16:1) in iOP9 cells, representing 29% of total FA (versus 9% in uOP9 or sOP9 cells, p=0.007) (Figures 2D, E). This result was associated to a reduction of 18 carbon FAs in iOP9 cells and a trend towards a consistent reciprocal enrichment of 18 carbon FAs in sOP9 cells: stearic acid (18:0, sOP9 11% vs. iOP9 4%, p=0.02), oleic acid (18:1, sOP9 26% vs. iOP9 16%, p=0.07) and linoleic acid (18:2 n-6, sOP9 4% vs. iOP9 1%, p=0.007). The most abundant PUFA species was arachidonic acid (20:4 n-6). In relative terms, linoleic (18:2 n-6) and arachidonic acid (20:4 n-6) were significantly enriched in the sOP9-adipocytes at 5% of total FA while making up only 1% of total FA in iOP9-adipocytes. Notably, the ratio of palmitoleic acid (16:1) versus its saturated form (stearic acid, 16:0) in iOP9 adipocytes was three times higher than in sOP9 adipocyte cultures or uOP9 control cells (Figure 2E). The ratio of oleic acid (18:1) versus its saturated form (stearic acid, 18:0) showed a similar but non-significant trend (Figure 2F). These results are very similar to those obtained on rats' tibiae when comparing lipid profiles from constitutive adipocytes versus regulated adipocytes (1). Our data is also congruent with the results shown for rabbit BMAds when comparing FA composition of rabbit BMAs from rBMAd-rich versus cBMAd-rich sites ((35) and summarized in Table 1).

Overall, these results indicate that, at the population level, sOP9 adipocytic cultures share transcriptional similarities in the adipocyte differentiation program with iOP9 cells, but are less lipidated and present lower abundance of unsaturated FAs. This constellation would be consistent with our hypothesis that sOP9 adipocytic cultures present similarities with regulated BMAds, and thus an enrichment in saturated FA, as compared to cBMAd-like iOP9 adipocytic cultures. Given the heterogeneous lipidation of sOP9 adipocytic cultures and the inevitably bulk nature of our RT-PCR and HPLC-based analysis, we set out to validate our hypothesis through a single cell analysis pipeline that could directly compare sOP9 and iOP9 adipocytes on their relative FA acid composition at the single cell level.

3.2 Raman microspectroscopy detects unsaturated spectra at the single lipid droplet level in spontaneous and induced OP9-derived adipocytes.

Raman microspectroscopy represents a powerful yet non-invasive and label-free method to assess the lipid composition of adipocytes *in vitro*. The unsaturation ratio is recognized as a measure of the proportion of unsaturated FA obtained by the ratio of the peak area assigned to unsaturated bonds (C=C) divided by the peak area assigned to saturated bonds (CH2) (Equation 1) (60–63).

$$Unsaturation\ \ ratio = \frac{A(\nu C = C)}{A(\nu CH_2)} \quad (1)$$

Equation 1: Lipid unsaturation ratio measured by Raman microspectroscopy.

Our feasibility test with Raman microspectroscopy imaging showed that it was possible to acquire Raman spectra at single lipid droplet (LD) resolution in our model (Figure 3). After 17 days of culture, Raman spectra, representative of the molecular composition of individual LDs, were acquired for sOP9 and iOP9 adipocytes through high resolution Raman imaging. No analysis was performed for the undifferentiated (uOP9) condition as it presented with very few, if any, LDs. Raman images of individual adipocytes were processed by PCA. The PCA shows that a mixture of spectra exists between the adipocytes but also within the LDs themselves, as illustrated by the Raman images (Figures 3B, E). In Figure 3C, the PC1 scores (96.68%) show a representative spectrum rich in unsaturated lipids for the iOP9 adipocyte shown in Figures 3A, B. In Figure 3F, the PC1 scores (95.69%) show a spectrum representative of a saturated rich lipids for the sOP9 adipocyte shown in Figures 3D, E. Figure S4 shows the additional variation captured by PC2 and PC3 (<5%) for the same two adipocytes shown in Figure 3. We conclude that LDs composed of predominantly unsaturated-rich or saturated-rich lipids can be identified through Raman microspectroscopy within OP9-derived adipocytes at single LD resolution.

3.3 Raman microspectroscopy reveals differential predominance of unsaturated spectra in large lipid droplets from induced adipocytes

In order to determine if significant differences exist in the unsaturation ratio of FAs accumulated within sOP9 versus iOP9

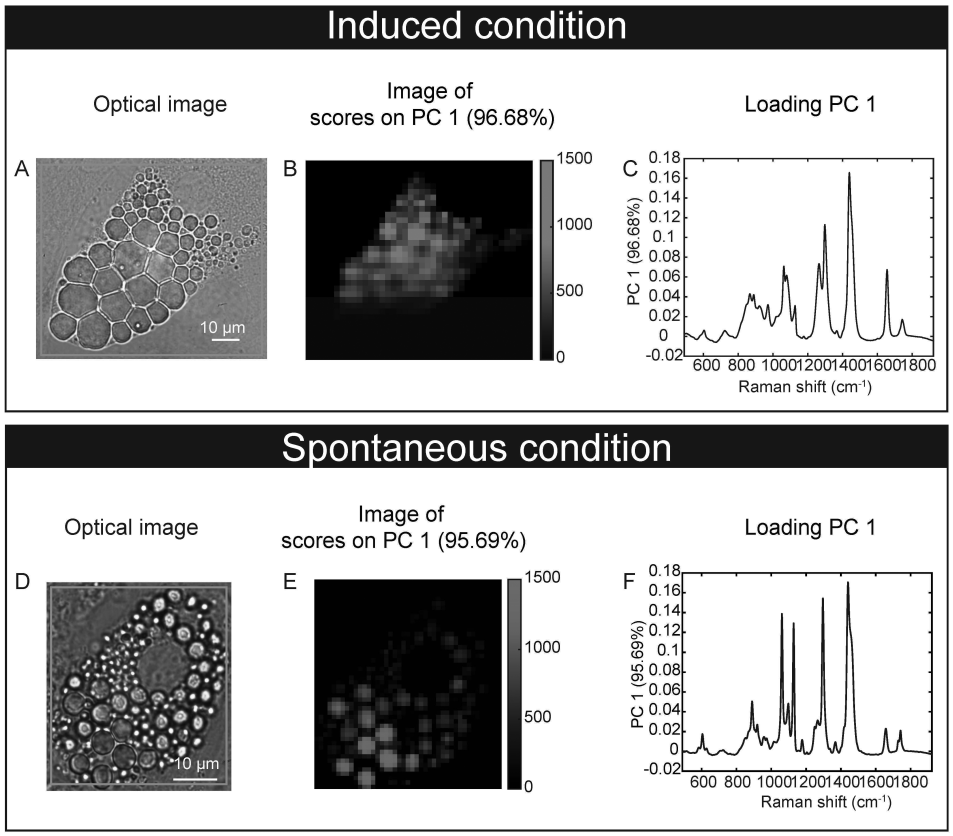

FIGURE 3
Raman microspectroscopy detects unsaturated spectra at the single lipid droplet level in spontaneous and induced adipocytes. **(A)** An optical image of an adipocyte in the induced condition (iOP9) analyzed by Raman imaging. **(B)** Raman image of the scores of PC1 in induced condition. Pixels in black represent a score of PC1 equal to zero, which corresponds to the absence of PC1. Pixels in shades of blue correspond to the contribution of PC1. **(C)** Loading PC1 is characteristic of a spectrum of unsaturated lipid-rich and captures more than 95% of the variation. **(D)** An optical image of an adipocyte in spontaneous condition (sOP9) analyzed by Raman imaging. **(E)** Raman image of the scores of PC1 in spontaneous condition. Pixels in black represent a score of PC1 equal to zero, which corresponds to the absence of PC1. Pixels in shades of red correspond to the contribution of PC1. **(F)** Loading PC1 is characteristic of a spectrum of saturated lipid-rich. The Raman images of the scores and the loadings of PC2 and PC3 capture less than 2% and are presented in supplementary files (Figure S4).

adipocytes, we thus proceeded to the acquisition of Raman spectra from individual LD in both conditions and throughout 3 separate experimental campaigns (iOP9: n = 138 adipocytes and 2971 spectra; sOP9: n = 120 adipocytes and 2944 spectra; lateral resolution 1-2µm), and combined all data for aggregated principal component (PC) analysis in both conditions. Figure S5 shows the classification of spectra using unsupervised hierarchical cluster analysis, which predicted three main categories: saturated-rich, unsaturated-rich and mixture. The representative spectrum of each category is shown in Figure 4A. PCA was then performed on the averaged spectra per adipocyte. The PC1 loading plot contains characteristic spectra where the positive peaks correspond to saturated lipids (1061, 1129, and 1296 cm-1, represented in red for Figures 4A, B) and the negative peaks correspond to unsaturated lipids (1080, 1267, and 1655 cm-1, represented in blue for Figures 4A, B) (60). PC1 captures 78.20% of the variability of the overall dataset, and separates the Raman spectra based on the saturated-rich and unsaturated-rich profiles (Figure 4B). On the PCA score plot, each point represents an averaged spectrum per adipocyte (Figure 4C). Most of the spectra from iOP9-adipocytes (81%) form a cluster in the negative score along PC1, while the spectra of sOP9-adipocytes are scattered along PC1. This indicates that the molecular composition of LDs in sOP9-adipocytes is heterogeneous compared to iOP9-adipocytes, and that iOP9-adipocytes are enriched in unsaturated-rich lipids. Score plots in Figures 4C, D are equivalent, but the points in Figure 4C are colored according to PC1 scores, and the points in Figure 4D are colored according to the culture condition. Specifically, the points in dark red and dark blue in Figure 4C correspond to Raman spectra of saturated-rich and unsaturated-rich lipids, while intermediate colors point to Raman spectra of a rather balanced mixture of saturated and unsaturated lipids. PCA analysis shows that LDs in iOP9-adipocytes are mainly rich in

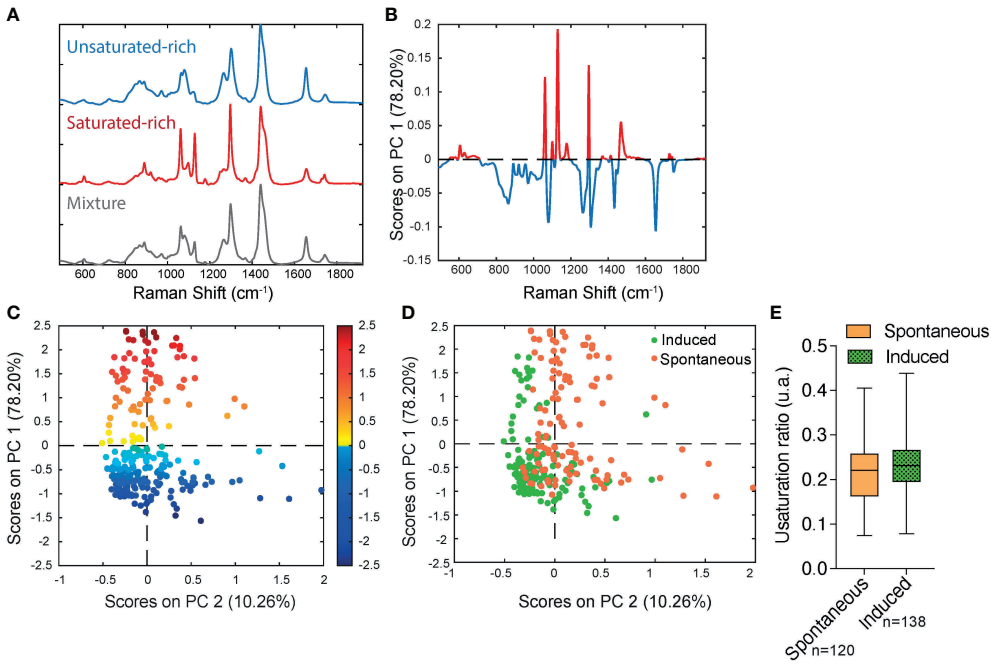

FIGURE 4
Raman microspectroscopy reveals predominance of unsaturated spectra in induced adipocytes, with heterogeneity in the unsaturation ratio for the spontaneous condition. **(A)** Representative Raman spectrum of saturated-rich, unsaturated-rich lipids and mixture identified by unguided hierarchical cluster analysis. **(B)** Loading plot PC1 indicates the discriminant peaks for saturated versus unsaturated designation, the color is associated to the attribution of specific Raman bands: saturated in blue, unsaturated in red (n = 3 independent experiments, pooled for PCA analysis). **(C)** PCA score plot of Raman spectra labelled according to spontaneous (orange) and induced (green) OP9-adipocytes. **(D)** The same PCA score plot as **(C)** labelled according to the assignment of Raman spectra as saturated (red) and unsaturated (blue) lipids based on the PC1 loading determined by **(B)** For panels C and D, each point is a single adipocyte with all its lipid droplet data points averaged. n (induced) = 138 adipocytes, 2971 spectra; n (spontaneous) = 120 adipocytes, 2944 spectra. **(E)** Unsaturation ratios of spontaneous and induced at adipocyte level. The unsaturation ratio of sOP9 adipocytes is not different from iOP9 adipocytes (P = 0.0855 by Mann-Whitney test).

unsaturated lipids, while LDs in sOP9-adipocytes are composed of a rather balanced mixture of unsaturated and saturated lipids (Figure 4D). However, when comparing the averaged raw unsaturation ratio (based on averaged spectra per adipocyte) we found no significant difference between iOP9 adipocytes and sOP9 adipocytes (Figure 4E). At the adipocyte level, both conditions have a similar averaged unsaturation ratio. This result is explained by PCA analysis which shows that LDs of both conditions are not solely composed of either uniformly saturated or unsaturated lipids, but rather by different mixtures thereof. We thus took advantage of the 1-2µ resolution of our setup and performed the analysis at the single LD level.

First, we hypothesized that the smaller diameter of LDs in sOP9 adipocytes may be related to their lower unsaturation ratio, owing to the higher mobilization rate of unsaturated FAs (64). We thus plotted LD diameter versus unsaturation ratio (Figures 5A, B). The LD diameter did not correlate with the unsaturation ratio. Specifically, correlation analysis for the LD diameter to unsaturation ratio shows that the parameters are not linearly correlated in either condition (Figures 5A, B, R^2spont=0.0013; R^2ind=0.0107). Even when the spectra are separated according the 3 types of lipids (saturated-rich, unsaturated-rich and mixture) the LD diameter and the unsaturation ratio are not linearly correlated. All the R^2 are inferior to 0.05 (Figure S6). Since, no correlation was observed, the LD diameter and the unsaturation ratio were explored separately.

The averaged LD diameter was significantly lower ($p<0.0001$) in the sOP9-adipocytes (5.24 ± 1.85µm) than the iOP9-adipocytes (7.87 ± 3.83µm) (Figure 5C). When we further separated LDs by type of lipids, we found that saturated-rich, unsaturated-rich or mixture LDs are not different in their average composition when originating from iOP9 or sOP9 adipocytes, but unsaturated LDs are more frequent in iOP9s while saturated LDs are more frequent in the sOP9 condition (Figures 5D, E; S5B). Unsaturated-rich LDs are overall bigger in size than saturated-rich LDs, with a predominance in iOP9 adipocytes, particularly above the diameter of 10 µm. In iOP9

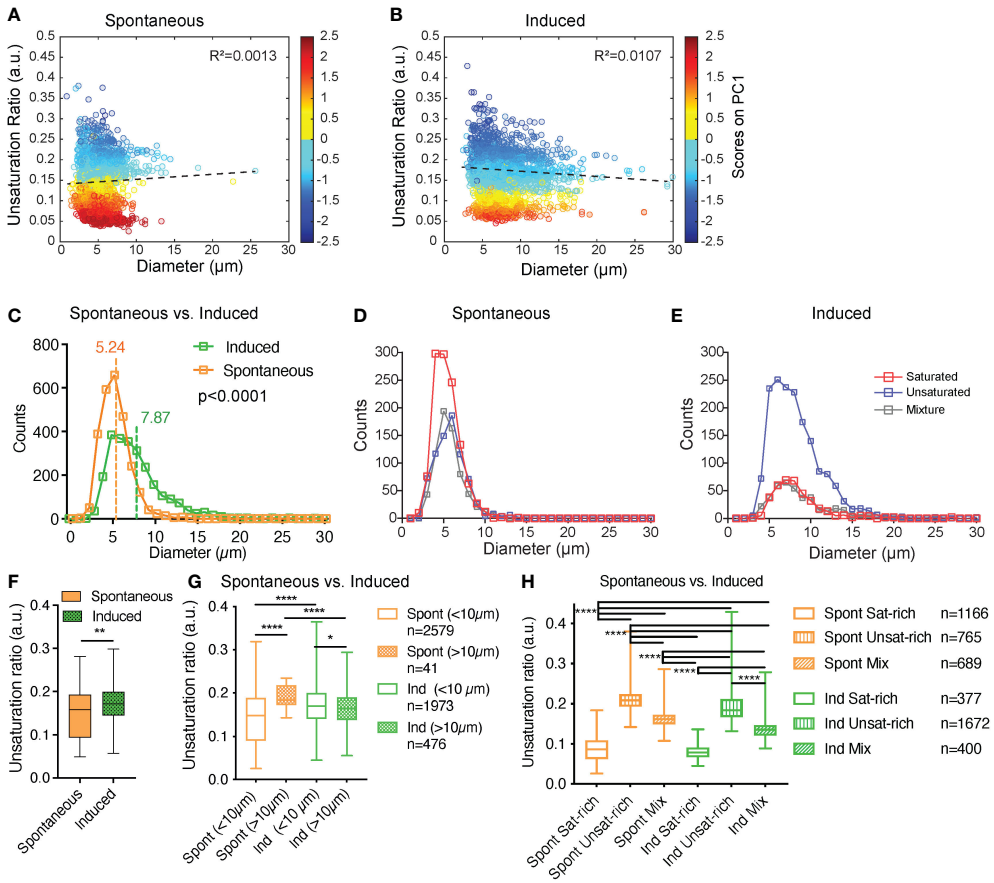

FIGURE 5
Induced adipocytes are composed of larger lipid droplets than spontaneous adipocytes, but there is no overall correlation between lipid droplet diameter and unsaturation ratio. **(A, B)** Unsaturation ratio as a function of the diameter of the LDs for sOP9 versus iOP9 adipocytes (n = 3 independent experiments, pooled for LD analysis). The low R2 for both conditions indicates that the diameter of the LDs is not correlated with the unsaturation ratio. Dashed lines represent the correlation line. The Y axis is colored as function of the score of PC1. The circles in dark blue corresponds to LDs identified as unsaturated rich. The circles in dark red correspond to LDs identified as saturated-rich. The circles in yellow and light blue correspond to LDs identified as mixture. **(C)** Histogram for frequency of LDs as a function of the diameter for the spontaneous and induced condition. Vertical lines show the mean diameter of the LD for each condition. The mean diameter of LDs is 5.24µm (±1.85µm) and 7.87 µm (±3.83µm) for sOP9 adipocytes and iOP9 adipocytes, respectively. The LDs mean diameter of sOP9-adipocytes is significantly lower compared to iOP9-adipocytes ($P < 0.0001$, Mann-Whitney test). **(D, E)** When separated according to LD type a trend toward larger unsaturated lipid droplets in the induced condition is observed. **(F)** Unsaturation ratios of sOP9 versus iOP9 at LD level. LDs from iOP9 adipocytes have a higher mean unsaturation ratio compared to LDs from sOP9 adipocytes. ($P < 0.0014$, Mann-Whitney test). **(G)** At single droplet resolution, larger droplets (>10µm) have a higher unsaturation ratio as compared to smaller lipid droplets, while smaller droplets (<10µm) in induced OP9-adipocytes (n = 1973) have a higher unsaturation ratio than those of spontaneous OP9-adipocytes (n = 2579). Highest unsaturation ratio overall is seen in large droplets from spontaneous OP9-adipocytes (n = 41). **(H)** Unsaturation ratio as a function of the condition (spontaneous and induced) and the nature of the lipid (saturated-rich, unsaturated-rich and mixture). *$P < 0.05$, ****$P < 0.001$ by Kruskal-Wallis test. The lipid droplet of spontaneous unsaturated-rich have the higher unsaturation ratio compared to induced unsaturated-rich. **p<0.01.

adipocytes, the number of unsaturated-rich LDs is higher compared to sOP9 adipocytes for LD diameter superior to 10 µm.

Then, the averaged unsaturation ratio per condition were obtained from individual spectra of LDs. The unsaturation ratio of iOP9 condition (0.17 ± 0.05) is significantly higher than sOP9 condition (0.14 ± 0.05, p=0.0014). Also on average, LDs of iOP9 condition have more unsaturated-rich lipids compared to the LDs in sOP9 condition. Since differences are observed between sOP9 and iOP9 around a LD diameter of 10 µm (Figure 5E), the unsaturation ratio of LDs was investigated as function of the threshold of 10 µm (Figure 5G). The larger LDs (>10µm) have the highest unsaturation ratio compared to smaller LDs. Smaller LDs (<10µm) from iOP9 adipocytes have a higher unsaturation ratio compared to sOP9-adipocyte. Then, we investigated the unsaturation ratio as a function of the 3 types of LDs, namely saturated-rich, mixture or unsaturated-rich. Although we found consistent differences between the three classes of LDs, there

were no significant differences between LDs of the same class in sOP9 adipocytes versus iOP9-adipocytes (Figure 5H). Not surprisingly, mixture LDs showed the greatest heterogeneity in their unsaturation ratio (Figure 5H). Overall, we conclude from this data that iOP9 adipocytes contain significantly bigger LDs and more frequently unsaturated LDs than sOP9 adipocytes. In vivo, both higher LD diameter and higher FA unsaturation are characteristics of cBMAds, while smaller LD diameter and lower unsaturation ratio are characteristics of rBMAds. We could not find a consistent relationship between LD diameter and unsaturation ratio.

3.4 Hematopoietic support capacity of sOP9-adipocytes is superior to that of iOP9-adipocytes

Another in vivo property of rBMAds as compared to cBMAds is their differential capacity to serve as a supportive niche to hematopoietic progenitor cells. Indeed, cBMAds are associated to the hematopoietic poor -yellow- regions of the marrow, while rBMAds are associated to the hematopoietic-rich -red- regions of the marrow. To determine whether sOP9 versus iOP9 cultures behave different in terms of hematopoietic support, we co-cultured murine hematopoietic stem and progenitor cells (HSPCs) isolated as cKit+Lin-Sca1+ (KLS) cells for seven days with the differentiated OP9 cells at a ratio of 1 HSPC to 10 OP9 cells. As in previous work (65), this high ratio of KLS to OP9 cells serves to avoid dispersion due to HSPC heterogeneity and avoids downstream stochastic, clone effects on analysis secondary to differences in the content of the most primitive and thus proliferative HSPCs across wells, which although small, would be exponentially exaggerated after co-culture. At the end of the seven-day co-culture period, flow cytometric analysis revealed that total hematopoietic expansion of 2,000 seeded HSPCs was 4.5-fold lower ($p<0.0001$) when iOP9 cultures were used as feeder as compared to the sOP9 condition (Figure 6A). Of note, total hematopoietic cells in suspension were significantly lower in the iOP9 versus sOP9 condition ($p<0.05$) whereas the more immature progenitor cells that are typically in close contact and adherent to the feeder cells were proportionally lower in the sOP9 condition. This suggests that iOP9 cultures may preferentially favor support of the more primitive hematopoietic progenitors, which is congruent with previous data from purified human BMAd as compared to undifferentiated stromal cells (9). The more hematopoietic progenitor supportive function of the sOP9 condition is also illustrated by the quantification of colonies formed by day 7 of co-culture (Figure 6B). The total number of hematopoietic colonies per initial number of HSPCs seeded, was significantly higher in the sOP9 coculture (0.13 colonies per initial KLS seeded) than in the iOP9 coculture (0.01 colonies per initial KLS seeded). All three colony categories, from the shiny consisting of more mature hematopoietic cells to the mixed and cobblestone colonies which contain the most immature hematopoietic progenitors were significantly increased ($P<0.05$) in the sOP9 condition. To understand to which extent secreted factors from either condition contributed to hematopoietic expansion, HSPCs were cultured for two days in the absence of feeder cells but in the presence of different concentrations of 48-hour conditioned media from either uOP9, sOP9 or iOP9 cultures. For the iOP9 condition we tested both a short (5 + 2

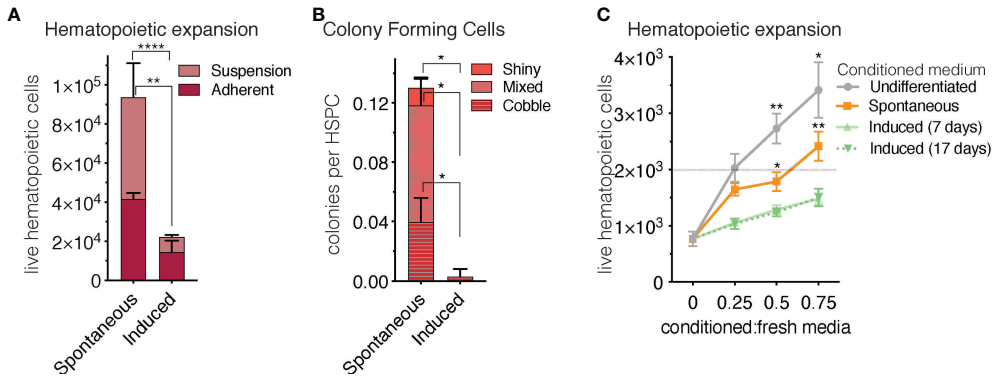

FIGURE 6
Short-term co-culture of OP9-adipocytes with hematopoietic stem and progenitor cells favours hematopoietic expansion in the spontaneous condition. **(A)** Total hematopoietic cell expansion of 2000 initial HSPCs after seven days in co-culture (including cells in adherent and cells in suspension) is significantly higher ($p < 0.0001$) when hematopoietic stem and progenitor cells, HSPCs, ($cKit^+Lin^-Sca1^+$, KLS) are co-seeded with spontaneous- compared to induced OP9 adipocytes. **(B)** The colony forming capacity of HSPCs seeded with spontaneous OP9 adipocytes is significantly higher ($P < 0.05$) than when cultured with induced OP9 adipocytes. **(C)**, Total hematopoietic expansion (in the absence of stroma) after two-day co-culture of 2000 HSPCs in conditioned medium from OP9 cultures comprising increasing ratios of conditioned-to-fresh media. ****$P < 0.0001$, **$P < 0.01$, *$P < 0.05$ by Bonferroni's multiple comparisons test. Error bars represent mean ± s.d. (n = 3 biological replicates).

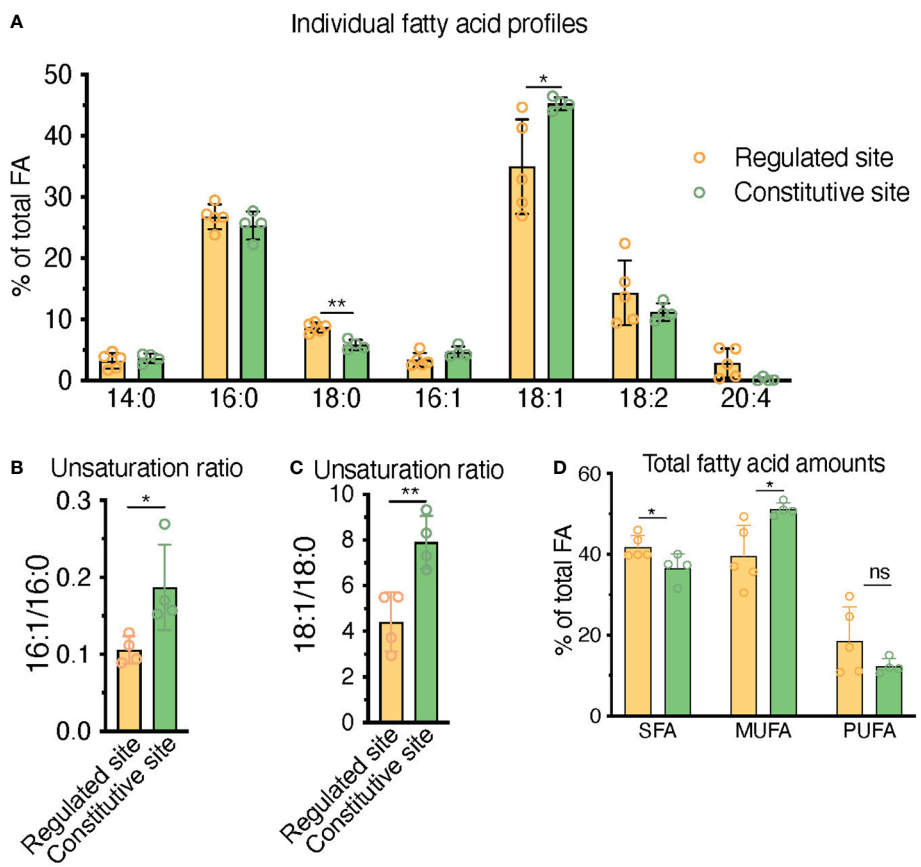

FIGURE 7
HPLC fatty acid quantification of primary human BM samples confirms a higher unsaturation ratio in constitutive BMAd-rich marrow (femoral head) versus regulated BMAd-rich marrow (ileac crest post-chemotherapy). **(A–C)** HPLC analysis of lipids isolated from human iliac crest bone marrow aspirates after induction chemotherapy (regulated site, labile marrow) or from the bone marrow of femoral specimens collected upon hip replacement surgery (constitutive site, stable marrow). **(A)** Higher unsaturation content in stable versus labile marrow oil reveal nuances of individual saturated, mono-, and polyunsaturated lipid species. **(B, C)** Greater unsaturation ratios in the human marrow from the constitutive site versus the regulated siten. **(D)** **P < 0.01, *P< 0.05 by student's t-test. Error bars represent mean ± s.d. (n = 4 experiments from independent donors). Regulated site (iliac crest): 3 females, 1 male (age = 55 ± 12 years). Constitutive site (hip replacement): 3 males, 1 female (age = 68 ± 10 years).

days) and a long (17 + 2 days) DMI adipogenesis induction protocol (Figure 7C). Hematopoietic expansion was greatest for HSPCs cultured in the highest concentration of undifferentiated-conditioned medium. HSPCs cultured in conditioned medium from iOP9-adipocytes did not show a significant expansion after two days in culture, independently of the length of the iOP9 DMI induction protocol. However, the conditioned medium from sOP9 cultures was substantially more supportive to HSPC maintenance than iOP9, although less than those cultured in conditioned media from undifferentiated OP9 cells. This effect increased with higher ratios of conditioned-to-basal medium. We therefore conclude that the *in vitro* hematopoietic progenitor support capacity of sOP9 cultures is superior to that of iOP9 cultures, aligning with the in vivo functionality of regulated versus constitutive BMAds.

3.5 HPLC fatty acid quantification in primary human samples confirms a higher unsaturation ratio in constitutive BMAd-rich marrow (femoral head) versus regulated BMAd-rich marrow (iliac crest post-chemotherapy)

In order to contextualize and validate the value of the FA unsaturation ratio used throughout this work as a surrogate marker for regulated versus constitutive BMAds, we set to test whether we could find differences in the unsaturation ratio of lipids extracted from one of the most extreme BM remodeling scenarios. Patients suffering from acute leukemias receive intensive aplastic chemotherapy, a regime that eliminates leukemic cells but also virtually all short-term hematopoietic

progenitors in the BM, leading to a rapid adipocytic conversion of the marrow. BMAds formed in this context should represent a stereotypical example of rBMAd, and we thus set out to compare the unsaturation ratio of lipids obtained from iliac crest samples from these patients as compared to the lipid fraction obtained from surgical debris of adult patients undergoing elective hip replacement surgery, which is thought to represent a cBMAd-rich site. Analysis of these primary human BM lipid samples reflected a preferential enrichment of MUFAs in the post-chemotherapy iliac crest BM samples (regulated BMAd site) versus the femoral head BM samples (constitutive BMAd site) from hip replacement surgery (39.6% versus 51.2%, p=0.02) to the detriment of PUFAs (18.6% versus 17.0% p=0.80) and SFAs (41.8% and 36.6%, p=0.04) (Figure 7D). While rapid conversion to adipocytic marrow is induced by chemotherapy, and thus iliac crest samples are interpreted as rBMAd-rich, the differences in fatty acid profiles displayed could also be an inherent function of the anatomical site. The largest difference between FA species in the regulated versus constitutive marrow sites was seen in the 18:1 to 18:0 unsaturation ratio (4.40 versus 7.91, p=0.007), and the 16:1 versus 16:0 unsaturation ratio (0.11 versus 0.19, p=0.031) (Figures 7B, C). We thus conclude that human BM samples from a rBMAd-rich site in the context of BM remodeling driven by hematopoietic demand present a lower unsaturation ratio, as measured by 16:1/16:0 -and 18:1/18:0- FA content, than samples obtained from a cBMAd-rich site, which complements previously reported results for rabbit and rats marrow at steady-state (1, 35–37) as summarized in Table 1.

Taken together, we conclude that the spontaneous versus induced OP9 *in vitro* adipogenesis model presented here replicates key differences in lipid droplet size, FA unsaturation ratio and hematopoietic support respectively associated *in vivo* to regulated versus constitutive BMAd subtypes. We additionally validate the value of the 16:1/16:0 FA unsaturation ratio as a surrogate marker to segregate rBMAd-rich versus cBMAd-rich tissues both *in vivo* and for our *in vitro* model, and the feasibility of Raman microspectroscopy to reveal equivalent differences in the unsaturation ratio at the single adipocyte level.

4 Discussion

BMAds constitute a distinct fat depot with low responsiveness to cold and insulin, overall relative resistance to lipolysis, and high expression of adiponectin as compared to subcutaneous fat depots (39, 66, 67). Two BMAd subtypes have been described based on their differential response to physiological and metabolic stimuli: the more stable so-called constitutive (cBMAd) depots, preferentially located in the distal parts of the skeleton, and the more labile so-called regulated (rBMAd) adipocytes, which are interspersed within the hematopoietic marrow in more proximal skeletal sites. Due to their fragility and location within the bone cavity, access to live BMAd cells for functional and cell trajectory analysis is not trivial, especially for murine BMAd depots where BM adipose tissue volume is very limiting. Although possibly limited on the extrapolation of specific metabolic behaviors (39), *in vitro* models of adipogenesis from undifferentiated stromal progenitors have been proposed as a complementary tool to study BMAd at the cellular level, so as to facilitate both gene function studies and cell behavior analysis [reviewed in (34, 68)]. To our knowledge, no *in vitro* model has been described to recapitulate some or all of the differential characteristics of the in vivo defined rBMAd versus cBMAd depots. Here we present a model of BM adipogenesis in the form of a differential *in vitro* culture system for BM-derived OP9 stromal cells. When classically induced by an adipogenic cocktail (iOP9s) OP9-derived adipocytes resemble cBMAds and, when allowed to spontaneously differentiate by confluency in serum-containing conditions (sOP9s), they resemble rBMAds in lipid droplet size, overall lipid saturation, 16:1/16:0 FA unsaturation ratio and hematopoietic supportive properties. Indeed, we validated the value of the 16:1/16:0 FA unsaturation ratio, already described as a discriminating factor for cBMAd and rBMAd depots in rabbit and rat homeostatic tissues, in both human BM and as a marker of cBMAd-like (iOP9) versus rBMAd-like (sOP9) *in vitro* cultures. Furthermore, we have extended the reproducibility of the 16:1/16:0 FA unsaturation ratio as a discriminating factor to highly remodeled rBMAd depots in the context of patients undergoing intensive ablative chemotherapy. It is worth noting that the robustness of differences in the 16:1/16:0 FA unsaturation ratio in our model [summarized in Table 1 (1, 69], as opposed to other proposed FA pairs (e.g. 18:1/18:0), is somehow surprising and may be associated to the low mobilization rate for palmitate (16:0) and palmitoleate (16:1) (64, 70). Further studies should mechanistically address the relative contribution of de novo lipogenesis and FA re/uptake in lipid composition differences underlying the 16:1/16:0 FA unsaturation ratio. Indeed, at the RNA level, sOP9 adipocytes had significantly higher expression of Lpl, which mediates fatty acid uptake for storage, while iOP9 adipocytes had increased expression of Atgl, the key enzyme that initiates hydrolysis of TAGs.

After HPLC-based lipid composition analysis of OP9 cultures at the cell population level, and given the relative heterogeneity of *in vitro* adipogenic cultures (68), we implemented a novel application of Raman microspectroscopy to measure lipid unsaturation heterogeneity at the single cell level, with individual LD resolution and in a label-free manner. This approach allowed us to focus lipid composition analysis exclusively on mature adipocytes and not on the remaining unlipidated stromal component. Previous studies have shown the application of Coherent anti-Stokes Raman microspectroscopy to embryonic stem cells undergoing adipogenic differentiation, showing a measure of chemical lipid saturation composition and an increase in LD accumulation with

10.3389/fendo.2022.1001210

TABLE 2 List of general abbreviations.

Abbreviation	Definition
ACTb	Actin beta
AdipoQ	Adiponectin
Angpt1	Angiopoietin 1
ANOVA	Analysis of variance
ATGL	Adipose triglyceride lipase
Ap2	Activating protein 2
BM	Bone marrow
BMAd	Bone marrow adipocyte
BMAT	Bone marrow adipose tissue
BMSC	Bone marrow stromal cell
CA	Cluster of analysis
CAR cell	CXCL12 abundant reticular cell
cBMAd	Constitutive bone marrow adipocyte
cDNA	Complementary deoxyribonucleic acid
CEBPa	CCAAT Enhancer Binding Protein Alpha
CFU	Colony-forming unit
CGL	Congenital generalized lipodystrophy
cKit	Kit proto-oncogene, receptor tyrosine kinase
CXCL12	C-X-C motif chemokine ligand receptor 12
DMI	Cocktail for Dexamethasone, IBMX and insulin
DNA	Deoxyribonucleic acid
DNL	*De novo* lipogenesis
EDTA	Ethylenediaminetetraacetic acid
EGFP	Enhanced green fluorescent protein
ER	Endoplasmic reticulum
FA	Fatty acid
FABP4	Fatty acid binding protein 4
FACS	Fluorescence-activated cell sorting
FADS	Fatty acid desaturase
FBS	Fetal bovine serum
HKGs	Housekeeping genes
^{1}H-MRS	proton magnetic resonance spectroscopy
HPLC	High performance liquid chromatography
HSC	Hematopoietic stem cell
HSL	Hormone sensitive lipoase
HSPC	Hematopoietic stem and progenitor cell
IBMX	isobutylmethylxanthin
IMDM	Iscove's Modified Dulbecco's Medium
iOP9	induced OP9 cell
KitL	cKit ligand
KLS	cKit^{+}Lineage^{-}Sca1^{+}
LD	Lipid droplet
LPL	lipoprotein lipase
mRNA	Messenger ribonucleic acid
MRI	Magnetic resonance imaging
MUFA	Monounsaturated fatty acid
M-CSF	Macrophage colony-stimulating factor
MEMα	Minimum Essential Medium alpha
ORO	Oil red O
PC	Principle component
PCA	Principle component analysis
PCR	Polymerase chain reaction
PFA	Paraformaldehyde
PI	Propidium iodide
PLIN	Perilipin
PPARγ	Peroxisome proliferator-activated receptor gamma
PTRF	Polymerase I and transcript-release factor
P/S	Penicillin/Streptomycin
PUFA	Polyunsaturated fatty acid
rBMAd	Regulated bone marrow adipocyte
RNA	Ribonucleic acid
ROS	Reactive oxygen species
RT-qPCR	Real-time quantitative polymerase chain reaction
Sca1	Stem cell antigen 1
Scd	Stearyl-CoenzymeA desaturase
SCF	Stem cell factor
SD	Standard deviation
SFA	Saturated fatty acid
sOP9	spontaneous OP9 cell
STR	Short tandem repeats
TAG	Triacylglycerols
uOP9	Undifferentiated OP9 cell

differentiation (71, 72). While, very interestingly, individual LDs within one adipocyte appear to have an inhomogeneity in their chemical composition, this was not further analyzed. Raman microspectroscopy has allowed for the characterization of LD lipid composition in animal and *in vitro* models. Lipid droplets have been measured directly in the endothelial layer of murine aortic sections, pointing to smaller LDs induced by TNFalpha preferentially containing more unsaturated lipids whereas larger LDs were more rich in saturated lipids (73). Another Raman-based study showed interesting differences in the pattern of distribution between saturated FA species (palmitic acid -16:0- and stearic acid -18:0), which were evenly distributed in broad areas of the cell, and unsaturated FA species (oleic acid -18:1- and linoleic acid -18:2-), which were concentrated in LDs, after exposure and uptake in macrophages (74). The effect of the high fat diet was evaluated on the lipidic composition of perivascular adipocytes in a mouse model. The size of the LDs was increased as an adaptive response to the excessive lipid income. In an in-vitro study, the effect of TNF-α on endothelial HMEC-1 cells during 24h was monitored by Raman microspectroscopy. The composition and the distribution of cellular lipids was modified upon exposure to TNF-α, and the increase in LD size was concomitant with the formation LDs

TABLE 3 List of fatty acid abbreviations.

Abbreviation	Definition	Formula	IUPAC Name
14:1	Myristoleic acid	$C_{14}H_{26}O_2$	(Z)-tetradec-9-enoic acid
16:0	Palmitic acid	$C_{16}H_{32}O_2$	hexadecanoic acid
16:1n-7	Palmitoleic acid	$C_{16}H_{30}O_2$	(Z)-hexadec-9-enoic acid
16:1n-10	Sapienic acid	$C_{16}H_{30}O_2$	(Z)-hexadec-6-enoic acid
18:0	Stearic acid	$C_{18}H_{36}O_2$	octadecanoic acid
18:1n-9	Oleic acid	$C_{18}H_{34}O_2$	(Z)-octadec-9-enoic acid
18:2n-6	Linoleic acid	$C_{18}H_{32}O_2$	(9Z,12Z)-octadeca-9,12-dienoic acid
20:4n-6	Arachidonic acid	$C_{20}H_{32}O_2$	(5Z,8Z,11Z,14Z)-icosa-5,8,11,14-tetraenoic acid

composed of unsaturated rich lipids (75, 76). However, none of these studies provide supporting statistical analysis for an univocal association between LDs size and molecular composition. In all, we found Raman microspectroscopy to be robust for the measurement of the unsaturation ratio at the lipid droplet level. Congruently to the HPLC-derived data, we could thus confirm at the single adipocyte level the higher unsaturation ratio of iOP9 lipids as compared to the sOP9 condition. It is worth noting that the overall differences in unsaturation ratio were more pronounced when measured with HPLC analysis (1.02 ± 0.27 for iOP9-cultures versus 0.19 ± 0.11 sOP9-cultures, p=0.0004, Figure 2E), than with Raman (0.17 ± 0.05 for iOP9-cultures versus 0.14 ± 0.05 sOP9-cultures, p=0.014, Figure 5F). This difference could be related to the sample bias, as HPLC analysis was done in lipid extracts from the bulk culture while Raman microspectroscopy acquired spectra from mature adipocytes only, or to the method itself. For the HPLC analysis, the unsaturation ratio is calculated from the contribution of isolated and purified lipids. On the other hand, Raman analysis is done inside the LD where lipids are mixed. The unsaturation ratio is calculated from the contribution of the mixture of lipids which hamper the signal. Indeed, the small differences we report in the unsaturation ratio are in the range of previous Raman studies cited above, although differences are more pronounced if only the more defined fractions are considered (unsaturation-rich versus saturated-rich, Figure S5).

Diseases of lipodystrophy may provide insights into the formation of BMAds and the selective accumulation of FAs that we are struggling to understand (1, 77). Congenital generalized lipodystrophy (CGL) is a family of diseases that include a complete or partial loss of adipose depots, which reveal important insights into the consequences of genetic deficiencies involved in adipocytic maturation and function [reviewed in (77)] and may point us in the direction of the underlying nature of BMAd formation. One of the best understood CGL mouse models within the context of BMAd research are the caveolae associated protein 1 deficient mice (*Cav1*, also known as *Ptrf-/-*), which contain BMAT only in the tail vertebrae and very distal tibia with a loss of BMAds at the tibia-fibula junction and proximal thereof (1, 78–80), thus indicating a rBMAd-specific loss. This is accompanied by a small increase in cortical bone mineral content in adult male mice and a large increase in trabecular number and cortical bone mineral content in females (1). The differential effect on BMAT upon *Cavin1/Ptrf* loss of function, points toward a differential regulation of LD formation in regulated versus constitutive BMAds. Alternatively, differences in unsaturated lipid ratios could be involved in the specific sensitivity of BMAds to such a mutation. More recently, diphtheria-toxin mediated ablation of Adipoq-Cre expressing cells also revealed differences in BMAd plasticity throughout the long bones in "fat-free" mice. In particular BMAds were increasingly present in the mid-diaphysis with age (81, 82). Furthermore, specific depletion of BMAds through a double conditional Osterix and Adipoq-dependent strategy caused severe reduction in rBMAds with a milder reduction in the cBMAd mass, while ATGL (Pnpla2 gene) loss in BMAd through the same strategy caused massive rBMAd expansion in the mid diaphysis (83, 84). To what extent these discrepancies are due to divergent transcriptional programs or part of a stabilization of the adipocytic differentiation program remains to be determined. Moreover, seipin-deficient lymphoblastoid cell-lines derived from patients suffering congenital generalized lipodystrophy type 2 were shown to have an increased proportion of SFAs with a decrease in MUFAs, which are the principle products of Scd1, indicating decreased Scd1 activity. LD number and size were increased compared to control (85). Impaired Δ9-desaturase activity in nematodes also led to decreased TAG accumulation and LD size that could not be rescued completely by supplemented dietary oleate (86). Therefore, it appears that LD size is at least partially driven by the ability of Scd1 to synthesize unsaturated FAs. Although our results did not show a strong correlation of LD size with lipid unsaturation, we did observe that the largest LDs were always predominantly unsaturated. Taken together, this points to tissue-specific regulation of lipid composition independently of nutrient and metabolite availability, and possibly to sequential stages of LD (and adipocyte) maturation in the sOP9 versus the iOP9 conditions. Overall, it is tempting to suggest a continuum with smaller LD being mostly saturated, an intermediate stage of LD maturation that are of largely mixed composition, and the

most mature LDs that are large and unsaturated. Follow-up studies should address this hypothesis through Raman microspectroscopy in the context of inhibition versus activation of lipolysis and reuptake with relation to lipid droplet and adipocyte size. Extrapolation to the *in vivo* scenario should be done with caution, as the primary mechanism of lipid remodeling in primary human BMAd has been shown to be independent of ATGL-mediated lipolysis (39).

Finally, we found that sOP9-adipocytes are more supportive to hematopoiesis than iOP9-adipocytes, as seen by their capacity to form hematopoietic colonies and to support hematopoietic expansion. This agrees with reports of adiponectin expressing BM pre/adipocytes -including so-called Adipo-CAR cells- being necessary for hematopoietic expansion (13, 87, 88), whereas mature BMAds rather inducing HSCs quiescence or reduced proliferation (8, 9, 12, 89). Of note, depletion of recently described marrow adipocyte lineage precursors (MALPs) did not affect hematopoiesis, at least in homeostasis (90). The reduced proliferation of hematopoietic progenitors in iOP9 adipocytic cocultures was replicated in a dose-dependent manner through condition media experiments (Figure 6C), pointing to availability of soluble factors as one of the implicated mechanisms. Indeed, previous data revealed a higher expression of the hematopoietic supportive factors C-X-C Motif Chemokine Ligand 12 (Cxcl12) and c-Kit Ligand (KitL) in undifferentiated OP9 cultures versus OP9-derived adipocytes analogous to iOP9s (44), and the regulation of BM stromal cell differentiation precisely *via* Cxcl12 (91). Note however that the undifferentiated OP9 condition was shown even more supportive of hematopoietic proliferation than sOP9s (Figure 6). In congruence with previous in vivo data (12), this observation in the OP9 system suggests that hematopoiesis is favored when mature marrow adipocytes are absent. We therefore suggest an optimum of maturation along the adipocytic differentiation axis with regard to hematopoietic support, in particular through at least limited expression of Angpt1, SCF, and Cxcl12 that are attenuated in terminally differentiated adipocytes (92). Taken together, our results indicate that, at the population level, sOP9 adipocytic cultures share similarities in terms of hematopoietic support with the labile rBMAds of the red marrow, while iOP9 adipocytic cultures impair rapid hematopoietic progenitor proliferation as described for the stable cBMAds of the yellow marrow.

The mechanisms for differential hematopoietic support in vivo are still poorly understood, but extrapolation from the collective findings of the field suggests that cBMAd-dense regions of the distal skeleton maintain HSCs, while rBMAd-containing red marrow would contribute to expansion of their progenitors, possibly through increased FA transfer (83). Most HSCs have low mitochondrial potential and rely mainly on anaerobic glycolysis, while downstream progenitors rely on high energy production through mitochondrial oxidative phosphorylation (93–95). Previous studies have also revealed that HSCs and leukemic cells can rely on PPAR-mediated FA oxidation (96), with activation of oxidative metabolism being a predictive factor for leukemic stem cell behavior (97). Indeed, we have shown that BM stromal cells with lower overall lipid content (sOP9 cultures) associate to increased hematopoietic expansion capacity compared with more mature BMAds that are high in lipid content (iOP9 cultures). Specific differences in FA of BMAds may contribute to the nuances of differential hematopoietic support. For example, palmitic acid was shown to have a lipotoxic effect on hematopoietic-supportive osteoblasts, and high levels are present in aged and osteoporotic bone associated with decreased hematopoiesis (98, 99). This may in part explain the overt myeloproliferation that is seen on the aged skeleton. Of note, in the current study, the stromal OP9 cell line was selected for its adipocytic differentiation potential. The inherent M-CSF deficiency may influence outcomes with regard to the hematopoietic supportive function. Previous studies have shown lymphoid and myeloid support of bone marrow adipocytes, although the extent of hematopoietic support as a function of the extent of adipocytic differentiation has not been addressed. In future studies, a comparison to marrow stromal cell lines without cytokine expression defects is warranted to provide a more representative understanding of the marrow hematopoietic and adipocytic lineages.

Future studies to understand the functional metabolic differences of rBMAd-like sOP9 versus cBMAd-like iOP9 adipocytes should focus on *in vitro* lipase- and desaturase-inhibition, complemented by the study of their role in BMAd-deficient animal models (such as the Atgl-KO or Scd1-KO) to better understand the role of rBMAd vs cBMAd FA mobilization on hematopoiesis. Altogether, our results open avenues for future work on the OP9-adipocyte system to understand the mechanisms underlying BMAd heterogeneity and its impact on both hematopoiesis and bone health.

Data availability statement

The raw data supporting the conclusions of this article has been published as DOI: 10.17632/wdm9gvz3bm.1, which can be downloaded at https://data.mendeley.com/datasets/wdm9gvz3bm.

Ethics statement

The studies involving human participants were reviewed and approved by Commission d'étique Canton de Vaud (CER-VD). The patients/participants provided their written informed consent to participate in this study.

Author contributions

JT planned experiments, analyzed and interpreted the results. GF performed Raman acquisitions, interpreted and analyzed the results and compiled the corresponding figures. AD and NB performed HPLC analyses. JT, CB, and DNT performed *in vitro* culture experiments. VC performed co-cultures. GF and LD performed statistical analyses for Raman data. JT, GF, AD, CC, and ON interpreted the Raman and HPLC data. GD and ON designed and optimized OP9 differentiation protocols and associated hematopoietic support assays. ON and GP initiated the project, while CC and ON co-supervised the project. ON and JT wrote the manuscript, GF and CC significantly edited the manuscript. All authors contributed to the article and approved the submitted version.

Funding

JT, VC, and ON were financed by Swiss National Science Foundation (SNSF) grants PP00P3_176990 and PP00P3_183725 (to ON), the Anna Fuller cancer fund (JT and ON) and UNIL unrestricted funds to ON. DT was funded by the Whitaker Fellowship program in Bioengineering. CB was financed by Sinergia funding CRSII5_186271.

Acknowledgments

OP9 cells were generously provided by T. Nakano, Kyoto University, Japan, *via* the Daley Lab. MS5 stromal cells were generously provided by Prof. Gary Gilliland, C3H10T1/2 and MC3T3 stromal cells by Prof. Peter Hauschka (both at Children's Hospital Boston), and AFT024 as well as BFC012 from Prof. Rudolf Jaenisch (Whitehead Institute, Massachusetts Institute of Technology). We are very grateful to Aurélien Oggier and Silvia Vaz Ferreira Lopes for technical help with qPCR experiments and to the support of the EPFL Flow Cytometry Core Facility for flow cytometric sorting and EPFL Bioscreening Facility for Digital Holographic Microsocopy imaging. This collaborative work was made possible by the networking opportunities facilitated by the Bone Adiposity in HEalth and Disease (BoneAHEAD) Network consortium, and by the International Bone Marrow Adiposity Society (BMAS).

Conflict of interest

The authors declare that the research was conducted in the absence of any commercial or financial relationships that could be construed as a potential conflict of interest.

Publisher's note

All claims expressed in this article are solely those of the authors and do not necessarily represent those of their affiliated organizations, or those of the publisher, the editors and the reviewers. Any product that may be evaluated in this article, or claim that may be made by its manufacturer, is not guaranteed or endorsed by the publisher.

Supplementary material

The Supplementary Material for this article can be found online at: https://www.frontiersin.org/articles/10.3389/fendo.2022.1001210/full#supplementary-material

References

1. Scheller EL, Doucette CR, Learman BS, Cawthorn WP, Khandaker S, Schell B, et al. Region-specific variation in the properties of skeletal adipocytes reveals regulated and constitutive marrow adipose tissues. *Nat Commun* (2015) 6:7808. doi: 10.1038/ncomms8808

2. Kricun ME. Red-yellow marrow conversion: Its effect on the location of some solitary bone lesions. *Skeletal Radiology.* (1985) 14(1):10–9. doi: 10.1007/BF00361188

3. Tratwal J, Bekri D, Boussema C, Sarkis R, Kunz N, Koliqi T, et al. MarrowQuant across aging and aplasia: A digital pathology workflow for quantification of bone marrow compartments in histological sections. *Front Endocrinol* (2020) 11:480. doi: 10.3389/fendo.2020.00480

4. Doucette CR, Horowitz MC, Berry R, MacDougald OA, Anunciado-Koza R, Koza RA, et al. A high fat diet increases bone marrow adipose tissue (MAT) but does not alter trabecular or cortical bone mass in C57BL/6J mice. *J Cell Physiol* (2015) 230(9):2032–7. doi: 10.1002/jcp.24954

5. Scheller EL, Khandaker S, Learman BS, Cawthorn WP, Anderson LM, Pham HA, et al. Bone marrow adipocytes resist lipolysis and remodeling in response to β-adrenergic stimulation. *Bone* (2019) 118:32–41. doi: 10.1016/j.bone.2018.01.016

6. Craft CS, Scheller EL. Evolution of the marrow adipose tissue microenvironment. *Calcified Tissue Int* (2017) 100(5):461–75. doi: 10.1007/s00223-016-0168-9

7. Horowitz MC, Berry R, Holtrup B, Sebo Z, Nelson T, Fretz JA, et al. Bone marrow adipocytes. *Adipocyte* (2017) 6(3):193–204. doi: 10.1080/21623945.2017.1367881

8. Ambrosi TH, Scialdone A, Graja A, Gohlke S, Jank AM, Bocian C, et al. Adipocyte accumulation in the bone marrow during obesity and aging impairs stem cell-based hematopoietic and bone regeneration. *Cell Stem Cell* (2017) 20(6):771–784.e6. doi: 10.1016/j.stem.2017.02.009

9. Mattiucci D, Maurizi G, Izzi V, Cenci L, Ciarlantini M, Mancini S, et al. Bone marrow adipocytes support hematopoietic stem cell survival. *J Cell Physiol* (2018) 233(2):1500–11. doi: 10.1002/jcp.26037

10. Mattiucci D, Naveiras O, Poloni A. Bone marrow "Yellow" and "Red" adipocytes: Good or bad Cells ? *Curr Mol Bio Rep* (2018) 4:117–22. doi: 10.1007/s40610-018-0098-6

11. Wei Q, Frenette PS. Niches for hematopoietic stem cells and their progeny. *Immunity.* (2018) 48(4):632–48. doi: 10.1016/j.immuni.2018.03.024

12. Naveiras O, Nardi V, Wenzel PL, Hauschka PV, Fahey F, Daley GQ. Bone-marrow adipocytes as negative regulators of the haematopoietic microenvironment. *Nature.* (2009) 460(7252):259–63. doi: 10.1038/nature08099

13. Zhou BO, Yu H, Yue R, Zhao Z, Rios JJ, Naveiras O, et al. Bone marrow adipocytes promote the regeneration of stem cells and haematopoiesis by secreting SCF. *Nat Cell Biol* (2017) 19(8):891–903. doi: 10.1038/ncb3570

14. Tratwal J, Rojas-Sutterlin S, Bataclan C, Blum S, Naveiras O. Bone marrow adiposity and the hematopoietic niche: A historical perspective of reciprocity, heterogeneity, and lineage commitment. *Best Pract Res Clin Endocrinol Metab* (2021) 35(4):101564. doi: 10.1016/j.beem.2021.101564

15. Ghali O, Broux O, Falgayrac G, Haren N, van Leeuwen J, Penel G, et al. Dexamethasone in osteogenic medium strongly induces adipocyte differentiation of mouse bone marrow stromal cells and increases osteoblast differentiation. *BMC Cell Biol* (2015) 16(1):9. doi: 10.1186/s12860-015-0056-6

16. Campos V, Rappaz B, Kuttler F, Turcatti G, Naveiras O. High-throughput, nonperturbing quantification of lipid droplets with digital holographic microscopy. *J Lipid Res* (2018) 59(7):1301–10. doi: 10.1194/jlr.D085217

17. Stiebing C, Schmölz L, Wallert M, Matthäus C, Lorkowski S, Popp J. Raman imaging of macrophages incubated with triglyceride-enriched oxLDL visualizes translocation of lipids between endocytic vesicles and lipid droplets. *J Lipid Res* (2017) 58(5):876–83. doi: 10.1194/jlr.M071688

18. Guo Y, Cordes KR, Farese RV, Walther TC. Lipid droplets at a glance. *J Cell Science.* (2009) 122(6):749–52. doi: 10.1242/jcs.037630

19. Ehehalt R, Füllekrug J, Pohl J, Ring A, Herrmann T, Stremmel W. Translocation of long chain fatty acids across the plasma membrane – lipid rafts and fatty acid transport proteins. *Mol Cell Biochem* (2006) 284(1–2):135–40. doi: 10.1007/s11010-005-9034-1

20. Schaffer JE, Lodish HF. Expression cloning and characterization of a novel adipocyte long chain fatty acid transport protein. *Cell.* (1994) 79(3):427–36. doi: 10.1016/0092-8674(94)90252-6

21. Thiam AR, Beller M. The why, when and how of lipid droplet diversity. *J Cell Science.* (2017) 130(2):315–24. doi: 10.1242/jcs.192021

22. Kimmel AR, Sztalryd C. The perilipins: Major cytosolic lipid droplet–associated proteins and their roles in cellular lipid storage, mobilization, and systemic homeostasis. *Annu Rev Nutr* (2016) 36(1):471–509. doi: 10.1146/annurev-nutr-071813-105410

23. Zimmermann R. Fat mobilization in adipose tissue is promoted by adipose triglyceride lipase. *Science.* (2004) 306(5700):1383–6. doi: 10.1126/science.1100747

24. Zechner R, Zimmermann R, Eichmann TO, Kohlwein SD, Haemmerle G, Lass A, et al. FAT SIGNALS - lipases and lipolysis in lipid metabolism and signaling. *Cell Metab* (2012) 15(3):279–91. doi: 10.1016/j.cmet.2011.12.018

25. Unger RH, Clark GO, Scherer PE, Orci L. Lipid homeostasis, lipotoxicity and the metabolic syndrome. *Biochim Biophys Acta (BBA) - Mol Cell Biol Lipids.* (2010) 1801(3):209–14. doi: 10.1016/j.bbalip.2009.10.006

26. Ouchi N, Parker JL, Lugus JJ, Walsh K. Adipokines in inflammation and metabolic disease. *Nat Rev Immunol* (2011) 11(2):85–97. doi: 10.1038/nri2921

27. Carta G, Murru E, Banni S, Manca C. Palmitic acid: Physiological role, metabolism and nutritional implications. *Front Physiol* (2017) 8. doi: 10.3389/fphys.2017.00902

28. Ly LD, Xu S, Choi SK, Ha CM, Thoudam T, Cha SK, et al. Oxidative stress and calcium dysregulation by palmitate in type 2 diabetes. *Exp Mol Med* (2017) 49 (2):e291. doi: 10.1038/emm.2016.157

29. Gillet C, Spruyt D, Rigutto S, Dalla Valle A, Berlier J, Louis C, et al. Oleate abrogates palmitate-induced lipotoxicity and proinflammatory response in human bone marrow-derived mesenchymal stem cells and osteoblastic cells. *Endocrinology.* (2015) 156:4081–93. doi: 10.1210/en.2015-1303

30. Miranda M, Pino AM, Fuenzalida K, Rosen CJ, Seitz G, Rodríguez JP. Characterization of fatty acid composition in bone marrow fluid from postmenopausal women: Modification after hip fracture. *J Cell Biochem* (2016) 117(10):2370–6. doi: 10.1002/jcb.25534

31. Tencerova M, Ferencakova M, Kassem M. Bone marrow adipose tissue: Role in bone remodeling and energy metabolism. *Best Pract Res Clin Endocrinol Metab* (2021) 35(4):101545. doi: 10.1016/j.beem.2021.101545

32. Bravenboer N, Bredella MA, Chauveau C, Corsi A, Douni E, Ferris WF, et al. Standardised nomenclature, abbreviations, and units for the study of bone marrow adiposity: Report of the nomenclature working group of the international bone marrow adiposity society. *Front Endocrinol (Lausanne).* (2020) 10:923. doi: 10.3389/fendo.2019.00923

33. Craft CS, Li Z, MacDougald OA, Scheller EL. Molecular differences between subtypes of bone marrow adipocytes. *Curr Mol Biol Rep* (2018) 4(1):16–23. doi: 10.1007/s40610-018-0087-9

34. Tratwal J, Labella R, Bravenboer N, Kerckhofs G, Douni E, Scheller EL, et al. Reporting guidelines, review of methodological standards, and challenges toward harmonization in bone marrow adiposity research. report of the methodologies working group of the international bone marrow adiposity society. *Front Endocrinology.* (2020) 11:65. doi: 10.3389/fendo.2020.00065

35. Tavassoli M, Houchin DN, Jacobs P. Fatty acid composition of adipose cells in red and yellow marrow: A possible determinant of haematopoietic potential. *Scandinavian J Haematology.* (1977) 18(1):47–53. doi: 10.1111/j.1600-0609.1977.tb01476.x

36. Ren J, Dimitrov I, Sherry AD, Malloy CR. Composition of adipose tissue and marrow fat in humans by 1H-NMR at 7 Tesla. *J Lipid Res* (2008) 49(9):2055–62. doi: 10.1194/jlr.D800010-JLR200

37. Beekman KM, Regenboog M, Nederveen AJ, Bravenboer N, Akkerman EM, Maas M. Gender- and age-associated differences in bone marrow adipose tissue and bone marrow fat unsaturation throughout the skeleton, quantified using chemical shift encoding-based water–fat MRI. *Front Endocrinology.* (2022) 13:10. doi: 10.3389/fendo.2022.815835

38. Maciel JG, de Araújo IM, Carvalho AL, Simão MN, Bastos CM, Troncon LEA, et al. Marrow fat quality differences by sex in healthy adults. *J Clin Densitometry.* (2017) 20(1):106–13. doi: 10.1016/j.jocd.2016.08.002

39. Attané C, Estève D, Chaoui K, Iacovoni JS, Corre J, Moutahir M, et al. Human bone marrow is comprised of adipocytes with specific lipid metabolism. *Cell Rep* (2020) 30(4):949–958.e6. doi: 10.1016/j.celrep.2019.12.089

40. Lucas S, Tencerova M, von der Weid B, Andersen TL, Attané C, Behler-Janbeck F, et al. Guidelines for biobanking of bone marrow adipose tissue and related cell types: Report of the biobanking working group of the international bone marrow adiposity society. *Front Endocrinol* (2021) 12:744527. doi: 10.3389/fendo.2021.744527

41. Moore KA, Ema H, Lemischka IR. *In vitro* maintenance of highly purified, transplantable hematopoietic stem cells. *Blood.* (1997) 89(12):4337–47. doi: 10.1182/blood.V89.12.4337

42. Kim K, Doi A, Wen B, Ng K, Zhao R, Cahan P, et al. Epigenetic memory in induced pluripotent stem cells. *Nature.* (2010) 467(7313):285–90. doi: 10.1038/nature09342

43. McKinney-Freeman SL, Naveiras O, Daley GQ. Isolation of hematopoietic stem cells from mouse embryonic stem cells. *Curr Protoc Stem Cell Biol* (2008) 4 (1):1F.3.1–1F.3.10. doi: 10.1002/9780470151808.sc01f03s4

44. Naveiras O. *Novel determinants of the hematopoietic microenvironment in development and homeostasis.* (Harvard University: ProQuest Dissertations Publishing (2009), 3351000.

45. Rueden CT, Schindelin J, Hiner MC, DeZonia BE, Walter AE, Arena ET, et al. ImageJ2: ImageJ for the next generation of scientific image data. *BMC Bioinf* (2017) 18(1):529. doi: 10.1186/s12859-017-1934-z

46. During A. Lipid determination in bone marrow and mineralized bone tissue: From sample preparation to improved high-performance thin-layer and liquid chromatographic approaches. *J Chromatogr A.* (2017) 1515:232–44. doi: 10.1016/j.chroma.2017.08.004

47. Taylor SC, Nadeau K, Abbasi M, Lachance C, Nguyen M, Fenrich J. The ultimate qPCR experiment: Producing publication quality, reproducible data the first time. *Trends Biotechnol* (2019) 37(7):761–74. doi: 10.1016/j.tibtech.2018.12.002

48. Vandesompele J, Preter KD, Roy NV, Paepe AD. Accurate normalization of real-time quantitative RT-PCR data by geometric averaging of multiple internal control genes. *Genome Biol* (2002) 3:research0034.1. doi: 10.1186/gb-2002-3-7-research0034

49. Feugier P, Li N, Jo DY, Shieh JH, MacKenzie KL, Lesesve JF, et al. Osteopetrotic mouse stroma with thrombopoietin, c-kit ligand, and flk-2 ligand supports long-term mobilized CD34 $^{+}$ hematopoiesis *in vitro*. *Stem Cells Dev* (2005) 14(5):505–16. doi: 10.1089/scd.2005.14.505

50. Dexter TM, Allen TD, Lajtha L. Conditions controlling the proliferation of haemopoietic stem cells *in vitro*. *J Cell Physiol* (1977) 91(3):335–44. doi: 10.1002/jcp.1040910303

51. Dexter T, Lajtha L. Proliferation of haemopoietic stem cells in vitro. *Br J Haematology* (1974) 28(4):525–30. doi: 10.1111/j.1365-2141.1974.tb06671.x

52. Dexter TN, Testa NG. Differentiation and proliferation of hemopoietic cells in culture. *Methods in cell biology* (1976) 14:387–405. doi: 10.1016/s0091-679x(08)60498-7

53. Westen H, Bainton DF. Association of alkaline-phosphatase-positive reticulum cells in bone marrow with granulocytic precursors. *J Exp Med* (1979) 150(4):919–37. doi: 10.1084/jem.150.4.919

54. Baccin C, Al-Sabah J, Velten L, Helbling PM, Grünschläger F, Hernández-Malmierca P, et al. Combined single-cell and spatial transcriptomics reveal the molecular, cellular and spatial bone marrow niche organization. *Nat Cell Biol* (2020) 22(1):38–48. doi: 10.1038/s41556-019-0439-6

55. Gao J, Yan XL, Li R, Liu Y, He W, Sun S, et al. Characterization of OP9 as authentic mesenchymal stem cell line. *J Genet Genomics* (2010) 37(7):475–82. doi: 10.1016/S1673-8527(09)60067-9

56. Wolins NE, Quaynor BK, Skinner JR, Tzekov A, Park C, Choi K, et al. OP9 mouse stromal cells rapidly differentiate into adipocytes: characterization of a useful new model of adipogenesis. *J Lipid Res* (2006) 47(2):450–60. doi: 10.1194/jlr.D500037-JLR200

57. Yoshida H, Hayashi SI, Takahiro K, Ogawa M, Nishikawa S, Okamnura H, et al. The murine mutation osteopetrosis is in the coding region of the macrophage colony stimulating factor gene. *Nature* (1990) 345(6274):442–4. doi: 10.1038/345442a0E

58. Nakano T, Kodama H, Honjo T. Generation of lymphohematopoietic cells from embryonic stem cells in culture. *Science New Series.* (1994) 265(5175):1098–101. doi: 10.1126/science.8066449

59. Gubelmann C, Schwalie PC, Raghav SK, Roder E, Delessa T, Kiehlmann E, et al. Identification of the transcription factor ZEB1 as a central component of the adipogenic gene regulatory network. *Elife.* (2014) 3:e03346. doi: 10.7554/eLife.03346

60. Czamara K, Majzner K, Pacia MZ, Kochan K, Kaczor A, Baranska M. Raman spectroscopy of lipids: a review. *J Raman Spectroscopy.* (2015) 46(1):4–20. doi: 10.1002/jrs.4607

61. Kochan K, Maslak E, Krafft C, Kostogrys R, Chlopicki S, Baranska M. Raman spectroscopy analysis of lipid droplets content, distribution and saturation level in non-alcoholic fatty liver disease in mice. *J Biophotonics.* (2015) 8(7):597–609. doi: 10.1002/jbio.201400077

62. Le TT, Duren HM, Slipchenko MN, Hu CD, Cheng JX. Label-free quantitative analysis of lipid metabolism in living caenorhabditis elegans. *J Lipid Res* (2010) 51(3):672–7. doi: 10.1194/jlr.D000638

63. Wu H, Volponi JV, Oliver AE, Parikh AN, Simmons BA, Singh S. *In vivo* lipidomics using single-cell raman spectroscopy. *Proc Natl Acad Sci USA* (2011) 108(9):3809–14. doi: 10.1073/pnas.1009043108

64. Raclot T, Groscolas R. Differential mobilization of white adipose tissue fatty acids according to chain length, unsaturation, and positional isomerism. *J Lipid Res* (1993) 34(9):1515–26. doi: 10.1016/S0022-2275(20)36944-3

65. Tavakol DN, Tratwal J, Bonini F, Genta M, Campos V, Burch P, et al. Injectable, scalable 3D tissue-engineered model of marrow hematopoiesis. *Biomaterials.* (2020) 232:119665. doi: 10.1016/j.biomaterials.2019.119665

66. Suchacki KJ, Tavares AAS, Mattiucci D, Scheller EL, Papanastasiou G, Gray C, et al. Bone marrow adipose tissue is a unique adipose subtype with distinct roles in glucose homeostasis. *Nat Commun* (2020) 11(1):3097. doi: 10.1038/s41467-020-16878-2

67. Cawthorn WP, Scheller EL, Learman BS, Parlee SD, Simon BR, Mori H, et al. Bone marrow adipose tissue is an endocrine organ that contributes to increased circulating adiponectin during caloric restriction. *Cell Metab* (2014) 20(2):368–75. doi: 10.1016/j.cmet.2014.06.003

68. Dufau J, Shen JX, Couchet M, De Castro Barbosa T, Mejhert N, Massier L, et al. *In vitro* and *ex vivo* models of adipocytes. *Am J Physiology-Cell Physiol* (2021) 320(5):C822–41. doi: 10.1152/ajpcell.00519.2020

69. Tavassoli M. Marrow adipose cells. histochemical identification of labile and stable components. *Arch Pathol Lab Med* (1976) 100(1):16–8.

70. Raclot T, Oudart H. Selectivity of fatty acids on lipid metabolism and gene expression. *Proc Nutr Soc* (1999) 58(3):633–46. doi: 10.1017/S002966519900083X

71. Masia F, Glen A, Stephens P, Borri P, Langbein W. Quantitative chemical imaging and unsupervised analysis using hyperspectral coherent anti-stokes raman scattering microscopy. *Anal Chem* (2013) 85(22):10820–8. doi: 10.1021/ac402303g

72. Masia F, Glen A, Stephens P, Langbein W, Borri P. Label-free quantitative chemical imaging and classification analysis of adipogenesis using mouse embryonic stem cells. *J Biophotonics.* (2018) 11(7):e201700219. doi: 10.1002/jbio.201700219

73. Pacia MZ, Sternak M, Mateuszuk L, Stojak M, Kaczor A, Chlopicki S. Heterogeneity of chemical composition of lipid droplets in endothelial inflammation and apoptosis. *Biochim Biophys Acta (BBA) - Mol Cell Res* (2020) 1867(6):118681. doi: 10.1016/j.bbamcr.2020.118681

74. Sugiyama T, Hobro AJ, Pavillon N, Umakoshi T, Verma P, Smith N. Label-free raman mapping of saturated and unsaturated fatty acid uptake, storage, and return toward baseline levels in macrophages. *Analyst.* (2021) 146(4):1268–80. doi: 10.1039/D0AN02077J

75. Majka Z, Czamara K, Janus J, Kępczyński M, Kaczor A. Prominent hypertrophy of perivascular adipocytes due to short-term high fat diet. *Biochim Biophys Acta (BBA) - Mol Basis Disease.* (2022) 1868(2):166315. doi: 10.1016/j.bbadis.2021.166315

76. Czamara K, Majzner K, Selmi A, Baranska M, Ozaki Y, Kaczor A. Unsaturated lipid bodies as a hallmark of inflammation studied by raman 2D and 3D microscopy. *Sci Rep* (2017) 7(1):40889. doi: 10.1038/srep40889

77. Scheller EL, Rosen CJ. What's the matter with MAT? marrow adipose tissue, metabolism, and skeletal health: Marrow adipose tissue and skeletal health. *Ann New York Acad Sci* (2014) 1311(1):14–30. doi: 10.1111/nyas.12327

78. Hayashi YK, Matsuda C, Ogawa M, Goto K, Tominaga K, Mitsuhashi S, et al. Human PTRF mutations cause secondary deficiency of caveolins resulting in muscular dystrophy with generalized lipodystrophy. *J Clin Invest* (2009) 119(9):2623–33. doi: 10.1172/JCI38660

79. Ding SY, Lee MJ, Summer R, Liu L, Fried SK, Pilch PF. Pleiotropic effects of cavin-1 deficiency on lipid metabolism. *J Biol Chem* (2014) 289(12):8473–83. doi: 10.1074/jbc.M113.546242

80. Ding SY, Lee MJ, Summer R, Liu L, Fried SK, Pilch PF. Pleiotropic effects of cavin-1 deficiency on lipid metabolism. *J Biol Chem* (2014) 289(12):8473–83. doi: 10.1074/jbc.M113.546242

81. Zou W, Rohatgi N, Brestoff JR, Zhang Y, Scheller EL, Craft CS, et al. Congenital lipodystrophy induces severe osteosclerosis. *Baron R editor. PloS Genet* (2019) 15(6):e1008244. doi: 10.1371/journal.pgen.1008244

82. Zhang X, Robles H, Magee KL, Lorenz MR, Wang Z, Harris CA, et al. A bone-specific adipogenesis pathway in fat-free mice defines key origins and adaptations of bone marrow adipocytes with age and disease. *eLife.* (2021) 10:e66275. doi: 10.7554/eLife.66275

83. Li Z, Bowers E, Zhu J, Yu H, Hardij J, Bagchi DP, et al. Lipolysis of bone marrow adipocytes is required to fuel bone and the marrow niche during energy deficits. *eLife.* (2022) 11:e78496. doi: 10.7554/eLife.78496.sa2

84. Li Z, Bagchi DP, Zhu J, Bowers E, Yu H, Hardij J, et al. Constitutive bone marrow adipocytes suppress local bone formation. *JCI Insight* (2022) 1:e160915. doi: 10.1172/jci.insight.160915

85. Boutet E, El Mourabit H, Prot M, Nemani M, Khallouf E, Colard O, et al. Seipin deficiency alters fatty acid Δ9 desaturation and lipid droplet formation in berardinelli-seip congenital lipodystrophy. *Biochimie.* (2009) 91(6):796–803. doi: 10.1016/j.biochi.2009.01.011

86. Shi X, Li J, Zou X, Greggain J, Rødkær SV, Færgeman NJ, et al. Regulation of lipid droplet size and phospholipid composition by stearoyl-CoA desaturase. *J Lipid Res* (2013) 54(9):2504–14. doi: 10.1194/jlr.M039669

87. Aoki K, Kurashige M, Ichii M, Higaki K, Sugiyama T, Kaito T, et al. Identification of CXCL12-abundant reticular cells in human adult bone marrow. *Br J Haematology.* (2021) 193(3):659–68. doi: 10.1111/bjh.17396

88. Zhang Z, Huang Z, Ong B, Sahu C, Zeng H, Ruan HB. Bone marrow adipose tissue-derived stem cell factor mediates metabolic regulation of hematopoiesis. *Haematologica.* (2019) 104(9):1731–43. doi: 10.3324/haematol.2018.205856

89. Spindler TJ, Tseng AW, Zhou X, Adams GB. Adipocytic cells augment the support of primitive hematopoietic cells *In vitro* but have no effect in the bone marrow niche under homeostatic conditions. *Stem Cells Dev* (2014) 23(4):434–41. doi: 10.1089/scd.2013.0227

90. Zhong L, Yao L, Tower RJ, Wei Y, Miao Z, Park J, et al. Single cell transcriptomics identifies a unique adipose lineage cell population that regulates bone marrow environment. *Elife.* (2020) 9:e54695. doi: 10.7554/eLife.54695.sa2

91. Tzeng YS, NC C, YR C, HY H, WP C, Lai DM. Imbalanced osteogenesis and adipogenesis in mice deficient in the chemokine Cxcl12/Sdf1 in the bone mesenchymal Stem/Progenitor cells. *J Bone Mineral Res* (2018) 33(4):679–90. doi: 10.1002/jbmr.3340

92. Oh I, Ozaki K, Miyazato A, Sato K, Meguro A, Muroi K, et al. Screening of genes responsible for differentiation of mouse mesenchymal stromal cells by DNA micro-array analysis of C3H10T1/2 and C3H10T1/2-derived cell lines. *Cytotherapy.* (2007) 9(1):80–90. doi: 10.1080/14653240601016374

93. Takubo K, Nagamatsu G, Kobayashi CI, Nakamura-Ishizu A, Kobayashi H, Ikeda E, et al. Regulation of glycolysis by pdk functions as a metabolic checkpoint for cell cycle quiescence in hematopoietic stem cells. *Cell Stem Cell* (2013) 12(1):49–61. doi: 10.1016/j.stem.2012.10.011

94. Yu WM, Liu X, Shen J, Jovanovic O, Pohl EE, Gerson SL, et al. Metabolic regulation by the mitochondrial phosphatase PTPMT1 is required for hematopoietic stem cell differentiation. *Cell Stem Cell* (2013) 12(1):62–74. doi: 10.1016/j.stem.2012.11.022

95. Suda T, Takubo K, Semenza GL. Metabolic regulation of hematopoietic stem cells in the hypoxic niche. *Cell Stem Cell* (2011) 9(4):298–310. doi: 10.1016/j.stem.2011.09.010

96. Ito K, Carracedo A, Weiss D, Arai F, Ala U, Schafer ZT, et al. A PML-PPARδ pathway for fatty acid oxidation regulates haematopoietic stem cell maintenance. *Nat Med.* (2012) 18(9):1350–8. doi: 10.1038/nm.2882

97. Farge T, Saland E, de Toni F, Aroua N, Hosseini M, Perry R, et al. Chemotherapy-resistant human acute myeloid leukemia cells are not enriched for leukemic stem cells but require oxidative metabolism. *Cancer Discovery.* (2017) 7(7):716–35. doi: 10.1158/2159-8290.CD-16-0441

98. Al Saedi A, Bermeo S, Plotkin L, Myers DE, Duque G. Mechanisms of palmitate-induced lipotoxicity in osteocytes. *Bone.* (2019) 127:353–9. doi: 10.1016/j.bone.2019.06.016

99. Singh L, Tyagi S, Myers D, Duque G. Good, bad, or ugly: the biological roles of bone marrow fat. *Curr Osteoporosis Rep* (2018) 16(2):130–7. doi: 10.1007/s11914-018-0427-y

Frontiers in Endocrinology

Explores the endocrine system to find new therapies for key health issues

The second most-cited endocrinology and metabolism journal, which advances our understanding of the endocrine system. It uncovers new therapies for prevalent health issues such as obesity, diabetes, reproduction, and aging.

Discover the latest Research Topics

See more →

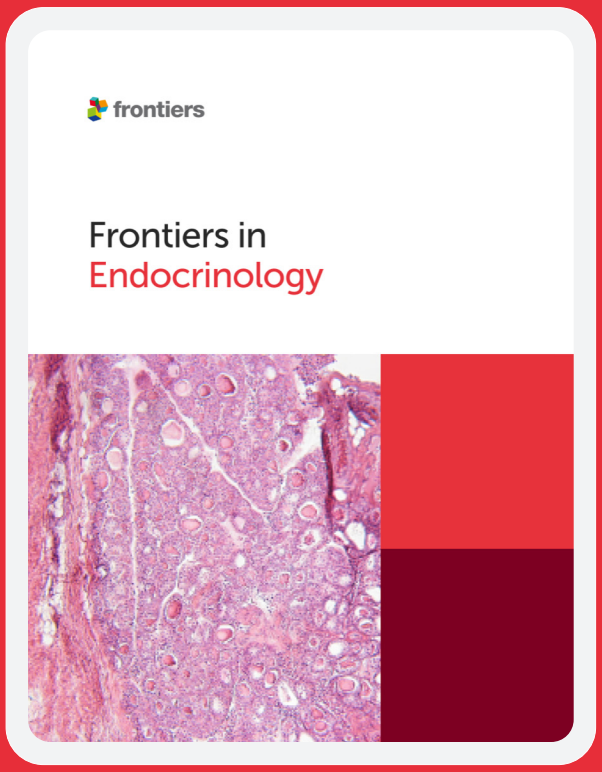

Frontiers

Avenue du Tribunal-Fédéral 34
1005 Lausanne, Switzerland
frontiersin.org

Contact us

+41 (0)21 510 17 00
frontiersin.org/about/contact